Nuclear Energy and the Environment

Green Separation
Techniques

Separations
Chemistry

Radiation
Chemistry

Nuclear Power
Plant

Fuel Recycle

Repository
Chemistry

EDITED BY

Chien M. Wai
and Bruce J. Mincher

Nuclear Energy and the Environment

ACS SYMPOSIUM SERIES **1046**

Nuclear Energy and the Environment

Chien M. Wai, Editor
Department of Chemistry
University of Idaho

Bruce J. Mincher, Editor
Aqueous Separations and Radiochemistry Department
Idaho National Laboratory

Sponsored by the
ACS Division of Nuclear Chemistry and Technology and ACS
Division of Industrial and Engineering Chemistry

American Chemical Society, Washington, DC

The paper used in this publication meets the minimum requirements of American National Standard for Information Sciences—Permanence of Paper for Printed Library Materials, ANSI Z39.48n1984.

PRINTED IN THE UNITED STATES OF AMERICA

Foreword

The ACS Symposium Series was first published in 1974 to provide a mechanism for publishing symposia quickly in book form. The purpose of the series is to publish timely, comprehensive books developed from the ACS sponsored symposia based on current scientific research. Occasionally, books are developed from symposia sponsored by other organizations when the topic is of keen interest to the chemistry audience.

Before agreeing to publish a book, the proposed table of contents is reviewed for appropriate and comprehensive coverage and for interest to the audience. Some papers may be excluded to better focus the book; others may be added to provide comprehensiveness. When appropriate, overview or introductory chapters are added. Drafts of chapters are peer-reviewed prior to final acceptance or rejection, and manuscripts are prepared in camera-ready format.

As a rule, only original research papers and original review papers are included in the volumes. Verbatim reproductions of previous published papers are not accepted.

ACS Books Department

Table of Contents

Preface

A renewed global interest in nuclear power is underway due to concerns about the contribution of combustion of fossil fuels to climate change and the unreliability of the supply of fossil fuels. Nuclear power is currently an important source of carbon-free, safe, and domestic energy in many countries. However, concerns about nuclear waste disposal and the proliferation of nuclear weapons have hindered its expanded use and continued development. As world demand for energy continues to rise, it is recognized that nuclear energy will be required to meet this demand in an environmentally sustainable manner. Responsible management of nuclear wastes, more efficient processes for conversion of uranium to energy, and effective and secure techniques for recycling used nuclear fuel are some of the key issues which must be addressed in order to develop sustainable nuclear energy technologies for the 21st century.

This book is based on the papers presented at a recent and very successful symposium entitled *Nuclear Energy and the Environment* held at the 238th American Chemical Society (ACS) National Meeting in Washington, DC, August 16-20, 2009. The 3-day ACS symposium was well attended with participants from Canada, France, Germany, Japan, Sweden, Taiwan, and the USA discussing research ideas and progress in separation of actinides and fission products, green separation techniques, radiation effects, and repository chemistry. This book starts with an overview of challenges in actinide separation chemistry for advanced nuclear fuel cycles and roadmaps of new cleanup technologies by the U.S. Department of Energy. It is followed by 3 sections covering recent research and development in separations chemistry, radiation chemistry, and repository chemistry. The book documents reasons to be optimistic for the future of nuclear power and challenges facing nuclear scientists and engineers today.

We acknowledge support from the ACS Nuclear Chemistry and Technology Division and the Separation Science and Technology Subdivision of the ACS Division of Industrial and Engineering Chemistry for the symposium. The ACS Books Department is thanked for their encouragement and support in the publication of the book. Finally, we thank the authors for their contributions and the reviewers for their time and valuable comments.

Chien M. Wai
Department of Chemistry
University of Idaho, Moscow, Idaho 83844

Bruce J. Mincher
Aqueous Separations and Radiochemistry Department
Idaho National Laboratory, Idaho Falls, Idaho 83415

Acknowledgement

The editors thank the following associate editors for their help in organizing the symposium, editing manuscripts, and greatly improving the quality of the final symposium series book: Linfeng Rao, Dean R. Peterman, Sydney S. Koegler, and Marsha J. Lambregts.

Introduction

Chapter 1

The Nuclear Renaissance: Producing Environmentally Sustainable Nuclear Power

Bruce J. Mincher*

Aqueous Separations and Radiochemistry Department, Idaho National Laboratory, P.O. Box 1625, Idaho Falls, ID 83415-6180 USA
bruce.mincher@inl.gov

A renewed global interest in nuclear power, the so-called nuclear renaissance, is underway. Energy demand continues to rise, and it is now recognized that nuclear energy will be required to meet this demand. The long-term environmental sustainability of expanded nuclear power production will require more efficient processes for the conversion of uranium to energy. Thus, for purposes of increased efficiency of energy production and to reduce the amount of waste interred in a repository it is likely that the reprocessing of spent nuclear fuel, or "closed" fuel cycle, will be more widely adopted in the future. This will be a major component of the development of environmentally sustainable nuclear power. This chapter introduces the symposium book documenting the latest research from around the world with a goal of creating an environmentally sustainable nuclear power industry. Held 16-20 August, 2009 in Washington DC, USA, the symposium hosted scientists from the fuel cycle countries of Canada, China, Germany, Sweden, France, Japan and the USA. The scientists in attendance presented plans and progress for the aqueous separation of fission products and the minor actinides to improve the efficiency of power generation and to minimize the amount of material requiring geological disposal.

Introduction

A renewed global interest in nuclear power, the so-called nuclear renaissance, is underway. As developed and developing countries continue to expand their populations and economies, energy demand continues to rise, and it is now recognized that nuclear energy will be required to meet this demand. The ascendance of nuclear power is being driven by both political and environmental concerns. The sources of fossil fuels are unreliable. Political turmoil frequently interrupts supply resulting in unpredictable prices. These facts were recognized early by France, which became the first nation to make a major commitment to nuclear electricity generation following the oil embargo of the 1970s. France now generates nearly 80% of its power domestically from a fleet of nearly 60 nuclear reactors. More recently, natural gas supplies to Europe have also proven to be unreliable, and while no other European country has yet announced an expansion in nuclear power plant construction that result seems to be inevitable. Meanwhile, Japan, China, India and the USA are expanding their commitments to nuclear power as a domestic source of energy.

In addition to problematic supplies are concerns about the possible contribution of fossil fuels to climate change. A final product of the burning of oil, coal and natural gas is CO_2, which is a greenhouse gas. The concentration of CO_2 in Earth's atmosphere is about 380 ppmv, with a pre-industrial revolution value of 280 ppmv being estimated. Although there is not a consensus (*1*), many believe that the increase in CO_2 concentration is raising the average global temperature. Some governments are considering nuclear power as a carbon-free source of energy in an attempt to meet CO_2 emission reduction goals.

Nuclear power is already an important source of safe, domestic, carbon-free energy. For example about 20% of electricity consumed in the USA and 30% in Europe is produced in nuclear reactors. The percentage as base-load electricity is even higher. However, concerns about waste disposal and weapons proliferation have until now made its expanded adoption politically untenable. Proposals for the new nuclear fuel cycle are designed to address these concerns. The back end of the fuel cycle, where uranium is recycled and long-lived radioactive waste is treated has received special attention.

The long-term environmental sustainability of expanded nuclear power production will require more efficient processes for the conversion of uranium to energy. Like fossil fuels, the earth contains a finite supply of uranium. This uranium must be mined, refined and enriched at significant cost prior to fuel fabrication. The light-water reactors in common use today recover only ~1% of the energy potential of the uranium that is used to construct a fuel element (*2*). The once-through, or "open" fuel cycle, where used reactor fuel is simply disposed in a geological repository is clearly not sensible given this low efficiency of energy extraction. Recovery of unfissioned uranium will significantly extend the reactor fuel inventory into the future. For example, it has been estimated that the recovery of uranium and/or plutonium results in 15% (*2*) to 30% (*3*) natural uranium savings. There are additional cost savings in reduced needs for uranium enrichment.

About 10,500 t of used fuel are already discharged yearly from more than 400 nuclear reactors around the world (*4*). The rate of spent fuel generation could reach 15,000 t by 2050 (*5*) and this spent fuel contains appreciable quantities of actinides and fission products, some with very long half-lives. For example, 1 t of UO_2 fuel, after 30 GW days of burn-up, contains 950 kg U, 9 kg Pu, 75 g Np, 140 g Am, 47 g Cm and 31 kg fission products (*6*). With half-lives ranging from 433 years for [241]Am to 2.4 million years for [237]Np, the α-emitting actinide nuclides determine the radiotoxicity of the waste for periods of time on a geological scale. The partitioning of these radionuclides and their transmutation to short-lived isotopes will significantly reduce the long-term hazard (*7*). Thus, for purposes of increased efficiency of energy production and to reduce the amount of waste interred in a repository it is likely that the reprocessing of spent nuclear fuel, or "closed" fuel cycle, will be more widely adopted in the future than currently. Thus, the development of the future closed fuel cycle will be a major component of the development of environmentally sustainable nuclear power.

This symposium book documents the latest research from around the world with a goal of creating an environmentally sustainable nuclear power industry. Held 16-20 August, 2009 in Washington DC, USA, the symposium hosted scientists from the fuel cycle countries of Canada, China, Germany, Sweden, France, Japan and the USA. The scientists and students in attendance presented plans and progress for the aqueous separation of fission products and the minor actinides to improve the efficiency of power generation and to minimize the amount of material requiring geological disposal. Although much progress has been made, significant challenges remain. These challenges are being overcome by the science-based approaches of dedicated researchers, as revealed in the symposium. This includes not only the development of new separations processes, some being nonaqueous, but also responsible disposition of the final waste-form following separations, as well as development of the analytical techniques necessary for both. The remediation of previously contaminated sites, mainly contaminated by cold-war activities rather than by power generation, is also a concern in the demonstration to a suspicious public that nuclear power is environmentally sustainable.

Alternatives to PUREX

Aqueous reprocessing currently begins with the chopping and dissolution of the used reactor fuel in nitric acid. The resulting acidic and highly radioactive solution is then contacted with an appropriate organic solvent to selectively recover desired metal ions. Although no longer practiced in the USA, the PUREX (Plutonium Uranium Refining by EXtraction) solvent extraction process for the recycle of light-water reactor fuels has been in use for decades. Consisting of 30% tributyl phosphate (TBP) in an alkane diluent, the process can either partition uranium separately or co-extract uranium, neptunium, and plutonium depending on how the valence states of the latter metals are set during pre-treatment. The history of its development and use over six decades has been reviewed by McKay (*8*). The metal-loaded solvent is then stripped to recover the uranium and/or

neptunium and plutonium and recycled for further contacts with newly dissolved fuel.

Both aqueous and non-aqueous alternative extraction processes are under development. Among aqueous processes under development are the use of alkylamides which provide good separation factors for the partitioning of U and Pu from fission products and therefore have been proposed as replacement compounds for TBP (*9*). The most mature example is the European DIAMEX (DIAmide EXtraction) process, based upon the malonamide dimethyl dioctyl hexylethoxymalonamide (DMDOHEMA) (*10*). A related diglycolamide extractant *N*, *N*, *N'*,*N'*-tetraoctyl-3-oxapentane-1,5-diamide (TODGA) has received study in Europe and Japan (*11*). Unlike TBP, the amides do not contain phosphorous. This may be an important advantage in that they are incinerable, simplifying the waste disposal of spent solvents. This is referred to as the CHON principal, in which ligand design favors molecules containing only C, H, O and N atoms. Other benefits include the production of relatively benign radiolysis products. The potential advantages and uses of amides as actinide extractants were reviewed by Gasparini and Grossi (*12*). This symposium contains several papers discussing the use of amidic compounds as actinide extractants.

Several research groups reported the development of non-aqueous separation strategies. The demonstration of the direct dissolution of oxides by ligand assisted SFE, containing the CO_2-soluble TBP•HNO_3 complex, opens up novel opportunities for fuel reprocessing while minimizing secondary waste generation. The separation of uranium from lanthanide fission products is possible directly from their oxides by proper selection of operating temperature and pressure. Supercritical CO_2 and ionic liquids are green separations reagents because they minimize secondary waste and rely on relatively harmless diluents for their metal complexing agents. Their use in reprocessing and in uranium recovery from waste is reviewed here.

Minor Actinide Separations

Traditionally, the remaining fission products such as Cs, Sr and the lanthanides, as well as the minor actinides Np, Am and Cm have been disposed as high-level waste following the PUREX extraction. Most current plans call for vitrification of the waste, and storage of the glass inside metal containers disposed in a geological repository. However, these minor actinides are the major contributors to the radiotoxicity of the high-level waste after 1000 years of decay time. Their presence has provoked requirements that propose to guarantee the integrity of the waste forms over unimaginably long periods of time. Current fuel cycle proposals call for the removal and fission of the minor actinides in fast reactors. Their conversion into short-lived fission products, in the process known as partitioning and transmutation, would eliminate the risks associated with their long-term underground storage.

Neptunium can be partitioned using the PUREX process given careful attention to valence control; however, trivalent Am and Cm require the development of new approaches. Their separation from the fission-product

lanthanides is one of the more formidable challenges associated with the design of the advanced fuel cycle. The lanthanides represent about a third of the total fission product inventory and they have very similar chemical properties. They also have large neutron capture cross sections and poor metal alloy properties and thus they can not be incorporated into fast reactor fuel. A separation amenable to currently existing aqueous solvent extraction processes is therefore desired, and the current approaches being studied around the world were presented in this symposium.

Among them, the TALSPEAK (Trivalent Actinide Lanthanide Separation by Phosphorous reagent Extraction from Aqueous Komplexes) process is favored in the USA. It is, however, a complicated process and although it has undergone flow-sheet testing much remains to be elucidated about the mechanism by which the lanthanides are complexed and extracted by diethylhexylphosphoric acid (HDEHP) while the actinides are complexed and retained in the aqueous phase by diethylenetriaminepentaacetic acid (DTPA) in the presence of molar amounts of lactic acid (*13*). The lactic acid buffer allows for $\alpha_{Am/Eu}$ separation factors of ~ 90, with the use of most other buffer systems being somewhat less selective. A novel approach to combine TALSPEAK and TRUEX (TRansUranic EXtraction) into one step to simplify the currently-proposed fuel cycle has been proposed and is discussed here. Simplification of current proposals is considered to be necessary prior to practical implementation.

In European work, current investigation into trivalent actinide/trivalent lanthanide partitioning is focused on a process called SANEX (Selective ActiNide EXtraction). SANEX adheres to the CHON principal by using heterocyclic nitrogen donor ligands in combination with diamides to selectively extract the trivalent actinides from an actinide/lanthanide acidic solution. Kolarik (*14*) and Ekberg et al (*15*) have reviewed the history of the development of these heterocyclic nitrogen donor ligands including attempts to improve their radiolytic and hydrolytic stability. Among the most promising of these compounds are various derivatives of the 2,6-bistriazinylpyridines (BTPs). Separation factors as high as $\alpha_{Am/Eu}$ of ~ 120 for extractions from 1 M HNO_3 have been achieved (*16*)..

Other techniques for separation of the trivalent actinides from the trivalent lanthanides are also being considered. Among them are the use of higher oxidation states of americium (*17*), and the use of soft-donor-S ligands such as dithiophosphinic acids, and column chromatographic techniques based on the BTPs as discussed in this symposium. Each of these techniques is less mature than TALSPEAK or SANEX but nonetheless show promise in achieving this difficult separation.

Radiation Chemistry

The design of successful separations for the nuclear fuel cycle relies on the use of reagents that are stable in an acidic radioactive environment. Hydrolysis and radiolysis of ligands, diluents and solvent modifiers can have deleterious effects on metal distribution ratios, separation factors and solvent physical properties (*18*, *19*). For example, the introduction of solvent reconditioning steps to the PUREX process was necessary to remove TBP degradation products which

interfered with separation factors for uranium and fission products, which adds to the cost and complexity of process design. For the new fuel cycle increased attention is being given to these issues, and the evolution of the ligands in the DIAMEX and SANEX processes shows a series of structural modifications that have evolved meant to address them. The radiolytic production of transient reactive radical species from irradiated solution such as •OH and •NO$_3$ and their reactions with solution constituents are now recognized to be major sources of radiation damage. The increased attention being devoted to radiation chemistry in solvent design is reflected in the fact that an entire session of the symposium was devoted to this phenomenon. Overviews of the chemistry of irradiated nitric acid, and for radiation chemistry in solvent extraction are provided here. Research findings related to specific solvent systems being developed for separation of the trivalent actinides from the trivalent lanthanides are also presented.

A common source of undesirable products in irradiated nitric acid is due to nitration reactions and the mechanism of radiolytic nitration is given special attention where it is shown that under acidic conditions much nitration is due to the radiolytic production of nitrous acid. By far, most radiation chemical research has been performed with γ-sources, despite that a great deal of α-activity is to be expected in the fuel dissolution. Given the much higher linear energy transfer of the α-particle it might be expected that its effects would be different. A comparison of both radiation sources in the radiolytic degradation of DMDOHEMA interestingly reports that α-effects were less severe. A recent Japanese report has come to a similar conclusion for TODGA radiolysis (*20*). Radiation effects are not a black box, and research into the mechanisms of solvent system radiolysis should help to design more robust systems with less demanding solvent reconditioning needs.

Chemistry in the Repository

Following the separations described above the fuel dissolution contains primarily the lanthanides and possibly other fission products such as Cs and Sr, depending on whether these latter activities have been removed in a dedicated step (*21*). In the absence of the actinides the amount of time required for decay to low levels is greatly decreased. Most scenarios call for the vitrification of such radioactive waste as a glass, to be contained in metal canisters destined for deep disposal in a geological repository. Low-level waste might simply be grouted prior to disposal. In countries devoted to the once-through, open fuel cycle, used fuel elements are proposed to be containerized and then disposed in a deep repository. Canada, for example, uses natural uranium in its reactors and will not likely need to reprocess to recover unfissioned [235]U. The corrosion of UO$_2$ under repository conditions is discussed here. Multiple engineered barriers will provide containment of the radioactive materials in isolation from the environment. Among them are the non-leachable waste forms themselves, being glass or metal-clad oxide fuels. These are stored in appropriate canisters, which are embedded in absorbent clays such as bentonite. Repository locations will be selected in the most appropriate available geologically stable locations.

Despite these precautions it must be assumed that after many thousands of years the containment canisters will be breached. Additionally, many surface sites remain radioactively contaminated primarily due to weapons production and testing associated with the cold war and the testing of experimental reactors. For these reasons major research efforts continue to be devoted to the behavior of radionuclides, especially the actinides, in the environment and the remediation of contaminated sites. Once released to the environment, the mobility and transport of the actinides to sites remote from that release will be limited by their speciation. The form in which they occur will be determined by chemical and biological processes. Among important chemical process are carbonate formation, redox cycling or hydrolysis as discussed here.

Conclusion

This symposium brought together many of the scientists and engineers working globally to ensure a continued supply of clean nuclear energy for growing economies and populations. Environmentally sustainable nuclear energy production requires the recycling of uranium from used light water reactor fuels, and the partitioning and transmutation, rather than the geological disposition, of the minor actinides. Several approaches are being investigated world-wide. Some amount of shorter-lived radioactive waste will still require deep geological disposition, and the chemistry of the repository is also being investigated to provide an understanding of the best containment strategies and the behavior of radionuclides in the environment. Taken in sum, the science-based approach to used fuel recycling and waste disposal revealed in this symposium illustrates that the environmental responsibilities of future nuclear energy production are being given serious attention. Progress is being made in the difficult issues of actinide/lanthanide separations and understanding radionuclide speciation. This is necessary for the successful fulfillment of the nuclear energy renaissance now in progress.

References

1. Plimer, I. *Heaven and Earth: Global Warming, the Missing Science*. Conner Court Publishing: Ballan, Victoria, Australia, 2009.
2. Boullis, B. In Proceedings of ISEC 2008, International Solvent Extraction Conference; Moyer, B. A., Ed.; 2008; Volume 2, p 29.
3. Paviet-Hartmann, P.; Lineberry, M.; Benedict, R. Nuclear Fuel Reprocessing. In *Nuclear Engineering Handbook*; Kok, K. D., Ed.; CRC Press: Boca Raton, FL, 2009; pp 315−366.
4. *Implications of Partitioning and Transmutation in Radioactive Waste Management*; Technical Report Series, ISSN 0074-1914, No. 435; International Atomic Energy Agency: Vienna, 2004.
5. Laidler, J. J. In Proceedings of ISEC 2008, International Solvent Extraction Conference; Moyer, B. A., Ed.; 2008; Volume 1, p 695.

6. Benedict, M.; Pigford, T. H.; Levi, H. W. *Nuclear Chemical Engineering*, 2nd ed.; McGraw-Hill: New York, 1981.

7. *Actinide and Fission Product Partitioning and Transmutation-Status and Assessment Report*; Organisation for Economic Co-operation and Development, Nuclear Energy Agency (OECD-NEA): Paris, 1999.

8. McKay, H. A. C. Introduction. In *Science and Technology of Tributyl Phosphate*; Schulz, W. W., Navratil, J. D., Eds.; CRC Press: Boca Raton, FL, 1984; Volume 1, pp 1−14.

9. Thiollet, G.; Musikas, C. *Solvent Extr. Ion Exch.* **1989**, *7*, 813–827.

10. Berthon, L.; Morel, J. M.; Zorz, N.; Nicol, C.; Virelizier, H.; Madic, C. *Sep. Sci. Technol.* **2001**, *36*, 709–728.

11. Modolo, G.; Asp, H.; Schreinemachers, C.; Vijgen, H. *Solvent Extr. Ion Exch.* **2007**, *25*, 703–721.

12. Gasparini, G. M.; Grossi, G. *Solvent Extr. Ion Exch.* **1986**, *4*, 1233–1271.

13. Nilsson, M.; Nash, K. L. *Solvent Extr. Ion Exch.* **2007**, *25*, 665–701.

14. Kolarik, Z. *Chem. Rev.* **2008**, *108*, 4208–52.

15. Ekberg, C.; Fermvik, A.; Retegan, T.; Skarnemark, G.; Foreman, M. R. S.; Hudson, M. J.; Englund, S.; Nilsson, M. *Radiochim. Acta* **2008**, *96*, 225–333.

16. Geist, A.; Hill, C.; Modolo, G.; Foreman, M. R. St. J. *Solvent Extr. Ion Exch.* **2006**, *24*, 463–483.

17. Mincher, B. J.; Martin, L. R.; Schmitt, N. C. *Inorg. Chem.* **2008**, *47*, 6984–6989.

18. Pikaev, A. K.; Kabakchi, S. A.; Egorov, G. F. *Radiat. Phys. Chem.* **1988**, *31*, 789–803.

19. Mincher, B. J.; Modolo, G.; Mezyk, S. P. *Solvent Extr. Ion Exch.* **2009**, *27*, 1–25.

20. Sugo, Y.; Taguchi, M.; Sasaki, Y.; Hirota, K.; Kimura, T. *Radiat. Phys. Chem.* **2009**, *78*, 1140–1144.

21. Riddle, C. L.; Baker, J. D.; Law, J. D.; McGrath, C. A.; Meikrantz, D. H.; Mincher, B. J.; Peterman, D. R.; Todd, T. A. *Solvent Extr. Ion Exch.* **2005**, *23*, 449–461.

Overview

Chapter 2

Separations Research for Advanced Nuclear Fuel Cycles

T. A. Todd*

Laboratory Fellow and Director, Fuel Cycle Science and Technology, Division Idaho National Laboratory, P.O. Box 1625, Idaho Falls, ID 83415
***terry.todd@inl.gov**

The United States Department of Energy has been conducting research into advanced separation methods for the recycle of used nuclear fuel components for the last decade. Separation of certain used fuel constituents allows for improved waste management (by developing waste forms tailored for specific long-lived radioisotopes) and transmutation of long-lived actinide elements. One incentive for processing used fuel is to reduce the time that the overall radiotoxicity of the used fuel is greater than that of natural uranium ore. Spent fuel must be managed for geologic time scales (300,000+ years) while fuel that is processed to recycle and transmute actinide elements requires management for engineering time scales (hundreds of years). Efficient separation processes are needed for treatment of current light water reactor used fuel and future fast transmutation fuel (metal or oxide). Low process losses and product purity sufficient to meet fuel specifications are needed.

Introduction

The United States has recently commissioned a "blue ribbon commission" to provide recommendations for developing a safe, long-term solution to managing the Nation's used nuclear fuel and nuclear waste (*1*). One strategy that will likely be considered by the commission is the treatment of used nuclear fuel to recycle actinide elements for their unused energy value, as well as to transmute higher actinides. The United States Department of Energy has been researching advanced separation methods for the recycle of used nuclear fuel components

for about the last decade (*2*, *3*). The focus of the current research program is long-term, science-based research into advanced recycle technologies. Paramount to any transmutation scenario is the separation of transuranium actinides, primarily plutonium, neptunium, americium and curium from the rest of the used fuel constituents. A number of technologies have been recently studied and demonstrated in laboratory-scale experiments (*4*, *5*). Additional examples are provided in the following chapters of this symposium series book.

The potential benefits of separating out the actinides from used fuel for reuse include utilizing their unused energy potential and transmutation to shorten the time they are radioactive. Used nuclear fuel that is directly disposed to a repository retains a radiotoxicity (relative to natural uranium ore) that requires management of the fuel for several hundred thousand years. By separating the actinides and recycling them into reactors (either thermal or fast) the radiotoxicity decreases dramatically and for the scenario of recycle in fast spectrum reactors, is less radiotoxic than natural uranium ore in several hundred years. This equates to the responsible management of nuclear wastes for *geologic* time scales in the case of direct disposal or *engineering* time scales in the case of separation/transmutation. There are still some very long lived fission products that would require disposal in a repository, (iodine-129, technetium-99 and Cs-135), but because their half-lives are very long (15.9 million years, 213,000 years, and 2.3 million years, respectively) their specific activity (i.e. radiotoxicity) is quite low. The radiotoxicity (normalized to natural uranium ore) for used fuel directly disposed and with the uranium and transuranics recycled is shown in Figure 1.

Additionally, any geologic repository will have to manage heat from the decay of used fuel or radioactive waste products. By removing plutonium and americium from the fuel, transmuting and not placing it in the repository, the peak long-term heat load in the repository is greatly reduced. This was a major benefit for the proposed Yucca Mountain repository, and would likely benefit other repository designs as well, but to a lesser extent.

The U.S. separations research program has recently shifted from an applied process development/demonstration focus to a more fundamental research program. It is recognized that any successful process must have a solid understanding of the process chemistry before it could be successfully implemented. A primary focus of the research program it to develop robust, simplified methods of minor actinide separation (americium or americium and curium) from lanthanides. Research into thermodynamics, kinetics, coordination chemistry, radiation chemistry and interfacial transport mechanisms is currently underway for aqueous and electrochemical technologies. Additionally, research into innovative separation technologies, involving reactive gases and/or volatility and alternative process chemistries such as carbonate chemistry is in progress.

Minor Actinide Separation

The U.S. Fuel Cycle Research and Development (FCR&D) program is researching new methods of separating the minor actinides (Am, Cm) from
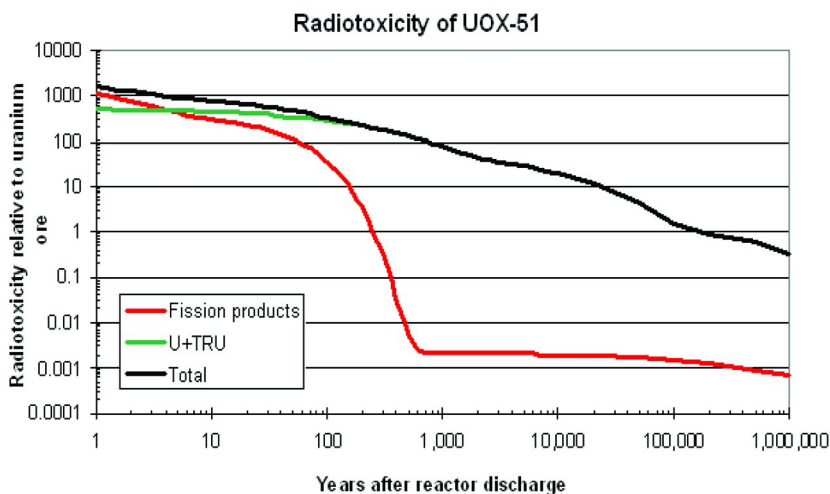
Figure 1. Used nuclear fuel radiotoxicity vs. time (see color insert)

lanthanides, as well as methods to partition americium from curium. Specific areas of research are focused on:

- Developing a more robust one-step An/Ln separation process
- Developing a broad operating envelope of An/Ln separation processes through better fundamental understanding
- Developing a viable method to separate Am from Cm and Ln
- Establishing a strong scientific basis for future process selection

The primary benefit of this research is expected to be a significant simplification of fuel recycle methods, resulting in overall improvement in economics and increased acceptability of the nuclear fuel cycle.

One of the underlying aspects of developing a one-step An/Ln separation process as well as developing a broad operating envelope and scientific basis, is to understand the competing factors in current separation processes such as the TALSPEAK process (6). This process, and related processes such as the SANEX process (7), rely on the strong complexation of actinides and lanthanides by an organic extractant such as di-2-ethylhexylphosphoric acid (HDEHP), and the complexation of the actinides in the aqueous phase by another complexant such as diethylenetriaminepentacetic acid (DTPA), in the presence of a buffer such as lactic acid. Investigations of the thermodynamic and kinetic effects of the TALSPEAK process have led to the development of a preliminary thermodynamic model. However, this model predicts a different pH dependence on An (III) and Ln (III) distribution ratios than is observed experimentally (8). Possible causes for this discrepancy include ternary metal complex formation involving lactate and HDEHP in the organic phase, a ternary metal complex formation involving lactate and DTPA in the aqueous phase, activity coefficient variation, possible micellization behavior, and kinetic effects. It is expected that as a greater understanding of the TALSPEAK chemistry is developed, this knowledge will

translate to other An/Ln separation chemistry applications (such as alternative extractants) as well.

Purposeful manipulation of ternary metal complexes in the aqueous phase in a TALSPEAK-type extraction system is another avenue of research being investigated to effect Am/Cm selectivity. Research into appropriately sized aqueous complexants has shown some promise in fitting the secondary ligand in the open coordination site, making complexation more favorable for the slightly larger Am (III) cation.

Another approach to a simplified An (III) separation is the combining of the extractants of the TRUEX and TALSPEAK processes. The hypothesis being explored is that the combined extractant would extract An (III) and Ln (III) elements in nitric acid with selective stripping of An (III) occurring in a buffered, complexant solution. This approach is discussed in Chapter 10 by Lumetta et al.

Molecular modeling is being employed to identify and select targets for synthesis of soft-donor ligands in the bis(dithiophosphinic) acid family. This effort is focused on identifying ligands that are designed for optimal Am(III) binding, and therefore provide some selectivity for Am over Cm and the lanthanides.

The above methods seek to identify ligands or ligand systems that selectively complex Am(III) in the presence of Ln(III). In a different approach, selective extraction of Am (V) or (VI) from Cm (III) and Ln (III) has been demonstrated in organic solvents (*9*). The greatest challenge with this approach is being able to hold the Am in the higher oxidation state long enough to extract it. Another approach would be to extract Am (III) with Cm (III) and Ln (III) in a TRUEX-like extractant, and then selective strip Am (V) from the loaded solvent. A third approach would be to utilize an actinyl-selective complexant that would stabilize Am in the penta- or hexavalent state.

Electrochemical methods for separation of Am (IV) or (VI) from Cm (III) and Ln (III) in room temperature ionic liquids is another approach being investigated.

Finally, methods to separate Am (III) from Ln (III) using alkaline carbonate conditions or inorganic ion exchangers are also being investigated. It can be seen that this science-based approach is investigating multiple possible solutions to the problem of actinide separations, and is thus expected to yield an optimal solution.

Fundamental Separations Research

Understanding the fundamental properties of separation processes is a major effort of the FCR&D program. A key activity that supports the minor actinide separation activities is developing an understanding of the thermodynamic and kinetic behavior of the trivalent actinides and lanthanides in the TALSPEAK process using microcalorimetry, fluorescence and conventional spectrophotometric techniques, radiochemical techniques, and stopped flow kinetics. This work builds on recently developed methodologies and will focus on a) studying the behavior of the fundamental thermodynamic parameters $\Delta G°$, $\Delta H°$ and $\Delta S°$ in relation to changes in the extraction media; b) characterization of the solution chemistry parameters for the actinides and lanthanides within the operational envelope of the TALSPEAK process. It is envisaged that the results of

these studies will be useful in improving the TALSPEAK process and/or provide a useful starting point for the development of alternative Am/Cm separation methods.

Another key area of research is the area of radiation chemistry (*10*, *11*). Radiation chemistry may adversely affect the separations process in a number of ways. In addition to direct radiation damage, the formation of free radicals in solution may also damage organic solvents indirectly. Gamma and alpha radiolysis are of particular interest, as well as understanding radiolysis mechanisms needed to develop predictive tools/models. In the past, most work involved performing solvent extraction experiments on irradiated solvents. Today, a more fundamental chemical investigation includes steady state radiolysis and identification of decomposition products as well as pulse radiolysis to understand the kinetics of free radical reactions with solutes. These data will be important in the overall development of any separation process in the presence of high radiation fields that exist in used nuclear fuel.

Electrochemical Technologies

Electrochemical technologies offer another approach to processing used nuclear fuel (*12*). This approach is particularly important for the recycle of transuranic elements from metal fast reactor fuel. The current research approach utilizes electrochemical separation in a molten KCl/LiCl salt phase. The focus of R&D for electrochemical technology will be to demonstrate key technical issues directly related to the feasibility of a sustainable electrochemical technology. Of particular importance are TRU recovery (losses and purity), understanding of the process operating envelope over a broad range of conditions, removal of TRU and fission products from salt (to enable salt recycle and improve economics) development and optimization of spent salt and metallic waste forms, and on-line near-real time process monitoring and control.

Transformational Separation Technologies

A new area of research is in the area of innovative separation technologies that could result in a new approach to used fuel treatment, beyond conventional methods using nitric acid dissolution/solvent extraction or electrochemical processing in molten salts. This approach may utilize alternative media (e.g. ionic liquids, supercritical fluids, alkaline chemistry, gaseous phase, etc) to facilitate advanced separation methods. The goal of any new process would be to simplify processing, and maintain needed selectivity.

Summary

Treatment of used nuclear fuel to separate actinides and recycle them for additional energy and transmutation of long-lived isotopes can provide substantial benefit in the long-term management of used fuel. For a closed fuel cycle to be cost effective, new approaches to used fuel separations are being investigated, as well

as developing a greater understanding of the fundamental chemistry of separation processes.

Acknowledgments

References

1. Secretary Chu Announces Blue Ribbon Commission on America's Nuclear Future, 2010. U.S. Department of Energy. http://www.energy.gov/news/8584.htm.
2. Todd, T. A.; Felker, L. K.; Vienna, J. D.; Bresee, J. C.; Lesica, S. *The Advanced Fuel Cycle Initiative Separations and Waste Campaign: Accomplishments and Strategy*. In Proceedings of Global 2009, Paris, September 2009.
3. Todd, T. A.; Wigeland, R. A. Advanced Separation Technologies for Processing Spent Nuclear Fuel and the Potential Benefits to a Geologic Repository. In *Separations for the Nuclear Fuel Cycle in the 21st Century*; Lumetta, G. J., Nash, K. L., Clark, S. B., Friese, J. I., Eds.; ACS Symposium Series 933; American Chemical Society: Washington, DC, pp 41−55.
4. Periera, C.; Vandegrift, G. F.; Regalbuto, M. C.; Bakel, A. J.; Laidler, J. J. *A Summary of the Lab-Scale Demonstrations of UREX+ Processes at Argonne National Laboratory*. In Proceedings of Global 2007, Boise, ID, September 2007.
5. Jubin, R. T.; et al. *CETE R&D at the Oak Ridge National Laboratory Supporting Management of Nuclear Waste*. In Proceedings of Waste Management '09, Phoenix, AZ, March 2009.
6. Weaver, B.; Kappelmann, F. A. *J. Inorg. Nucl. Chem.* **1968**, *30*, 263–272.
7. Hill, C.; Guillaneux, D.; Berthon, L. *SANEX-BTP Process Development Studies*. In Proceedings of the International Solvent Extraction Conference (ISEC), 2002; 1205−1209.
8. Nilsson, M.; Nash, K. L. *Solvent Extr. Ion Exch.* **2009**, *27*, 354–377.
9. Mincher, B. J.; Martin, L. R.; Schmitt, N. C. *J. Inorg. Chem.* **2008**, *47*, 6984–6989.
10. Mincher, B. J.; Modolo, G.; Mezyk, S. P. *Solvent Extr. Ion Exch.* **2009**, *27*, 1–25.
11. Martin, L. R.; Mexyk, S. P.; Mincher, B. J. *J. Phys. Chem. A.* **2009**, *113*, 141–145.
12. Li, S. X.; Johnson, T. A.; Westphal, B. R.; Goff, K. M.; Benedict, R. W. *Experience for Pyrochemical Processing of Spent EBR-II Driver Fuel*. In Proceedings of Global 2005, Tsukuba, Japan, October 2005.

Chapter 3

Challenges for Actinide Separations in Advanced Nuclear Fuel Cycles

K. L. Nash* and J. C. Braley

Chemistry Department, Washington State University, P.O. Box 644630, Pullman, WA 99164-4630
*knash@wsu.edu

During more than five decades of deployment, a great deal of both scientific and engineering insight has been gained into the application of solvent extraction to the challenge of processing spent nuclear fuel. Though no chemical separation process is without limitations, the ability to employ continuous operations, to tune process efficiency and to take advantage of more than 50 years of industrial-scale experience all argue for the continuation of solvent extraction-based processing of nuclear fuels into the 21st Century. A great deal of research is underway globally to support new options for advanced aqueous separations. With the integration of sound waste management practices into spent fuel processing, solvent extraction can still be a workhorse for the operation of advanced nuclear fuel cycles. In this presentation, selected features of the current state of the actinide separations art will be discussed emphasizing options and prospects for the future.

Introduction

With the accidental discovery of radioactivity by Becquerel at the end of the 19th Century and the purposeful identification of previously unknown naturally-occurring radioactive elements by Marie and Pierre Curie in the subsequent decade, humanity was launched into a century of unprecedented progress in our understanding of the physical world we occupy. Among the many new developments that occurred during the 20th Century in the physical sciences, arguably none is more important than the demonstration of the vast power that

could result from transformations of the nuclei of atoms, i.e., nuclear chemistry. Einstein's postulate of the equivalence of mass and energy, $E=mc^2$, led to the Manhattan Project and the development of explosives based on the transmutation of uranium isotopes.

Applications of nuclear chemistry in the context of World War II began a decades-long quest for new elements and even more energetic materials. Most important among them was element 94, plutonium. Though uranium had been used for the preparation of decorative glasses as early as 79 AD (*1*), elements heavier than U were unknown prior to their creation in cyclotrons and nuclear reactors starting in the late 1930's. Transuranium elements may very well have been present in the early decades of the solar nebula that eventually produced our solar system, but their lifetimes were too short to have survived the intervening billions of years. Of the actinides, only uranium and thorium (and their short-lived radioactive decay progeny) survived. At about the same time, the nuclear reaction that led to the destruction of uranium, fission, was also demonstrated (though not initially understood as such). With the synthesis of the transuranium elements and demonstration of the ability to sustain a nuclear chain reaction with some isotopes of these elements, first the nuclear weapons and then years later the nuclear power industries were born.

The eventual end of World War II was almost certainly hastened by the development of nuclear weapons. Unfortunately, the vast power available in these materials led almost immediately after WWII to the Cold War, which involved five nuclear weapons states, but was driven primarily by the United States and the former Soviet Union. Ever more destructive (and sophisticated) nuclear explosive devices were designed and manufactured, requiring the creation of many tons of plutonium and highly enriched uranium and yielding an enormous radiotoxic legacy of less useful byproducts. The fissile materials used for these weapons, ^{235}U or ^{239}Pu, were prepared either via isotope separation (^{235}U from natural uranium) or transmutation of ^{238}U followed by chemical separations of ^{239}Pu from a blend of uranium and fission products. The initial separations of plutonium isotopes were done using precipitation methods, within a few years progressing to increasingly efficient solvent extraction processes. Solvent extraction separations still dominate the options for processing of nuclear fuels today.

In the following, some description of the historical development of nuclear fuel cycles for weapons and energy production purposes will be discussed in the context of contemporary issues of weapons proliferation, cleanup of the weapons complex and possible future applications of this separation technology for increasing CO_2 emissions-free energy. Much of the separations chemistry has been discussed previously in a comprehensive review of the current state of the art in nuclear fuel processing (*2*).

History of Closed Loop Fuel Cycles in the U.S.

As noted above, the application of closed loop nuclear fuel cycles in the U.S. had its origins in the Manhattan Project. As ^{235}U was necessarily isolated by isotope separation based fundamentally on the volatility of UF_6, closed loop

fuel cycles are really only relevant to the production of plutonium. Weapons-grade plutonium was produced by short term irradiations of natural or slightly enriched uranium fuel elements in graphite-moderated reactors built at the Hanford site in central Washington state. The reactor design was fundamentally defined by Fermi's experiments conducted at the University of Chicago in 1942 (*3*). To ensure a predominance of ^{239}Pu in the product, the uranium fuel elements were subjected to a comparatively short residence time in the reactor. Following a short period of cooling to allow the short-lived radioactive isotopes to decay, the fuel elements were dissolved and subjected to chemical separations using a co-precipitation process based on $BiPO_4$. This process relied on the variable oxidation states of plutonium for its separation from the uranium, fission products and other transuranium elements that were produced in the reactor. Several cycles of re-dissolution and precipitation were applied to improve the purity of the plutonium product. This process was overall relatively inefficient and in fact offered no means of recovering the valuable uranium to enable its recycle back to the reactor for additional plutonium production. But it was the only technology that could be quickly scaled up to produce the required kilogram amounts of Pu that were needed for weapons production.

To improve the efficiency of plutonium production at Hanford, the $BiPO_4$ Process was supplanted in the early 1950s by processes based on solvent extraction. The REDOX process, also based on the manipulation of plutonium oxidation states and using extraction of Pu and U from $Al(NO_3)_3$ solutions by methyl(isobutyl)ketone (aka, hexone), was introduced. This process proved far more efficient (in terms of both product recovery and waste generation) than the $BiPO_4$ Process that it ultimately replaced. Because hexone is a comparatively weak Lewis base, it was necessary to employ $Al(NO_3)_3$ as a salting agent to allow sufficient extraction of uranium and plutonium. The need for a salting agent unfortunately amplified the quantity of secondary wastes produced as a byproduct of plutonium production. This extractant proved to be unacceptably flammable and in addition to have moderate chemical toxicity. At the same time in the United Kingdom, the BUTEX process, which employed butyl cellosolve as the extractant and extraction from nitric acid media, was employed to produce plutonium for weapons production.

The third iteration for plutonium production in the U.S. weapons program was the shift from the REDOX process to the PUREX (Plutonium Uranium Recovery by Extraction) Process. In this system, the hexone extractant solution was replaced by a solution of tri-*n*-butylphosphate (TBP) in odorless kerosene. The aqueous phase was the dissolver solution for the irradiated fuel, 2-4 M HNO_3; no additional salting agent was required to support efficient phase transfer. Like the REDOX Process, this system was able to accomplish selective isolation of plutonium and uranium (as their nitrate salts) from a mix of fission products and other transuranium elements (*4*). The chemical equilibria that govern this separation are

$$Pu^{4+} + 4\ NO_3^- + 2\ TBP_{org} = Pu(NO_3)_4(TBP)_{2\ org}$$

and

$$UO_2^{2+} + 2\ NO_3^- + 2\ TBP_{org} = UO_2(NO_3)_2(TBP)_{2\ org}$$

TBP is not sufficiently strong to extract trivalent (Am^{3+}, Cm^{3+} or Pu^{3+}) or pentavalent (NpO_2^+) actinide ions and also rejects most fission products, though it does extract HNO_3. Plutonium is removed from the extractant phase by contact with a reducing nitric acid solution (containing Fe^{2+} or U^{4+}) which transforms Pu^{4+} to Pu^{3+}. UO_2^{2+} can be stripped with dilute HNO_3 and any excess removed by scrubbing with Na_2CO_3.

Modifications and improvements of PUREX continue to be made around the world. It remains the only large-scale fuel recycling process in operation. PUREX is used in commercial fuel reprocessing applications in France, the United Kingdom, Japan, Russia and India today; in the U.S., a commercial used fuel reprocessing facility operated briefly at West Valley in New York during the 1970s. Operations were terminated because of some operational difficulties, but primarily as a measure to reduce opportunities for nuclear weapons proliferation. A similar plant constructed in Barnwell, South Carolina never began hot operations. Reprocessing to produce plutonium for weapons use continued at the Hanford site and at the Savannah River Site (using PUREX) until the late 1980s. Emphasis in the field at that point shifted to the notion of applying aqueous separations technologies to the cleanup of the weapons complex. This effort continues today and will for many decades into the future.

21st Century Nuclear Fuel Cycle Challenges

At the beginning of the 21st Century, the nuclear energy and weapons landscape has changed somewhat from that existing prior to the end of the Cold War:

- There are at present at least nine confirmed nuclear weapons states.
- More than 400 nuclear power generating units are in operation globally generating approximately 17% of the total electricity that is consumed planet-wide.
- There are no operational geologic repositories for the permanent disposal of either used nuclear fuel or high level wastes from reprocessing, though research continues in several nations with the goal of identifying an appropriate location for such repositories (multiple repositories will likely be created, as nuclear nations retain responsibility for management of wastes from either power plant or reprocessing operations). One geologic repository operates in the U.S. that accepts defense wastes contaminated with transuranium elements (the Waste Isolation Pilot Plant (WIPP) in New Mexico).
- International terrorism has become a greater issue – the possibility of nuclear terrorism has thus become a greater fear than that of a nuclear exchange between nations.
- Concerns about the global climate (and the possible/probable connection between fossil fuel combustion and climate change) have arisen, spurring

demand for energy production approaches that release smaller amounts of greenhouse gases into the atmosphere, for which fission based nuclear power is well suited.

- The peak of oil production from accessible underground resources is believed to have been passed.
- Demands for primary energy by rapidly industrializing countries like China, India, Brazil and Russia are increasing.

The primary concerns for society arising from nuclear power production are prevention of the proliferation of nuclear weapons to additional states (or sub-national groups) and the isolation of the byproducts of fission (fission products and transuranium elements) from the accessible surrounding environment. The weapons proliferations issue appears in general to have three solutions, probably mutually supporting:

- "Guns, guards and fences" to prevent these materials from falling into the hands of people who might choose to divert them to illicit uses
- Recycling radioactive materials (of primary concern are the transuranium elements) back into reactors to maintain the self-protecting shield of highly radioactive fission products while at the same time…
- Transmuting the long-lived radiotoxic isotopes to decrease their potential to do damage to the environment and to the human ecosystem.

The first element of these is an obvious requirement. The second and third are related and require chemical treatment to separate the important elements, create irradiation targets and recycle them back into nuclear reactors where they are transmuted into shorter-lived byproducts. It is possible to recycle reactor grade plutonium back to light water reactors at least once and possibly twice, but beyond that fast neutron spectrum reactors (e.g., those cooled by sodium) are required for efficient transmutation. Fast reactors can also be used to transmute other actinides (of primary interest are $^{241, 243}$Am, ^{237}Np) and excess uranium containing substantial amounts of ^{236}U. This recycle improves the overall utilization of the energy value of the transuranium elements, but more importantly protects these elements from diversion to weapons and shortens the lifetime of the radiotoxic isotopes. With reprocessing and full recycle, the required time for isolation of the byproducts from the accessible environment can be reduced from 10^5 or 10^6 years to less than 1000.

Two particular hazards arising from mismanagement (or accident) of the byproducts of fission are the possibility of airborne release (for example, in the event of a particularly unlucky and violent meteor strike, volcanic activity or human intervention) or the more likely scenario of contamination of ground and surface waters by radioactive materials released from a repository. The short-lived fission product radioactivity for the most part decays away within a couple of decades. The isotopes that remain include alpha emitting transuranium elements, intermediate to long-lived fission products like ^{137}Cs and ^{90}Sr and mobile species like the moderately long-lived ^{99}Tc, ^{135}Cs and ^{129}I isotopes. The ^{137}Cs and ^{90}Sr dominate the radiotoxicity of used fuel from a few years after

discharge from the reactor until about 300 years. Without any processing of the fuel, all transuranium elements are retained in the fuel and disposed to a geologic repository. From 300 to about 4,000 years the radiotoxicity is dominated by [241]Am. From 4,000 to 70,000 years the radiotoxicity is dominated by plutonium isotopes and from 70,000 to about 2,100,000 years by [237]Np. In a closed fuel cycle in which plutonium is recycled, the toxicity of the high level wastes is dominated by [241, 243]Am isotopes between several hundred years and 70,000 and by [237]Np from 70,000 to 2,100,000 years. If all transuranium elements are removed and transmuted, the radiotoxicity of the residue returns to that of uranium ore when the ^{137}Cs and ^{90}Sr have passed about 10 half-lives after discharge from the reactor.

The single pass open fuel cycle (as nuclear electricity is created in the U.S.) involves no processing of the fuel as it is removed from the reactor. The used fuel bundle is considered the waste form and there is no secondary processing. The operation of the single pass fuel cycle was adopted as official policy in the U.S. during the 1970s as a strategic response to the danger of nuclear weapons proliferation. Due to the radiation field produced by the fission products in the used fuel, this material was considered to be "self-protecting" hence proliferation resistant. Its disposal into a mined repository was considered within the context of the day to render the fuel as adequately protected from weapons diversion. In the absence of a functional geologic repository, this characterization is less certain. As demand increases for additional nuclear power, this approach becomes more questionable on practical grounds, as the additional fuel value of the discharged fuel might be considered more as a resource than a waste product. It is not clear that adequate supplies of economically recoverable uranium reserves are available to fuel increased application of this important energy technology beyond a few centuries if a single pass fuel cycle is employed; with the breeding of fissile material from [238]U and [232]Th, adequate supplies for at least several thousands of years can be projected.

Closed loop management of the nuclear fuel cycle can be approached to different degrees of completeness. As closed loop recycling is practiced today in France, the United Kingdom, Japan and Russia, the PUREX process operates and recovered reactor grade plutonium is recycled once as MOX fuel through light water reactors. The recovered uranium is suitable for reuse, but at present freshly mined uranium is used instead. The increased content of [236]U (and the presence of traces of [232]U and [233]U) makes the recycled uranium less desirable for reuse in light water reactors. In France this material is maintained as a "strategic reserve". With the development and application of advanced separation systems in conjunction with fast neutron spectrum reactors or accelerator transmutation systems, it will some day be possible to envision nuclear fuel cycles in which fissile material can be recycled repeatedly and actinides transmuted to improve both waste management and energy production. Such systems would be capable of extracting energy from the uranium discharged from light water reactor fuel reprocessing plants and transuranium elements as well. A further advantage of such a transmutation system would be improved proliferation resistance, as each pass of plutonium isotopes through reactors makes them both less attractive for weapons diversion and keeps it in the company of highly radioactive fission products emitting lethal amounts of penetrating radiation. Effective strategies for

proliferation-proofing the nuclear fuel cycle will demand substantial international cooperation.

Nuclear fuel cycle reprocessing research being conducted around the world addresses various possible options for advanced processing of irradiated nuclear fuels. The PUREX process is robust, has enjoyed the benefit of more than 50 years of research and process experience and undergoes continued refinement. If the goal of fuel processing remains recycling uranium and plutonium, PUREX will suffice as an acceptable technological solution. However, as discussed above a number of adjustments are being studied around the world for more advanced processing options. These processes target specifically several options for recovery of actinides individually or as a group. Problematic fission products like ^{135,137}Cs, ^{90}Sr, ^{99}Tc, ^{129}I, noble gases (Xe and Kr) and the lanthanides are targets for the development of separations processes to aid in their disposal.

During the past several decades, the U.S. separations effort has focused on the development of processes and reagents to support cleanup of the former weapons complex. This focus has led to the development of the SREX (strontium extraction), CSEX (cesium extraction) and TRUEX (transuranic element extraction) processes and reagents that enable them. During the same period, the French-led European program has focused on the development of CHON (carbon, hydrogen, oxygen, nitrogen) reagents for actinide management in advanced fuel processing, which has led to the development of diamide extractants (and the DIAMEX process) and a class of compounds based on bis-triazinyl pyridine and bipyridine ligands. The basic features of advanced processes under development are summarized in Tables I and II.

Uranium and Plutonium Extraction

PUREX is the industry standard and benefits from 50+ years of plant scale experience. Advances designed to support improvements in partitioning efficiency continue to be made in basic PUREX chemistry, mainly to increase the predictability of neptunium partitioning in the system. In the advanced fuel cycle research effort in the U.S., a principle limitation of the PUREX process is the essential design characteristic that permits the isolation of a pure plutonium product, which is considered unacceptable because of weapons proliferation concerns. To minimize the opportunities for production of a pure Pu stream, various options for advanced management strategies that blend U, Np, and Pu have been proposed. The UREX process modifies PUREX through the addition of acetohydroxamic acid, which complexes plutonium(IV) and maintains Np in the pentavalent oxidation state to allow selective extraction of uranium. Most of the Tc present in the fuel accompanies U(VI) into the TBP phase in UREX. Plutonium extraction can be accomplished in a number of different options, mixed with uranium, neptunium or all of the transuranium elements depending on the choice of extractants and aqueous conditions. In at least one version of UREX, Np and Pu are subsequently coextracted in the TBP-based NPEX process.

Table I. Separations methods for oxidized species in used fuel

Radionu-clide	Process	Comments	Status
Uranium	PUREX	Typically TBP in dodecane. Separates Pu(IV) and U(VI). Np can be recovered as Np(VI) or retained in raffinate as Np(V).	Industry standard
	UREX	Addition of AHA to PUREX process aqueous phase prevents Pu extraction and promotes Tc extraction. U and Tc are separated by selective stripping.	Pilot plant scale, SRS
Technetium	UREX	99.7% of Tc could theoretically be extracted. 97% recovery has been demonstrated at lab-scale.	Pilot plant scale, SRS
TRU Elements	TRUEX	CMPO added to TBP in dodecane. Extracts actinides and lanthanides over fission products. An(III) and Ln(III) separated from higher valent species by selective stripping.	Commercialized in Japan
	DI-AMEX	Diamide extractant DMDBTDMA or DMDOHEMA dissolved in TPH extracts actinides and lanthanides from acidic solutions.	Developed in France. Hot demonstration at ATALANTE facility
	TRPO	Mixture of tri-alkyl phosphine oxides extracts actinides. Selective stripping recovers U, Pu, Np, and An(III).	Developed in China. Hot demonstrations in Germany and China
	TBP Extraction	Using valence adjusting chemicals and complexing agents can separately recover U, Pu, and Np but not Am/Cm.	Based on PUREX (NPEX process)
	TODGA	Tridentate diamide extractant tetraoctyldiglycolamide extracts actinides and lanthanides from acidic solutions.	Extractant aggregation in the organic phase. Process scale and analytical applications possible/known

Table II. Separations methods for low valent species in used fuel

Radionuclide	Process	Comments	Status
Am, Cm from Ln	TALSPEAK	DTPA complexes An(III) and HDEHP as extracts Ln(III) from acidic streams.	Hot cell demonstration
	"Reverse" TALSPEAK	An(III) and Ln(III) are both extracted. DTPA (and carboxylic acid) is then used to strip An from Ln	
	DIDPA	Modified TALSPEAK. DIDPA is the extractant.	Hot cell demonstration with actual waste
	SETFICS	Modified TRUEX process. Uses DTPA complexant and modified CMPO extractant.	Not tested with actual waste
	PALADIN	Malonamide co-extracts An(III) and Ln(III) from acid stream. HDEHP extractant and DTPA complexant selectively strips actinides.	Successfully tested
	SANEX processes	Selective extraction of An(III) from Ln(III): Cyanex 301 uses R_2PSSH as extractant. ALINA uses two extractants a dithiophosphinic acid and trioctylphosphine oxide. BTPs and TMAHDPTZ w/ octanoic acid have been used as neutral extractants.	Demonstrated with Am, Ln mixtures and genuine wastes
Cs and Sr	UNEX (or FPEX or CCD-PEG)	Allows extraction of Cs and Sr with An and Ln. A dicarbollide extracts Cs+, PEG synergizes Sr^{2+} extraction by CCD^-, a phosphine oxide extracts the actinides. Selective stripping with guanidine and DTPA separates Sr^{2+}, Cs^+ from actinides.	Small-scale tests at INEEL and larger-scale demo in Russia

Trivalent Lanthanide/Actinide Isolation from Mixed Fission Products

Having a variety of accessible oxidation states, there are a number of options available for the selective partitioning of U, Np, and Pu from other transuranic elements and fission products. Both the PUREX and UREX processes under normal operating conditions reject trivalent transuranic elements and fission product lanthanides (along with most of the rest of the fission products). This feature, an advantage for the production of weapons plutonium in PUREX, represents a limitation in the context of managing

wastes from plutonium production or in advanced nuclear fuel cycle processing schemes. During the 1980's Horwitz and coworkers led the development of the carbamoylmethylphosphine oxide (CMPO) extractants and the TRUEX process, a process designed to remove and recover trivalent actinides and lanthanides from PUREX raffinates or dissolved tank wastes.

The conventional TRUEX process (*5*) uses octyl(phenyl)-N,N-diisobutylcarbamoyl-methylphosphine oxide, CMPO (Figure 1), a bifunctional phosphine oxide extractant, to selectively partition An(III) nitrate complexes along with fission product lanthanides away from all remaining fission products. The combination of an amide functional group with the phosphine oxide serves to reduce the negative impact of mineral acid extraction on metal nitrate extraction efficiency. In most forms of TRUEX, tributylphosphate (TBP, Figure 1), is employed as a phase modifier and/or supporting extractant to increase overall efficiency. In at least one version of the UREX process, the TRUEX stage is based on the use of diphenyl-N,N-dibutylcarbamoylmethyl phosphine oxide in a polar sulfone diluent. This process has been subjected to considerable testing up through the pilot scale with actual wastes and adapted to chromatographic separations via extraction chromatography. This extraction system can also support partitioning of plutonium, neptunium and uranium, but (relative to PUREX/UREX) is limited by the solubility of metal complexes, hence is better suited for application as a complement to PUREX rather than a replacement for it.

Various studies of spent fuel partitioning that have been conducted around the world have resulted in the development of several other approaches to this process step. For example, the comparable European process uses a diamide extractant (*6*, *7*), e.g. N,N′-dimethyl-N,N′-dioctyl-hexylethoxydiamide, DMDOHEMA (Figure 1), to co-extract An/Ln under conditions similar to those employed for CMPO. This bifunctional extractant similarly resists the negative impact of mineral acid extraction and provides the added benefit of producing innocuous degradation products. Studies initiated in Japan (*8*, *9*) using a diglycolamide, N,N,N′N′-tetraoctyl-3-oxapentanediamide, TODGA (Figure 1), have shown that a tridentate diamide offers additional interesting separation options. In the partitioning program developed in China, monofunctional trialkylphosphine oxide extractants, TRPO (*10*, *11*), have been employed in conjunction with a necessary denitration step. An/Ln co-extraction can also be accomplished using a cation exchanging extractant such as bis(2-ethylhexyl) phosphoric acid, HDEHP (*12*) or di(isodecyl) phosphoric acid, DIDPA (*13*, *14*). As is true for the TRPO process, cation exchangers can only be used after the acidity of the feed is reduced below that of dissolved spent fuel. In contrast, extraction by CMPO or diamide extractants requires high nitrate concentrations, usually provided by HNO_3.
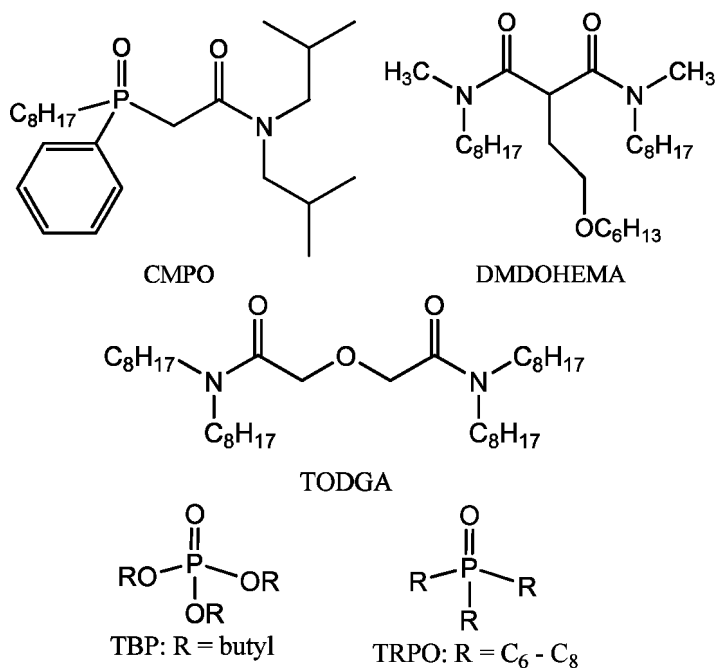
Figure 1. Extractants examined for the isolation of trivalent actinides and lanthanides from fission products.

Trivalent Lanthanide-Actinide Separations

Lanthanides compete with actinides for neutrons in a reactor, hence the mutual separation of the groups is required in advanced nuclear fuels cycles in which transmutation of actinides is the ultimate objective. The chemistry of trivalent actinides and lanthanides are nearly identical except for slightly stronger interaction of actinides with soft (S, Cl-) or less-hard (N) donor atoms. The first demonstration of this effect was made by Diamond and coworkers in the separation of Am^{3+} from Pm^{3+} (*15*). Many different approaches based on complex ligands bearing S or N atoms (in either the aqueous or organic phase) or from chloride or thiocyanate media have been investigated.

Once the actinides and lanthanides are extracted from other fission products, there are a couple of options available to proceed with the group separation. One alternative is to strip both groups of metals into an aqueous phase and subsequently treat this phase with a 2nd extraction step to separate An from Ln. Examples of such steps are TALSPEAK (*16*) or SANEX processes (*17, 18*). Another option is to selectively strip the actinides into an aqueous phase using a selective complexing agent in the strip solution, leaving the lanthanides in the organic phase and thereby accomplishing group separation. This type of selective strip is used in the CTH-process (*19–21*), to selectively strip An from an organic solvent of HDEHP in kerosene loaded with actinides and lanthanides. This is commonly referred to as reverse TALSPEAK. A similar approach is used in the Japanese SETFICS process

(*22–24*) in which CMPO first co-extracts An(III) and Ln(III) nitrates and actinides selectively stripped using DTPA.

The TALSPEAK Process

The Trivalent Actinide - Lanthanide Separation by Phosphorus reagent Extraction from Aqueous Komplexes (TALSPEAK) process addresses the most challenging separation task within the UREX+ design – group separation of fission product lanthanides from trivalent transplutonium elements (Figure 2). In TALSPEAK the selective separation of trivalent transplutonium actinides from lanthanides results from a competitive complexation of the metal ions by a hydrophobic acidic organophosphorus extractant ($(RO)_2PO_2H$, most commonly HDEHP) and a hydrophilic polyaminopolycarboxylate complexant (e.g., DTPA) in an aqueous phase containing a high concentration of a carboxylic acid buffer (typically lactic acid). The opposing preferences for binding the members of f-block elements facilitates the separation: the phosphoric acid extractant partitions lanthanides to the organic phase, while the buffered polyaminopolycarboxylic acid aqueous phase retains the trivalent actinides. Developed in the late 1960s at Oak Ridge National Laboratory (*16*), the process is currently considered to be ready for technological deployment. Its integration into the UREX+3 process flow scheme demands careful attention to phase preparation prior to contact.

HDEHP: R = 2-ethylhexyl
DIDPA: R = diisodecyl

DTPA

Lactic Acid
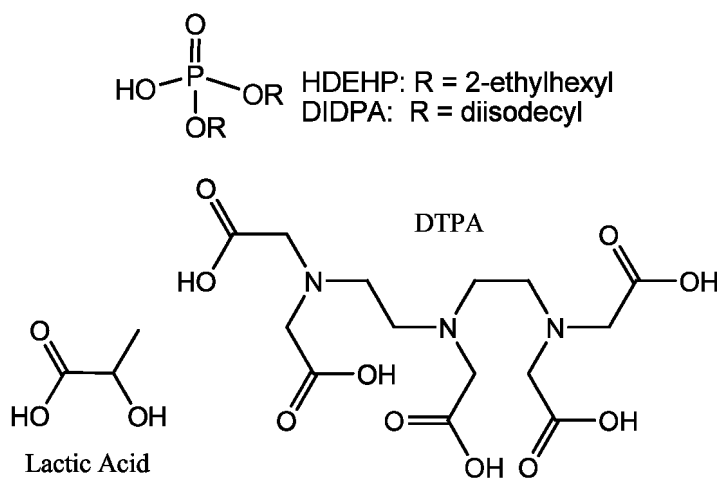
Figure 2. Structures of TALSPEAK components.

The general set of operational conditions that have been considered in various attempts at developing the TALSPEAK process include the following:

- Baseline TALSPEAK uses HDEHP in 1,4-diisopropylbenzene (0.3 - 0.7 M)
- Other phosphorous reagents that have been tested include 2-ethylhexyl phenylphosphonic acid, DIDPA, CMPO
- Other organic diluents tested, aliphatic diluents increased distribution ratios but decreased group separation efficiency.
- Several aminopolycarboxylates have been examined – DTPA (0.05 M) is generally considered to give the best overall performance.
- Several carboxylic acid buffers have been considered

    - Lactate has emerged as the first choice based on overall group separation factors and solubility (> 1 M); citrate has also received serious consideration
    - Observations have been made that indicate that lactate partitions into the organic phase at high metal loading – mixed lanthanide-lactate-extractant complexes have been suggested as being responsible.
    - Lactate is known to play an important role in extraction kinetics, in radiation stability and in maintaining solubility of solute species.

Recent investigations of TALSPEAK chemistry have revealed fresh insights into the chemistry of the process:

- Thermodynamic calculations reveal that Ln/An partitioning derives from a balance between two strong complexants (HDEHP/DTPA) pulling in opposite directions. The trans-lanthanide pattern of complex stability (in both the organic and aqueous phases) is important.
- Thermodynamic data describing the interactions of the process components (metal ions, lactate, extractant, DTPA) predicts a different pH dependence from that observed in process development studies
- Lactic acid partitions to organic phase (whether complexed to extracted lanthanide ions or not). It functions as a pH buffer, accelerates the cation phase transfer reaction and affords a measure of radiation protection to the DTPA and HDEHP reagents.
- Kinetics (homogeneous and phase transfer) are very complex
- Supramolecular organization of solute molecules in the organic phase appears to be likely.
- Incomplete understanding of interactions between components hinders application to other separation platforms, hence further investigations offer significant opportunities for process improvement.

Several processes have been developed and tested, with mixed success, for applicability of TALSPEAK-like chemistry for An(III)/Ln(III) separations, as follows.

CTH Process

As mentioned above, instead of the conventional approach of selectively extracting lanthanides from trivalent actinides, it is possible to operate this separation system utilizing selective stripping of the trivalent actinides from an organic phase containing both lanthanides and trivalent actinides using a solution of diethylenetriamine-N,N,N′,N″,N″-pentaacetic acid, DTPA in buffered lactic acid as the stripping agent. Such a system was extensively tested and used as a part of a process for treating high-level liquid waste from spent nuclear fuel in the CTH-process (Chalmers Tekniska Högskola) (*19–21*). In the final stage of the CTH process, americium, curium and the lanthanides are co-extracted away from the other fission products by HDEHP. The loaded organic phase is then contacted with the DTPA – buffered lactic acid solution to selectively strip the actinides, hence, reversed TALSPEAK. This system was successfully tested on actual spent fuel, however difficulty in controlling pH, crucial for long-term operation, was identified as a problem.

DIDPA

HDEHP used as the extracting agent in TALSPEAK has the disadvantage of giving low distribution ratios for trivalent metals at low p[H$^+$]. Tachimori and coworkers (*13*, *14*) investigated the possibility of replacing HDEHP with DIDPA. The results showed that DIDPA was able to extract americium and neodymium at a higher acidity than HDEHP, but with a decrease in separation factor between the two elements. One benefit of this process is the possibility to work at a lower p[H$^+$], though DTPA will not tolerate a p[H$^+$] below about 2.5. In practice, the DIDPA process operates under conditions similar to TALSPEAK or reverse TALSPEAK.

SETFICS

As mentioned above, the TRUEX process utilizes a neutral bidentate organophosphorus ligand, CMPO, to selectively co-extract trivalent actinide and lanthanide nitrates from other fission products. The SETFICS process (Solvent Extraction for Trivalent f-elements Intra-group separation in CMPO-complexant System) (*22–24*), takes advantage of the opportunity to co-extract the two groups of metals and introduces selective stripping of the trivalent actinides using DTPA (*16*). In effect, this process more closely resembles a reverse-TALSPEAK separation. The CMPO (often used in conjunction with TBP), also extracts nitric acid, so the organic phase must be deacidified before the selective stripping since DTPA may otherwise precipitate. The SETFICS process is considered as

a part of the advanced aqueous reprocessing system NEXT (<u>N</u>ew <u>EX</u>traction system for <u>T</u>RU recovery) developed in Japan (*25*). Studies of this system reveal issues associated with incomplete understanding of the fundamental chemistry governing process operations.

GANEX

In the GANEX (<u>G</u>roup <u>A</u>cti<u>N</u>ide <u>EX</u>traction) process (*26*), currently under development by the CEA in France, HDEHP is combined with DMDOHEMA in TPH (branched aliphatic hydrocarbon diluent) to co-extract trivalent actinides and lanthanides. The trivalent actinides are subsequently stripped using an aqueous solution of citric acid and (N-hydroxyethyl)ethylenediamine-N,N′,N′-triacetic acid (HEDTA), directly comparable to the TALSPEAK or reverse TALSPEAK stripping solution.

These methods for separating An(III) from Ln(III) by first co-extracting and selectively stripping have achieved some success. Different extractants call for different stripping conditions, but the common denominator is that a polyaminopolycarboxylate ligands, e.g. DTPA or HEDTA, and probably a buffering solution are required. Mixtures of extractants have been tested to some extent in SETFICS and GANEX. There are obvious benefits to accomplishing the selective removal of actinides immediately after the co-extraction step to avoid having to strip both groups into an aqueous phase only to introduce a 2nd extraction step. These several examples also indicate the attractiveness of this approach (combining extraction steps for more efficient partitioning). The mixed successes reported have been accomplished despite incomplete understanding of how TALSPEAK chemistry actually operates.

Of course, continued research also addresses the development of new reagents and processes for their application. Among the newest reagents are the following:

- Cyanex 301, bis 2,4,4(trimethylpentyl)dithiophosphinic acid ($R_2PS(SH)$) is a commercially available solvent extraction reagent that contains a pair of sulfur atoms that are available for the formation of lipophilic metal ion coordination compounds. Cyanex 301 finds its primary application in hydrometallurgical separations of d transition metals. However, Chen and coworkers have reported actinide/lanthanide separation factors of greater than 5,000 in laboratory studies (*27–29*). Unfortunately, Cyanex 301 is very susceptible to hydrolytic and radiolytic degradation and the resulting mono thio or dioxo phosphinic acids exhibit poor ability to distinguish trivalent actinides from lanthanides.
- To improve the stability and compatibility with more acidic media in dithiophosphinic acids, Modolo and coworkers have prepared and tested Di(p-chlorophenyl)dithiophosphinic acid extractants (with TBP or TOPO as a phase modifier) as reagents for this important separation. The chlorophenyl derivative is more stable than Cyanex 301 and more acidic (so able to function in media of higher acidity), but suffers lower group separation factors (*30*).

- In the late 1990s, Kolarik first reported the synthesis of pyridine-2,6 bistriazine complexants that demonstrate americium/europium separation factors of about 100 (*31*). This result has inspired a considerable research effort involving much of the European community and a variety of studies of similar polyaza extractant molecules elsewhere. Like the dithiophosphinic acids, the BTP and related bistriazinyl-bipyridyl (BTBP) reagents suffer some susceptibility to hydrolytic and radiolytic degradation.

Other Fission Products of Interest

Among the remaining fission products, the four noted above (^{135,137}Cs, ^{90}Sr, ^{99}Tc, ^{129}I) are of primary concern for their radiotoxicity. The precious metals Pd, Rh, and Ru are of interest for their potential utility for applications as catalysts. Reagents and processes for the selective extraction of Cs^+ and Sr^{2+} have been developed, mainly centering on reagents capable of exercising a size selective recognition of these ions, crown ethers and calixarenes most significantly. In the UREX process, the FPEX process relies on these size recognition reagents. These ions can also be successfully removed using solvent that includes a polar fluorinated sulfone diluent (FS-13), polyethylene glycol (PEG-400) phase modifier and chlorinated cobalt dicarbollide (HCCD) primary extractant. The removal of these isotopes at the head end of an advanced processing scheme would have the desirable effect of reducing radiolytic degradation later in the process, though it is unclear whether this improvement would have an effect proportional to the expense of operating an additional separation process. In the UREX+ process suite, technetium can be largely managed as a byproduct of uranium extraction, as noted above. Iodine would be controlled in advanced processing applications by volatilization during fuel dissolution.

Conclusions

At the beginning of the 21st Century, the combined effects of an apparent global temperature increase (that may be of anthropogenic origin), increasing industrialization of former third world countries, a growing global population and declining availability of at least some fossil carbon resources, it is becoming increasingly apparent that all forms of primary power production must be considered. Nuclear power is attractive in this regard, as the energy density of the fuel is high, it is useful for little else and is a resource that if fully exploited could supply a considerable percentage of primary power for thousands of years. The byproduct wastes are dangerous because of their radioactivity/radiotoxicity and because of the possibility that they could be diverted to the creation of weapons of mass destruction. But unlike other primary energy production methods that consume fossil fuels, virtually all wastes produced are confined in the fuel (and can be recovered and concentrated from the byproduct wastes of processing of irradiated fuel).

The following observations can be made about the potential impacts of increased reliance on fission based nuclear power:

- More nuclear power globally will combat the potential climatic effects of CO_2 emission, but …
- More nuclear power will deplete known reserves of uranium faster, thus….
- Faster depletion of reserves will encourage adoption of breeder reactor cycles and full recycle of fissile materials.
- Any strategies for expansion must be nuclear weapons proliferation resistant.
- Keeping TRUs in the fuel cycle improves energy utilization and reduces their suitability for weapons diversion.
- No amount of recycling or processing will eliminate the need for a geologic repository thus even with full recycle and transmutation of the most obnoxious byproducts it will still be necessary to have repositories in suitable (preferably reducing) environments.
- Increased production of the radioactive byproducts of fission will increase the need for more complete understanding of environmental and ecological fate and transport.
- Advanced (fast neutron spectrum) reactors will be needed as TRUs are to be recycled.
- An(III)/Ln(III) separation will be needed for transmutation.
- It will be important to develop the next generation workforce.
- International cooperation will be essential.
- Continued investment will be needed in research and infrastructure – recent reports in Scientific American and Chemical & Engineering News reveal that a shockingly small percentage of the U.S. GDP has been expended on energy research during the past 30 years; the fraction spent on nuclear power is below that needed to sustain an industry. The issue of energy supplies is certain to remain a serious concern for the foreseeable future, hence the issue demands far more attention than it has received.

To define the research challenges of fission based nuclear power, the following list of priority issues is offered. The challenges faced by the 21st Century nuclear fuel cycle include the following:

- Finding an appropriate location for one or more high level geologic repositories for high level wastes from reprocessing or used nuclear fuel. Separate facilities will be needed for low and intermediate level radioactive wastes, which are fundamentally different in composition, but containing the same mixes of isotopes.
- Cleaning up the weapons complex, where wastes needing treatment exist in alkaline conditions, require solid liquid separations and waste immobilization for an outcome that will likely produce no useful byproducts (aside from preservation of environmental quality).

- It will be necessary to achieve a deep understanding of the behavior of actinides in the environment (whose unique properties of near-neutral pH, dilute solutions, solid-liquid interactions, colloid transport phenomena may be most important).
- Managing used fuel in a geologic repository will take on a somewhat different profile depending on whether an open or closed fuel cycle operation is conducted.
- In a single pass open fuel cycle, the irradiated fuel is the waste form, hence waste-environment interactions are defined by the fuel-environment interaction.
- In a closed loop fuel cycle, several categories of wastes replace the spent fuel waste form of the open fuel cycle, low level, intermediate level (not at present a defined waste category in the U.S., but used in other countries that do recycle used fuel) and high level waste glass.
- Used fuel reprocessing can be approached for U, Pu recycle to LWRs only, or for a more complete partitioning and transmutation scheme in which advanced burner and breeder reactors will be deployed and transmutation will be practiced to reduce long-term radiotoxicity of the wastes. In the short term, it appears that aqueous processing and separations from acidic solutions (or buffered acidic media) will most probably be utilized.
- Used fuel reprocessing for transmutation in NGNP will attempt to transmute all actinide isotopes (that are not readily consumed in thermal reactors). Such reprocessing systems will likely generate high radiation levels during processing and the possible introduction of "dry" (pyrometallurgical) processing methods.
- In any case, prevention of the proliferation of nuclear weapons will be an essential component.

References

1. *CRC Handbook of Chemistry and Physics*, 86th ed.; Lide, D. R., Ed.; CRC Press: Boca Raton, FL, 2005; Chapter 4, p 33.
2. Nash, K. L.; Madic, C.; Mathur J. N.; Lacquemont, J. Actinide Separation Science and Technology. In *The Chemistry of Actinides and Transactinide Elements*; Morss, L. R., Katz, J. J., Edelstein, N., Fuger, J. , Eds.; Springer: Dordrecht, The Netherlands, 2006; Chapter 24, pp 2622−2798.
3. Rhodes, R. *The Making of the Atomic Bomb*; Simon & Shuster: New York, 1986.
4. Musikas, C.; Shulz, W. W.; Liljenzin, J.-O. Solvent Extraction in Nuclear Science and Technology. In *Principles and Practices of Solvent Extraction*; Rydberg, J., Musikas, C., Choppin, G. R.; Eds., Marcel Dekker: New York, 2004; Chapter 12, pp 507−557.
5. Schulz, W. W.; Horwitz, E. P. *Sep. Sci. Technol.* **1988**, *23*, 1191.

6. Madic, C.; Hudson, M. J.; Liljenzin, J.-O.; Glatz, J.-P.; Nannicini, R.; Facchini, A.; Kolarik, Z.; Odoj, R. *Prog. Nucl. Energy* **2002**, *40* (3−4), 523–526.

7. Madic, C.; Blanc, P.; Condamines, N.; Baron, P.; Berthon, L.; Nicol, C.; Pozo, C.; Lecomte, M.; Philippe, M.; Masson, M.; Hequet, C.; Hudson, M. J. *Actinide Partitioning from HLLW Using the DIAMEX Process*, Proceedings of the Fourth International Conference on Nuclear Fuel Reprocessing and Waste Management, RECOD'94, London, April 24−28, 1994.

8. Sasaki, Y.; Sugo, Y.; Suzuki, S.; Tachimori, S. *Solvent Extr. Ion Exch.* **2001**, *19*, 91–103.

9. Morita, Y.; Sasaki, Y.; Tachimori, S. Actinide separation by TODGA extraction. *JAERI-Conf.* **2002**, 255−260.

10. Zhu, Y.; Jiao, R.; Wang, S.; Fan, S.; Liu, B.; Zheng, H.; Chen, S. *An Extractant (TRPO) for the Removal and Recovery of Actinides from High Level Radioactive Liquid Waste*, ISEC'83, Denver, CO, 1983.

11. Zhu, Y.; Song, C. L. *Recovery of Neptunium, Plutonium and Americium from Highly Active Waste, Trialkyl Phosphine Oxide Extraction*, Proceedings of Transuranium Elements, 200th American Chemical Society National Meeting, Washington, DC, August 26–31, 1990; Morss, L. R., Fuger, J., Eds.; American Chemical Society; Washington, DC, 1992, pp 318–330.

12. Choppin, G. R.; Nash, K. L. *Radiochim. Acta* **1995**, *70/71*, 225.

13. Morita, Y.; Glatz, J. P.; Kubota, M.; Koch, L.; Pagliosa, G.; Roemer, K.; Nicholl, A. *Solvent Extr. Ion Exch.* **1996**, *14*, 385.

14. Morita, Y.; Tachimori, S.; Koma, Y.; Aoshima, A. *Studies on Actinide Separation Process from High-Level Liquid Waste*; Department of Materials Science, Tokai Research Establishment, Japan Atomic Energy Research Institute: Tokai-mura, Naka-gun, Ibaraki-ken, Japan, 2002; pp i−iv, 1−20.

15. Diamond, R. M.; Street, K.; Seaborg, G. T. *J. Am. Chem. Soc.* **1954**, *76*, 1461.

16. Weaver, B.; Kappelmann, F. A. *TALSPEAK, A New Method of Separating Americium and Curium from the Lanthanides by Extraction from an Aqueous Solution of an Aminopolyacetic Acid Complex with a Monoacetic Organophosphate or Phosphonate*; ORNL-3559; Oak Ridge National Laboratory : Oak Ridge, TN, August 1964.

17. Hill, C.; Guillaneux, D.; Berthon, L.; Madic, C. SANEX-BTP process development studies. *J. Nucl. Sci. Technol.* **2002** (Suppl. 3), 309–312.

18. Magnusson, D.; Christiansen, B.; Foreman, M. R. S.; Geist, A.; Glatz, J. P.; Malmbeck, R.; Modolo, G.; Serrano-Purroy, D.; Sorel, C. *Solvent Extr. Ion Exch.* **2009**, *27*, 97.

19. Liljenzin, J. O.; Persson, G.; Svantesson, I.; Wingefors, S. *Radiochim. Acta* **1984**, *35*, 155.

20. Svantesson, I.; Hagstrom, I.; Persson, G.; Liljenzin, J.-O. *J. Inorg. Nucl. Chem.* **1980**, *42*, 1037–1043.

21. Svantesson, I.; Hagstrom, I.; Persson, G.; Liljenzin, J.-O. *Radiochem. Radioanal. Lett.* **1979**, *37*, 215–222.

22. Koma, Y.; Watanabe, M.; Nemoto, S.; Tanaka, Y. *Solvent Extr. Ion Exch.* **1998**, *16*, 1357.

23. Ozawa, M.; Koma, Y.; Nomura, K.; Tanaka, Y. *J. Alloys Compd.* **1998**, *271-273*, 538–543.
24. Koma, Y.; Koyama, T. M.; Nemoto, S.; Tanaka, Y. *J. Nucl. Sci. Technol.* **1999**, *36*, 934–939.
25. Nakahara, M.; Sano, Y.; Koma, Y.; Kamiya, M.; Shibata, A.; Koizumi, T.; Koyama, T. *J. Nucl. Sci. Tech.* **2007**, *44*, 373.
26. Miguirditchian, M.; Chareyre, L.; Heres, X.; Hill, C.; Baron, P.; Masson, M. In Proceedings of Advanced NuclearFuel Cycles and Systems (GLOBAL 2007), Boise, ID, September 9−13, 2007; American Nuclear Society: La Grange Park, IL, 2007; p 1692.
27. Zhu, Y.; Chen, J.; Zhou, R. *Solvent Extr. Ion Exch.* **1996**, *14* (1), 61–68.
28. Tian, G.; Zhu, Y.; Xu, J. *Solvent Extr. Ion Exch.* **2001**, *19*, 993–1015.
29. Chen, J.; Tian, G.; Jiao, R.; Zhu, Y. A hot test for separating americium from fission product lanthanides by purified Cyanex 301 extraction in centrifugal contactors. *J. Nucl. Sci. Technol.* **2002** (Suppl. 3), 325–327.
30. Modolo, G.; Odoj, R. *Solvent Extr. Ion Exch* **1999**, *17* (1), 33–53.
31. Kolarik, Z.; Mullich, U.; Gassner, F. *Solvent Extr. Ion Exch.* **1999**, *17*, 1155.

Chapter 4

Roadmapping New Cleanup Technologies in the U.S. Department of Energy's Office of Environmental Management

John R. Wiley[*,1,†] **and Edwin Przybylowicz**[2,†]

¹National Research Council, Midland, Texas
²Eastman Kodak Company, Webster, New York
***johnrwis@gmail.com**
†Retired.

The Department of Energy's Office of Environmental Management is at about the midpoint in its efforts to clean up the nation's former nuclear weapons material production sites. DOE estimates that the cleanup will require another 30 years during which about two-thirds of the approximately $300 billion life-cycle cleanup cost will be incurred. To enhance its efforts to develop new technologies that can make the cleanup safer and more efficient, EM prepared an engineering and technology roadmap in 2008 at the request of Congress. The EM roadmap was the subject of a study by the National Academies. This paper extends that study to recognize the synergism between the EM cleanup and environmental issues that will arise from future applications of nuclear energy. In both instances, science and technology roadmaps can be valuable tools for inspiring and focusing the kinds of research that are described in other chapters of this Symposium Series book.

Introduction

The U. S. Department of Energy (DOE) is at about the midpoint in its efforts to clean up massive amounts of waste and environmental contamination that resulted from Cold War-era production of nuclear weapons materials. Serious efforts to treat high-level radioactive waste stored in million-gallon tanks began in the mid-1970s even while production operations were still ongoing (*1*, *2*). DOE

established its Office of Environmental Management (EM), the office charged with site cleanup, in 1989. DOE has estimated that completing its site cleanup will require another 30 years and cost between $205 billion and 260 billion during that time (*3*).

Since its inception, EM has maintained an office charged with providing new, advanced technologies to help make the cleanup effort "faster, cheaper, and safer." Congress, DOE, and technology developers held high expectations, and funding for EM technology development rose to over $400 million in fiscal year 1995. Since then, however, funding for technology development has generally declined. Recent funding levels through fiscal year 2009 were in the range of about $20-40 million (*4*).

While there have been important, new, science-based technologies introduced into the EM cleanup program (*5*), most observers would agree that waste management technology development has moved slowly—especially compared to new areas of applied science such as biotechnology, information technology, alternative energy, and nanotechnology. Many would question whether nuclear waste management presents a fertile field for major new technical advances at all.

It was in this context that in 2007 Congress requested EM to prepare an engineering and technology roadmap. The roadmap was to help guide EM's technology development by identifying science and technology gaps in the cleanup program and laying out a plan to address these gaps. EM's Office of Engineering and Technology (EM-20) requested that the National Research Council of the National Academies (NRCNA) assist the roadmapping activity. The NRCNA has a long history of advising DOE and its predecessors about how to deal with Cold War-era "legacy" wastes (*6–8*).

To provide the requested assistance, the NRCNA convened a study committee, which visited four major DOE cleanup sites (the Oak Ridge Reservation, TN; the Hanford Reservation, WA; the Idaho National Laboratory; and the Savannah River Site, SC) and held six public information-gathering meetings between March 2007 and April 2008. The authors of the present paper, Edwin P. Przybylowicz and John R. Wiley served respectively as chairman and NRCNA staff director of the study. The final report from the study was released in February 2009 (*9*).

This paper extends a presentation about the EM roadmap, based on the NRCNA committee study, that was given by one of the authors (Wiley) during the symposium on Nuclear Energy and the Environment at the ACS 238th National Meeting, August 2009. In the present paper, the authors include their own experiences in technology development and application in both the commercial and DOE sectors to suggest how roadmapping can help make future research more effective in addressing environmental issues at the DOE sites and also those that will be associated with expanded future uses of nuclear energy.

EM Technology Gaps Needing Research

The NRCNA 2009 report (*9*) presented a set of technology gaps identified by the study committee as required by its task statement. For its study, the committee considered a gap to be "a shortfall in available knowledge or technology that could

prevent EM from accomplishing a cleanup task on its expected schedule and/or budget" ((*9*), p.5). Gaps were organized according to categories used by EM in its Engineering and Technology Roadmap (*10*). These categories and the gaps identified in NRCNA 2009 (*9*) are described below.

Waste Processing

Gaps identified in this area dealt primarily with high-level waste, which is stored in large tanks and bins at DOE's, Hanford, Idaho, and Savannah River sites. The main gaps are as follow:

- Substantial amounts of waste may be left in tanks/bins after their cleanout—especially in tanks with obstructions, compromised integrity, or associated piping.
- Increased vitrification capacity may be needed to meet schedule requirements of EM's high-level waste programs.
- The baseline tank waste vitrification process significantly increases the volume of high-level waste to be disposed.
- Low-activity streams from tank waste processing could contain substantial amounts of radionuclides.

These gaps are specific to the nature of DOE waste produced under the duress of the Cold War and waste management practices of that era—for example, wastes from different nuclear fuel reprocessing methods were comingled, and storage requirements greatly increased the waste volume and created hard-to-remove solids. Developing improved or new technologies to help close these gaps is an important opportunity for applied research and development (R&D) during the next five to ten years. R&D approaches for closing the gaps are described in NRCNA 2009 (*9*).

Future, advanced fuel cycles will certainly avoid waste management "mistakes" dating from 60 years ago. Future high-level wastes most likely will be in relatively small volumes of homogeneous liquids. Such wastes will, however, be thermally and radioactively more energetic than the aged and diluted DOE legacy wastes. This may be exacerbated by high-burn-up fuels and actinide-burning reactor cycles to eliminate most long-lived actinides in the waste, but which yield higher concentrations of fission products. Borosilicate glass made with Joule-heated melters, the current baseline technology for stabilizing DOE wastes for disposal, will probably be unsuitable for advanced fuel cycle waste, and completely new waste processing technologies will have to be developed.

Other technology gaps for waste processing as identified in NRCNA 2009 (*9*) are:

- New facility designs, processes, and operations usually rely on pilot-scale testing with simulated rather than actual wastes.
- A variety of wastes and nuclear materials do not yet have a disposition path.

R&D to bridge these gaps will likely be as relevant for advanced fuel cycles as for DOE's legacy waste. For example, reliance on non-radioactive simulants for process tests is generally driven by the long time and high expense of constructing radioactive pilot facilities—typically a large fraction of that needed to construct the actual full-scale facility. Use of computer modeling will certainly increase in the future, but such models necessarily rely on identifying and incorporating all essential attributes of the actual waste that can affect process design.

Finally, we note that, absent a deep geologic repository at Yucca Mountain, at present there is no disposal pathway for high-level wastes from the DOE sites or from future reprocessing. In addition, future reprocessing may produce wastes that do not fit well into today's regulatory categories of high-level or low-level wastes. Specifically, efforts to reduce the volume of high-level waste from future reprocessing may lead to substantial amounts of wastes that would today fall into the category of "greater-than-Class C" low-level waste. This is an awkwardly defined category for which there are few disposal pathways (*11*, *12*).

Groundwater and Soil Remediation

Contamination from radioactive and/or hazardous chemicals has reached groundwater at all four of the DOE sites visited by the NRCNA committee. Technology gaps that impact on-site remediation are as follow:

- The behavior of contaminants in the subsurface is poorly understood.
- Site and contaminant source characteristics may limit the usefulness of EM's baseline subsurface remediation technologies.
- The long-term performance of trench caps, liners, and reactive barriers cannot be assessed with current knowledge.
- The long-term ability of cementitious materials to isolate wastes is not demonstrated.

Environmental remediation at the DOE sites is unusually complicated because a wide variety of wastes were previously discharged to the environment—cribs, seepage basins, unlined burial trenches. Gaps identified in this area are specific to the EM cleanup sites visited by the study committee, and R&D approaches to close these gaps are described in NRCNA 2009 (*9*).

While new applications of nuclear energy will not repeat the environmental mistakes of the past, R&D to fully understand the geoscience of disposal systems will remain a requisite. For example, some analysts assert that a major scientific flaw in the Yucca Mountain repository was its oxidizing environment in which UO_2 (the chemical form of uranium in spent nuclear fuel) is thermodynamically unstable (*13*). New efforts to establish a geologic repository for high-level wastes and spent fuels must rest on sound geoscience.

Future waste disposals and environmental protection will continue to rely on specially designed barriers in deep-geologic and near-surface facilities. R&D to fundamentally improve long-term barrier performance, predictability, and construction will be necessary for both DOE site cleanup and future nuclear energy applications. Cementitious materials (concrete, grout) will remain

ubiquitous for use as barriers, as matrices to contain wastes, and for building new facilities.

Facility Deactivation and Decommissioning (D&D)

Buildings for the reactors, separations plants, and most other facilities at DOE production sites were not designed with D&D as a consideration. Highly contaminated plutonium facilities at Rocky Flats and the reactors at Hanford have been successfully deactivated and decommissioned with mostly conventional construction technologies, but major challenges, such as the fuel reprocessing "canyons" at Hanford and Savannah River remain. Technology gaps identified by the study committee were:

- D&D work relies on manual labor for building characterization, equipment removal, and dismantlement.
- Removing contamination from building walls, other surfaces, and equipment can be slow and ineffective.
- Personal protective equipment tends to be heavy, hot, and limits movement of workers.

D&D work is a notable example of DOE and policy makers' decisions to accept risks, which can presumably be managed, for the current generation of workers in order to alleviate potential risks to future generations. Approaches for R&D described in NRCNA 2009 (*9*) and previously (*14*) highlight remote technologies such as robotics that could eliminate the need for workers to enter hazardous areas.

Future nuclear facilities probably will be designed with at least some consideration of their eventual D&D. However, construction cost will inevitably play a major role in such considerations and push design decisions toward minimizing near-term costs. D&D will likely remain a long-term challenge for all nuclear facilities.

In addition to end-of-life D&D, maintenance at future facilities may be a source of risks to workers. Maintenance was a primary consideration in the design of DOE's original production complex, but it appears that DOE's new facilities, e.g., the Hanford Waste Treatment Plant, the SRS Mixed Oxide Fuel Fabrication Facility, are being designed to be "turnkey" operations with much less concern for maintenance or possible needs for major process modifications. In the authors' experience and views, expectations for nearly turn-key, maintenance-free operations are unlikely to be fulfilled. Needs for improved robotics, other remote maintenance techniques, and personal protective gear will continue to be opportunities for R&D.

Capabilities To Be Maintained to Support R&D

In addition to identifying technology gaps that could affect the DOE site cleanup, the NRCNA committee was tasked to identify personnel expertise

and physical infrastructure that DOE should maintain at its sites and national laboratories to bridge the gaps and support its next 30 years of cleanup activities. At the outset, the committee observed that expertise and infrastructure are complementary—technical experts cannot do their work without adequate infrastructure (buildings and equipment), and infrastructure is useless without qualified personnel to operate it. The committee adopted the word "capability" to refer collectively to expertise and infrastructure, and agreed on the following set of capabilities:

- Handling radioactive materials,
- Conducting engineering and pilot-scale tests,
- Determining contaminant behavior in the environment, and
- Utilizing state-of-the-art science to develop advanced technologies.

One might observe that the first two refer more to the physical infrastructure to support R&D, the third refers more to an R&D activity, and the last looks forward to future R&D. In fulfilling its task, the NRCNA committee described these four capabilities rather broadly and refrained from endorsing specific capabilities to be maintained at specific sites, although examples were provided for illustration.

The capability to handle highly radioactive materials is central to sustaining the EM cleanup for the next 30 years. Existing national laboratory and DOE site facilities provide unique capabilities for handling liter or larger quantities of actual high-level tank waste and other radioactive materials from former production activities. Equivalent capabilities do not exist in university laboratories or in the commercial sector.

The capability to conduct engineering and pilot-scale tests—for example to determine basic process parameters like heat and mass transfer or whether equipment is appropriately designed—is not unique to the DOE sites and national laboratories. Such capability is common in the commercial sector and in university engineering departments. The committee recommended that, as a matter of practicality, DOE should maintain some of its specialized engineering test facilities, for example the tank mock-up facilities at Hanford and Savannah River, and "high-bay" buildings for testing large pieces of equipment.

University, production site, and national laboratory personnel frequently collaborate to understand the geohydrology and other factors that determine contaminant behavior at the DOE sites. While capability to conduct geoscientific research is widely distributed, the sites themselves are unique field laboratories for tests and measurements to develop and confirm conceptual understanding and predictive models. Records, databases, and knowledge among experienced personnel who are well acquainted with site history are necessary for maintaining this capability.

These three capabilities—handling radioactive materials, conducting engineering tests, and understanding the environmental behavior of site contamination—are essential for EM to bring its site cleanup work to a successful conclusion during the next 30 years. They will also be essential to support future uses of nuclear energy, especially advanced fuel cycles. The national laboratories must not lose their basic radiochemical, engineering, and field capabilities as, for

example, more attention is given to computer modeling of contaminant behavior and waste processing.

While direct discharges to the environment will not be allowed in future applications of nuclear energy, wastes and possible contamination from new applications will present new R&D needs. Separation processes will probably produce wastes in different chemical forms than DOE's legacy waste. The spectrum of waste radionuclides will be different due to higher fuel burnup and possibly actinide burning as noted previously in this paper. Efforts to reduce the volume of wastes designated as high-level, which must be disposed in a deep geological repository, will probably result in greater amounts (both curies and volume) being disposed in near-surface facilities. Sound geoscience and engineering bases will be necessary to establish the safety of these practices—to ensure that future generations do not regard our "modern" environmental practices to be as naïve as we regard those of the Cold War era.

Lastly, the study committee stated that during the remaining 30 years of cleanup, EM must maintain the capability to utilize new, state-of-the-art science. New scientific discoveries and enhanced understanding of fundamental scientific principles will lead to opportunities for technologies that cannot be envisioned today. Goals for EM's cleanup will change as public expectations for "how clean is clean" evolve, and possibly as the understanding of radiation's health effects advances. EM would not be expected to maintain its own state-of-the-art scientific programs, but rather to maintain a cadre of personnel who could understand and collaborate with investigators in the basic and applied sciences. To this end, EM must maintain a presence in the national laboratories and also establish partnerships with other federal, university, and commercial-sector R&D programs, as discussed in the next section of this report.

Leveraging R&D for Environmental Management

Broadly-speaking, leveraging R&D assets is becoming an attractive alternative in today's economic and rapidly changing technology environments. Leveraging R&D assets requires the "pooling together" of R&D funds, personnel resources, and even infrastructure from several organizations to pursue a common set of R&D objectives that can benefit all the participants. Leveraging can provide state-of-the art-technology at a reduced cost to each of the participating organizations. Along with its other tasks, the NRCNA committee was asked to identify opportunities for EM to better leverage its limited R&D funds.

To be successful, leveraging requires effective working partnerships or strategic alliances between the organizations involved with the technology development (*15*). The more common "go it alone" R&D project, while providing exclusivity, is supported by a single organization and as such the project can be expensive and isolated. Sometimes, the lack of cross-fertilization of ideas and solutions from different viewpoints can lead to less effective results from the R&D.

Earlier in this paper, it was noted that historically R&D in EM was supported at substantially higher levels than it is today. The decrease in R&D support of

its work, at a time when EM is facing some of the most challenging tasks in the cleanup program, may have resulted from less than expected results from the earlier investments as well as the competition for R&D budgets from other, higher profile programs within DOE or a combination of the two. The net result is less available R&D funding for research to support the more complex, challenging cleanup problems that EM is facing today and will be during the next 30 years as they work to clean up the toughest legacy waste problems.

In its report, the committee defined "opportunities to leverage" as those collaborations or co-investments between EM and other organizations—government, academic, and private sector—to achieve synergistic production of new knowledge, knowledge transfer and application to clean-up problems, reduction in timetables, and efficiency improvements in personnel and infrastructure utilization. These types of opportunities must be specifically identified by EM as it goes forward in order to maximize the return on its R&D investment by leveraging it with other organizations that have complementary capabilities and are interested in advancing science and technology objectives in areas of common interest with those of EM. To do this requires that EM attract and maintain strong scientists and technologists who can not only provide an effective interface with partnering organizations, but can provide a *quid pro quo* of capabilities that other partnering organizations seek. While EM probably cannot maintain a critical mass of expertise in certain scientific and technological fields, the opportunity to partner with other capable institutions and organization can act as an incentive to attract good scientists and technologists to the EM organization.

Much has been studied and written about success factors in these strategic alliances or leveraging opportunities (*15*), which needn't be repeated here. The essence of creating an effective partnership is for each partner in the collaboration to have a strong incentive for their participation. Given the challenges that lie ahead for EM in cleaning up complex legacy nuclear wastes: (1) the limited funds that are likely to be available for such tasks and (2) the continued deterioration of present containment mechanisms (buildings, soil and groundwater plume expansion, decay of tanks and tank containment), which will make the cleanup task even more complex as time goes on, EM has strong motivation to seek out the best technology possible to clean up these wastes in a safe, cost-effective and rapid manner. In so doing, not only will EM address its most urgent needs, but EM will also be providing the basis of technology for the handling of nuclear waste from future energy generation programs and production.

Conclusions

In its final report, the NRCNA committee provided nearly a dozen findings and recommendations to assist EM improve its 2008 roadmap, especially for sustaining R&D to close the gaps described in the report and for establishing R&D partnerships with other organizations (*9*). The four conclusions in this paper are a distillation of the committee's findings and recommendations along with the authors' own perspectives. We address these conclusions primarily to those who

have responsibilities for administering R&D funding relevant to nuclear energy and the environment and to those who seek this funding.

1. Funding of Mission-Directed R&D Is an Appropriate and Essential Role for DOE's Programmatic Offices Such as EM and the Office of Nuclear Energy (NE).

The NRCNA committee noted that site cleanup contractors provide much if not most of the funding for cleanup R&D. This is mainly for "as needed" research to address specific short-term issues. Such a limited scope for R&D funding is not likely to provide the necessary technology advances to address site cleanup and nuclear energy environmental challenges over the next 30 years.

The committee's interim report (*16*) compared the funding of R&D by cleanup contractors to the industry practice of funding product-related R&D through business units. Business units, driven by the profit/loss bottom line, usually make investments only for short-term results and incremental product improvements. In industry, the longer-term (5 to 10 years or more) investments that are more likely to result in new product and process concepts are usually supported at the corporate level. By direct analogy with industry, DOE program offices such as EM and NE should support longer-term, visionary, strategic, yet mission-oriented R&D.

The committee did not overlook the DOE Office of Science (SC), which is DOE's primary funder of cutting-edge science and applied R&D. Rather, it recommended that SC be a key partner with which EM leverages R&D. The former EM Science Program, in which EM evaluated R&D proposals for relevance to site cleanup needs and SC evaluated the proposals for scientific merit, was cited by the committee as an excellent example of partnering.

2. The EM Roadmap Can Be an Excellent Tool for EM to Communicate Its R&D Needs ("Technology Gaps"), the Time Frame for Addressing Them, Possibilities for Partnering with Other R&D Organizations, and Its R&D Accomplishments.

Roadmapping is being used increasingly by private-sector and governmental organizations. The committee strongly endorsed the concept of the 2008 EM roadmap, but found numerous ways to improve it. For example, the roadmap did not include timelines for bringing new technologies to bear on cleanup needs. R&D toward new technologies must be keyed to site cleanup milestones. If the technologies are not available when needed, then their potential to reduce costs, technical risks, or cleanup time will not be realized.

EM should consider its roadmap to be a living document and update it regularly. The committee recommended updates at least every four years not only to remain current with milestones and technical challenges of the cleanup program, but also to help ensure carryover of R&D projects and their rationales into new administrations. EM was aware of this need and requested that the committee release its final report in time to assist the transition in early 2009. We, the authors of this paper, also note that opportunities for EM to partner with

other organizations will continue to change. The roadmap must stay up to date to reflect these changes if it is to be an effective tool for leveraging EM R&D. The EM cleanup will have a dynamic relationship with the further development of nuclear energy during the next 30 years.

3. The Roadmap Can Be an Important Tool for Inspiring R&D.

Both the 2008 EM roadmap (*10*) and the 2009 NRCNA report (*9*) list technology gaps that can have major impacts on EM's cleanup schedule and budget. These lists and their accompanying commentary on R&D approaches to bridge the gaps raise opportunities for researchers to tie their work to EM's most significant cleanup technology needs. Synergism between creative research and problems for which solutions can have major, positive impacts is most likely to lead to the kinds of technological breakthroughs envisioned when EM was established with its own R&D office in1989. Research proposals that build on this synergism will be well positioned to receive DOE funding.

Finally, we would add that researchers can benefit from future roadmaps of the waste management and environmental challenges that will arise from expanded uses of nuclear energy. New fuel cycle technologies will produce wastes for which known disposal paths will probably be sub-optimal or perhaps inappropriate. Some of these likely future challenges were described earlier in this paper. As in the case for EM's cleanup work, synergisms between creative research and major practical problems can lead to transformational new technologies. We encourage NE and other appropriate organizations, for example the Nuclear Energy Institute, to roadmap these challenges.

4. Researchers Are Encouraged to Seek Opportunities To Form Collaborations—Those Including Academic, National Laboratory, and Industry Researchers Are Especially Encouraged.

The leveraging of R&D resources is becoming increasingly important, as described by NRCNA 2009 (*9*) and in this paper. Much R&D, especially that most likely to have major impacts on problems of energy, the environment, and waste management, has become more expensive and also more interdisciplinary. The committee observed that "EM's Office of Engineering and Technology does not have the resources necessary to sustain all of the capabilities that are necessary for its R&D work" (*9*). Similarly in commenting on a recent review of NASA's manned space flight program, which found that NASA does not have enough money to carry out its current plan for a lunar landing in 2020, the author of a letter to *Science* stated that "Our national space dilemma can be solved by including international partners at all stages of future expensive manned space projects, from planning, to design, to use" (*17*).

During the future 30 years of the EM cleanup and as applications of nuclear energy expand, environmental technology gaps and new issues are likely to be best addressed by R&D partnerships. Each member of a partnership can bring a different set of needs and resources to the table—detailed understanding of a problem, specialized or perhaps unique scientific and technical personnel and

infrastructure, and financial assets. Through this kind of leveraging, innovative R&D projects that are beyond the ability of any of the individual partners can be sustained.

The NRCNA committee was tasked to identify capabilities at the DOE sites and national laboratories that should be maintained to support EM's 30-year cleanup program. Such capabilities, as described in the committee's report and in this paper, might provide the core on which R&D proposals and partnerships are developed. In forming a partnership for the purpose of leveraging research assets, each partner must have a strong incentive for participating, and each member must be able to share in all the benefits of the collaboration.

We hope that this paper, in conjunction with NRCNA 2009 (*9*) and DOE's present and future technology roadmaps, will provide useful ideas and guidance for all involved in research in the area of nuclear energy and the environment.

References

1. Wiley, J. R. Decontamination of alkaline radioactive waste by ion exchange. *Ind. Eng. Chem. Process Des. Dev.* **1978**, *17*(67).
2. Wiley, J. R. Preparations for High-Level Defense Waste Immobilizaton at Savannah River Plant. In *Effluent and Environmental Radiation Surveillance*; ASTM Special Technical Publication 698; Kelley, J. J., Ed.; American Society for Testing and Materials: Philadelphia, PA, 1980.
3. FY 2010 Congressional Budget Request, Environmental Management, Defense Nuclear Waste Disposal, Nuclear Waste Disposal; DOE/CF-039; U.S. Department of Energy: Washington, DC, 2009; p 17. http://www.cfo.doe.gov/budget/10budget/Content/Volumes/Volume5.pdf.
4. The FY 2010 request for technology development was $105 million including $50 million for Hanford tank cleaning technology. FY 2010 Congressional Budget Request, Environmental Management, Defense Nuclear Waste Disposal, Nuclear Waste Disposal; DOE/CF-039; U.S. Department of Energy: Washington, DC, 2009; p 18. http://www.cfo.doe.gov/budget/10budget/Content/Volumes/Volume5.pdf.
5. Moyer, B. A.; Birdwell, J. F., Jr.; Bonnesen, P. V.; Delmau, L. H. Use of Macrocycles in Nuclear-Waste Cleanup: A Real-World Application of a Calixcrown in Technology for the Separation of Cesium. In *Macrocyclic Chemistry Current Trends and Future*; Gloe, K., Ed.; Springer: Dordrecht, 2005; pp 383−405.
6. *Linking Legacies: Connecting the Cold War Nuclear Weapons Production Processes to their Environmental Consequences*; DOE/EM-0319; Office of Environmental Management, U.S. Department of Energy: Washington, DC, January 1997.
7. *The Disposal of Radioactive Waste on Land*; National Research Council of the National Academies, National Academies Press: Washington, DC, 1957. http://books.nap.edu/catalog.php?record_id=10294.
8. *Science and Technology Needs for DOE Site Cleanup: Workshop Summary*; National Research Council of the National Academies,

National Academies Press: Washington, DC, 2007. http://www.nap.edu/catalog.php?record_id=11932.

9. *Technical and Strategic Advice for the Department of Energy, Office of Environmental Management's Development of a Cleanup Technology Roadmap*; National Research Council of the National Academies, National Academies Press: Washington, DC, 2009. http://www.nap.edu/catalog.php?record_id=12603.

10. *Engineering and Technology Roadmap: Reducing the Uncertainty in the EM Program*; Office of Environmental Management, U.S. Department of Energy: Washington, DC, March 2008.

11. *Improving the Regulation and Management of Low-Activity Radioactive Wastes: Final Report*; National Research Council of the National Academies, National Academies Press: Washington, DC, 2006. http://www.nap.edu/catalog.php?record_id=11595.

12. Wiley, J. R. Why We Need Better Management of Low-Activity Radioactive Waste. *Radwaste Solutions*, May/June 2005.

13. Ewing, R. C.; Macfarlane, A. Nuclear waste: Yucca Mountain. *Science* **2002**, 296, 659−660, DOI: 10.1126/science.1071886, in Policy Forum.

14. *Research Opportunities for Deactivating and Decommissioning Department of Energy Facilities*; National Research Council of the National Academies, National Academies Press: Washington, D.C., 2001. http://www.nap.edu/catalog.php?record_id=10170.

15. Slowinski, G.; Sagal, M. W. *The Strongest Link: Forging a Profitable and Enduring Corporate Alliance*; American Management Association: New York, 2003.

16. Letter to Mr. Mark Gilbertson, Deputy Assistant Secretary for Engineering and Technology, Office of Environmental Management, U.S. Department of Energy. In *Technical and Strategic Advice for the Department of Energy, Office of Environmental Management's Development of a Cleanup Technology Roadmap–Interim Report*; National Research Council of the National Academies, National Academies Press: Washington, DC, February 14, 2008. http://www.nap.edu/catalog.php?record_id=12165.

17. Howard, W. E., III. Space goals require worldwide participation. *Science* **2009**, *326*, 797, in Letters.

Separations Chemistry

Chapter 5

Green Separation Techniques for Nuclear Waste Management

Chien M. Wai*

Department of Chemistry, University of Idaho, Moscow, ID 83844
*cwai@uidaho.edu

Recent developments utilizing green solvents, ionic liquids and supercritical fluid carbon dioxide (sc-CO_2), for managing nuclear wastes are summarized in this chapter. Direct dissolution of uranium dioxide and lanthanide oxides in sc-CO_2 can be accomplished with a CO_2-soluble tri-n-butylphosphate-nitric acid complex. On-line separation of uranium and lanthanides dissolved in the sc-CO_2 phase can be achieved by a countercurrent stripping technique. Using room temperature ionic liquid coupled with sc-CO_2 for extraction of uranium from acidic solutions and for dissolution of solid uranium dioxide are also described. Potential applications of these green separation techniques for decontamination of nuclear wastes and for reprocessing spent fuels are discussed.

Introduction

Replacing traditional fossil fuels with environmentally sustainable energy sources is necessary for curbing the threat of global warming. Nuclear power is one of the known energy sources which is free of carbon emission and has a power production cost comparable to that of gas (*1*). Currently nuclear power contributes to about 20% of the electricity generated in the USA whereas in France over 80% of the electricity is generated by nuclear energy. One public concern for expanding use of nuclear energy in the USA is the economic and environmental issues associated with the wastes produced by nuclear power generation. Traditional methods of treating nuclear wastes and reprocessing spent fuel require acid solutions and organic solvents for dissolution and separation of radioactive elements with an unavoidable consequence of generating large

quantities of liquid wastes. Minimizing waste generation in the nuclear fuel cycle is an important factor to make nuclear energy environmentally sustainable and acceptable to the public. Utilizing green solvents for treating nuclear wastes and for reprocessing spent fuel is one approach of minimizing waste generation in the nuclear fuel cycle (*2*).

Supercritical fluid carbon dioxide (sc-CO_2) and ionic liquids (ILs) are considered green solvents for chemical reactions and separations (*3*, *4*). Research in utilizing sc-CO_2 as a solvent for dissolution and extraction of metal species started nearly two decades ago (*5*, *6*). The successful demonstration of extracting lanthanides and uranium from aqueous solutions using CO_2-soluble ligands in the early 1990s led to the speculation that sc-CO_2 extraction could be an attractive green technology for nuclear waste management because it does not require conventional liquid solvents. Later reports showed that direct dissolution of lanthanide oxides and uranium dioxide in sc-CO_2 could be achieved with a high efficiency using a CO_2-soluble TBP-nitric acid complex (*7–9*). These reports established the value of the supercritical fluid technology for management of nuclear wastes. Current industrial interest in supercritical fluid technology for nuclear waste management is demonstrated by a project undertaken by AREVA for recovering enriched uranium from the incinerator ash generated by the light-water reactor fuel fabrication process (*10*). The process is discussed in detail by S. Koegler in Chapter 6 of this book. Possibilities of utilizing sc-CO_2 technology for reprocessing spent nuclear fuels have also been investigated by other research projects (*11*, *12*).

Room temperature ionic liquids (RTILs) have unique properties including non-flammable nature, near zero vapor pressure and high solubility for a variety of ionic and neutral compounds (*1*, *13*, *14*). These properties make them attractive for replacing volatile organic solvents traditionally used in various liquid-liquid extractions. However, separation of dissolved metal species from RTILs by conventional methods such as acid stripping, distillation, or organic solvent back-extraction is often inefficient and results in production of secondary wastes. It is known that sc-CO_2 can dissolve in RTILs effectively whereas latter have negligible solubilities in the fluid phase (*15*). This property allows easy recovery of dissolved metal species in RTIL by sc-CO_2 without contamination or loss of the IL. A combination of IL dissolution and sc-CO_2 extraction may provide another green approach for managing nuclear wastes (*16*).

This chapter summarizes current status of sc-CO_2 extraction technology for nuclear waste management with an emphasis on industrial applications. Recent developments in IL dissolution of lanthanide and actinide oxides and their subsequent extraction and separation by sc-CO_2 are discussed. One unique property of RTILs is their unusual solvation character, which is reflected in their ability to dissolve both ionic species and neutral compounds. Little is known at the present time regarding the chemical environments of uranyl and other actinide species dissolved in RTILs. In this chapter, some information based on spectroscopic studies of uranyl species dissolved in a RTIL are also given to illustrate the coordination environments of uranyl in the ionic liquid phase.

Dissolution and Separation of Lanthanides and Actinides in Sc-CO$_2$

Direct dissolution of uranium dioxide (UO$_2$) in sc-CO$_2$ using a CO$_2$-soluble tri-n-butylphosphate (TBP)-nitric acid complex of the general form TBP(HNO$_3$)$_x$(H$_2$O)$_y$ is well-established in the literature. The complex is prepared by shaking TBP with concentrated nitric acid (15.5 M) leading to the formation of a Lewis acid-Lewis base complex in the TBP phase (*17*). The composition of the complex is controlled by the relative amounts of TBP and the acid used in the preparation. With an equal volume of TBP and concentrated nitric acid, the complex formed has a chemical composition of TBP(HNO$_3$)$_{1.8}$(H$_2$O)$_{0.6}$ (Figure 1). Because TBP is highly soluble in sc-CO$_2$, it serves as a carrier for introducing HNO$_3$ into the supercritical fluid phase with a minimum amount of water. The HNO$_3$ in the complex oxidizes UO$_2$ from +4 oxidation state to the +6 oxidation state uranyl ion (UO$_2$)$^{2+}$ followed by the formation of UO$_2$(NO$_3$)$_2$(TBP)$_2$, which is soluble in the supercritical fluid phase. According to one report, UO$_2$(NO$_3$)$_2$(TBP)$_2$ has a solublility of 0.45 moles per liter in sc-CO$_2$ at 40 °C and 200 atm (*18*). This is close to the uranium concentration utilized in the PUREX (plutonium uranium extraction) process. The supercritical fluid dissolution method, which combines dissolution and extraction of uranium dioxide in sc-CO$_2$ in one step without formation of an aqueous phase, is attractive for treating uranium containing wastes. In conventional solvent-based extraction processes, uranium dioxide is first dissolved in an acid solution (typically 3-6 M nitric acid) followed by extracting the dissolved uranyl ions from the acid solution into an organic solvent (such as dodecane or kerosene) containing TBP. The sc-CO$_2$ dissolution/extraction process produces far less liquid wastes compared with conventional solvent-based extraction methods.

The sc-CO$_2$ dissolution process is particularly effective for removing uranium from densely packed solid materials because sc-CO$_2$ is capable of penetrating into small pores in solid matrixes. One example is the extraction of enriched uranium from incinerator ash generated by the light-water nuclear reactor fuel fabrication process (*9*, *19*). The fuel fabrication process involves conversion of enriched UF$_6$ gas (about 3.5% ^{235}U) to solid UO$_2$ for nuclear power production. Disposable solid waste generated by the process is reduced by a factor of about 1/20 through a carefully controlled incineration process. The incinerator ash contains approximately 8-10% by weight of enriched uranium, a valuable material for the nuclear industry. Some gadolinium (Gd), which is added to the fuel as a neutron absorber, is also present in the ash.

AREVA NP in Richland, Washington has recently demonstrated that sc-CO$_2$ containing TBP(HNO$_3$)$_{1.8}$(H$_2$O)$_{0.6}$ is very effective for removing uranium from the incinerator ash. Gadolinium and some alkaline earth metals are also dissolved in the sc-CO$_2$ phase. Recovery of uranium from the sc-CO$_2$ phase is achieved by a countercurrent column stripping process illustrated in Figure 2. In this process, the sc-CO$_2$ carrying the dissolved gadolinium and uranium is fed into a stripping column from the bottom while nitric acid is introduced into the column through a nozzle from the top. The highly acidic aqueous phase strips the Gd^{3+} into the aqueous phase. The aqueous phase containing Gd^{3+} is collected in a reservoir at
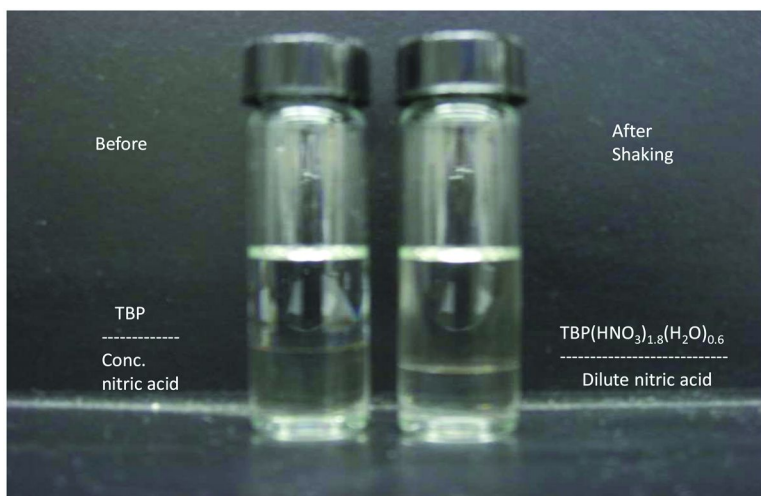
Figure 1. Preparation of TBP(HNO₃)₁.₈(H₂O)₀.₆ extractant by shaking an equal volume (5 mL each) of TBP and concentrated nitric acid (15.5 M); left: before shaking; right: after shaking.

the bottom of the column. The exiting sc-CO_2 from the first column is fed into a second column from the bottom and water is introduced into the column from the top. If the acidity of the aqueous phase in contact with the sc-CO_2 is low, $(UO_2)^{2+}$ can be stripped into the aqueous phase. TBP and some uranium remaining in the sc-CO_2 phase are recycled for repeated extraction of the ash. Separation of gadolinium and uranium in this process is based on the fact that $UO_2(NO_3)_2(TBP)_2$ and $Gd(NO_3)_3(TBP)_x$ exist in the sc-CO_2 phase at different HNO_3 concentrations. Typically, Gd is stripped around 3-4 M nitric acid whereas UO_2 is stripped at <0.5M nitric acid concentration. After removing uranium from the incinerator ash, the ash can be classified as a different type of waste and disposed of accordingly.

The incinerator ash is difficult to treat by conventional acid dissolution methods. The success of the AREVA process suggests the sc-CO_2 dissolution/ extraction technology may be used to recovery uranium and other fissionable actinides (e.g. plutonium and thorium) from refractory solid materials such as spent nuclear fuels. The sc-CO_2 countercurrent stripping technology developed by AREVA is significant because it provides a means for on-line separation and collection of dissolved lanthanides and actinides in conjunction with supercritical fluid extraction. This technology may have a number of applications in nuclear waste management. For example, the counter-current stripping process can be modified for separation of uranium and plutonium in a sc-CO_2 stream by altering the oxidation state of Pu(IV) using a reducing agent following the chemistry of the PUREX process. It is conceivable that separation of Th(IV) and U(VI) in a sc-CO_2 stream can also be achieved using the counter-current stripping technology.

An attempt to evaluate the feasibility of extracting uranium and plutonium from spent nuclear fuel using the supercritical fluid dissolution/extraction technique was conducted in Japan a few years ago (*11*). The so-called
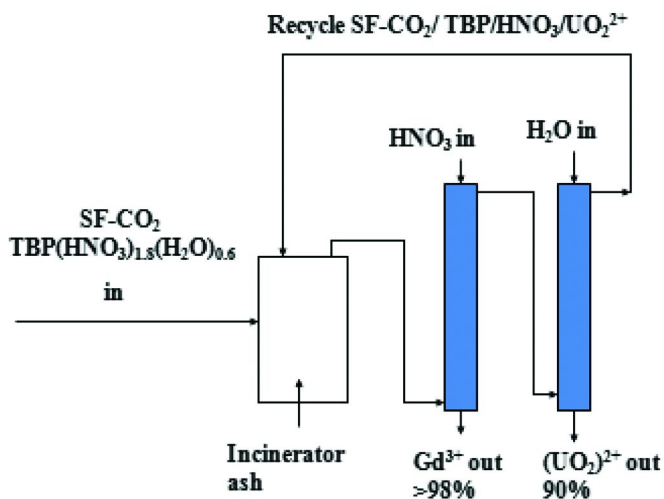
Figure 2. Schematic diagram illustrating the AREVA sc-CO$_2$ process for recovering enriched uranium from incinerator ash

"Super-DIREX" (supercritical fluid direct extraction) process demonstrated that uranium and plutonium in irradiated uranium fuel can be extracted by sc-CO$_2$ containing a TBP-nitric acid extractant (*11*). The details of the Super-DIREX project are not totally described in the literature. Nevertheless, the project illustrates the interest of the nuclear industry in utilizing the sc-CO$_2$ technology for spent fuel reprocessing applications. In Russia, the use of β-diketones as extractants for recovering uranium from spent fuel was investigated (*12*). The feasibility of using β-diketones for extracting actinides including plutonium and americium from soil into sc-CO$_2$ was demonstrated by scientists from Idaho National Lab (INL) in recent years (*20*). Studies on sc-CO$_2$ extraction of thorium and uranium from solid materials have been reported by scientists from India (*21*). These studies may provide a foundation for applying sc-CO$_2$ technology to wastes associated with the thorium-based fuel cycle. Conversion of uranium oxides to anhydrous uranyl nitrate using liquid dinitrogen tetraoxide (N$_2$O$_4$) is a well known chemial reaction reported nearly 50 years ago (*22*). This reaction has been used recently by Chinese scientists for converting lanthanide oxides and by Russian scientists for converting uranium dioxide to their nitrates for sc-CO$_2$ extraction with TBP (*23*, *24*). Supercritical fluid-based dissolution/extraction technology apparently has received world-wide attention in recent years for its potential applications in nuclear waste management and in spent fuel reprocessing. Its application to decontamination of nuclear wastes and to recover valuable materials from the wastes is well illustrated by the AREVA project described in this section. However, its applications to reprocessing spent nuclear fuels require much work in the future, including understanding chemistry of actinides and various fission products in sc-CO$_2$ and design of complicated engineering systems for sc-CO$_2$ processing.

Ionic Liquid and Supercritical Fluid Hyphenated Dissolution/Extraction Techniques

Using room-temperature ionic liquids (RTILs) as media for treating nuclear wastes has been an active research area in recent years (*14*, *16*). One type of RTIL consisting of 1-butyl-3-methylimidazolium (BMIM) cation and an fluorinated anion such as [BMIM][Tf$_2$N] where Tf$_2$N = *bis*-(trifluoromethane)sulfonamide anion is commonly used for extraction of metal ions because they are hydrophobic and stable in contact with water. However, separation of dissolved metal species from RTILs by conventional methods such as acid stripping, distillation, or organic solvent back-extraction is often inefficient and may cause cross-contamination due to their mutual solubility. It is known that supercritical carbon dioxide (sc-CO$_2$), can dissolve in RTILs effectively whereas RTILs have negligible solubility in the supercritical CO$_2$ fluid phase (*15*). This property allows easy recovery of dissolved metal species in RTIL by sc-CO$_2$ extraction without contaminating or losing the IL. In addition, the solvation strength of sc-CO$_2$ is known to depend on density, which can be tuned by varying temperature and pressure of the fluid phase. Therefore, some degree of selectivity during extraction of metal species from IL into sc-CO$_2$ may be achieved by manipulating the density of the fluid phase.

Recent reports show that uranyl ions dissolved in 3 M nitric acid can be effectively extracted into [BMIM][Tf$_2$N] containing TBP at room temperature (*16*). The absorption spectra of uranyl in the aqueous phase and in the IL phase are given in Figure 3. The chemical environment of the dissolved uranyl species in the IL phase is not known. Experimental data indicate that the uranyl species dissolved in the IL can be recovered quantitatively using sc-CO$_2$ at 40 °C and 200 atm and the final product is UO$_2$(NO$_3$)$_2$(TBP)$_2$ (*16*). In this three-phase extraction process, the IL serves as a recyclable medium for extraction and concentration of uranium from the acid solution under ambient pressure (Figure 4). One advantage of this approach is that it would significantly reduce the volume of the uranium-containing solution for high-pressure supercritical fluid extraction and separation. After removing uranium, the RTIL can be reused for continuous extraction of uranyl ions from the acid solution with addition of TBP. The two-step ionic liquid and supercritical fluid coupled extraction technique appears attractive for treating liquid wastes containing uranium. However, this technique is not suitable for removing uranium oxides from solid wastes because the process requires dissolution of uranium oxides in a nitric acid solution first that would result in acidic liquid waste generation.

Direct dissolution of uranium dioxide in [BMIM][Tf$_2$N] at room temperature and ambient pressure can be achieved using the TBP-nitric acid complex, TBP(HNO$_3$)$_{1.8}$(H$_2$O)$_{0.6}$ (*25*). The complex is miscible with [BMIM][Tf$_2$N] forming a homogeneous one phase at a volume ratio of TBP(HNO$_3$)$_{1.8}$(H$_2$O)$_{0.6}$: [BMIM][Tf$_2$N] = 1:5. With stirring, the black UO$_2$ powder in the IL gradually dissolves and turns the color of the IL phase to bright yellow. Uranium dioxide is apparently oxidized by the nitric acid from TBP(HNO$_3$)$_{1.8}$(H$_2$O)$_{0.6}$ to form uranyl ions in the IL phase. The rate of dissolution of UO$_2$ with TBP(HNO$_3$)$_{1.8}$(H$_2$O)$_{0.6}$ in the IL solution monitored by UV/Vis absorption spectra appears to follow a

pseudo first-order reaction initially. Figure 5 shows a plot of $\ln[(A_\infty - A)/A_\infty]$ versus time for the absorbance of uranyl peaks (at 437 nm and at 452 nm) measured in the IL phase during the dissolution process, where A is the absorbance at time t and A_∞ is the maximum absorbance when t becomes very large. The rate constant (slope of the straight line) is 0.028 min^{-1}, suggesting a half-life of about 25 min for the initial dissolution process. This means after 50 min, about 75% of the initial UO_2 should be dissolved in the IL phase.
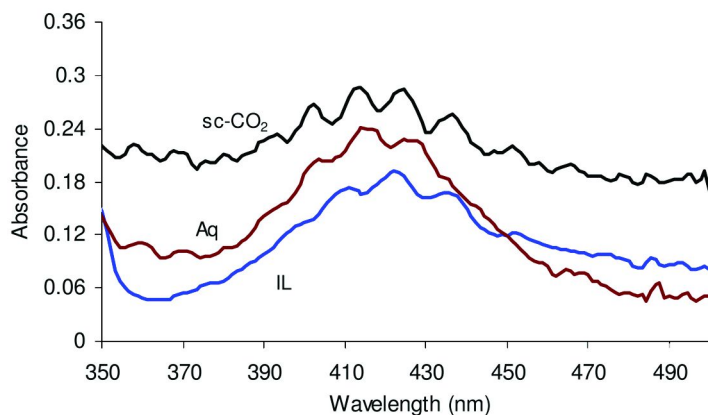
Figure 3. UV-Vis spectra of U(VI) in aqueous (3 M nitric acid), RTIL ([BMIM][Tf₂N]) and sc-CO₂ phases
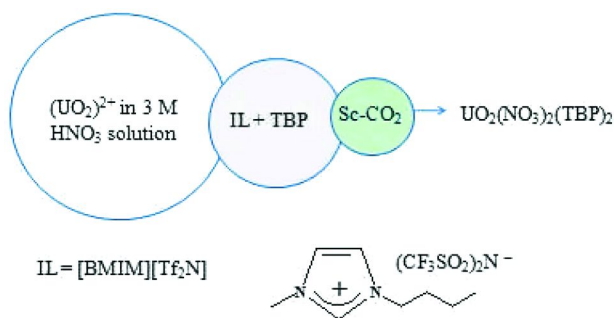
Figure 4. Ionic liquid and sc-CO₂ coupled extraction of uranyl ions from nitric acid solution

Figure 5. Plot of ln[(A∞–A)/A∞] versus time for the dissolution of UO$_2$ in [BMIM][Tf$_2$N] containing TBP(HNO$_3$)$_{1.8}$(H$_2$O)$_{0.6}$

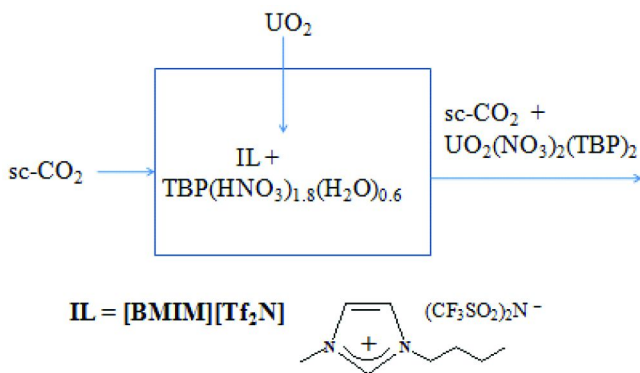*Figure 6. Schematic diagram illustrating direct dissolution of UO$_2$ in [BMIN][Tf$_2$N] coupled with sc-CO$_2$ extraction.*

The dissolution process can be envisioned to involve a number of steps including diffusion of TBP(HNO$_3$)$_{1.8}$(H$_2$O)$_{0.6}$ to the UO$_2$ surface, oxidation of UO$_2$ to uranyl on the UO$_2$ surface, and diffusion of uranyl species from the solid surface to the IL phase. Diffusion of the uranyl species from the UO$_2$ surface to the IL phase is probably a main factor controlling the rate of dissolution of UO$_2$. Deviation from the linear relationship after 60 min possibly indicates occurrence of other processes which would affect the steady diffusion of uranyl at higher concentrations in the IL phase. The solubility of UO$_2$ in [BMIM][Tf$_2$N] is estimated to be around 0.4 moles per liter at room temperature. The UV/Vis

spectra of uranyl species dissolved in the IL phase does not reveal much information about its chemical environment. Understanding the coordination environment of the dissolved uranyl species in IL is important for applying the technology to complex nuclear waste systems. It is known that the Raman active uranyl symmetrical stretching mode (O=U=O) is sensitive to changes in the uranyl coordination environment. Complexation of the uranyl ion weakens the O=U=O bonds and causes the symmetrical stretching mode to shift to lower frequency. Some Raman studies have been carried out in our lab recently. Preliminary Raman data show the uranyl species dissolved in the IL phase with $TBP(HNO_3)_{1.8}(H_2O)_{0.6}$ has a symmetrical stretching mode at 860 cm^{-1}. If only $UO_2(NO_3)_2 \cdot 6H_2O$ is dissolved in the IL without the TBP-nitric acid complex, the O=U=O symmetrical strenching mode occurs at 868 cm^{-1}. The Raman data suggest that the uranyl species dissolved by $TBP(HNO_3)_{1.8}(H_2O)_{0.6}$ in the IL is coordinated with TBP. The dissolved uranyl species can be rapidly transferred to sc-CO_2 at 40 °C and 200 atm. The final uranium compound extracted into the sc-CO_2 phase is $UO_2(NO_3)_2(TBP)_2$. No aqueous phase is formed in either the IL dissolution process or in the supercritical fluid extraction process. Thus, an IL and sc-CO_2 hyphenated dissolution/extraction process shown in Figure 6 may provide another green technique for managing uranium contaminated solid wastes.

Conclusions

The need for renewable and emission free energy sources is obvious in order to alleviate the threat of global warming. Nuclear energy is carbon emission free and has been used for power generation for half of a century. One public concern regarding expansion of nuclear energy for power generation in the USA is the economic and environmental issues associated with managing nuclear wastes. Using green solvents such as supercritical carbon dioxide and room temperature ionic liquids for recycling uranium and for treating wastes generated by the nuclear fuel cycle appears to be a promising approach to minimize the problems associated with nuclear wastes. These emerging green separation techniques will probably play a significant role for managing nuclear wastes in the 21st century.

Acknowledgments

References

1. Lewis, N. S. Powering the planet. *MRS Bull.* **2007**, 32, 808−820. www.mrs.org/bulletin.
2. Wai, C. M. Supercritical Fluid Extraction of Radionuclides: A Green Technology for Nuclear Waste Management. In *Nuclear Waste Management: Accomplishments of the Environmental Management Science Program*;

Wang, P. W., Zachry, T., Eds.; ACS Symposium Series 943; American Chemical Society: Washington, DC., 2006; Chapter 9, pp 161−170.

3. Binnemans, K. *Chem. Rev.* **2007**, *107*, 2592–2614.
4. Wai, C. M. Metal Processing in Supercritical Carbon Dioxide. In *Supercritical Fluid Technologies in Materials Science and Engineering: Synthesis, Properties, and Application*; Sun, Y. P., Ed.; Marcel Dekker: New York, 2002; Chapter 10, pp 351−386.
5. Laintz, K. E.; Wai, C. M.; Yonker, C. R.; Smith, R. D. *Anal. Chem.* **1992**, *64*, 2875–2878.
6. Lin, Y.; Brauer, R. D.; Laintz, K. E.; Wai, C. M. *Anal. Chem.* **1993**, *65*, 2549–2552.
7. Tomioka, O.; Enokida, Y.; Yamamoto, I. *J. Nucl. Sci. Technol.* **1998**, *35*, 513–514.
8. Samsonov, M. D.; Wai, C. M.; Lee, S. C.; Kulyako, Y.; Smart, N. G. *Chem. Commun.* **2001**, 1868–1869.
9. Tomioka, O.; Meguro, Y.; Iso, S.; Yoshida, Z.; Enokida, Y.; Yamotomo, I. *J. Nucl. Sci. Technol.* **2001**, *38*, 461–462.
10. Smith, T.; Thomas, J. Radioactive Waste Not Wasted with New Green Chemistry Technology. *Radwaste Solutions*, September/October 2008, pp 32−35.
11. Shimada, T.; Ogumo, S.; Ishihara, N.; Kosaka, Y.; Mori, Y. *J. Nuc. Sci. Technol.* **2002** (3), 757–760.
12. Murzin, A. A.; Babain, V. A.; Shadrin, A. Ui.; Smirnov, I. V.; Lumpov, A. A.; Gorshkov, N. I.; Miroslavov, A. E.; Muradymov, M. Z. *Radiochemistry* **2002**, *44* (5), 423–427.
13. Dietz, M. L.; Dzielawa, J. A. *Chem. Commun.* **2001**, 2124–2125.
14. Billard, I.; Gaillard, C. *Radiochim. Acta* **2009**, *97*, 355–359.
15. Blanchard, L. A.; Hancu, D.; Beckman, E. J.; Brennecke, J. F. *Nature* **1999**, *399*, 28–29.
16. Wang, J. S.; Sheaff, C. N.; Yoon, B.; Addleman, R. S.; Wai, C. M. *Chem. Eur. J.* **2009**, *15*, 4458–4463.
17. Enokida, Y.; Tomioka, O.; Lee, S.; Rustenholts, A.; Wai, C. M. *Ind. Eng. Chem. Res.* **2003**, *42*, 5037–5041.
18. Carrott, M. J.; Waller, B. E.; Smart, N. J.; Wai, C. M. *Chem. Commun.* **1998**, 373–374.
19. Koegler, S. *Abstract NUCL-043*; 238th American Chemical Society National Meeting, Washington, DC, August 16−20, 2009.
20. Fox, R. V.; Mincher, B. J. Supercritical Fluid Extraction of Plutonium and Americian from Soil Using Beta-Diketone and Tributyl Phosphate Complexants. In *Supercritical Carbon Dioxide-Separations and Processes*; Gopalan, A. S., Wai, C. M., Jacobs, H. K., Eds.; ACS Symposium Series 860; American Chemical Society: Washington, DC., 2003; Chapter 4, pp 36−49.
21. (a) Kumar, P.; Rao, A.; Ramakumar, K. L. *Radiochim. Acta* **2009**, *97*, 105−112. (b) Kumar, R.; Sivaraman, N.; Vadivu, E. S. *Radiochim. Acta* **2003**, *91*, 197−201.
22. Gibson, G.; Katz, J. J. *J. Am. Chem. Soc.* **1951**, *73*, 5436–5438.

23. Bondin, V. V.; Bychkov, S. I.; Revenko, Y. A. *Radiochemistry* **2008**, *50*, 253–255.
24. Zhu, L. Y.; Duan, W. H.; Xu, J. M. *Chin. J. Chem. Eng.* **2009**, *17*, 214–218.
25. Wai, C. M. *Abstract NUCL-042*; 238th American Chemical Society National Meeting, Washington, DC, August 16−20, 2009.

Development of a Unique Process for Recovery of Uranium from Incinerator Ash

Sydney S. Koegler*

AREVA NP Inc., 2101 Horn Rapids Road, Richland, WA 99354
*****sydney.koegler@areva.com**

A unique new industrial process has been developed that recovers uranium from incinerator ash produced by nuclear fuel fabrication plants. The process utilizes nitric acid and tri-n-butylphosphate (TBP) dissolved in supercritical carbon dioxide to extract uranium oxide directly into the supercritical fluid without a separate acid dissolution step. The process was developed in phases beginning with bench-scale feasibility tests and concluding with pilot plant demonstration tests. The bench-scale feasibility experiments tested basic chemistry and the ability of the process to extract uranium from incinerator ash. Pilot-scale tests determined practical operating conditions and scale-up factors for the design and implementation of a full-scale process. AREVA NP Inc. completed construction of a full-scale ash uranium plant in 2009 that will allow safe and environmentally friendly uranium recovery from ash and other low-uranium materials that would otherwise be uneconomic if done by conventional methods.

Introduction

In 2003 AREVA NP Inc. (then Framatome) in cooperation with the University of Idaho began developing a unique new process to recover uranium from incinerator ash. The program was driven by a need for a lower cost and more environmentally satisfactory way to recover uranium from the 30-plus metric tons of incinerator ash produced at the Richland nuclear fuel fabrication site during 20 years of burning uranium-contaminated combustible waste.

Nuclear fuel fabrication combustible waste comprises paper wipes and rags, shoe covers, worn-out protective clothing, plastic, and other materials that have become contaminated with uranium during uranium fuel fabrication for the nuclear power industry. The high cost of direct disposal of combustible waste drove AREVA to install an incinerator in the early 1980's to reduce the volume of waste with plans to eventually recover the enriched uranium contained in the ash. Incineration of the combustible waste reduces its mass by 20 to one, and hence its disposal cost is greatly reduced, but the ash still contains valuable enriched uranium. AREVA tested recovery of the uranium from incinerator ash using its nitric acid dissolution and solvent extraction processes, but found that these processes were costly and produced undesirable wastes, and therefore, a replacement technology was needed. Although a supercritical (SC) CO_2 uranium recovery process held the promise of a more efficient, cleaner method, it required significant development work to implement a commercially viable process. This chapter describes the development process.

Process Description

Carbon dioxide is an excellent solvent for certain organics under supercritical conditions, i.e. temperature greater than 31°C and pressure greater than 73 bar (1070 psi), and its solvent properties can be modified by adjusting temperature and pressure. The efficacy of the SC CO_2 process for uranium recovery lies in the unique properties of the supercritical fluid. Because SC CO_2 has gas-like properties (low viscosity and surface tension) it can flow easily through a bed of ash. Its liquid-like properties, relatively high-density and solvation properties, make it possible for it to extract metals directly into the SC fluid without a separate acid dissolution step.

The AREVA SC CO_2 uranium recovery process is based on technology developed jointly with University of Idaho (*1*). It recovers uranium from ash and other low-uranium content material using a tri-n-butylphosphate (TBP) and nitric acid complex, $TBP(HNO_3)x(H_2O)_y$, dissolved in SC CO_2. The SC CO_2 process is an improvement upon the existing AREVA uranium recovery processes for low-uranium materials that use a nitric acid leach followed by TBP-dodecane solvent extraction. Although the existing process was demonstrated to be workable, the low-uranium-content uranyl nitrate solution produced by the traditional process makes uranium recovery via this route economically unattractive. The SC CO_2 process is better than the traditional solvent extraction process because it recovers a larger fraction of the uranium, eliminates the separate nitric acid dissolution step, and is less costly to operate. Environmental performance is also improved with the SC CO_2 process because it requires no NOx treatment and produces no off-gas treatment effluent, and it creates an easy-to-handle solid waste ash residue.

Feasibility Tests

The development of the SC CO_2 process began with feasibility testing. Dr. Chien Wai and his associates at the University of Idaho showed that uranium oxide can be dissolved in SC CO_2 with the use of tributyl phosphate (TBP) as a cosolvent and nitric acid as an oxidizer (2–4). This chemistry is similar to that of the Plutonium Uranium Extraction (PUREX) process developed in the 1960s for recycle of spent nuclear fuel. Bench-scale feasibility tests carried out at AREVA demonstrated that the SC CO_2 process could extract uranium directly from incinerator ash. The goals of the feasibility tests were to determine if uranium could be effectively extracted from incinerator ash and then separated from the other co-dissolved metals so that the uranium could be recycled in AREVA's fuel fabrication process.

Uranium Extraction Feasibility Test Results

The experimental set-up for the uranium extraction tests is shown in Figure 1. For the extraction tests the nitric-acid-saturated TBP was placed in a cell and SC CO_2, supplied by a high-pressure syringe pump, was pumped into the cell and carried the TBP into a extraction chamber containing the ash test sample. The ash, SC CO_2, and TBP were held at temperature for a prescribed amount of time and then discharged to a lower-pressure separation chamber where the CO_2 vaporized and the TBP separated from the CO_2 gas. The TBP was then analyzed for uranium to determine extraction efficiency.

The bench-scale tests demonstrated that the key parameters for uranium extraction are temperature, pressure, TBP concentration in the SC CO_2, nitric acid content of the TBP, and extraction time. The temperature and pressure determine the density of the SC CO_2 and the TBP solubility. A higher temperature also improves the reaction kinetics and hence the extraction rate. However, a higher temperature also decreases the SC CO_2 density and with it the solubility of TBP. Higher nitric acid content increases the oxidation rate of UO_2 to the uranyl ion (UO_2^{+2}). For these tests the TBP was saturated with the maximum nitric acid possible in a single-stage batch contact before its use in the SC CO_2 test. An important result of the batch feasibility tests was that under the proper conditions more than 90 percent of the uranium could be extracted from incinerator ash in less than four hours.

Chemical Separations Feasibility Test Results

Another objective of the feasibility tests was to determine if once the uranium was extracted from the incinerator ash, it could be separated from the other co-extracted materials to purify it for recycle in the AREVA uranium fuel fabrication process. In the chemical separations tests TBP which had been loaded with uranium in the extraction tests was contacted with an aqueous phase containing various amounts of water and nitric acid. It was expected, based on extraction data from the PUREX process that a separation could be made between
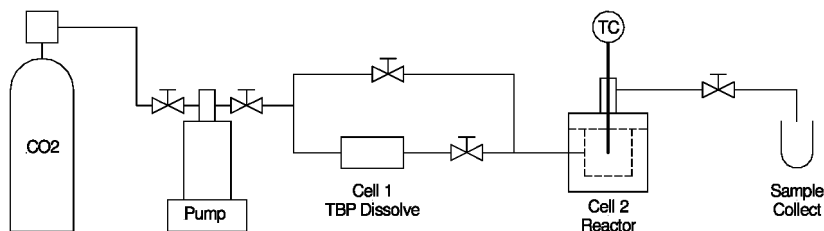
Figure 1. Bench-Scale SC CO₂ Setup for Uranium Extraction Tests.

the uranium and metals, but the performance under supercritical conditions was unknown.

The experimental setup for the separations tests was similar to the extraction test setup. The uranium-loaded TBP was placed in a cell through which SC CO_2 was pumped to carry it into a reaction cell. The reaction cell contained the aqueous phase comprising various concentrations of nitric acid. The TBP-SC CO_2 solution and aqueous phase solution were mixed for a specified time and then transferred through a pressure reduction valve to a low pressure vessel to separate the CO_2 gas from the TBP and aqueous solutions. The TBP and aqueous samples were then analyzed for uranium, metals, and acid content. The distribution coefficients (metal concentration in TBP divided by concentration in aqueous) are shown for uranium and other co-extracted metals in Figures 2 and 3.

The separations test data showed that the uranium distribution coefficient was much higher than the distribution coefficients of the other metals at high nitric acid concentrations. This implied that uranium could be partitioned from the other metals in a "scrub" step. In the scrub step, at a suitable nitric acid concentration, the contaminating metals will transfer to the nitric acid aqueous phase leaving the uranium behind in the TBP phase. The test data also showed that uranium has a low distribution coefficient at a low nitric acid concentration and therefore uranium could be removed from the TBP after its purification in a "strip" step using water or diluted acid.

Pilot Plant Tests

The next phase in the development of the SC CO_2 uranium recovery process was pilot plant testing. The pilot plant tests included one-pass experiments to test individual process steps, a series of continuous pilot-plant tests where the entire process was tested as a unit, and intermediate-scale column tests that used a larger separation column to determine scale-up parameters for the chemical separations (scrub and strip) steps.

Extraction Test Apparatus

The pilot plant extraction test apparatus comprised two, one-liter, stainless steel extraction vessels with removable baskets, and auxiliary equipment including pumps, heaters, and hold tanks. The extractor vessels used for the batch
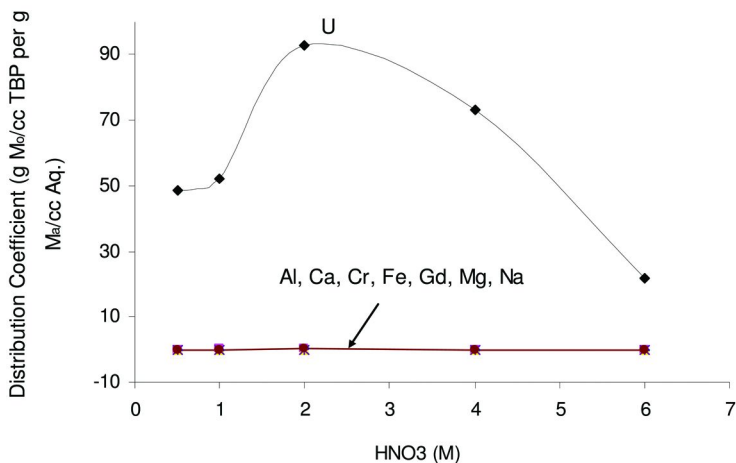
Figure 2. Uranium Distribution Coefficient as a Function of Free HNO₃ Concentration
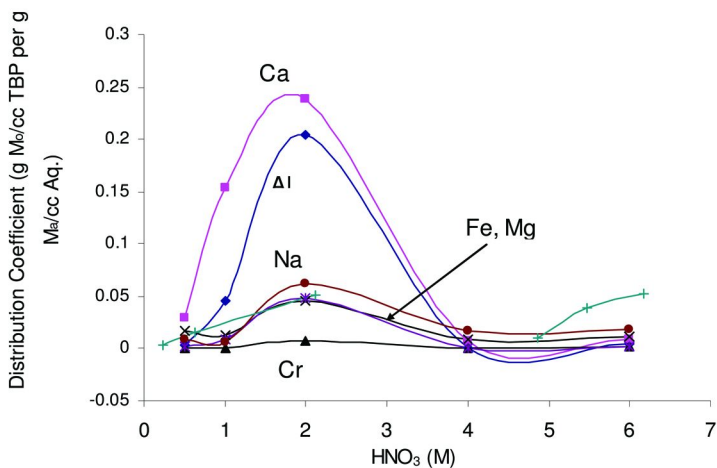

Figure 3. Metals Distribution Coefficients as Functions of Free HNO₃ Concentration

extraction tests are shown in Figure 4. The extractor vessels, CO_2 vaporization tank, CO_2 pressure-let-down valves, and feed lines were heated with electric resistance heaters controlled by stand-alone controllers using surface-mounted thermocouples. Incinerator ash or other low-uranium feed material was placed in the extractor baskets and the TBP-HNO₃-SC CO_2 extractant solution was pumped through the static material in either down-flow or up-flow mode. When using the up-flow configuration, a sintered metal frit-and holder screwed into the lid kept the ash from being carried out with the SC CO_2 extraction solution.

Figure 4. Pilot Plant Extraction Vessels Used for Uranium Recovery from Incinerator Ash

Key Pilot Plant Extraction Test Results

The pilot plant extraction tests confirmed that time, temperature, and nitric acid concentration are key parameters for uranium extraction from incinerator ash. The extraction tests also demonstrated that ash particle size is important and that uranium extracts differently from ash obtained by burning different types of combustible material.

Uranium extracted from the ash initially at a relatively constant rate and gradually decreased with time as the uranium was depleted as shown in Figure 5. Extraction at 70°C for four-to-six hours removed more than 90 percent of the uranium from the ash. Increasing the temperature from 50°C to 70°C greatly increased the uranium extraction rate. However, TBP-dodecane solvent extraction experience has shown that temperatures above about 70°C can degrade TBP, producing dibutyl phosphate (DBP) and phosphoric acid. DBP tends to extract uranium, but does not allow the uranium to be stripped out with water under normal process conditions. Therefore, extraction temperatures above 70°C must be avoided. Figure 6 shows that uranium extraction efficiency increases as the nitric acid concentration in the TBP increases. Increasing the free TBP nitric acid content from 3.6 $\underline{M}$ to 6.0 $\underline{M}$ significantly improved the extraction rate.

Effect of Other Parameters on Uranium Extraction

Ash produced from different sources of combustible material extracted differently. Uranium extracted more easily from ash produced from a mix of combustible material containing mainly paper and wood as opposed to ash
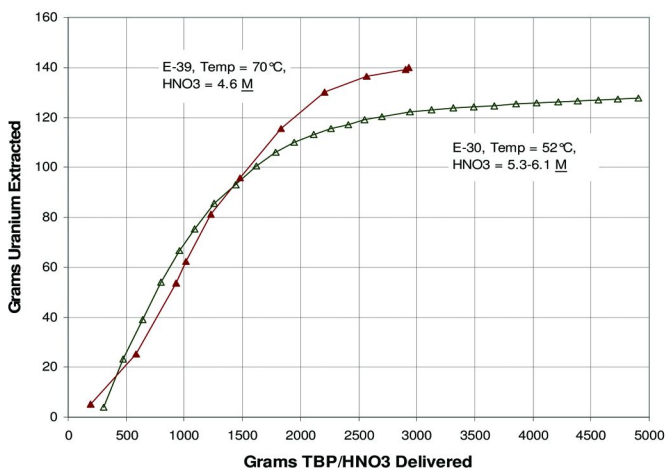
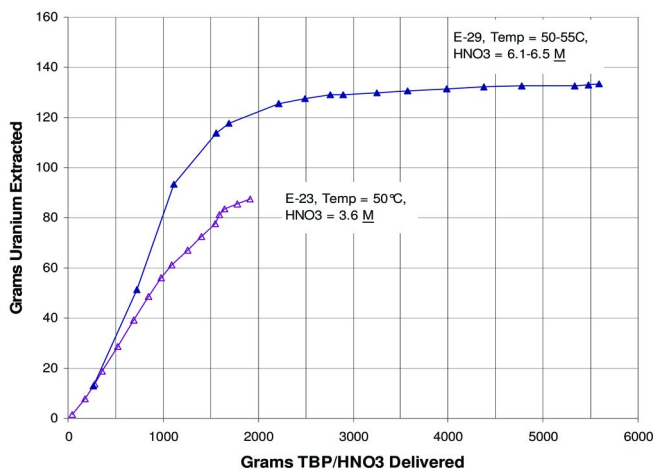Figure 5. Effect of Time and Temperature on Uranium Extraction

Figure 6. Effect of TBP Nitric Acid Concentration on Uranium Extraction

produced from another mix of combustible material with a higher fraction of plastics. Although the two types of ash were produced in the same incinerator at approximately the same temperature and residence time, they varied in density, pH, and particle size. These parameters may have affected the ability of the TBP-HNO_3-SC CO_2 mixture to intimately contact and extract uranium form the ash particles. It is likely that incinerator ash or other uranium-containing material from any new source will require a test to determine extraction parameters before sending it to the full-scale plant.

Chemical Separation Test Results

The chemical separation tests demonstrated the steps necessary to purify the uranium extracted from the incinerator ash in a form suitable for recycle in the

AREVA fuel-fabrication process. The separations processes tested in the chemical separation experiments were uranium purification (scrubbing), uranium removal (stripping), and acidification of TBP. The separations tests used a packed column to provide contact for mass transfer between the SC CO2-TBP stream and an aqueous stream. Two different one-inch (0.025 m) inside-diameter (ID) packed-bed columns were used in the tests. The smaller column had a packing height of 31 inches (0.8 m) and the taller column had a packed height of 81.5 inches (2.1 m). The taller column is shown in Figure 7. The columns were heated by wrapping them in electrical heat tape. Several packing materials were tested, including stainless steel mesh and stainless steel and ceramic rings.

Water or nitric acid scrub/strip solution (aqueous phase) was pumped into the column near the top through a spray nozzle and droplets flowed downward, while a SC CO_2-TBP solution (organic phase) was pumped into the column near the bottom and flowed upward. The heavier aqueous phase coalesced at the bottom of the column below the SC CO_2-TBP inlet point and was removed from the column. The organic phase was discharged from the top of the column through a pressure-reduction valve into a phase-separation tank where the liquid TBP/ uranium solution separated from the vaporized CO_2 and the CO_2 was discharged to the vent system.

Acidification of TBP

A single batch contact between pure TBP and 70 percent (15.6 M) nitric acid produces a TBP-nitric acid solution containing about 3.6 M nitric acid. The TBP nitric acid content can be increased substantially by contacting the TBP with nitric acid in a counter-current column. A series of TBP acidification tests were conducted with the separations columns to test the counter-current acidification of TBP. The nitric acid concentration in the organic (TBP-CO_2) and aqueous phases exiting the columns was determined by titrating the solutions with sodium hydroxide.

The tests showed that TBP-nitric solution acid concentration was directly proportional to the aqueous nitric acid concentration injected at the top of the column. There was also a small effect of the aqueous-to-organic flow ratio. There was little difference in organic solution nitric acid concentration between tests run at different flow rates, or between tests run on the 0.8m and 2.1m columns.

Nitric Acid Scrub Test Results

Several "scrubbing" tests were conducted in which the TBP/HNO_3/uranium solution (organic) from the extraction tests was re-dissolved in SC CO_2 and pumped upward through the packed column while a nitric acid scrub solution was pumped downward through the column. The purpose of the scrub step is to cause the contaminating materials that were co-extracted with the uranium to be transferred into the nitric acid scrub stream while the uranium remains in the TBP-SC CO_2 stream. The scrub column experiments tested the effects of scrubbing parameters including stream flow rate and nitric acid concentration on contaminate removal from the uranium-TBP stream and uranium loss to

the aqueous-scrub stream. Concentrations of uranium and contaminants were measured in both the aqueous and organic phases at the conclusion of each test.

The scrubbing experiments tested varying aqueous and organic flows with nitric acid at concentrations between 0.5 and 10 molar sprayed into the top of the column. The effect of column height was also tested. Scrub solution nitric acid concentration and flow rate affected both the contaminant removal efficiency and uranium loss (uranium scrubbed out with contaminants). Higher scrub feed nitric acid concentration and flow improved the removal of contaminants from the organic (TBP-SC CO_2) stream. Uranium lost to the aqueous scrub increased with the scrub flow rate and was higher in the taller column than the shorter column. An important implication of these results is that there is an inherent trade off between uranium purification and uranium loss to the aqueous effluent. The same parameters that improve uranium purity (high flow, high acid concentration) also cause more uranium to be lost to the aqueous effluent.

Uranium Stripping Test Results

Uranium was removed from the purified organic stream in stripping tests with water. The same pilot-plant equipment was used in the stripping tests as had been used in the TBP acidification and uranium purification (scrubbing) tests. For the stripping tests, purified TBP-HNO_3-Uranium solution from the scrubbing tests was re-dissolved in SC CO_2 and pumped upward through the packed column as deionized water was pumped downward through the column. The uranium content was measured in the organic and aqueous phases at the conclusion of each test to determine uranium stripping efficiency.

Uranium stripping efficiency is a function of the nitric acid concentration of the organic feed, the organic-to-aqueous flow ratio, and the column height. In general higher aqueous flows improved uranium stripping. As would be expected, the uranium stripped more readily under low-acid conditions, from either increasing the water flow or with a lower acid content in the organic. The water addition rate, however, is limited by the potential for column flooding and by the need to avoid excessive dilution of the uranyl nitrate which is to be recycled into the AREVA chemical conversion process.

Intermediate-Scale Tests

In 2008, AREVA installed an intermediate-scale separations column to help scale up the SC CO_2 uranium recovery process. AREVA determined that data from the small, one-inch columns was not sufficient to provide the design basis for the full-scale process and that tests at an intermediate scale were necessary to reduce scale-up risks. The objectives of the intermediate-scale tests were to determine acceptable column configurations, including height and diameter, and optimize process parameters for the separations columns planned for the full-scale plant.

Figure 7. Small (0.8 m) Scrub/Strip Column

Test Apparatus

The intermediate-scale column test equipment comprised an 18-foot (5.5 m) tall, three-inch (0.77 m) ID column (Figure 8) and supporting pumps, tanks, and instrumentation. The column was fabricated in three, six-foot-long (1.8 m) sections so that aqueous strip and scrub solutions (water and nitric acid) could be fed into the column at the top and at each junction. The column was wrapped in a copper water-heating coil and insulated to maintain a constant temperature. All feed streams, liquid CO_2, TBP, water, and HNO_3 were preheated in a tube-in-pipe heat exchanger. Because of the larger inventory of process solutions and CO_2 the column and supporing equipment skid were placed inside enclosures to contain any CO_2 leaks.

For each test TBP feed material generated in extraction tests in the small pilot plant was mixed with SC CO_2, heated, and fed to the bottom of the column. Acid or water was pumped to the column from the skid to remove impurities or strip out uranium. The TBP-SC CO_2 mixture exited the top of the column and was sent back to the skid where it was depressurized and sent to the TBP-CO_2 separator. The TBP from the separator was collected and analyzed and the gaseous CO_2 was condensed and recycled.

Figure 8. Intermediate-Scale Column

Key Intermediate-Scale Test Results

Flow tests conducted with various packing materials demonstrated the operating flow rates achievable before flooding (aqueous carryover with SC CO_2-TBP) occurred. The tests were made using SC CO_2 and TBP near the expected operating pressure and temperature with water introduced at the top of the column. Tests at the maximum flow capacity of the pilot plant CO_2 and TBP feed pumps with the smallest-size packing produced a small amount of aqueous carryover (about 1 percent of the total water input), no carryover occurred when the water to CO_2-TBP ratio was reduced sufficiently. The column was more susceptible to flooding with smaller packing, but there was a trade off.

Smaller-size packing also provided a larger surface area, and therefore, better mass transfer.

The intermediate-scale experiments tested various configurations for uranium purification (scrubbing). The best configuration for impurities decontamination - other than gadolinium - was with the top third of the column used for water scrub and the bottom two thirds of the column used for nitric acid scrub. Gadolinium decontamination, however, was better with the top two thirds of the column used for water decontamination. This implies that there will be a trade-off between decontamination factors for different contaminants when setting parameters in the large-scale system. The nitric acid concentration in the scrub stream was the second-most important process parameter for scrubbing, with high nitric acid producing the best decontamination.

Uranium was removed in stripping tests from the SC CO_2-TBP mixture as uranyl nitrate by a counter-current downward flow of water. The column configuration, packing size, and acid concentration had an impact on uranium removal. As expected the taller column removed more uranium and smaller-diameter packing performed better than larger packing. This was due to better mass transfer from the higher specific surface area of the smaller packing. Uranium stripping was better for lower nitric acid concentrations.

Full-Scale Process Implementation

AREVA completed construction of its full-scale industrial ash uranium recovery process in late 2009. The facility is designed to implement a clean and cost-effective SC CO_2 uranium recovery process with the capacity to treat AREVA's ash and that of potential customers. The facility is to be operated under AREVA's Nuclear Regulatory Commission (NRC) special nuclear materials license and, as such, must meet NRC requirements for nuclear and industrial safety. Prior to beginning installation, AREVA conducted an integrated safety analysis in which the impact of process design and expected operating parameters on nuclear, industrial, and chemical safety was analyzed. AREVA's integrated safety analysis had a significant impact on the final design of the process, especially in the areas of improved material handling, chemical and ergonomic safety, and nuclear criticality safety.

The SC CO_2 uranium-recovery process is installed in an existing uranium chemical conversion building on the Richland, Washington site and covers approximately 1100 square feet of a high-bay room. The process utilizes much of the building's existing infrastructure, including utilities and intermediate storage tanks. Because of the potential for personnel exposure to uranium and harmful chemicals, the process equipment is installed in a ventilated enclosure. Most process operations are automated and manual operations are conducted through glove ports. The process comprises four main operations, 1) ash pail in feed and extractor basket loading, 2) uranium extraction, 3), uranium purification and 4) spent-ash handling.

Incinerator ash is supplied to the system in pails of approximately five-gallon capacity. The ash-storage pails move from the in-feed bucket queue into a

containment hood for processing. The containment hood encloses the ash processing equipment that includes a crusher, a tumbler/mixer, and the extraction basket loading station. Ash clinkers may be present, so the contents of each pail are sifted and clinkers are routed through a crusher for size reduction. The ash and processed clinkers are then blended together and transferred into an extraction basket. The basket is then placed into an extraction vessel for uranium extraction. The extraction module is shown in Figure 9 being unloaded at the facility. An overhead crane is used to move the baskets in and out of the extractors. The extractor vessels are designed to preclude accidental opening under pressure.

The uranium purification module comprises the counter-current packed columns, feed tanks and pumps, and a heat exchanger to preheat streams fed to the columns. Each countercurrent column contains a packing material that facilitates mass transfer between the SC CO_2-TBP and aqueous liquid phases. Personnel exposure to CO_2 or aerosols from a release of the working fluid is precluded by primary and secondary containment that have management measures in place to ensure that they are available and reliable when needed.

At the completion of an extraction cycle an operator removes the spent ash basket from the extractor vessel using an overhead crane and places it in the uranium assay station. Two separate uranium assays are performed before the basket is allowed to move from the assay station to the emptying station. The spent ash residue is packaged in drums suitable for disposal at a licensed nuclear waste disposal site. The spent-ash handling operation is also enclosed in a ventilated glove box to protect the operator from contact with hazardous dust.

Figure 9. Extraction Module Delivery

Conclusions

AREVA, in cooperation with University of Idaho, spent six years in developing and implementing an innovative new process for uranium recovery from incinerator ash and other low-uranium-content materials based on supercritical CO_2 technology. Implementation of the technology required several stages of bench-scale and pilot-plant development. AREVA and University of Washington engineers and scientists designed and operated bench-scale and pilot-plant scale equipment at AREVA's Richland, Washington fuel fabrication facility that developed the chemistry, process, and equipment necessary to implement a commercial-scale process. In 2009, AREVA finished construction of a full-size, industrial ash-uranium recovery facility at its Richland, Washington plant that will be operational in 2010. The new ash uranium-recovery process is important to AREVA because it allows economic recovery of enriched uranium from incinerator ash using a safe, environmentally friendly technology.

References

1. Wai, C. M.; Koegler, S. S. Method and System for Recovering Metal from Metal-Containing Materials. U.S. Patent 7,686,865, March 30, 2010.
2. Lin, Y.; Smart, N. G.; Wai, C. M. *Environ. Sci. Technol.* **1995**, *29*, 2706–2711.
3. Enokida, Y.; Yamamoto, I.; Wai, C. M. Extraction of Uranium and Lanthanides from Their Oxides with a High-Pressure Mixture of TBP-HNO$_3$-H$_2$O-CO$_2$. In *Supercritical Carbon Dioxide Separations and Processes*; Gopalan, A. S., Wai, C. M., Jacobs H. K., Eds.; ACS Symposium Series 860; American Chemical Society: Washington, DC, 2003; pp10−22
4. Wai, C. M.; Smart, N. G.; Lin, Y. Extraction of Metals and/or Metalloids from Acidic Media Using Supercritical Fluids and Salts. U.S. Patent 5,770,085, June 23, 1998.

Supercritical Fluid Extraction of Mixed Wastes: PAH, PCB, Uranium and Lanthanum in Solid Matrices

Joanna S. Wang,[1] WenYen Chang,[2] HuaKwang Yak,[3] and KongHwa Chiu*,[4]

[1]Department of Chemistry, University of Idaho, Moscow, ID 83844, USA
[2]Department of Natural Sciences, National Science Council, Taipei, Taiwan 107, ROC
[3]Department of Chemistry, ChungYuen Christian University, ChungLi, Taiwan 330, ROC
[4]Department of Applied Science, National DongHwa University, Hualien, Taiwan 907, ROC
***ckh@mail.ndhu.edu.tw**

A sequential two-step supercritical fluid extraction technique has been developed for treating mixed wastes containing organic compounds (polychlorinated biphenyls and polyaromatic hydrocarbons) and metals (uranium and lanthanum). In the first step, the organic contaminants are extracted with neat supercritical fluid carbon dioxide at 250 atm and 150 °C. The extraction efficiencies for the organic compounds are around 93-100%. In the second step, a TBP (tri-*n*-butylphosphate)-nitric acid ligand is added to the system to extract uranium and lanthanum from the solid at 75 °C and a supercritical fluid density of 0.77 g/mL. The extraction efficiency for uranium is over 90% and lanthanum around 80%. This sequential supercritical fluid extraction technique appears promising for large-scale treatment of mixed wastes.

Introduction

Radioactive wastes arise in many forms from a wide range of activities, particularly from the operation of nuclear power plants and processes associated

with nuclear research and isotope production. Uses of radioisotopes in medical diagnostic research, pharmaceutical and biotechnology developments also generate radioactive wastes (*1–4*). Mixtures of trans-uranium elements (TRU) or low level wastes (LLW) with toxic and hazardous substances are defined as mixed wastes by the Resource Conservation and Recovery Act (RCRA). Spent nuclear fuel, high-level radioactive waste and trans-uranic radioactive waste are three categories of nuclear wastes. Hazardous wastes include metallic compounds, organic solvents, and toxic organic materials such as polychlorinated biphenyls (PCBs) and poly aromatic hydrocarbon (PAHs). PCBs are particularly harmful to human health and environments. The Department of Health and Human Services (DHHS) (*5*) has concluded that PCBs can be anticipated to be carcinogens. Many existing mixed wastes containing such toxic compounds and radioisotopes have to be treated to acceptable levels for safe discharge into the environment.

Solvent extraction is extensively used in the nuclear waste treatment and nuclear fuel reprocessing (*6*, *7*). In the PUREX (Plutonium Uranium Extraction) process, acid dissolution followed by solvent extraction, typically kerosene containing an organophosphorous reagent, is used to recover uranium and plutonium separately from irradiated fuel. Organic chelation has been widely used for selective separation of metals from aqueous solutions in solvent extraction (*6*, *8*). Similar technologies have also been proposed for treating soils containing radioactive wastes. Acid dissolution usually leads to many hazardous by-products and environmental problems. The use of liquid–liquid solvent extraction can generate large quantity of organic wastes. To remove toxic organic compounds from solid wastes, solvent reflux methods are often used. The Soxhlet process, for example, would generate organic liquid wastes. Therefore, there is a great need to have an improved method for treatment of mixed wastes using green solvents which would minimize secondary waste generation.

Supercritical fluid carbon dioxide (Sc-CO_2), as a green extraction medium, offers an attractive alternative over the conventional methods such as the PUREX and Soxhlet processes. The SFE technique has several advantages over the conventional solvent extraction methods (*9*). Extraction efficiency in SFE is enhanced due to the rapid mass transfer in the supercritical fluid phase. Efficient and rapid separation of extracted substances from CO_2 can be achieved by simply venting CO_2 into the atmosphere. SFE for extraction of organic compounds such as PCBs and PAHs is well-established in the literature (*10–13*). However, it has seldom been applied to the mixed waste treatment.

This paper describes a sequential SFE method to efficiently separate organic and radioactive materials in mixed wastes into different fractions. PCBs (IUPAC #77, IUPAC #209) and PAH congeners (chrysene) are used as model organic compounds. We select uranium and lanthanum as representative metals in this mixed waste study. The matrix effect is studied by spiking the toxic organic compounds, uranium and lanthanum in different solid matrices including filter paper, sea sand, and soil. Extraction conditions including temperature, pressure, CO_2 density, and time are optimized, and two different ligands (TTA-TBP and TBP/HNO_3) are used for metal extraction.

Experimental

Chemicals

Uranium and lanthanum standard solutions were obtained from EM Science (Gibbstown, NJ, USA) and used as received. Sea sand (washed, S25–500) was purchased from Fisher Scientific Inc. (NJ, USA). Chloroform and hexane were purchased from EM Science (Gibbstown, NJ, USA), and from J.T. Baker, respectively. SFE grade carbon dioxide (purity of 99.99%) was supplied by Oxarc, Spokane, WA. USA. Tri-n-butylphosphate (TBP) ($\geq$ 97%) was obtained from Aldrich Chemical Company, Inc. (Milwaukee, WI) and used as received. HNO_3 (Sigma-Aldrich) was used directly. IUPAC #77 (3, 3′, 4, 4′-tetrachlorobiphenyl), IUPAC #209 (decachlorinated PCB), and a PAH compound chrysene (about 300 µg/mL) were obtained from Ultra Scientific (North Kingston). Internal standard fluoranthene was supplied by Sigma Chemicals Co. (USA). De-ionized water (Millipore Milli-Q system, Bedford, MA) was used for the preparation of all aqueous solutions.

Instruments and Facilities

Supercritical fluid extractions were performed by an ISCO syringe pump (model 260D, Lincoln, NE, USA) connected to a series of stainless steel vessels placed in an oven (Varian 3700, USA). The flow of Sc-CO_2 was controlled manually by a high pressure outlet valve. A schematic diagram of the experimental apparatus is shown in Figure 1. A fused silica capillary (inner diameter: 100 µm, length 25 cm) from Polymicro Technologies, Phoenix, USA, was used as a restrictor in the extraction of PCB and PAH processes. For the extraction of U and La, a PEEK tube, as a restrictor, was used. The outlet end of the restrictor was placed in a glass tube containing a trap solvent (hexane or chloroform) to collect the extracted analytes. A high-resolution gas chromatograph combined with a flame ionization detector (FID) (Hewlett Packard, HP 5890A) was used for analyzing the organic compounds.

Sample Preparation

Three spiked solid matrices were studied: filter paper (Whatman No.1), washed sea sand and soil. A standard mixture of PCBs and PAHs containing two PCB congeners, IUPAC #77 (3, 3′, 4, 4′-tetrachlorobiphenyl) and IUPAC #209 (decachlorinated biphenyl), and one PAH compound: chrysene (about 300 µg/mL/congener) was used as the source of the organic compounds. Samples were prepared by spiking with 100 µL (or 100 µg, at 1000 µg/mL concentration) of each of the standard mixtures of PCBs, PAHs, UO_2 and lanthanum. The solvent was evaporated at room temperature for 2 h. After that the sample was loaded into the extraction vessel and placed in the oven.

Two ligands, i.e., $TBP(HNO_3)_{0.7}(H_2O)_{0.7}$ and TTA-TBP, were used in the extraction of metals. The extractant, $TBP(HNO_3)_{0.7}(H_2O)_{0.7}$, was prepared as described previously (*14*). A TTA-TBP complex was prepared by adding 0.111 g
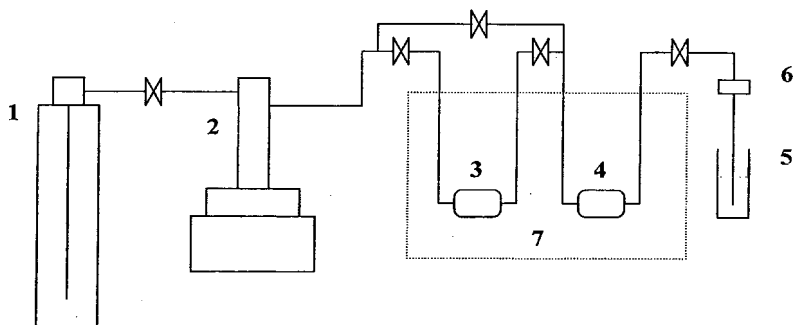
Figure 1. Schematic diagram of the experimental system for the mixed waste treatment in Sc-CO₂: (1) CO₂ cylinder, (2) syringe pump, (3) ligand cell, (4) extraction cell, (5) collection vial, (6) heater for the PEEK restrictor, (7) heating oven.

of solid TTA to 1 mL TBP. The ligand (3 mL of $TBP(HNO_3)_{0.7}(H_2O)_{0.7}$ or 1 mL TTA-TBP) was placed in a separate vessel in the oven as shown in Figure 1.

Supercritical Fluid CO₂ Extraction

In the first step, extraction of PCBs and PAHs was performed at 250 atm, 150 °C with 20 min static time followed by 20 min dynamic time with a flow rate of 1.5 mL/min. During dynamic extraction, the analytes were trapped in hexane (20 mL). The PCB/PAH extract was concentrated by evaporating the solvent to about 2 mL using a slow nitrogen flow. Internal standard fluoranthene (100 µL) was added to the sample before the analysis. The PCB/PAH extract was analyzed by a high-resolution gas chromatograph/flame ionization detector. Separation of the compounds was carried out on a DB-5 column (J&W Scientific, Folsom, CA, USA, 30 m, 0.32 mm, 0.25 µm). Sample (1 µL) was injected at 280 °C. Helium gas(purity 99.9%, Oxarc, WA, USA) was used as a carrier gas. The oven temperature was held at 70 °C for 1 min, then increased at a rate of 10 °C/min to 300 °C, where it was held for 5 min. Concentrations of the analytes were calculated by comparing the peak area ratio between extracted compounds to the internal standard.

In the second step, CO₂ was delivered to the sample vessel through the ligand vessel, carrying the dissolved $TBP(HNO_3)_{0.7}(H_2O)_{0.7}$ into the extraction cell and converting uranium and lanthanide into CO₂-soluble metal complexes. Static extraction time was fixed at 10 min and the dynamic time was optimized from 5 min up to 80 min with flow rate of 1 mL/min. Extracted metals were collected in 20 mL of chloroform. Back extraction of the extracted metals was performed by adding 3 mL of HNO_3 (8 N) to the trap solution and shaking for 3 min. The aqueous phase was separated and the organic phase was washed twice with 3 mL of deionized water. The amount of the extracted metal ions was later analyzed by an ICP-AES (Perkin Elmer ICP optima 3000 XL, USA). The wavelengths of 385.9 nm and 408.7 nm were used for U and La analyses, respectively.
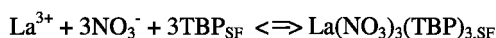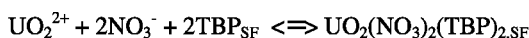
Results and Discussion

Two steps are used for treatment of mixed wastes in this study. The first step is for separation of organic compounds, PCBs and PAHs, which is followed by the second step, i.e., extraction of metals.

Extraction Efficiency for Organic Compounds

Extraction of the natural soil showed that there was no detectable level of PCBs/PAHs in the solid matrix. Extraction efficiencies of PCBs and PAHs standards directly from the vessel (without the soil) were about 96-100%. This indicated that the SFE trapping technique was workable and no loses of PCBs/PAHs occurred during the sample treatment and analysis. PCB and PAH compounds were effectively extracted (93-100%) from all three solid matrices under the conditions of 250 atm pressure and 150 °C. Milder conditions were studied as well, but the extraction efficiency of chrysene decreased as the temperature or pressure descended to 100 °C or 200 atm. Since 150 °C and 250 atm showed the best results for extraction of the organic analytes in soil, this condition was adopted for mixed waste applications.

Extraction Efficiency for Metals

The behavior of La and U in the complex formation with TBP/HNO_3 can be described by the following equations:

$$UO_2^{2+} + 2NO_3^- + 2TBP_{SF} \iff UO_2(NO_3)_2(TBP)_{2,SF}$$

$$La^{3+} + 3NO_3^- + 3TBP_{SF} \iff La(NO_3)_3(TBP)_{3,SF}$$

where SF stands for supercritical fluid. Extraction of metals from solid matrix with different ligands showed that a higher extraction efficiency can be achieved with the TBP/HNO_3 complex than the TTA-TBP complex (Figure 2). This is probably due to the higher solubility of TBP/HNO_3 complex in the supercritical fluid (*15*). The extraction of metals from sea sand and filter paper was easier than from natural soil. This is probably because natural soil has more active sites to bind the metal ions than filter paper or sea sand matrices. Extraction efficiency of uranium was near 80% from natural soil even with the ligand TTA-TBP. Only 55-70% of the spiked lanthanum was extracted under the conditions of 65 °C and 250 atm using $TBP(HNO_3)_{0.7}(H_2O)_{0.7}$. The extraction efficiency for lanthanum was lower than that of uranium in all cases (Figure 2).

The trap solvent (hexane) was analyzed after the first extraction. Results confirmed that lanthanum was not dissolved in neat CO_2 during the process of extraction of organic compounds. The low SFE efficiency for lanthanum was most likely due to its strong interactions with the solid matrices.
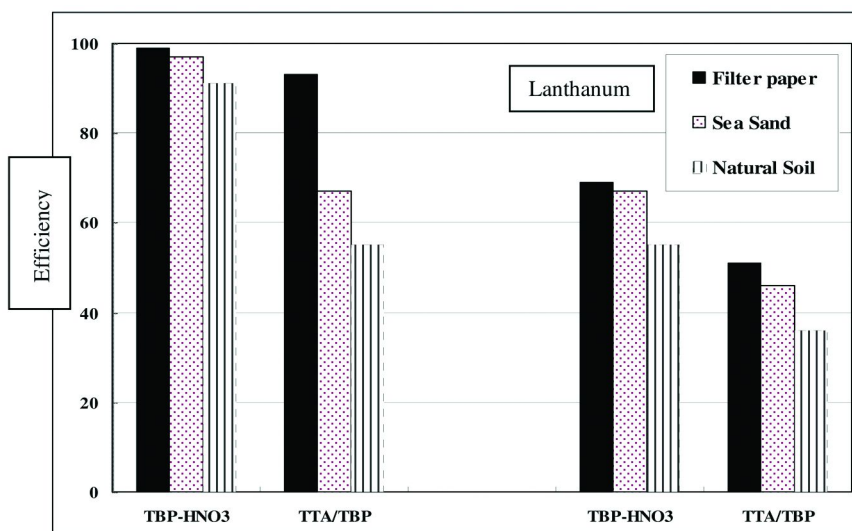
Figure 2. SFE of uranium and lanthanum from solid matrices at 65 °C and 250 atm. The left part is for uranium extraction and the right part is for lanthanum extraction. The extraction efficiencies are calculated for the first and second step extractions.

Mixed Waste Extraction

In Table I, the optimal conditions for Sc-CO$_2$ extraction of the mixed waste are presented.

Effects of Density and Temperature

In SFE, one of the most promising advantages is that the density of CO$_2$, can be continuously tuned over a wide range by adjusting the pressure and temperature. The solubility of an analyte in the Sc-CO$_2$ phase depends on the density of the Sc-CO$_2$. The following equation explains the correlation between the solubility of solute and the CO$_2$ density (*16*).

$$\text{Log S}_{SF} = p\text{LogD} + q$$

where S$_{SF}$ is the solubility of a solute in Sc-CO$_2$ with a specific density (D). Constant *p* is related to the solvation strength of the solute and *q* is a temperature-dependent constant that involves thermal properties including solvation heat and volatility of the solute. Therefore, to improve the extraction efficiency of metals from solid matrices, the major Sc-CO$_2$ extraction parameters, i.e. temperature, pressure, and fluid density, should be studied.

When the Sc-CO$_2$ density was below 0.6 g/mL, the extraction efficiency of uranium was over 60%, whereas less than 20% of lanthanum was extracted from the sea sand (Figure 3). When the fluid density exceeded 0.6 g/mL, the extraction of lanthanum was significantly enhanced, reaching 67 % at 0.77 g/mL.

Table I. Sequential SFE of spiked mixed waste (PCBs and PAHs + U and La) as % recovery from different solid matrices

Matrices	First Extraction % with Neat CO_2[a]			Second Extraction % with TBP-HNO$_3$ in CO_2[b]	
	PCB #77	PCB #209	Chrysene	U	La
Filter Paper	100	100	99	90	85
Sea Sand	98	97	92	90	85
Natural soil	95	96	93	85	77

[a] 150 °C, 250 atm, 20 min static and 20 dynamic extraction time.   [b] 75 °C, 295 atm, 10 min static and 80 dynamic extraction time.
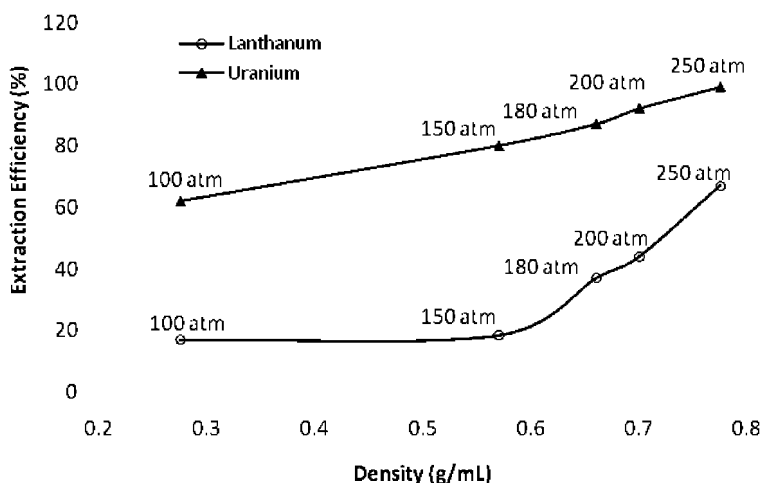
Figure 3. Effect of Sc-CO_2 density on the extraction of U and La from sea sand at a constant temperature of 65 °C.

At a constant CO_2 density (0.77 g/mL), elevation of temperature resulted in a significant improvement on the extraction of both uranium and lanthanum from sea sand (Figure 4). Uranium can be efficiently extracted at a low temperature (55 °C), whereas a high extraction efficiency for lanthanum can only be obtained at 75 °C. We did not perform experiments higher than 75 °C due to the apparatus limitation. However, with extended extraction time (up to 80 min dynamic time), approximately 89% of the spiked lanthanum could be extracted at temperature of 75 °C and CO_2 density of 0.77 g/mL.

The result indicates that in extraction of lanthanum from solid matrices, more harsh extraction conditions and a longer extraction time are required in order to reduce the interactions between lanthanum ions and matrix. Formation of lanthanum complex with TBP(HNO$_3$)$_{0.7}$(H$_2$O)$_{0.7}$ is not as effective as that of uranium. As temperature increases, a better extraction efficiency is obtained which suggests that lanthanum probably can react more effectively with the ligand at higher temperatures.
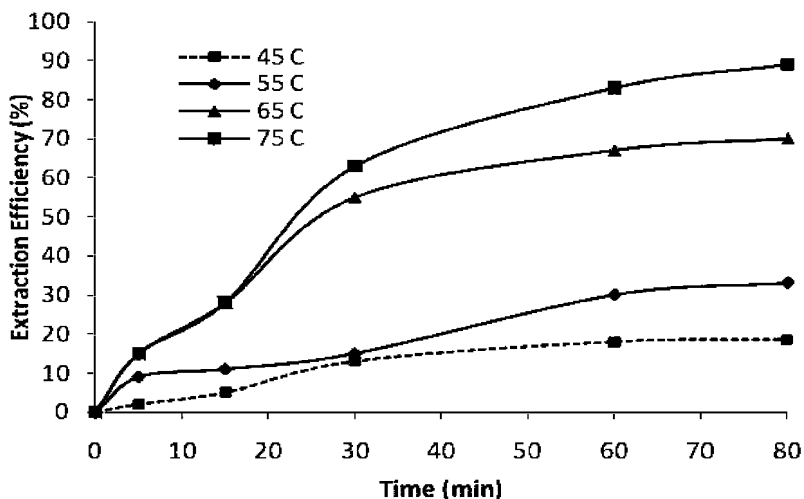
Figure 4. Effect of temperature on the extraction of La from sea sand at a constant CO$_2$ density of 0.77 g/mL.

Conclusions

A sequential two-step Sc-CO$_2$ extraction process can be used to treat mixed-wastes which contain both radioactive materials and hazardous organic compounds. First, organic compounds such as PAHs and PCBs are separated from solid matrices by neat Sc-CO$_2$ extraction. In the second step, radioactive elements such as uranium and lanthanides are extracted using a proper complexing agent. Generally speaking, the Sc-CO$_2$ extraction efficiency is lower in the "naturally" occurring matrices such as soil. This could be caused by strong interactions between the matrix and the contaminants. The density of the Sc-CO$_2$ phase can be adjusted by temperature and pressure to achieve optimum extraction efficiencies. This sequential extraction method represents an environmentally friendly green technology for treating mixed wastes. The Sc-CO$_2$ technology appears suitable for large-scale treatment of mixed wastes containing lanthanides, actinides, and toxic organic compounds.

References

1. Kemp, R. V.; Bennet, D. G.; White, M. J. *Environ. Int.* **2006**, *32*, 1021–1032.
2. Andrade, C.; Martínez, I.; Castellote, M.; Zuloaga, P. *J. Nucl. Mater.* **2006**, *358*, 82–95.
3. Plećaš, I.; Dimovic, S. *Prog. Nucl. Energy* **2006**, *48*, 629–633.
4. Melville, G.; Liu, S. F.; Allen, B. J. *Appl. Radiat. Isot.* **2006**, *64*, 979–988.
5. U.S. Department of Health & Human Services. http://www.hhs.gov/.
6. Minezewski, J.; Chwastowska, J.; Dybezynski, R. In *Separation and Preconcentration Methods in Inorganic Trace Analysis*; Ellis Harwood/Halsted Press: Chichester, England, 1982; pp 97−282.

7. Alegret, S.; Masson, M. R. In *Development in Solvent Extraction*; Ellis Harwood Limited: Chichester, England, 1988; Chapter 11, pp 177−188.
8. Wai, C. M. In *Preconcentration Techniques for Trace Elements*; Alfassi Z. B., Wai, C. M., Eds.; CRC Press: Boca Raton, FL, 1991; Chapter 4, pp 101−32.
9. Lin, Y.; Smart, N. G.; Wai, C. M. *Trends Anal. Chem.* **1995**, *14*, 123–133.
10. Berg, B. E.; Lund, H. S.; Kringstad, A.; Kvemheim, A. L. *Chemosphere* **1999**, *38*, 587–599.
11. Miller, D.; Hawthorne, S. B.; Clifford, A. A. *J. Supercrit. Fluids* **1997**, *10*, 57–63.
12. Morselli, L.; Sabbioni, M.; Zappoli, S.; Quattroni, G. *Fresenius Environ. Bull.* **1995**, *4*, 463–468.
13. Berset, J. D.; Holzer, R. *J. Chromatogr., A.* **1999**, *852*, 545–558.
14. Enokida, Y.; ElFatah, S. A.; Wai, C. M. *Ind. Eng. Chem. Res.* **2002**, *41*, 2282–2286.
15. Samsonov, M. D.; Wai, C. M.; Lee, S. C.; Kulyako, Y.; Smart, N. G. *Chem. Commun.* **2001**, 1868–1869.
16. Rao, A.; Kumar, P.; Ramakumar, K. L. *Radiochim. Acta* **2008**, *96*, 787–798.

Chapter 8

Actinide(III) Recovery from High Active Waste Solutions Using Innovative Partitioning Processes

Giuseppe Modolo[*]

Institut für Energieforschung, Sicherheitsforschung und Reaktortechnik (IEF-6), Forschungszentrum Jülich GmbH, 52425 Jülich, Germany
[*]**E-mail: g.modolo@fz-juelich.de**

The selective partitioning of minor actinides from the fission products and separate treatment by transmutation can considerably improve long-term safety of the residual waste for its subsequent future disposal in a deep underground repository. The present chapter will summarize about the ongoing research activities at Forschungszentrum Jülich (FZJ) in the field of actinide partitioning using innovative solvent extraction processes. European research over the last few decades, i.e. in the NEWPART, PARTNEW and the recent EUROPART programs, has resulted in the development of a multicycle process for minor actinide partitioning. In this respect, numerous European partners cooperate closely in European projects. These multicycle processes are based on the co-separation of trivalent actinides and lanthanides (e.g. DIAMEX process), followed by the subsequent trivalent actinide/lanthanide group separation in the SANEX process. Apart from optimizing the properties of the solvent for optimal extraction and separation efficiency, extractant stability is a critical issue to be studied. In this chapter, we will focus mainly on the development of flowsheets for the recovery of americium and curium from high active waste solutions, and testing them in mixer-settler and centrifugal contactors. The scientific feasibility of the processes developed will be demonstrated on a laboratory scale using synthetic and genuine fuel solution. The future direction of research for the development of new

processes within a new European project (ACSEPT) is briefly discussed in the conclusion.

Introduction

Reducing the radiotoxicity of spent nuclear fuel is an important objective to ensure the sustainability of nuclear energy. This objective can be attained by recovering the long-lived elements from the spent fuel constituents and their conversion into short-lived or stable nuclides by irradiation in a dedicated reactor, the so-called partitioning and transmutation strategy (*1*).

Plutonium, the main contributor to radiotoxicity can already be recovered today by the PUREX process, which with some modifications can also recover neptunium (advanced PUREX). In order to achieve a significant reduction in the radiotoxicity of spent fuel, we must also remove americium and curium. These trivalent minor actinides, however, are not currently industrially separated and they remain with the fission products in high level liquid waste, which is vitrified and prepared for final disposal. This is not due to a lack of interest in separating these elements but rather due to the fact that they cannot be extracted with tributylphosphate (TBP) within the PUREX process (*2*). The chemical similarity of trivalent actinides (An) and lanthanides (Ln) combined with the unfavourable mass ratio necessitate very demanding and complex process steps. Processes developed over the last 20 years are predominantly based on the combined extraction of actinides and lanthanides from the PUREX raffinate followed by their subsequent group separation. A distinction is made here between two process variants (*1*).

In the single-cycle processes, An(III) + Ln(III) are simultaneously separated. Following this, the trivalent actinides are selectively back-extracted (stripped) from the loaded organic phase, e.g. using diethylenetriaminepentaacetic acid (DTPA). The most important developments in terms of this process include the reversed TALSPEAK (USA), DIDPA (Japan) and SETFICS (Japan) processes (*2*). The multicycle processes, on the other hand, make use of different extractants. Following the joint co-separation of An(III) + Ln(III) from the fission product solution, e.g. using TRUEX (USA), TRPO (China), DIAMEX (France), the next process step involves the joint back-extraction of trivalent An + Ln. This is followed by selective An(III)/Ln(III) separation using a highly selective extractant, e.g. CyMe$_4$BTBP (*3*).

The advantage of the latter method is the high purity of the actinide(III) product and a lower volume of secondary waste. This chapter provides an overview of important process developments for actinide separation achieved within the scope of European collaborative projects during the EU 3rd, 4th and 5th Framework Programmes (*4–6*). Particular attention will be devoted to developments at Forschungszentrum Jülich, which were made possible through close cooperation with partners in the EU projects. The strategy employed for actinide separation is shown in Figure 1.
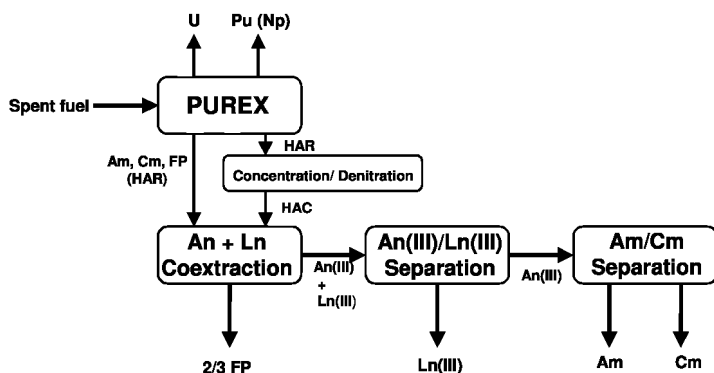
Figure 1. European partitioning strategy for the separation of all actinides from spent fuel

DIAMEX Process Developments

During the 1980s, the family of malonamides were developed for the extraction of actinides from high level liquid fission product solutions (*7*). From the multitude of synthesized compounds, dimethyldibutyltetradecyl malonamide (DMDBTDMA) (Figure 2) was found to have the most promising properties for use in extraction processes (*8*). The DIAMEX process was successfully tested using real waste solution for the first time in 1993 in the CEA's Fontenay-aux-Roses research centre (*9*). It was continuously further developed within European collaborative projects (*10–13*). In the EU's 4th Framework Programme NEWPART (*4*), Forschungszentrum Jülich was involved in the development of an optimized DIAMEX process in cooperation with ENEA Saluggia and Politechnico di Milano (PoliMi). This new DIAMEX-III process used 1 mol/L DMDBTDMA in TPH (branched aliphatic solvent) as an extractant instead of 0.5 mol/L (DIAMEX-I) or 0.65 mol/L (DIAMEX-II). Increasing the diamide concentration from 0.5 to 1.0 mol/L significantly increased the capacity of the extractant. This in turn decreased the tendency to third-phase formation and also allowed the process to be conducted at high HNO_3 concentrations. In order to prevent the co-extraction of Zr and Mo, oxalic acid was used. It was added to the feed (PUREX raffinate) in advance and to the scrubbing solution during the process. A spiked test (i.e. synthetic PUREX raffinate with [241]Am, [152]Eu and ^{137}Cs tracers) was successfully performed in 1998 at Forschungszentrum Jülich in a 16-step mixer-settler set-up (*14*). The corresponding flowsheet was developed with the aid of a computer model at PoliMi. In this test, more than 99.99 % An(III) and lanthanides were removed and a high decontamination versus the fission products including Mo and Zr was achieved.

In the NEWPART project, more than twenty different malonamides were synthesized and tested in terms of their suitability for actinide extraction (*4*, *15*). In addition, intensive studies were conducted on hydrolysis and radiolysis stability (*16*, *17*). Molecule optimizations ultimately led to a new DIAMEX reference molecule (Figure 2): the N,N′-dimethyl-N,N′-dioctylhexylethoxy malonamide (DMDOHEMA). Its suitability for use in the process was demonstrated in a range

of hot tests with real fuel solution, both at CEA in Marcoule and at the Institute for Transuranium Elements (ITU) in Karlsruhe (*18*).

Currently, during reprocessing in the PUREX process, the high active raffinate (HAR) is concentrated and then denitrated for subsequent vitrification. The volume of the product, which is known as high active concentrate (HAC), is reduced by a factor of 15 compared to HAR. In view of an industrial application, the high active process flows (compared to HAR) are also reduced, as is the size of the processing unit. In the PARTNEW project, three partners (ITU, CEA and FZJ) were collaborating on the development of a DIAMEX process for separating An(III) from HAC (*19*).

As a result of the very high metal concentrations in HAC, the question arises as to how the co-extraction of certain transition metals (Zr, Mo, Pd, etc.) together with the trivalent actinides and lanthanides can be avoided. Such co-extraction would inevitably lead to third-phase formation and the failure of the separation process. Against this background, cold concentration and denitration experiments were performed with simulated HAR solutions. In these optimization experiments, parameters were developed that then led to a successful hot demonstration (concentration-denitration). In these hot tests, a real fuel solution was used as the basis to prepare a HAC solution with a concentration factor of 10 and an acidity of 4 mol/L. The loss of actinides in the accruing precipitation was very low at < 0.04 % (*20*).

In batch shaking experiments, the thermodynamic distribution data were determined for the HAC-DIAMEX process and a flowsheet as shown in Figure 3 was generated using computer code simulations. In order to minimize the risks (third-phase formation, precipitation, etc.) during a hot test, a cold DIAMEX test was first performed at Forschungszentrum Jülich using a centrifugal extractor battery (*21*). A simulated HAC solution (identical metal concentrations to real HAC) was used with the radionuclides ^{241}Am, ^{244}Cm, ^{134}Cs, ^{152}Eu (each 6.25 MBq/L). The extractant consisted of 1 mol/L DMDOHEMA dissolved in an aliphatic solvent (TPH). The aim of the DIAMEX test was to separate > 99 % of the actinides(III) together with the lanthanides(III) and to achieve high decontamination factors versus the other HAC elements. As can be inferred from the findings of Modolo et al. (*21*), these ambitious goals were achieved in a 16-step process.

Based on the positive results of spiked tests (Figure 3), a hot DIAMEX experiment was subsequently successfully performed in the hot cell facility at ITU, Karsruhe. The findings are discussed in detail in (*22*, *23*). Almost identical results were generated with the same flowsheet as shown in Figure 4. With the exception of technetium (97.8 % remained in the solvent), most of the fission products were not extracted (with the exception of Ln). Here, oxalic acid and HEDTA also very effectively prevented the co-extraction of Mo, Zr and Pd. The studies described here on the development of a new partitioning process very clearly demonstrate the transferability of simulated process conditions to real process conditions. This was shown both for the preparation of HAC as well as for the subsequent DIAMEX test. This makes optimization experiments both easier and cheaper under hot-cell conditions.
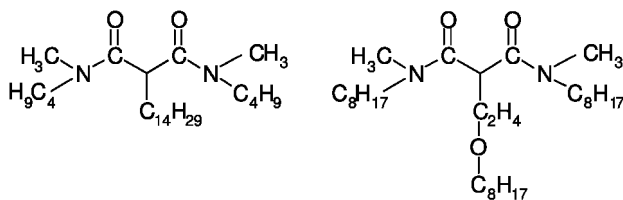
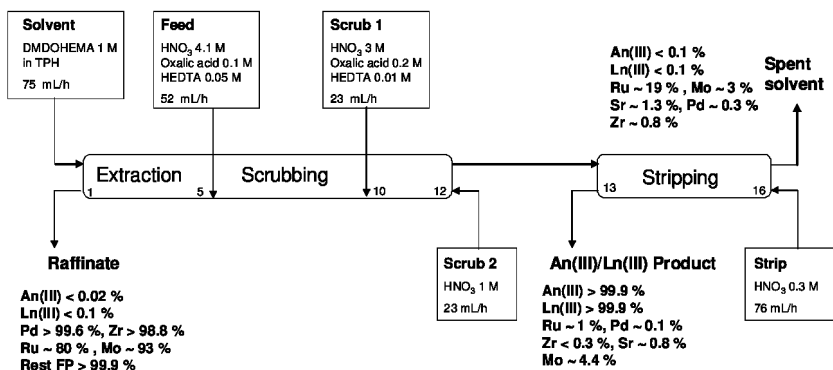*Figure 2. The structures of DMDBTDMA (left) and DMDOHEMA (right)*

Figure 3. Flowsheet and main results of the spiked DIAMEX-HAC carried out at FZJ/Jülich in 2003
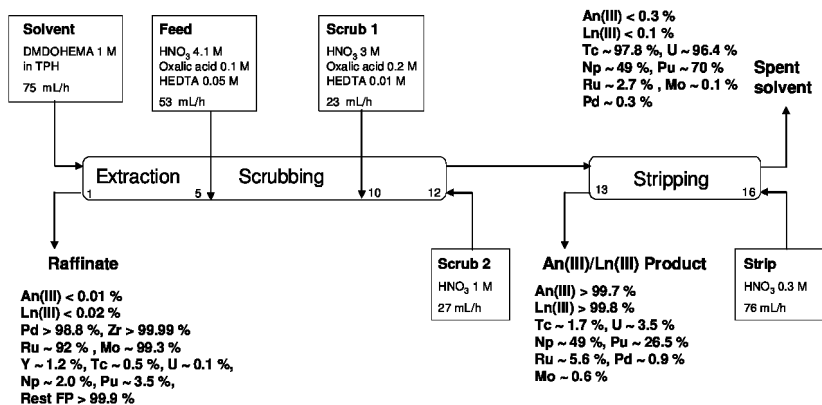

Figure 4. Flowsheet and main results of the hot DIAMEX-HAC carried out at ITU/Karlsruhe in 2003

TODGA-Based Process Developments

In the early 1990s, Stephan et al. (*24*) reported on the extraction of different metals using multidentate ligands such as diglycolamides (DGA). The DGA substance class with an ether group between both amide functions resembles the malonamides and therefore also satisfies the CHON principle. During the late 1990s, Japanese scientists recognized that these ligands are particularly suitable for extracting actinides from acidic waste solutions (*25*).

Extensive extraction studies were performed with this very promising substance class (*26–28*). The change from a bidentate ligand (e.g. malonamide) to a tridentate diglycolamide not only significantly increased the affinity for trivalent actinides but also for the lanthanides. Different DGAs were synthesized and the N,N,N′,N′-tetraoctyl-3-oxapentan-diamide (TODGA, Figure 5) was found to have the best properties in terms of extraction, solubility in aliphatic solvents and stability. However, TODGA had a tendency to form a third phase in aliphatic solvents such as n-dodecane, particularly at high metal and HNO_3 concentrations (*29*).

Within the scope of the PARTNEW project, the aggregation behaviour of TODGA was studied in n-dodecane as a solvent. With the aid of small-angle X-ray and neutron scattering experiments, it was shown that the reason for third-phase formation was the van der Waals interaction at low temperatures (*30*). Other basic studies with TODGA and related compounds can be found in the literature, but almost no studies exist on process development including demonstration (*31–39*). This motivated Modolo et al. to develop a continuous reversible partitioning process, which was successfully tested for the first time in 2003 in centrifugal contactors at Forschungszentrum Jülich (*40*). However, high oxalic acid concentrations of up to 0.4 mol/L were added to the PUREX raffinate in order to suppress the extraction of Zr and Mo on the one hand and third-phase formation on the other. At such high oxalic acid concentrations, a slow precipitation of trivalent actinides and lanthanides was observed in the PUREX raffinate. This also led to low oxalate precipitations in the scrubbing steps of the continuous process. This inevitably led to low actinide(III) losses.

Following this, Modolo et al. optimized the partitioning process and suggested a new continuous process in which the extractant was a mixture of 0.2 mol/L TODGA and 0.5 mol/L TBP in TPH (*41*). The addition of TBP not only improved the hydrodynamic properties but also increased the loading capacity of the extractant and reduced the tendency to third-phase formation. In 2006, Forschungszentrum Jülich performed two tests in centrifugal extractors in cooperation with the Institute for Transuranium Elements (ITU) and CEA Marcoule (*42*).

In the second test run (see Figure 6) with 28 stages (4 extraction steps, 12 scrubbing steps and 12 back-extraction steps), 99.99 % of the actinides and lanthanides were selectively extracted and back-extracted from a PUREX raffinate. Problems were caused only by Ru, which was co-extracted (10 % of initial amount) and remained in the spent solvent.

Based on these positive results, a hot process run was demonstrated at the end of 2006 in ITU's centrifugal extractor battery with almost identical results (*43*). The most important results are summarized in Figure 7. The extraction of the problem nuclides Sr, Zr, Mo and Pd was efficiently prevented in both test runs thanks to the complexants oxalic acid and HEDTA, as well as the acid concentration settings in the scrubbing steps. Ru exhibited peculiar behaviour in both process runs. In the spiked tests, 10 % (18 % in the hot test) was co-extracted and approx. 7.5 % (17 % in the hot test) remained in the spent solvent following the scrub and strip. The An(III)/Ln(III) product was very pure in both continuous tests and contained less than 0.1 % Sr, Zr and Pd and 1.8 % (1 % hot test) Ru.
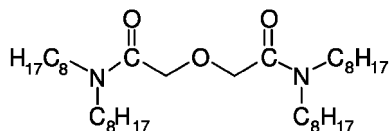
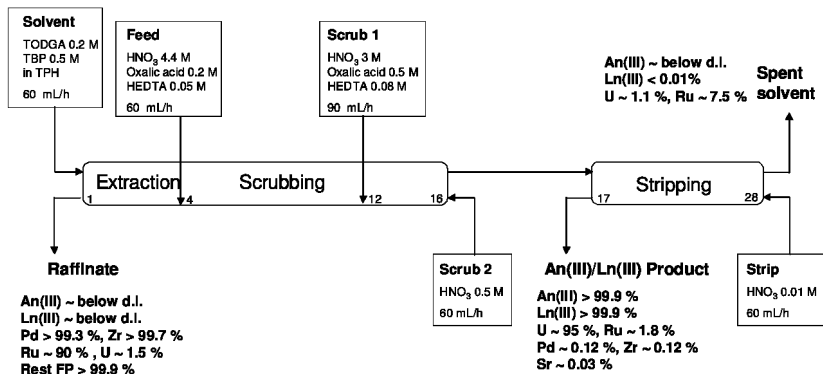*Figure 5. The structure of TODGA*

Figure 6. Flowsheet and main results of the spiked TODGA-based process carried out at FZJ/Jülich in 2006

In summary, we can say that the solvent composed of TODGA and TBP in an aliphatic solvent is particularly suitable for separating actinides from a process solution containing numerous fission products. This was demonstrated with a synthetic and a genuine PUREX raffinate with an optimized flowsheet. The main objective (> 99.9 % actinide separation) and a high fission product decontamination were achieved. The results generated are comparable with those for the DIAMEX processes further developed in France and the EU (*43*).

As TODGA has much higher An(III) + Ln(III) distribution coefficients than DMDOHEMA, it follows that the extraction is much more efficient. However, this is at the expense of complicated scrubbing and a multistep back-extraction. Furthermore, it should be noted that more waste is generated in the TODGA/TBP process (raffinate, dilution of the feed by a factor 3.5) than in the DIAMEX process (dilution of the feed by a factor of 2). The acidity of the An(III)/Ln(III) product also differs significantly for a subsequent actinide(III)/lanthanide(III) separation. Depending on the extractant used, the acidity can however be adjusted slightly. The behaviour of ruthenium needs to be further investigated in both processes (TODGA and DIAMEX), particularly in terms of the regeneration of the spent solvent.

Selective Actinide(III)/Lanthanide(III) Separation

The extraction systems described above separate the trivalent actinides together with the lanthanides from most of the fission products (e.g. Cs, Sr, Mo, Zr, etc.) in the liquid radioactive PUREX raffinate. For the transmutation of the minor actinides, any excess lanthanides (nuclear poison) must once again be
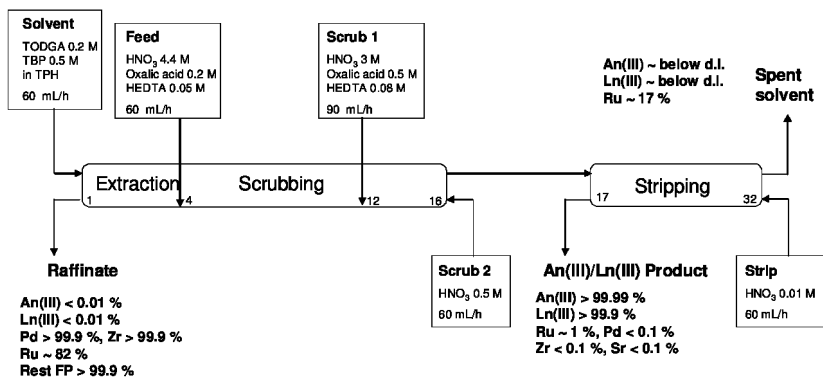
Figure 7. Flowsheet and main results of the hot TODGA-based process carried out at ITU/Karlsruhe in 2006

separated. As a result of the chemical and physical similarity of both element groups, group extraction is only possible using extractants or complexants containing soft donor atoms, such as N, S, CI, as they evidently have a stronger interaction with trivalent actinides (*2*).

Many extraction systems with relatively low An(III)/Ln(III) separation factors are described in the literature, but these systems are of little interest for technical application. Systems with a high selectivity are also described, but they are extremely complex (e.g. high salt loads, secondary waste), and they are incompatible with the partitioning processes described previously (*44–46*).

In the following, we will therefore only outline the most important European developments that have been tested with synthetic and real process solutions on a laboratory scale. The SANEX concept (Selective ActiNide EXtraction) which aims to selectively extract trivalent actinides was first proposed by Musikas et al. (*47*). In the early 1980s, the authors discovered two selective An(III)/Ln(III) extraction systems comprising soft N- or S-donor atoms, which subsequently formed the basis for the development of more efficient extractants.

Within the scope of the multinational EU project NEWPART (*4*), the continuous development of extractants containing the N donor led to the discovery of 2,6-bis (5,6-dialkyl-1,2-4-trizazin-3-yl) pyridines (BTPs). An overview and historic look back at solvent extraction using nitrogen donor ligands is given in the review by Ekberg at al. (*48*). At the end of the 1990s, BTPs discovered by Kolarik et al. (*49, 50*) achieved very high Am/Eu separation factors > 100 in strong nitric acid solutions (> 1mol/L). The unusually good extraction behaviour of BTPs was intensively studied (*51–53*) and many basic studies were conducted to characterize the actinides(III) and lanthanides(III) BTP complexes in an effort to find reasons for this high selectivity. Following this, continuous tests were conducted with real fuel solutions (after DIAMEX process) at the Institute for Transuranium Elements (ITU) in Karlsruhe, Germany, and at CEA in Marcoule, France (*54, 55*). Very good separation results were achieved, although owing to insufficient stability against hydrolysis and radiolysis BTPs tended to degrade.

Having clarified the decay mechanism (*56, 57*), modified BTPs (CyMe4BTP, see Figure 8) with protective side rings were synthesized at the University of

Reading in England (*58*). These BTPs have an even higher selectivity with Am/Eu separation factors of > 1000 and they are extremely resistant to hydrolysis. Within the EU project Europart, however, it was not possible to develop a continuous process. Evidently, the trivalent actinides form extremely stable CyMe₄BTP complexes, which prevent back-extraction (*59*).

Finally, a new class of heterocyclic N-donor SANEX ligands was developed by Foreman et al. (*60–64*), namely 6,6´-bis(5,6-dialkyl)-[1,2,4]triazin-3-yl)-[2,2´]bipyridines (BTBPs), which exhibit extraction properties that are just as good as BTPs. A summary of the extraction properties of the reference molecule CyMe₄BTBP (see Figure 9) can be found in Geist et al. (*3*). The slow extraction kinetics were significantly improved with a phase transfer catalyst, such as the malonamide DMDOHEMA.

However, continuous tests on extraction and back-extraction using a single centrifuge showed that even at low process flows, equilibrium values could not be achieved (*65*). Despite this, at the beginning of 2008, a hot test was successfully conducted for this SANEX process with a 16-stage flowsheet at ITU, Karlsruhe (*66*). The product fraction contained more than 99.9 % Am(III) and Cm(III) and less than 0.1 % Ln(III). These promising results are summarized in Figure 10.

At Forschungszentrum Jülich, Modolo et al. developed an alternative process (*67*). The extractant comprised 0.015 mol/L CyMe₄BTBP in n-octanol. However, instead of 0.25 mol/L DMDOHEMA, only 0.005 mol/L TODGA was used to improve the extraction kinetics. This system showed comparably good extraction properties and the process was successfully demonstrated at Forschungszentrum Jülich in February 2008.

In this 20-stage process with 12 extraction steps, 4 scrubbing steps and 4 back-extraction steps, >99.9 % Am(III), Cm(III) and Cf(III) were separated, and the product fraction contained less than 0.1 % of the initial lanthanides (Figure 11).

The hot testing of this process (possibly at ITU, Karlsruhe) is one of the tasks of our collaborative future programme. The SANEX process variant developed at Forschungszentrum Jülich appears to be very promising for two reasons: replacing DMDOHEMA with TODGA increases the solubility of BTBPs, and the regeneration of the extractant is easier.

Americium/Curium Separation by the LUCA Process

The separation of adjacent trivalent actinides represents an even more challenging task than the An(III)/Ln(III) separation. In principal, both elements could be transmuted together in a fast reactor or ADS system. However, because of the high heat decay and neutron emission of curium, any dry or wet fabrication process will require remote handling and continuous cooling in hot cells behind thick concrete shielding. The development of a simple, compact and robust fabrication process appears to be a great challenge (*69*).

Therefore, an effective method for separating Am from Cm prior to re-fabrication is a major prerequisite for the discussion of further fuel cycle scenarios. It is known that separating of americium from curium is a very difficult due to the very similar properties of these elements. Numerous techniques,
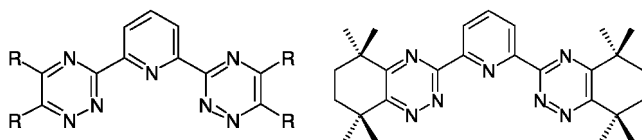
Figure 8. The 2,6-bis(5,6-dialkyl-1,2,4-trizazin -3-yl) pyridines (BTPs, left) and 2,6-bis(5,5,8,8-tetramethyl-5,6,7,8-tetrahydro-benzol[1,2,4]-triazin -3-yl) pyridine (CyMe₄BTP, right).
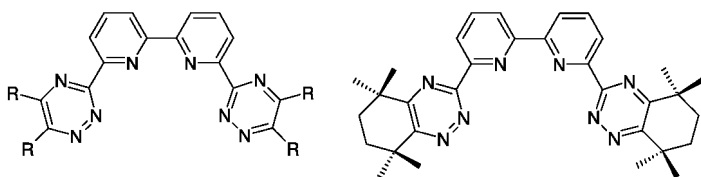

Figure 9. The 6,6́-bis(5,6-dialkyl-[1,2,4]-triazin -3-yl) –[2,2́] bipyridines (BTBPs, left) und 6,6́-bis(5,5,8,8-tetramethyl-5,6,7,8-tetrahydro-benzol[1,2,4]-triazin-3-yl)–[2,2́] bipyridine. (CyMe₄BTBP, right)
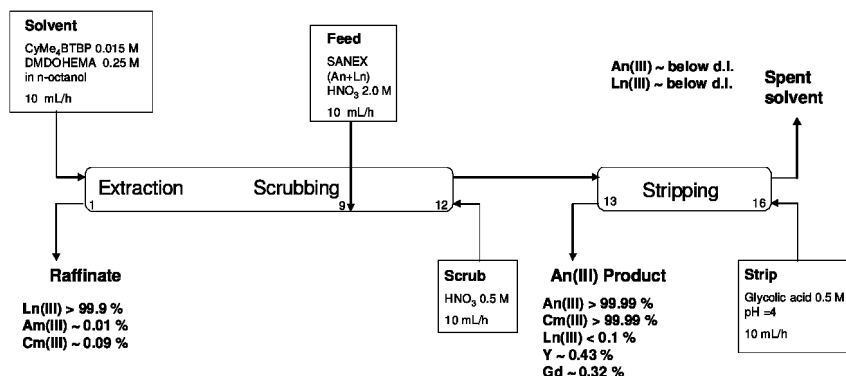

Figure 10. Flowsheet and main results of the hot SANEX CyMe₄BTBP/ DMDOHEMA process carried out at ITU/Karlsruhe in 2008

including high-pressure ion exchange, extraction chromatography, and solvent extraction using e.g. di(2-ethyl-hexyl)phosphoric acid (HDEHP) have been used for Am(III)/Cm(III) separation and purification (*1*, *2*). However, the Am/Cm separation factors were low and do not exceed 3, necessitating a large number of stages in order to obtain a pure product. The best separation of transplutonium elements has been obtained using methods based on the various oxidation states of the separated elements.

Contrary to Cm, Am can be oxidized in aqueous solutions to oxidation states higher than III, i.e. IV, V and VI. Nevertheless, these Am oxidation states are thermodynamically unstable in acidic aqueous solutions. The solvent extraction of hexavalent Am has been studied by several authors (*70–72*). Within the PARTNEW project, CEA developed a novel option for Am/Cm separation based
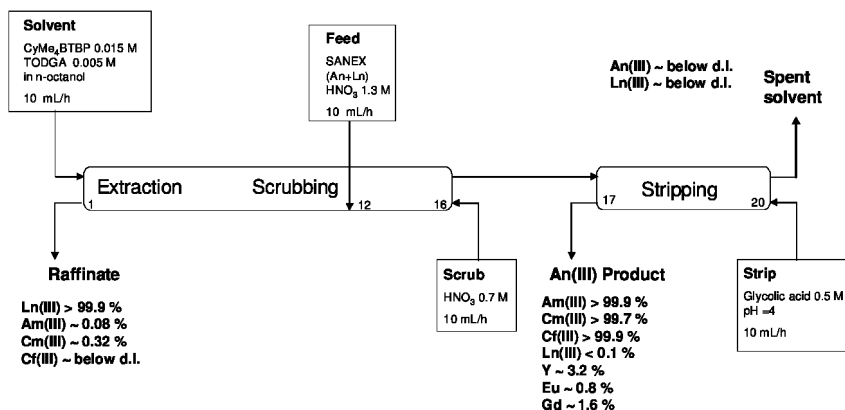
Figure 11. Flowsheet and main results of the spiked SANEX CyMe₄BTBP/TODGA process carried out at FZJ/Jülich in 2008

on the difference of the affinity of the DIAMEX extractant (DMDOHEMA) for Am(III) and Cm(III) (*5, 73*).

Since the Am(III)/Cm(III) separation factor of 1.6 is low, this process requires a large number of stages. Nevertheless, a flowsheet comprising 24 extraction, 24 scrubbing and 8 stripping stages was successfully tested in 2002 using surrogate solutions without significant difficulties. The performance of this test was good, as was predicted by calculations: more than 99.9 % of each actinide was recovered. 0.6 % Am was found within the Cm product solution, 0.7 % Cm within Am product solution, and only 0.02 % Am and 0.01 % Cm remained in the stripped solvent.

The synergistic mixture (Figure 12) composed of bis(chlorophenyl)-dithiophosphinic acid [(ClPh)₂PSSH] and tris(2-ethylhexyl) phosphate (TEHP) shows a very high affinity for actinides(III) over lanthanides(III). Am(III)/Eu(III) separation factors is over 3000. Surprisingly high Am(III)/Cm(III) separation factors of 6 – 10 were also reported by Modolo et al (*74, 75*). Based on the extraordinary extraction properties of the above synergistic mixture, the LUCA process (*76*) was invented for the selective recovery of Am(III) from an aqueous nitric acid solution containing trivalent actinides (i.e. Am(III), Cm(III) and Cf(III)) and trivalent lanthanides.

LUCA is the acronym for "Lanthaniden Und Curium Americum separation". Optimization studies were carried out to define the best conditions for extraction, scrubbing and stripping. In addition to the batch extraction studies, a single-stage extraction experiment was conducted to obtain more data on the system kinetics, and to generate data required for the flowsheet calculations.

After the data was collected, a 24-stage flowsheet was designed, and the final assessment was performed in a counter-current test using miniature centrifugal contactors (*77*). The results of this counter current test (Figure 13) showed, that the difficult recovery of Am(III) is possible from an acidic solution containing a mixture of trivalent actinides (Am(III), Cm(III) and Cf(III)) and Eu(III) as a lanthanide representative. The LUCA process can be used after a co-extraction process (e.g. after DIAMEX) for the selective extraction of Am(III), leaving Cm(III) together with the lanthanides in the raffinate fraction. Alternatively, the

process can also be run after a SANEX process (e.g. CyMe₄BTBP) for mutual Am/Cm separation.

In the future, we plan to optimize the formulation of the extractant composition, i.e. by changing the diluent. The promising results obtained here with a surrogate solution should also allow a hot demonstration to be performed in the near future with a genuine process solution. We are confident, that the aromatic dithiophosphinic acids under real process conditions (0.1 - 0.3 mol/L HNO_3, total doses up to 0.5 MGy) are sufficiently stable within the LUCA process. However, at higher acidities (> 0.5 mol/L HNO_3, e.g. during stripping) considerable degradation (by oxidation) of $(ClPh)_2PSSH$ was observed in a former study (*78*). Oxidation of the ligand can be suppressed by adding HNO_2 scavengers or using hydrochloric acid as a stripping medium.

Conclusion

Research on partitioning in the European Union (EU) is at such an advanced stage that serious consideration is being given to the industrialization of some separation processes. The leading nation here is France with its ambitious R&D programme on partitioning and transmutation. After decades of research in this area, separating minor actinides (americium and curium) from the PUREX raffinate still poses just as a big a challenge as in the past. The feasibility has already been demonstrated with the aid of a multicycle process (e.g. DIAMEX, TODGA, SANEX) on a laboratory scale using genuine fuel solutions. The challenge now is to optimize the developed processes in terms of their transferability and to work towards industrial process maturity. This will only be possible in the form of a large international project, and is being addressed in the EU follow-on project ACSEPT (*68*).

Within the framework of this international project, the focus is also on developing innovative processes. The objectives include simplifying processes developed in the past and reducing the number of cycles. The direct separation of trivalent actinides from the fission product solution (direct SANEX) is not yet viable as the necessary highly selective and stable extractants are not yet available. However, intensive research is being conducted on their development. Furthermore, tests must be performed to determine whether the processes developed to date are also suitable for future reactor concepts of the third and fourth generation (GEN IV). In some GEN IV concepts, for example, the aim is to jointly recycle all transuranium elements (Np, Pu, Am, Cm). A separation technology adapted for these concepts is therefore essential. Within the framework of the ongoing EU project ACSEPT (2008 - 2012), grouped actinides extraction (GANEX concept) is therefore being studied in order to fulfil the requirements for future issues.
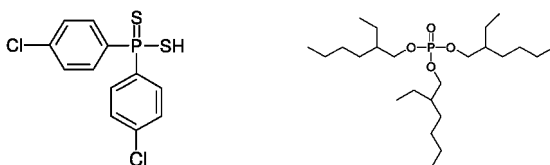
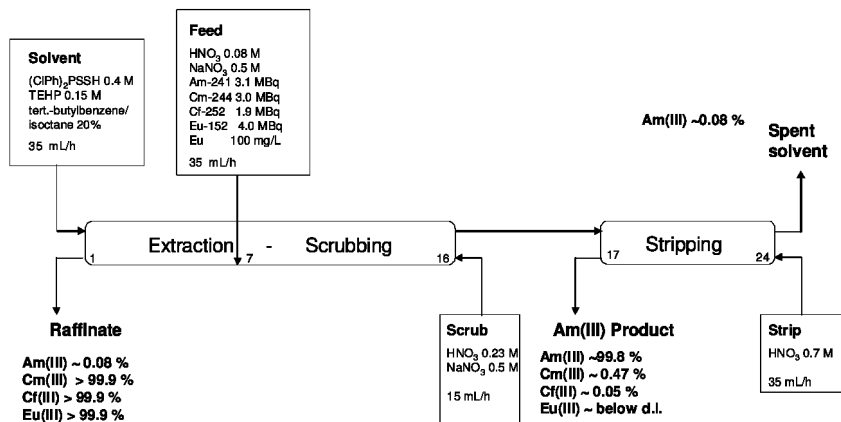*Figure 12. Synergistic mixture of (ClPh)₂PSSH and TEHP used in the LUCA process*

Figure 13. Flowsheet and main results of the LUCA process for Am/Cm separation carried out at FZJ/Jülich in 2008

Acknowledgments

References

1. *Actinide and Fission Product Partitioning and Transmutation: Status and Assessment Report*; Nuclear Energy Agency (NEA), Organisation for Economic Co-operation and Development (OECD): Paris, 1999.
2. Nash, K. L. Separation Chemistry for Lanthanides and Trivalent Actinides. In *Handbook on the Physics and Chemistry of Rare Earths*; Gschneidner, K. A., Jr., Eyring, L., Choppin, G. R., Lander, G. H., Eds.; 1994; Chapter 121, pp 197−235.
3. Geist, A.; Hill, C.; Modolo, G.; Foreman, M. R. St.-J.; Weigl, M.; Gompper, K.; Hudson, M. J.; Madic, C. *Solvent Extr. Ion Exch.* **2006**, *24*, 463–483.
4. Madic, C.; Hudson, M. J.; Liljenzin, J. O.; Glatz, J. P.; Nannicini, R.; Facchini, A.; Kolarik, Z.; Odoj, R. *New Partitioning Techniques for*

Minor Actinides; European Report, EUR 19149; European Commission: Luxembourg, 2000.

5. Madic, C.; Testard, F.; Hudson, M. J.; Liljenzin, J. O.; Christiansen, B.; Ferrando, M.; Facchini, A.; Geist, A.; Modolo, G.; Gonzales-Espartero, A.; De Mendoza, J. *PARTNEW−New Solvent Extraction Processes for Minor Actinides−Final Report*; CEA Report 6066; 2004.

6. Madic, C.; Hudson, M. J.; Baron, P.; Ouvrier, N.; Hill, C.; Arnaud, F.; Espartero, A. G.; Desreux, J.-F.; Modolo, G.; Malmbeck, R.; Bourg, S.; De Angelis, G.; Uhlir, J. *European Research Programme for Partitioning of Minor Actinides within High Active Wastes Issuing from the Reprocessing of Spent Nuclear Fuels (EUROPART)*, Proceedings of the FISA 2006, Luxembourg, 2006.

7. Cuillerdier, C.; Musikas, C.; Hoel, P.; Nigond, L.; Vitart, X. *Sep. Sci. Technol.* **1991**, *26*, 1229.

8. Cuillerdier, C.; Musikas, C.; Nigond, L. *Sep. Sci. Technol.* **1993**, *28*, 155.

9. Madic, C.; Blanc, P.; Condamines, N.; Baron, P.; Berthon, L.; Nicol, C.; Pozo, C.; Lecomte, M.; Philippe, M.; Masson, M.; Hequet, C.; Hudson, M. J. *Actinide Partitioning from HLLW Using the DIAMEX Process*, Proceedings of RECOD 1994, London, 1994.

10. Baron, P.; Charbonnel, M. C.; Nicol, C.; Berthon, L. *State of Advancement of DIAMEX Process*, Proceedings of GLOBAL 1997, Yokohama, Japan, 1997.

11. Madic, C.; Hudson, M. J *High-Level Liquid Waste Partitioning by Means of Completely Incinerable Extracts*; European Report EUR 18038; European Commission: Luxembourg, 1998.

12. Courson, O.; Malmbeck, R.; Lebrun, M.; Pagliosa, G.; Römer, K.; Sätmark, B.; Glatz, J.-P. *Radiochim. Acta* **2000**, *88*, 857−863.

13. Malmbeck, R.; Courson, O.; Pagliosa, G.; Römer, K.; Sätmark, B.; Glatz, J.-P.; Baron, P. *Radiochim. Acta* **2000**, *88*, 865−871.

14. Facchini, A.; Amato, L.; Modolo, G.; Nannicini, R.; Madic, C.; Baron, P. *Sep. Sci. Technol.* **2000**, *35* (7), 1055−1068.

15. Spjuth, L.; Liljenzin, J. O.; Hudson, M. J.; Drew, M. G. B.; Iveson, P. B.; Madic, C. *Solvent Extr. Ion Exch.* **2000**, *18*, 1.

16. Berthon, L.; Morel, J. M.; Zorc, N.; Nicol, C.; Virelizier, H.; Madic, C. *Sep. Sci. Technol.* **2001**, *36* (5−6), 709.

17. Mincher, B. J.; Modolo, G.; Mezyk, St. P. *Solvent Extr. Ion Exch.* **2009**, *27* (4), 579−606.

18. Serrano-Purroy, D.; Baron, P.; Christiansen, B.; Malmbeck, R.; Sorel, C.; Glatz, J.-P. *Radiochim. Acta* **2005**, *93* (3), 351−355.

19. Modolo, G.; Seekamp, S.; Vijgen, H. *DIAMEX Process Developement to Separate Trivalent Actinides from High Active Concentrates*, Proceedings of ICEM 2003: The 9th International Conference on Radioactive Waste Management and Environmental Remediation, Oxford, England, 2003.

20. Serrano-Purroy, D.; Christiansen, B.; Glatz, J.-P.; Malmbeck, R.; Modolo, G. *Radiochimica Acta* **2005**, *93* (3), 357−361.

21. Modolo, G.; Vijgen, H.; Serrano-Purroy, D.; Christiansen, B.; Malmbeck, R.; Sorel, C.; Baron, P. *Sep. Sci. Technol.* **2007**, *42*, 439−452.

22. Serrano-Purroy, D.; Baron, P.; Christiansen, B.; Glatz, J.-P.; Madic, C.; Malmbeck, R.; Modolo, G. *Sep. Purif. Technol.* **2005**, *45* (2), 157–162.

23. Madic, C.; Boullis, B.; Baron, P.; Testard, F.; Hudson, M. J.; Liljenzin, J.-O.; Christiansen, B.; Ferrando, M.; Facchini, A.; Geist, A.; Modolo, G.; Espartero, A. G.; De Mendoza, J. *J. Alloys Compd.* **2007**, *444−445*, 23−27.

24. Stephan, H.; Gloe, K.; Beger, J.; Mühl, P. *Solvent Extr. Ion Exch.* **1991**, *9* (3), 459–469.

25. Sasaki, Y.; Choppin, G. R. *Anal. Sci.* **1996**, *12*, 225–230.

26. Sasaki, Y.; Choppin, G. R. *Radiochim. Acta* **1998**, *80*, 85–88.

27. Sasaki, Y.; Sugo, Y.; Suzuki, S.; Tachimori, S. *Solvent Extr. Ion Exch.* **2001**, *19*, 91–103.

28. Tachimori, S.; Sasaki, Y.; Suzuki, S. *Solvent Extr. Ion Exch.* **2002**, *20* (6), 687–699.

29. Yaita, T.; Herlinger, A. W.; Thiyagarajan, P.; Jensen, M. P. *Solvent Extr. Ion Exch.* **2004**, *22*, 553−571.

30. Nave, S.; Modolo, G.; Madic, C.; Testard, F. *Solvent Extr. Ion Exch.* **2004**, *22* (4), 527–551.

31. Narita, H.; Yaita, T.; Tachimori, S. *Solvent Extr. Ion Exch.* **2004**, *22*, 135–145.

32. Suzuki, H.; Sasaki, Y.; Sugo, Y.; Apichaibuol, A.; Kimura, T. *Radiochim. Acta* **2004**, *92*, 463–466.

33. Zhu, Z. X.; Sasaki, Y.; Suzuki, H.; Suzuki, S.; Kimura, T. *Anal. Chim. Acta* **2004**, *527*, 163−168.

34. Sasaki, Y.; Zhu, Z. X.; Sugo, Y.; Suzuki, H.; Kimura, T. *Anal. Sci.* **2005**, *21*, 1171−1175.

35. Sasaki, Y.; Rapold, P.; Arisaka, M.; Hirata, M.; Kimura, T.; Hill, C.; Cote, G. *Solvent Extr. Ion Exch.* **2007**, *25* (2), 187–204.

36. Sugo, Y.; Sasaki, Y.; Tachimori, S. *Radiochim. Acta* **2002**, *90*, 161–165.

37. Morita, Y.; Sasaki, Y.; Tachimori, S. *Development of TODGA Extraction Process for High-Level Liquid Waste: Preliminary Evaluation of Actinide Separation by Calculation*, Proceedings of Global 2001, Paris, 2001.

38. Ansari, S. A.; Pathak, P. N.; Manchanda, V. K.; Husain, M.; Prasad, A. K.; Parmar, V. S. *Solvent Extr. Ion Exch.* **2005**, *23*, 463–479.

39. Tian, G.; Wang, J.; Shen, Y.; Rao, L. *Solvent Extr. Ion Exch.* **2005**, *23*, 519–528.

40. Modolo, G.; Vijgen, H.; Schreinemachers, C.; Baron, P.; Dinh, B. *TODGA Process Development for Partitioning of Actinides(III) from PUREX Raffinate*, Proceedings of GLOBAL 2003, New Orleans, 2003.

41. Modolo, G.; Asp, H.; Schreinemachers, C.; Vijgen, H. *Solvent Extr. Ion Exch.* **2007**, *25*, 703–721.

42. Modolo, G.; Asp, H.; Vijgen, H.; Malmbeck, R.; Magnusson, D.; Sorel, C. *Solvent Extr. Ion Exch.* **2008**, *26* (1), 62–76.

43. Magnusson, D.; Christiansen, B.; Glatz, J.-P.; Malmbeck, R.; Modolo, G.; Serrano-Purroy, D.; Sorel, C. *Solvent Extr. Ion Exch.* **2009**, *27* (1), 26–35.

44. Baybarz, R. D.; Weaver, B. S.; Kuiser, H. B. *Nucl. Sci. Eng.* **1963**, *17*, 457–462.

45. King, L. J.; Bigelow, J. E.; Collins, E. D. In *Transplutonium Elements: Production and Recovery*; Navratil, J. D., Schulz, W. W., Eds.; ACS Symposium Series 161; American Chemical Society: Washington, DC, 1981; pp 133−145.

46. Ensor, D. D.; Jarvinen, G. D.; Smith, B. F. *Solvent Extr. Ion Exch.* **1988**, *6*, 439.

47. Musikas, C.; Vitorge, P.; Pattee, D. *Progress in Trivalent Actinide Lanthanide Group Separation*, Proceedings of International Solvent Extraction Conference, Denver, CO, 1983.

48. Ekberg, C.; Fermvik, A.; Retegan, T.; Skarnemark, G.; Foreman, M. R. S.; Hudson, M. J.; Englund, S.; Nilsson, M. *Radiochim. Acta* **2008**, *96* (3−4), 225–233.

49. Kolarik, Z.; Müllich, U.; Gassner, F. *Solvent Extr. Ion Exch.* **1999**, *17* (1), 23–32.

50. Kolarik, Z.; Müllich, U.; Gassner, F. *Solvent Extr. Ion Exch.* **1999**, *17* (5), 1155–1170.

51. Drew, M. G. B.; Guillaneux, D.; Hudson, M. J.; Iveson, P. B.; Russell, M. L.; Madic, C. *Inorg. Chem. Commun.* **2001**, *4*, 12–15.

52. Iveson, P. B.; Rivière, C.; Guillaneux, D.; Nierlich, M.; Thuéry, P.; Ephritikhine, M.; Madic, C. *Chem. Commun.* **2001**, 1512–1513.

53. Denecke, M. A.; Rossberg, A.; Panak, P. J.; Weigl, M.; Schimmelpfennig, B.; Geist, A. *Inorg. Chem.* **2005**, *44* (23), 8418–8425.

54. Hill, C.; Heres, X.; Calor, J.-N.; Guillanex, D.; Mauborgne, B.; Rat, B.; Rivalier, P.; Baron, P. *Trivalent Actinides/Lathanides Separation Using Bis-triazinyl-pyridines*, Proceedings of GLOBAL 1999, Jackson Hole, WY, 1999.

55. Hill, C.; Guillaneux, D.; Berthon, L.; Madic, C. *J. Nucl. Sci. Technol.* **2002**, *3*, 309–312.

56. Mincher, B. J.; Modolo, G.; Mezyk, St. P. *Solvent Extr. Ion Exch.*, in press.

57. Hill, C.; Berthon, L.; Madic, C. *Study of the Stability of BTP Extractants under Radiolysis*, Proceedings of GLOBAL 2005, Tsukuba, Japan, 2005.

58. Hudson, M. J.; Boucher, C. E.; Drew, M. G. B.; Foreman, M. R. St. J.; Harwood, L. M.; Hill, C.; Madic, C.; Marken, F.; Youngs, T. G. A. *New J. Chem.* **2006**, *30*, 1171–1183.

59. Modolo, G. Unpublished data.

60. Drew, M. G. B.; Foreman, M. R. St. J.; Hudson, M. J.; Madic, C. *Inorg. Chem. Commun.* **2005**, *8*, 239–241.

61. Foreman, M. R. St. J.; Hudson, M. J.; Geist, A.; Madic, C.; Weigl, M. *Solvent Extr. Ion Exch.* **2005**, *23* (5), 645–662.

62. Foreman, M. R. St. J.; Hudson, M. J.; Drew, M. G. B.; Hill, C.; Madic, C. *Dalton Trans.* **2006**, 1645–1653.

63. Foreman, M. R. S.; Hudson, M. J.; Geist, A.; Madic, C.; Weigl, M. *Solvent Extr. Ion Exch.* **2005**, *23* (5), 645–662.

64. Nilsson, M.; Ekberg, C.; Foreman, M.; Hudson, M.; Liljenzin, J.-O.; Modolo, G.; Skarnemark, G. *Solvent Extr. Ion Exch.* **2006**, *24*, 823–843.

65. Magnusson, D.; Christiansen, B.; Glatz, J.-P.; Malmbeck, R.; Modolo, G.; Serrano-Purroy, D.; Sorel, C. *Radiochim. Acta* **2009**, *97* (3), 155–159.

66. Magnusson, D.; Christiansen, B.; Foreman, M. R. S.; Geist, A.; Glatz, J.-P.; Malmbeck, R.; Modolo, G.; Serrano-Purroy, D.; Sorel, C. *Solvent Extr. Ion Exch.* **2009**, *27* (2), 97–106.

67. Modolo, G.; Sypula, M.; Geist, A.; Hill, C.; Sorel, C.; Malmbeck, R.; Magnusson, D.; Foreman, M. R. St. J. *Development and Demonstration of a New SANEX Process for Actinide(III)−Lanthanide(III) Separation Using a Mixture of CyMe₄BTBP and TODGA as Selective Extractant*, Proceedings of the 10th OECD/NEA P&T Meeting, Mito, Japan, 2008.

68. Bourg, S.; Caravaca, C.; Ekberg, C.; Hill, C.; Rhodes, C. *ACSEPT, Toward the Future Demonstration of Advanced FuelTreatments*, Proceedings of Global 2009, Paris, 2009.

69. Pillon, S.; Somers, J.; Grandjean, S.; Lacquement, J. *J. Nucl. Mater.* **2003**, *320*, 36–43.

70. Mason, G. W.; Bollmeier, A. F.; Peppard, D. F. *J. Inorg. Nucl. Chem.* **1970**, *32*, 1011–1022.

71. Myasoedov, B. F. *J. Alloys Compd.* **1994**, *231/214*, 290–299.

72. Madic, C.; Lecomte, M.; Baron, P.; Boullis, B. *C.R. Physique* **2002**, *3*, 797–811.

73. Myasoedov, B. F.; Maryutina, T. A.; Litvina, M. N.; Malikov, D. A.; Kulyako, Yu. M.; Spivakov, B. Ya.; Hill, C.; Adnet, J.-M.; Lecomte, M.; Madic, C. *Radiochim. Acta* **2005**, *93*, 9–15.

74. Modolo, G.; Odoj, R. *Solvent Extr. Ion Exch.* **1999**, *17* (1), 33–53.

75. Modolo, G.; Nabet, S. *Solvent Extr. Ion Exch.* **2005**, *23*, 359–373.

76. Modolo, G.; Odoj, R. *Method for Separating Trivalent Americium from Trivalent Curium*. European Patent EP 1664359B1, March 1, 2007.

77. Modolo, G.; Kluxen, P.; Geist, A. *Radiochim. Acta*, in press.

78. Modolo, G.; Seekamp, S. *Solvent Extr. Ion Exch.* **2002**, *20* (2), 195–210.

Chapter 9

Combining Octyl(phenyl)-N,N-diisobutyl-carbamoylmethylphosphine Oxide and Bis-(2-ethylhexyl)phosphoric Acid Extractants for Recovering Transuranic Elements from Irradiated Nuclear Fuel

Gregg J. Lumetta,[*,1] **Jennifer C. Carter,**[1] **Artem V. Gelis,**[2] **and George F. Vandegrift**[2]

[1]Pacific Northwest National Laboratory, P.O. Box 999, MSIN P7-25, Richland, Washington 99352
[2]Argonne National Laboratory, Chemical Technology Division, Argonne, Illinois 60439
[*]E-mail: gregg.lumetta@pnl.gov

Advanced concepts for closing the nuclear fuel cycle include separating Am and Cm from other fuel components. Separating these elements from the lanthanide elements at an industrial scale remains a significant technical challenge. We describe here a chemical system in which a neutral extractant—octyl(phenyl)-N,N-diisobutyl-carbamoylmethyl-phosphine oxide (CMPO)—is combined with an acidic extractant—bis-(2-ethylhexyl)phosphoric acid (HDEHP)—to form a single process solvent (with dodecane as the diluent) for separating Am and Cm from the other components of irradiated nuclear fuel. Continuous variation experiments in which the relative CMPO and HDEHP concentrations are varied indicate a synergistic relationship between the two extractants in the extraction of Am from buffered diethylenetriaminepentaacetic acid (DTPA) solutions. A solvent mixture consisting or 0.1 M CMPO + 1 M HDEHP in dodecane offers acceptable extraction efficiency for the trivalent lanthanides and actinides from 1 M HNO_3 while maintaining good lanthanide/actinide separation factors in the stripping regime (buffered DTPA solutions with

pH 3.5 to 4). Using citrate buffer instead of lactate buffer results in improved lanthanide/actinide separation factors.

Introduction

Advanced concepts for closing the nuclear fuel cycle typically include separating the minor actinides (i.e., Am and Cm) from other fuel components. The reason for separating these elements stems from the long-term impacts of these elements on the performance of geologic repositories for irradiated fuel. Separating these elements from the material going to the repository and subsequently transmuting these elements to stable or short-lived nuclides would greatly reduce the long-term risks associated with nuclear power. Separating Cm also has near-term benefits for the repository in reducing the heat load. Recent efforts in the United States have considered separating the transuranic (TRU) elements (Np, Pu, Am, Cm) from irradiated nuclear fuel as a single group. Including the minor actinides with the Pu renders the Pu less desirable for weapons production and thus improves the proliferation resistance of the fuel cycle compared to conventional fuel recycling schemes (which separate pure Pu) (*1*).

One of the critical challenges in this regard is separating the TRU elements (especially Am and Cm) from the lanthanide fission products. The lanthanides are generally neutron poisons and thus reduce the efficiency of transmutation processes for the TRU elements. Although there are active programs worldwide investigating the separation of TRU elements from the lanthanides, recent work in the United States has focused on the "UREX+" suite of separation processes. One disadvantage of this approach is the process complexity. For example, in the "UREX+1a" concept for irradiated fuel recycling, a series of four solvent extraction processes are proposed to partition the fuel into useful products and fission-product waste (*2*). Combining systems to reduce the complexity of materials handling has significant potential benefit. Two processes that might be suited to "blending" are the Transuranic Extraction (TRUEX) process and the Trivalent Actinide-Lanthanide Separations by Phosphorus-reagent Extraction from Aqueous Complexes (TALSPEAK) process.

The TRUEX process extracts the TRU elements (Np, Pu, Am, Cm) and the lanthanide fission products from the other fission products from 1 to 3 M HNO_3. This is achieved by extracting the TRU elements with octyl(phenyl)-N,N-diisobutyl-carbamoylmethylphosphine oxide (CMPO, Figure 1a) into an aliphatic hydrocarbon diluent. Tri-butyl phosphate (TBP) is added to the TRUEX solvent as a modifier to prevent third-phase formation at high solvent loading (*3*). The TALSPEAK process uses bis-(2-ethylhexyl)phosphoric acid (HDEHP, Figure 1b) as the extractant (*4*). In this case, an aqueous-soluble complexant, diethylenetriaminepentaacetic acid (DTPA), is used to complex the actinide ions and prevent their extraction into the organic phase (or to strip the actinides from the organic phase in the so-called "reverse TALSPEAK" method). Because DTPA binds the lanthanide ions less strongly than the actinide ions, the

lanthanides are extracted by HDEHP in the presence of DTPA, thereby achieving a separation of the lanthanides from the actinides.

In UREX+1a, the TALSPEAK process is applied to the TRU/lanthanide product from TRUEX to separate the TRU elements from the lanthanides. In this report, we describe a process in which the TRUEX and TALSPEAK functions are combined into a single solvent extraction process, referred to here as "TRUSPEAK." In the TRUSPEAK process, the TRUEX extractant (CMPO) is combined with the TALSPEAK solvent (HDEHP in dodecane). In doing this, it was envisioned that the CMPO chemistry would dominate under conditions of high acidity ($\geq$ 1 M HNO$_3$), resulting in co-extraction of the TRU and lanthanide elements into the organic phase. After suitable scrubbing steps, contacting the loaded solvent with a buffered solution of DTPA at pH ~3 to 4 would result in a condition in which the HDEHP chemistry dominates, and the system should behave in a manner analogous to a "reverse TALSPEAK" process. The greater affinity of DTPA for the TRU ions versus the lanthanides should cause the TRU to be selectively stripped into the aqueous phase, thereby separating them from the lanthanides.

Other authors have recently suggested combining neutral and acidic extractants to produce solvent systems for separating lanthanides from actinides. Watanabe et al. (5) reported on a system in which N,N,N',N'-tetrakis(2-methylpyridyl)-ethylenediamine (TPEN) is combined with HDEHP in 1-octanol. This work indicated a synergistic effect between TPEN and HDEHP in the extraction of Am(III), whereas no such synergy was observed for the Eu(III) extraction. Presumably, the relatively soft nature of the nitrogen donor groups in TPEN display preference for Am(III), which is a slightly softer acid than Eu(III). The separation factor of Am over Eu was ~80 when the solvent phase consisted of 0.002 M TPEN and 0.004 M HDEHP in 1-octanol, and the aqueous phase consisted of 0.001 M Eu and 0.1 M NH$_4$NO$_3$ at pH 4.3. Replacing the 1-octanol diluent in this system with dodecane resulted in a decline in the Am/Eu separation factor and precipitation or third phase formation above 80 vol% dodecane. Gannaz et al. (6) used a somewhat different approach in which the neutral malonamide extractant, N,N'-dimethyl-N,N'-dioctylhexylethoxy-malonamide (DMDOHEMA), was combined with di-n-hexylphosphoric acid (HDHP) in dodecane. This system is more analogous to the TRUSPEAK concept in that trivalent lanthanides and actinides are extracted from nitric acid solutions. Above 1 M HNO$_3$ the extraction behavior of DMDOHEMA dominates. Below 1 M HNO$_3$, the extraction is dominated by HDHP, although DMDOHEMA does appear to have some influence on the extraction mechanism. No synergistic effect between DMDOHEMA and HDHP was observed. The selective stripping of the actinides from the lanthanides was not described for the DMDOHEMA/HDHP system. Dhami et al. (7) investigated the combination of CMPO and HDEHP in a normal paraffin diluent, which in essence was the first description of the TRUSPEAK concept. In that work, a solvent formulation consisting of 0.2 M CMPO + 0.3 M HDEHP in n-paraffin was used. The results were promising, but the Am(III) distribution coefficients for extraction from nitric acid were found to be less than observed for the TRUEX process. Selective stripping of Am(III) was shown to be possible using a stripping solution consisting of 0.05 M DTPA + 0.4

M formic acid + 0.4 M hydrazine hydrate at pH 2 to 4. Thus, the work of Dhami et al. demonstrated the potential for combining CMPO and HDEHP into a single process solvent for separating trivalent actinides from the trivalent lanthanides, but the system they described was not optimized.

We describe here our initial investigations of the TRUSPEAK concept. This initial work focused primarily on assessing the feasibility of the concept and determining the effects of changes to the solvent formulation or the aqueous-phase chemistry on the potential to separate lanthanides from americium(III).

Experimental

TRUSPEAK Solvent

CMPO was procured from Strem Chemicals, Inc., Newburyport, MA. HDEHP was obtained from Eastman Kodak (Rochester, NY) and Aldrich (Milwaukee, WI). Normal dodecane was also obtained from Aldrich. The HDEHP and n-dodecane were used as-received.

The CMPO was purified as follows. The CMPO (81.79 g) was dissolved in 180 mL of heptane. Dowex 50WX8-200 (60 to 170 mesh; 10.3 g) cation exchange resin was added. [Before use, the Dowex 50WX8-200 was twice washed with deionized water (~6 mL/g resin), three times with methanol (~3 mL/g resin), and finally, three times with heptane (~3 mL/g resin).] After stirring the CMPO solution with the cation exchange resin for 2 h, 2.3 g of Dowex 1-X8 (20 to 50 mesh) anion exchange resin was added, and the mixture was stirred for another 2 h. [The Dowex 1-X8 was converted from the chloride form to the hydroxide form by treating with 1 M NaOH (5 mL/g resin) and then repeatedly washing with deionized water.] The resins were removed from the solution by filtration, and the heptane solution of CMPO was washed twice with 100 mL each 0.25 M Na_2CO_3, then twice with 100 mL 0.1 M HNO_3, and finally twice with 100-mL portions of deionized water. The solution was dried over anhydrous sodium sulfate and then was concentrated by ~50% using a rotary evaporator. The concentrated CMPO solution was stored in a freezer for 10 days to induce crystallization. Excess heptane was decanted, and the white crystalline solid was dried *in vacuo* yielding 75.51 g of purified CMPO.

The following is a typical description of preparing the initial prototypic TRUSPEAK solvent, which consisted of 0.2 M CMPO + 1 M HDEHP in n-dodecane. CMPO (2.038 g, 5.0 mmol) and HDEHP (8.062 g, 25 mmol) were stirred together in a glass beaker until the CMPO had dissolved. The resulting solution was quantitatively transferred to a 25-mL volumetric flask and diluted to 25-mL with n-dodecane. Before use, the prototypic TRUSPEAK solvent was washed successively with 1) 1 M NaOH/4 M NaCl (three washes at organic-to-aqueous ratio of 5), 2) 1 M HNO_3 (one wash at organic-to-aqueous ratio of 1; two washes at organic-to-aqueous ratio of 5), and 3) deionized water (three washes at organic-to-aqueous ratio of 2.5). Each washing step was performed by gently shaking the washing mixture, centrifuging, and then withdrawing the aqueous phase. Other formulations of the TRUSPEAK solvent were prepared in a similar manner.
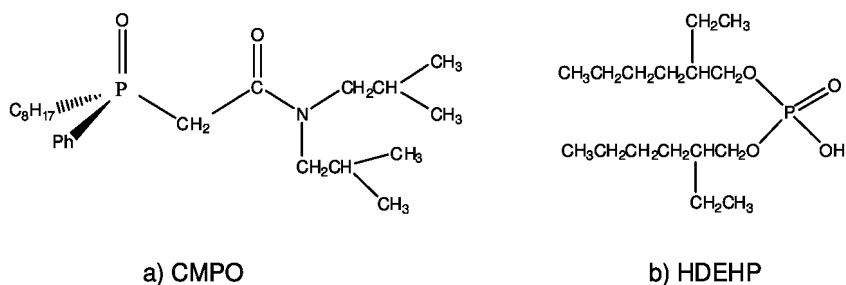
Figure 1. Chemical structures of the extractants used in a) the TRUEX process and b) the TALSPEAK process

Distribution Measurements

Americium and Eu distribution coefficients were usually measured in a competitive manner, using [241]Am and [155]Eu tracers, although single isotopes were used in selected cases. The relative activities of these isotopes in the organic and aqueous phases were determined by gamma spectroscopy using an intrinsic germanium detector. The gamma peaks at 59 keV and 86 keV were measured for [241]Am and [155]Eu, respectively. The [241]Am activity was corrected for the contribution from the 60 keV [155]Eu peak. The aqueous phases were prepared by mixing stock lactate or citrate solutions with a stock DTPA solution and adjusting the pH with ammonium hydroxide. For measurements of the equilibrium pH, 1.5-mL aliquots of the aqueous solutions were shaken for 1 h with 1.5-mL of the TRUSPEAK solvent. After centrifuging, the aqueous phase was separated and the pH measured using a Ross® combination electrode. To measure the Am and Eu distribution coefficients, 0.5-mL aliquots of the aqueous solution were spiked with [241]Am and [155]Eu tracers. The solution was then contacted with 0.5-mL of the TRUSPEAK solvent by vortex mixing for 1 min, and the solution was shaken for 3 h using a hand-action shaker. (Preliminary kinetic experiments indicated that 1-h shaking was sufficient to reach equilibrium.) The mixture was centrifuged, and 0.2-mL aliquots of each phase were taken for gamma spectroscopy. The extraction experiments from pure nitric acid solutions were performed similarly.

To determine the distribution coefficients for the lanthanide ions, aqueous solutions (1.5 M lactate or citrate; 0.05 M DTPA) containing a mixture of the following elements (0.001 M each) were prepared: Nd, Sm, Eu, Gd, Tb, and Dy. Solutions of variable pH were prepared by adjusting the pH with aqueous ammonium hydroxide. Each solution was sampled for analysis before equilibration with the TRUSPEAK solvent. The solutions (1.5 mL) were contacted with an equal volume of the TRUSPEAK solvent by shaking for 3 h. The mixtures were centrifuged, and the aqueous phase was separated. The final pH of the aqueous phase was determined; then it was sampled for analysis. The aqueous solution before and after equilibration was analyzed by inductively coupled plasma mass spectrometry (ICP-MS) to determine the Nd, Sm, Eu, Gd, Tb, and Dy concentrations. The concentration of these elements in the organic phase was determined by difference.

Results and Discussion

The influence of the CMPO-to-HDEHP ratio on the Am(III) and Eu(III) distribution behavior was investigated with a continuous-variation experiment to determine if there is a synergistic interaction between the CMPO and HDEHP. Solvent solutions were prepared with a total concentration of CMPO plus HDEHP equal to 0.2 M in dodecane, but with a varying mole fraction of CMPO. These solvent mixtures were contacted with an aqueous solution consisting of 0.05 M DTPA/1.5 M lactate at pH 3.6 and spiked with [241]Am and [155]Eu. Figure 2 presents the results of this experiment. The Eu distribution coefficients decrease steadily, but not linearly, with increasing mole fraction of CMPO. This suggests a weak synergistic interaction between CMPO and HDEHP in the extraction of Eu. On the other hand, the Am distribution coefficient initially increases with increasing CMPO mole fraction, reaching a maximum at a CMPO mole fraction of 0.1 to 0.2, and then decreases with a further increase in the CMPO mole fraction. This indicates that there is a substantial synergistic interaction between CMPO and HDEHP in the Am extraction.

The data in Figure 2 also show that the Eu/Am separation factor ($SF_{Eu/Am}$ = the Eu distribution coefficient divided by the Am distribution coefficient) increases rapidly as the CMPO mole fraction drops below 0.2. At a CMPO mole fraction of 0.1, the $SF_{Eu/Am}$ is 28 under the conditions used to collect the data in Figure 2. However, under those conditions, the CMPO concentration was too low to achieve practical extraction of Am and Eu from nitric acid solutions. To determine if the high $SF_{Eu/Am}$ would be maintained at higher CMPO concentrations, the extraction of Am(III) and Eu(III) was determined at a constant CMPO mole fraction of 0.1, but with increasing total [CMPO] + [HDEHP]. As seen in Figure 3, the $SF_{Eu/Am}$ drops precipitously above [CMPO] + [HDEHP] = 0.2 M, and levels out at approximately 10 to 12. The reason for this behavior is not obvious. But the $SF_{Eu/Am}$ at the higher [CMPO] + [HDEHP] concentrations is sufficiently high to achieve efficient separation of Am from Eu. For most of the remaining experiments to be discussed, a TRUSPEAK solvent formulation of 0.1 M CMPO + 1 M HDEHP in dodecane was used. This formulation provided the best balance between efficiently extracting the trivalent lanthanides and actinides from nitric acid solution and selectively stripping the actinides from the loaded solvent.

Figure 4 illustrates the Am(III) and Eu(III) distribution coefficients for extraction from nitric acid solutions into 0.1 M CMPO + 1 M HDEHP in dodecane. The extraction behavior of Am and Eu under these conditions is quite different than observed for the TRUEX process in that the distribution coefficients decrease with increasing nitric acid concentration. This observation is consistent with behavior described in the report by Dhami et al. (*7*). At low nitric acid concentration, extraction by HDEHP becomes dominant. This should simplify scrubbing of the loaded solvent in that careful control over the nitric acid concentration is not required. That is, the nitric acid can be scrubbed from the extractant phase without the possibility of losing the extracted Am and Eu (because partitioning to the organic phase increases as HNO_3 is removed).
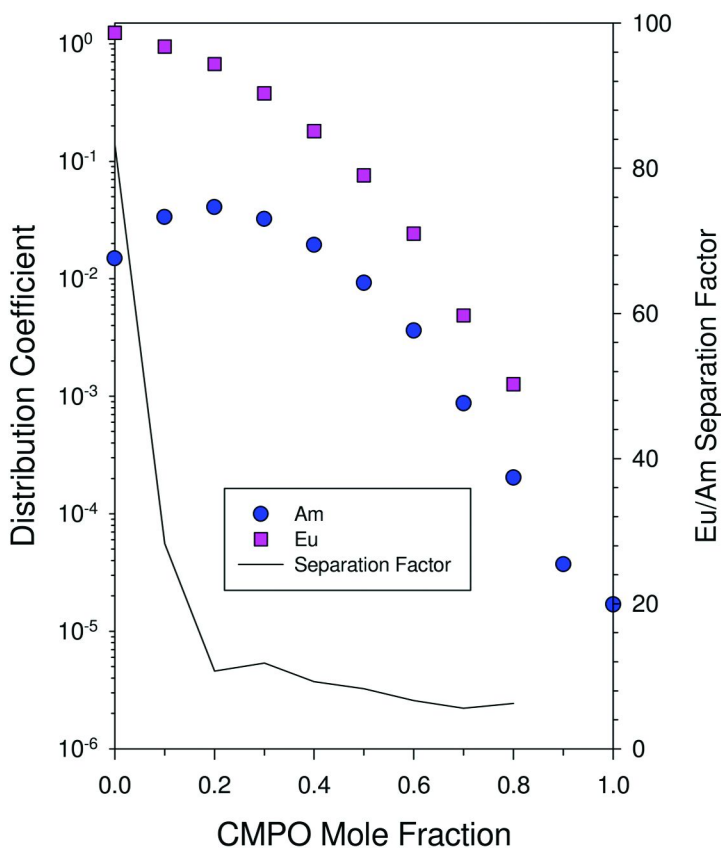
Figure 2. Extraction of Am and Eu by CMPO/HDEHP/dodecane with varying mole fraction of CMPO at 1.5 M lactate, 0.05 M DTPA, pH 3.6; total [CMPO] + [HDEHP] = 0.2 M.

The suppression of Am and Eu extraction at higher nitric acid concentration compared to the TRUEX process suggests that additional extraction stages or higher organic flow rates would be required for this formulation of the TRUSPEAK solvent compared to the traditional TRUEX solvent. However, since the Am and Eu distribution coefficients remain greater than 1 up to ~2 M HNO_3, a viable process should be achievable. Based on the data available, operation of the TRUSPEAK extraction at ~1 M HNO_3 would be preferable since the Am and Eu distribution values are comparable to those for TRUEX at that nitric acid concentration. The Sr and Cs distribution coefficients for the 0.1 M CMPO + 1 M HDEHP solvent formulation as a function of nitric acid concentration were determined using [85]Sr and ^{137}Cs tracers, respectively. For initial nitric acid concentrations ≥ 1 M, the organic-phase [85]Sr and ^{137}Cs concentrations were below the detection limit. At 0.1 M HNO_3, the D_{Sr} was 0.016, and the D_{Cs} was 0.0014. So the extraction of these two elements should be insignificant in the TRUSPEAK process. However, the behavior of other fission products, especially Zr and Mo, remains to be determined.
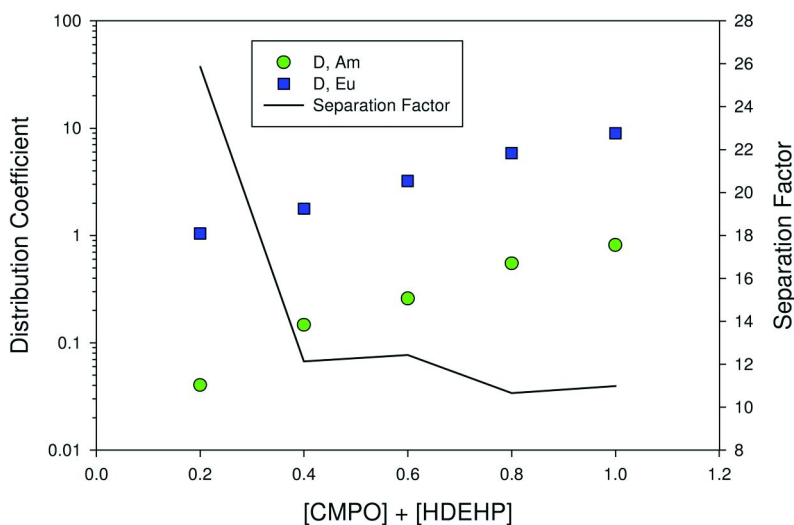
Figure 3. Extraction of Am and Eu by CMPO/HDEHP/dodecane with constant mole fraction of CMPO of 0.1, but variable total [CMPO] + [HDEHP]; 1.5 M lactate, 0.05 M DTPA, pH 3.4 to 3.6.
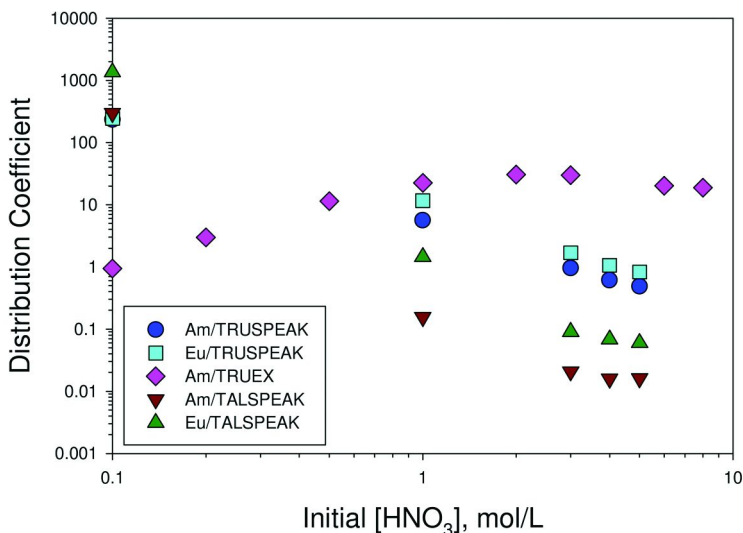
Figure 4. Extraction of Am and Eu by 0.1 M CMPO/1 M HDEHP/dodecane as a function of initial nitric acid concentration. Also shown are the Am distribution coefficients for the TRUEX process (0.2 M CMPO/1.4 M TBP/normal paraffin hydrocarbon; ref. (8); the TRUEX data are plotted against the equilibrium [HNO₃] rather than the initial. The Am and Eu distribution coefficients for the TALSPEAK solvent (1 M HDEHP in dodecane) are also presented for comparison.
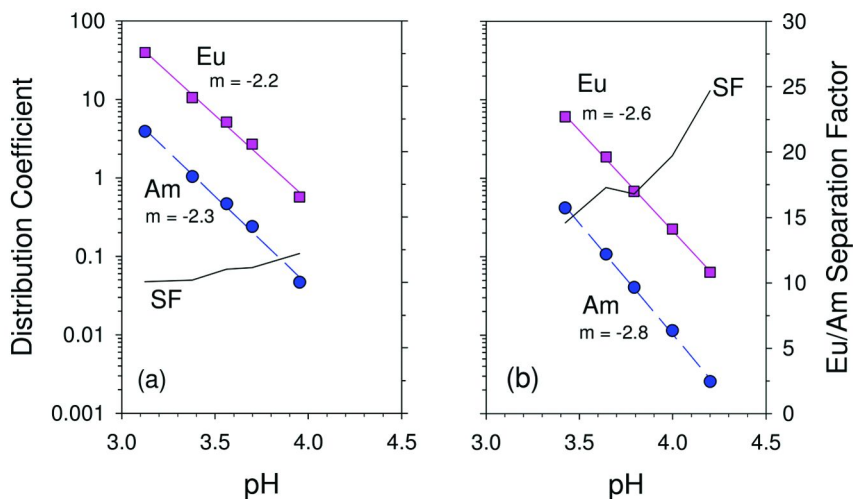
Figure 5. Extraction of Am and Eu by 0.1 M CMPO/1 M HDEHP/dodecane as a function of equilibrium pH at a) 1.5 M lactate and 0.05 M DTPA and b) 1.5 M citrate and 0.05 M DTPA.

Figure 5a shows the Am(III) and Eu(III) (tracer-level) distribution coefficients for extraction into 0.1 M CMPO + 1 M HDEHP from 1.5 M lactate + 0.05 M DTPA solutions as a function of pH. The trend of decreasing distribution coefficient with increasing pH is consistent with the behavior normally seen in the TALSPEAK process (*4*). The logD vs pH plots are linear within the pH region examined, with slopes of about -2, suggesting that 2 moles of H$^+$ is transferred to the aqueous phase for every mole of M^{3+} extracted. In the absence of lactate ion or DTPA, the extraction of trivalent lanthanides and actinides is described in terms of the HDEHP dimer as:

$$M^{3+}(aq) + 3(HA)_2(org) \leftrightarrow M(AHA)_3(org) + 3H^+(aq) \tag{1}$$
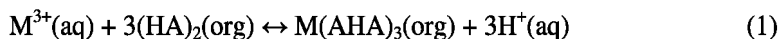
where A represents the deprotonated form of HDEHP (*4*). This is supported by slopes of -3 in the logD vs pH plots (*9*). On the other hand, plots of logD$_{Cm}$ vs pH for extraction into HDEHP from lactate solutions give slopes of -2, suggesting the extraction reaction (*10*):

$$M^{3+}(aq) + L^-(aq) + 2(HA)_2(org) \leftrightarrow ML(AHA)_2(org) + 2H^+(aq) \tag{2}$$
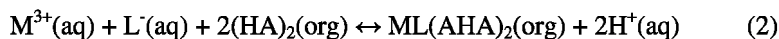
where L$^-$ = lactate ion.
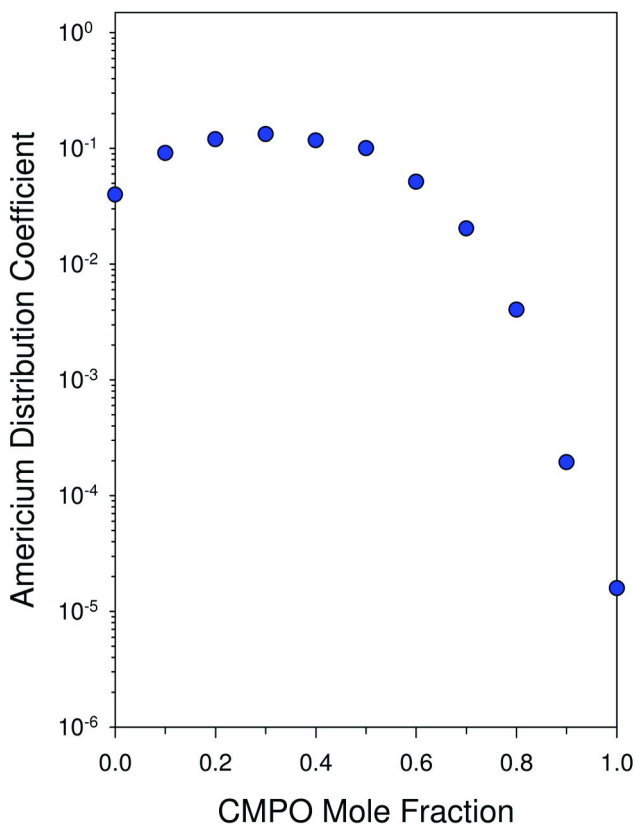
Figure 6. Extraction of Am and Eu by CMPO/HDEHP/dodecane with varying mole fraction of CMPO at 1.5 M lactate, 0.05 M DTPA, pH 3.6; total [CMPO] + [(HDEHP)₂] = 0.2 M.

A modified version of the continuous variation experiment was performed to further explore the nature of the extracted Am species in the synergistic CMPO/HDEHP system. In this case, $[CMPO] + [(HDEHP)_2]$ was held constant at 0.2 M so that the dependence on the HDEHP dimer concentration could be evaluated. Figure 6 illustrates the results of this experiment. Again, the data show a definitive synergism between CMPO and HDEHP in the extraction of Am from 1.5 M lactate/0.05 M DTPA/pH 3.6. The maximum in the continuous variation plot occurs at ~0.3 CMPO mole fraction, suggesting that the extracted Am species contains one CMPO for every two HDEHP dimers. Based on this and the -2 slope of the $\log D_{Am}$ vs pH plot (Figure 5a), the following extraction reaction is postulated:

$$Am^{3+}(aq) + L^-(aq) + CMPO(org) + 2(HA)_2(org) \leftrightarrow$$

$$[ML(AHA)_2 \cdot CMPO](org) + 2H^+(aq) \quad (3)$$
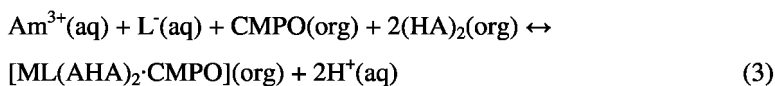
Reaction 3 should be viewed as a hypothesis at this point. Further experimental work is required to provide more definitive proof for this reaction. The inclusion of lactate ion in Equation 3 is particularly problematic because

the extraction of Am from 0.05 M DTPA at pH 3.5 into 0.2 M CMPO + 1 M HDEHP/dodecane decreases as a function of lactate concentration. So this is a matter for further investigation.

Replacing the lactate buffer with a citrate buffer was investigated based on previous work done on a citrate-based TALSPEAK process (*11*). Using citrate ion instead of lactate ion to buffer the aqueous phase resulted in an increase in the Eu/Am separation factor (Figure 5b). The increased separation factors ($SF_{Eu/Am}$ ~ 15 to 25) would result in improved process efficiency compared to the lactate system.

The extraction behaviors for Nd, Sm, Eu, Gd, Tb, and Dy were determined for the 1.5 M citrate/0.05 M DTPA system as a function of pH using 0.1 M CMPO + 1 M HDEHP/dodecane as the extraction solvent. The extraction behavior was similar to that seen for Am and tracer-level Eu with slopes of approximately -2 for the logD vs pH plots (Figure 7a). These data were used to determine the lanthanide/americium separation factors. Figure 7b presents a plot of the $SF_{Ln/Am}$ as a function of the ionic radius (*12*) of the lanthanide ions. For this solvent formulation, the Sm/Am separation factor is lowest among the lanthanide ions examined. This observation is somewhat different than that reported by Del Cul et al. (*11*) in which the minimum in the $SF_{Ln/Am}$ occurs at Nd. This suggests that CMPO also influences the extraction behavior of the light lanthanides; that is, the extraction of Nd appears to be enhanced relative to that of Sm in the presence of CMPO. Further investigations into the fundamental chemistry underlying the combined CMPO/HDEHP extraction system are underway in our laboratories.
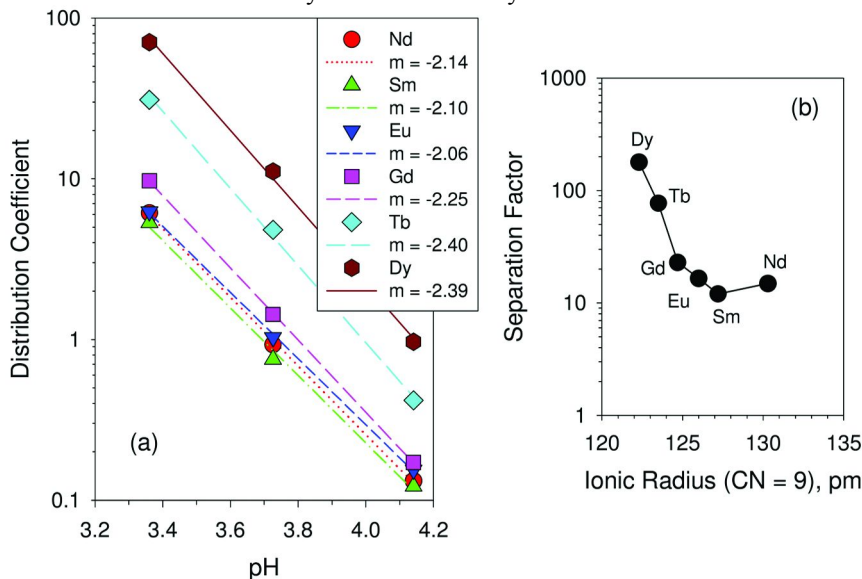
Figure 7. a) Extraction of Nd, Sm, Eu (macro), Gd, Tb, and Dy by 0.1 M CMPO/1 M HDEHP/dodecane as a function of equilibrium pH at 1.5 M citrate and 0.05 M DTPA. b) Ln/Am Separation Factors for Nd, Sm, Eu, Gd, Tb, and Dy achieved by extraction with 0.1 M CMPO/1 M HDEHP/dodecane as a function of ionic radius at pH 3.7, 1.5 M citrate, and 0.05 M DTPA.

Acknowledgments

References

1. Todd, T. A.; Wigeland, R. A. In *Separations for the Nuclear Fuel Cycle in the 21st Century*; Lumetta, G. J., Nash, K. L., Clark, S. B., Friese, J. I., Eds.; ACS Symposium Series 933; American Chemical Society: Washington, DC, 2006; pp 41−55.
2. Mincher, B. J.; Modolo, G.; Mezyk, S. P. *Solvent Extr. Ion Exch.* **2009**, *27*, 1–25.
3. Horwitz, E. P.; Kalina, D. G.; Diamond, H.; Vandegrift, G. F.; Schulz, W. W. *Solvent Extr. Ion Exch.* **1985**, *3*, 75−109.
4. Nilsson, M.; Nash, K. L. *Solvent Extr. Ion Exch.* **2007**, *25*, 665–701.
5. Watanabe, M.; Mirvaliev, R.; Tachimori, S.; Takeshita, K.; Nakano, Y.; Morikawa, K.; Chikazawa, T.; Mori, R. *Solvent Extr. Ion Exch.* **2004**, *22*, 377–390.
6. Gannaz, B.; Chiarizia, R.; Antonio, M. R.; Hill, C.; Cote, G. *Solvent Extr. Ion Exch.* **2007**, *25*, 313–337.
7. Dhami, P. S.; Chinis, R. R.; Gopalakrishnan, V.; Wattal, P. K.; Ramanujam, A.; Bauri, A. K. *Sep. Sci. Technol.* **2001**, *36*, 325–335.
8. Seefeldt, W. B; Tse, P.-K.; Fredrickson, D. R.; Reichley-Yinger, L.; Chaiko, D. J.; Kwok, J. D.; Lorton, S.; Sabau, C. S.; Sedlet, J.; Shinn, W.; Simonzadeh, N.; Vandegrift G. F. *The Generic TRUEX Model: Experimental Data Base Generated in Support of the Model*; ANL-89/19; Argonne National Laboratory, Argonne, IL, 1989; Vol. 3.
9. Peppard, D. F.; Mason, G. W.; Maier, J. L.; Driscoll, W. J. *J. Inorg. Nucl. Chem.* **1957**, *4*, 334–343.
10. Kosyakov, V. N.; Yerin, E. A . *J. Radioanal. Chem.* **1980**, *56*, 93−104.
11. Del Cul, G. D.; Bond, W. D.; Toth, L. M.; Davis, G. D.; Dai, S.; Metcalf, D. H. *Citrate-Based "TALSPEAK" Lanthanide−Actinide Separation Process*; ORNL/TM-12785; Oak Ridge National Laboratory: Oak Ridge, TN, 1994.
12. Huheey, J. E. *Inorganic Chemistry: Principles of Structure and Reactivity*; Harper & Row: New York, 1978; pp 71−74.

Chapter 10

Development of a Novel GANEX Process

Emma Aneheim,* **Christian Ekberg, Anna Fermvik,**
and Mark R. S. Foreman

Nuclear Chemistry and Industrial Materials Recycling,
Chalmers University of Technology,
Gothenburg, Sweden, SE-41296
***emma.aneheim@chalmers.se**

The waste from nuclear power plants has to be isolated from man and his environment for about 100,000 years to be considered safe. It has been suggested that if the long-lived actinides could be separated from the spent fuel and transmuted, the isolation time could be shortened to about 1,000 years. This, however, requires selective separation of parts of the waste. The partitioning for transmutation research in Europe has for the major part taken place within several European Union Framework Programmes. Within the projects NEWPART, PARTNEW and EUROPART a process scheme for the partitioning of nuclear waste from the PUREX process was developed. The scheme includes the DIAMEX, SANEX and SESAME-processes among which both the DIAMEX and SANEX process has been successfully tested on genuine spent fuel. However, in the latest EU Project ACSEPT, which started in 2008, another approach towards partitioning is being investigated. This is the so called GANEX (Group ActiNide EXtraction) process. In the GANEX process all the actinides in the dissolved spent fuel are extracted as a group and hence separated from the lanthanides as well as the rest of the fission and corrosion/activation products. A novel GANEX process has been developed at Chalmers university of Technology in Sweden. This new process utilizes the properties of already well known extractants by combining BTBP and TBP into one solvent. The system is able to extract U, Np, Pu and Am from strong nitric acid and simultaneously separate these

elements from the lanthanides. This is done with sufficiently high distribution ratios and separation factors without the need for any redox control.

Introduction

Spent nuclear fuel is one of the main problems associated with the use of nuclear power. Many countries have selected the so called "Once though" cycle where the spent nuclear fuel is treated as a waste and disposed of in final repositories, often under ground. These repositories are planned to keep the waste isolated from contact with humans or other biotopes for more than 100 000 years. An option to this handling is the reprocessing aimed at recovering the uranium and plutonium from the waste in order to make new fuel, so called mixed oxide (MOX) fuel. However, even in this case the remaining nuclides such as neptunium, americium and curium require a very long storage time. In recent years the idea of partitioning and transmutation has become increasingly popular. The main idea is to take the remaining solution after the reprocessing and then separate out the long lived elements for further irradiation and fission into shorter lived fission products. By applying this strategy the storage time of the nuclear waste would have been reduced to less than 1000 years and the energy utilization had increased (*1*).

Over the years several processes and flow sheets for the separation for transmutation have been designed, e.g. TRUEX, TALSPEAK, TRPO, DIDPA, UNEX, DIAMEX and SANEX. Of these, DIAMEX and SANEX have been developed in Europe and are discussed in detail below. However, this chapter deals with the development of a fairly new concept, the so called GANEX (Group ActiNide EXtraction) process. The main idea behind it is, as the name suggests, to simultaneously remove all the actinides from dissolved spent fuel, after the bulk part of the uranium has been removed. This renders a separation of the actinides from the lanthanides as well as the rest of the fission and corrosion/activation products in one operation. The actinides can then be selectively stripped for transmutation purposes (*2*).

Background

Partitioning in Europe

In Europe the development of liquid-liquid partitioning for transmutation has for the major part taken place within several European Union Framework Programs (EU FP). The partitioning research started already in the third EU FP with only two partners (CEA and University of Reading) but the first larger joint European research project started in 1996 and continued until 1999 within the scope of the fourth EU FP. The project was called NEWPART (New Partition Technology) (*1*) and had seven participating institutes from five different countries; the Department of Nuclear Chemistry, Chalmers (Sweden), CEA (France), University of Reading (UK), ENEA (Italy), Transuranium Institute,

Forschungszentrum Karlsruhe and Forschungszentrum Jülich (all three in Germany).

NEWPART was considered to be very successful and was therefore in the year 2000 followed by another project within the fifth EU FP called PARTNEW (Partitioning: New Solvent Extraction Processes for Minor Actinides). The project had now expanded to include 11 partners and lasted for a total of 36 months. During that time e.g. 189 different molecules were prepared and tested as minor actinide extractants and as reagents for An(III)/Ln(III) separations (*3, 4*).

After the major progress made in PARTNEW another project followed called EUROPART (EUROpean Research Programme for the PARTitioning of Minor Actinides) (*5*). EUROPART lasted from 2004 to 2007 and included 24 members situated in 11 EU countries plus two partners from Australia and Japan. The scope of the project was to comprise the continuation of not only PARTNEW but also two additional fifth EU FP projects; Calixpart (*6*) and Pyrorep (*7*). The PARTNEW project only dealt with An/Ln separation using solvent extraction with various nitrogen donor ligands or e.g. malonamides while the Calixpart project considered solvent extraction with ligands of the calixarene type. In the case of Pyrorep the separation was made by molten salts or molten metal techniques and hence in EUROPART, all three of these fields were studied.

Since March 2008 the fourth project, ACSEPT (Actinide Separation for Transmutation) (*8*), is running, now within the seventh EU FP. ACSEPT has 34 partners from 12 EU countries and 2 non EU countries (Australia and Japan). The project is divided into four domains: Hydrometallurgy, Pyrometallurgy, Process integration and Teaching and education. The calixarene research within hydrometallurgy has more or less disappeared but the pyroprocesses introduced in EUROPART still remains. A new angle within the ACSEPT project is the process integration domain where the idea is to make the small scale laboratory research industrially viable by modelling it into a real life process. Another new feature is the education and training domain where all the members, which have their own specific field of knowledge, get the oportunity to learn from each other and thereby produce better researchers within the field of partitioning.

Extraction Process Development in Europe

During the different EU projects mentioned above, the strategy for the partitioning work in Europe has changed its focus as progress within the area has been made. During the EUROPART project a full extraction scheme for the reprocessing process was developed (*5*). The scheme that can be seen in Figure 1 was developed under many years and several projects.
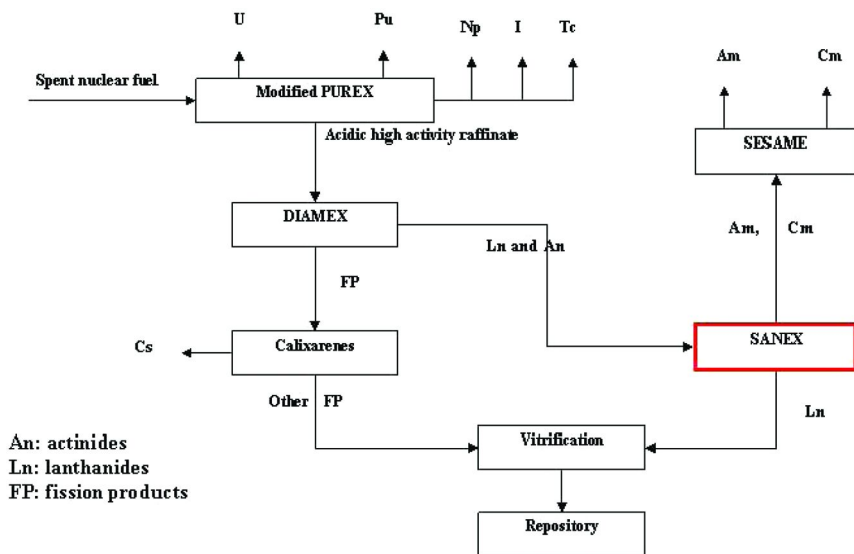
Figure 1. Extraction scheme for the partitioning of spent nuclear fuel (5).

The development started already in NEWPART where the first aim was to co-extract actinides and lanthanides from a PUREX raffinate. The PUREX process is already implemented in several European countries like France and the UK which is why this was a natural step for reprocessing of the minor actinides. The co-extraction method developed was called the DIAMEX (**DIAM**ide **EX**traction (*1*)) process, which as the name suggests uses a di-amide for the extraction of both actinides and lanthanides. During PARTNEW the DIAMEX process was further developed and several bis-malonamides were prepared and tested. Some of which showed interesting extraction properties. The basic chemistry of the promising extracting agents was also further investigated. In addition, several flow-sheets were developed and in 2005, on the verge between PARTNEW and EUROPART a successful hot test of the process with genuine spent fuel was performed at the European Commissions Joint Research Center - Institute for Transuranium Elements (ITU). The fuel was run through a small scale PUREX process to produce the PUREX raffinate that was used as the water phase for the DIAMEX process. The hot test was performed using the di-amide DMDOHEMA (DiMethyl-DiOctyl-HexaEthoxy-MalonAmide) and the recovery of Am and Cm was over 99.9%. Hence the test was considered to be very successful (*9*).

In parallel with the development of the DIAMEX process was the next step in the partitioning scheme developed. This step, which aims at extracting the trivalent actinides into an organic phase and hence separating them from the lanthanides, would follow after the stripping of both the actinides and lanthanides that were co-extracted in the DIAMEX process. This separation was to be called the regular SANEX (**S**elective **A**cti**N**ide **EX**traction) or r-SANEX process (*10*). Under the PARTNEW project several different approaches to the SANEX process was investigated, among two were the use of polydentate N-bearing ligands and the bis-(substituted phenyl)-di-thiophosphinic acid + neutral ligand

synergistic mixtures. Numerous studies of both these systems solvent extraction thermodynamics and mechanisms were made and supplemented by molecular modeling and testing in centrifugal contactor batteries. Further studies of the SANEX process were made also during EUROPART and a promising extraction system consisting of CyMe₄-BTBP in octanol was chosen for hot testing. The CyMe₄-BTBP molecule has been developed by improving the properties of a long row of successive nitrogen donor ligands such as TERPY, TPTZ, BTP and hemi-BTP (*11*). A final hot test with an optimised SANEX process on actual PUREX raffinate were however not realised until just after EUROPART. Then it was shown that the suggested process using CyMe₄-BTBP in octanol worked quite well (*12*). The major difficulty was however the kinetics of extraction, which with this system was a bit slow.

The development of the very last step of the entire reprocessing process was started already during the NEWPART project. This step, that follows after the SANEX process, deals with the separation of Am and Cm from each other. The process that was developed then was the so called SESAME (Selective Extraction of Americium by Electrochemical Method) process (*13*, *14*). During PARTNEW two new solvent extraction systems were also found to be promising for An separation. One of them was based on a single malonamide and the other based on a synergic mixture containing a chlorinated di-phosphinic acid. Two separation flowsheets were developed and tested using these two systems. The synergetic system was then further developed under EUROPART into the LUCA process (*15*). Besides this not much progress on the An partitioning process was made during EUROPART except as a byproduct of the development of actinide selective ligands like BODO, that could separate Am from Cm with a separation factor of around 5 (*16*).

After these successful results the research on both DIAMEX and r-SANEX continues within the ACSEPT project but with more basic investigations of the two extraction systems, like radiolytic stability, stripping conditions etc. The search for new extracting molecules for An/Ln co-extraction and separation and similar is thus diminished. Within ACSEPT, these areas of basic investigations are however not the main focus but instead process simplifications by reducing the number of steps in the entire reprocessing process are investigated. A reduction in the number of steps in a solvent extraction process is very important since it could result in a considerable reduction in not only the capital investment required to build an industrial plant but also the size of the plant, the running costs and the final decommissioning costs (*17*). This decrease in extraction steps is realized within two new extraction processes which are under development and that both differ from the original extraction scheme (Figure 1) used in the previous projects. One process is a further development of the r-SANEX process which is called the innovative SANEX (i-SANEX) and the other one is the GANEX process.

In the i-SANEX process actinides and lanthanides are firstly co-extracted into an organic phase with a di-amide (e.g. TODGA) just like in the DIAMEX process. Secondly however, there is a selective back extraction of the actinides with a hydrophilic complexing agent, separating them from the lanthanides. For a schematic explanation of the process see Figure 2.
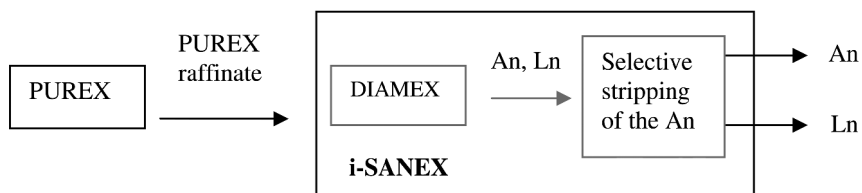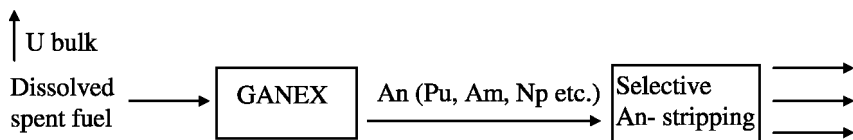
Figure 2. Schematic picture of the i-SANEX process

Figure 3. Schematic picture of the GANEX process

As can be seen in Figure 2, the i-SANEX process is quite similar to the American reversed TALSPEAK process. This processes is however quite complicated and therefore not well understood and difficult to control (*18*).

The GANEX process (for a schematic picture see Figure 3) is today under development in at least three different ways among the members of ACSEPT. The rest of this article will however only deal with the Swedish model developed at Chalmers University of Technology in Gothenburg.

Development of a Novel GANEX Extraction System

The Chalmers idea behind the new GANEX system was to combine two well known extractants that display complementing properties i.e. extraction of trivalent actinides and hence separation from the trivalent lanthanides as well as extraction of tetra- penta- and hexavalent actinides. With these properties of the extraction system there would be no need for redox control of e.g. Pu. This ternary system consists of cyclohexanone as the diluent and the two extractants BTBP and TBP. TBP already has a well documented ability to extract uranium and plutonium directly from dissolved spent fuel (*19*) while BTBP molecules on the other hand are known to be able to extract trivalent and pentavalent actinides and hence separate them from the trivalent lanthanides (*20, 21*).

When developing the extraction process first of all, three basic demands need to be met:

1. The organic system has to be able to withstand the strong acidic conditions present (an acidity of 4M HNO_3 has been set as standard for GANEX experiments within the ACSEPT project) when extracting directly from dissolved spent fuel.
2. The system has to be able to extract all of the actinides.
3. The system has to be able to separate all the actinides from the lanthanides.

If the system is found to meet these demands and hence is worth investigating further, then several other important questions have to be considered:

4. Can the system perform the extractions and separations after having received a large dose of radiation?
5. Does the system extract any fission- or corrosion-/activation-products?
6. How does the system perform under the heavy metal loading conditions that will be when extracting directly from dissolved spent fuel?

When dealing with a two phase system like the Chalmers concept it is also important to see if the two extractants extract independently of each other. If so, then a future computer modelling of the system would be much simplified.

How the Chalmers novel GANEX extraction process meets the demands listed above is presented below.

1. Stability towards Strong Acid

TBP is a chemical that has been used within the PUREX process for a long time and that has been very well investigated. It is therefore long known and documented that TBP, to a very small degree, is degraded by nitric acid to di-butyl phosphate, mono-butyl phosphate and finally phosphoric acid (22) which however does not affect the extraction in a negative way. Some of the BTBP molecules on the other hand are much sensitive to acid and would be rapidly degraded under such a harsh environment as 4M nitric acid but for instance the CyMe$_4$-BTBP (Figure 4) has shown a good stability towards nitric acid (23). This is because the CyMe$_4$-BTBP side chains do not provide any opportunity for hydrogen abstraction on the benzylic carbons.

Due to these properties of the extractants the GANEX system are stable towards strong acid. The diluent, cyclohexanone has however been observed to be totally miscible with nitric acid of high concentration but since the high amount of TBP in the GANEX organic system prevents it from being miscible with the water phase, this is not a problem.
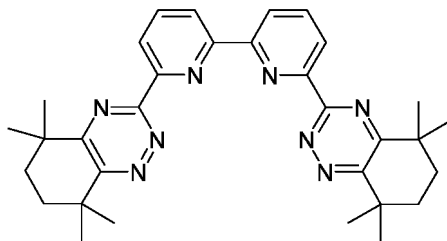
Figure 4. Molecular structure of CyMe$_4$-BTBP
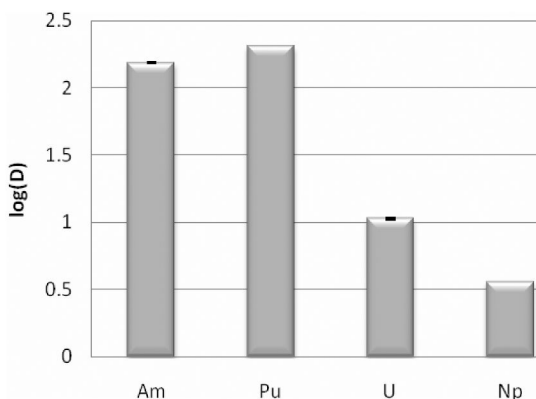
Figure 5. Extraction of actinides (^{241}Am, ^{238}Pu, ^{235}U, ^{237}Np) from 4M HNO₃ with 0.01M CyMe4-BTBP and 30% TBP in cyclohexanone.

2. Actinide Extraction

Extractions of the different actinides U, Np, Pu and Am were performed from 4M HNO₃ with the new GANEX system consisting of 0.01M of CyMe4-BTBP and 30% TBP in cyclohexanone (*24*).

As can be seen in Figure 5, all actinides are readily extracted with the GANEX system from strong acid.

3. An/Ln Separation

Extractions of several lanthanides (La, Nd, Ce, Sm, Eu) were performed with the system to confirm that it could separate them from the actinides as proposed. All lanthanides except Eu was used in the form of inactive salts in as realistic concentrations as possible in the extraction experiments. This means concentrations close to those that can be found in dissolved spent fuel. The europium was however added as ^{152}Eu in trace amounts (*24*).

The experiments rendered separation factors between the actinides and the lanthanides that looked very promising even when comparing to the lanthanide that is extracted the most (Eu). When comparing the extraction of the actinides to the extraction of the lanthanide that is the most abundant in spent fuel (Nd) the result looks even better (Table I). Np is the actinide which has the lowest SF towards the lanthanides but it is still sufficiently high.

**Table I. Separation Factors for the actinides (U, Np, Pu, Am) and two
different lanthanides (Nd, Eu) after extraction from 4M HNO₃ with 0.01M
BTBP-CyMe4 + 30% TBP in cyclohexanone**

Elements	Separation factor
Am / Eu	160
Pu / Eu	210
U / Eu	11
Np / Eu	3.5
Am / Nd	1700
Pu / Nd	2300
U / Nd	120
Np / Nd	38

4. Radiolytic Stability

TBP has long been used in the PUREX process where the conditions are more or less the same as they would be in a future GANEX process. The radiolytic degradation of TBP is therefore well known and was not considered to be a problem to the Chalmers concept.

The radiolytic behavior of the other extractant, CyMe4-BTBP is however a little bit more uncertain. It has been shown that the molecule can be degraded by γ-radiation (*25*) but it has also been shown for other BTBPs that the degradation is dependent on the diluents as well as the dose rate (*26*). Due to this, further investigations of the radiolytic behavior of the GANEX system are necessary even though preliminary results look promising.

5. Fission- and Corrosion/Activation-Product Extraction

When extracting several corrosion/activation products (Fe, Ni, Cr, Co, Mn) and fission products (Rb, Sr, Y, Zr, Mo, Ru, Rh, Pd, Ag, Cd, Sb, Te, Cs, Ba) with the GANEX system it was found that a few of the metals were undesirably extracted (*24*). Three metals were identified as the most troublesome ones (Pd, Zr and Mo). This is however not an insurmountable problem and there are different ways to approach it. One way is to insert an extraction step before the actual GANEX process where the troublesome elements are extracted. Another approach is to add water soluble complexants to the aqueous phase which hinders the extraction of the unwanted elements in the GANEX process. Previously oxalic acid has been used in i.e. the DIAMEX process as a water soluble complexing agent to stop the extraction of troublesome fission products like zirconium and molybdenum (*9*). This is however not applicable in the GANEX process since it is known that oxalic acid precipitates plutonium.

There are some molecules that look promising for the prevention of fission product extraction. One of these is dioctyl sulfide that together with kerosene

could be used in a pre extraction step of Pd (*27*). Another one is methionine that has been known to form complexes with Pt and hence could be used as a water soluble complexing agent for Pd (*28*). A third molecule is mannitol which has been reported to form Mo complexes and therefore could be used to prevent the extraction of this and other metals in the GANEX process (*29*).

6. Metal Loading Conditions

An extraction experiment has been performed where the actinides ([235]U, [237]Np, [238]Pu and [241]Am) and one lanthanide ([152]Eu) have been added in trace amounts to a 4M nitric acid water phase loaded with fission products. The metals present were Rb, Sr, Y, Zr, Mo, Rh, Pd, Ag, Cd, Sb, Cs, Ba, La, Ce, Nd, Sm and Te in realistic concentrations (*9*, *30*, *31*) rendering a total concentration of over 9000ppm (*24*).

The distribution rations were somewhat lowered for Am and Pu compared to the case without metal loading but the D for both U and Np stayed the same. Since the D for Eu was decreased this actually rendered an average increase in separation factor (Table II).

Conclusion

With the support from several European Union Framework Programs much European research within the area of partitioning for transmutation has been conducted during the last 10-15 years. This research has, after many great achievements, in Europe led to the GANEX process. The concept of a GANEX process would bring large benefits industrially by implementing only a very few extraction steps compared to the extraction scheme PUREX-DIAMEX-SANEX-SESAME previously investigated. The novel GANEX extraction process developed at Chalmers University of Technology in Sweden meet many of the basic demands necessary for a viable partitioning process, indicating that GANEX could be a possible future process alternative.

Table II. An/Ln Separation Factors for extraction with 0.01M CyMe₄-BTBP and 30% TBP in cyclohexanone from metal loaded (>9000ppm) 4M HNO₃

Elements	*Separation factor*
Am / Eu	101
Pu / Eu	363
U / Eu	91
Np / Eu	28

References

1. Madic, C.; Hudson, M. J.; Liljenzin, J-O.; Glatz, J. P.; Nannicini, R.; Facchini, A.; Kolarik, Z.; Odoj, R. Final Report, European Union Project FI4I-CT-96-0010, European Commission Project Report EUR 19149; European Commission: Luxembourg, 2000.
2. Miguirditchian, M.; Chareyre, L.; Hérès, X.; Hill, C.; Baron, P.; Masson, M. *GANEX*, Proceedings from Global 2007, Boise, ID, September 2007.
3. Madic, C.; Testard, M.; Liljenzin, J-O.; Christiansen, B.; Ferrando, M.; Faccini, A.; Geist, A.; Modolo, G.; Gonza Mendoza, J. Final Report, CEA-R-6066; CEA-Valrho: Marcoule, France, 2004.
4. Madic, C.; Hudson, M. J.; Liljenzin, J.-O.; Glatz, J.-P.; Nannicini, R.; Facchini, A.; Kolarik, Z.; Odoj, R. *Prog. Nucl. Energy* **2002**, *40* (3−4), 523–526.
5. Hill, C.; Arnaud-Neu, F.; Espartero, A. G.; Desreux, J.-F.; Modolo, G.; Bourg, S.; Malmbeck, R.; Caravaca, C.; Harrison, M.; De Angelis, G.; Uhlir, J.; Ouvrier, N.; Madic, C. EUROPART, Final Activity Report, Contract F16W-CT-2003-508 854; 2007.
6. Arnaud-Neu, F.; Böhmer, V.; Casensky, B.; Casnati, A.; Desreux, J.-F.; Gruner, B.; Grüttner, C.; De Mendoza, J.; Pina, G.; Selucky, P.; Verboom, W.; Wipff, G. Final Report, European Union Project FIKW-CT- 2000-00088, Final Technical Report 6466; March 31, 2004.
7. Pyrometallurgical Processing Research Programme, Final Report, September 2000–August 2003, Contract FIKW-CT-2000-00049; 2003.
8. Bourg, S.; Caravaca, C.; Ekberg, C.; Hill, C.; Rhodes, C. Paper 9185, Proceedings from Global 2009, Paris, September 6−11, 2009.
9. Serrano-Purroy, D.; Baron, P.; Christiansen, B.; Malmbeck, R.; Sorel, C.; Glatz, J.-P. *Radiochim. Acta* **2005**, *93* (6), 351–355.
10. Madic, C.; Hudson, M. J.; Liljenzin, J.-O.; Glatz, J.-P.; Nannicini, R.; Facchini, A.; Kolarik, Z.; Odoj, R. *Prog. Nucl. Energy* **2002**, *40* (3–4), 523–6.
11. Ekberg, C.; Fermvik, A.; Retegan, T.; Skarnemark, G.; Foreman, M. R. S.; Hudson, M. J.; Englund, S.; Nilsson, M. *Radiochim. Acta* **2008**, *96* (4−5), 225–233.
12. Magnusson, D.; Christiansen, B.; Foreman, M. R. S.; Geist, A.; Glatz, J.-P.; Malmbeck, R.; Modolo, G.; Serrano-Purroy, D.; Sorel, C. *Solvent Extr. Ion Exch.* **2009**, *27* (2), 97–106.
13. Adnet, J. M.; Donnet, L.; Brossard, P.; Bourges, J. Process for the Electrochemical Oxidation of Am(III) to Am(VI) Usable for Separating Americium from Spent Nuclear Reprocessing Solutions. U.S. Patent 5609745, 1996.
14. Donnet, L., Adnet, J. M., Faure, N., Bros, P., Brossard, P., Josso, F. Session II, Proceedings of the 5th OECD-NEA International Information Exchange Meeting on Actinide and Fission Product Partitioning and Transmutation, Mol, Belgium, 1998.
15. Modolo, G., Odoj, R. Method for Separating Trivalent Americium from Trivalent Curium. European Patent EP 1664359B1, March 1, 2007.

16. Andersson, S.; Ekberg, C.; Foreman, M. R. S.; Hudson, M. J.; Liljenzin, J.-O.; Nilsson, M.; Skarnemark, G.; Spahiu, K. *Solvent Extr. Ion Exch.* **2003**, *21* (5), 621–636.
17. Ritcey, G. M. *Solvent Extraction Principles and Practice*, 2nd ed.; Rydberg, J., Cox, M., Musikas, M., Choppin, G., Eds.; Marcel Dekker, Inc: New York, 2004; pp 324−333.
18. Nilsson, M.; Nash, K. *Solvent Extr. Ion Exch.* **2007**, *25* (6), 665–701.
19. Burger, L. L. *J. Phys. Chem.* **1958**, *62* (5), 590–593.
20. Retegan, T.; Dubois, I.; Ekberg, C.; Fermvik, A.; Johnson Wass, T.; Skarnemark, G. *Solvent Extr. Ion Exch.* **2007**, *25*, 417–431.
21. Drew, M. G. B.; Foreman, M.; Hill, C.; Hudson, M.; Madic, C. *Inorg. Chem. Commun.* **2005**, *8* (3), 239–241.
22. Burger, L. L. *Prog. Nucl. Energy* **1959**, *2*, 307–319.
23. Geist, A.; Hill, C.; Modolo, G.; Foreman, M. R. S.; Weigl, M.; Gompper, K.; Hudson, M. J.; Madic, C. *Solvent Extr. Ion Exch.* **2006**, *24* (4), 463–483.
24. Aneheim, E.; Ekberg, C.; Fermvik, A.; Foreman, M. R S.; Retegan, T.; Skarnemark, G. Nuclear Chemistry and Industrial Materials Recycling; Chalmers University of Technology: Gothenburg, Sweden, unpublished.
25. Magnusson, D.; Christiansen, B.; Malmbeck, R.; Glatz, J.-P. *Radiochim. Acta* **2009**, *97*, 497–502.
26. Fermvik, A.; Laurance, B.; Ekberg, C.; Englund, S.; Retegan, T.; Zorz, N. *Dalton Trans.* **2009** (32), 6421–6430.
27. Torgov, V. G.; Tatarchuk, V. V.; Druzhinina, I. A.; Korda, T. M.; Renard, E. V. *At. Energy* **1996**, *80* (4), 251–256.
28. Davidson, Y. Y.; Chang, S.-C.; Norman, R. E. *Dalton Trans.* **1995**, *77*.
29. Hedman, B. *Acta Cryst.* **1977**, *B33*, 3077–3083.
30. Malmbeck, R.; Courson, O.; Pagliosa, G.; Römer, K.; Sätmark, B.; Glatz, J.-P.; Baron, P. *Radiochim. Acta* **2000**, *88* (12), 865–871.
31. Garcia Alonso, J. I.; Thoby-Schultzendorff, D.; Giovanonne, B.; Glatz, J.-P.; Pagliosa, G.; Koch, L. *J. Anal. At. Spectrom.* **1994**, *9*, 1209.

Chapter 11

Extraction Chromatographic Separation of Trivalent Minor Actinides Using *i*Hex-BTP/SiO₂-P Resin

N. Surugaya,* Y. Sano, M. Yamamoto, A. Kurosawa, and T. Hiyama

Japan Atomic Energy Agency, 4-33 Muramatsu, Tokai, Ibaraki 319-1194, Japan
***surugaya.naoki@jaea.go.jp**

The separation of trivalent minor actinides (Am(III) and Cm(III)) from lanthanides is a challenging issue because of difficulties associated with their mutual similarity in chemical behavior. However, this separation is important for the future nuclear fuel cycle for environmental friendship. Extraction chromatographic separation of the long-lived trivalent minor actinides has been performed to study the potential application of 2,6-bis(5,6-di-*iso*-hexyl-1,2,4-triazin-3-yl)-pyridine (*i*Hex-BTP) impregnated into a porous silica support coated with styrene-divinylbenzene copolymer (SiO₂-P). The adsorption and elution characteristics of Am(III) and Cm(III) in nitric acid medium have been investigated to separate them from lanthanides using a column packed with *i*Hex-BTP/SiO₂-P resin. Depending on the concentration of nitric acid solution as well as aqueous flow rate, a certain condition allowed us to selectively recover the fractions containing Am(III) and Cm(III) from a sample solution derived from the PUREX raffinate.

Introduction

Trivalent minor actinides like Am(III) and Cm(III) are present in nuclear wastes generated from spent nuclear fuel reprocessing activities. Their separation is important because the minor actinides with long half-life and high radiological toxicity are highly abundant in irradiated nuclear fuel (*1, 2*). Nowadays group partitioning used to reprocess spent nuclear fuels through a number of

stages as shown in Figure 1 is under investigation for future nuclear cycle in Japan. Uranium in dissolved spent nuclear fuels is coarsely separated by crystallization. Uranium, plutonium and neptunium are co-recovered by the extraction with tri-butyl phosphate (TBP). The minor actinides are separated from lanthanides and fission products by extraction chromatography (*3*, *4*) using extractants like octylphenyl-N,N-diisobutylcarbomoyl phosphine oxide (CMPO), bis triazinyl pyridine (BTP), N,N,N′,N′-tetraoctyl diglycolamide (TODGA), and di-(2-ethylhexyl) phosphoric acid (HDEHP). Americium and curium are mutually separated using ion exchange. Currently, extraction chromatography is being investigated for the separation of minor actinides from lanthanides by combination utilization of several ligands (Figure 1).

Extraction chromatography offers several advantages over conventional liquid-liquid extraction: less organic material is required, no third phase formation occurs, phase modifiers are not necessary, the equipment is simple and compact, and a rapid operation is possible. Therefore, extraction chromatography may be a suitable option for the separation of minor actinides from lanthanides as a part of advanced nuclear fuel cycle.

The mutual separation of minor actinides and lanthanides is generally very difficult due to the similarity in their chemical behavior. Some potential extractants have been proposed to facilitate the separation of Am and Cm from lanthanides. In 1999 Kolarik *et al.* firstly reported that BTP is one of the strongest candidates (*5*, *6*). The BTP containing nitrogen atom, which is a soft donor, has a greater extraction selectivity for 5f elements compared to 4f elements through the covalent coordination (*7–11*). Recent studies have been performed using 2,6-bis-(5,6-dialkyl-1,2,4-triazine-3-yl)-pyridine (R-BTP) derivatives like 2,6-bis-(5,6-dibutyl-1,2,4-triazine-3-yl)-pyridine (*n*Bu-BTP) (*12*) and its isomer *i*-Bu-BTP (*13*). In this study, we investigated the performance of 2,6-bis(5,6-di-*i*-hexyl-1,2,4-triazin-3-yl)-pyridine (*i*Hex-BTP), whose longer alkyl side-chains might facilitate the selective separation of minor actinides (Figure 2) and decrease its solubility in nitric acid. A series of preliminary experiments using *i*Hex-BTP in liquid-liquid extraction systems actually suggested that Am and Cm have high distribution ratios and separation factors from lanthanides in 1-3 M nitric acid media.

In this paper, *i*Hex-BTP was impregnated into a porous silica support coated with styrene-divinylbenzene copolymer (SiO$_2$-P) for the extraction chromatographic separation. The resulting *i*Hex-BTP/SiO$_2$-P resin has been used for a series of separation tests for Am and Cm existing in a real sample of highly radioactive liquid waste generated by the current PUREX process. This paper describes the experimental results and the adsorption characteristics of the *i*Hex-BTP/SiO$_2$-P resin based on the extraction chromatography using the sample solutions containing 1 and 3M nitric acid media.
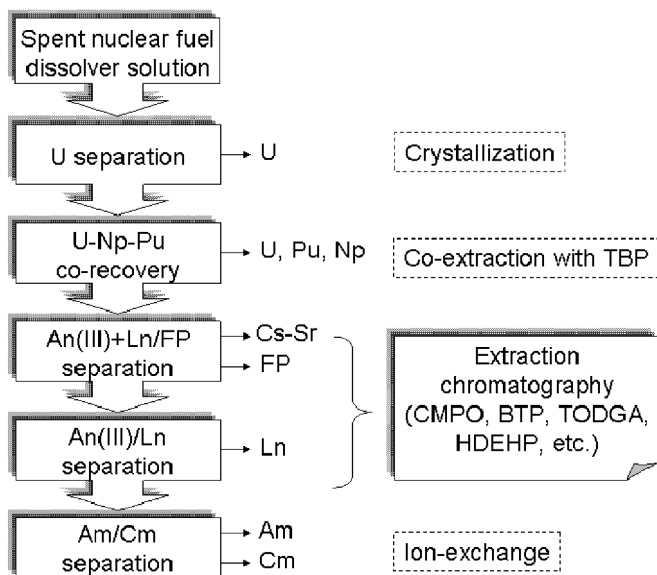
Figure 1. An advanced separation process for nuclear fuel cycle planed for the future in Japan (Extraction chromatography is under investigation as an option for separation of An(III) from Ln using several ligands).
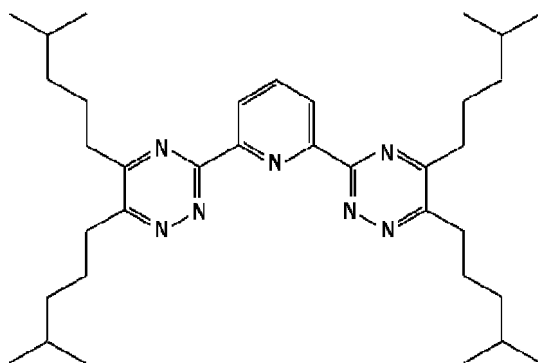

Figure 2. 2,6-bis(5,6-di-iso-hexyl-1,2,4-triazin-3-yl)-pyridine (iHex-BTP).

Experimental

Materials

The SiO$_2$-P resin was prepared according to the published procedures (*2*, *3*) using spherical silica particles with a diameter of 40-60 μm, a mean pore size of 600 nm, and a pore fraction of 0.69. The *i*Hex-BTP extractant obtained from the Institute of Research and Innovation was impregnated into the SiO$_2$-P resin based on the reported procedure. The extractant was placed in a glass flask and diluted with dichloromethane as a diluent. Subsequently, the dried SiO$_2$-P particles were added to the solution. The mixture was then shaken mechanically for 2h at room temperature. The diluent was evaporated under reduced pressure and the residue was finally dried up in vacuo. The weight ratio of *i*Hex-BTP to SiO$_2$-P resin was approximately 1:2. The *i*Hex-BTP/SiO$_2$-P resin was transferred into a φ0.8 cm × h4 cm Bio-Rad poly-prep column with a bed volume of 2 mL. All commercially available chemicals like nitric acid were of analytical grade and were used without further purification. The water used for buffer preparation was deionized, sub-boiled, distilled, and further purified using the Milli-Q academic purification system. Radiotracers, [241]Am and [244]Cm, for analytical calibration were obtained from laboratory stocks. Stock standard solutions were prepared from reagent grade chemicals obtained from Wako Chemical Co., Inc. for other metal ions.

The nuclear waste sample was derived from a PUREX raffinate, which was generated at the Tokai Reprocessing Plant of the Japan Atomic Energy Agency. The reprocessed spent fuels originated from the advanced thermal reactor FUGEN (Burn-up = 17.2 GWd/t, cooling time ≈ 2800 d). Major fission product (FP) elements selected in the sample included La, Ce, Nd, Sm, Eu, Gd, Sr, Y, Zr, Mo, Ru, Pd, and Ba, which were dissolved in 3 M nitric acid medium. The concentrations of Am and Cm were 35 and 0.56 mg/L, respectively. The highly radioactive sample was treated in shielded analytical facilities.

Separation Tests

The column packed with *i*Hex-BTP/SiO$_2$-P resin was first conditioned using a nitric acid solution (1 or 3 M) at a volume that was 30 times greater than the bed volume. Then, a sample solution of 1 mL was introduced into the packed column using a custom made pipetting device. The nitric acid concentration was about 3 M in the original sample. Sample loading was carried out using the original sample or its diluted solution, which was adjusted to 1 M by adding 0.01 M nitric acid. Taking advantage of the high affinity and selectivity of the *i*Hex-BTP stationary phase for trivalent minor actinide species in nitric acid media, 3 or 1 M nitric acid (8 mL) was passed through the column to wash off the lanthanides and other fission products. Water (15 mL) was subsequently added to elute Am and Cm. All the fractions were collected as 0.5 mL in the course of the experiment. The chromatographic separations were performed at room temperature by gravity flow with no pressure added. The flow rate was about 0.1-0.4 mL/min. Each collected fraction was diluted with 1 M nitric acid (500-5000-fold dilution) for subsequent measurements. An Elan 6000 inductively coupled plasma mass

spectrometer (Perkin Elmer) was used to analyze [241]Am and [244]Cm. An SPS 7700 inductively coupled plasma atomic emission spectrometer (Seiko Instrument) was used to analyze other elements. Each instrument was installed in a containment glove-box for handling radioactive sample solutions.

Results and Discussion

Extraction Chromatographic Behavior and Acid Dependence of Extraction Chromatographic Separation

The chromatographic separation profiles of Am, Cm, and other selected FP elements in the sample are shown in Figure 3a. The nitric acid concentration was 3 M in the sample and washing solution, and the flow rate was 0.3-0.4 mL/min. The relative elemental concentrations determined in each fraction with respect to the initial sample, C/C_0, were plotted as a function of effluent volume. The plots show that almost all elements, except Am, Cm and a part of Sm and Eu, were eluted with 3 M nitric acid during the column wash step, while Am and Cm were eluted immediately with addition of water. The chromatographic behavior of Am and Cm was quite similar. This experiment also reveals that Sm and Eu appeared both in nitric acid and water fractions, indicating that Am and Cm could be separated from the FP elements, except a part of Sm and Eu. The distribution coefficient K_d of each element was calculated by:

$$K_d = \sum \frac{C_0 - C_{si}}{C_{si}} \times \frac{V}{W} \qquad (1)$$

where C_0 denotes the initial concentration of element in the sample. C_{si} is the concentration of element in ith eluted fraction (1 or 3 M nitric acid); V is the volume of aqueous phase and W is the weight of dried resin. K_d values calculated for selected representative elements are listed in Table 1. The separation factor between minor actinides (Am, Cm) and the adsorptive lanthanides (Sm, Eu) which was calculated as the ratio of their K_d values, was about 10; this is not high enough to separate them completely. It is also noted that Pd adsorbed strongly on the resin and was not eluted in water.

A similar experiment was carried out for the sample solution containing 1 M nitric acid and 1 M nitric acid was used as washing solution at a flow rate of about 0.1 mL/min (Figure 3b). This flow rate was slower than in the previous experiment, because the flow rate control was unreliable in gravity experiments. In this experiment, Am and Cm were eluted with addition of water and the water fractions did not contain Sm and Eu. In addition, Pd was not detected in the original sample in this experiment. This fortuitous observation may indicate the potential of Pd precipitation under these experimental conditions and/or under sample storage circumstances in the hot cell. Moreover, Ru concentration was not determined because of analytical problems. Despite missing some experimental data, K_d values for the analyzed elements are summarized in Table 1. The separation factor between Am/Cm and other elements, including Sm and Eu, was found to be about 10^1 to 10^2. As the result, a large number of the coexisting matrix

elements showed no or little effect on the separation, and they were separated from Am and Cm fractions. Excellently selective separation and recovery of Am and Cm was therefore achieved by adjusting the nitric acid concentration to 1 M using extraction chromatography with *i*Hex-BTP/SiO$_2$-P resin.
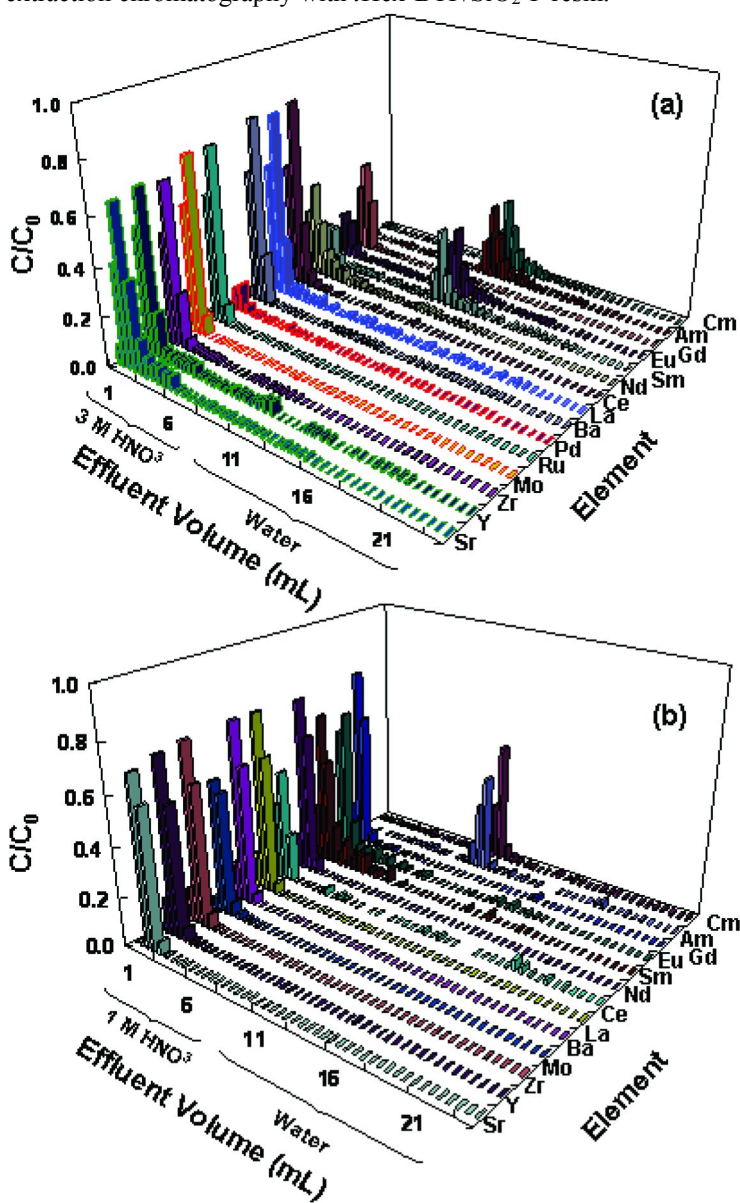

Figure 3. Extraction chromatographic profiles of selected elements with iHex-BTP/SiO$_2$-P resin. Sample: PUREX raffinate, temperature: 25°C, nitric acid concentration: (a) 3 M, and (b) 1M, flow rate: (a) 0.3-0.4 mL/min. and (b) 0.1 mL/min.

Table 1. Distribution coefficients, K_d, of selected elements obtained from extraction chromatographic separation with *i*Hex-BTP/SiO$_2$-P resin at different nitric acid concentrations using a PUREX raffinate sample[a]

Element	Distribution coefficient, K_d	
	at 3 M	at 1 M
Sr	44	83
Y	48	71
Zr	65	71
Mo	71	85
Ru	81	-
Pd	250	-
Ba	57	70
La	53	68
Ce	62	71
Nd	70	70
Sm	161	47
Eu	164	62
Gd	101	72
Am	989	1374
Cm	1608	592

[a] Temperature: 25°C.

Recovery Yield

Table 2 shows recovery yields for the elements in the extraction chromatographic separation with the *i*Hex-BTP/SiO$_2$-P resin using the sample solutions containing 3 and 1 M nitric acid, respectively. The recovery yields of Am and Cm were 50-60% which are much less than 100%, suggesting possible hydrolysis of Am and Cm nitrates in elution with water. The use of a very dilute nitric acid solution (0.1-0.01 M) as eluent may be able to prevent the hydrolysis. Moreover, elution of Am, Cm, and other elements using nitric acid or water by gravity flow is subject to slow kinetics, which causes these elements to remain attached to the resin. In addition, radiolytic degradation of *i*Hex-BTP/SiO$_2$-P resin may be one of the reasons for incomplete recovery.

Table 2. Recovery yields of selected elements in extraction chromatographic separation with *i*Hex-BTP/SiO₂-P resin using a PUREX raffinate sample[a]

Element	Recovery yield, %	
	at 3 M HNO₃ sample	at 1 M HNO₃ sample
Sr	115	67
Y	115	76
Zr	76	77
Mo	71	60
Ru	62	-
Pd	26	-
Ba	92	77
La	92	77
Ce	79	58
Nd	73	77
Sm	82	105
Eu	78	94
Gd	53	82
Am	60	50
Cm	58	60

[a] Temperature: 25°C.

Conclusions

We demonstrated that extraction chromatography using a column packed with *i*Hex-BTP/SiO₂-P resin is a suitable technique for the selective separation and recovery of trivalent minor actinides like Am(III) and Cm(III) from lanthanides existing in highly radioactive nuclear waste. Although more comprehensive experiments are required, the optimal nitric acid concentration in this study was found to be 1 M in the sample solution to achieve high separation factors for Am and Cm from lanthanides. Thus, the nitric acid concentration should be adjusted to 1 M prior to separation. We observed that Am and Cm elution recovery using water was incomplete. Overall, approximately 60% of Am and Cm was recovered in both tests using the sample solutions with 1 and 3 M nitric acid, respectively. Nevertheless, the separation procedures and experimental results described above are useful for further optimizing separation and recovery conditions using the *i*Hex-BTP/SiO₂-P resin for extraction chromatography. An unexpected finding was the observation of strong affinity of Pd to the *i*Hex-BTP/SiO₂-P resin. Some complexing agents may be useful to remove the adsorbed Pd for repeatedly using the resin packed in the column.

References

1. Wei, Y.-Z.; Hoshi, H.; Kumagai, M.; Asakura, T.; Morita, Y. *J. Alloys Compd.* **2004**, *374*, 447–450.
2. Hoshi, H.; Wei, Y.-Z.; Kumagai, M.; Asakura, T.; Morita, Y. *J. Alloys Compd.* **2006**, *408-412*, 1274–1277.
3. Wei, Y.-Z.; Kumagai, M.; Takashima, Y. *Nucl. Technol.* **2000**, *132*, 413–423.
4. Hoshi, H.; Wei, Y.-Z.; Kumagai, M.; Asakura, T.; Morita, Y. *J. Alloys Compd.* **2004**, *374*, 451–455.
5. Kolaric, Z.; Müllich, U.; Gassner, F. *Solvent Extr. Ion Exch.* **1999**, *17*, 23–32.
6. Kolaric, Z.; Müllich, U.; Gassner, F. *Solvent Extr. Ion Exch.* **1999**, *17*, 1155–1170.
7. Mathur, J. N.; Murali, M. S.; Nash, K. L. *Solvent Extr. Ion Exch.* **2001**, *19* (3), 357–390.
8. Jensen, M. P.; Bond, A. H. *J. Am. Chem. Soc.* **2002**, *124* (33), 9870–9877.
9. Miguirditchian, M.; Guillaneus, M. D.; Guillaumont, D.; Moisy, P.; Madic, C.; Jensen, M. P.; Nash, K. L. *Inorg. Chem.* **2005**, *44* (5), 1404–1412.
10. Modolo, G.; Nabet, S. *Solvent Extr. Ion Exch.* **2005**, *23*, 359–373.
11. Petit, L.; Adamo, C.; Maldivi, P. *Inorg. Chem.* **2006**, *45* (21), 8517–8522.
12. Wei, Y.-Z.; Hoshi, H.; Kumagai, M.; Asakura, T.; Uchiyama, G. *J. Nucl. Sci. Technol.* **2002**, *3*, 761–764.
13. Zhang, A.; Kuraoka, E.; Kumagai *J. Radioanal. Nucl. Chem.* **2007**, *273* (3), 455–464.

Recent Advances in the Development of the Hybrid Sulfur Process for Hydrogen Production

H. R. Colon-Mercado, M. C. Elvington, J. L. Steimke, T. J. Steeper, D. T. Herman, M. B. Gorensek, W. A. Summers, and D. T. Hobbs*

Savannah River National Laboratory, Savannah River Nuclear Solutions, LLC, Aiken, SC 29808
***david.hobbs@srnl.doe.gov**

Thermochemical processes are being developed to provide global-scale quantities of hydrogen. A variant on sulfur-based thermochemical cycles is the Hybrid Sulfur (HyS) Process, which uses a sulfur dioxide depolarized electrolyzer (SDE) to produce the hydrogen. In the HyS Process, sulfur dioxide is oxidized in the presence of water at the electrolyzer anode to produce sulfuric acid and protons. The protons are transported through a cation-exchange membrane electrolyte to the cathode and are reduced to form hydrogen. In the second stage of the process, the sulfuric acid by-product from the electrolyzer is thermally decomposed at high temperature to produce sulfur dioxide and oxygen. The two gases are separated and the sulfur dioxide recycled to the electrolyzer for oxidation. The Savannah River National Laboratory (SRNL) has been exploring a fuel-cell design concept for the SDE using an anolyte feed comprised of concentrated sulfuric acid saturated with sulfur dioxide. The advantages of this design concept include high electrochemical efficiency and small footprint compared to a parallel-plate electrolyzer design. This paper will provide a summary of recent advances in the development of the SDE for the HyS process.

Introduction

Alternative energy generation and storage systems are the subject of increased interest and innovative research to meet continually increasing energy demands in the face of a diminishing supply of nonrenewable fossil fuels. Hydrogen is an attractive energy carrier since it contains the highest energy per mass ratio of any conventional fuel. Transitioning to a hydrogen-based energy system will require significant scale-up compared to existing capabilities. These global-scale demands can be met by water electrolysis or through thermochemical water-splitting cycles. Water electrolysis offers several advantages over other production methods, however, the technology required and energy input can make hydrogen produced by this method expensive. Thermochemical water splitting cycles offer an alternative highly efficient route for hydrogen production (*1*, *2*). Among the many possible thermochemical cycles for the production of hydrogen, the sulfur-based cycles lead in overall energy efficiency.

The Hybrid Sulfur (HyS) Process is a sulfur-based two-step thermochemical-electrochemical hybrid cycle. In this process sulfuric acid is thermally decomposed at high temperature (900 °C) producing SO_2 [eqn 1]. H_2SO_4 saturated with SO_2 is then pumped into a SDE. The SDE electrochemically oxidizes sulfur dioxide to form sulfuric acid at the anode [eqn 2] and reduces protons to form hydrogen at the cathode [eqn 3]. The overall electrochemical reaction consists of the production of H_2SO_4 and H_2 [eqn 4], while the entire cycle produces H_2 and O_2 from H_2O with no side products [eqn 5].

$$H_2SO_4 \rightarrow SO_2 + \tfrac{1}{2}O_2 + H_2O \qquad [1]$$

$$SO_2 + 2H_2O \rightarrow H_2SO_4 + 2H^+ + 2e^- \qquad [2]$$

$$2H^+ + 2e^- \rightarrow H_2 \qquad [3]$$

$$SO_2 + 2H_2O \rightarrow H_2SO_4 + H_2 \qquad [4]$$

$$2H_2O \rightarrow 2H_2 + O_2 \qquad [5]$$
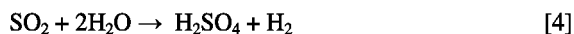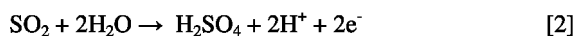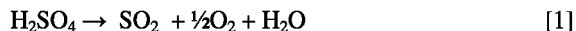
Sulfur dioxide oxidation has a reversible half-cell potential of -0.158 V (SHE), while low temperature water electrolysis has a reversible half cell potential of -1.23 V (SHE), thus the HyS process requires lower electrical energy input. Due to ohmic, kinetic, and mass transport overpotential losses, an operating cell potential of 0.6 V has been targeted for HyS electrolyzer operation at a current density of 500 mA cm^{-2}. This operating condition would result in an estimated overall process efficiency of 41% with approximately 30% of the energy input powering the electrolyzer.

The development of a liquid-fed HyS electrolyzer began in the late 1970s and continued until the early 1980s. At this stage of development, the SDE featured a parallel-plate filter-press type design with a separator/membrane to keep the anolyte and catholyte compartments separate (*4*). Approximately five years ago renewed interest in the HyS process initiated a review of the SDE design concept, since significant advances have occurred in electrochemical technology over the last 30 years, particularly in the development of hydrogen fuel cells. From this

review, SRNL adopted a fuel cell design concept for the SDE as shown in Figure 1 (*3*, *5*, *6*). The heart of the fuel cell is the membrane electrode assembly or MEA, which consists of the anode, cation-exchange membrane and cathode (see Figure 1). To optimize the performance of the SDE, we have investigated key properties of electrocatalysts and cation-ion exchange membranes. This paper presents a summary of these findings as well as results of work to identify operating conditions that limit the formation of an undesired sulfur-rich layer between the cathode and membrane.

Experimental

All membranes were hydrated prior to testing by immersing in deionized water. Commercially available membranes included perfluorinated sulfonic acid (PFSA) membranes (*7*) from DuPont and polybenzimidizole (PBI) (*8*) membranes from BASF. Experimental membranes included the following; (1) sulfonated Diels-Alder polyphenylenes (SDAPP) (*9*) from Sandia National Laboratories (SNL), (2) PFSA/fluorinated ethylene propylene (FEP) blends from Case Western Reserve University, and (3) perfluorocyclobutane-biphenyl vinyl ether (BPVE) and perfluorocyclobutane-biphenyl vinyl ether hexafluoroisopropylidene (BPVE-6F) polymer blends from Clemson University (*10*).

The chemical stability of the membranes was determined by immersing the membrane into a 9.2 M (60 wt%) H_2SO_4 at 80 °C for 24 hours. Following acid exposure, the membranes were rinsed and stored in deionized water. Each membrane was inspected for visible signs of chemical attack. Fourier transform infrared spectroscopy (FTIR) was used with the attenuated total reflectance (ATR) sampling technique to determine if chemical attack occurred. FTIR spectra were measured with a Jasco FT/IR-6300 instrument before and after exposure to the hot, concentrated sulfuric acid solution.
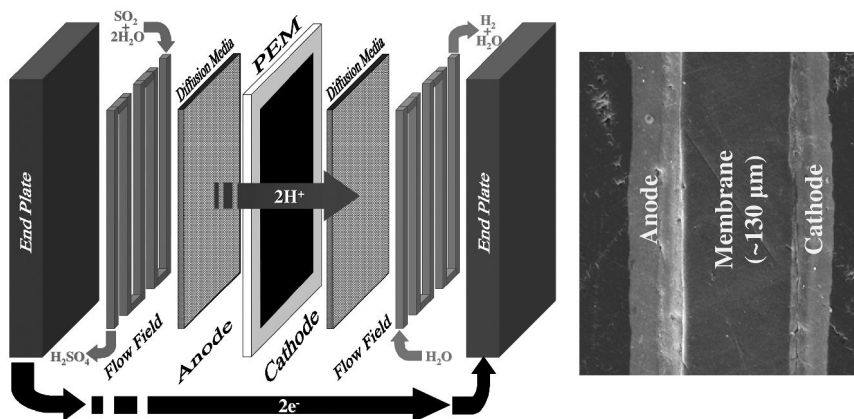
Figure 1. Schematic diagram of SDE (left) and scanning electron micrograph showing the anode (Pt/C), membrane (Nafion®) and cathode (Pt/C) regions of the membrane electrode assembly, MEA (right).
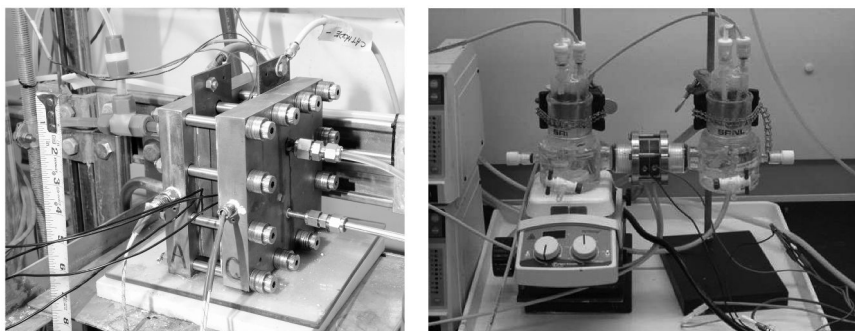
Figure 2. Photograph of single-cell electrolyzers with working area of 54.8 cm² (left) and 2.5 cm² (right).

Membrane transport of SO_2 was evaluated under non-polarized conditions using a permeation cell consisting of two glass chambers joined by a Teflon™ bridge where the membrane is secured. The bridge consists of a diffusion layer in the left chamber where acid saturated with SO_2 is pumped into the anolyte-membrane interface. Additionally, the diffusion media presses the membrane to the working electrode, which is supported by a perforated tantalum plate that provides electrical connection to the working electrode. Finally, a non-conductive diffusion media separates the tantalum support from the counter electrode in order to allow the flow of fresh acid pumped to the counter electrode without short circuiting the cell. Further details on the SO_2 transport measurement method as well as that for ionic conductivity and resistivity are provided in reference (*11*).

Evaluation of catalyst performance featured cyclic voltammetry (CV) and linear sweep voltammetry (LSV) using a Bioanalytical Systems (BAS) B/W electrochemical analyzer. Sulfuric acid solutions were prepared by diluting reagent grade sulfuric acid (Fisher Scientific) with deionized, distilled water. Prior to the measurements all solutions were purged of oxygen by bubbling nitrogen. For tests evaluating the oxidation of SO_2, we continuously bubbled gaseous SO_2 (Scott Specialty Gases) through the sulfuric acid solution. CVs were performed at a scan rate of 50 mV/sec and in a potential window between 1004 mV and -100 mV vs. Ag/AgCl (3M NaCl). LSVs were performed in the potential window between 804 mV and 104 mV vs. Ag/AgCl at a scan rate of 5 mV/sec. The experiments were carried out at temperatures ranging from 30 °C up to 70 °C and sulfuric acid concentrations of 30 – 70 wt%. The curves were repeated until a stable performance was obtained. Both CV and LSV measurements were performed starting from the anodic potential and going in the cathodic direction.

Electrolyzer performance of membranes and catalysts was evaluated by fabricating a MEA of appropriate size and installing the MEA in a SDE. Figure 2 provides photographs of the two experimental electrolyzers used in the performance testing. The larger SDE features a working area of 54.8 cm² and can be operated at temperatures of between 30 and 80 °C and pressures of 1 – 6 atmospheres. The smaller SDE has a working area of 2.5 cm² and can be operated at temperatures of between 30 and 80 °C at atmospheric pressure.

Results and Discussion

The SRNL concept for the SDE features a fuel cell design as shown schematically in Figure 2. Concentrated sulfuric acid containing dissolved SO_2 is pumped into the anolyte compartment and transported to the anode on the surface of the MEA. Protons produced at the anode transport across the cation-exchange membrane, reach the cathode and are reduced to form hydrogen. Hydrogen transports into the catholyte and exits the cell. Key components of the SDE include the anode, cathode and cation exchange membrane, which comprise the MEA for the cell (see Fig. 2), as well as current collector and flow fields for liquids and gases.

Flow fields for the anolyte and catholyte compartments used in the electrolyzer testing consisted of grooved graphite carbon pieces that are inserted into the thicker graphite carbon blocks along with either carbon paper (anode side) or carbon cloth (cathode side) placed between the carbon blocks and the MEA (see Figure 1). Stainless steel plates that are electrically isolated from the carbon blocks serve as endplates. These parts are sandwiched together in a filter-press arrangement and fastened with bolts. Heating elements are inserted into the endplates to provide auxiliary heating for higher temperature experiments.

Catalyst Testing

The anode and cathode materials are key components of the SDE to ensure that the electrolyzer operates at maximum energy efficiency with long lifetimes. Compared to the cathode, the kinetics of the electrochemical oxidation of SO_2 at the anode are very slow. Consequently, most of the inefficiencies of the electrolyzer arise from the anode reaction kinetics. Thus, to date we have focused on identifying materials that feature excellent catalytic activity and chemical stability for the oxidation of sulfur dioxide.

Fuel cells today feature electrodes comprised on fine metal powders supported on a carbon substrate. These types of materials can exhibit much different catalytic activity compared to the bulk metal powders that were used in the early development effort for the Hybrid Sulfur electrolyzer. The early testing featured a number of metals including platinum, palladium and other noble and transition metals (*12*). Of these, platinum received the most attention, although palladium was reported to be an excellent catalyst for the oxidation of sulfur dioxide. Thus, we investigated the performance of platinum and palladium supported on carbon as well as binary and ternary alloys of noble metals and transition metals.

Linear sweep voltammetry indicated the catalytic activity of both platinum deposited on carbon black (Pt/C) and palladium deposited on carbon black (Pd/C) changes with sulfuric acid concentration, temperature and with the number of cycles (*13*). A potential window of 0.30 V to 1.00 V vs. SHE was selected to avoid the reduction of SO_2 to S, which could passivate the catalyst surface, and avoid the dissolution of the metal catalysts at higher potentials (*14*). The open circuit voltage increased as the acid strength increases. For example, potentials for Pt/C measured 0.50 V, 0.56 V and 0.63 V vs. SHE in 3.5 M (30 wt%), 6.5 M (50 wt%) and 10.5 M (70 wt%) H_2SO_4 solutions, respectively. For Pd/C, the potentials measured 0.59

V, 0.66 V and 0.73 V vs. SHE, in the 3.5 M, 6.5 M and 10.4 M H_2SO_4 solutions, respectively. In addition to a lower open circuit voltage, Pt/C exhibited higher exchange currents than Pd/C over all H_2SO_4 solution concentrations. In general, the activation energy for sulfur dioxide on Pt/C was less than half of that measured for Pd/C (*13*).

Cyclic voltammetry of Pt/C and Pd/C in concentrated H_2SO_4 solutions revealed that platinum became activated and palladium became deactivated with increasing number of cycles. Figure 3 presents the measured current as a function of cycle number for the oxidation of sulfur dioxide in 3.5 M H_2SO_4 solution at 30 °C. Pt/C shows a modest current initially, which more than doubles with cycle number up to a maximum value of about 30 A/mg Pt after 12 cycles. After reaching a maximum value, the current remained constant with additional cycles. In contrast to Pt/C, Pd/C exhibits a much higher initial current (31.9 A/mg Pd), which rapidly diminishes with each cycle and falls by more than 98% after 35 cycles.

The enhancement of electrocatalytic activity for Pt/C during the cyclic voltammetry experiment likely reflects reduction of SO_2 to S or partially reduced SO_2 onto the catalysis surface. Sulfur-containing deposits are well known to change the electrode reactivity by altering the binding characteristics of surface sites (*15*). For Pd/C, loss of activity likely reflects attack of the palladium leading to sintering of the particles and overall deactivation. In view of these results and the greater stability of the Pt/C catalyst, we conclude that Pt/C is a superior electrocatalyst to Pd/C for SO_2 oxidation in concentrated H_2SO_4 solutions.

Note however, Pt/C shows evidence of deterioration when polarized in 70 wt% H_2SO_4 solution at 50 °C or higher. Operating conditions targeted for the SDE include H_2SO_4 concentrations as high as 70 wt% and temperatures of 120 – 140 °C. Thus, further development of the anode electrocatalyst is needed to provide a material that can successfully perform in concentrated H_2SO_4 solutions at elevated temperatures.

To this end we have more recently initiated studies of binary and ternary metal alloy powders as anode catalyst materials. Figure 4 provides Tafel plots for the baseline Pt/C material as well as a binary alloys, Pt/Co/C and Pt/Ru/C, and ternary alloys, Pt/Co/Cr/C, Pt/Co/Ni/C and Pt/Co/Ir/C. Under the test condition, the Pt/C baseline material exhibited an open-circuit potential of 0.507 V (vs. SHE). Three of the experimental catalyst materials exhibited lower open-circuit potential and exchange currents equal to that of Pt/C indicating higher catalytic activity. These alloys included Pt/Co/Cr/C (open-circuit potential = 0.485 V vs. SHE), Pt/Co/C (0.488 V) and Pt/Co/Ni/C (0.0.501 V). Testing is in progress to determine the stability and catalytic properties of these promising materials at higher H_2SO_4 concentrations and temperatures.
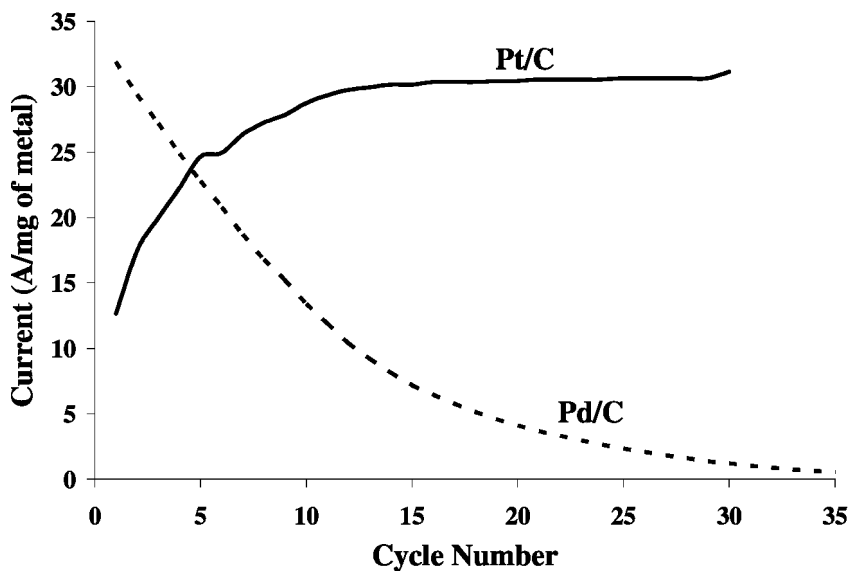
Figure 3. SO₂ Oxidation Current versus Cycle Number in 3.5 M H₂SO₄ solution at 30 °C.
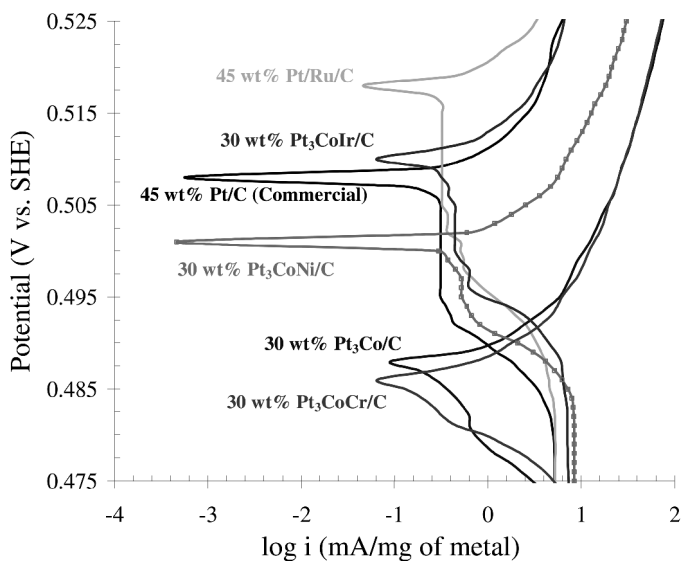
Figure 4. Tafel plots for Pt/C as well as binary and ternary alloys of Pt and other noble and transition metals

Ion-Exchange Membrane Testing

The ion-exchange membrane is a key component of the electrolyzer as it provides a physical and electrically-insulating barrier between the anode and cathode and serves as the electrolyte for conducting protons from the anode to the cathode. Key attributes of the ion exchange membrane are chemical stability to hot, concentrated H_2SO_4 solutions, electrically insulating, good ionic conductivity and low permeability to sulfur dioxide. From previous testing on the Hybrid Sulfur electrolyzer development as well as recent developments in fuel cell and industrial electrolyzers, the perfluorinated sulfonic acid (PFSA) class of membranes such as the Nafion® family offered by the E.I. DuPont Co. appeared especially suited for use in the electrolyzer. Other candidate membranes included (1) sulfonated Diels-Alder polyphenylene (SDAPP), (2) perfluoro-sulfonimide (PFSI), (3) perfluorocyclobutane-biphenyl vinyl ether (PBVE) and perfluorocyclobutane-biphenyl vinyl ether hexafluoroisopropylidene (PBVE-6F) polymer blends, (4) polyetheretherketone (PEEK) and (5) polybenzimidazole (BPI).

The chemical stability of the membranes in a corrosive environment was examined to provide insight into long-term performance. The PEEK family of membranes was found to be unstable in hot, concentrated H_2SO_4 solution and, therefore, is not a suitable material for this application. Testing indicated that all PFSA-type membranes exhibited no measurable degradation when exposed to 9.2 M H_2SO_4 solution for 24 hours at 80° C. Also, no degradation was observed for SDAPP, PBVE and PBVE-6F membranes. We did observe small changes in peak intensities in the 800 to 1200 cm^{-1} region for the Celtec V PBI membrane sample. We attribute the changes to the substitution of H_2SO_4 for H_3PO_4 in the membrane. No other spectral shifts are observed for the PBI membrane indicating the polymer backbone remained intact during the test.

The membranes exhibiting excellent chemical stability were further evaluated to determine SO_2 transport characteristics, conductivity and performance in a bench-scale liquid –fed electrolyzer. Table 1 provides a summary listing of the membrane characteristics. The reported conductivity is the through-plane conductivity and current density is that measured in the 2.5 cm^2 single cell electrolyzer operated at a potential of 1.0 V at 80 °C and atmospheric pressure.

The Nafion® 115 membrane showed a high through-plane conductivity (0.0241 S cm^{-1}) and good electrolyzer performance (270 mA cm^{-2}) at 80 °C, while having among the highest measured SO_2 transport (6.10 x 10^{-8} cm^2 s^{-1}). Nafion® 211, which is a much thinner membrane, exhibited a much lower conductivity (0.0159 S cm^{-1}), but lower (i.e., better) SO_2 transport (5.09 x 10^{-8} cm^2 s^{-1}) and excellent electrolyzer performance (393 mA cm^{-2}) compared to the Nafion® 115 membrane. Introduction of a layer of fluorinated ethylene propylene (FEP) to a PFSA membrane produced a material (Case Western PFSA/FEP blend) with much lower SO_2 transport (1.99 x 10^{-8} cm^2 s^{-1}). Note, however, that this membrane exhibited a lower conductivity (0.0096 S cm^{-1}) and poorer electrolyzer performance (228 A cm^{-2}) compared to the baseline Nafion® 115 membrane.

Table 1. SO$_2$ flux, SO$_2$ transport, conductivity, and current density (performance in HyS electrolyzer) is shown along with membrane thickness for a number of commercially available and experimental membranes

Supplier	Membrane Classification	Thickness (μm)	SO$_2$ Flux (mol SO$_2$ s^{-1} cm^{-2}) x 10^{-9}	SO$_2$ Transport (cm^2 s^{-1}) x10^{-8}	Conductivity (S cm^{-1})	Current Density (mA cm^{-2})
Dupont Nafion® 115	PFSA	127	5.23	6.10	0.0241	270
Dupont Nafion® 211	PFSA	25	21.8	5.09	0.0159	393
Case Western Reserve University	PFSA-FEP Blend	53	4.09	1.99	0.0096	228
Sandia National Laboratories	SDAPP	50-85	11.1	7.79	0.0328	286
Clemson University	BPVE	18	21.2	3.50	0.0048	320
Clemson University	BPVE/BPVE-6F 1:1 Blend	16	16.2	2.37	0.0063	337
Clemson Univeristy	BPVE/BPVE-6F 2:1 Blend	19	17.6	3.07	0.0109	335
BASF Celtec-V	PBI	100	2.14	1.99	nd	344

The SDAPP membrane exhibited excellent proton conductivity (0.0328 S cm^{-1}) and good electrolyzer performance (286 A cm^{-2}). However, the SO_2 transport (7.79 x 10^{-8} cm^2 s^{-1}) was the highest of any tested membrane. The perfluorinated cyclobutyl-based membranes supplied by Clemson University also show promise for this application. The BPVE and BPVE/BPVE-6F blends all showed reduced SO_2 transport, lower conductivity and better electrolyzer performance compared to the baseline Nafion® 115 membrane. The PBI membrane, Celtec-V, performed very well in the electrolyzer with low SO_2 transport (1.99 x 10^{-8} cm^2 s^{-1}).

Membrane testing has identified a number of candidate materials in addition to the current baseline material, Nafion® 115. Modifications to the Nafion®-class of membranes as well as new types of fluorinated polymers have been shown to reduce SO_2 transport while maintaining good performance in a bench-scale electrolyzer at 80 °C. Hydrocarbon membranes such as the SDAPP and PBI materials also are attractive candidates based on testing results described above as well as the potential for even better performance at higher temperatures. For example, preliminary results indicate excellent current densities at low cell voltages in tests with these experimental membranes in a SO_2-gas fed electrolyzer.

Sulfur Layer Formation

Cell voltage is influenced by a number of operating parameters and conditions including the current density, cell temperature, concentration of sulfur dioxide in the anolyte, anolyte flowrate, membrane type and thickness and concentration of sulfuric acid. Over the course of testing various MEAs in the single cell electrolyzer (see Fig 2), it was observed that the cell voltage generally increased while maintaining constant current conditions (*16*). The small gradual increase in cell voltage suggested that there may be chemical and/or physical changes to the MEA over the course of a test. Thus, after a 100-hour test, we recovered the MEA from the cell and used scanning electron microscopy (SEM) to determine if there were any visible signs of change.

Figure 5 shows a SEM image of MEA-12 indicating a sulfur-rich layer between the cathode and membrane that is almost as thick as the membrane. The layer is conductive as evidenced by the small increase in cell voltage. However, as a result of the layer formation, the MEA is becoming thicker and is pushed into the flow field channels. The expansion of the MEA into the flow channel also increases the pressure drop by restricting flow in the flow field. Ultimately, the formation of the sulfur-rich layer would result in mechanical failure of the MEA. Additional tests established that the sulfur-rich layer began forming within about 10 hours of cell operation. Interestingly, the sulfur-rich layer is not observed when the electrolyzer is operated at atmospheric pressure or with a gas fed anolyte.

MEA-12
(Nafion® 115)

Pt: 0.50 wt%
C: 35.7 wt%
S: 58.7 wt%
F: 5.0 wt%

Pt: 0.32 wt%
C: 42.6 wt%
S: 49.7 wt%
F: 7.3 wt%

Pt: 2.2 wt%
C: 57.5 wt%
S: 14.4 wt%
F: 25.9 wt%

Pt: 20.9 wt%
C: 69.5 wt%
S: 5.2 wt%
F: 4.4 wt%

Membrane thickness

Pt: 14.3 wt%
C: 80.8 wt%
S: 4.9 wt%

Cathode

Anode
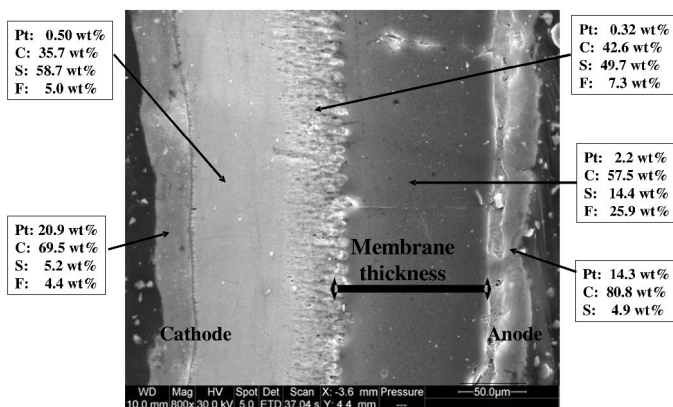
Figure 5. SEM image of MEA-12 showing a sulfur-rich layer between the cathode and membrane. Elemental content is that determined qualitatively by energy dispersive analysis of x-rays.

The formation of a sulfur-layer at the cathode and membrane interface is believed to be due to chemical reactions involving sulfur dioxide that has reached the cathode/membrane interface. These reactions include sulfur dioxide reacting with hydrogen to form hydrogen sulfide (reaction 6) and hydrogen sulfide reacting with sulfur dioxide to form elemental sulfur (reaction 7) (*16*). Reaction 6 is more energetically favored than reaction 7 and is preferable in that hydrogen sulfide is a gas and would not likely form a physical layer to the degree that elemental sulfur would under the cell operating conditions.

$$SO_2 + 3H_2 = H_2S + 2H_2O \qquad [6]$$

$$2H_2S + SO_2 = 3S + 2H_2O \qquad [7]$$
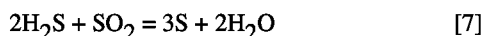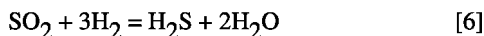
We hypothesized that by minimizing the amount of sulfur dioxide that reaches the cathode, we could limit reactions to that of reaction 6 and not form a sulfur-rich layer in the MEA. Changes that would minimize sulfur dioxide reaching the cathode/membrane interface include (1) reducing the concentration of sulfur dioxide in the anolyte, (2) increase the current density to consume more sulfur dioxide at the anode, (3) increase the net water flux from the cathode to anode and (4) decrease the permeability of the membrane to sulfur dioxide. Thus, we conducted additional tests to determine if the sulfur-rich layer could be eliminated by modifying the electrolyzer operating conditions.

The MEA-31 test featured the same MEA construction as that of MEA-12, but under operating conditions that reduced the sulfur dioxide concentration in the anolyte, operated at relatively high current density and at a catholyte pressure of about 15 psig higher than that of the anolyte. This test operated continuously for 50 hours at 80 °C. Figure 6 shows a plot of the normalized cell voltage versus elapsed hours of cell operation. In the MEA-12 test, the normalized cell voltage

increased from about 1.5 V to 1.9 V over the 100-hour test duration. In the MEA-31 test, there was no measured change in the cell voltage over the 50-hour test duration (see Figure 6). Furthermore, as shown in Figure 7, SEM analysis of MEA-31 after the test revealed no evidence of a sulfur-rich layer. Thus, reducing the concentration of sulfur dioxide that reaches the cathode/membrane interface appears to be successful in preventing a sulfur-rich layer forming over a 50-hour test duration. Additional experiments are planned to confirm that this mode of operation will prevent the sulfur-rich layer over longer test durations.
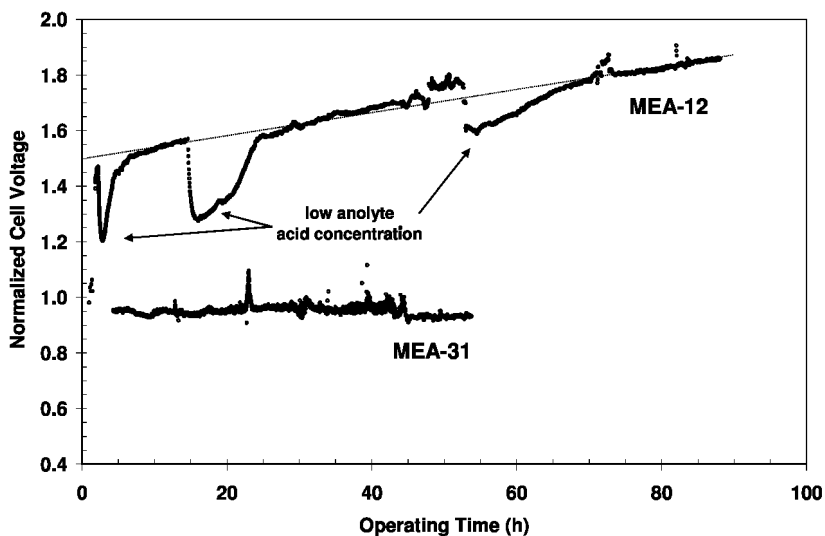
Figure 6. Normalized cell voltage of single cell electrolyzer experiments in which sulfur-rich layer formed (MEA-12) and did not form (MEA-31).
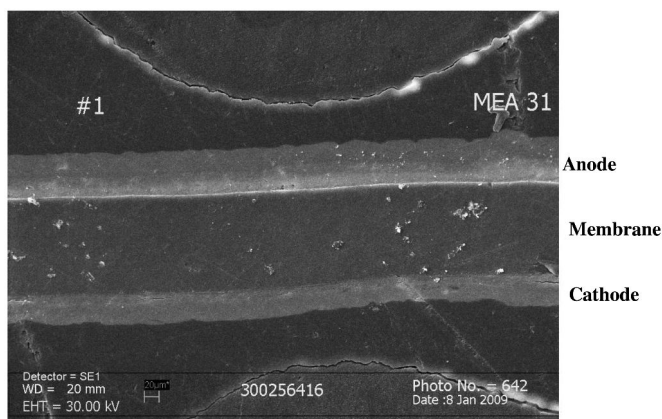
Figure 7. SEM image of MEA-31 showing the absence of a sulfur-rich layer between the cathode and membrane after 50-hours of continuous electrolyzer operation.

Conclusions

Catalyst testing indicates that Pt/C exhibits superior performance and stability compared to Pd/C for the oxidation of SO_2 in concentrated sulfuric acid solutions. Binary and ternary alloys containing platinum and other metals such as Co, Cr and Ni show promise as alternate anode materials. Based on the properties and performance characteristics of a variety of ion-exchange membranes, we have identified a number of candidate membranes for the sulfur dioxide-depolarized electrolyzer. At high operating pressures, we have observed the rapid formation of a sulfur-rich layer between the cathode and the Nafion® membrane in the liquid-fed electrolyzer. This layer can be eliminated in the short term by modifying the electrolyzer operating conditions to reduce the quantity of SO_2 that passes beyond the anode layer in the MEA. Continued membrane development is needed to produce materials with lower SO_2 transport characteristics and high conductivity. We are currently modifying the bench-scale testing equipment to allow membrane and catalyst testing at higher temperatures (> 100 °C).

Acknowledgments

References

1. Udagawa, J.; Aguiar, P.; Brandon, N. P. *J. Power Sources* **2007**, *166*, 127.
2. Funk, J. E. *Int. J. Hydrogen Energy* **2001**, *26*, 185.
3. Gorensek, M. B.; Staser, J. A.; Stanford, T. G.; Weidner, J. W. *Int. J. Hydrogen Energy* **2009**, *15*, 6089–6095.
4. *A Study on the Electrolysis of Sulfur Dioxide and Water for the Sulfur Cycle Hydrogen Production Process*; AESD-TME-3043; Westinghouse Electric Corporation: Columbus, OH, July 1980.
5. Steimke, J. L.; Steeper, T. J. *Characterization Testing of H₂O-SO₂ Electrolyzer at Ambient Pressure*; Technical Report WSRC-TR-2005-00310; Westinghouse Savannah River Company: Aiken, SC, August 1, 2005.
6. Steimke, J. L.; Steeper, T. J. *Characterization Testing and Analysis of Single Cell SO₂ Depolarized Electrolyzer*; Technical Report WSRC-STI-2006-00120; Washington Savannah River Company: Aiken, SC, September 15, 2006.
7. Mauritz, K. A.; Moore, R. B. *Chem. Rev.* **2004**, *104*, 4535–4585.

8. Xiao, L.; Zhang, H.; Scanlon, E.; Ramanathan, L. S.; Choe, E.; Rogers, D.; Apple, T.; Benicewicz, B. C. *Chem. Mater.* **2005**, *17*, 5328–5333.

9. Fujimoto, C. H.; Hickner, M. A.; Cornelius, C. J.; Loy, D. A. *Macromolecules* **2005**, *38*, 5010–5016.

10. Jin, J.; Stanbro, J.; Van Derveer, D.; Smith, D. W. *PMSE Prepr.* **2004**, *91*, 504–505.

11. Elvington, M. C.; Colón-Mercado, H.; McCatty, S.; Stone, S. G.; Hobbs, D. T. *J. Power Sources* **2010**, *195*, 2823–2829.

12. Lu, P. W. T.; Ammon, R. L *J. Electrochem. Soc.* **1980** (127), 2610–2616.

13. Colón-Mercado, H. R.; Hobbs, D. T. *Electrochem. Commun.* **2007** (9), 2649–2653.

14. Morales, I. R.; Beber, M.; Nart, F. C. *Electrochim. Acta* **1997** (42), 617.

15. Glipa, X.; Bonnet, B.; Mula, B.; Jones, D. J.; RozieÁre, J. *J. Mater. Chem.* **1999**, *9*, 3045–3049.

16. Steimke, J. L.; Steeper, T. J.; Herman, D. T.; Colón-Mercado, H. R.; Elvington, M. C. *Method to Prevent Sulfur Accumulation inside Membrane Electrode Assembly*; Technical Report SRNS-STI-2009-00134; Savannah River Nuclear Solutions: Aiken, SC, September 15, 2009.

Green Process for Uranium Separations Utilizing Molybdenum Trioxide

Mohamed Chehbouni,[1] Hamed Al-Busaidi,[2] and Allen W. Apblett*,[2]

**[1]Department of Chemistry, Computer, and Physical Sciences,
Southeastern Oklahoma State University, Durant, OK 74701
[2]Department of Chemistry, Oklahoma State University, Stillwater, OK 74078
*allen.apblett@okstate.edu**

Molybdenum trioxide can absorb uranium from aqueous solution with a capacity of up to 165 % by weight. The mechanism of this process is a chemical reaction that produces an insoluble uranium molybdenum oxide mineral oxide called umohoite, $UMoO_6 \cdot 2H_2O$. The reaction between MoO_3 and aqueous uranyl acetate was found to be first order in each reactant with a rate constant of 0.084 L/mol·min. A 'green" process was developed whereby MoO_3 adsorbed uranium from aqueous solution and then the uranium and molybdenum trioxide were separated by treatment with aqueous ammonia. The resulting ammonium uranate solid was isolated by filtration and the aqueous ammonium molybdate was converted back to MoO_3 by heating. The recovery of uranium was 98.9%.

Introduction

All aspects of nuclear energy production can have a potential toll on the environment. While the spent fuel produced by commercial, defense, and isotope-production reactors is an obvious hazard, fuel fabrication and reprocessing, and uranium mining, milling, and extraction activities also produce radioactive wastes that require safe disposal. In the past, insufficient attention to this problem has led to the contamination of soil and ground water with large quantities of radioactive substances, especially at U.S. Department of Energy facilities (*1*). For example, the concentration of uranium in contaminated soil and mine tailings was found to be 0.012% and 0.002–0.11% percent, respectively

(*2*). The Fry Canyon site in Utah provides a good example of the dangers of uranium mine tailings. The uranium concentrations measured in groundwater at this site were as high as 16,300 ppb with a median concentration of 840 ppb before remedial actions were taken (*3*). Uranium contamination can result from human activities other than the generation of nuclear energy (*4*, *5*). In particular, phosphate fertilizers are an important contributor of uranium to groundwater since they often contain uranium at an average concentration of 150 ppm (*6*). The depleted uranium ammunition used as armor penetrators in several military conflicts has also been demonstrated as a source of drinking water contamination (*7*)

The contamination of ground water with uranium can also arise from natural sources. Uranium will solubilize over a wide range of pH when bedrock consisting mainly of uranium-rich granitoids and granites are exposed to soft, slightly alkaline bicarbonate waters under oxidizing conditions. These conditions occur widely throughout the world. For example, in Finland exceptionally high uranium concentrations up to 12,000 ppb are found in wells drilled in bedrock (*8*). Concentrations of uranium up to 700 ppb have been found in private wells in Canada (*9*) while a survey in the United States of drinking water from 978 sites found a mean concentration of 2.55 ppb (*10*). However, some sites in the United States, such as the Simpsonville-Greenville area of South Carolina, have serious contamination with uranium. At that location, high amounts of uranium (30 to 9900 ppb) were found in 31 drinking water wells (*11*) as a consequence of the presence of veins of pegmatite in the area. While uranium in ground water is problematic for drinking water supplies, it is also a resource that could be tapped to augment the supply of uranium for energy generation. What is required is a simple efficient method to remove the uranium in the form of a useful resource while at the same time perhaps generating purified drinking water.

Animal testing and studies of occupationally exposed people have shown that the major health effect of uranium is not due to radiation but is a result of chemical kidney toxicity (*12*). Functional and histological damage to the proximal tubulus of the kidney have been observed (*13*). The effects of long-term environmental uranium exposure in humans are uncertain but there is an association of uranium exposure with increased urinary glucose, alkaline phosphatase, and β-microglobulin excretion (*14*) as well as increased urinary albumin levels (*15*) As a result of such studies, the World Health Organization has proposed a guideline value of 2 ppb for uranium in drinking water while the US EPA has specified a limit of 30 ppb.

Current practices for treatment of municipal water supplies practices are not effective for removing uranium. However, it has been reported that uranium removal can be accomplished by a variety of processes such as modification of pH or chemical treatment (often with alum) or a combination of the two (*16*). Several sorbents have been shown to be useful for removal of uranium from water. Activated carbon, iron powder, magnetite, anion exchange resin and cation exchange resin were shown to be capable of adsorbing more than 90% of the uranium and radium from drinking water. However, two common household treatment devices were found not to be totally effective for uranium removal (*11*).

Molybdenum hydrogen bronze (also called molybdenum blue), HMo_2O_6, was previously investigated for application in removal of uranium from aqueous solution and possible use in a cyclic process for recovery of actinides and heavy metals (*17*). It was thought that the protons would provide ion exchange sites on the material in its reduced form while oxidation would remove these sites and release the toxic metals in concentrated form. However, it was discovered that oxidation of the blue reagent occurred during the adsorption process so that the reagent turned from blue to yellow. It was also found that the uptake of uranium (122% by weight) exceeded the expected capacity based on the number of protons present i.e. the proton concentration is 3.46 mEq/g while the uranium adsorption was 5.14 mEq/g. Analysis of the product from uranium uptake revealed that the bronze had reacted with uranium to produce the mineral iriginite, $UMo_2O_9 \cdot 3H_2O$. The reaction of HMo_2O_6 was found to be very selective for uranium, other actinides, and heavy metals. The oxidation of the Mo(V) centers in the bronze was found to be due to reaction with molecular oxygen as the layered structure was disassembled by reaction with uranyl ions. This result suggested that prior reduction of MoO_3 to HMo_2O_6 was unnecessary for uranium adsorption, a hypothesis that was proven in subsequent work (*18*).

Experimental

All reagents were commercial products of ACS Reagent grade purity or higher and were used without further purification. Water was purified by reverse osmosis followed by deionization. Bulk pyrolyses at various temperatures were performed in an air atmosphere in a digitally-controlled muffle furnace using approximately 1 g samples, a ramp of 10°C/min and a hold time of 4 hr. X-ray powder diffraction (XRD) patterns were recorded on a Bruker AXS D-8 Advance X-ray powder diffractometer using copper K_α radiation. Crystalline phases were identified using a search/match program and the PDF-2 database of the International Centre for Diffraction Data (*19*). Scanning Electron Microscopy (SEM) photographs were recorded using a JEOL Scanning Electron Microscope. Uranium concentrations of aqueous solutions were determined by XRF spectroscopy on a Thermo Electron QuanX XRF spectrometer. A calibration curve for the instrument was generated using a NIST-traceable standard at 5 different concentrations that bracketed the region of interest.

Reaction of MoO₃ with Uranyl Acetate

MoO_3 (1.00 g, 6.95 mmol) was added to 100 ml of a 0.100 M uranyl acetate solution (10.0 mmol) and the mixture was heated at reflux for 7 days. Upon cooling, a yellow solid was isolated by filtration through a fine sintered glass filter. After drying in vacuum at room temperature, the yield of yellow solid was found to be 3.23 g. Thermal gravimetric analysis indicated a water content of 9.24%. XRD analysis after firing at 600°C indicated the formation of $UMoO_6$. Overall, the yield of this product was 2.97 g or 99.7% based on MoO_3. Infrared spectrum

(DRIFTS, solid diluted in KBr, cm^{-1}): 3582 w, 3513 vs, br, 3195 w, 2928 w, 2150 w, 1630 s, 1611 s, 1402 s, 918 vs, 889 vs, 859 vs, 821 vs, 724 m, 642 m, 541 m.

Kinetic Studies of Uranium Uptake Using MoO$_3$

Excess of MoO$_3$ (5 mmol, 0.72 g) was reacted at room temperature with 100 ml of an aqueous solution of 0.250 mmol of uranium acetate that was buffered with sodium acetate / acetic acid (pH of 4.7). The mixture was stirred magnetically and aliquots of 5 ml of the reaction mixture were withdrawn at regular intervals and the concentration of uranium and the pH were determined. This experiment was repeated in the presence of 10, 15, and 20 mmol of MoO$_3$. The rate constant of the reaction for each experiment was determined and the overall order of the reaction was established.

Recovery of Uranium and Molybdenum Trioxide

Uranium was recovered from the uranium molybdate phase by treatment with a strong base. In this procedure, 1.00 g of the uranium/molybdenum trioxide product was stirred overnight with 100 ml of a 15% solution of ammonium hydroxide. The reaction mixture was separated by filtration through a 20 μm nylon membrane filter. The solid product was washed copiously with distilled water and then dried in a vacuum desiccator to yield 0.701 g of a yellow solid that was subsequently identified as ammonium uranate, $(NH_4)_2U_3(OH)_2O_9\cdot2H_2O$, by XRD analysis. The filtrate was evaporated and the solid obtained was determined to be ammonium molybdate by XRD analysis.

Results and Discussion

A prolonged reaction of molybdenum trioxide with an aqueous solution of uranyl acetate was performed in order to determine the maximum uptake of uranium and identify the product of the reaction. After one week, the MoO$_3$ had absorbed 165% by weight of uranium, and amount that equates to 6.94 millimoles of uranium per gram of MoO$_3$ and surpasses the 122% by weight observed for HMo$_2$O$_6$ (*17*). The uranium-containing products in both cases have the characteristic yellow color of hexavalent uranium and the infrared spectra of products are consistent with a structures consisting of hydrated uranyl ions and molybdenum oxide octahedra. These results imply that the differences in uranium uptake are due to varying ratios of uranium to molybdenum in the product rather than to differences in uranium oxidation states.

X-ray powder diffraction analysis (Figure 1) of the solid product from uranium uptake by MoO$_3$ revealed that it consisted mainly of the mineral umohoite [(UO$_2$)MoO$_4$(H$_2$O)](H$_2$O) in contrast to the iriginite, [(UO$_2$)Mo$_2$O$_7$(H$_2$O)$_2$](H$_2$O), that was produced by the reaction of HMo$_2$O$_6$ with uranyl acetate. In the latter case it appears that the presence of a proton and, initially, a Mo(V) center stops the adsorption of uranium at one equivalent per two moles of molybdenum oxide. The XRD pattern of the product from the reaction of uranyl acetate with

MoO$_3$ contains several unidentified peaks, the strongest of which is centered at approximately 2θ = 15°. It is believed that these correspond to a more hydrated form of UMoO$_6$ than umohoite. Supporting evidence for this hypothesis was provided by thermal gravimetric analysis, which clearly demonstrated a water content of 9.24% or approximately 2.43 molar equivalents of water per UMoO$_6$ formula unit. Also, when the product from the reaction between uranyl acetate with MoO$_3$ was not dried before XRD analysis, the peaks for the proposed hydrated phase were significantly more intense than they were in the dried sample. Finally, heating of the uranyl acetate/MoO$_3$ product to 600°C produced phase-pure UMoO$_6$ (Figure 1), eliminating the possibility of the presence of a crystalline phase with a different ratio of uranium to molybdenum other than one to one.

The reaction of MoO$_3$ with uranyl ions to produce umohoite appears to preserve part of the structure of MoO$_3$. The latter compound is composed of MoO$_6$ octahedra that are interconnected through corner linking to form infinite chains. These chains are further linked by edge-sharing to form double-layer sheets. These stack together via Van der Waals forces to give the final layered structure (Figure 2) (*20*).

Reaction of uranyl ion with MoO$_3$ leads to separation of the edge-shared chains of MoO$_6$ octahedra. These chains are intercalated with chains of UO$_7$ decahedra to yield umohoite with a new layered structure shown in Figure 3 (*21*).

The structural changes suggests that the mechanism of the reaction might involve pulling out of chains of molybdenum oxide octahedral as the uranyl ions react with MoO$_3$. Such a reaction would be expected to give a fibrous product as it does in the reaction of molybdenum hydrogen bronze with uranyl nitrate. However, the SEM image of the MoO$_3$/uranyl acetate product provided in Figure 4 shows square plates and rectangles. Notably, the new particles are much smaller than those of the MoO$_3$ reagent used. This result suggests a second mechanistic possibility in which the molybdenum trioxide particles are completely dissolved in a dissolution/precipitation process that generates new particles with different morphologies. Unfortunately, the experiments that were performed cannot confirm this mechanism. Future experiments with large single crystals of molybdenum trioxide may shed further light on the mechanism. Previously, complete morphological rearrangement was also seen for the reaction of HMo$_2$O$_6$ with uranyl acetate (*17*).

An important parameter for application of MoO$_3$ in removal of uranium from water is the rate of reaction under ambient conditions. Therefore, the kinetics of the uranium uptake reaction were determined under condition where the MoO$_3$ was present in excess. Under these conditions, plotting the natural logarithm of uranium ion concentration versus time yields a straight line (Figure 5), demonstrating that the reaction is first order in the uranyl ion. The slope of the plots yielded the rate constants listed in Table 1.
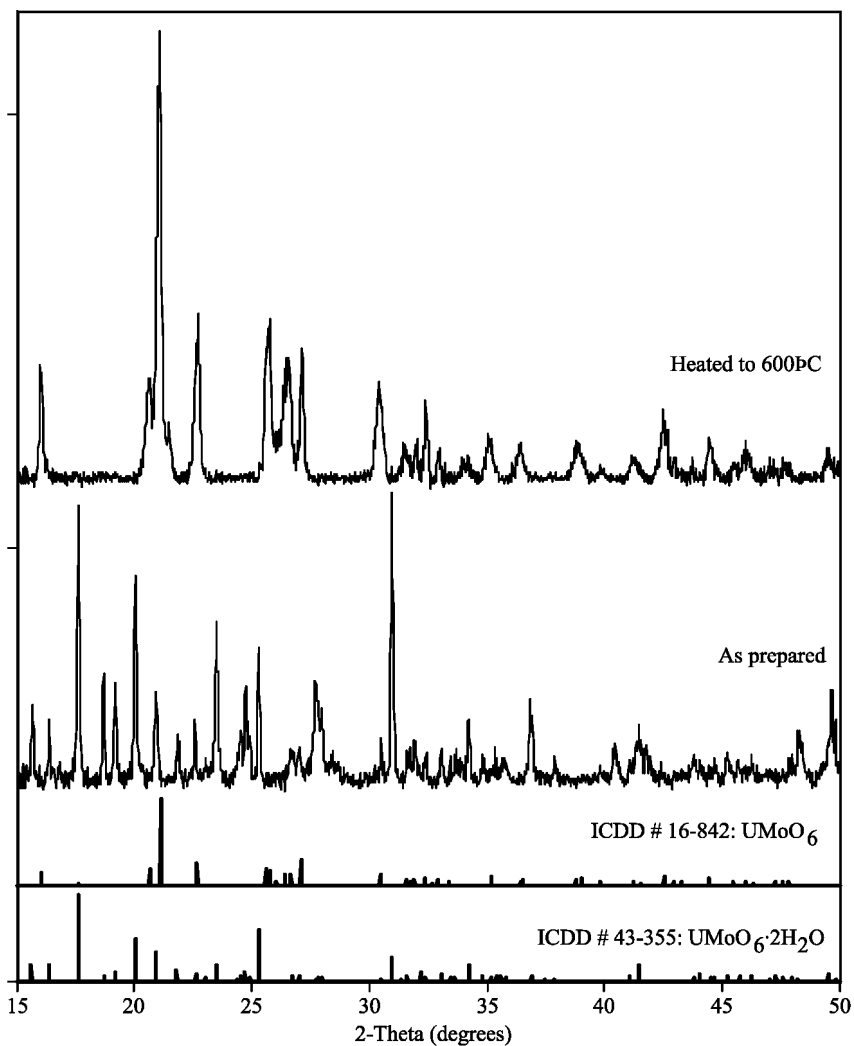
Figure 1. XRD patterns of product from reaction of uranyl acetate with MoO₃ as isolated and after heating to 600°C.
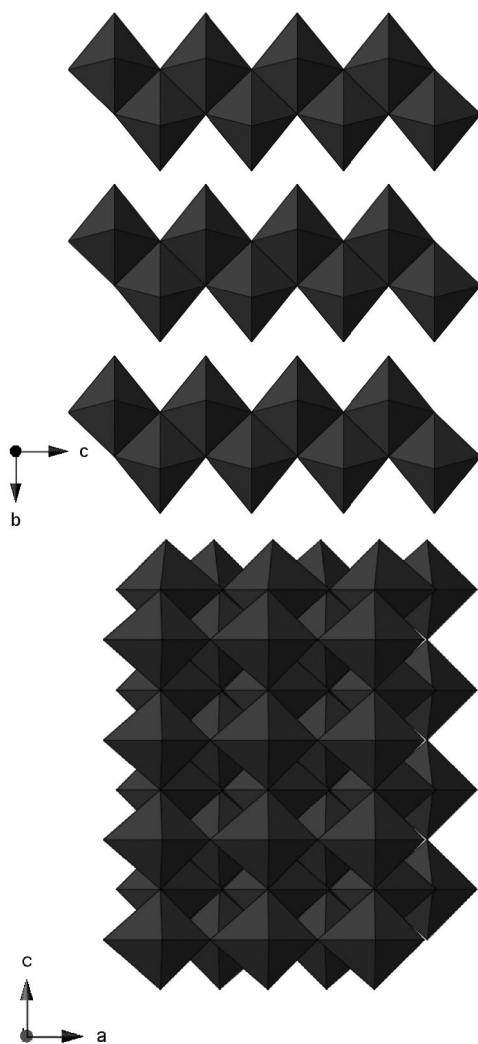
Figure 2. Layered structure of MoO₃ viewed down the a axis (left) and the c axis (right).
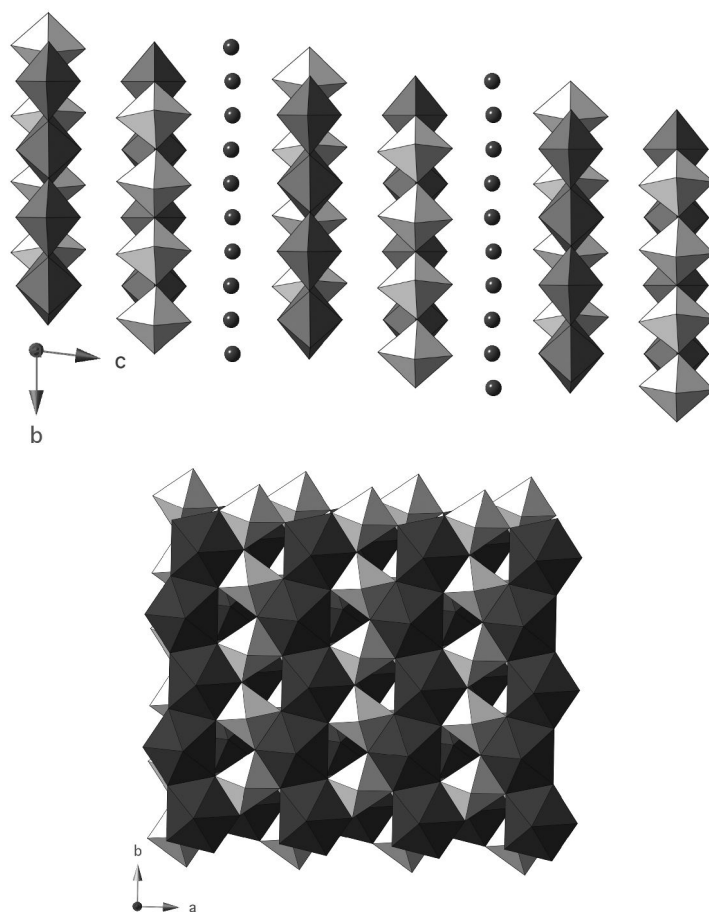
Figure 3. Structure of umohoite viewed down the axis (left) and the c axis (right). Lighter shaded octahedra are MoO_6 while darker shaded decahedra are UO_7 (21). Spheres are water.

Table 1. Rate Constants for Varying MoO_3 Concentrations

Concentration (M)	K_{obs} (min^{-1})
0.05	0.0042
0.10	0.0080
0.15	0.0120
0.20	0.0165
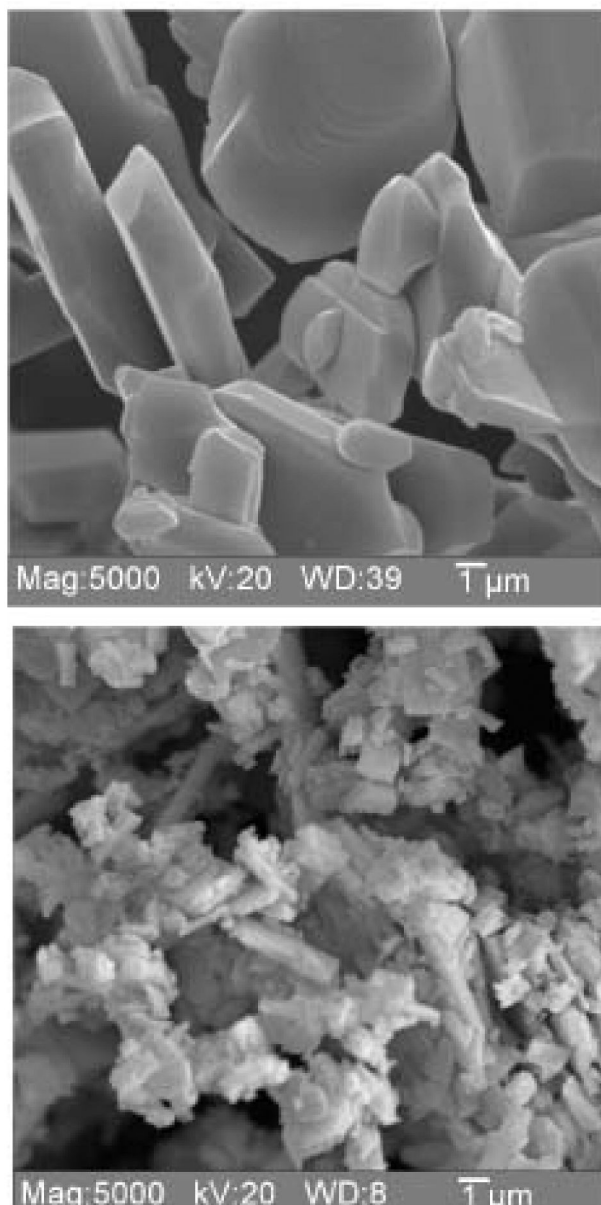
Figure 4. SEM pictures of molybdenum trioxide (top) and the product from its reaction with uranium acetate (bottom).
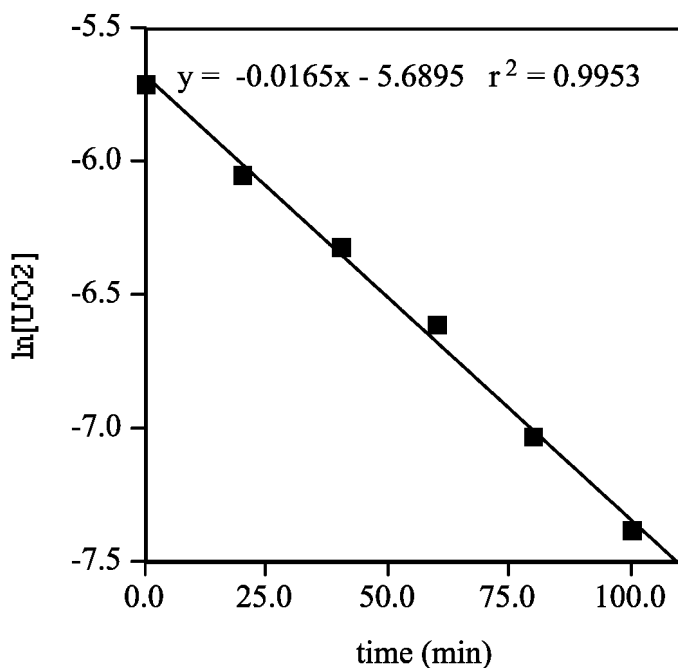
Figure 5. Pseudo-first order kinetics for the reaction of 0.20 mmol of MoO₃ with 100 ml of 0.025 M UO₂²⁺.

The order of the reaction in molybdenum trioxide was determined by plotting the logarithm of k_{obs} versus the logarithm of the concentration of MoO_3 (Figure 6). The slope of the resulting graph was 1.0, indicating that the reaction is first order in MoO_3. Therefore, the reaction is first order in both MoO_3 and in UO_2^{2+} overall follows a second-order rate law (Equation 1). The rate constant was derived from a plot of k_{obs} versus the concentration of MoO_3, Figure 7, that gave a slope of 0.084 L/mol·min. Note that the "concentration" of MoO_3 is being expressed in terms of molarity despite the fact that it is an undissolved solid. Since the reaction transforms one solid into another, it is difficult to give a rate constant in terms of surface area.

$$\text{Rate} = k[\text{MoO}_3][\text{UO}_2^{2+}] \qquad (1)$$
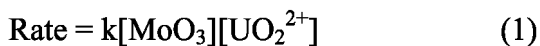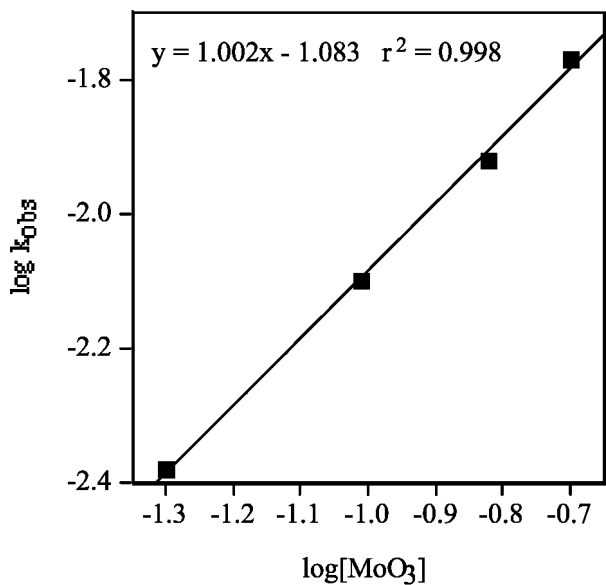
Figure 6. Order of reaction in MoO₃.
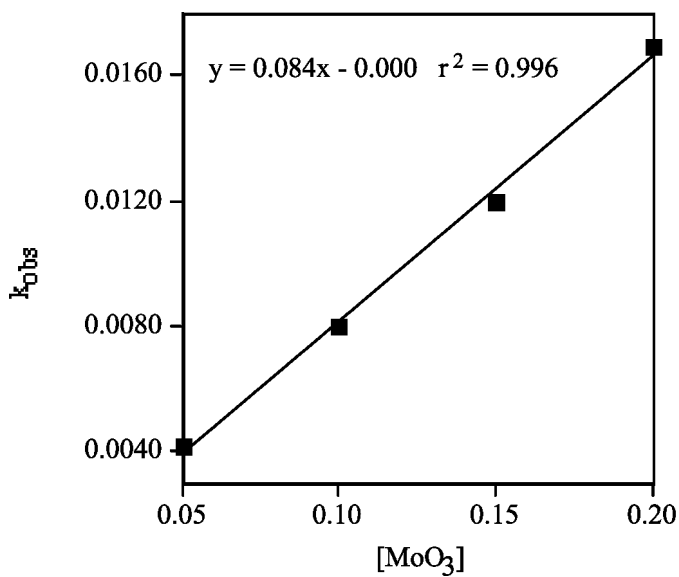
Figure 7. k_{obs} versus [MoO₃].
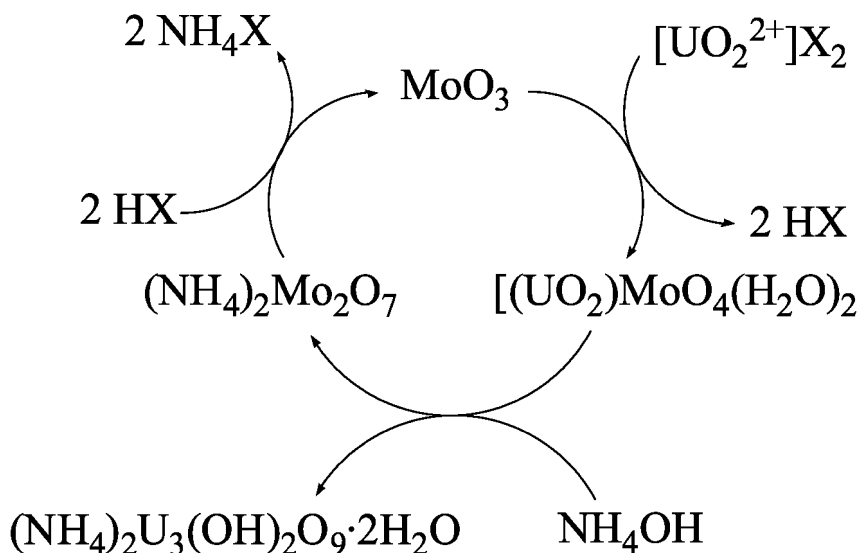
Figure 8. Green cycle for uranium removal from water.

The uranyl molybdate product (umohoite) obtained on the reaction of molybdenum bronze with uranyl nitrate was treated with a 15% solution of ammonium hydroxide. The reaction was stirred for 12 hours and the reaction mixture was separated by filtration. The X-ray powder diffraction pattern of the residue corresponded to ammonium uranate $\{(NH_4)_2U_3(OH)_2O_9.2H_2O\}$, which has applications in the nuclear power industry. The ammonium uranate can be further converted to UO_3 upon heating to 600°C. The recovery of uranium was 98.9 %. Evaporation of the filtrate produced ammonium molybdate, $\{(NH_4)_2(Mo_2O_7)\}$, that was identified by XRD. Molybdenum trioxide (MoO_3) could be recovered on heating the ammonium molybdate product to 242°C as determined by thermal gravimetric analysis. Hence a complete cycle for uranium concentration can be developed in which the only reagents consumed are ammonium hydroxide. Potentially the ammonia could be recovered and reused to yield a process with no waste products (Figure 8).

Conclusions

In conclusion, it has been demonstrated that molybdenum trioxide has an extremely high capacity for absorption of uranium by a reaction that generates the insoluble mineral umohoite. MoO_3 has considerable promise for application in environmental remediation, water treatment, and uranium recovery from ores.

References

1. Riley, R. G.; Zachara, J. M.; Wobber, F. J. *Chemical Contaminants on DOE Lands and Selection of Contaminant Mixtures for Subsurface Science Research*; DOE/ER-0547T; U.S. Department of Energy: Washington, DC, 1992.

2. Oluwole, A. F.; Ajayi, O.; Ojo, J. O.; Balogun, F. A.; Obioh, I. B.; Adejumo, J. A.; Ogunsola, O. J.; Adepetu, A.; Olaniyi, H. B. *Nucl. Instrum. Methods Phys. Res., Sect. A* **1994**, *353*, 499–502.

3. *Field Demonstration of Permeable Reactive Barriers To Remove Dissolved Uranium from Groundwater, Fry Canyon, Utah*; EPA 402-C-00-001; U.S. Environmental Protection Agency: Washington, DC, 2000.

4. Cothern, C. R.; Lappenbusch, W. L. *Health Phys.* **1983**, *45*, 89.

5. Dreesen, D. R.; Williams, J. M.; Marple, M. L.; Gladney, E. S.; Perrin, D. R. *Environ. Sci. Technol.* **1982**, *16*, 702.

6. Spalding, R. F.; Sackett, W. M. *Science* **1972**, 629.

7. *Depleted Uranium in Bosnia and Herzegovina Post-Conflict Environmental Assessment*, revised ed.; United Nations Environment Programme: Switzerland, 2003.

8. Salonen, L. In *Future Groundwater Resources at Risk*; Soveri, J., Suokko, T., Eds.; International Association of Hydrological Sciences: Wallingford, U.K., 1994; p 77−81.

9. Moss, M. A.; McCurdy, R. F.; Dooley, K. C.; Givner, M. L.; Dymond, L. C.; Slayter, J. M.; Courneya, M. M. In *Chemical Toxicology and Clinical Chemistry of Metals*; Brown, S., Savory, J., Eds.; Academic Press: London, 1983; p 149−152.

10. *Occurrence and Exposure Assessment for Uranium in Public Drinking Water Supplies*; EPA 68-03-3514; U.S. Environmental Protection Agency: Washington, DC, 1990.

11. Navratil, J. D. *Arch. Oncol.* **2001**, *9*, 257–260.

12. Taylor, D. M.; Taylor, S. K. *Rev. Environ. Health* **1997**, *12*, 147–157.

13. Haley, D. P. *Lab. Invest.* **1982**, *46*, 196–208.

14. Zamora, M. L.; Tracy, B. L.; Zielinski, J. M.; Meyerhof, D. P.; Moss, M. A. *Toxicol. Sci.* **1998**, *43*, 68–77.

15. Mao, Y.; Desmeules, M.; Schaubel, D.; Bérubé, D.; Dyck, R.; Brûlé, D.; Thomas, B. *Environ. Res.* **1995**, *71*, 135–140.

16. White, S. K.; Bondietti, E. A. *J. Am. Water Works Assoc.* **1983**, *75*, 374.

17. Kiran, B. P.; Apblett, A. W.; Chehbouni, M. *Ceram. Trans.* **2003**, *143*, 385–394.

18. Chehbouni, M.; Apblett, A. W. *Ceram. Trans.* **2006**, *176*, 15–23.

19. Powder Diffraction File; PDF-2; International Centre for Diffraction Data: Newtown Square, PA, 2009.

20. Hsu, Z. Y.; Zeng, H. C. *J. Phys. Chem. B* **2000**, *104*, 11891–11898.

21. Krivovitchev, S. V.; Burns, P. C. *Can. Mineral.* **2000**, *38*, 717–726.

Alpha Spectrometry of Thick Samples for Environmental and Bioassay Monitoring

T. M. Semkow,[*,1] **A. J. Khan,**[1] **D. K. Haines,**[1] **A. Bari,**[1] **G. Sibbens,**[2]
S. Pommé,[2] **S. E. Beach,**[1] **I. AlMahamid,**[1] **and G. L. Beach**[1]

**[1]Wadsworth Center, New York State Department of Health,
Albany, NY 12201, USA**
**[2]European Commission, Joint Research Centre, Institute for Reference
Materials and Measurements, Retieseweg 111, B-2440 Geel, Belgium**
[*]tms15@health.state.ny.us

A projected future increase in nuclear energy options requires the development of new and improved methods for monitoring of radioactivity in the environment. Alpha spectrometry of thick samples offers, with certain limitations, rapid identification and quantification of α radioactivity in a variety of environmental and bioassay matrices. This method is particularly suitable for radiological emergency response. Detailed discussion is presented of novel algorithms for fitting of α-particle spectra for samples ranging from weightless to moderately thick. A successful test of the thick-sample α spectrometry method during the Empire09 Radiological Emergency Exercise is described, consisting of the identification of ^{241}Am in a bioassay matrix.

1. Principles of Thick-Sample α Spectrometry

There is an ongoing need for rapid α radionuclide identification in a range of matrices for monitoring of the environment, for bioassay, and for various levels of emergency response. Although mass spectrometry offers the highest sensitivity for long-lived α emitters, it requires sophisticated instrumentation and it suffers from sample homogeneity issues in real samples. Traditional α spectrometry consists of electroplating, coprecipitation, or vacuum evaporation

of an α emitting radionuclide, followed by measurement of it's α spectrum. It offers good sensitivity; however, sample preparation time can be relatively long.

Thick-sample α spectrometry is concerned with radioactivity measurement from a matrix which has radionuclide distributed throughout its bulk. This method had been tested for matrices such as evaporated water, soil, co-precipitated samples of leached air filters, concrete and urine (1–4).

The method for, water which yields reasonably uniform residues (4), consists of evaporation, flaming of the planchet holding the sample, and α spectrometric radioactivity assessment using grid ionization chamber (GIC). The complete method can be rapid (a few hours), if the levels of radioactivity are moderate ($\geq$ 3 mBq L^{-1}), or reasonably fast (1 day) for low-levels of radioactivity (sub-mBq L^{-1}). The slowest step of the method is the counting, if low detection limit is desired. Many features of GIC are useful for thick-sample α spectrometry, such as the large sample area, the high efficiency, the lack of recoil contamination, and the low background. Use of GIC at elevated pressure can prevent violent outgassing of samples, which could be a potential problem in vacuum measurements. There is no need for ^{242}Pu recovery tracer, which is necessary in other methods. Some of the problems associated with the GIC include temperature gain shifts and potential contamination caused by internal counting. Thick-sample α spectrometry can also be performed with a Si detector (2).

A detailed, 3-dimensional calibration of GIC efficiency as a function of both α energy and the residue mass was performed using standards of ^{238}U, ^{230}Th, ^{239}Pu, ^{241}Am, and ^{244}Cm (4). This calibration is common for several matrices. In addition to evaporated drinking water, it is valid for any environmental sample that can be prepared as a uniform layer. Specifically, this method can be used for evaporated residues of surface water, acid wash or leachate of materials, as well as urine. The method can also be used for finely grained solid matrices but not for samples composed of large and separated grains.

Examples of thick-sample α-particle spectra are depicted in Figure 1. Several samples containing ^{230}Th tracer and increasing masses of water residues were measured by GIC. It is seen that as the mass of the residue increases, the α peak becomes broader and less intense due to self-absorption of α particles in the sample. For the highest residue masses, the α peak disappears altogether, and the spectrum resembles a step function. However, the energy information is retained in the intercept of the right-hand side of the spectrum with the energy axis. All spectra exhibit a similar intercept owing to the fact that some unattenuated α particles are emitted from the surface (even for the thickest sample). A useful correlation was determined for the α energy E_α from the intercept energy E_i

$$E_\alpha(\text{MeV}) = E_i(\text{MeV}) - 0.03. \qquad (1)$$

Compared to α spectrometry of thin sources (with mass thicknesses of less than 0.1 mg cm^{-2}), spectrometry of thick sources has limited ability of simultaneous resolution of several α peaks, as can be inferred from Figure 1. Nevertheless, it can quantify a major radioactivity component and simultaneously a second minor radioactivity component having α energy higher than that of the major component.
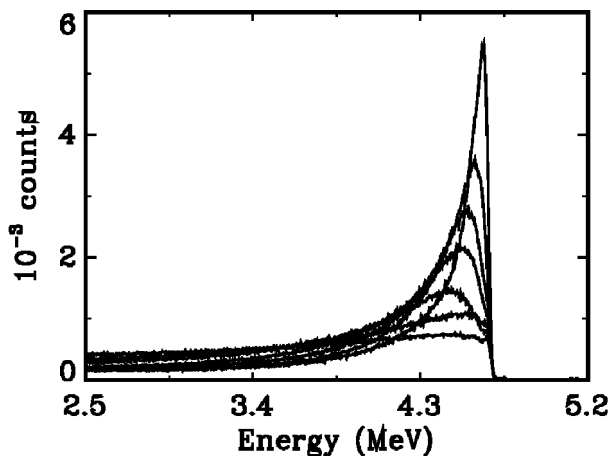
Figure 1. ^{230}Th alpha energy spectra from evaporated water residues of mass thicknesses (from the top): 0.16, 0.43, 0.68, 0.92, 2.1, 3.8, and 5.7 mg cm^{-2}.

2. Algorithms for Fitting Thick-Sample α-Particle Spectra

The spectra depicted in Figure 1 can be quantified by either the summation of counts in the region (which is described in Section 3) or by fitting of the spectral algorithms discussed in this Section. A novel algorithm was investigated for the fitting thick-sample α-particle spectra. The algorithm uses a power function for the left tail of the α peak (5) and was generalized to a fractional power, given by eq 2a, representing the observation that self-absorption has been described by the fractal power function (6). The α peak is given by the generalized exponent (GE) in eq 2b. If x is abbreviated as a spectrum channel number, and p_i, $i = 1,...,9$, denote spectral shape parameters, the spectral algorithm $g(x,\{p_i, i = 1,...,9\})$ is given by

$$g(x,\{p_i, i = 1,...,9\}) = \begin{cases} \dfrac{p_1}{(1 - x/p_2)^{p_3}} + p_4, & x < p_5, \quad (2a) \\[2mm] p_7 \exp\left\{-|x - p_6|^{p_9}/p_8\right\}, & x \geq p_5. \quad (2b) \end{cases}$$

The peak maximum is located at $x = p_6$. Equation 2b becomes Gaussian for $p_9 = 2$. Because the two functions 2a and 2b are logarithmically matched at $x = p_5$, the parameters p_1 and p_4 can be calculated as follows:

$$p_1 = \frac{p_2 p_7 p_9}{p_3 p_8}\left(1 - \frac{p_5}{p_2}\right)^{p_3+1} (p_6 - p_5)^{p_9-1} \exp\left\{-(p_6 - p_5)^{p_9}/p_8\right\}, \quad (3a)$$

$$p_4 = p_7 \exp\left\{-(p_6 - p_5)^{p_9}/p_8\right\}\left[1 - \frac{p_9}{p_3 p_8}(p_2 - p_5)(p_6 - p_5)^{p_9-1}\right]. \quad (3b)$$

Equation 2 describes the main α peak in the spectrum. Additional α peaks can be included in the spectrum by assuming that their shapes are the same as the

171

main peak shape, while their positions are shifted left by y_j channels from the main peak's position, and their intensities are p_j fractions of the main peak's intensity, where index $j \geq 10$. As many peaks can be included as needed. The final algorithm for the α-particle spectrum is given by eq 4,

$$f(x,\{y\},\{p\}) = g(x,\{p_i, i=1,\ldots,9\})$$

$$+ \sum_{j \geq 10} p_j g(x + y_j, \{p_i, i = 1,\ldots,9\}). \quad (4)$$

In addition to GE, two other algorithms for fitting of the α peak were investigated: fractional quadratic (FQ) and fractional polynomial (FP), given by eqs 5a and 5b, respectively:

$$g(x,\{p_i, i=1,\ldots,9\}) = \begin{cases} p_7 - p_8 \left\{ (x/p_6)^{p_9} - 1 \right\}^2, & x \geq p_5, \quad (5a) \\ \\ p_7 - |x - p_6|^{p_9} / p^8, & x \geq p_5. \quad (5b) \end{cases}$$

For both the FQ and FP algorithms, the left-side tail is taken from eq 2a. Additional relationships, not reproduced here, were derived for p_1 and p_4 from logarithmic matching of eqs 5a and 5b with eq 2a.

The fitting of f from eq 4 to an α-particle spectrum is a non-linear problem. The program GAPQ (General Alpha-Peak Quadruple precision) has been written in Fortran 95 (7, 8) to accomplish this task, based on a non-linear Neyman χ^2 minimization and the Levenberg-Marquardt convergence technique (8–10). In the course of the minimization, all parameters p are fitted, except for p_1 and p_4, which are calculated according to eq 2 or similar. In addition, y_j values are fixed to produce the best fit. We normally include two α peaks in the spectrum (the main peak and a satellite), even if they are not resolved in the measurement. Therefore, the minimum number of fitting parameters is 10. Initial values of the parameters are guessed by the program from the shape of the spectrum. The program also calculates the variation coefficient of the fitted function $v(f) = \sigma(f)/f$ (10). The minimization takes approximately 0.1 s per iteration on an HP rx2660 Itanium workstation.

Example fits for selected cases are listed in Table 1 and are reproduced in Figs. 2 and 3.

It is seen from rows 1 and 2 of Table 1 that the GE algorithm provides excellent fits to the experimental spectra, for mass thicknesses up to about 1 mg cm^{-2}. The fitted curves in Figs. 2 and 3 are barely distinguishable from the plotted data. It is also seen that, for thick samples, the FQ algorithm (row 3) performed worse than did the GE algorithm, whereas the FP algorithm (row 4) performed slightly better than did the GE algorithm, based on the maximum possible value of the sample mass thickness. Overall, all these algorithms, while performing well for mass thicknesses ≤ 1.3 mg cm^{-2}, fail for mass thicknesses exceeding approximately 1.3 mg cm^{-2}. This failure is due to numerical reasons: the logarithm of the ratio of the

Table 1. Selected results from the fits

Radionuclide	Mass thickness (mg cm⁻²)	Peak algorithm	Number of iterations	χ^2 per degfree	Figure in text
^{238}U	0.11	GE	133	1.07	2
^{238}U	0.96	GE	464	1.06	3
^{238}U	0.53	FQ	7	1.26	NA
^{238}U	1.3	FP	74	1.06	NA
^{240}Pu	≈ 0	GE	14	1030	4

largest to the smallest fitted parameter p exceeds the computer precision, causing the Hessian matrix in the χ^2 minimization to be singular.

While the developed algorithms were designed for the thick samples, we also tested the GE algorithm for a high-resolution α-particle spectrum from a weightless, vacuum-evaporated source of ^{240}Pu (*11*). This source was prepared for the study of α emission probabilities from ^{240}Pu. The corresponding α-particle spectrum, depicted in Fig. 4, contains 3.6×10^8 counts and exhibits an exceptional energy resolution of 10 keV. Four peaks from ^{240}Pu are visible: α_0, α_{45}, α_{149}, α_{310}, as well as a small impurity from ^{241}Pu.

The fit, consisting of 13 parameters, included all 5 peaks simultaneously: 4 peaks from ^{240}Pu and 1 from ^{241}Pu. The fitted curve is shown in Fig. 4, indicating a very good fit for more intense peaks, but a poor fit of the tail section distant from the main peaks. Nevertheless, the minor peaks were fitted. The large χ^2 in Table 1 (row 5) is not indicative of a poor fit, but rather of the exceptional statistical sample of over 10^8 counts, leading to an underestimation of the uncertainties. Therefore, even the slightest deviation of the fitted curve from the measured data increased χ^2 considerably.

From the fitted parameters p_j, $j \geq 10$ (in this case p_{10}, p_{11}, p_{12}), and if we neglect the contribution from ^{241}Pu (p_{13}), we can calculate α-particle emission probabilities for ^{240}Pu, abbreviated as Q_k, $k = 0,1,2,3$, according to

$$Q_0 = \frac{1}{1 + \sum_{j \geq 10} p_j}, \tag{6a}$$

$$Q_k = \frac{p_{k+9}}{1 + \sum_{j \geq 10} p_j}, \quad k \geq 1. \tag{6b}$$

Furthermore, one can, from the fitted variation coefficients $v(f)$ and $v(p_j)$, calculate variation coefficients of the α-particle emission probabilities, abbreviated as $v(Q_k)$:

$$v^2(Q_0) = v^2(f) + \sum_{n \geq 1} Q_n^2 v^2(p_{n+9}), \tag{7a}$$
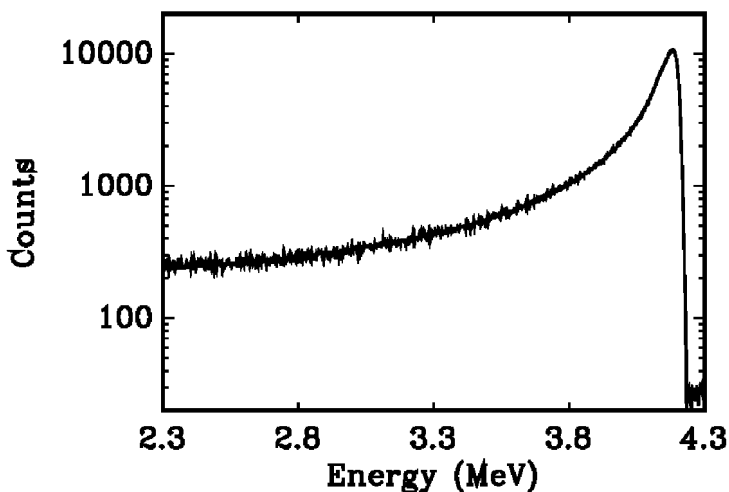
Figure 2. ^{238}U alpha energy spectrum and fit for evaporated water residue of 0.11 mg cm^{-2} mass thickness.

$$v^2(Q_k) = v^2(f) + Q_0^2 \left\{ \left[\left(1 + \sum_{\substack{n \geq 1 \\ n \neq k}} p_{n+9} \right)^2 v^2(p_{k+9}) \right] + \sum_{\substack{n \geq 1 \\ n \neq k}} p_{n+9}^2 v^2(p_{n+9}) \right\}, \quad k \geq 1. \quad (7b)$$

Then, $\sigma(Q_k)$ can be calculated. The results are given in Table 2.

The emission probabilities for peaks 0, 1, and 2 in Table 2 agree well with those obtained by other fitting methods (*11*). The uncertainty of the peak-3 emission probability exceeds the value of the emission probability as well as the uncertainties obtained from other fitting methods. The reason for that is the poor fit of the tail section distant from the main peak.

3. ^{241}Am Identification in Empire09

The Federal Radiological Monitoring and Assessment Center's Empire09 Radiological Emergency Exercise was held in Albany, NY on June 2-5, 2009. The exercise scenario called for simultaneous explosions of two Radiological Dispersal Devices, containing ^{137}Cs and ^{241}Am.

Several spiked environmental and bioassay samples were available to the participants in the exercise. We describe below an α identification in a urine sample, using thick-sample α spectrometry method. The 3-mL sample taken for analysis contained 1 pCi mL^{-1} (1 nCi L^{-1}) activity concentration. The sample was quickly digested with concentrated HNO$_3$ and H$_2$O$_2$, evaporated, flamed, and
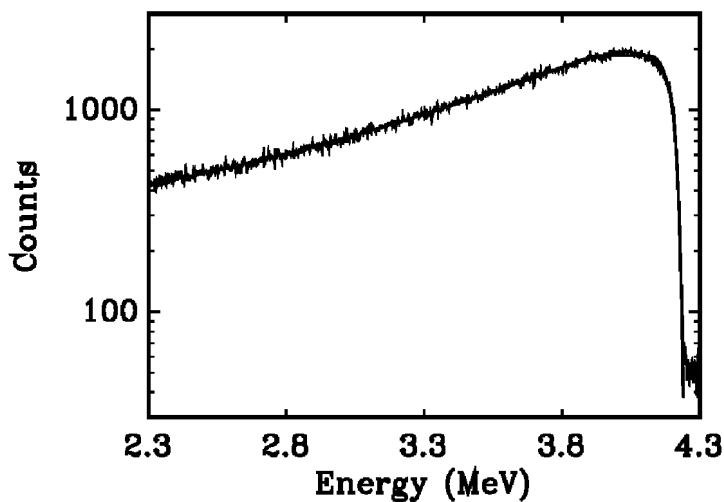
Figure 3. ^{238}U alpha energy spectrum and fit for evaporated water residue of 0.96 mg cm^{-2} mass thickness.
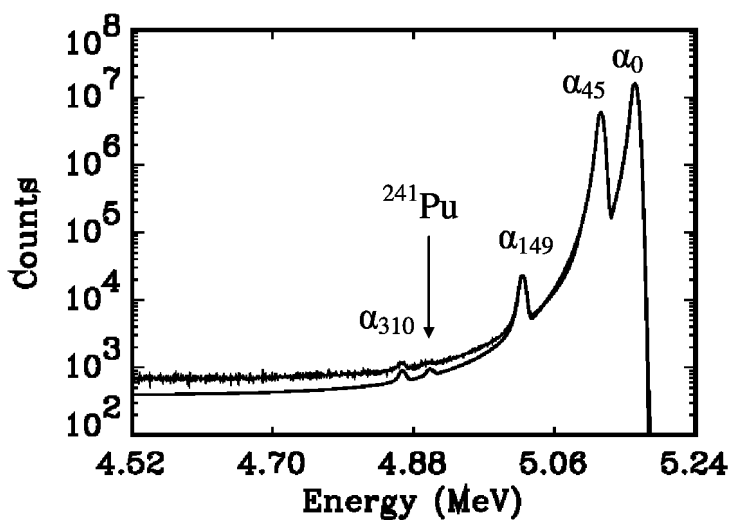
Figure 4. ^{240}Pu alpha energy spectrum and fit for vacuum-evaporated source.

measured on the GIC for 1000 min. The resultant α-particle spectrum is depicted in Fig. 5.

The intercept of the right-hand side of the spectrum with the energy axis yielded 5.52 MeV, from which an α energy of 5.49 MeV was calculated using eq 1. This value identified [241]Am as a radionuclide, which was confirmed by γ spectrometry. The sample residue had mass thickness of 1.32 mg cm^{-2}, corresponding to a GIC efficiency of 0.239 (4). The spectrum in Fig. 5 contains 1535 counts in the region between 3 and 6 MeV. From the above data we calculated an activity concentration of 0.965 ± 0.075 (95 % CL) nCi L^{-1}, in close agreement with the spiked concentration. Counting for shorter period of about 300 min would still have been sufficient for α identification and quantification; however, with reduced accuracy.

Table 2. Calculated alpha emission probabilities for [240]Pu and their 1σ least-significant digit uncertainties

Alpha-peak index k	Alpha branch	Alpha energy (keV)	Q_k (%)
0	α_0	5168	72.79(9)
1	α_{45}	5123	27.12(8)
2	α_{149}	5021	0.089(6)
3	α_{310}	4864	0.0012(15)
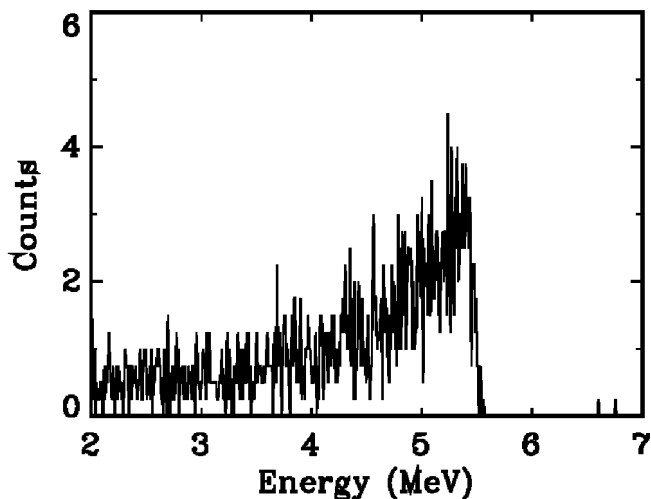
Figure 5. [241]Am alpha energy spectrum for evaporated bioassay residue of 1.3 mg cm^{-2} mass thickness.

4. Conclusions

A novel algorithm has been described for the fitting of α-particle spectra. The algorithm consists of a generalized exponent for the α peak and a power function for the left-side tail. The algorithm performs well for α-particle spectra for samples ranging from weightless to about 1 mg cm^{-2} mass thickness. The algorithm fails for thicker samples, for numerical reasons. Additional algorithm development will be required for samples thicker than 1 mg cm^{-2}.

Thick-sample α spectrometry was successfully applied to rapid ^{241}Am identification and quantification in the context of the Empire09 Radiological Emergency Exercise. Our thick-sample α spectrometric method emerges as a useful rapid technique for α radiation identification in an emergency situation, arising from the use of nuclear energy, or from nuclear incidents.

References

1. Sill, C. W. Rapid monitoring of soil, water, and air dusts by direct large-area alpha spectrometry. *Health Phys.* **1995**, *69*, 21–33.
2. Farmer, D. E.; Steed, A. C.; Sobus, J.; Stetzenbach, K.; Lindley, K.; Hodge, V. F. Rapid identification and analysis of airborne plutonium using a combination of alpha spectroscopy and inductively coupled plasma mass spectrometry. *Health Phys.* **2003**, *85*, 457–465.
3. Scarpitta, S. C.; Miltenberger, R. P.; Gaschott, R.; Carte, N. Rapid analytical technique to identify alpha emitting isotopes in water, air-filters, urine, and solid matrices using a Frish grid detector. *Health Phys.* **2003**, *84*, 492–501.
4. Semkow, T. M.; Khan, A. J.; Haines, D. K.; Bari, A. Rapid alpha spectroscopy of evaporated liquid residues for emergency response. *Health. Phys.* **2009**, *96*, 432–441.
5. García-Toraño, E.; Aceña, M. L. Nolin: Nonlinear analysis of complex alpha spectra. *Nucl. Instrum. Methods* **1981**, *185*, 261–269.
6. Semkow, T. M.; Jeter, H. W.; Parsa, B.; Parekh, P. P.; Haines, D. K.; Bari, A. Modeling of alpha mass-efficiency curve. *Nucl. Instrum. Methods Phys. Res., Sect. A* **2005**, *538*, 790–800.
7. Press, W. H.; Teukolsky, S. A.; Vetterling, W. T.; Flannery, B. P. *Numerical Recipes in Fortran 90*; Cambridge University Press: Cambridge, U.K., 1996.
8. Akin, E. *Object-Oriented Programming via Fortran 90/95*; Cambridge University Press: Cambridge, U.K., 2003.
9. Press, W. H.; Teukolsky, S. A.; Vetterling, W. T.; Flannery, B. P. *Numerical Recipes in Fortran*; Cambridge University Press: Cambridge, U.K., 1992.
10. Bevington, P. R.; Robinson, D. K. *Data Reduction and Error Analysis for the Physical Sciences*; McGraw-Hill: Boston, MA, 2003.
11. Sibbens, G.; Pommé, S.; Altzitzoglou, T.; García-Toraño, E.; Janβen, H.; Dersch, R.; Ott, O.; Martín Sánchez, A.; Rubio Montero, M. P.; Loidl, M.; Coron, N.; de Marcillac, P.; Semkow, T. M. Alpha-particle emission probabilities in the decay of ^{240}Pu. *Appl. Radiat. Isot.* **2009**, submitted for publication.

Radiation Chemistry

An Overview of Selected Radiation Chemical Reactions Affecting Fuel Cycle Solvent Extraction

Bruce J. Mincher*

Aqueous Separations and Radiochemistry Department, Idaho National Laboratory, P.O. Box 1625, Idaho Falls, ID 83415-6180 USA
***Bruce.Mincher@inl.gov**

Aqueous solvent extraction for the recovery of uranium and plutonium from dissolved nuclear fuel has been used successfully since the advent of the nuclear age. Following decades of PUREX operating experience in several countries, new solvent extraction processes are now being developed worldwide to extract additional long-lived radionuclides , including especially the minor actindes. These must be partitioned from the lanthanides in what is an especially challenging separation. These new processes rely on specialty ligands as metal complexing agents. They must be reasonably stable to hydrolytic and radiolytic degradation in the acidic, irradiated biphasic system. Solvent system degradation may lead to decreases in ligand concentration, production of interfering degradation products, and changes in solvent viscocity and phase separation parameters. Therefore, research is underway in the USA, Europe and Asia with a goal of understanding these affects on solvent extraction efficiency for specific systems. This chapter presents an overview of the important reactions that are common to all solvent extraction systems with reference to recent research findings at Idaho National Lab (INL) and elsewhere. It is shown that indirect radiolysis by reaction with radiolytically produced reactive species such as hydroxyl radical, radical cations and nitrous acid is responsible for much ligand and diluent degradation.

Understanding these reactions requires a combination of steady-state and pulsed irradiation experiments and solvent extraction distribution ratio measurements.

Introduction

The hydrolytic and radiolytic stabilities of solvent extraction formulations are key parameters determining the expense and ultimate success of a proposed process. Ligand and diluent degradation decreases solvent extraction efficiency by reducing the distribution ratios of the extracted metal species, reducing separation factors by the production of degradation products that are complexing agents, and/or by interfering with post-extraction phase separation by changing the physical parameters of the solvent (*1*). Solvent recycle lifetimes are reduced, and radioactively-contaminated spent solvents are difficult and expensive to dispose. Understanding the nature of solvent degradation is thus important to the design of a successful system. In recent years much research has been devoted to the design of numerous new systems to support the advanced fuel cycle, and the hydrolysis and radiolysis of these systems is an active area of investigation worldwide.

Since solvent extraction ligands are typically present as low concentration constituents of an alkane diluent in contact with aqueous nitric acid, hydrolytic reactions occur due to contact with nitric acid while most radiation energy is absorbed by the bulk diluent and acid. Direct ligand radiolysis is a minor effect with most radiation damage occurring due to the reaction of the ligand and diluent with the products of bulk diluent and acid radiolysis. These species may be transient, as with inorganic radicals, or relatively stable as with radiolytically produced hydrogen peroxide and nitrous acid. The suite of important reactive species produced by water (*2*), alkane (*3*), and nitric acid (*4–7*) radiolysis are shown respectively in eqs 123:

$$H_2O \text{ -}\backslash\!\backslash\!\backslash\text{-} \rightarrow {}^{\bullet}OH + e^{-}_{aq} + H^{\bullet} + H_2O_2 + H_3O^{+} + H_2 \qquad (1)$$

$$CH_3(CH_2)_nCH_3 \text{ -}\backslash\!\backslash\!\backslash \rightarrow e^{-}_{sol} + CH_3(CH_2)_nCH_3^{\bullet +} +$$

$$CH_3(CH_2)_nCH_2^{\bullet} + {}^{\bullet}CH_3 + H^{\bullet} + H_2 \qquad (2)$$

$$HNO_3 \text{ -}\backslash\!\backslash\!\backslash \rightarrow {}^{\bullet}NO_2 + {}^{\bullet}NO_3 + HNO_2 \qquad (3)$$
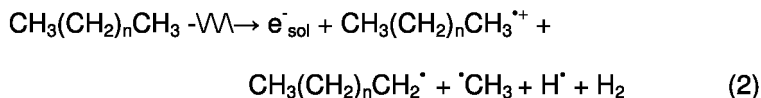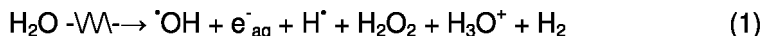
These equations are not meant to be stoichiometric, rather they illustrate the products to be expected in irradiated solution. The strongly oxidizing hydroxyl radical (${}^{\bullet}OH$) of eq 1 is an important water radiolysis product capable of reaction with organic compounds; however, the produced aqueous electron (e^{-}_{aq}) and hydrogen atom ($H^{\bullet}$) are of less importance in the solvent extraction system because they are scavenged by reactions with acidity (*2*), nitrate ion (*8*), and dissolved oxygen (*2, 9*) to produce less reactive species. These reactions, and their associated aqueous bimolecular rate constants are shown in eqs 4567:

$$e^-_{aq} + H^+ \rightarrow H^\bullet \qquad\qquad k = 2.3 \times 10^{10}\ M^{-1}s^{-1} \qquad (4)$$

$$e^-_{aq} + NO_3^- \rightarrow NO_3^{-2\bullet} \qquad\qquad k = 9.7 \times 10^9\ M^{-1}s^{-1} \qquad (5)$$

$$e^-_{aq} + O_2 \rightarrow {}^\bullet O_2^- \qquad\qquad k = 1.9 \times 10^9\ M^{-1}s^{-1} \qquad (6)$$

$$H^\bullet + O_2 \rightarrow HO_2^\bullet \qquad\qquad k = 2.1 \times 10^{10}\ M^{-1}s^{-1} \qquad (7)$$

The $^\bullet OH$ radical reacts by addition to unsaturated organic species to produce hydroxylated derivatives, or by electron transfer or $^\bullet H$ atom abstraction to produce carbon-centered radical products.

The radiolysis of alkanes shown in eq 2 produces the alkane radical cation $(CH_3(CH_2)_nCH_3^{\bullet+})$, which may undergo charge transfer reactions with solutes if the ionization potential of the solute is less than that of the diluent. Aromatic diluents, with their low ionization potentials may thus stabilize ligands in irradiated solution (10). The neutral organic radicals produced in eq 2 ($CH_3(CH_2)_nCH_2^\bullet$ and $^\bullet CH_3$) are electrophilic species that may react with solutes (11), or by addition to other radicals (12). Dissolved oxygen will also react with carbon-centered radicals to produce peroxyl radicals, which stabilize by a number of mechanisms to produce oxidized derivatives such as organic acids, alcohols and ketones (13), as shown in eqs 8 and 9:

$$CH_3(CH_2)_nCH_2^\bullet + O_2 \rightarrow CH_3(CH_2)_nCH_2OO^\bullet \qquad (8)$$

$$CH_3(CH_2)_nCH_2OO^\bullet \rightarrow acids, alcohols, ketones \qquad (9)$$
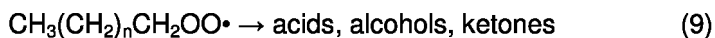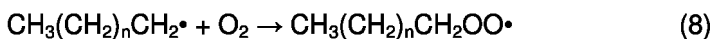
The production of nitrogen-centered radicals and nitrous acid from irradiated nitric acid is shown in eq 3. The $^\bullet NO_3$ radical is an electrophilic species that may add to unsaturated organic compounds, or react by electron transfer or $^\bullet H$ atom abstraction reactions similarly to the $^\bullet OH$ radical (14). Its reactions are typically slower than those of the $^\bullet OH$ radical. The $^\bullet NO_2$ radical is less reactive; however, both N-centered radicals may add to carbon-centered radicals to produce nitrated derivatives.

The generation of nitrous acid in eq 3 is the more important result of the irradiation of nitric acid with consequences to nuclear solvent extraction. Although its maximum concentration will be limited by radiolytic production of H_2O_2, as shown in eq 10, steady state concentrations sufficient to cause nitration and to alter metal oxidation states occur (15–17).

$$H_2O_2 + HNO_2 \rightarrow HOONO \rightarrow H^+ + NO_3^- + H_2O \qquad (10)$$
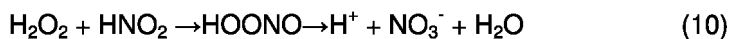
As eqs 12345678910 illustrate, a disparate array of reactive species acting in competition for solutes are created in the irradiated solvent extraction system. The yields and affects of these species with regard to final stable products depend on the nature of the diluent, ligands and radiation source. The following sections provide

examples of these reactions with reference to specific solvent extraction systems using data from the literature and current work at Idaho National Lab (INL).

Oxidative Reactions of the •OH Radical

The •OH radical is produced during water radiolysis with high yield and is the most powerful aqueous oxidizing agent with a potential of 2V (*2*). The yield in neutral water is 0.27 μmol Gy^{-1} for low linear energy transfer (LET) β,γ radiation (*2*). The yield is lower, at ~ 0.05 μmol Gy^{-1} for high LET radiation such as 5 MeV α particles (*18*). Reaction rate constants with organic molecules are typically high, in the range of ≥ 10^9 M^{-1} s^{-1}, thus these reactions are highly competitive and important in irradiated aqueous solution. The •OH radical aqueous reaction rate constant with tributyl phosphate has been measured at 5.0 x 10^9 M^{-1} s^{-1}, resulting in •H atom abstraction, shown in eq 11 (*19*):

$$\bullet OH + (C_4H_9O)_3PO \rightarrow (C_4H_9O)_2(\bullet C_4H_8O)PO + H_2O \qquad (11)$$
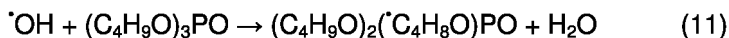
The resulting TBP radical is the source of dibutylphosphoric acid (eq 12) (HDBP); responsible for decreased separation factors in the partitioning of U from Zr in the PUREX process (*20*):

$$(C_4H_9O)_2(\bullet C_4H_8O)PO + H_2O \rightarrow \quad \bullet C_4H_8OH + \\ (C_4H_9O)_2POO^- + H^+ \qquad (12)$$
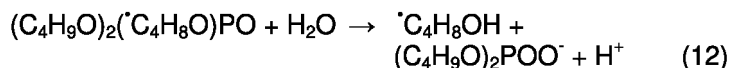
Dissolved oxygen is also implicated in HDBP production, resulting in the TBP peroxyl radical (eq 13) by addition to the C-centered radical product of TBP (*21*) in eq 12, followed by superoxide elimination and hydrolysis as shown in eq 14-15 (*22*):

$$(C_4H_9O)_2(\bullet C_4H_8O)PO + O_2 \rightarrow \\ (C_4H_9O)_2P(O)\text{-}O\text{-}(C_4H_8)OO^\bullet \qquad (13)$$

$$(C_4H_9O)_2P(O)\text{-}O\text{-}(C_4H_8)OO^\bullet \rightarrow \\ O_2^{\bullet-} + (C_4H_9O)_2P(O)\text{-}O\text{-}(C_4H_8)^+ \qquad (14)$$

$$(C_4H_9O)_2P(O)\text{-}O\text{-}(C_4H_8)^+ + H_2O \rightarrow (C_4H_9O)_2P(O)\text{-}O^- + \\ C_3H_7CHO + 2H^+ \qquad (15)$$
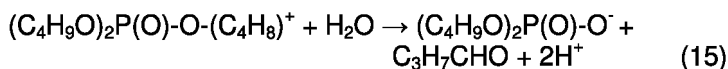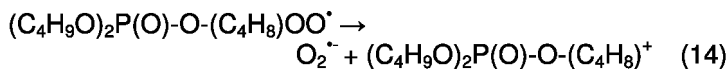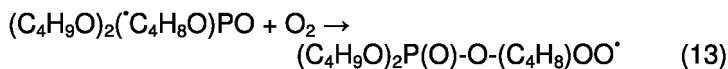
Although the rate constant for the reaction in eq 13 is unknown, peroxyl radical formation typically occurs at about ~ 10^9 M^{-1} s^{-1} (*13*).

Hydrogen atom abstraction reactions are implicated in many other ligand degradation mechanisms. Using low-temperature electron-spin-resonance (ESR) analysis to identify produced organic radicals in irradiated crown ethers, the radical product shown in eq 16 has been identified (*23*):

$$+ \cdot OH \rightarrow \qquad + H_2O \qquad (16)$$
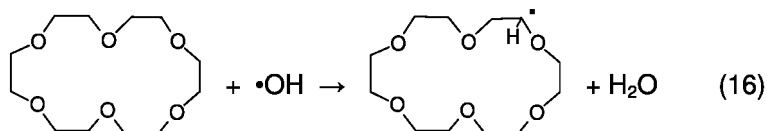
This C-centered radical might then add dissolved oxygen, as was shown above for the TBP radical (eq 13), or may disproportionate, resulting in ring opening to produce a linear polyether, as shown in eq 17:

$$2 \left[\quad \right] \rightarrow$$

$$+ \qquad (17)$$
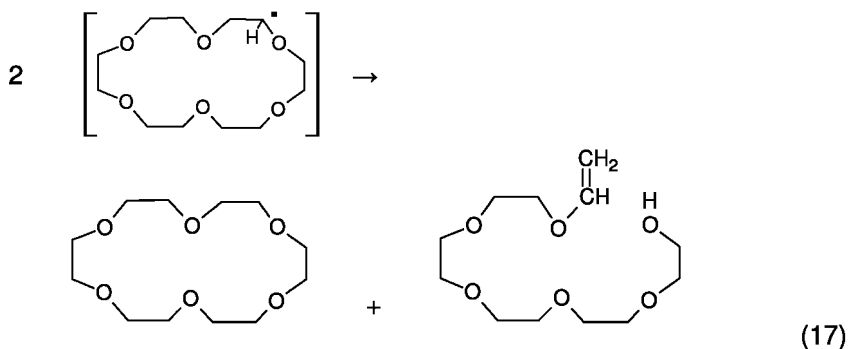
Ring opening to produce linear products has been reported for the 12-carbon cyclic ether dicyclohexano-18-crown-6 when irradiated in aqueous nitric acid (*24*). This crown ether is used in the CSSX and FPEX solvent extraction processes for Cs and Sr extraction. The produced linear ethers contained 3, 5 or 6-carbon chains indicating multiple C-O bond ruptures. The most abundant product contained 4 carbons, with a yield of 0.04 µmol Gy^{-1} for initially 0.005 M crown ether. While linear ethers may also act as solvent extraction ligands, they can be expected to have lower efficiency and selectivity compared to crown ethers.

Carbon-O bonds preferentially rupture in comparison to C-C bonds. This knowledge has been used to advantage in the design of the malonamide dimethyl dioctyl hexylethoxymalonamide (DMDOHEMA) (*25*), used in the DIAMEX actinide extraction process. In recognition that radiolysis is unavoidable in the irradiated solvent, the ligand molecule was designed with a sacrificial ether linkage situated between its diamide functional groups. Upon scission of the C-O bond relatively harmless dealkylated diamide and alcohol products result.

Unfortunately, the C-N bond is also subject to radiolytic rupture, probably also following ·H atom abstraction. Products such as amines and acidamides are produced in irradiated diamide solution, as shown in eq 18:

$$+ H_2O \rightarrow \qquad\qquad (18)$$
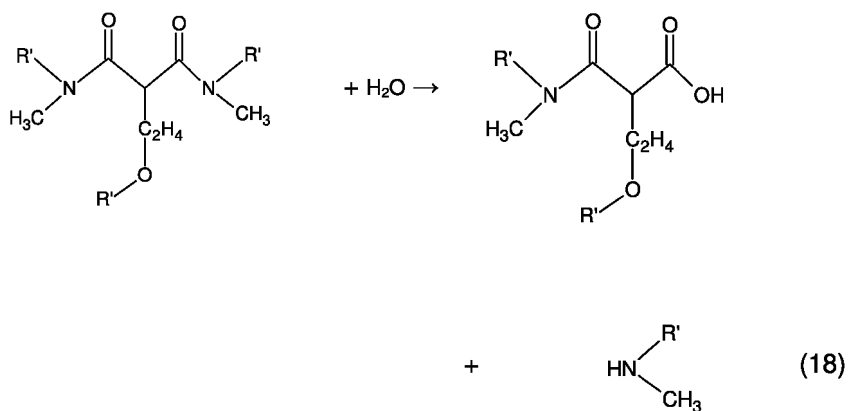
Decarboxylation of the acidamide in eq 18 produces a stable monoamide product. The presence of these produced species in irradiated solvent necessitates the implementation of solvent washing steps prior to solvent recycling, as has also been traditionally implemented for the PUREX process (*26*).

Analogous reactions are reported for the radiolysis of the TRUEX processes neutral organophosphorous amide actinide extractant octyl(phenyl)-*N,N*-diisobutylcarbamoylmethyl phosphine oxide (CMPO), shown in eq 19 (*27, 28*):

$$+ H_2O \rightarrow \qquad\qquad (19)$$
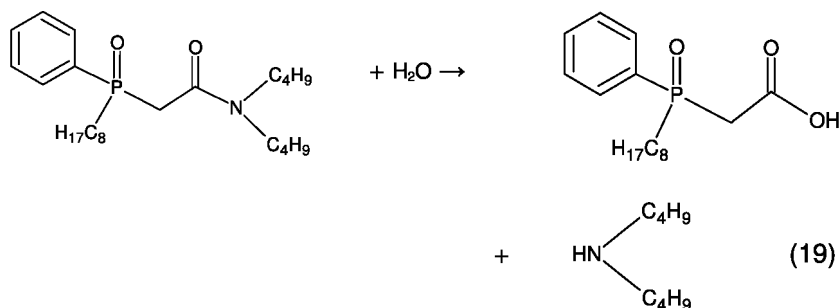
In this case, the acidic organophosphorous product of eq 19 is a complexing agent that is soluble in the organic phase and has been shown to interfere with stripping when dilute acids are used for back extraction. Decarboxylation of the acidic product produces a phosphine oxide that maintains forward extraction distribution ratios, as described in eq 20:

$$\rightarrow \qquad\qquad + CO_2 \qquad (20)$$
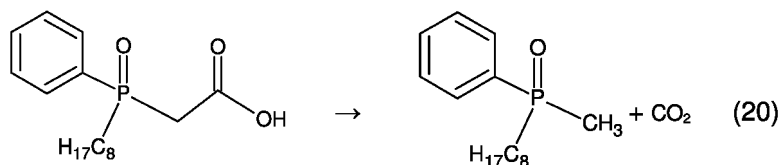
Another important reaction of the •OH radical is addition to unsaturated organic species, including phenyl rings. This reaction, which initiates a series of

further reactions, is used to advantage in water treatment by advanced oxidation processes (AOPs) to mineralize aromatic pollutants (*29*). It is disadvantageous in the solvent extraction system due to the resulting decreases in ligand concentration. The addition of the ·OH radical to the FPEX/CSSX solvent modifer 1-(2,2,3,3,-tetrafluoropropoxy)-3-(4-sec-butylphenoxy)-2-propanol (Cs-7SB) is shown in eq 21:

$$(21)$$
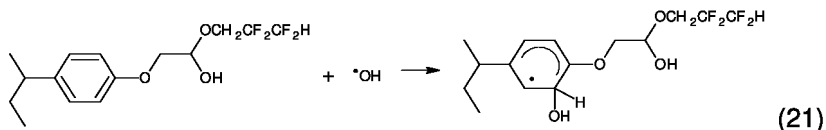
Although the reaction depicted in eq 21 has not been specifically observed for Cs-7SB, it is well-known for other aromatic functional groups. Under oxygen-deficient conditions phenolic products may result. Alternately, the resulting carbon-centered radical may add dissolved oxygen to initiate ring opening reactions, shown in eqs 22-23:

$$(22)$$

$$(23)$$
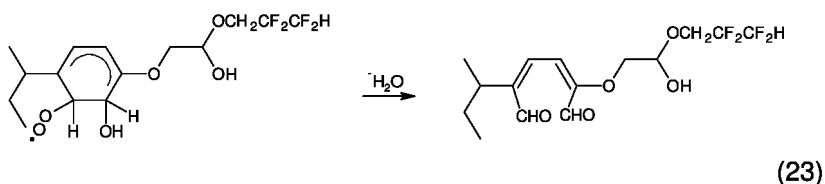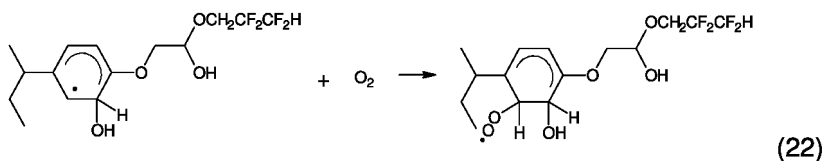
Diluent Radical Cations

The stability imparted to ligands by aromatic diluents is well known, although unfortunately aromatic compounds are unpopular for use in bulk amounts due to health and safety concerns. The protection afforded to solutes is due to their lower ionization potentials. Direct radiolysis of the diluent proceeds via a primary ionization event to produce an electron. The energetic electron generates other ionization events until it becomes thermalized and solvated. The other product is the diluent radical cation (eq 2). The main reaction of the radical cation is charge transfer to ionize a reaction partner, which will occur with ligands if their ionization potential is lower than that of the diluent. This has been shown for the glycolamide actinide extractant *N,N,N',N'*-tetraoctyl-3-oxapentane-1,5-diamide (TODGA) when irradiated in dodecane or octane solution (*30, 31*). As expected, the addition of benzene to dodecane solutions or the use of aromatic diluents decreases TODGA decomposition due to their low ionization potentials.

Glycolamide derivatives containing aromatic functional groups also exhibited higher radiation stability, possibly due to intramolecular energy transfer to the benzyl ring.

The products of TODGA radiolysis under these conditions included dioctylamine, dioctylacetamide, dioctylglycolamide, and dioctylformamide (*30*, *31*). The presence of nitric acid did not enhance radiolytic degradation but did favor cleavage of the C-N bond to form the amine and acidic products over C-O bond cleavage to form acetamide and glycolamide. Post-irradiation solvent-extraction performance of 0.2 M TODGA in an alkane diluent both with and without the presence of nitric acid indicated a gradual decrease in D_{Am} with absorbed dose (*32*). Nine degradation products of irradiated 0.1 M TODGA in alkane diluent were determined in the absence of the aqueous phase (*33*). These included products of C-N bond rupture to eliminate one or more octyl groups from the amide nitrogen and generation of secondary amines. The glycolamide and acetamide products of C-O bond cleavage were also detected.

Another example of a diluent radical cation reaction is provided by the direct radiolysis of TBP (*34*). Tributylphosphate is used at the high concentration of ~ 30% in the PUREX process and direct radiolysis can be expected according to eq 24:

$$(C_4H_9O)_3PO \text{ -\hspace{-0.3em}\raisebox{0.2ex}{\scriptsize\it\char`\~\char`\~}\hspace{-0.3em}} \rightarrow e^-_{sol} + (C_4H_9O)_3PO^{\bullet+} \qquad (24)$$
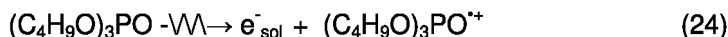
Intramolecular hydrogen bonding between the phosporyl oxygen and a butoxy hydrogen atom next forms a six or seven-membered ring, which decomposes to produce protonated HDBP and the butene radical, as shown in eq 25. Loss of the proton creates HDBP in eq 26:

$$(C_4H_9O)_3PO^{\bullet+} \rightarrow (C_4H_9O)_2P(OH)OH^+ + CH_2=CHCH^{\bullet}CH_3 \quad (25)$$

$$(C_4H_9O)_2P(OH)OH^+ \rightarrow (C_4H_9O)_2POOH + H^+ \qquad (26)$$
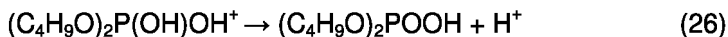
Radiolytic and Hydolytic Nitration Reactions

The nitration of ligands and diluents occurs in the biphasic system even in the absence of irradiation, although product yields are higher in the irradiated system. Non-radiolytic or thermal nitration has been discussed with other nitric acid oxidation reactions under the category "hydrolysis" in the literature. Using anisole as a model compound it was shown that the major nitrated products in both irradiated and unirradiated solution are the same and consist of the ortho-, and para-substituted nitroanisoles and nitrophenol (*35*). These are the products of the nitrous acid catalyzed reaction. In acidic solution nitrous acid reacts to produce the nitrosonium ion (*36*):

$$HNO_2 + H^+ \rightarrow NO^+ + H_2O \qquad (27)$$

Nitrosonium ion is a powerful nitrating agent which reacts with both saturated and unsaturated organic compounds to produce nitroso derivatives, which then oxidize

in nitric acid solution to create the nitro derivatives, shown for an example aromatic compound in eqs 28–29–30:

$$NO^+ + ArH \rightarrow ArHNO^+ \tag{28}$$

$$ArHNO^+ \rightarrow ArNO + H^+ \tag{29}$$

$$ArNO + HNO_3 \rightarrow ArNO_2 + HNO_2 \tag{30}$$

Nitrous acid is regenerated in eq 30. For an alkane diluent the resulting products are nitroparaffins, the enol form of which (eq 31) are complexing agents that are not removed by solvent reconditioning procedures (*37, 38*). Rearrangement of nitropraffins produces hydroxamic acids, which are complexing and reducing agents for the actinide metals (eq 32) (*39*). Hydroxamic acids hydrolyze to produce oxidation products such as carboxylic acids but have been shown to occur at small, steady-state concentrations in irradiated solution (*40*). These deleterious effects of diluent nitration have been reported for the PUREX (*41*) and TRUEX (*27*) solvent extraction systems, and will also be present in other solvent formulations relying on alkane diluents.

$$RCH_2N=O(O) \leftrightarrow RCH=NO(O)^- \tag{31}$$

$$RCH_2NO_2 \rightarrow RCONHOH \tag{32}$$
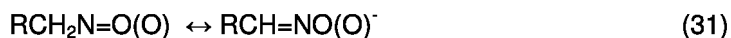
Ligands and/or solvent modifiers also become nitrated. Nitrated products derived from TBP (*42*), Cs-7SB (*43*) and various calixarenes have all been reported (*44*). Yields of these products are higher under irradiation and irradiated solvents develop yellow or yellowish orange tints. Nitrated calixarenes have been identified by mass spectrometric analysis, and the resulting steric interference decreased D_{Cs} (*44*).

The N-centered radical $\cdot NO_2$ has been identified as a nitrating agent in the gas phase for atmospheric chemistry although its reactions are typically slow and non-competitive in the acidic condensed phase. For example, the rate constants for the reactions of $\cdot NO_2$ with TBP (*19*) and Cs-7SB (*45*) have been measured at $< 10^6$ M^{-1} s^{-1}. In contrast, the $\cdot NO_3$ radical is more electrophilic and reactive, having rate constants of 4.3 x 10^6 M^{-1} s^{-1} for TBP (*19*), and 2.7 x 10^9 M^{-1}s^{-1} for Cs-7SB (*45*). The very fast rate constant for the Cs-7SB reaction is indicative of an electron transfer or hydrogen abstraction reaction, rather than an addition to produce a nitrated derivative (*14*). However, these fast reactions produce C-centered radicals in analogy with the similar reactions by $\cdot OH$ radicals reported above, which may then add N-centered radicals to create nitrated products. An example is shown for TBP in eq 33 (*46*):

$$\cdot NO_2 + (C_4H_9O)_2(\cdot C_4H_8O)PO \rightarrow (C_4H_9O)_2(OC_4H_8NO_2)PO \tag{33}$$
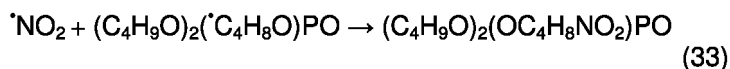
Experiments with anisole in irradiated neutral sodium nitrite solution have shown that $\cdot NO_2$ radical is capable of addition to aromatic compounds in the condensed phase, providing low yields of ortho-, meta-, and para-nitroanisole (*35*). The meta-product is present at the highest concentration, reflecting the statistical substitution of the aromatic ring expected from $\cdot NO_2$ radical addition. This reaction is not significant in irradiated acidic solution, where nitrous acid catalyzed nitration predominates.

Conclusion

Although not an exhaustive list, some major radiolytic reactions of consequence to solvent extraction in the irradiated biphasic system have been presented. Except for high-concentration constituents, direct radiolytic reactions are less important than indirect reactions with reactive species produced from the diluents. Since the irradiated solvent is acidic and aerated, reactions of the produced solvated electron and hydrogen atom are expected to be mitigated by scavenger reactions. However, the oxidizing hydroxyl radical, and to a lesser extent the N-centered radicals will react with ligand molecules to produce dealkylated, hydroxylated and nitrated derivatives. Radiolytically-produced nitrous acid is an important nitrating agent in this system. In addition to solvent extraction experiments, steady-state and pulse radiolysis techniques are necessary to fully understand these reaction mechanisms. There are many opportunities for future research given the large number of new ligands now being considered worldwide for advanced fuel cycle applications.

Acknowledgments

References

1. Pikaev, A. K.; Kabakchi, S. A.; Egorov, G. F. *Radiat. Phys. Chem.* **1988**, *31*, 789–803.
2. Buxton, G. V.; Greenstock, C. L.; Helman, W. P.; Ross, A. B. *J. Phys. Chem. Ref. Data* **1988**, *17*, 513–886.
3. Spinks, J. W. T.; Woods, R. J. *An Introduction to Radiation Chemistry*, 3rd ed.; John Wiley and Sons: New York, 1990; pp 364−392.
4. Katsumura, Y.; Jiang, P. Y.; Nagaishi, R.; Oishi, T.; Ishigure, K. *J. Phys. Chem.* **1991**, *95*, 4435–4439.
5. Bugaenko, L. T.; Roshchektaev, B. M. *Khimiya Vysokikh Energii* **1971**, *5*, 472–474.
6. Jiang, P.-Y.; Nagaishi, R.; Yotsuyanagi, T.; Katsumura, Y.; Ishigure, K. *J. Chem. Soc., Faraday Trans.* **1994**, *90*, 93–95.

7. Benderskii, V. A.; Krivenko, A. G.; Ponomarev, E. A.; Fridovich, N. V. *Sov. Electrochem.* **1987**, *23*, 1343–1348.
8. Elliot, A. J. *Radiat. Phys. Chem.* **1989**, *34*, 753–758.
9. Gordon, S.; Hart, E. J.; Thomas, J. K. *J. Phys. Chem.* **1964**, *68*, 1262–1264.
10. Bellido, A. V.; Rubenich, M. N. *Radiochim. Acta* **1984**, *36*, 61–64.
11. Schreiner, P. R.; von Ragué Schleyer, P.; Schaefer, H. F., III *J. Am. Chem. Soc.* **1995**, *117*, 453–461.
12. Hill, C.; Berthon, L.; Madic, C. *Study of the Stability of BTP Extractants under Radiolysis*, Global 2005 Conference on Nuclear Energy Systems for Future Generation and Glocal Sustainability, Tsukuba, Japan, October 9−13, 2005.
13. von Sonntag, C.; Schuchmann, H.-P. In *Peroxyl Radicals*; Alfassi, Z. B., Ed.; John Wiley and Sons: New York, 1997; pp 173−234.
14. Neta, P.; Huie, R. E. *J. Phys. Chem.* **1986**, *90*, 4644–4648.
15. Bhattacharyya, P. K.; Veeraraghavan, R. *Int. J. Chem. Kinet.* **1977**, *9*, 629–640.
16. Bugaenko, L. T.; Roshchektaev, B. M. *Khimiya Vysokikh Energii* **1971**, *5*, 472–474.
17. Vladimirova, M. V.; Kulikov, I. A.; Savel´ev, Yu. I. *High Energy Chem.* **1969**, *3*, 526–527.
18. Lefort, M.; Tarrago, X. *J. Phys. Chem.* **1959**, *63*, 833–836.
19. Mincher, B. J.; Mezyk, S. P.; Martin, L. R. *J. Phys. Chem.* **2008**, *112*, 6275–6280.
20. Burr, J. G. *Radiat. Res.* **1958**, *8*, 214–221.
21. Khaikin, G. I. *High Energy Chem.* **1998**, *32*, 287–289.
22. Clay, P. G.; Witort, M. *Radiochem. Radioanal. Lett.* **1974**, *19*, 101–107.
23. Kuruc, J. *J. Radioanal. Nucl. Chem. Lett.* **1990**, *145*, 205–213.
24. Draye, M.; Favre-Reguillon, A.; Foos, J.; Guy, A. *Radiat. Phys. Chem.* **2008**, *77*, 581–584.
25. Berthon, L.; Morel, J. M.; Zorz, N.; Nicol, C.; Virelizier, H.; Madic, C. *Sep. Sci. Technol.* **2001**, *36*, 709–728.
26. Bisel, I.; Camès, B.; Faucon, M.; Rudloff, D.; Saucerotte, B. *DIAMEX-SANEX Solvent Behavior under Continuous Degradation and Regeneration Operation*, Global 2007 Conference on Advanced Nuclear Fuel Cycles and Systems; Boise, ID, September 9−13, 2007.
27. Nash, K. L.; Rickert, P. G.; Horwitz, E. P. *Solvent Extr. Ion Exch.* **1989**, *7*, 655–675.
28. Nash, K. L.; Gatrone, R. C.; Clark, G. A.; Rickert, P. G.; Horwitz, E. P. *Sep. Sci. Technol.* **1988**, *23*, 1355−1372.
29. Mincher, B. J.; Cooper, W. J. In *Chemical Degradation Methods for Wastes and Pollutants: Environmental and Industrial Applications*; Environmental Science and Pollution Control Series 26; Tarr, M. A., Ed.; Marcel Dekker Publishers: New York, 2003; pp 305−341.
30. Sugo, Y.; Sasaki, Y.; Tachimori, S. *Radiochim. Acta* **2002**, *90*, 161–165.
31. Sugo, Y.; Izumi, Y.; Yoshida, Y.; Nishijima, S.; Saski, Y.; Kimura, T.; Sekine, T.; Kudo, H. *Radiat. Phys. Chem.* **2007**, *76*, 794–800.

32. Modolo, G.; Asp, H.; Schreinemachers, C.; Vijgen, H. *Solvent Extr. Ion Exch.* **2007**, *25*, 703–721.
33. Mincher, B. J.; Modolo, G.; Mezyk, S. P. *Solvent Extr. Ion Exch.* **2009**, *27*, in press.
34. Wilkinson, R. W.; Williams, T. F. *J. Chem. Soc.* **1961**, 4098–4107.
35. Mincher, B. J.; Elias, G.; Martin, L. R.; Mezyk, S. P. *J. Radioanal. Nucl. Chem.* **2009**, in press, DOI: 10.1007/s 10967-009-0156-x.
36. Turney, T. A.; Wright, G. A. *Chem. Rev.* **1959**, *59*, 497–513.
37. Stieglitz, L.; Becker, R. *Kerntechnik* **1985**, *46*, 76–80.
38. Tripathi, S. C.; Bindu, P.; Ramanujam, A. *Sep. Sci. Technol.* **2001**, *36*, 1463–1478.
39. Lane, E. S. *Nucl. Sci. Eng.* **1963**, *17*, 620–625.
40. Hao-xin, H.; Guo-hui, Z.; Shu-bin, H. *Radiochim. Acta.* **1988**, *46*, 159–162.
41. Tahraoui, A.; Morris, J. H. *Sep. Sci. Technol.* **1995**, *30*, 2603–2630.
42. Lasage, D.; Virelizier, H.; Jankowski, C. K.; Tabet, J. C. *Spectroscopy* **1997**, *13*, 275–290.
43. Mincher, B. J.; Mezyk, S. P.; Bauer, W. F.; Elias, G.; Riddle, C. L.; Peterman, D. R. *Solvent Extr. Ion Exch.* **2007**, *25*, 593–601.
44. Lamare, V.; Dozol, J.-F.; Allain, F.; Virelizier, H.; Moulin, C.; Jankowski, C.; Tabet, J.-C. In *Calixarenes for Separations*; Lumetta, G. J., Rogers, R. D., Gopalan, A. S., Eds.; ACS Symposium Series 757; American Chemical Society: Washington DC, 2005, pp 26−43.
45. Mincher, B. J.; Mezyk, S. P., unpublished data.
46. He, H.; Lin, M.; Muroya, Y.; Kudo, H.; Katsumura, Y. *Phys. Chem. Chem. Phys.* **2004**, *6*, 1264–1268.

Chapter 16

Aqueous Nitric Acid Radiation Effects on Solvent Extraction Process Chemistry

Stephen P. Mezyk,*,[1] Thomas D. Cullen,[1] Gracy Elias,[2] and Bruce J. Mincher[2]

[1]Department of Chemistry and Biochemistry, California State University, Long Beach, 1250 Bellflower Blvd., Long Beach, CA 90840
[2]Aqueous Separations and Radiochemistry Department, Idaho National Laboratory, P.O. Box 1625, Idaho Falls, ID 83415-6150
*smezyk@csulb.edu

The use of aqueous nitric acid is ubiquitous in the nuclear industry especially as the diluent for dissolved used fuel in nuclear solvent extraction processes. These acidic solutions are therefore exposed to the radioactive decay energy from the actinides and fission products contained in the fuel. The radiolysis of aqueous nitric acid produces a mixture of radical and molecular species especially the $\cdot NO_2$ and $\cdot NO_3$ radicals. We have measured the absorbance of these radicals in pulse-irradiated 6.0 M nitric acid and find that at this acidity no $\cdot NO_2$ species was detectable. This, coupled with slow rate constants for reaction of $\cdot NO_2$ with many organic solutes, suggests that $\cdot NO_3$ radical is the more important reactive species. However, most literature values for $\cdot NO_3$ reaction with organic solutes have been made in acetonitrile, rather than aqueous acidic solution, so here we have compared values available in both solvents, including our own measurements, to obtain a quantitative correlation between the two solvents. The implications for the mechanism of the reaction with some ligand solutes are discussed.

Introduction

Every year some 10,000 tonnes of spent fuel is discharged from nuclear reactors across the world. For the majority of this fuel that is ultimately slated for repository disposal, the prior partitioning of the long-lived alpha emitters and high-yield fission products would reduce its long-term radiotoxicity and significantly shorten the time needed for safe confinement (*1*). Planned partitioning strategies for light-water reactor fuels are likely to be based on solvent-extraction technologies. These technologies would selectively remove the uranium, plutonium, and minor actinide actinides from the remainder of the fission products. All of these extraction systems will have to work under highly acidic and radioactive conditions.

Therefore, the design and implementation of a practical reprocessing system requires extraction ligands that are robust. In the aqueous phase, or at the aqueous-organic interface in the solvent extraction process where the metal ion complexation occurs, both thermal and radiolytically-induced degradation of the ligands and solvents will occur. The full understanding of this chemistry, particularly establishing the quantitative impact of the radiolysis occurring in aqueous nitric acid solutions, will potentially allow the minimization of interfering ligand degradation chemistry (*2*).

The radiolysis of nitric acid solutions has been extensively studied for many years (*3*). The $NO_3^•$ radical is one of the most important intermediates formed by radiolysis of nitric acid solutions and many investigations have been carried out on its formation mechanisms (*2, 4–11*) and yields (*2, 8, 9*). These investigations have identified two major $NO_3^•$ formation pathways in aqueous acidic media; through the reaction of hydroxyl radicals ($^•OH$) with undissociated nitric acid molecules (*2*):

$$^•OH + HNO_3 \rightarrow H_2O + NO_3^• \qquad k_1 = 1.4 \text{ x } 10^8 \text{ M}^{-1} \text{ s}^{-1} \qquad (1)$$
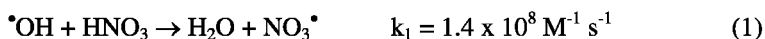
and the direct action of radiation on nitrate anions:

$$NO_3^- \text{ -}\land\!\land\!\land\!\rightarrow NO_3^• + e_{aq}^- \qquad (2)$$
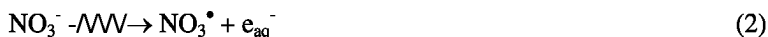
The reaction of nitrate anions with H_2O^+ has also been proposed (*9*):

$$H_2O^+ + NO_3^- \rightarrow H_2O + NO_3^• \qquad (3)$$

The chemical reactivity of the $NO_3^•$ radical has been well-studied in the gas phase (*12–14*) due to its important nighttime chemistry in the atmosphere. In the solution phase a number of rate constants for $NO_3^•$ radical reactions in acetonitrile (*15–22*) have also been determined, but only a few investigations have studied this radicals' reactions in aqueous solution (*2, 10, 18, 21, 23–29*). Moreover, much less study on the $NO_3^•$ radical reactivity has been done in other solvents (*10, 18*).

The purpose of this study was to establish $NO_3^•$ radical reactivities for some important ligands used in nuclear waste reprocessing, and to gain insight into the mechanisms of this reactivity through the use of model ligands under anticipated acidic, real-world, reprocessing conditions. The correlation of measured rate constants in acetonitrile and acidic water has also performed, in order to establish

a predictive capability for larger reprocessing ligands that are only sparingly soluble in acidic aqueous solution.
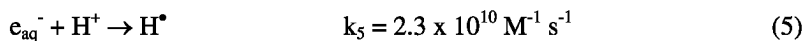
Experimental

All of the chemicals used in this study (Fischer, Sigma-Aldrich) were of reagent grade or higher purity, and used as received. Aqueous 6.0 M HNO_3 solutions were made by diluting concentrated nitric acid with Millipore Milli-Q, charcoal-filtered (TOC <13 ppb), deionized (>18.0 MΩ) water. At this acidity, some 20% of the nitic acid exists in its non-dissociated form (*2*). Care was taken to ensure that all chemical solutions cooled to room temperature before use.

The radiolysis of neutral pH water gives a mixture of radicals and molecular products according to the following equation (*30*):

$$H_2O -\text{/\/\/\/}\rightarrow [0.28]^{\bullet}OH + [0.27]e_{aq}^{-} + [0.06]H^{\bullet}$$
$$+ [0.07]H_2O_2 + [0.05]H_2 + [0.27]H_3O^{+} \qquad (4)$$
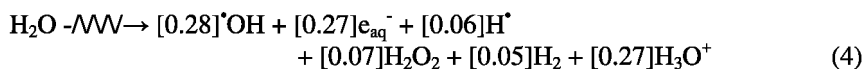
The coefficients of each species are absolute yields in μmol Gy^{-1}. Under these highly acidic conditions, no free hydrated electrons exist, as fast reaction with protons to form hydrogen atoms, and nitrate ions to form $NO_3^{2-\bullet}$, occurs by:

$$e_{aq}^{-} + H^{+} \rightarrow H^{\bullet} \qquad\qquad k_5 = 2.3 \text{ x } 10^{10} \text{ M}^{-1} \text{ s}^{-1} \qquad (5)$$

$$e_{aq}^{-} + NO_3^{-} \rightarrow NO_3^{2-\bullet} \qquad\qquad k_6 = 9.7 \text{ x } 10^{9} \text{ M}^{-1} \text{ s}^{-1} \qquad (6)$$
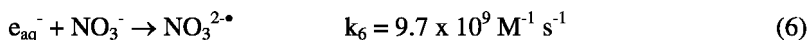
To improve our initial yield of $NO_3^{\bullet}$ radicals, formed by reactions (1) and (2), the nitric acid solutions were pre-saturated with N_2O gas, which converted some hydrated electrons into $^{\bullet}OH$ radicals, via the reaction

$$e_{aq}^{-} + N_2O (+ H_2O) \rightarrow {}^{\bullet}OH + OH^{-} + N_2 \quad k_7 = 9.1 \text{ x } 10^{9} \text{ M}^{-1} \text{ s}^{-1} \qquad (7)$$
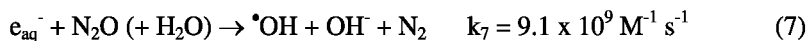
All radicals were generated by irradiating the 6.0 M HNO_3 solutions with an 8 MeV electron beam, generated by a linear accelerator at the University of Notre Dame Radiation Laboratory. This system has been described in detail previously (*31*). This accelerator system gives 2-10 ns pulses of electrons, of doses ranging from 3-15 Gy, and the resulting chemical reactions were observed on the microsecond timescale using a transient absorption detection system (*32*). These irradiation conditions gave $NO_3^{\bullet}$ radical concentrations of the order of 10-20 μM, with solute concentrations chosen to ensure pseudo-first-order kinetics were maintained. Recombinant water radiolysis products, such as hydrogen peroxide, react slowly on time scales that are much too long to interfere with these radical measurements.

A continuous-flow cuvette was used to prevent build-up of interfering absorptions due to long-lived products. Solution flow rates were adjusted so that each pulse irradiation was performed on a fresh sample, and multiple traces (*5–20*) were averaged to produce a single kinetic trace.

Absolute hydroxyl radical concentrations (dosimetry) were measured using the transient absorption of $(SCN)_2^{\bullet-}$ at 475 nm, using 0.010 M potassium

thiocyanate (KSCN) in N_2O-saturated solution at natural pH (*33*). These measurements were performed daily.

Rate constant error limits reported here are the combination of experimental precision and estimated compound purities.

Results and Discussion

The electron pulse radiolysis of only a 6.0 M HNO_3 aqueous solution gave a transient spectrum (see Figure 1) whose characteristic absorption bands between 550 and 700 nm identified this absorption as being due to the $NO_3^{\bullet}$ radical. The $NO_3^{\bullet}$ radical absorption spectrum in the gas phase is sharper than seen here, and slightly red-shifted (*34, 35*). Our spectrum is shown in comparison to that obtained by the laser flash photolysis of cerium(IV) ammonium nitrate under the same conditions, and also for that of $NO_2^{\bullet}$, which is obtained by the $^{\bullet}OH$ radical oxidation of the nitrite ion (*36*).

$$^{\bullet}OH + NO_2^- \rightarrow OH^- + NO_2^{\bullet} \qquad k_8 = 6.0 \times 10^9 \ M^{-1} \ s^{-1} \qquad (8)$$

One marked difference for our spectrum under these highly acidic conditions is seen in the wavelength range 300 – 450 nm, where the literature peaks for the two radicals was not observed. While the flash photolysis spectrum could have some interference from the remaining Ce(IV) product, the $NO_2^{\bullet}$ radical absorption would have been expected to have been formed from the subsequent decay of any formed $NO_3^{2-\bullet}$ (*30*):

$$NO_3^{2-\bullet} + H^+ \rightarrow {}^{\bullet}NO_2 + OH^- \qquad k_9 = 2 \times 10^{10} \ M^{-1} \ s^{-1} \qquad (9)$$

$$NO_3^{2-\bullet} + H_2O \rightarrow {}^{\bullet}NO_2 + 2OH^- \qquad k_{10} \sim 1 \times 10^5 \ s^{-1} \qquad (10)$$
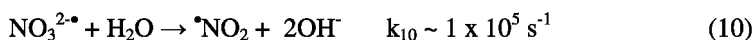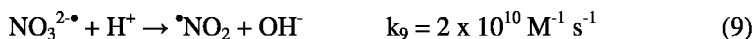
or through reaction of the formed hydrogen atoms with nitrate (*37*):

$$H^{\bullet} + NO_3^- \rightarrow {}^{\bullet}OH + NO_2^- \qquad k_{11} = 5.6 \times 10^6 \ M^{-1} \ s^{-1} \qquad (11)$$

followed by $NO_3^{\bullet}$ oxidation of nitric acid (*2*):

$$NO_3^{\bullet} + HNO_2 \rightarrow HNO_3 + NO_2^{\bullet} \qquad k_{12} = 8.0 \times 10^6 \ M^{-1} \ s^{-1} \qquad (12)$$
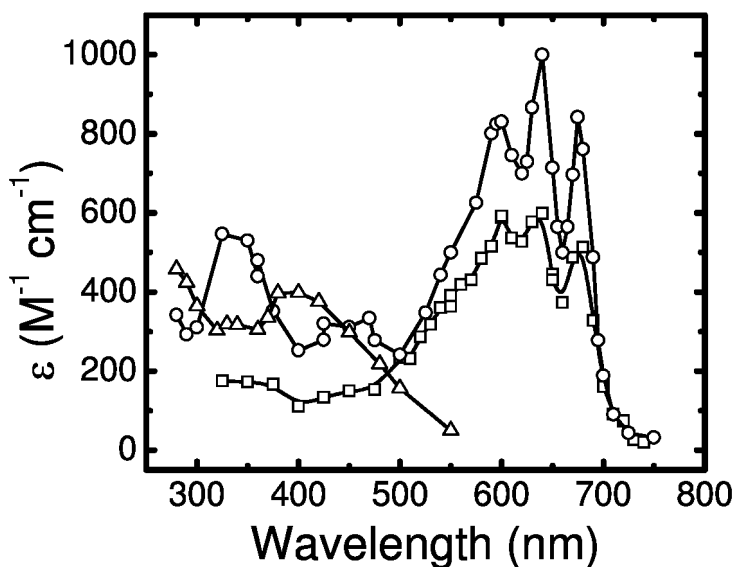
Figure 1. Measured spectrum of NO$_3$• radical (squares) in 6.0 M HNO$_3$ in comparison to the literature spectra for NO$_3$• (circles, from Ce(NO$_3$)$_6^{3-}$ photolysis) and NO$_2$• (triangles, from •OH radical oxidation of NO$_2^-$).

The lack of NO$_2$• radical formation suggests that under these highly acidic conditions, an alternative decay pathway of the NO$_3^{2-}$• radical occurs. One possibility is perhaps through the formation of H$_2$NO$_3$:

$$NO_3^{2-\bullet} + 2H^+ \rightarrow H_2NO_3 \tag{13}$$

which might be a more stable species than the intermediate monoprotonated radical formed by single proton addition to NO$_3^{2-}$• (Equation 9).

However, the NO$_3$• radical kinetics can still be determined through monitoring the absorbance change at 640 nm (see Figure 2). The lifetime of the NO$_3$• radical in only the acidic solution is long, > 50 μs, and the decay follows first-order kinetics. Upon addition of a solute, the decay becomes faster, and by plotting the fitted exponential decay kinetic paramaters against the solute concentration, the second-order rate constant can be determined. This is shown for NO$_3$• radical reaction with lactic acid in Figure 2b:

$$NO_3^\bullet + CH_3CH(OH)CO_2H \rightarrow products \quad k_{14} = (2.15 \pm 0.17) \times 10^5 \tag{14}$$
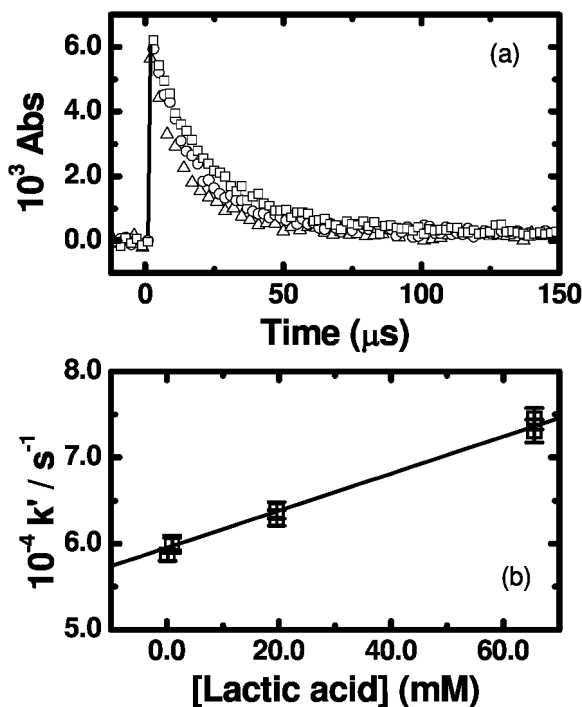
Figure 2. a) Decay of the NO₃• radical at 640 nm in N₂O-saturated 6.0 M HNO₃ with 0.141 (squares),, 19.58 (circles) and 65.57 (triangles) mM lactic acid added. b) Transformed second order plot of fitted pseudo-first-order decay kinetics of (a) plotted against lactic acid concentration. Solid line is weighted linear fit, corresponding to reaction rate constant of $k = (2.15 \pm 0.17) \times 10^5$ M^{-1} s^{-1} ($R^2 = 0.990$).

Table 1. Summary of NO₃• radical reaction rate constants for some ligands used in nuclear waste reprocessing

Ligand	k_{NO3} M^{-1} s^{-1}
Lactic acid	$(2.15 \pm 0.17) \times 10^5$
Tributyl phosphate	$(4.3 \pm 0.7) \times 10^6$
Cs7SB	$(2.71 \pm 0.03) \times 10^9$

Table 2. Summary of measured NO₃˙ reaction rate constants for compounds in acetonitrile and acidic water. Values of this study in bold

Chemical	log_{10} k_{CH_3CN}	log_{10} k_{H_2O}
Methanol	6.37	5.32
Ethanol	6.83	6.29
1-Propanol	6.71	6.33
1-Butanol	6.84	6.28
tert-Butanol	5.36	4.75
1-Pentanol	6.83	6.38
1-Hexanol	6.79	6.52
1-Heptanol	6.90	6.56
1-Octanol	6.93	6.76
Propen-3-ol	8.35	8.34
Ethylene Glycol	6.82	5.88
Acetone	5.38	3.64
Acetaldehyde	7.36	5.69
Benzene	6.0	**6.0**
Anisole	9.36	**9.65**
4-methylanisole	10.11	**9.69**
Toluene	8.11	**9.23**
3-nitrotoluene	5.78	**7.45**
1,2-Dimethylbenzene	9.57	**9.39**
1,3-Dimethylbenzene	9.23	**9.11**
1,4-Dimethylbenzene	9.79	**9.03**

Kinetic data obtained by this approach for several extraction ligands that had sufficient solubility in water are summarized in Table 1. These rate constants varied over four orders of magnitude with the faster values observed for species containing aromatic rings. It has previously been shown that in the condensed phase, the NO₃˙ radical can react via both electron or hydrogen atom transfer, depending on the ionization potential of the solute. The latter reaction occurs for simple aliphatic alcohols, (see Table 2 for measured literature values) (*30*) where H˙ atom abstraction occurs from the –OH group (*21*). Analyses of these data showed a sub-group reactivity of ~7 x 10⁴ M⁻¹ s⁻¹, ~7 x 10⁵ M⁻¹ s⁻¹ and 2.4 x 10⁶ M⁻¹ s⁻¹ for primary, secondary, and tertiary carbon hydrogen atom abstraction,

respectively (*23*). These reaction rate constants are slower than the corresponding values determined in acetonitrile, utilizing laser flash photolysis (*15–22*).

However, the relative $NO_3^\bullet$ reactivity in acetonitrile also occurs similarly; it has been shown that formation of an initial complex between $NO_3^\bullet$ and aromatic alkylbenzenes in CH_3CN which decays in <20 ns either by hydrogen atom transfer or by deprotonation to form a radical cation depending on the oxidation potential of the substrate (*15*). It was found that radical cation formation occurred for species with an ionization potential of less than 8.4eV whereas for higher solute ionization potentials benzyl radicals were formed.

The direct comparison of nitrate radical reactivity with aromatic-containing solutes in aqueous solution was significantly hampered by the limited data available (*30*). As many of the extraction ligands planned for real-world extraction usage have aromatic moieties, we measured reaction rate constants for $NO_3^\bullet$ with several prototypical simple aromatic species. These data were obtained as for lactic acid (see Figure 2), and the measured data are also summarized in Table 2. As expected from the acetonitrile data, much faster reaction rate constants were obtained for aromatic compounds.

The correlation of $NO_3^\bullet$ radical reactivity with solute structure has been investigated previously, with plots of log(k) vs C-H bond strength. (*23, 26*), Hammett sigma parameters (*16, 19*), ionization energies (*17, 21*) and indirect correlations with Marcus and Rehm-Weller theories (*19, 20*), and sulfate radicals (*28*) reported. However for a more direct comparison, we have chosen to follow the method of Ito *et al.* (*21*) in plotting the logarithm of the measured rate constant in acetonitrile against the same parameter in water. These data are shown in Figure 3, and a very good correlation is observed with the exception of two compounds: toluene and 3-nitrotoluene. The $NO_3^\bullet$ reaction with toluene has been shown to have a significant deuterium isotope effect in acetonitrile (*17*) suggesting that some hydrogen atom abstractions dominate in this solvent. In water, however, it's possible that electron abstraction is the major mechanism, resulting in a faster reaction rate constant. It is assumed that similar reactions could occur for the mono-nitrated toluene.

The remaining rate constant data were well fitted by the equation

$$\log_{10} k_{CH3CN} = (1.674 \pm 0.332)*\log_{10} k_{H2O} + (0.827 \pm 0.045) \qquad (15)$$

The very good ($R^2 = 0.95$) linear correlation for the $NO_3^\bullet$ reaction rate constants observed for most of these simple organic species suggests that more complex organic ligand rate constants could be extrapolated to acidic water solutions from acetonitrile measurements. This is important because many of the molecules proposed for use as metal complexing agents in nuclear solvent extraction have been purposefully designed to be insoluble in water, and aqueous solutions are not readily prepared for kinetic investigation. These species will, however, be exposed to reaction with the $NO_3^\bullet$ radical in the solvent extracation process.
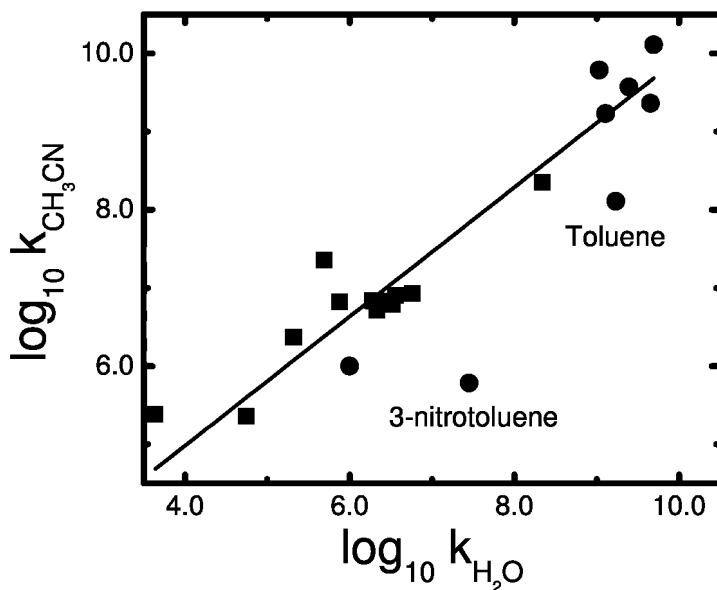
Figure 3. Correlation plot for rate constants measured in acetonitrile against those in acidic water. Black squares are previous literature data, circles are data of this study. Solid line represents linear fit (excluding values for toluene and 3-nitrotoluene) with slope 1.674 ± 0.332, intercept 0.827 ± 0.045 and $R^2 = 0.95$

Acknowledgments

References

1. *Actinide and Fission Product Partitioning and Transmutation: Status and Assessment Report*; ISSN 0074-1914; Nuclear Energy Agency (NEA)/Organisation for Economic Co-operation and Development (OECD): Paris, 1999.
2. Katsumura, Y.; Jiang, P. Y.; Nagaishi, R.; Oishi, T.; Ishigure, K. *J. Phys. Chem.* **1991**, *95*, 4435–4439.
3. Polevi, P.; Ross, A. B. *Radiat. Phys. Chem.* **1987**, *29*, 161–174.
4. Daniels, M. *J. Phys. Chem.* **1966**, *70*, 3022–3024.
5. Broszkiewicz, R. K. *Int. J. Appl. Radiat. Isot.* **1967**, *18*, 25–32.
6. Daniels, M. *J. Phys. Chem.* **1969**, *73*, 3710–3717.
7. Hamill, W. H. *J. Phys. Chem.* **1969**, *73*, 1341–1347.

8. Pikaev, A. K.; Sibirskaya, G. K.; Shirshov, E. M.; Glazunov, P. Ya.; Spitsyu, V. I. *Dokl. Akad. Nauk SSSR* **1974**, *215*, 645–648.

9. Kozlowska-Milner, E.; Broszkiewicz, R. K. *Radiat. Phys. Chem.* **1978**, *11*, 253–260.

10. Broszkiewicz, R. K.; Kozlowska-Milner, E.; Blum, A. *J. Phys. Chem.* **1981**, *85*, 2258–2262.

11. Kozlowska-Milner, E. *Appl. Radiat. Isot.* **1987**, *38*, 517–520.

12. Cabanas, B.; Baeza-Romero, M. T.; Martin, P.; Salgado, S.; Villanueva, F.; Monedero, E.; Martinez, E. *Recent Res. Dev. Phys. Chem.* **2007**, *9*, 137–157.

13. Atkinson, R. Atmospheric Oxidation. In *Handbook of Property Estimation Methods for Chemicals*; Boethling, R. S., Mackay, D., Eds.; CCR Press, LLC: Boca Raton, FL, 2000; pp 335−354.

14. Wayne, R. P.; Barnes, I.; Biggs, P.; Burrows, J. P.; Canosa-Mas, C. E.; Hjorth, J.; Le Bras, G.; Moortgat, G. K.; Perner, D.; Poulet, G.; Restelli, G.; Sidebottom, H. *Atmos. Environ., Part A* **1991**, *25A*, 1–203.

15. Del Giacco, T.; Baciocchi, E.; Steenken, S. *J. Phys. Chem.* **1993**, *97*, 5451–5456.

16. Ito, O.; Akiho, S.; Iino, M. *J. Phys. Chem.* **1989**, *93*, 4079–4083.

17. Ito, O.; Akiho, S.; Iino, M *J. Org. Chem.* **1989**, *54*, 2436–2440.

18. Alfassi, Z. B.; Padmaja, S.; Neta, P.; Huie, R. E. *J Phys. Chem.* **1993**, *97*, 3780–3782.

19. Baciocchi, E.; del Giacco, T.; Murgia, S. M.; Sebastiani, G. V. *Tetrahedron* **1988**, *44*, 6651–6660.

20. Baciocchi, E.; del Giacco, T.; Murgia, S. M.; Sebastian, G. V. *J. Chem. Soc., Chem. Commun.* **1987**, 1246–1248.

21. Ito, O.; Akiho, S.; Iino, M. *Bull. Chem. Soc. Jpn.* **1989**, *62*, 1606–1611.

22. Akiho, S.; Ito, O.; Iino, M. *Int. J. Chem. Kinet.* **1989**, *21*, 667–676.

23. Neta, P.; Huie, R. E. *J. Phys. Chem.* **1986**, *90*, 4644–4648.

24. Dogliotti, L.; Hayon, E. *J. Phys. Chem.* **1967**, *71*, 3802–3808.

25. Exner, M.; Herrmann, H.; Zellner, R. *Ber. Bunsen-Gen.* **1992**, *96*, 470–477.

26. Herrmann, H.; Exner, M.; Zellner, R. *Geochim. Cosmochim. Acta* **1994**, *58*, 3239–3244.

27. Exner, M.; Herrmann, H.; Zellner, R. *J. Atmos. Chem.* **1994**, *18*, 359–378.

28. Shastri, L. V.; Huie, R. E. *Int. J. Chem. Kinet.* **1990**, *22*, 505–512.

29. Mincher, B. J.; Mezyk, S. P.; Martin, L. R. *J. Phys. Chem. A.* **2008**, *112*, 6275–6280.

30. Buxton, G. V.; Greenstock, C. L.; Helman, W. P.; Ross, A. B. *J. Phys. Chem. Ref. Data* **1988**, *17*, 513–886.

31. Whitman, K.; Lyons, S.; Miller, R.; Nett, D.; Treas, P.; Zante, A.; Fessenden, R. W.; Thomas, M. D.; Wang, Y. *Linear Accelerator for Radiation Chemistry Research at Notre Dame 1995*, Proceedings of 1995 Particle Accelerator Conference and International Conference of High Energy Accelerators, Dallas, TX, 1996.

32. Hug, G. L.; Wang, Y.; Schoneich, C.; Jiang, P. Y.; Fessenden, R. W. *Radiat. Phys. Chem.* **1999**, *54*, 559–566.

33. Buxton, G. V.; Stuart, C. R. *J. Chem. Soc., Faraday Trans.* **1995**, *91*, 279–282.

34. Graham, R. A.; Johnson, H. S. *J Phys. Chem.* **1978**, *82*, 254–268.
35. Mitchell, D. N.; Wayne, R. P.; Allen, J.; Harrison, R. P.; Twin, R. J. *J. Chem. Soc., Faraday Trans. 2* **1980**, *76*, 785–793.
36. Logager, T.; Sehested, K. *J. Phys. Chem.* **1993**, *97*, 6664–6669.
37. Mezyk, S. P.; Bartels, D. M. *J. Phys. Chem. A* **1997**, *101*, 6233–6237.

Chapter 17

Nitration Mechanisms of Anisole during Gamma Irradiation of Aqueous Nitrite and Nitrate Solutions

Gracy Elias,*,[1] Bruce J. Mincher,[1] Stephen P. Mezyk,[2] Thomas D. Cullen,[2] and Leigh R. Martin[1]

[1]Idaho National Laboratory, P.O. Box 1625, Idaho Falls, ID 83415, U.S.A.
[2]California State University-Long Beach, 1250 Bellflower Blvd., Long Beach, CA 90840, U.S.A.
*Corresponding Author. Phone: (208) 526-0979. Fax: (208) 526-0603. E-mail gracy.elias@inl.gov.

The nitration of aromatic compounds in the condensed phase is of interest to nuclear waste treatment applications. This chapter discusses our investigation of radiolytic aromatic nitration mechanisms in the condensed phase toward understanding the nitration products created during nuclear fuel reprocessing. The nitration reactions of anisole, a model aromatic compound, were studied in γ-irradiated acidic nitrate, neutral nitrate, and neutral nitrite solutions. The nitrated anisole product distributions were the same with and without radiation in acidic solution, although more products were formed with radiation. In the irradiated acidic condensed phase, radiation-enhanced nitrous acid-catalyzed nitrosonium ion electrophilic aromatic substitution followed by oxidation reactions dominated over radical addition reactions. Neutral nitrate anisole solutions were dominated by mixed nitrosonium/nitronium ion electrophilic aromatic substitution reactions, but with lower product yields. Irradiation of neutral nitrite anisole solution resulted in a statistical substitution pattern for nitroanisole products, suggesting non-electrophilic free radical reactions involving the $\cdot NO_2$ radical.

Introduction

The ligands proposed for use in nuclear fuel reprocessing including some that contain aromatic functional groups will be exposed to highly radioactive aqueous nitric acid solutions, and many have been shown to undergo nitration in irradiated acidic solution (1–3). Some nitration products of the modifier, Cs-7SB, were found in the FPEX (Fission Product Extraction) formulation used for Cs extraction in the presence of nitric acid (1). The selectivity of ligands for the complexation of certain actinides and lanthanides may be affected by nitration products found in the nitric acid system. The radiolytic degradation of a ligand can reduce the ligand concentration, thus depressing the forward extraction distribution ratios. The degradation products may also act as complexing agents that increase forward extraction distribution ratios, or complex undesirable elements to reduce the selectivity of the solvent extraction system (4). Degradation can also affect ligand solubility, viscosity and other solvent properties. In irradiated nitric acid systems, some of these reactions presumably occur due to reactions with radiolytically-produced nitrogen-centered radicals like $\cdot NO$, $\cdot NO_2$ and $\cdot NO_3$.

In concentrated nitric acid solution, substitution of a nitro group for a hydrogen atom on the aromatic ring occurs in electrophilic or free radical reactions. Conventional "thermal" nitration occurs with high positional selectivity through electrophilic aromatic substitution via the nitronium ion, shown in Equations 1-2 (5) for a concentrated nitric acid solution.

$$2HNO_3 \rightarrow NO_2^+ + NO_3^- + H_2O \tag{1}$$

$$ArH + NO_2^+ \rightarrow ArNO_2 + H^+ \tag{2}$$

Electrophilic nitration in nitric acid solution is also catalyzed by nitrous acid under conditions of high acidity. Nitrous acid protonates and dissociates to produce the nitrosonium ion NO^+, as shown in Equation 3. The nitrosonium ion is electrophilic and reacts with aromatic compounds as shown in Equations 4 and 5 to produce a nitroso product (6):

$$HNO_2 + H^+ \rightleftharpoons NO^+ + H_2O \tag{3}$$

$$ArH + NO^+ \rightarrow ArHNO^+ \tag{4}$$

$$ArHNO^+ \rightarrow ArNO + H^+ \tag{5}$$

Nitroso species are readily oxidized to form the corresponding nitro products (7):

$$ArNO + HNO_3 \rightarrow ArNO_2 + HNO_2 \tag{6}$$

Nitrous acid is continually generated in nitric acid solution via nitric acid oxidation of solutes. The ortho/para ratio for the nitrated products for this type of reaction is < 1, and it depends on the type of aromatic substrate and the acidity of the solution (8, 9). Thus, in acidic solution, nitration may occur by a combination of NO_2^+ and NO^+ ion electrophilic aromatic substitution reactions, with low yields of meta products.

Titov (*10*) discussed the mechanism of radical aromatic nitration. The direct reaction with aromatic compounds is shown in Equation 7 (*11*):

$$ArH + \cdot NO_2 \rightarrow \cdot ArHNO_2 \tag{7}$$

The hydrogen atom abstraction reaction to produce a stable nitrated aromatic product is shown below (*5*):

$$\cdot ArHNO_2 + \cdot NO_2 \rightarrow ArNO_2 + HNO_2 \tag{8}$$

The nitration of aromatic compounds by the less electrophilic $\cdot NO_2$ radical is reported to occur without positional selectivity, resulting in a statistical distribution of 40% ortho, 40% meta and 20% para-substituted products (*12*) except when steric considerations reduce the abundance of the ortho-isomer. The $\cdot NO_3$ radical is more electrophilic and more reactive than the $\cdot NO_2$ radical and its reactions with organic compounds are generally reported to occur via hydrogen atom abstraction and electron transfer to produce carbon-centered radical products (*13*).

In this chapter, we report experiments designed to elucidate the mechanism of the nitration of anisole in γ-irradiated aqueous nitric acid. Anisole ($C_6H_5\text{-}OCH_3$) is highly reactive towards nitration and thus large amounts of products may be generated at moderate absorbed radiation doses. Since a suite of radical and ionic reactive species are produced in this system, solutions of nitric acid, neutral nitrate and neutral nitrite were irradiated in separate experiments to isolate selected reactive species. Following irradiation, the stable products were measured using high performance liquid chromatography (HPLC). Pulse radiolysis techniques were used to measure reactions of the $\cdot NO_2$ and $\cdot NO_3$ radicals with anisole and related compounds to elucidate these mechanisms kinetically.

Experimental Methods

Saturated and known concentrations of reagent-grade neat compounds of anisole were prepared in 6 M HNO_3, 6 M $NaNO_3$, and $NaNO_2$ (0.05, 0.1, 0.5 and 1 M) solutions. The acid, neutral nitrate and neutral nitrite solutions were chosen to maximize production of the $\cdot NO_3$ radical or $\cdot NO_2$ radical. These were then sparged with N_2 to remove oxygen and to provide adequate mixing. Oxygen was eliminated to minimize peroxyl radical formation and subsequent loss of products to ring-opening reactions which would lead to decreased concentrations of the nitro aromatic products that were the object of this study. Aliquots of the prepared acidic and neutral solutions of anisole were then transferred to 1 mL glass vials for irradiation. Hydrazine, a nitrous acid scavenger, was used in unirradiated solutions of anisole and 6 M HNO_3 to investigate nitrous acid catalyzed nitration of anisole in nitric acid.

Irradiations were performed using a Nordion Gammacell 220E (Ottawa, Canada) [60]Co γ-source with a nominal dose rate of 12 kGy h[-1]. The samples were exposed in a series of absorbed doses, including an unirradiated control, by varying the duration of exposure to the γ-ray source. Dosimetry was performed using GafChromic (Goleta, CA, USA) radiochromic films, traceable to Fricke dosimetry. The temperature in the irradiator sample chamber was 50 °C.

The linear accelerator (LINAC) electron pulse radiolysis system at the Radiation Laboratory, University of Notre Dame, was used for the reaction rate constant determinations in this study. During rate constant measurements, the solution vessels were sparged with a minimum amount of nitrogen gas necessary to prevent air ingress. Solution flow rates in these experiments were adjusted so that each irradiation was performed on a fresh sample. Dosimetry was performed using N_2O-saturated, 1.00 x 10^{-2} M KSCN solutions at λ = 475 nm, ($G\varepsilon$ = 5.2 x 10^{-4} m2 J^{-1}) with average doses of 3-5 Gy per 2-3 ns pulse. All measurements were conducted at a room temperature of 18 ± 1 °C.

For HPLC analyses, a 10 µL injection volume was analyzed using a Shimadzu HPLC (Shimadzu LC-10 AD VP pumps, CTO-10 AC VP column oven, SIL-HTc autosampler and a SPD-M10A VP photo-diode array detector and Class VP software) and a Supelco 25 cm x 4.6 mm, 5 µm C-18 column at 55 °C. Methanol and water (55:45) at a flow rate of 0.5 mL min^{-1} was used isocratically with a run time of 30 minutes and the analytes were detected at a wavelength of 254 nm. The approximate retention time for anisole was 15 minutes. Products were identified by comparison of the retention times and UV spectra to standard compounds. All results are the means of the triplicate analyses.

For GC-MS analyses, a Shimadzu GC system (GC-MS QP 2010, AOC-5000 auto injector, and GCMS solution software) coupled to a quadrupole mass spectrometer operating in electron impact ionization (EI) mode was used. The GC separation was performed using a Restek XTI-5 capillary column with a length of 30.0 m x 0.25 mm id and a film thickness of 0.25 µm. The oven temperature was programmed as follows: 40 °C (3 min.); 5 °C/min to 100 °C; 50 °C/min to 250 °C (2 min.). 1 µL injection of sample with a split ratio of 15.0 was used for anisole products analysis in the extracted methylene chloride solution.

Results and Discussion

Kinetic Study

Direct radiolysis of HNO_3 gives radiolysis products of both HNO_3 and water as shown in Equations 9101112.

$$H_2O \xrightarrow{\text{-/\/\/\/-}} {}^{\bullet}OH + e_{aq}^{-} + H^{\bullet} + H_2 + H_2O_2 + H^{+} \tag{9}$$

$$HNO_3 \xrightarrow{\text{-/\/\-}} e^{-} + HNO_3^{+} \rightarrow H^{+} + e^{-} + {}^{\bullet}NO_3 \tag{10}$$

$$NO_3^{-} \xrightarrow{\text{-/\/\-}} e^{-} + {}^{\bullet}NO_3 \tag{11}$$
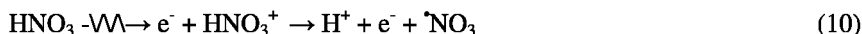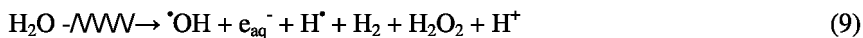
The aqueous electrons (e_{aq}^{-}) will immediately be converted to $^{\bullet}H$ atoms (*14*):

$$e_{aq}^{-} + H^{+} \rightarrow H^{\bullet} \qquad k_{12} = 2.3 \times 10^{10} M^{-1} s^{-1} \tag{12}$$
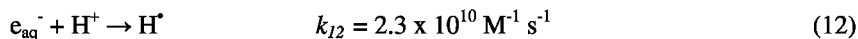
Both $^{\bullet}NO_3$ and $^{\bullet}NO_2$ transient absorption spectra were measured (the peak absorption maximum $^{\bullet}NO_3$, 640 nm; $^{\bullet}NO_2$, 400 nm) here and the production of $^{\bullet}NO_3$ is favored over $^{\bullet}NO_2$ in the nitric acid medium.

The transient absorption spectrum of the $^{\bullet}NO_2$ radical was measured in N_2O-sparged 0.10 M sodium nitrite solution. Under these conditions, $^{\bullet}NO_2$ radicals are produced through the reaction of $^{\bullet}OH$ radicals with nitrite ion as shown in Equation 13:

$$^{\bullet}OH + NO_2^- \rightarrow OH^- + {^{\bullet}NO_2} \quad k_{13} = 1.1 \times 10^{10} \text{ M}^{-1} \text{ s}^{-1} \tag{13}$$
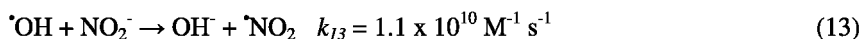
The relatively high concentration of nitrite in this system means that reactions with the formed e_{aq}^- and $^{\bullet}H$ atoms also occur (eq. 141516):

$$e_{aq}^- + NO_2^- \rightarrow {^{\bullet}NO_2^{2-}} \tag{14}$$

$$^{\bullet}NO_2^{2-} + H_2O \rightarrow 2OH^- + {^{\bullet}NO} \qquad k_{15} = 3.8 \times 10^9 \text{ M}^{-1} \text{ s}^{-1} \tag{15}$$

$$H^{\bullet} + NO_2^- \rightarrow {^{\bullet}OH} + NO^-/OH^- + {^{\bullet}NO} \qquad k_{16} = 1.6 \times 10^9 \text{ M}^{-1} \text{ s}^{-1} \tag{16}$$

For rate constant (k) determinations, the rate of change of the decay kinetics at the peak absorption maximum ($^{\bullet}NO_3$, 640 nm; $^{\bullet}NO_2$, 400 nm) was observed. Typical kinetic data are shown for the $^{\bullet}NO_3$ radical reaction with anisole in Table 1. By plotting these fitted pseudo-first-order rate constants against anisole concentration, a second-order rate constant of $(4.42 \pm 0.05) \times 10^9$ M^{-1} s^{-1} was obtained. For the $^{\bullet}NO_2$ radical measurements, no significant change in the rate of decay of transient absorbance was determined, even at the highest solute concentrations used. The k value for anisole was found to be $< 2 \times 10^5$ M^{-1} s^{-1}.

Steady-State Radiolysis: Acidic Nitrate, Neutral Nitrate and Neutral Nitrite Solutions

Acid-catalyzed nitration occurs typically by electrophilic aromatic substitution where the isomer distributions show very low concentration of the meta isomers (*15*). Figure 1 shows the results of anisole nitration measured using HPLC. Both ortho- and para-nitroanisoles were produced, but the lack of meta-nitroanisole suggests that nitration occurred via the electrophilic substitution mechanism (*12*). The HPLC analysis also showed the ingrowth of para-nitrophenol, dinitrophenols, and nitrous acid. The main nitration products, nitroanisoles and nitrophenols, were confirmed using GC-MS. The overall ortho/para ratio of nitroanisoles in all anisole samples was ~0.35, which is characteristic of nitrosonium ion (NO$^+$) dominated electrophilic substitution catalyzed by nitrous acid (*7, 16*). The nitrous acid scavenger hydrazine reduced the nitroanisole concentration by over two orders of magnitude (see Figure 2), and the ortho/para ratio for the mono-nitrated products changed from 0.35 to >1. This change in product ratios indicated the absence of nitrous acid catalyzed nitrosonium electrophilic substitution. In addition, the absence of p-nitrophenol, dinitrophenols, and color formation in these solutions supports this cconclusion (*16*). Under these conditions the nitration mechanism is due to nitronium ion (NO$_2^+$) electrophilic aromatic substitution (*5*). In the presence of radiation, the

amounts of nitrated products and the rate of these reactions increased due to the radiolytically-enhanced production of nitrous acid (*17*) as shown in Figure 3.

Table 1. Kinetic data for ·NO₃ radical reaction with anisole

Anisole Concentration (μM)	k (s⁻¹)
93	$(4.46 \pm 0.05) \times 10^5$
203	$(9.5 \pm 0.2) \times 10^5$
338	$(1.46 \pm 0.02) \times 10^6$
661	$(3.01 \pm 0.05) \times 10^6$
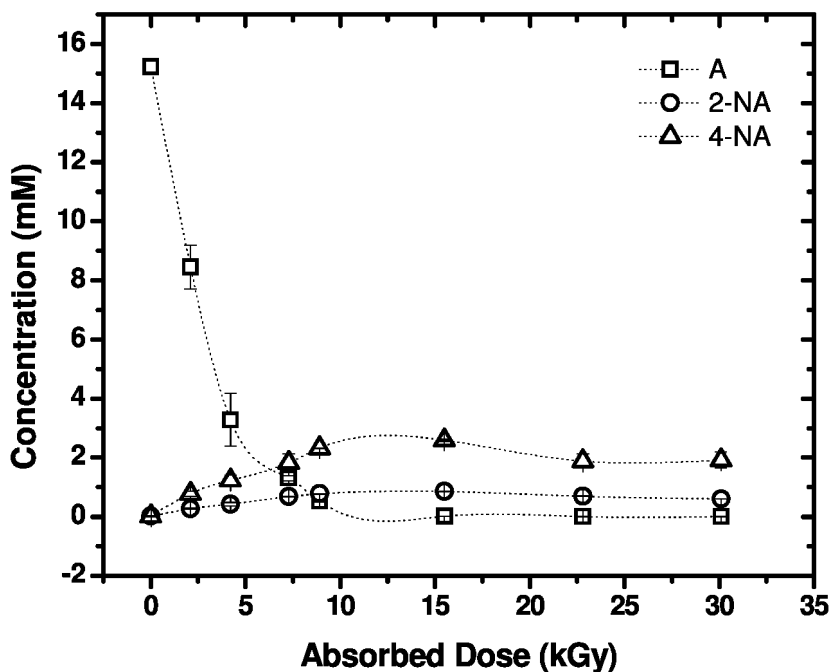
Figure 1. The loss of anisole (A) and production of 2-nitroanisole (2-NA) and 4-nitroanisole (4-NA) for irradiated anisole in 6 M nitric acid. Reported errors are the standard deviation of triplicate measurements.
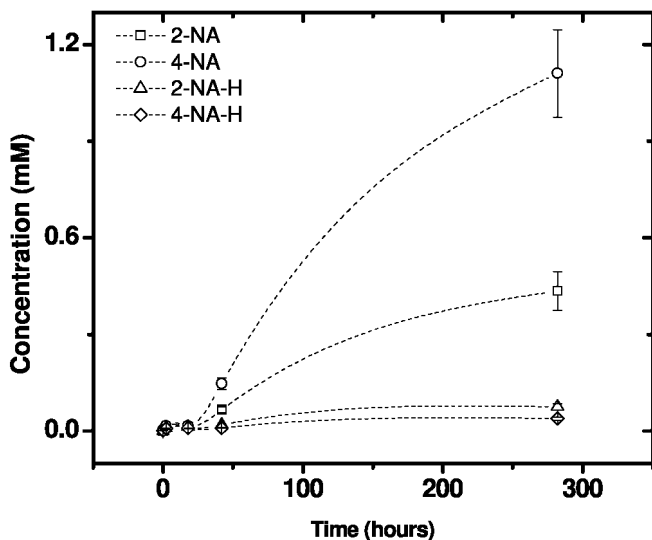
Figure 2. The trend (fitted lines) for the ingrowth of 2-nitroanisole (2-NA) and 4-nitroanisole (4-NA) for thermal anisole reaction with 6 M HNO3 in the presence and absence of the nitrous acid scavenger hydrazine (H). Errors shown are the calculated method errors applied to each individual measurement, (13.9 % for 2-NA and 12.2 % for 4-NA).
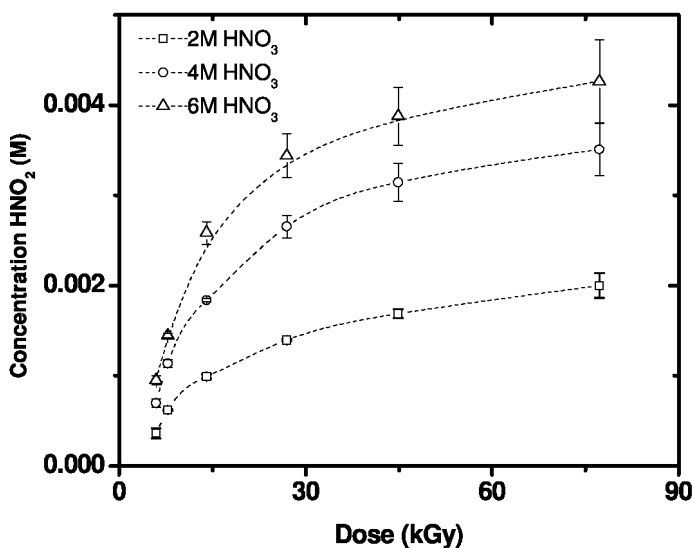
Figure 3. The production of nitrous acid with irradiation of nitric acid of different concentrations. Reported errors are the standard deviation of triplicate measurements.
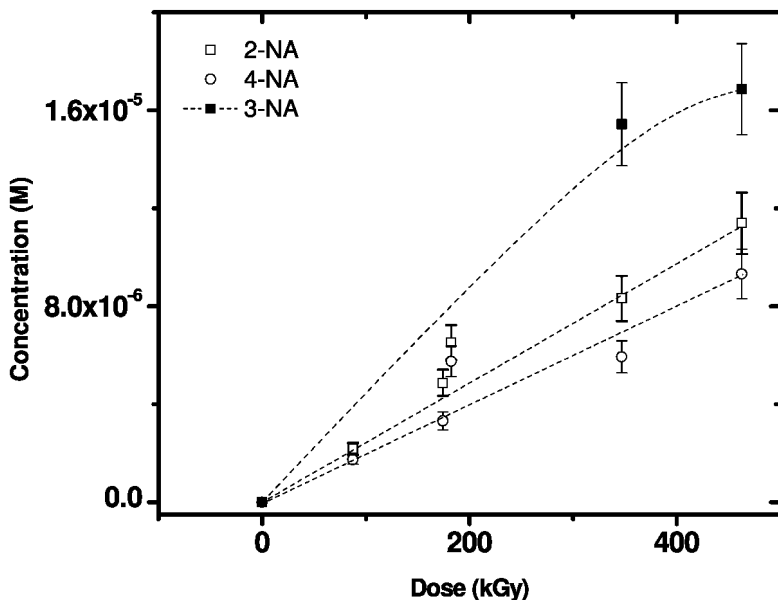
Figure 4. The production of 2-nitroanisole (2-NA), 3-nitroanisole (3-NA) and 4-nitroanisole (4-NA) as a function of absorbed dose in irradiated anisole in 0.5 M sodium nitrite solution. Errors shown are the calculated method errors applied to each individual measurement, (13.9 % for 2-NA 11.0% for 3-NA and 12.2 % for 4-NA).

Anisole in irradiated neutral nitrate solution produced 2-nitroanisole, 4-nitroanisole, 2-nitrophenol, and 4-nitrophenol. Production of 4-nitroanisole was predominant over 2-nitroanisole showing a prevalence of nitrous acid catalyzed electrophilic substitution reaction. The concentrations of the nitroisomers were a factor of 10-100 less than those produced in the acidic media. Formation of 2-nitrophenol is characteristic of free radical reactions (*18*), whereas the 4-nitrophenol formation is characteristic of nitrous acid catalyzed electrophilic reaction (*17*). This product distribution suggests that a combination of electrophilic nitration with NO^+, NO_2^+, and free radical reactions with $^\bullet OH$ and $^\bullet NO_2$ occurs in irradiated neutral sodium nitrate solution.

In irradiated sodium nitrite solution, only the $^\bullet NO_2$ radical is present, in equilibrium with its addition product N_2O_4. The UV/Vis spectrum of NO_2 in irradiated solution confirmed the dominance of NO_2 radical under these conditions. The decomposition rate of anisole irradiated in neutral nitrite solution was slow. The concentration of all three nitroanisole isomers produced in irradiated 0.5 M sodium nitrite solution at different irradiation doses is shown in Figure 4. It can be seen that the overall concentration of meta-nitro isomer (concentration at lower doses not given in Figure 4 because it co-eluted with anisole at lower concentrations) was higher compared to those of the ortho and para-nitro isomers. The nitroanisole distribution was 30-50% for 2- and 3-nitroanisoles and 20% for 4-nitroanisole. This is in qualitative agreement

with the statistically random distribution resulting from $\cdot NO_2$ radical reactions with toluene, reported by Olah *et al.* (*12*). The product 2-nitrophenol was also detected in 0.1 M sodium nitrite solution at 346.9 kGy, characteristic of free radical reaction mechanisms in the presence of $\cdot OH$ and $\cdot NO_2$ (*18*).

Conclusion

The reaction mechanisms of anisole, the simplest aryl alkyl ether and a strong ortho-para director, in nitric acid, neutral nitrate, and neutral nitrite solutions under γ- and pulse radiolysis were investigated in this research. HPLC with UV detection was primarily used to assess the reaction products. The distribution of nitrated derivatives of anisole in acidic solution with the predominance of para-nitroanisole was the same with and without irradiation, although the concentration of products was higher in the irradiated solution. For anisole in the irradiated acidic condensed phase, radiation-enhanced nitrous acid-catalyzed electrophilic aromatic substitution dominated over radical addition reactions. Experiments with neutral nitrate/anisole solutions showed a mixture of nitronium and nitrosonium ion reactions, and small amounts of free-radical reaction products, but with lower product yields than for the nitrous acid catalyzed reactions in acidic solution. Nitroanisole products in neutral nitrite/anisole solution occurred in a statistical fashion, suggesting a non-electrophilic free radical reaction involving the $\cdot NO_2$ radical. However, the $\cdot NO_2$ radical reaction is unlikely to be an important pathway in the acidic condensed phase due to its low reaction rate constants. Thus, the predominant products expected in irradiated acid solution are due to the enhanced nitrous acid catalyzed reaction resulting from radiolytic generation of nitrous acid.

Acknowledgments

References

1. Mincher, B. J.; Mezyk, S. P.; Bauer, W. F.; Elias, G.; Riddle, C.; Peterman, D. R. *Solvent Extr. Ion Exch.* **2007**, *25*, 593.
2. Lamare, V.; Dozol, J. F.; Allain, F.; Virelezier, H.; Moulin, C.; Jankowski, C. K.; Tabet, J. C. Behavior of Calix[4]arene Crown 6 under Irradiation. In *Calixarenes for Separations*; Lumetta, G. J, Rogers, R. D., Gopalan, A. S., Eds.; ACS Symposium Series 757; American Chemical Society: Washington, DC, 2000; Chapter 5.
3. Lamouroux, C.; Aychet, N.; Lelie'vre, A.; Jankowski, C. K.; Moulin, C. *Rapid Commun. Mass Spectrom.* **2004**, *18*, 1493.

4. Mincher, B. J.; Elias, G.; Martin, L. R.; Mezyk, S. P. *J. Radioanal. Nucl. Chem.* **2009**, *282*, 645.
5. Olah, G. A.; Malhotra, R.; Narang, S. C. *Nitration, Methods, and Mechanisms*. Wiley-VCH: New York, 1989; pp 11−12, 201.
6. Atherton, J. H.; Moodie, R. B.; Noble, D. R.; Sullivan, B. O. *J. Chem. Soc., Perkin Trans. 2* **1997**, 663.
7. Ridd, J. H. *Acta Chem. Scand.* **1998**, *52*, 11.
8. Barnett, J. W.; Moodie, R. B.; Schofield, K.; Weston, J. B.; Coombes, R. G.; Golding, J. G.; Tobin, G. D. *J. Chem. Soc., Perkin Trans. 2* **1977**, 248.
9. Turney, T. A.; Wright, G. A. *Chem. Rev.* **1959**, *59*, 497.
10. Titov, A. I. *Tetrahedron* **1963**, *19*, 557.
11. Peluso, A.; Del Re, G. *J. Phys. Chem.* **1996**, *100*, 5303.
12. Olah, G. A.; Lin, H. C.; Olah, J. A.; Narang, S. C. *Proc. Natl. Acad. Sci. U.S.A.* **1978**, *75*, 1045.
13. Neta, P.; Huie, R. E. *J. Phys. Chem.* **1986**, *90*, 4644.
14. Buxton, G. V.; Greenstock, C. L.; Helman, W. P.; Ross, A. B. *J. Phys. Chem. Ref. Data* **1988**, *17*, 513.
15. Olah, G. A.; Narang, S. C.; Olah, J. A.; Lammertsma, K. *Proc. Natl. Acad. Sci. U.S.A.* **1982**, *79*, 4487.
16. Dix, L. R.; Moodie, R. B. *J. Chem. Soc., Perkin Trans. 2* **1986**, 1097.
17. Jiang, P.-Y.; Nagaishi, R.; Yotsuyanagi, T.; Katsumura, Y.; Ishigure, K. *J. Chem. Soc., Faraday Trans.* **1994**, *90*, 93.
18. Halfpenny, E.; Robinson, P. L. *J. Chem. Soc.* **1952** (Part I), 939.

Radiolytic Degradation of Heterocyclic Nitrogen Containing Ligands from Low Dose-Rate Gamma Sources

Anna Fermvik,*,1 Mikael Nilsson,2 and Christian Ekberg3

1Nuclear Chemistry, Chalmers University of Technology, Kemivägen 4, SE-412 96 Gothenburg, Sweden
2Department of Chemical Engineering and Materials Science, University of California–Irvine, 916 Engineering Tower, Irvine, CA 92697-2575, USA
3Industrial Materials Recycling, Department of Chemical and Biological Engineering, Chalmers University of Technology, Kemivägen 4, SE-412 96 Gothenburg, Sweden
*anna.fermvik@chalmers.se

Chemical processes intended for the separation of various elements in used nuclear fuel will inetvitably take place in an environment exposed to ionizing radiation. Solutions used in liquid-liquid extraction processes must therefore be resistant towards radiolysis. This study presents a collection of radiolysis experiments with BTP and BTBP type molecules carried out at Chalmers University of Technology over a period of several years. The molecules both aim to extract trivalent actinides into an organic phase while leaving lanthanides in the aqueous phase. Detailed knowledge about the radiolysis behavior of BTP and BTBP type molecules can enhance the design of new, more radiolytically stable extractants and facilitate any future implementation of triazine containing ligands in an industrial process. Results show that many factors, *e.g.* dose rate and diluent composition, influence the radiolytic stability of these molecules. There are also strong indications that the radiolysis products of the BTBP ligand are still able to coordinate and extract metal ions, effectively altering the chemical equilibrium constants.

Introduction

The current debate about the global climate and the need for carbon-neutral energy production have made nuclear power production an interesting alternative to coal and oil power. However, concerns are raised regarding the long-term storage of the used nuclear fuel material. Partitioning and Transmutation (P&T) is a concept aiming at decreasing the long-term radiotoxicity of used nuclear fuel. This concept focuses on chemical treatment of used nuclear fuel by separating different elements by means of some separation process, *e.g.* liquid-liquid extraction as a classic example. In the well established PUREX process (*1*) the uranium and plutonium are separated from the rest of the spent fuel and can then be used to produce so called mixed oxide (MOX) fuel and again used to fuel nuclear reactors. The acidic raffinate resulting from the PUREX process can be further treated and desired metal ions can be separated by different means.

One process, intended for the challenging separation of trivalent actinides (An) from trivalent lanthanides (Ln), is the SANEX (Selective ActiNide EXtraction) process. The separation of these chemically similar groups of metals is a key to enable production of transmutation targets, mainly due to the large neutron cross section of some of the lanthanides. Long-lived actinides can then be transformed into stable or short-lived nuclides by neutron bombardment. This would decrease the amount of waste and also the storage time required in order for the spent nuclear fuel to be regarded as safe. The separation of the two groups of elements is realized using a soft electron donor. Both actinides and lanthanides are considered as hard bases according to Lewis hard acid-base theory, but the actinide can display softer tendencies making them bind stronger to soft bases than would the lanthanides. In a SANEX process a soft, nitrogen containing, donor ligand is used as extractant and dissolved in a selected diluent.

In order to be considered a good extractant for the SANEX process a number of criteria (*2*) should be fulfilled, *e.g.* high enough solubility of formed metal complexes in the organic phase, selective towards the solutes that are to be separated and hydrolytic and radiolytic stability. Numerous compounds have been investigated over the years and from these studies the extractants have become more and more suitable for their purpose and fulfill more and more demands (*3*). One family of compounds, the BTPs (*2,6-bis-(1,2,4-triazine-3-yl)pyridines*) (*4*), were suggested as extractants for nuclear reprocessing by Kolarik et al. (*5*). They possess one important property that the earlier similar extractants lacked: they could form complexes with americium (Am) using nitrates to balance the +3 charge, thus avoiding the previous need for addition of an acidic synergist in the organic phase (*3*). However, the BTPs showed a serious weakness, namely a general lack of stability towards both radiolysis and chemical degradation (*6–10*). In addition, the complexes tended to be too strong, hence preventing efficient back-extraction (*3*). The successor to BTP was the BTBP (*6,6'-bis(5,6-dialkyl-[1,2,4-]triazin-3-yl)-2,2'-bipyridines)* with an additional aromatic nitrogen heterocyclic ring. The group of compounds was designed to increase the stability compared to the BTPs and also to allow for back-extraction. Especially one BTBP, the so called CyMe$_4$-BTBP, proved to be a suitable extractant and has been used as reference molecule for SANEX hot tests (*11*).

Derivatives of different BTP and BTBP molecules are made by changing the side groups attached to the triazine rings, see Figure 1, but attempts have also been made with additions of tert-butyl group to one of the pyridine rings (*12*). The choice of side groups has shown to potentially have a high impact on the radiolytic stability of the molecule (*10*). Other factors that influence the effect of radiolysis on the BTP/BTBP molecules include the composition of the diluent (*8*, *13*) and the absence or presence of an aqueous phase during irradiation (*14*).

There is a distinction between direct and indirect radiolysis (*7*), sometimes referred to as primary and secondary radiolysis (*15*). Direct radiolysis refers to reactions caused by energy transfer from the radiation itself to the molecule of interest, while indirect radiolysis is chemical reactions between the molecule and free radicals or other species formed in the direct radiolysis. Thus, indirect radiolysis processes can theoretically proceed after the irradiation has stopped. In the type of solvent extraction experiments discussed here, the extractant is generally present at concentrations around 5-10 mM, hence the relative concentrations of BTP/BTBP to the diluent is very low. Thus, the probability of direct interaction between the extractant and the radiation is low, and the degrading reactions are most likely indirect, or secondary, reactions. Since the indirect radiolysis processes are reactions involving reactive species formed in the radiolysis of the diluent, the choice of diluent plays an important role in the radiolytic reactions. If the diluent is stable towards radiolysis there will be few radicals formed and secondary processes are unlikely.

For a given organic system the radiolytic behaviour can also be changed by altering the type of radiation, *i.e.* LET-values (*16*, *17*), and the dose rate (*18–21*). The estimated dose rate to an organic phase in a SANEX type process is between 29 and 14300 Gy/h, depending on *e.g.* fuel type and burn-up (*22*). This corresponds to an annual dose of between 250 kGy and 125 MGy. Other studies (*23*) have indicated similar results with the argument that since the SANEX process mainly deals with alpha emitters (the high active beta-emitters having been previously removed) the dose to the solution is around 0.6 kGy per cycle. This study presents a collection of radiolysis experiments with BTP and BTBP type molecules carried out at Chalmers University of Technology over a period of several years. Experiences gained during these studies have resulted in altered methodologies for carrying out the investigations and the intensity of the ^{60}Co-gamma source decreased by at least one half-life which is reflected in the fact that dose rates changed between different experiments. However, the studies still allow for direct comparisons and are presented in close to chronological order. First, the general behavior regarding change in distribution ratios and separation factors as a function of the received dose is discussed for BTP and BTBP type extractants. Then detailed studies are presented, starting with the inhibition of BTP radiolysis by addition of various scavengers. The radiolysis of BTBPs is discussed by varying different factors including the side groups, the diluent and finally the dose rate.

Experimental

Chemicals

All extracting ligands were synthesized and supplied by the University of Reading, UK, and was used without further purification. The structures are given in Figure 1. The diluents used were 1-hexanol (>99%, Sigma Aldrich or 98%, Merck), cyclohexanone (>99.5%, Sigma Aldrich), nitrobenzene (pro analysi, Fisher Scientific Company) and tert-butyl benzene (99%, Sigma Aldrich).

The following chemicals were used for the aqueous phases: $HClO_4$ (titrisol, Riedel de Haën), HNO_3 (FIXANAL, Sigma Aldrich), $NaClO_4$, (>99%, Merck), $NaNO_3$ (>99% pro analysi, Merck) and ultrapure water (Milli-Q gradient, Millipore®, >18MΩ). The solution containing americium (^{241}Am) and europium (^{152}Eu) was prepared from laboratory stock solutions (*13*) and contained up to approximately 2 MBq/mL ^{241}Am and/or 0.4 MBq/mL ^{152}Eu.

Irradiation

The low dose rate γ irradiations were performed in a ^{60}Co source (Gamma cell 220, Atomic Energy of Canada Ltd) with a dose rate of between 40 and 12.5 Gy/h, depending on when the study was done. Additional high dose rate γ irradiations (900-1650 Gy/h) were carried out in a ^{137}Cs source in CEA, Marcoule (IBL637, CISBio International). Samples were removed from the source after various periods of time to achieve a span of various doses. Samples were also taken from reference solutions left outside the γ source. This was done in order to take the possible ageing of the solvent into account when making the evaluations.

Analysis of the BTBP concentration after irradiation was performed at the Academy of Sciences of the Czech Republic (*24*).

Extraction

The organic samples (250-500 µL) were contacted with an equal amount of aqueous phase, spiked with ^{241}Am and/or ^{152}Eu. If the diluent was cyclohexanone, both phases were pre-equilibrated prior to contact due to the mutual solubility of water and cyclohexanone (*25*). The samples were contacted for a time period long enough to assure that chemical equilibrium had been reached. The samples were then centrifuged to facilitate phase separation. Aliquots of each phase were taken for gamma measurements using high purity germanium (HPGe) detectors (Oretc, Gamma Analyst GEM 23195 and EG&G Ortec) for samples containing both Am and Eu. For samples containing only one radioactive isotope (Am or Eu) a NaI(Tl) solid scintillation well type detector (Intertechnique GC-4000) was used.

The aqueous phases were prepared to 1 M anion concentration (nitrate or perchlorate) to minimize the effect of activity changes during extraction. The initial acidity was adjusted to 0.01 M H^+ by the addition of corresponding mineral acid (nitric or perchloric acid). Although the initial concentration of BTP or BTBP ligand was lower than what would be expected during actual treatment of spent nuclear material the concentration of metal ions was sufficiently low to avoid
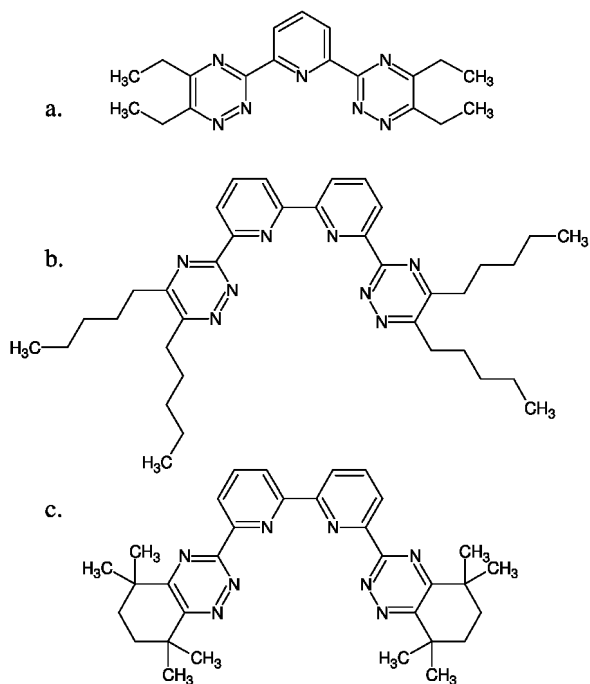
Figure 1. Structures of the ligands used in the experiments:
a.) 2,6-di(5,6-diethyl-1,2,4-triazin-3-yl)pyridine (C2-BTP), b.)
6,6'-bis(5,6-dipentyl-[1,2,4]triazin-3-yl)-[2,2']bipyridine (C5-BTBP) and c.)
6,6-bis(5,5,8,8-tetramethyl-5,6,7,8-tetrahydro-benzo-[1,2,4]triazin-3-yl)-
[2,2']bipyridine (CyMe4-BTBP).

loading. The main objective of these studies was to investigate how different chemical systems reacted to radiation and not to mimic process conditions.

Results

Previous studies of BTP and BTBP type ligands indicate the general extraction mechanism given below. For BTP is has been established that three ligands surround the metal ion in the organic phase. For BTBP molecules it has been found that two ligands surround the metal ions (*9*), although depending on experimental conditions there may be deviations from this.

$$M^{3+} + y\overline{L} + 3X^- \rightleftarrows \overline{ML_y(X)_3}$$
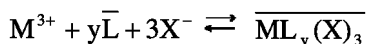
M is a trivalent metal ion such as Am or Eu, L is the BTP or BTBP ligand where y is 3 or 2, respectively. X is an anion, in this case nitrate or perchlorate. A line over a species indicates its presence in the organic phase.

As mentioned above BTP and BTBP favor the extraction of americium over europium. Table I below shows distribution ratios and separation factors for Am and Eu for unirradiated solvents used in this study. Although in this study the

extraction of Eu using a BTP ligand was not studied previous investigations have shown that using BTP results in at least on order of magnitude higher separation factor between Am and Eu than using BTBP. It can also be seen that using perchlorate instead of nitrate tends to increase the extraction efficiency of metal ions in these systems.

The values in Table I were reproduced by several studies and are shown in figures below as the point at 0 Gy received dose. Early work on radiolysis using BTP and BTBP were interpreted by assuming that a decrease from this initial distribution ratio was directly related to a decrease in extractant concentration based on the chemical equilibrium in the reaction shown above. This may not be strictly correct as was shown in later studies.

Inhibiting Radiolysis by Small Additions of Diluent Modifiers

It is known that benzene has a protective effect on molecules during irradiation by absorbing some of the energy and its ability to scavenge radiolysis products. Owing to these beneficial properties we investigated the effect of adding three different benzene derivatives, tert-butyl benzene (TBB), anisole and nitrobenzene, to a solution containing C2-BTP in hexanol.

The result of 10% (per volume) addition of each benzene derivative on the effect of distribution rations at different doses are shown in Figure 2. For comparison the distribution ratios for americium in hexanol with no additives is also included.

The results from Figure 2 indicate that nitrobenzene is an effective additive to reduce the effect of gamma radiolysis during americium extraction using BTP. It is also clear that TBB has essentially no effect on the stability compared to pure hexanol. For anisole, with its single ether oxygen, there seems to be a protective effect at low doses. However, at doses above 2 kGy the distribution ratios follow the same trend as for using TBB or no additives suggesting degradation of the BTP ligand. Based on these results the effect of smaller additions of nitrobenzene, from 0 to 10 %, was investigated. These experiments showed that an addition as small as 1% improved the stability of C2-BTP significantly. It was also seen that additions between 5% and 10% showed only small relative differences indicating that large additions are not necessary and that there is no linear effect. The degradation of BTP in hexanol was attributed to reactions with solvated electrons or α-hydroxy hexyl radicals from hexanol radiolysis. However, this conclusion was based on discussions rather than experimental evidence (*8*). It is important to note that only the organic phase was irradiated. If the organic solution would be irradiated in contact with an aqueous phase (of low to modearate adicity) the effect of the solvated electron would be decreased and Figure 2 may look different.

Varying the Side Groups

Experiments were carried out irradiating two different solutions, based on the same diluent, cyclohexanone, but with different extracting agents. The extractants used were CyMe4-BTBP and C5-BTBP, see Figure 1. As can be seen in Figure 3 below, metal extraction studies using the two irradiated solutions result in different

Table I. Extraction of americium and europium using unirradiated BTP and BTBP containing organic solutions

Solvent	Aqueous phase	D_{Am}	D_{Eu}	$SF_{Am/Eu}$
0.0018 M C2-BTP in nitrobenzene	0.01 M $HClO_4$, 0.99 M $NaClO_4$, traces of ^{241}Am	1300	-	-
0.005 M C5-BTBP in cyclohexanone	0.01 M HNO_3, 0.99 M $NaNO_3$, traces of ^{241}Am + ^{152}Eu	38.5	0.21	180
0.005 M C5-BTBP in hexanol	0.01 M HNO_3, 0.99 M $NaNO_3$, traces of ^{241}Am + ^{152}Eu	3.28	0.026	126
0.005 M CyMe$_4$-BTBP in cyclohexanone	0.01 M HNO_3, 0.99 M $NaNO_3$, traces of ^{241}Am + ^{152}Eu	4.31	0.039	112

extraction trends. For C5-BTBP in cyclohexanone, a decrease in extraction of Am is observed as the dose is increased. The distribution ratios of europium remain relatively stable with a possible slight decrease. The decrease is clearly larger for Am, resulting in a dramatic decrease in the separation factor ($SF_{Am/Eu}$). For CyMe$_4$-BTBP on the other hand, the metal extraction seems to be increasing with dose, and the separation factor remains more or less constant ($SF_{Am/Eu} \approx 110$-115).

Figure 3 shows distribution ratios for americium and europium from radiolysis studies carried out several years apart, resulting in different dose rates. The open symbols in Figure 3 represent experiments carried out at a later date at lower dose rates. It is clear that the experiments are reproducible with the exception of the extraction of americium using C5-BTBP where experiments carried out at a lower dose rate indicate a higher stability of the ligand. It is not entirely clear why there is a difference in the data. One important aspect to take into account is that C5-BTBP in cyclohexanone has been observed to be unstable with time and loose some of its extracting capacity as the solution ages (*10*), while CyMe$_4$-BTBP solutions appear to be stable (*13, 19*). Therefore reference solutions were kept outside the irradiation sources and the extraction capacity for these solutions was examined at the beginning and at the end of the experiments. The solvent containing CyMe$_4$-BTBP showed the same distribution ratios for both fresh and aged samples, confirming the stability in time. For C5-BTBP, the observation was made that for the more recent study, carried out at the lower dose rate, the distribution ratios for the reference sample kept outside the gamma source decreased over time. The data in Figure 3 have been corrected for this decrease. This indicates that the C5-BTBP ligand was in fact unstable in cyclohexanone even outside of a radiation field. This effect was not observed in the previous experiments using a different C5-BTBP sample, albeit the solution did not spend the same time in the gamma source due to the higher dose rate. Another aspect to take into account is the thermal effect. The low dose rate was low enough to not cause any temperature change during irradiation. This was however not controlled for the higher dose rate and a change in temperature may affect the degradation and consequently possibly also the distribution ratios. It is
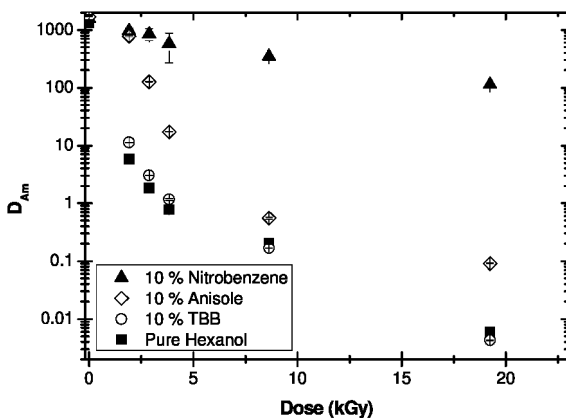
Figure 2. Distribution ratio for Am using various solvents consisting of 0.0018 M C2-BTP in hexanol with 10% additives irradiated to various doses (8). The aqueous phase comprised 0.01 M HClO₄, 0.99 M NaClO₄ and trace amounts of ²⁴¹Am.
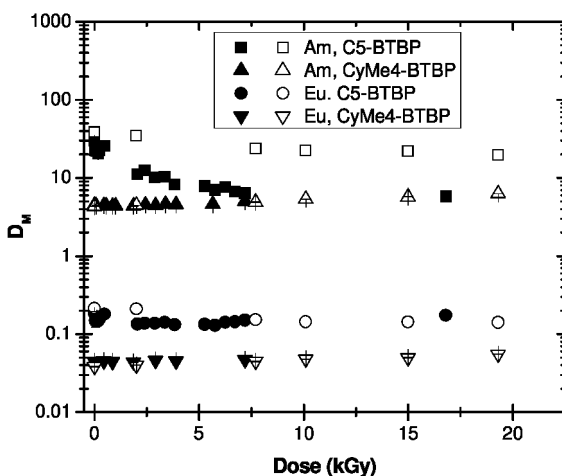
Figure 3. Distribution ratios of Am and Eu for two irradiated solvents; 0.005 M CyMe₄- or C5-BTBP in cyclohexanone. The aqueous phase contained 1 M total nitrate, 0.01 M nitric acid and trace amounts of ²⁴¹Am or ¹⁵²Eu. The open symbols represent experiments carried out at ~12.5 Gy/h dose rate while the closed symbols represent experiments carries out at ~40 Gy/h and ~30 Gy/h for C5-BTBP and CyMe₄-BTBP respectively.

also possible that trace impurities in the ligand samples may affect the distribution ratios for americium. A solvent containing C5-BTBP in hexanol instead of cyclohexanone is much more stable with time, but the decrease upon irradiation follows the same pattern as for cyclohexanone as shown below (10).

The cyclic side groups in CyMe₄-BTBP make the molecule more resistant towards radiolysis than BTBP's that have non cyclic carbon chains attached to

the triazine rings. In general, the radiolytic stability is considered to be higher for molecules with cyclic structures than for non cyclic molecules (*26*). The long carbon chains attached to the triazine rings in C5-BTBP are likely very sensitive towards radiolysis. Especially the carbon in the alpha position of the triazine ring has proven to be susceptible to chemical and radiolytical attacks (*27*).

Varying the Diluent

It has previously been shown that a change of diluent affects extraction properties of BTBPs such as D, SF and extraction kinetics (*28*, *29*). The diluent effect on radiolysis was therefore studied for two solvents containing 0.005 M C5-BTBP in either hexanol or cyclohexanone. The results are shown in Figure 4 and it can be seen that all four curves for the distribution ratio show a decrease in extraction as the solvent receives more dose. However, the decrease appears to be larger when the diluent is hexanol instead of cyclohexanone. Distribution ratios of americium are affected to a larger degree than ratios of europium. The difference in decrease between the two metals results in a decreasing $SF_{Am/Eu}$, as mentioned in the previous section and also shown in Figure 4.

However, as also mentioned in the previous section, the solvent consisting of C5-BTBP in cyclohexanone may not only be degraded by the radiation but also by ageing. With hexanol being the diluent the solvent is remarkably more stable and the degradation due to ageing during the time of these irradiations is negligible (*10*). The ageing of C5-BTBP in cyclohexanone has been subtracted to the overall degradation (the results from the irradiated solution), showing only the radiolytic degradation.

Varying the Dose Rate

Different dose rates might yield different radiolysis products, and also affect the yield of various products (*20*, *21*, *30*). Some radiolysis reactions might be favoured by a higher dose rate while some might be disfavoured or not affected at all (*20*). The two irradiation sources employed in this study had dose rates of either approximately 12.5 Gy/h or between 900-1600 Gy/h, depending on the placement in the source. In an industrial separation process of spent nuclear fuel the dose rate will depend on numerous factors such as fuel type and burn-up, cooling, pre-treatment, dilutions etc. BTBP radiolysis has previously been reported in both dose rate dependant systems (*18*) as well as systems independant of dose rate (*19*). However, in the study of dose rate dependant systems (*18*) the authors also points out that there might be other reasons for the different behaviour during irradiation than the dose rate, e.g. time of irradiation and oxygen content.

Solutions containing either C5- or CyMe$_4$-BTBP in cyclohexanone were irradiated with the two different dose rates and the results are presented in Figure 5, where D_{Am} is plotted as a function of the received dose. For the points representing the low dose rate results for C5-BTBP, the decrease due to ageing has been subtracted. It took around 1600 hours (~2 months) to reach 20 kGy with the low dose rate while it took only 19 hours to reach the same dose with the high dose rate.

For C5-BTBP the two curves look very similar, apart from the points at the lowest dose. Since the ageing has been subtracted, the results indicate that the irradiation alone affects the solution to the same extent whether it is given by a high or a low dose rate. CyMe$_4$-BTBP in cyclohexanone showed a larger increase in D$_{Am}$ with the low dose rate compared to high dose rate. Since the solvent is stable over time ageing effects do not apply here, hence the difference between the two dose rates must be due to another reason. Even though ageing of the molecule is not the cause, the difference can still be connected to the variation in irradiation time for the two series, since a longer irradiation time meant more time for various reactions to take place. Although the primary radiolysis reactions are very fast and the products are short-lived (10^{-12}-1 s), more stable reaction products with lifetimes in the region of 10-10^9 s or more can also be formed (*31*). These may in turn continue to react with solute molecules for a long period of time. If the sample is put in a freezer, as the samples in this study were after irradiation, these reactions may be slowed down or impeded. Furthermore, if the solutions would be irradiated in contact with an aqueous solution the life-time of some of the radicals may change and other long lived radicals may need to be taken into account.

Change in BTBP Concentration upon Irradiation

For the previous experimental results the assumption has been made that a decrease in distribution ratios is directly related to a decrease in extractant concentration. However this may not be the case and the concentration of ligand after irradiation should always be analyzed when possible. Thus, several of the BTBP samples discussed above was further analyzed to establish the change in BTBP concentration with dose (*32*). For C5-BTBP a clear decrease with increased dose was observed, and this is consistent with the decrease in extraction illustrated above. Figure 6 illustrates the decrease in C5-BTBP concentration in irradiated solvents with either hexanol or cyclohexanone as diluent. The degradation is larger when the diluent is hexanol and this agrees with the results from the extractions: the decrease in distribution ratios is larger in hexanol. However, the decrease in concentration is in general much larger than the decrease in extraction. For example, the concentration of C5-BTBP in hexanol reaches zero after 14 kGy but as can be seen in Figure 4 there is still a significant metal extraction even at doses above 14 kGy. This suggests that at least some of the degradation products must also extract metal ions to a certain extent. Analysis of aqueous solutions after contact with irradiated organic solutions showed no traces of C5-BTBP or any degradation products, hence the decrease in extraction is not caused by a change in water solubility.

For samples containing CyMe$_4$-BTBP the concentration of BTBP remained constant at all doses up to 19.3 kGy, in the range of the experimental error during transport, handling and HPLC analysis (ca. 2%). Thus, no explanation to the increasing extraction with increased dose could be given. Since the concentration remains the same evaporation of the diluent, resulting in a higher extractant concentration and thus higher distribution ratios, can be ruled out as the cause of the increasing extraction.
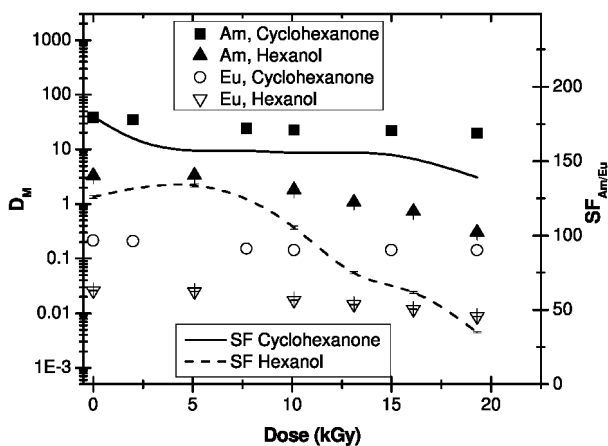
Figure 4. Log D (left) and SF$_{Am/Eu}$ (right) as a function of the dose for two solvents; 0.005 M C5-BTBP dissolved in either hexanol or cyclohexanone. For the solvent containing cyclohexanone as diluent the effect of ageing upon D and SF has been subtracted. The lines used to indicate the separation factors are only there to guide the eye to the general trend of the curves. It does not reflect any modeling attempts.
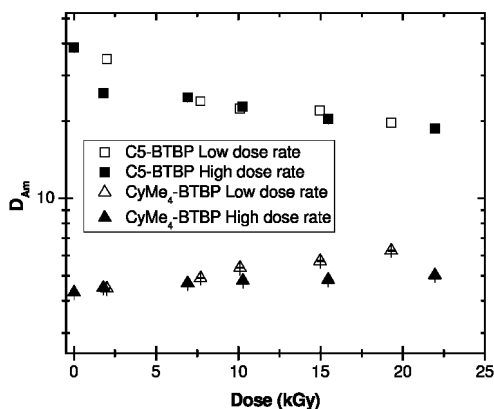
Figure 5. Distribution ratio for Am for a solvent consisting of 0.005 M C5-BTBP or CyMe$_4$-BTBP in cyclohexanone and irradiated to various doses with two different dose rates. The low dose rate was approximately 12.5 Gy/h and the high dose rate was approximately 1.6 kGy/h. The aqueous phase comprised 0.01 M HNO$_3$, 0.99 M NaNO$_3$ and trace amounts of [241]Am and [152]Eu. For the low dose rate curve the effect of ageing has been taken into consideration (by subtracting the decrease caused by ageing alone). For no dose (0 kGy) the points for low and high dose rate overlap.

Discussion

As mentioned above, cyclic structures are generally more stable towards radiolysis than non cyclic structures (*26*) and that is one reason for the higher

225
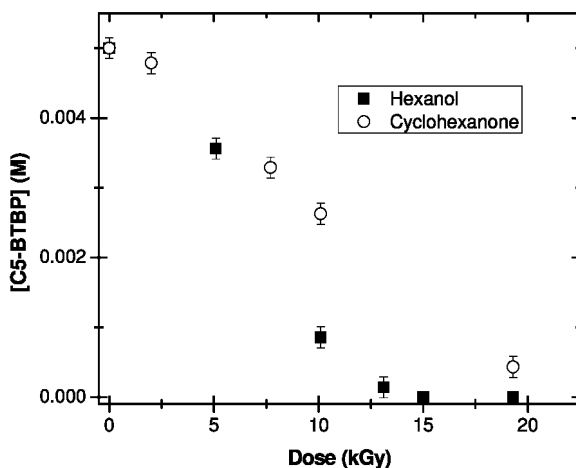
Figure 6. C5-BTBP concentration as a function of the received dose. The irradiated solution initially contained 0.005 M C5-BTBP in either cyclohexanone or hexanol and was irradiated with a ^{60}Co source with a dose rate of ca 12.5 Gy/h.

radiolytic stability of solvents containing cyclohexanone than corresponding solvents containing hexanol. In addition, the unsaturated bond in the ketone group in cyclohexanone increases the stability towards radiation compared to compounds with only saturated bonds (*33*). This general higher stability of cyclohexanone might result in a lower yield of reactive diluent degradation products that may react with the BTBP. Due to the stabilizing ketone group and the resonance structure the cyclohexanone radicals are less reactive than the hexanol radicals (*34*) and this might be yet another reason for the higher radiolytic stability of BTBP molecules in cyclohexanone. Also, the two diluents have different ionizing potentials (9.1 eV for cyclohexanone, 9.9 eV for hexanol) (*35*). Since the diluent may act as an "ionization sink" via charge transfer from radical cations (*15*, *36*, *37*), a diluent with a lower ionizing potential can to some extent help protect the extractant from degradation.

In the case of additives it was found that a benzene-like, hence cyclical, structure itself was not enough to protect the BTP from radiolytic degradation. In this case the added electronegative group of the nitrobenzene or the ether oxygen of the anisole improved the stability. Especially the nitrobenzene showed remarkable improvement even at small concentrations. Nitrobenzene, just like cyclohexanone, have non-saturated bonds to the oxygen atoms which may be a key to the protective properties. Anisole showed some stabilizing effect but at higher doses the larger concentration of radiolysis products present may have resulted in a saturation effect and indirect radiolytic degradation of BTP resulted.

It is interesting to note that for C5-BTBP, although studies carried out at different times resulted in slight differences, the extraction of americium was suppressed to a higher degree than for europium, for both types of diluents tested (cyclohexanone and hexanol). Furthermore, the concentration of C5-BTPB was shown to decrease down to zero in hexanol at doses of ~15 kGy where the distribution ratios indicated that a large fraction of the americium was

still extracted. Previous radiolysis studies of BTP ligands (*27*) have indicated that products heavier that the initial BTP have been observed in the irradiated solutions. It seems very likely that there is in fact a degradation product still capable of complexing and extracting americium, although the extraction constant may be slightly lower. The europium complexation of this new ligand may be comparable to C5-BTBP which results in the lesser decrease in europium extraction and the decrease in separation factor. Clearly C5-BTBP has lower affinity for europium than americium and the effect of this new ligand would not be as pronounced for Eu-extraction.

One possible explanation to the heavier degradation products formed is that diluent radicals attach themselves to the BTP or BTBP structure. In the case of C2-BTP degradation it was established that the most likely protective effect of the nitrobenzene was by scavenging radicals of the hexanol molecule. Solvated electrons are equally well scavenged by TBB and nitrobenzene and were ruled out due to the difference in extraction versus dose dependencies in Figure 2. It is quite likely that a C5-BTBP molecule with an extra side chain will still coordinate metal ions, although without detailed information of the exact structure effects such as steric hindrance and the coordination number can only be guessed at.

Comparing BTP and BTBP it can be gathered that the BTP is less stable. In hexanol the distribution ratios decrease almost six orders of magnitude (essentially over the entire detectable range) while for BTBP exposed to a corresponding dose the distribution ratios for americium decreased approximately one order of magnitude. Clearly BTBP is an improvement over BTP when radiolytic degradation is considered.

Finally, to account for the effects of radicals formed in aqueous solutions it is necessary to carry out irradiations in two-phase systems. However, to be able to fully comprehend the degradation pathway radiation of organic phase alone does play an important role.

Conclusions

Just as the equilibrium in an extraction system is dependent on the composition and type of ligand used so is the effect of radiolysis dependant on many of the same variables. The possibility to form byproducts still capable of extracting metals complicates the analysis of the results and treating a decrease in distribution ratio as a direct decrease of ligand may prove erroneous. The goal of producing a ligand that is not affected by radiolysis, or finding an additive that will completely protect the ligand may never be fully realized. However, understanding the effect of radiolysis can help to compensate for its effects. For process development correcting for radiolysis by including a parameter that decreases the distribution ratios based on absorbed dose may produce a flow-sheet that will fail. A more accurate correction can be made by including the formation rate of degradation products and based on the ligand and the diluent the structure of the byproducts formed may be estimated. From known structures it should be possible to estimate distribution ratios using theoretical or semi-empirical models based on thermodynamics and group contribution theories.

The CyMe4-BTBP is more tolerant towards radiolysis than C5-BTBP although it has limitations as far as extraction kinetics and solubility are concerned. By careful choice of organic diluent this may to a certain degree be compensated for. In a corresponding manner the radiolytic stability of C5-BTBP may be improved by using cyclohexanone although the problem of chemical degradation over time still exists.

References

1. Lanham, W. B.; Runion, T. C. *Purex Process for Plutonium and Uranium Recovery*; Report ORNL-479; U.S. Army Environmental Command, 1949.
2. Madic, C.; Hudson, M. J. *High Level liquid Waste Partitioning by Means of Completely Incinerable Extractants*; Final Report, EUR 18038, European Commision Contract No. FI2W-CT91-0112; European Commission, 1998.
3. Ekberg, C.; Fermvik, A.; Retegan, T.; Skarnemark, G.; Foreman, M. R. S.; Hudson, M. J.; Englund, S.; Nilsson, M. *Radiochim. Acta* **2008**, *96* (4−5), 225–233.
4. Case, F. H. *Heterocycl. Chem.* **1971**, *8* (6), 1043–1046.
5. Kolarik, Z.; Müllich, U.; Gassner, F. *Solvent Extr. Ion Exch.* **1999**, *17* (1), 23–32.
6. Hill, C.; Berthon, L.; Bros, P.; Dancausse, J.-P.; Guillaneux, D. Proceedings of the 7th Information Exchange Meeting, Jeju, Republic of Korea, October 14−16, 2002.
7. Hudson, M. J.; Boucher, C. E.; Braekers, D.; Desreux, J. F.; Drew, M. G. B.; Foreman, M. R. S. J.; Harwood, L. M.; Hill, C.; Madic, C.; Marken, F.; Youngs, T. G. A. *New J. Chem.* **2006**, *30*, 1171–1183.
8. Nilsson, M.; Andersson, S.; Ekberg, C.; Foreman, M. R. S.; Hudson, M. J.; Liljenzin, J.-O.; Skarnemark, G. *Radiochim. Acta* **2006**, *94* (1), 103–106.
9. Nilsson, M.; Andersson, S.; Drouet, F.; Ekberg, C.; Foreman, M. R. S.; Hudson, M. J.; Liljenzin, J.-O.; Magnusson, D.; Skarnemark, G. *Solvent Extr. Ion. Exch.* **2006**, *24* (3), 299–318.
10. Fermvik, A. Licentiate Thesis, Chalmers University of Technology, Göteborg, Sweden, 2008.
11. Magnusson, D.; Christiansen, B.; Foreman, M. R. S.; Geist, A.; Glatz, J.-P.; Malmbeck, R.; Modolo, G.; Serrano-Purroy, D.; Sorel, C. *Solvent Extr. Ion Exch.* **2009**, *27* (2), 97–106.
12. Foreman, M., et al. Chalmers University of Technology, Göteborg, Sweden, unpublished work.
13. Retegan, T.; Ekberg, C.; Englund, S.; Fermvik, A.; Foreman, M. R. S.; Skarnemark, G. *Radiochim. Acta* **2007**, *95* (11), 637–642.
14. Fermvik, A.; Gruner, B.; Kvíčalová, M.; Ekberg, C. Chalmers University of Technology, Göteborg, Sweden, unpublished work.
15. Manion, A. P.; Burton, M. *J. Phys. Chem.* **1952**, *56*, 560–569.
16. Magee, J. L.; Chatterjee, A. In *Radiation Chemistry: Principles and Applications*; Farhataziz, Rodgers, M. A. J., Eds.; VCH Publishers, Inc.: Weinheim, Germany, 1987; Chapter 5.

17. Foldiak, G.; Roder, M. J.; Wojnarovits, L. *J. Radioanal. Nucl. Chem.* **1992**, *164* (1), 29–37.
18. Fermvik, A.; Ekberg, C.; Englund, S.; Foreman, M. R. S.; Modolo, G.; Retegan, T.; Skarnemark, G. *Radiochim. Acta.* **2009**, *6*, 319–324.
19. Magnusson, D. Ph.D. Thesis, Chalmers University of Technology, Göteborg, Sweden, 2008.
20. Bibler, N. E. *J. Phys. Chem.* **1971**, *75* (16), 2436–2442.
21. Rice, R. N.; Gorin, G.; Raff, L. M. *J. Phys. Chem.* **1975**, *79* (25), 2717–2722.
22. Magnusson, D.; Christiansen, B.; Malmbeck, R.; Glatz, J.-P. *Radiochim. Acta* **2009**, *97*, 497–502.
23. Logunov, M. V.; Voroshilov, Yu. A.; Starovoitov, N. P.; Shadrin, A. Yu.; Smirnov, I. V.; Kvasnitskii, I. B.; Tananaev, I. G.; Myasoedov, B. F.; Morgalyuk, V. P.; Kamiya, M.; Koma, I.; Koyama, T. *Radiochemistry* **2006**, *48* (1), 55–61.
24. Fermvik, A., Ekberg, C., Gruner, B., Kvíčalová, M. Chalmers University of Technology, Göteborg, Sweden, unpublished work.
25. Marcus, Y. In *Solvent Extraction Principles and Practice*, 2nd ed.; Rydberg, J., Cox, M., Musikas, C., Choppin, G., Eds.; Marcel Dekker, Inc.: New York, 2004; Chapter 2.
26. György, I.; Wojnarovits, L. In *Radiation Chemistry of Hydrocarbons*; Földiak, G., Ed.; Elsevier Scientific Publishing Company: Budapest, Hungary, 1981; Chapter 1.
27. Hill, C., Berthon, L., Madic, C. GLOBAL, Tsukuba, Japan, October 9−13, 2005.
28. Retegan, T.; Ekberg, C.; Fermvik, A.; Skarnemark, G. In *Scientific Basis for Nuclear Waste Management XXX*; Dunn, D. S., Poinssot, C., Begg, B., Eds.; Materials Research Symposium Proceedings; Materials Research Society: Warrendale, PA, 2007; Volume 985.
29. Retegan, T.; Ekberg, C.; Fermvik, A.; Foreman, M. R. S.; Skarnemark, G. *Solvent Extraction: Fundamentals to Industrial Applications*, Proceedings of ISEC 2008, Tucson, AZ, September 15−19, 2008; Volume 1, pp 545−550.
30. Abramson, F. P.; Firestone, R. F. *J. Phys. Chem.* **1966**, *70* (11), 3596–3605.
31. Swallow, A. J. In *Radiation Chemistry: Principles and Applications*; Farhataziz, Rodgers, M. A. J., Eds.; VCH Publishers, Inc.: Weinheim, Germany, 1987; Chapter 11.
32. Fermvik, A.; Berthon, L.; Ekberg, C.; Englund, S.; Retegan, T.; Zorz, N. *Dalton Trans.* **2009**, 6421–6430.
33. Briskman, B. A. In *Organic Radiation Chemistry Handbook*; Milinchuk, V. K., Tupikov, V. I., Eds.; Ellis Horwood Limited: Chichester, England, 1989; Chapter 1.
34. Clayden, J.; Greeves, N.; Warren, S.; Wothers, P. *Organic Chemistry*; Oxford University Press: New York, 2005; Chapter 39.
35. Ionization Potentials of Gas-Phase Molecules. In *CRC Handbook of Chemistry and Physics*, 75th ed.; Lide D. R., Frederikse, H. P. R., Eds.; CRC Press: Boca Raton, FL, 1994.
36. Sugo, Y.; Izumi, Y.; Yoshida, Y.; Nishijima, S.; Sasaki, Y.; Kimura, T.; Sekine, T.; Kudo, H.; *Radiat. Phys. Chem.* **2007**, *76*, 794–800.
37. Tahraoui, A.; Morris, J. H. *Sep. Sci. Technol.* **1995**, *30* (13), 2603–30.

Chapter 19

Kinetics and Efficiencies of Radiolytic Degradation in Lanthanide/Actinide Separation Ligands - NOPOPO

Katy L. Swancutt,[1] Stephen P. Mezyk,[*,1] Leigh R. Martin,[2] Richard D. Tillotson,[2] Sylvie Pailloux,[3] Manab Chakravarty,[3] and Robert T. Paine[3]

[1]Department of Chemistry and Biochemistry, California State University Long Beach, 1250 Bellflower Blvd., Long Beach, CA 90840
[2]Aqueous Separations and Radiochemistry Department, Idaho National Laboratory, P.O. Box 1625, Idaho Falls, ID 83415-6150
[3]Department of Chemistry, University of New Mexico, Albuquerque, NM 87131
***smezyk@csulb.edu**

The separation of trivalent lanthanides from actinides is one of the important steps in the selective partitioning of used nuclear fuel. However, these separations occur in the presence of a radiation field that degrades both ligands and solvents, potentially reducing the overall extraction efficiency. To quantitatively predict the impact of radiation under process scale extraction conditions, we have investigated the aqueous stability of one ligand that has shown promise for lanthanide/ actinide separations, 2,6-bis[(di(2-ethylhexyl)phosphino) methyl] pyridine N,P,P-trioxide (NOPOPO). In this study the stable products produced in radiolysis of NOPOPO, and two model analogues (2-methylphosphonic acid) pyridine N,P dioxide and 2,6-bis(methylphosphonic acid) pyridine N,P,P trioxide), have been determined. In addition the temperature-dependent reaction rate constants for the hydroxyl (•OH) radical reaction with these three species were also measured.

Introduction

Separation processes for the partitioning of the actinides from the fission products in used nuclear fuel are vital components of a sustainable closed nuclear fuel cycle. These processes are required to reduce the total volume of waste intended for storage as well as to lower the long-term radiotoxicity of the stored waste. Continuous research has been conducted with the goal of implementing new or improved extraction procedures and components; however, the chemical behavior of existing extraction components (ligands such as TBP, CMPO, lactic acid etc.) under the exposure of highly radioactive materials has not been investigated until recently (*1–4*). Furthermore, it has not been a standard practice to determine the possible effects of direct or indirect radiolytic degradation of potential separation ligands prior to their implementation. Existing ligands were chosen, often by the approach of trial and error, for their sufficient ability to function and relative resilience within their highly acidic and radiolytic working environment. Understanding the mechanisms and efficiencies of existing ligands could lend insight into the design of new ligands, while determining the radiation-induced degradation mechanisms of new ligands, prior to the trial and error process, could be a more cost effective form of evaluation. The aim of the research described here is to evaluate the radiation stability of a new ligand designed for the separation of trivalent actinides from trivalent lanthanides.

Separation of actinides from lanthanides is a particularly challenging step in waste remediation since at this stage of the process both classes of metals are in the trivalent oxidation state, have similar ionic radii, ligand reactivity, and are strongly hydrated in aqueous solution. However, new phosphinomethyl-pyridine-*N*-oxides have been shown to separate the two products (*5*). One of the new ligands of interest is the phosphonate 2,6-bis[(di(2-ethylhexyl) phosphino) methyl]pyridine N,P,P-trioxide (NOPOPO, abbreviated **I**, see Scheme 1). This ligand could be a possible substitute for CMPO in a TRUEX-based actinide partitioning process (*5*) as its simpler, symmetrical, geometry could translate into easier synthesis procedures, and ultimately into lower expense for the reagent. The pyridine *N*-oxide and phosphoryl oxygen's act as the trivalent actinide coordination sites (see Scheme 1). The long aliphatic chains confer good solubility in organic extractant phase, its extraction kinetics are rapid, and the back-extraction efficiency is good (*6, 7*).

However, before this extraction ligand can be considered for large-scale processing, its complete thermal and radiolytic stability under its anticipated conditions of use must be quantitatively established. In this study the stable products produced in the radiolysis of **I**, and two model analogues, 2-(methylphosphonic acid) pyridine N oxide (Scheme 1, **II**) and 2,6-bis(methylphosphonic acid) pyridine N,-oxide (Scheme 1, **III**,), have been determined to assist in the understanding of the radiolytically-induced degradation of this ligand. In addition, as the hydroxyl radical (•OH) is the most important oxidizing radical produced in the aqueous phase (*1*), we have determined the temperature-dependent reaction rate constants for the hydroxyl radical oxidation of **I**.
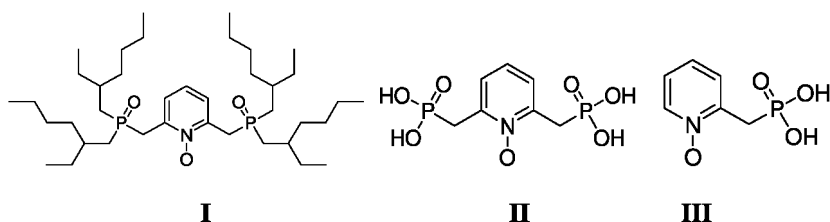
*Scheme 1. Chemical structures of compounds **I** (2,6-bis[di(2-ethylhexyl) phosphino) methyl]pyridine N,P,P-trioxide, also known as NOPOPO), 2,6-bis(methylphosphonic acid)pyridine N-oxide **II**, and 2-(methylphosphonic acid)pyridine N-oxide **III**.*

Experimental

Steady-State Irradiation Measurements

All chemicals (Aldrich) used in this study were reagent grade or higher and used as received without further purification. Samples of **I** (NOPOPO) were synthesized as described elsewhere (*5*). Aqueous solutions were made with ultrapure deionized water ($\geq$ 18 MΩ) obtained from a Millipore Milli-Q system. Static irradiations of 0.05 M NOPOPO in n-dodecane (Aldrich) were carried out at doses of 5, 10, 100 and 200 kGy using a ^{60}Co Gammacell 220E (MDS Nordion, Canada), with a dose rate of 9 kGy hr^{-1}, as based on radiochromic films traceable to standard Fricke dosimetry, at an internal temperature of ~48°C. After irradiation, these organic phases were used to perform solvent extraction experiments to determine the distribution coefficients for Am and Eu (from nitric acid media) as a function of absorbed dose to the organic phase. The organic phases were pre-equilibrated with fresh HNO$_3$ of the appropriate concentration before tracer experiments were performed. Acid concentrations were determined by titration with 0.1 M NaOH. All experiments were performed at ambient temperature.

Hydroxyl Radical Kinetics Measurements

The radiolysis of water gives a mixture of radicals and molecular products according to the following equation (*8*):

$$H_2O \text{ -}\wedge\wedge\wedge\rightarrow [0.28]^{\bullet}OH + [0.27]e_{aq}^{-} + [0.06]H^{\bullet}$$
$$+ [0.07]H_2O_2 + [0.05]H_2 + [0.27]H_3O^{+} \quad (1)$$
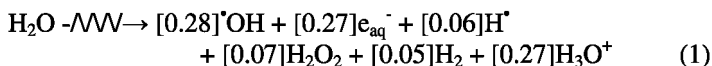
The coefficients next to each species are absolute yields (G-values) in μmol Gy^{-1}. Under anticipated large-scale operating conditions, the dissolved oxygen present will react with the reducing hydrated electron (e$_{aq}^{-}$) and hydrogen atom (H$^{\bullet}$) to produce the relatively inert HO$_2^{\bullet}$ species. The remaining $^{\bullet}$OH reaction with the NOPOPO ligand is likely to occur at the organic/aqueous interface in the extraction emulsion.

For the study of the $^{\bullet}$OH radical kinetics, the radiolytically-induced mix of radicals was generated by irradiating water with an 8 MeV electron beam,

generated by a linear accelerator at the University of Notre Dame Radiation Laboratory. This system has been described in detail previously (*9*). The accelerator gives 2-3 ns pulses of electrons, of doses ranging from 3-5 Gy, and the resulting chemical reactions were observed on the microsecond timescale using a transient absorption detection system (*10*). Recombinant water radiolysis products, such as hydrogen peroxide, react slowly on time scales that are much too long to interfere with these radical measurements.

To enhance our reaction kinetics measurements the hydroxyl radical was isolated from the mix of radicals by pre-saturating solutions with high-purity N_2O, which quantitatively converts hydrated electrons and some hydrogen atoms to $^\bullet OH$ according to (*8*):
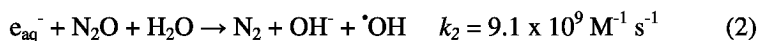
$$e_{aq}^- + N_2O + H_2O \rightarrow N_2 + OH^- + {}^\bullet OH \quad k_2 = 9.1 \times 10^9 \text{ M}^{-1}\text{s}^{-1} \quad (2)$$

$$^\bullet H + N_2O \rightarrow {}^\bullet OH + N_2 \quad\quad\quad\quad k_3 = 2.1 \times 10^6 \text{ M}^{-1}\text{s}^{-1} \quad (3)$$

Absolute hydroxyl radical concentrations (dosimetry) were measured using the transient absorption of $(SCN)_2^{\bullet-}$ at 475 nm, using 10^{-2} M potassium thiocyanate (KSCN) in N_2O-saturated solution at natural pH (*11*). These measurements were performed daily.

Aqueous solutions of **I**, **II** and **III** were made in high quality, Millipore Milli-Q, charcoal-filtered (TOC <13 ppb), deionized (>18.0 MΩ) water. However, the limited solubility of **I** was not sufficient for its necessary concentration to do direct, pseudo-first order rate constant measurements. Even for the lower concentrations required for competition kinetics (typically 5-20 μM) a small amount of non-oxidizable hexafluoroacetone co-solvent (*12*) was required to dissolve the ligand to this concentration.

A continuous-flow cuvette was used to prevent build-up of interfering absorptions due to long-lived products. Solution flow rates were adjusted so that each pulse irradiation was performed on a fresh sample, and multiple traces (5-35) were averaged to produce a single kinetic trace. Temperature control was achieved by flowing the ambient temperature solutions through a waterbath-fed condenser prior to irradiation. The solution temperature was measured immediately post-irradiation, using a thermocouple placed directly into the solution flow. The stability of the solution temperature was ± 0.3°C.

Rate constant error limits reported here are the combination of experimental precision and estimated compound purities.

Results and Discussion

Degradation due to Direct Effects: Steady-State Radiolysis

We initially completed a set of extractions with Am and Eu tracers using uni-rradiated 0.05 M NOPOPO in *n*-dodecane as a solvent. These experiments allowed us to compare our system and results to those reported by *Nash et al.* (*5*) to ensure our methodologies gave consistent results before commencing the radiolysis study. These experiments identified that the distribution coefficients (D = [M]*org*/[M]*aq*)

for Am and Eu were comparable in magnitude and acid dependence to those previously obtained (*5*), with the maximum D for both Am and Eu appearing at about 1.0 M HNO₃ (Figure 1). This Figure also shows the results of the distribution measurements made after the organic phase (0.05 M NOPOPO in dodecane) was irradiated to absorbed doses of 5, 7.5 and 10 kGy. At these low doses, D_{Am} and D_{Eu} showed little change indicating that the ligand has some resistance to direct radiolysis damage. However, when the absorbed dose to the organic phase was increased to 100 and 200 kGy, both D_{Am} and D_{Eu} decreased significantly (Figure 2). At 0.5M HNO₃ and above the magnitude of the decrease in metal ion extraction is approximately the same for both the americium and europium, as quantified by the separation factor $Sf_{Am/Eu}$ (Table I). However, at HNO₃ concentrations below this the $Sf_{Am/Eu}$ is seen to reduce as a result of D_{Am} reducing faster than D_{Eu}. These results suggest that NOPOPO degrades via several mechanisms. With little effect on the solvent extraction of Am and Eu at low doses, it seems reasonable to suggest that the main •OH radical reaction mechanism is via hydrogen atom abstraction from the alkyl groups of the NOPOPO ligands, as seen previously for TBP (*13*). However, once the ligand is exposed to more significant doses the degradation pathway may also incorporate damage to the ligand's metal binding site, most likely involving cleavage of one of the two phosphoryl side arms. Previous work supports this argument; (*5*) identified that the one armed 2-[(di-(2-ethylhexyl)phosphino) methyl] pyridine N,P-dioxide (NOPO) ligand performed poorly compared to NOPOPO for the solvent extraction of Am and Eu. The cleavage of a phosphoryl side arm at high doses would provide an adequate explanation of the observed drop in distribution coefficients for Am and Eu. Moreover, as the separation factors do not significantly change with increasing dose at higher acidity, the site of degradation must equally affect both metal ions. This might not be the case if the N-oxide were the site of the reaction. Radical damage here could lead to a "softer" donor ligand which we would expect to favor Am extraction and hence we would see an increase in the separation factors. In contrast to this at low aqueous phase acidity, there appears to be an as yet unidentified reaction on the ligand that results in the decrease of D_{Am} and hence the $Sf_{Am/Eu}$.

Degradation due to Indirect Effects: Hydroxyl Radical Kinetics

Due to the low solubility of the NOPOPO ligand in aqueous solution, no direct measurement of its reactivity with the hydroxyl radical was possible. Therefore, temperature-dependent rate constants were determined using SCN⁻ competition kinetics. The reaction of the hydroxyl radical with thiocyanate in N₂O-saturated solution gives the $(SCN)_2^{-•}$ transient (*8*):

$$•OH + SCN^- (+ SCN^-) \rightarrow (SCN)_2^{-•} + OH^- \quad k_4 = 1.05 \times 10^{10} \, M^{-1} \, s^{-1} \quad (4)$$
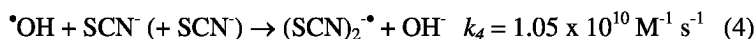
which occurs in competition with added ligand

$$•OH + I \rightarrow \text{non-absorbing products} \qquad k_5 \qquad (5)$$

The thiocyanate radical $(SCN)_2^{-•}$ has a strong absorption at 475 nm. Upon addition of **I** to a standard KSCN solution, Reactions (4) and (5) occur together, which
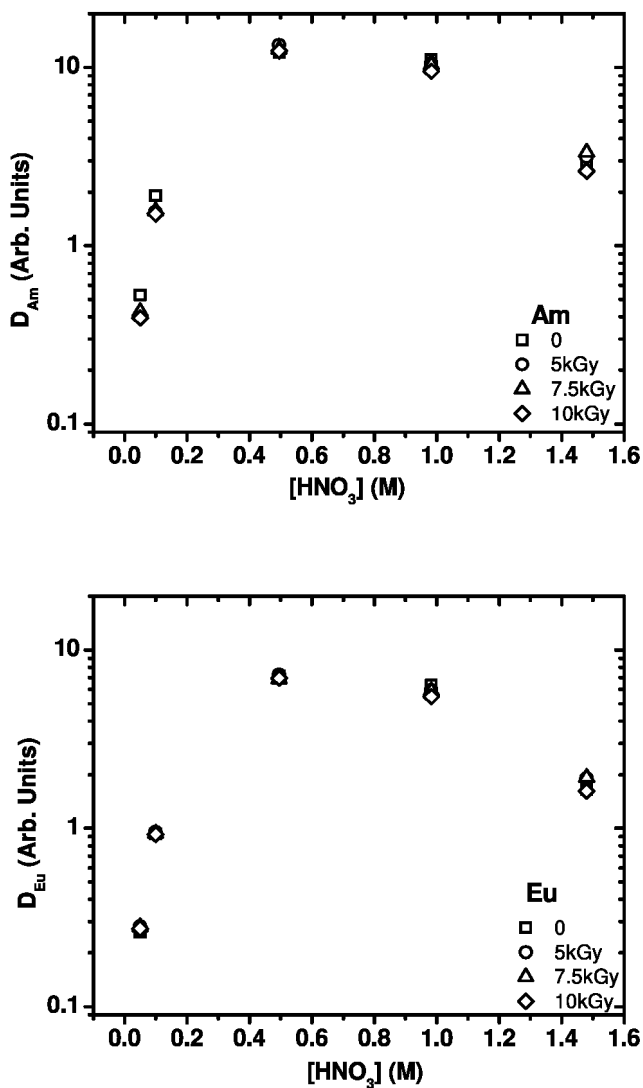
Figure 1. The effect of γ-irradiation on americium (upper data) and europium (lower data) extraction at various nitric acid concentrations. [HNO₃] = 0.05, 0.1, 0.5, 1 and 1.5 M, [NOPOPO] = 0.05 M in n-dodecane, γ-absorbed doses 0, 5, 7.5 and 10 kGy.
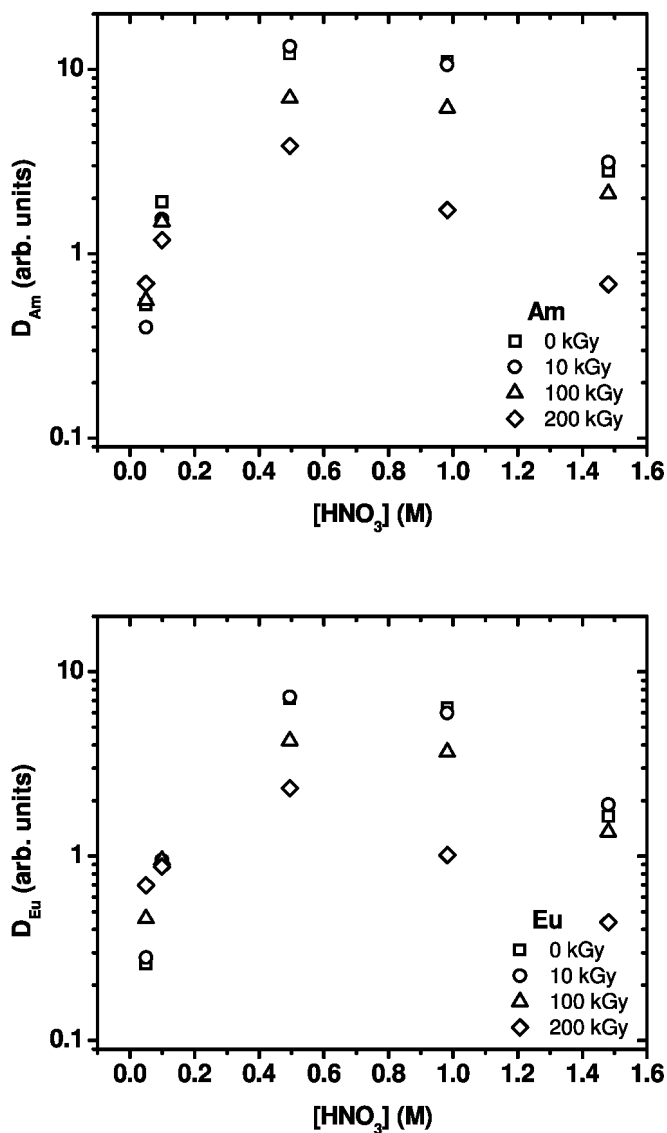
*Figure 2. The effect of γ-irradiation on americium (upper data) and europium
(lower data) extraction at various nitric acid concentrations. [HNO₃] = 0.05,
0.1, 0.5, 1 and 1.5 M, [NOPOPO] = 0.05 M in n-dodecane, γ-absorbed doses 0,
10, 100 and 200 kGy.*

lowers the total transient absorption. Typical $(SCN)_2^{-•}$ kinetic curves in the absence
and presence of **I** are shown in Figure 3. The decrease in limiting absorption with
increasing NOPOPO concentration can be modeled by analytically solving this
competition for the $^•OH$ radical, which gives

Table I. Separation factor(D_{Am}/D_{Eu}) at various acidities as a function of dose received to the organic phase

[HNO₃] (M)	$Sf_{Am/Eu}$			
	0 (kGy)	10 (kGy)	100 (kGy)	200 (kGy)
0.05	2.03	1.42	1.22	0.99
0.10	2.05	1.62	1.57	1.35
0.50	1.70	1.83	1.66	1.65
1.00	1.74	1.77	1.68	1.71
1.50	1.71	1.65	1.57	1.56

$$\frac{Abs^o(SCN)_2^{-\bullet}}{Abs(SCN)_2^{-\bullet}} = 1 + \frac{k_5}{k_4}\frac{[I]}{[SCN^-]} \tag{6}$$

where $Abs^o(SCN)_2^{-\bullet}$ is the peak transient absorption measured for only the SCN⁻ solution, and $Abs(SCN)_2^{-\bullet}$ is the reduced absorbance of the $(SCN)_2^{-\bullet}$ transient when **I** is present. As this analysis is dependent upon the initial hydroxyl radical concentration being constant for all the measurements, low concentrations of SCN⁻ (typically 30-40 μM) were deliberately used in this study, which minimized the impact of intra-spur scavenging of radicals (*14*).

A plot of ($Abs^o(SCN)_2^{-\bullet}/Abs(SCN)_2^{-\bullet}$) vs. ([**I**]/[SCN⁻]) gives a straight line of slope (k_5/k_4), as shown in Figure 4. From the known k_4 values (*8*), the k_5 rate constant can be calculated.

This was done at room temperature (23.3°C), with a specific •OH rate constant of $k_5 = (3.49 \pm 0.10) \times 10^9$ M⁻¹ s⁻¹, determined (see Table II for all rate constants of this study). These measurements were conducted over the temperature range 5.5 – 37.9°C (Figure 5). A good Arrhenius plot was obtained,with the fitted slope corresponding to an activation energy of 30.2 ± 4.1 kJ mol⁻¹.

To better elucidate the mechanism of •OH radical oxidation of **I**, reaction rate constants were also obtained for **II** and **III**, the two model compounds. As these two compounds have ionizable hydroxy groups rather than alkyl chains, the rate constant values would be expected to be pH-dependent. Therefore, specific •OH reaction rate constants for both model compounds were determined as for **I** over a wide range of pH (see Table II). To directly compare these model rate constants with the value for **I**, the anticipated large-scale process acidity of around pH = 1.0 was chosen, at room temperature (~23°C).

The individual rate constants for the model compound **III** slowed significantly with increasing protonation, suggesting that the majority of the •OH reaction was at the phosphorous atom in this molecule. Similar behavior for **II** was observed, but the changes were not as dramatic, suggesting that more of the hydroxyl radical oxidation occurred at the ring.
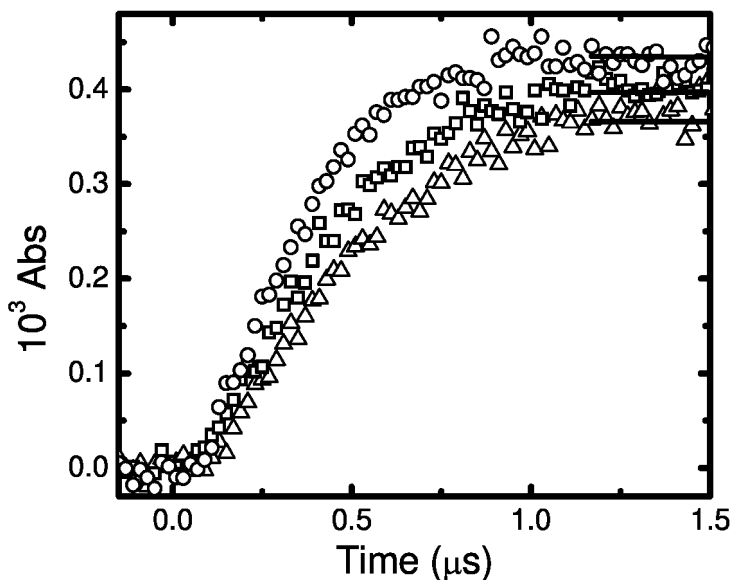
Figure 3. Measured (SCN)$_2$$^{-•}$ absorbance for N$_2$O-saturated, 35 μM KSCN with zero (○), 8.95 (□), and 13.93 (Δ) μM NOPOPO at natural pH and 37.9°C.

Figure 4. Competition kinetics plots for NOPOPO at 5.5°C (□) and 37.9°C (○) using N$_2$O-saturated SCN$^-$ as a standard at natural pH. Solid lines correspond to weighted linear fits, from which are determined specific rate constants of (1.47 ± 0.63) x 10^9 and (6.09 ± 2.7) x 10^9 M^{-1} s^{-1}, respectively.

However, the corresponding rate constants for these model compounds near pH =1, (6.66 ± 0.25) x 10^8 and (9.04 ± 0.23) x 10^8 M^{-1} s^{-1}, respectively, were much slower than observed for **I** (3.49 ± 0.10) x 10^9 M^{-1} s^{-1}). This supports

Table II. Summary of the absolute rate constants for hydroxyl radical oxidation of NOPOPO and each of the protonated states of model compounds II and III

Compound	pH	Temp. (°C)	$k_{\bullet OH}$ $(10^9 \ M^{-1}s^{-1})$
I (NOPOPO)		5.5	1.47 ± 0.63
		23.3	3.49 ± 0.10
		28.9	3.43 ± 0.47
		37.9	6.09 ± 0.27
II	1.3	23.1	0.66 ± 0.02
II	2.5	23.3	0.65 ± 0.01
II	4.7	22.6	0.99 ± 0.04
II	6.9	23.2	1.86 ± 0.07
II	9.97	23.9	1.45 ± 0.01
III	1.0	21.1	0.90 ± 0.02
III	4.36	21.1	1.87 ± 0.06
III	9.52	21.1	2.41 ± 0.19

Figure 5. Arrhenius plot for reaction of hydroxyl radical with NOPOPO in N₂O-saturated aqueous solution at natural pH. Solid line is linear fit, corresponding to an activation energy of 30.2 ± 4.1 kJ mol⁻¹ (R² = 0.96).

the conclusion that the •OH radical reaction occurs predominately at the long alkyl side-chains, as predicted earlier from the steady-state irradiation results. Thermodynamic considerations suggest that reaction at these chains would result in hydrogen atom abstraction to form a carbon-centered radical, but such reactions would not affect the actinide-coordinating moieties within this ligand. Thus it is seen that the aliphatic chains of **I** confer protective radiation resistance under

real-world processing conditions in addition to increasing the organic phase solubility of the ligand.

Conclusions

Steady state gamma-radiolysis of the NOPOPO ligand in n-dodecane showed that solvent extraction performance of Am and Eu was not affected by radiolysis of absorbed doses of up to 10 kGy at aqueous phase nitric acid concentrations ≥ 0.5 M. At absorbed doses of 100 and 200 kGy the extraction of Am and Eu was significantly reduced, although the separation factors remained similar for each [HNO_3] studied. At low nitric acid concentrations D_{Am} was seen to decrease with increasing dose resulting in a change in separation factor. This has lead to the conclusion that there are at least three possible ligand degradation pathways that need to be considered and identified.

The corresponding ˙OH rate constant measurements for **I**, and model compounds **II** and **III**, showed that the hydroxyl radical oxidation was rapid. The predominant reaction with **I** was concluded to be hydrogen atom abstraction from the aliphatic chains, with an activation energy of 30.2 ± 4.1 kJ mol^{-1}. In contrast, the smaller side-chains of the two model compounds allowed more oxidation to occur at the phosphorous atom or with the unsaturated ring.

Acknowledgments

References

1. Mincher, B. J.; Modolo, G.; Mezyk, S. P. *Solvent Extr. Ion Exch.* **2009**, *27*, 1–25.
2. Mincher, B. J.; Modolo, G.; Mezyk, S. P. *Solvent Extr. Ion Exch.* **2009**, *27*, 331–353.
3. Mincher, B. J.; Modolo, G.; Mezyk, S. P. *Solvent Extr. Ion Exch.* **2009**, *27*, 579–606.
4. Martin, L. R.; Mezyk, S. P.; Mincher, B. J. *J. Phys. Chem. A.* **2009**, *113*, 141–145.
5. Nash, K. L.; Lavallette, C.; Borkowski, M.; Paine, R. T.; Gan, X. *Inorg. Chem.* **2002**, *41*, 5849–5858.
6. Bond, E. M.; Engelhardt, U; Deere, T. P.; Rapko, B. M.; Paine, R. T. *Solvent Extr. Ion Exch.* **1997**, *15*, 381–400.

7.   Bond, E. M.; Engelhardt, U; Deere, T. P.; Rapko, B. M.; Paine, R. T.; FitzPatrick, J. R. *Solvent Extr. Ion Exch.* **1998**, *16*, 967–983.
8.   Buxton, G. V.; Greenstock, C. L.; Helman, W. P.; Ross, A. B. *J. Phys. Chem. Ref. Data* **1988**, *17*, 513–886.
9.   Whitman, K.; Lyons, S.; Miller, R.; Nett, D.; Treas, P.; Zante, A.; Fessenden, R. W.; Thomas, M. D.; Wang, Y. *Linear Accelerator for Radiation Chemistry Research at Notre Dame 1995*, Proceedings '95 Particle Accelerator Conference & International Conference of High Energy Accelerators, Dallas, TX, 1996.
10. Hug, G. L.; Wang, Y.; Schoneich, C.; Jiang, P. Y.; Fessenden, R. W. *Radiat. Phys. Chem.* **1999**, *54*, 559–566.
11. Buxton, G. V.; Stuart, C. R. *J. Chem. Soc., Faraday Trans.* **1995**, *91*, 279–282.
12. Mezyk, S. P.; Abud, E. M.; Swancutt, K. L.; McKay, G.; Dionysiou, D. D. Removing Steroids from Contaminated Waters Using Radical Reactions. In *Contaminants of Emerging Concern in the Environment: Ecological and Human Health Considerations*; Halden, R. U., Ed.; ACS Symposium Series 1048; American Chemical Society: Washington, DC, 2010; Chapter 9.
13. Mincher, B. J.; Mezyk, S. P.; Martin, L. R. *J. Phys. Chem. A* **2008**, *112*, 6275–6280.
14. LaVerne, J. A.; Pimblott, S. M. *Radiat. Res.* **1993**, *135*, 16–23.

Chapter 20

Effects of Aqueous Phase Radiolysis on Lactic Acid Under TALSPEAK Conditions

Leigh R. Martin,[*,1] **Bruce J. Mincher,**[1] **Stephen P. Mezyk,**[2] **Gracy Elias,**[3] **and Richard D. Tillotson**[1]

[1]**Aqueous Separations and Radiochemistry Department, Idaho National Laboratory, P.O. Box 1625, Idaho Falls, ID 83415-6150, USA**
[2]**Department of Chemistry and Biochemistry, California State University Long Beach, 1250 Bellflower Blvd., Long Beach, CA 90840, USA**
[3]**Chemistry and Radiation Measurements Department, Idaho National Laboratory, P.O. Box 1625, Idaho Falls, ID 83415, USA**
[*]**Leigh.Martin@inl.gov**

Understanding the radiolytic degradation behavior of the organic molecules involved in new or existing schemes for the recycling of used nuclear fuels is of major importance for sustaining a closed nuclear fuel cycle. The TALSPEAK process for the separation of the trivalent lanthanides from the trivalent actinides is one process that has been receiving increased attention in recent years. Despite this, there is still little known about the radiolysis effects on the aqueous phase complexants lactic acid and diethylenetriamine-N,N,N',N'',N''-pentaacetic acid (DTPA) used to accomplish this separation. This chapter discusses the results of our continued investigations into the radiolytic degradation of lactic acid in TALSPEAK aqueous phases and the resulting effects on the trivalent actinide/lanthanide separation.

Introduction

In closing the nuclear fuel cycle, it is becoming more important to remove the minor actinides from the high level waste (HLW) that is to be sent to a disposal facility. This is not only to reduce the amount of HLW but also to reduce the radiotoxicity and heat loading (*1*). Currently, the PUREX process is operated in

several countries to provide a limited recycle of used nuclear fuel. However, all solvent extraction processes employed to process commercial used nuclear fuels are subjected to radiation doses that can be on the order of kGy h^{-1} (*2*). These high radiation fields inevitably damage the reagents that are responsible for the separations. This can result in a simple reduction in the extraction efficiency (as the ligands are degraded) or as with the PUREX process, complicate the separation so much that a solvent washing step has to be introduced for solvent regeneration (*3, 4*).

As new processes are developed for the complicated separation of the minor actinides from the remainder of the fission products, the radiation chemistry of these systems becomes increasingly important. If the degradation mechanisms for the reagents that are used in these separations can be understood at the conceptual design phase, it becomes easier to develop methodologies for solvent clean-up and regeneration. Alternative approaches can also be considered, such as the addition of process-benign reagents that act as sacrificial molecules for the "active" ligands. An example of another development method can be seen in the French DIAMEX process. Here the organic phase ligand responsible for the separation has been designed with an ether linkage on a terminal alkyl chain that will preferentially cleave upon sustaining radiolytic damage, thus protecting the active site of the ligand (*5*). However, the resulting species may have reduced extraction efficiency and solubility in the organic phase.

In the US, the process that has been receiving the most attention recently for the separation of the trivalent lanthanides from the actinides is TALSPEAK (Trivalent Actinide Lanthanide Separations by Phosphorus-reagent Extraction from Aqueous Komplexes) (*6*). Originally developed at Oak Ridge National Laboratory, the separation is based on the unique properties of an aminocarboxylic acid diethylenetriamine N,N,N′,N″,N″-pentaacetic acid (DTPA, Figure 1) in a concentrated lactate buffer at pH 3.8. From this medium the trivalent lanthanides can be selectively removed using the generic organic phase extractant bis-(2-ethylhexyl) phosphoric acid (HDEHP, Figure 1). However, as identified in the recent review by Nilsson and Nash (*7*), despite the large volume of work performed on developing this process little is known about the radiation resistance of the key components and how radiolysis influences the separation. Interestingly, most reported work has focused on the organic phase extractant HDEHP (*8–10*) as opposed to the aqueous phase complexants lactic acid and DTPA (*11–13*). In a study on the radiolytic degradation of DTPA (*13*), precipitates were observed when the DTPA was in the presence of lanthanide ions at a dose of 160 kGy, which has obvious implications for process operation. Tachimori and Nakamura (*12*) reported that in a lactic acid/ lactate buffer, the extent of DTPA degradation was less than that in nitrate media of similar ionic strength, identifying that lactate acts as a protecting agent. Following on from Tachimori's work, a recent investigation by Martin *et al.* reported the rate constants for the •OH radical reaction with lactic acid and the lactate ion (*11*). For lactic acid, the room temperature rate constant (k_1) was identified as 5.24 x 10^8 M^{-1} s^{-1} while for the lactate ion (k_2) a slightly higher value of 7.77 x 10^8 M^{-1} s^{-1} was observed. There are no measurements of the •OH radical rate constant with DTPA at pH 3.8, although there are two reported at neutral pH 5.2 x 10^9 M^{-1} s^{-1} (*14, 15*) and 2.5 x 10^9 M^{-1} s^{-1} (*13*). At the anticipated

concentrations of lactic acid (0.5 M), lactate ion (0.5 M) and DTPA (50 mM) to be used in TALSPEAK a relative rates analysis shows that between 16-28% of the hydroxyl radical present will react with DTPA and not the lactate buffer. This analysis begins to provide an explanation of the observations of Tachimori and Nakamura however, for a more accurate analysis we need quantitative rate constant measurements for the $\cdot$OH/ DTPA reaction at this process relevant pH, and also to consider other transient reactive species such as $NO_3\cdot$ that are also present in irradiated solution.

Experimental

All chemicals (Aldrich) used in this study were reagent grade or higher and used as received without further purification. Solutions were made with ultrapure deionized water ($\geq$ 18 MΩ) obtained from a Millipore Milli-Q system.

The room temperature measurement of the nitrate radical reaction rate constant with (0.1, 1, 20 and 65 mM) lactic acid was performed using the electron pulse linear accelerator (LINAC) at the Radiation Laboratory, University of Notre Dame. Solutions for nitrate radical reaction rate constant measurements were 6.0 M HNO$_3$ sparged with N$_2$O. The irradiation and transient absorption detection system have been described elsewhere (2, 16).

Lactate buffer solutions for static irradiation were prepared from sodium lactate, the pH was adjusted by the addition of nitric acid. The irradiation source for these experiments was a ^{60}Co Gammacell 220E (MDS Nordion, Canada), with a dose rate of 9 kGyh^{-1} and an internal temperature of ~48°C. The pH of the lactate buffer solutions were measured before and after irradiation using a Ross combination pH electrode. For the solvent extraction experiments, a lactic acid/lactate buffer at pH 3.8 was irradiated in the absence of any DTPA and organic phase to doses of 5, 10, 100 and 200 kGy. After the irradiation DTPA was added to a concentration of 50mM (as anticipated for TALSPEAK). These solutions were then used to perform solvent extraction experiments with tracer americium and europium. The organic phase for these extractions was 0.17 M bis-diethylhexyl phosphoric acid (HDEHP) prepared from a purified stock solution.

Figure 1. (a) Lactic acid, (b) Bis-(2-ethylhexyl) phosphoric acid (HDHEP) and (c) Diethylenetriamine N,N,N',N'',N''-pentaacetic acid.

Figure 2. a) Decay of •NO₃ radical at 640 nm in N₂O-saturated 6.0 M HNO₃ with 0.141, 0.937, 19.58 and 65.57 mM lactic acid added. b) Transformed second order plot of pseudo-first-order decay kinetics of (a) plotted against lactic acid concentration. Solid line is weighted linear fit, corresponding to reaction rate constant of $k_2 = 2.15 \pm 0.17 \times 10^5$ M^{-1} s^{-1} ($R^2 = 0.990$).

High performance liquid chromatography was performed on selected samples of the lactate buffer and lactic acid after irradiation. A Shimadzu HPLC with photodiode array detector was used for the analysis of lactate. Biorad's Aminex HPX-87-H2 ion exclusion column (300 x 7.8 mm) was used for the separation with 0.01 N sulfuric acid as the eluent. The column temperature was maintained at 50°C and the column was equilibrated for one hour at 0.2 mL/min. flow rate. The flow rate was then gradually increased to 0.3, 0.4, 0.5, up to a final flow rate of 0.6 mL/min. An injection volume of 10 μL was used and the chromatograms were obtained at 210 nm. The retention time of lactate in this condition was ~13 min.

Results and Discussion

Nitrate Radical Reaction with Lactic Acid

The nitrate radicals for this study were generated by delivering fast pulses of electrons to solutions of 6.0 M nitric acid sparged with N_2O. Under these conditions the $NO_3^{\bullet}$ radicals are produced by the one of two mechanisms, either the direct radiolysis of HNO_3:

$$HNO_3 \xrightarrow{radiolysis} e^- + HNO_3^{\bullet+} \rightarrow H^+ + e^- + NO_3^{\bullet} \qquad (1)$$

or by the reaction with hydroxyl radical produced through the radiolysis of water (2, 17, 18):

$$H_2O \xrightarrow{radiolysis} {}^{\bullet}OH + e^- + H^{\bullet} + H^+ + H_2 + H_2O_2 \qquad (2)$$

$$HNO_3 + {}^{\bullet}OH \rightarrow H_2O + NO_3^{\bullet} \qquad k_3 = 1.4 \ \text{x} 10^8 \ \text{M}^{-1} \ \text{s}^{-1} \qquad (3)$$

The decay of the UV-vis absorbance of the nitrate radical was directly observed on the microsecond timescale (Figure 2a) to determine pseudo first order decay rates. These first order decay rates were then plotted vs. lactic acid concentration (Figure 2b). The slope of the linear fit corresponds to the second order rate constant which was determined to be 2.15 ± 0.17 x 10^5 M^{-1} s^{-1}. The slow rate constant for this reaction indicates that $NO_3^{\bullet}$ radical reaction with lactic acid will not be a significant contributor to the degradation of lactic acid in the TALSPEAK system. When we also consider that these separations systems will contain significant amounts of dissolved oxygen and are mildly acidic we can rule out any significant contribution to degradation from the hydrated electron and hydrogen atom as they are both rapidly consumed, Equations 3-4 (19–21):

$$e^- + H^+ \rightarrow H^{\bullet} \qquad\qquad k_4 = 2.3 \ \text{x} 10^{10} \ \text{M}^{-1} \ \text{s}^{-1} \qquad (4)$$

$$H^{\bullet} + O_2 \rightarrow HO_2^{\bullet} \qquad\qquad k_5 = 1.2 \ \text{x} 10^{10} \ \text{M}^{-1} \ \text{s}^{-1} \qquad (5)$$

This leaves the $^{\bullet}OH$ radical as the only transient radiolysis product likely responsible for the degradation of lactic acid and lactate ions in TALSPEAK.

Effect of Radiolysis on pH

Variation in aqueous solution pH from the radiolytic degradation of lactic acid could be problematic, as pH control is critical to the success of the TALSPEAK separation process. This was highlighted in recent work by Nilsson and Nash (22) where they reported significant decreases in distribution ratios for both the lanthanides and americium with increasing pH, although the separation factors remain the same. To investigate this potential problem, solutions of lactic acid at varying concentrations (1 mM, 10 mM and 1.0 M) were irradiated with a ^{60}Co source to absorbed doses of 5, 10, 100 and 200 kGy. In all cases the pH was seen to

increase as a function of increasing dose, see Figure 3. Despite these pH changes there was no discoloration observed in the irradiated solutions at any absorbed dose, and no precipitate formation. Nevertheless, these results show that as long as the lactate concentration is kept above 1.0 M, there should be little impact from radiolysis on the pH of the aqueous solution.

Effects of Radiolysis on Solvent Extraction Processes

As previously highlighted, radiolysis induced pH changes are not expected to be problematic in the TALSPEAK process, however the chemical products formed by the solution radiolysis may interfere. To elucidate the extent of this impact, distribution coefficients of americium and europium as a function of dose received to the lactate buffer were investigated, and are given in Figure 4. For americium there was found to be no change in the distribution coefficient (D_{Am}) regardless of the dose to the lactate buffer. For europium, D_{Eu} is seen to increase from 1.70 ± 0.06 at zero dose to a high of 2.31 ± 0.11 at a dose of 100 kGy, and then (within error) levels out to 2.08 ± 0.03 at a dose of 200 kGy. The change in D_{Eu} relates to an approximate 5% increase in the amount of Eu extracted. As there is no change observed to D_{Am}, with increasing dose to the lactate buffer, the separation factor for Eu from Am (given by D_{Eu}/D_{Am}) is also seen to increase slightly from 22 to 30 (Table I). These results suggest that the radiolysis products of the lactate buffer system influence the mechanism by which Eu is extracted. Conversely, the observation that there is no effect on D_{Am} with increasing dose to the lactate buffer is not unexpected. This is because in the TALSPEAK process we expect the chemistry of the trivalent actinides to be dominated by their interaction with DTPA. In addition to these experiments we investigated the stripping of Eu from the organic phase with 2.0 M nitric acid. These experiments were performed to establish if the degradation of the lactate buffer would lead to any species that could be extracted with the metal ion into the organic phase and inhibit the recovery of the trivalent lanthanides. The stripping distribution coefficients for Eu are given in Table II; and show that this ratio is constant within experimental error regardless of the dose. Moreover, we can infer from these data that all of the Eu is recovered from the organic phase. These results show that the degradation products from lactic acid/ lactate radiolysis should not significantly interfere with the TALSPEAK separation process.

Figure 3. Variation of pH in irradiated lactic acid solutions as a function of absorbed dose. (■) 0.001M lactic acid, (•) 0.01M lactic acid and (▲) 1.0 M lactic acid.

Figure 4. Distribution ratios for Eu and Am vs. absorbed dose to lactic acid/ lactate buffer for TALSPEAK extractions using 0.17M purified HDEHP. Error bars shown are standard deviations of triplicate measurements.

Table I. Separation factors (D$_{Eu}$/D$_{Am}$) as a function of dose to the lactate buffer

Dose (kGy)	Separation factor
0	22.3
5	27.8
10	29.1
100	30.2
200	29.7

Table II. Eu strip distribution coefficients as a function of dose to lactate buffer

Dose (kGy)	Strip D$_{Eu}$
0	0.0058
5	0.0061
10	0.0063
100	0.0061
200	0.0054

Figure 5. HPLC chromatograms showing (a) unirradiated lactic acid, (b) unirradiated lactate buffer, (c) 1.0 M lactic acid after 200 kGy irradiation and (d) 1.0 M lactate buffer after irradiation to 200 kGy

Stable Product Analysis

Irradiated and non-irradiated samples of pH 1 lactic acid and pH 3.8 lactate buffer at two concentrations (1 mM and 1.0 M) were analyzed by HPLC to identify significant degradation products. Both the 1 mM lactic acid and lactate buffer solutions were found to contain no evidence of lactate after irradiation to 200kGy, but several new peaks were observed in the HPLC trace.

In the samples containing an initial concentration of 1.0 M lactic acid or lactate buffer, similar new products were observed in addition to residual lactic acid/ lactate as illustrated in Figure 5. When comparing the chromatograms of the lactic acid and lactate buffer several differences are observed. The chromatogram for the lactate buffer after irradiation shows four new peaks at retention times of ∼ 8.7, 9.3, 10.8 and 18.3 mins. (Figure 5 (d)), whereas the chromatogram of the lactic acid (Figure 5 (c)) shows 6 new peaks at retention times of ∼ 8.9, 9.5, 10.16, 12.5, 15.7 and 25.7 mins (the peak at 13.4 is assumed to be lactate ion). The pair of peaks at around 8.9 and 9.4 min. retention time are expected to be the same products for both samples. The remaining peaks are seemingly different products, suggesting that the lactic acid and the lactate ion degradation pathways are different. Identification of individual product species is complicated by the pH of the solutions *e.g.* we expect that oxalic acid may well be one of the radiolysis products, as it can be produced by the combination of two formate radicals or via a Russell reaction (*23*). However, oxalic acid has two protons that can be removed with pK_1 at ∼1.2 and pK_2 at ∼4.19 (*23*), therefore at pH 3.8 we would expect both the $HC_2O_4^-$ and $C_2O_4^{2-}$ ions to be present at about a ratio of 70:30 % respectively, resulting in 2 peaks in the chromatogram. Other expected products may include lactate oligomers such as lactones or glyoxylic and acetic acids (*24*). Further, more detailed investigations into positive identification for each of the peaks observed is still underway.

Conclusions

We have identified the major transient species responsible for the degradation of lactic acid and the lactate ion in the TALSPEAK system to be the ˙OH radical. When irradiated, the pH of lactate buffer solutions has been shown to increase as a function of increased dose, this effect is more pronounced at lower concentrations of lactate. The solvent extraction experiments conducted here have shown that the products of radiolysis do not significantly affect TALSPEAK separation. Although D_{Eu} was seen to increase, there was no change in D_{Am} as a function of increased dose, resulting in a slightly increased separation factor. Despite this, Eu was successfully recovered from the organic phase. Finally, we have identified that the lactate ion and lactic acid degradation pathways differ and have begun stable product identifications.

Acknowledgments

References

1. Nash, K. L.; Lumetta, G. J.; Clark, S. B.; Friese, J. In *Separations for the Nuclear Fuel Cycle in the 21st Century*; Lumetta, G. J., Nash, K. L., Clark, S. B., Friese, J. Eds; ACS Symposium Series 933; American Chemical Society: Washington, DC, pp 3−20.
2. Mincher, B. J.; Mezyk, S. P.; Martin, L. R. *J. Phys. Chem. A* **2008**, *112*, 6275–6280.
3. Reif, D. J. *Sep. Sci. Technol.* **1988**, *23*, 1285–1295.
4. Blake, C. A., Jr.; Davis, W.; Schmitt, J. M. *Nucl. Sci. Eng.* **1963**, *17*, 626–637.
5. Berthon, L.; Morel, J. M.; Zorz, N.; Nicol, C.; Virelizier, H.; Madic, C. *Sep. Sci. Technol.* **2001**, *36*, 709–728.
6. Weaver, B.; Kappelmann, F. A. *TALSPEAK: A New Method of Separating Americium and Curium from the Lanthanides by Extraction from an Aqueous Solution of an Aminopolyacetic Acid Complex with a Monoacidic Organophosphate or Phosphonate*; ORNL-3559; Oak Ridge National Laboratory, Oak Ridge, TN, 1964.
7. Nilsson, M.; Nash, K. L. *Solvent Extr. Ion Exch.* **2007**, *25*, 665–701.
8. Tachimori, S.; Krooss, H.; Nakamura, H. *J. Radioanal. Chem.* **1978**, *43*, 53–63.
9. Schulz, W. W. *Nucl. Technol.* **1972**, *13*, 159–167.
10. Kulikov, I. A.; Milovanova, A. S.; Shesterikov, N. N.; Vladimirova, M. V. *Radiokhimiya* **1990**, *32*, 101–105.
11. Martin, L. R.; Mezyk, S. P.; Mincher, B. J. *J. Phys. Chem. A* **2009**, *113*, 141–145.
12. Tachimori, S.; Nakamura, H. *J. Radioanal. Chem.* **1979**, *52*, 343–354.
13. Bibler, N. E. *J. Inorg. Nucl. Chem.* **1972**, *34*, 1417–1425.
14. Cabelli, D. E.; Rush, J. D.; Thomas, M. J.; Bielski, B. H. *J. Phys. Chem.* **1989**, *93*, 3579–3586.
15. Thomas, V. G.; Srivastava, S. B.; Moorthy, P. N. *J. Radioanal. Nucl. Chem.* **1989**, *136*, 443–447.
16. Whitman, K.; Lyons, S.; Miller, R.; Nett, D.; Treas, P.; Zante, A.; Fessenden, R. W.; Thomas, M. D.; Wang, Y. *Linear Accelerator for Radiation Chemistry Research at Notre Dame*, IEEE Proceedings Particle Accelerator Conference and International Conference on High Energy Accelerators; Institute of Electrical and Electronics Engineers (IEEE): Dallas, TX, 1995; pp 131−133.
17. Shastri, L. V.; Huie, R. E. *Int. J. Chem. Kinet.* **1990**, *22*, 505–512.

18. Katsumura, Y.; Jiang, P. Y.; Nagaishi, R.; Oishi, T.; Ishigure, K.; Yoshida, Y. *J. Phys. Chem.* **1991**, *95*, 4435–4439.
19. Buxton, G. V.; Greenstock, C. L.; Helman, W. P.; Ross, A. B. *J. Phys. Chem. Ref. Data* **1988**, *17*, 513–886.
20. Asmus, K. D. *Methods Enzymol.* **1984**, *105*, 167–178.
21. Chin, M.; Wine, P. H. *J. Photochem. Photobiol., A* **1992**, *69*, 17–25.
22. Nilsson, M.; Nash, K. L. *Solvent Extr. Ion Exch.* **2009**, *27*, 354–377.
23. Vel Leitner, N. K.; Dore, M. *J. Photochem. Photobiol., A* **1996**, *99*, 137–143.
24. Stainforth, M.; O'Hanlon, M.; Khong, T. M. *J. Chromatogr., A* **1999**, *833*, 195–208.

DIAMEX Solvent Behavior under Continuous Degradation and Regeneration Operations

B. Camès,* I. Bisel, P. Baron, C. Hill, D. Rudloff, and B. Saucerotte

CEA, Nuclear Energy Division, Radiochemistry & Processes Department, SCPS, LPCP, F-30207 Bagnols sur Cèze, France
*beatrice.cames@cea.fr

Industrial implementation of partitioning processes based on solvent extraction requires solvent recycling with constant separation and physicochemical properties. In nuclear applications, both radiolysis and acidic hydrolysis lead to degradation products which need to be removed from solvent before its recycling. The long term evolution of DIAMEX process solvent (0.65M DMDOHEMA–HTP) under continuous degradation by acidic hydrolysis and γ-radiolysis was studied in the laboratory-scale MARCEL γ–irradiation facility, with and without alkaline treatment process (**AT**). With AT, analyses of organic phase showed the accumulation of only one degradation product, MDOHEMA, probably responsible for the molybdenum accumulation observed. Distribution coefficients of Zr, Pd, Fe and Nd, surface tension, refraction index, settling time, viscosity, and density were constant during the tests. Furthermore, no catalytic effect of fission and corrosion products was observed. These studies were consolidated by comparative α- and γ-radiolysis batch tests which showed that α-radiolysis and γ-radiolysis led to the same degradation products.

Introduction

As decreed by the French law of 30th December 1991, a 15-year research program was carried out by the CEA. Its objective was the investigation of separation processes for subsequent transmutation of long-lived radionuclides,

in order to significantly reduce the radiotoxicity of the final waste produced by the nuclear industry. The main targets were the minor actinides (MA) – i.e. neptunium, americium and curium – to be recovered quantitatively and selectively from PUREX (Plutonium - Uranium Refining by EXtraction) raffinate, the product of nuclear spent fuel reprocessing.

The reference strategy for separating MA from spent fuel is based on an adaptation of the PUREX process for the separation of Np, and the development of new liquid-liquid partitioning processes, called DIAMEX (DIAMide Extraction) and SANEX (Separation of ActiNides by Extraction), for the other minor actinides (Am and Cm).

Aims of the Studies

In the DIAMEX process, the use of a malonamide diluted in an aliphatic diluent permits the co-extraction of the Actinides (III) and the Lanthanides (III) from the waste. Different studies were performed to demonstrate the technical feasibility of this process: some focused on solvent stability, as the organic phase is degraded due to hydrolysis by aqueous nitric phases and radiolysis by fission products. The resulting degradation products modify the extraction and/or the hydrodynamic performances of the process. It is therefore necessary to remove these degradation compounds from the spent solvent by a specific treatment before recycling, and in parallel to have a fresh solvent supply. The extraction, separation, and hydrodynamic properties can thus be maintained.

To anticipate and scale-up the DIAMEX solvent behavior under continuous operations, two kinds of studies were realized:

- Batch studies to determine the parameters influencing the degradation kinetics of the extractant molecule, in particular the effects of γ and α radiation and those of acidic hydrolysis, and to establish the efficiency of solvent treatment.
- Long term tests to study the behavior over time of the solvent (hydrolysis effect, combined hydrolysis and radiolysis effects, impact of the solvent clean-up), the kinetics of solvent consumption and of degradation product accumulation, and the impact of these on process performances.

Experiments

Batch Studies

The Diamex Solvent

A DIAMEX solvent is an organic phase consisting of a malonamide diluted to 0.65 M in Hydrogenated TetraPropene (HTP). The reference molecule is N,N′-DiMethyl-N,N′-DiOctyl-Hexyl-Ethoxy-Malonamide (DMDOHEMA). This malonamide molecule's formula was optimized to minimize long-alkyl-chain degradation products (*1*).

Malonamide degradation under hydrolysis and radiolysis has been studied in detail using GC-FTIR and GC-MS techniques (*2*). The main degradation products identified in the organic solution after radiolysis or hydrolysis in presence of nitric acid aqueous phase were an amidic-acid (1), a monoamide (3), diamides (DMOHEMA (4) with a loss of octyl group and MDOHEMA (5) with a loss of methyl group), carboxylic acids and amines such as MethylOctyl Amine (2) (MOA) (Figure 1).

Degradation Conditions of DMDOHEMA

The diluted organic phase (0.65M or 1M) was pre-equilibrated with HNO_3 media (2 to 4M) to obtain different concentrations of HNO_3 in the organic phase, and then exposed to γ (^{60}Co or ^{137}Cs source) or α (^{244}Cm aqueous solution) radiation or to hydrolysis at 45°C in presence of HNO_3 aqueous phase.

Next, different analyses of the solvent were performed:

- Gas chromatography (GC) coupled with a flame ionization detector (FID) to quantify compounds with a molecular weight higher than 170 g/mol, such as amidic-acid, monoamide, MDOHEMA or DMOHEMA and the remaining DMDOHEMA.
- Potentiometric titration in nonaqueous medium to determine the concentration of amide and/or amine compounds, such as methyl octyl amine, and acidic species such as carboxylic acids.

Figure 1. Simplified scheme for radiolytic or hydrolytic degradation of DMDOHEMA

The solvent composed of DMDOHEMA 0.65M in HTP, pre-equilibrated with 3M HNO_3 media, was degraded either at 4 kGy·h^{-1} by α (^{244}Cm) or γ (^{60}Co) radiations, or by hydrolysis at 45°C in presence of 3M HNO_3 aqueous phase.

The monitoring of the remaining DMDOHEMA by GC-FID in all the degraded solutions allowed an estimation of the malonamide degradation kinetic. The results summarized in Figure 2 show that under these conditions, DMDOHEMA disappearance is linear with time under hydrolysis and α and γ radiolysis, according to an apparent zero order kinetics.

From the slope of the curves, the different apparent kinetic constants (k_1) are calculated:

- For hydrolysis at 45°C during 700 h, k_1^h = - 0.636 mmol·L^{-1}·h^{-1}.
- For radiolysis at 4 kGy·h^{-1} with a cumulated dose of 0.7 MGy (175h),

  ○ k_1^γ = - 1.666 mmol·L^{-1}·h^{-1} for gamma radiation
  ○ k_1^α = - 0.438 mmol·L^{-1}·h^{-1} for alpha radiation.

These results thus show that the impact of alpha radiation is 4 times slower than that of gamma radiation.

Figure 2. Evolution of the remaining DMDOHEMA after degradation, with duration. [DMDOHEMA]$_0$=0.65M in HTP pre-equilibrated with 3M HNO_3.

To complete these results, the influence of DMDOHEMA concentration, initial acidity of the organic phase and dose rate were studied.

The different degradation conditions are summarized in Table 1, the GC-FID analysis of the irradiated organic phases revealed that the variation of:

- The remaining DMDOHEMA concentration is linear with time, but different slope values (k_1^γ) are obtained.
- The plotting of these k_1^γ values increases linearly with dose rate, but different slope values (k_2^γ) are obtained.
- The plotting of these k_2^γ values increases linearly with acidity of the organic phase and leads to one slope value of $0.316.10^{-3}$ KGy^{-1} (Figure 3).

Table 1. Summary of the different irradiation conditions of the DMDOHEMA solution in HTP and of the apparent kinetic constants (k_1^γ and k_2^γ) obtained. γ source: ^{137}Cs or * ^{60}Co

[DMDOHEMA]$_0$ (M)	$[HNO_3]_0$ (M)	$[\overline{HNO_3}]_0$ (M)	Time (h)	Dose rate (KGy/h)	k_1^γ (mmol/L/h)	k_2^γ (mmol/L/KGy)
	2	0.25	461	1.0	-0.374	-0.335
			461	1.9	-0.610	
0.65	3	0.44	74	1.3	-0.545	-0.405
			234			
			330			
			479			
			461	1.9	-0.639	
			175	4.1*	-1.666	
	4	0.60	461	0.9	-0.404	-0.449
			461	1.9	*-0.594*	
1	3	0.73	461	1.0	-0.595	-0.510
			461	1.8	-0.883	
	4 (*3*)	1.0	188	4.0*	-2.293	-0.573

Figure 3. Evolution of the apparent kinetic constants (k_2^γ) with initial organic phase acidity for the different irradiated DMDOHEMA solutions

From these results, it seems that the kinetic of DMDOHEMA degradation is a function of 3 factors: initial nitric acid concentration in the organic phase, dose rate, and time, according to the following relationship:

$$[extractant]_t = \left(-k_3^\gamma \times [\overline{HNO_3}]_0 \times \dot{D} \times t \right) - \left(constant \times \dot{D} \times t \right) + [extractant]_0$$

$\dot{D}$: dose rate (KGy/h), t: radiolysis time (h), k_3^γ: consumption kinetic constant = $0.316.10^{-3}$ KGy^{-1} and constant = $0.265.10^{-3}$ KGy^{-1}

Degradation Product Accumulation

For the different degraded organic phases, GC-FID analyses also permitted quantification of the degradation products, such as monoamide (MOHOBA), amidic-acid (MOCHOBA) and diamide (MDOHEMA) only formed by radiolysis.

Potentiometric titration revealed that there were more amide and/or amine compounds and acidic species than those quantified by GC-FID. Except for the methyloctyl amide (MOA) characterized by its pKa value (9.8), the other products were not able to be identified. For these studies, they are called "light amide and/or amine" and "light acidic" compounds, because they have a molecular weight lower than the species quantified by GC-FID.

Figure 4 shows an example of quantification for all degradation products formed in the case of radiolysis at a dose rate of 4 KGy/h (^{60}Co).

Figure 4. Evolution of the degradation products with radiolysis duration. (^{60}Co irradiation, dose rate = 4 KGy/h, [DMDOHEMA]$_0$=0.65M, $\left[HNO_3\right]_0$= 0.44M

Removal of the Degradation Products

These degradation products must all be removed from the solvent if its performance is to be maintained. Different treatments were therefore tested, including washing with HNO$_3$ (0.1M), which is efficient towards MOA and carboxylic acids bearing less than 6 carbon atoms. The remaining products were monoamide, amidic-acid, MDOHEMA only in the case of radiolysis, and the light amides/amines or acid compounds. Table 2 summarizes the accumulation kinetic constants of these degradation products, estimated in the linear parts of the curves.

An additional alkaline treatment with 0.3M sodium hydroxide permitted the removal of:

- Amidic-acid and light acids, in the case of hydrolysis.
- Amidic-acid and half of light acids, in the case of radiolysis.

Table 2. Apparent kinetic constant values for degradation product accumulation, after HNO₃ 0.1M washing of degraded DIAMEX solvent (Pre-equilibrated solvent with HNO₃ 3M and radiolysis at 4 KGy/h or hydrolysis at 45°C)

k_I^γ (mmol.L⁻¹.h⁻¹)	Monoamide	Amidic acid	MDOHEMA	"Light*" Amides/ amines	"Light*" acids
Radiolysis	0.2	0.3	0.2	1.4	0.4
Hydrolysis	0.4	0.3	0	0.5	0.2

Impact of the Remaining Degradation Products

After solvent clean-up, the impacts of the remaining degradation products on the process performances were assessed.

The measurement of the phase Disengagement Time Ratio (DTR) permits the evaluation of the degraded solvent's hydrodynamic properties.

$$DTR = \frac{Disengagement\ Time\ of\ 80\%\ of\ 0.1M\ HNO_3\ after\ mixing\ with\ degraded\ solvent}{Disengagement\ Time\ of\ 80\%\ of\ 0.1M\ HNO_3\ after\ mixing\ with\ undegraded\ solvent}$$

Figure 5 shows that the DTR values:

- Do not completely depend on the diamide concentration.
- Depend on the presence of some of the remaining degradation products.

The impact of the remaining degradation products after 0.1M HNO₃ washing is low in the case of hydrolysed solvent and high for radiolysed solvent.

A 0.5M Na₂CO₃ treatment permitted the restoration of hydrolysed organic phase hydrodynamic performances, but was not sufficient for radiolytically degraded solvent.

Measurement of the different metal (americium or europium) distribution ratios between organic phases and a 3M HNO₃ aqueous phase showed (Figure 6) that the degradation products formed by radiolysis do not greatly affect the D_{Eu} or D_{Am} values, which decrease with decreasing DMDOHEMA concentration.

On the other hand, the degradation products formed by hydrolysis affect the D_{Eu} or D_{Am} values. The removal of some of these compounds by acido-basic treatments did not enable the restoration of the solvent's extracting properties.
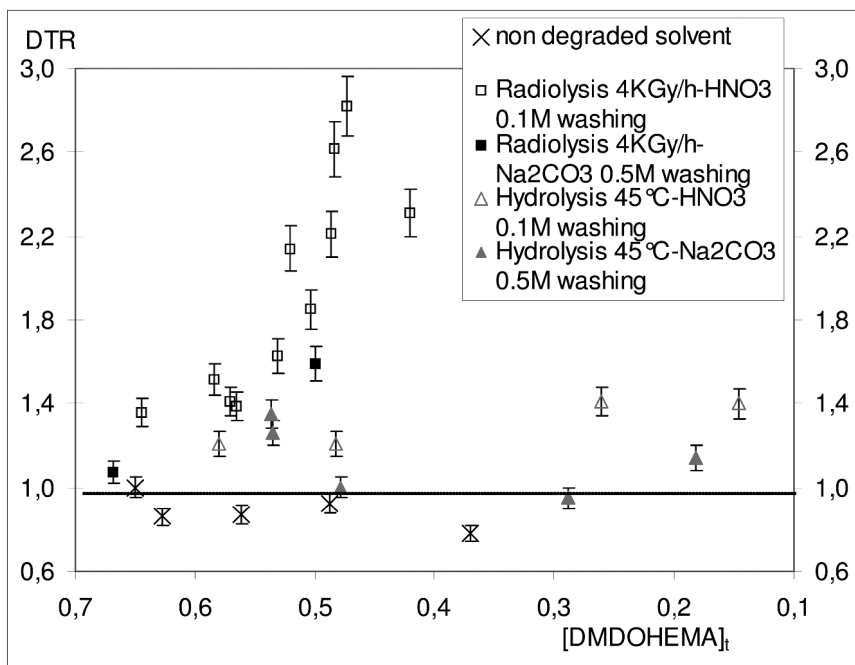
Figure 5. Evolution of the phase Disengagement Time Ratio (DTR) with DMDOHEMA concentration for non degraded or degraded solvent after acido-basic treatment

Continuous Operations

Methodology

The long term behavior of the DIAMEX solvent was studied in the MARCEL gamma irradiation facility.

On this process platform, all is automated and monitored to ensure the facility's safety: batteries of mixer settlers, centrifugal contactors (CC type 1, with a mixing chamber volume and a rotation speed lower than the CC type 2), pumps to feed in the aqueous solutions and the organic phase, scales to monitor the aqueous phase and level controllers for system safety.

All the liquid-liquid contactors are installed under laboratory hoods, except the irradiated reactor (with a ^{137}Cs source), located in the irradiator extension.

The chemical composition, the physico-chemical properties (refraction index, surface tension, DTR, density and viscosity) and extraction/separation performances (distribution ratios of Fe, Nd, Pd, Zr and Mo) were monitored.
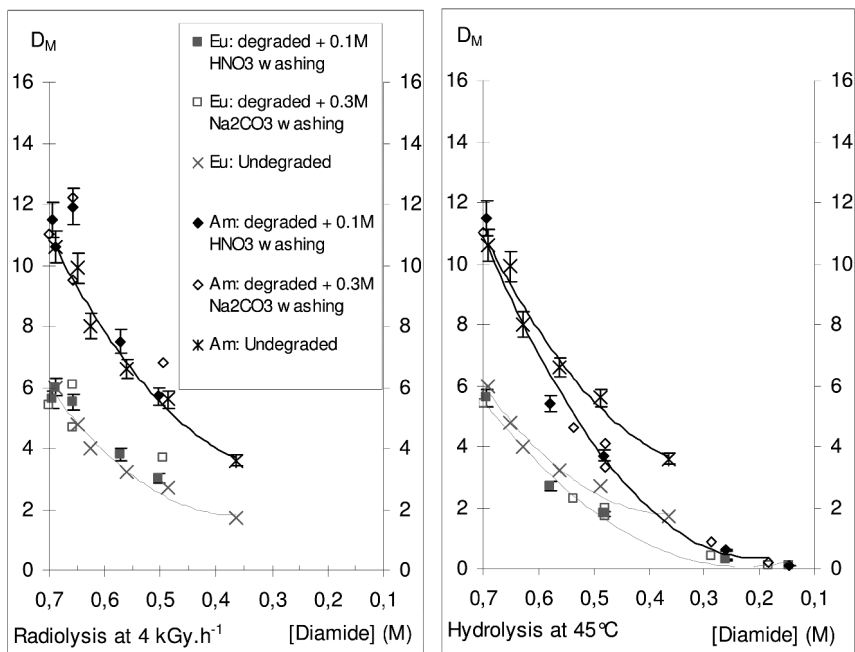
Figure 6. Distribution ratios of Am or Eu as a function of the DMDOHEMA concentration in the case of undegraded or hydrolysed or radiolysed (^{60}C) solvent. [DMDOHEMA]$_0$=0.65M, $\left[HNO_3\right]_0$= 0.44M

DIAMEX Flow-Sheet Scenarios

Different flow-sheets were tested on the process platform under penalizing chemical conditions. The solvent (DMDOHEMA 0.65M in HTP) was:

- spiked with 3M nitric acid and cations, neodymium only, or in addition to iron, molybdenum, zirconium, and palladium,
- submitted to hydrolysis at 40°C with a residence time of 2.5 hours, alone or coupled with gamma radiolysis at a dose rate of 1.3 kGy/h with a residence time of 6.25 hours,
- after scrubbing and stripping (0.1M HNO$_3$), the degraded solvent was either cleaned up with an alkaline treatment (**AT**) or not.

The main conditions are summarized in Table 3.

Table 3. Different DIAMEX flow-sheet scenarios tested on the Marcel process platform

Cations	Degradation	Alkaline Treatment	Test duration
Nd	Hydrolysis	None	222 h
Nd	Hydrolysis	NaOH 0.3M	262 h
Nd	Hydrolysis + Radiolysis	None	334 h
Nd	Hydrolysis + Radiolysis	NaOH 0.3M	298 h
Nd	Hydrolysis + Radiolysis	NaOH 0.3M	765 h
Nd, Fe, Mo, Zr, Pd	Hydrolysis + Radiolysis	NaOH 0.3M	446 h

The longest DIAMEX test with hydrolysis, radiolysis, Nd and alkaline treatment lasted 765 hours and corresponded to 43 solvent cycles, that is to say about 270 days of industrial operations for UOX2 spent fuels. The accumulated dose was 358 KGy, and the accumulated hydrolysis duration 104 h.

The monitoring of the DMDOHEMA concentration by GC-FID permitted an adjustment of the solvent to its nominal composition. From the addition of DMDOHEMA and HTP, it was possible to estimate the apparent rate constant of solvent consumption (k^{γ}).

For example, in the case of the DIAMEX long test (Figure 7), the k values were:

-   $k^{\gamma}_{DMDOHEMA}$ = 4.4 mmol/L/h hydrolysis (or 1.3 mmol/L/kGy)
-   k^{γ}_{HTP} = 69.4 mmol/L/h hydrolysis (or 20.2 mmol/L/kGy)

The more important consumption of HTP with regard to the DMDOHEMA (15 times more) is probably due to heating in the Centrifugal Contactors (CC) used for alkaline treatment, which increase the evaporation of HTP within these devices.

Furthermore, the comparison of this test with the others (Table 4) showed that:

-   the HTP evaporation is higher for the CC type 2 than for the CC type 1,
-   the degradation conditions were such that the radiolysis impact was 3 times higher than the hydrolysis effect.

Table 4. Estimation of the apparent rate constants of solvent consumption ($k\gamma$) for the different DIAMEX flowsheets tested on the Marcel platform

Flowsheets	$k\gamma_{DMDOHEMA}$ (mmol/L/h hydrolysis)	$k\gamma_{HTP}$ CC type 1 or 2	AT apparatus
Nd+ Hydrolysis	1.4	7.3	
Nd+ Hydrolysis+AT	2.4	20.9	CC type 1
Nd+ Hydrolysis + Radiolysis	3.9	19.1	
Nd+ Hydrolysis + Radiolysis	7.9	37.6	CC type 1
Nd+ Hydrolysis + Radiolysis+AT	4.4	69.4	CC type 2
Nd, Fe, Mo, Zr, Pd + Hydrolysis + Radiolysis+AT	5.7	76.3	CC type 2
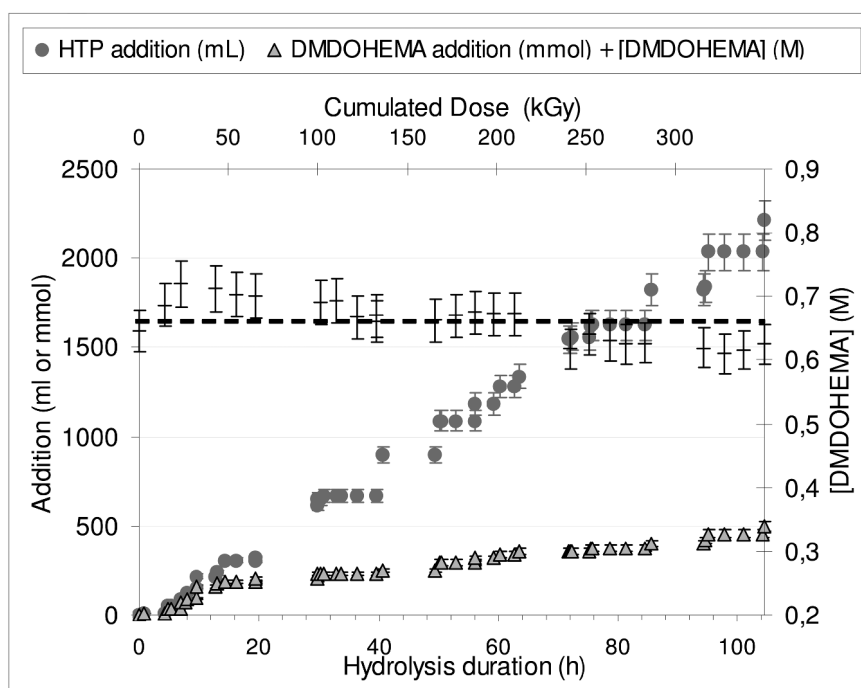
Figure 7. Variation of the extractant concentration and make-up volumes during the DIAMEX test: 765 h – Nd+ H+R+AT

For all these tests, the accumulation rate constants of the degradation products were estimated in the linear part of the curves (Table 5).

Table 5. Apparent kinetic constant values of degradation product accumulation for the different DIAMEX flowsheets

Flowsheets	$k\gamma_{monoamide}$	$k\gamma_{amidic-acid}$	$k\gamma_{MDOHEMA}$	$k\gamma_{\text{"light" acids}}$
	(mmol/L/h hydrolysis)			
Nd+Hydrolysis	0.2	0.5	0	0
Nd+Hydrolysis+AT	0	0	0	0
Nd+Hydrolysis+Radiolysis	0.1	0.6	0.4	0.7
Nd+Hydrolysis+Radiolysis+AT	0	0	0.3	0
Nd, Fe, Mo, Zr, Pd +Hydrolysis+Radiolysis+AT	0	0	0.3	0

The comparison of all these $k\gamma$ values allows the following assumptions:

- the amidic-acid is a primary degradation product formed by radiolysis or hydrolysis,
- MDOHEMA is a primary degradation product only formed by radiolysis,
- the monoamide is a secondary degradation product formed by degradation of amidic-acid, as it is not present in the solvent when the amidic-acid is removed by alkaline treatment,
- and the "light" acid compounds are primary degradation products only formed by radiolysis.

Moreover, the "light" amide/amine compounds detected in batch studies were not formed in continuous operations.

Therefore, the use of alkaline treatment for the DIAMEX process allows only MDOHEMA to accumulate.

Impact of the Degradation Products on the Physico-Chemical Properties and Performances of the Solvent

To study the impact of the degradation products on the process performances, different physico-chemical and distribution ratio measurements were monitored.

For all the flow-sheets tested, there is no impact of the remaining degradation products on the distribution ratios of Fe, Nd, Pd, and Zr, or on the refraction index and the surface tension. These species can however modify the DTR values, the density, the viscosity or the distribution ratio of Mo.

Table 6, which summarizes all the results, shows that for flowsheets with:

- neodymium only, the removal of some of the degradation products by alkaline treatment enabled the DTR values, the density and the viscosity to be stable,
- radiolysis degradation, the remaining degradation products led to molybdenum accumulation in the organic phase. In the case of the test

with all the cations including molybdenum, this phenomenon increased the density and the viscosity.

The Mo accumulation in the organic phase was probably due to one compound, MDOHEMA, because it was the only common degradation product accumulating in the solvent. Furthermore, the variation of Mo accumulation is linear with MDOHEMA concentration (Figure 8).

Table 6. Impact of the Diamex solvent degradation products on process performances

Flowsheets	DTR	Density	Viscosity	D_{Mo}
Nd+Hydrolysis	+31%	+0.4%	+4%	None
Nd+Hydrolysis+AT	None	None	None	None
Nd+Hydrolysis+Radiolysis	+22%	+1%	+22%	+338%
Nd+Hydrolysis+Radiolysis+AT	None	None	None	+272%
Nd, Fe, Mo, Zr, Pd +Hydrolysis+Radiolysis+AT	None	+1%	+25%	+0.2%/h hydrolysis
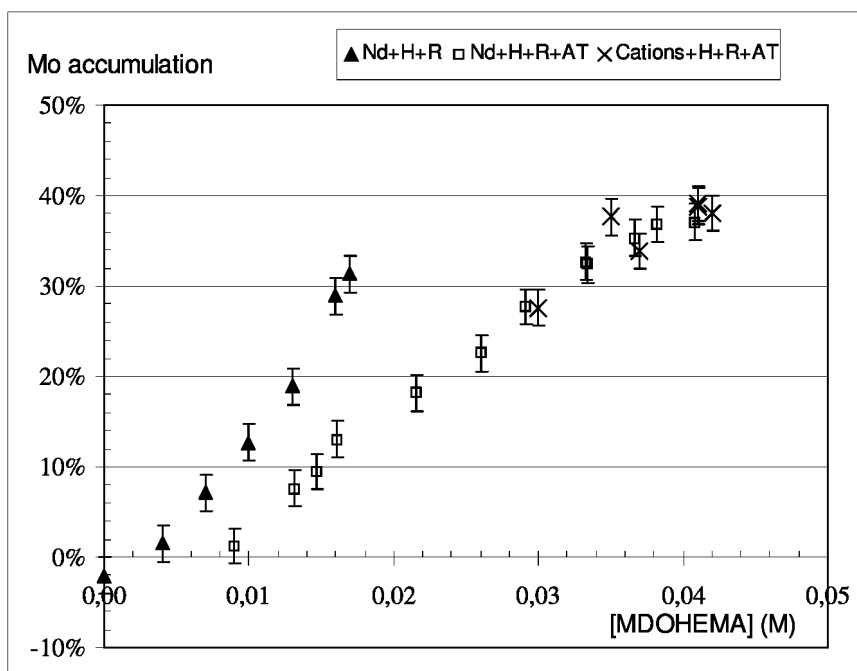
Figure 8. Variation of molybdenum in the solvent with MDOHEMA concentration for flowsheets with radiolysis

Figure 8 also shows that for the test with neodymium and hydrolysis and radiolysis degradation without alkaline treatment, the remaining "light" acid compounds probably contributed to this phenomenon.

Conclusion

The MARCEL gamma-irradiation facility enabled the long term evolution of DIAMEX process solvent to be studied. The longest test, with hydrolysis and radiolysis degradation and alkaline treatment, represented at least 270 days of industrial operations for UOX2 spent fuels and in fact probably more, as γ-radiation is 3 times more penalizing than α-radiation.

The batch studies showed that the DMDOHEMA consumption seems to depend only on nitric acid concentration in the organic phase, dose rate and time. Furthermore, these studies allowed an optimization of the acido-basic treatment efficiency for some of the degradation products (methyloctyl amine, amidic-acid and a part of the "light" species). The remaining degradation products are MDOHEMA, residual "Light" acid compounds, the monoamide and "Light" amide or amine compounds.

The continuous degradation/regeneration operations permitted the determination of the solvent consumption kinetic and the identification of the degradation processes. Methyloctyl amine, amidic-acid and MDOHEMA are primary degradation products formed by hydrolysis and/or by radiolysis. "Light" acid species, amide/amine compounds and monoamide are secondary degradation products, formed by radiolysis only or by hydrolysis.

Therefore, the use of an alkaline treatment permitted the removal of all the products formed by hydrolysis and/or radiolysis except one, MDOHEMA.

This compound has no impact on the physico-chemical properties of the solvent apart from the accumulation of molybdenum in the solvent, which increases its density (+1%) and viscosity (+25%). However, the MDOHEMA accumulation had no impact on DIAMEX process performances.

Additional studies will be realized to confirm the impact of this degradation product and to determine the concentration from which it will become problematic for the process.

References

1. Charbonnel, M. C.; Berthon, L. *Rapport Scientifique 1997*; CEA Report CEA-R-5801; Direction du Cycle du Combustible, 1998; pp 114−119.
2. Berthon, L.; Camès, B. *Rapport Scientifique 1999*; CEA Report CEA-R-5892; Direction du Cycle du Combustible, 2000; pp 206−211.
3. Berthon, L.; Charbonnel, M. C. In *Ion Exchange and Solvent Extraction: A Series of Advances*; Moyer, B. A, Ed.; CRC Press Taylor & Francis Group: Boca Raton, FL, 2010; Volume 19, pp 464−470.

Steady-State Radiolysis: Effects of Dissolved Additives

J. C. Wren[*]

Department of Chemistry, The University of Western Ontario, London, Ontario N6A 5B7, Canada
***jcwren@uwo.ca**

High energy, α, β and γ-radiation from nuclear fission and neutron activation products interacts with water by initially ionizing it. The ionized or excited water molecule undergoes a series of energy transfer processes, and decomposes into both oxidizing and reducing species, $\bullet OH$, H_2O_2, O_2, H_2, $\bullet H$, $\bullet O_2^-$ and $\bullet e_{aq}^-$, whose relative concentrations change considerably within a short time scale following the initial interaction. Under long-term continuous irradiation these species reach low, steady-state concentrations that can dictate the aqueous redox potential and, hence, materials corrosion processes. Understanding the impact of radiolysis is an important factor in the design, analysis and maintenance of materials in environments such as nuclear power plant coolant systems where high levels of radiation are present. Chemical additives may be used to effectively push the environment toward an optimal redox state to protect reactor components, but determination of the appropriate additive levels must take into account the influence of radiolysis on the system chemistry. The effects of chemical additives (pH-controlling agents, dissolved gases (O_2 and H_2) and dissolved corrosion products) on steady-state radiolysis chemistry have been investigated by both experiments and kinetic model analysis under long-term continuous irradiation conditions. The studies show there are three distinct regions of water radiolysis behaviour: pH < 4.5; 4.5 < pH < 9.7; and pH > 9.7 with the relative levels of radical and molecular radiolysis products changing substantially from one region to another. These studies show how changes in the

concentrations of key species that react with water radiolysis products influence the eventual steady-state concentrations by changing the rates of some reactions. Additives or dissolved species that can induce significant changes in the steady-state concentrations are those that can react with water radiolysis products in a catalytic manner.

1. Introduction

Understanding the factors that can affect the aqueous corrosion of materials used in nuclear power reactors is important for designers (material specifications) and operators (water chemistry control and corrosion monitoring). Corrosion kinetics depend on aqueous redox conditions and the physical and chemical nature of the alloys involved (*1, 2*). In addition to the normal corrosion challenges faced by materials in industrial environments, the materials used in nuclear reactor coolant systems must withstand high levels of ionizing radiation. Exposed to ionizing radiation, water decomposes into aggressive oxidizing and reducing species (including •OH, H_2O_2, O_2, •O_2^-). Understanding how radiation can change and control the redox chemistry in irradiated water systems is necessary if one needs to predict the corrosion potential in the system and the longevity of materials present.

The impact of high energy, ionizing radiation on physical systems has been subject to study for a long time. It is well known that the energy absorbed from incident radiation will ionize atoms and molecules, and break bonds to form unstable, highly reactive ions and radicals. The vast majority of these studies have focused on the short-term chemistry associated with absorption of incident energy delivered in short duration pulses. This effectively decouples short term processes from much longer term chemistry and makes the study of individual reactions more amenable. However, such studies do not fully explore the longer term chemistry that arises when a system is placed in a continuous, steady radiation field (or flux of incident energy) and the system is allowed to reach a steady-state chemical equilibrium. Under long-term irradiation conditions, the aggressive water radiolysis products quickly achieve low, but (pseudo) steady-state levels that can dictate the aqueous redox conditions in solution and, hence, the corrosion rate (*3–6*). This chapter discusses the more recent studies of water chemistry arising during steady-state radiolysis and the chemical environments that are created, with a focus on the impact of these environments on corrosion of metal alloys.

A consequence of corrosion is the formation and transport of dissolved or particulate corrosion products. In a circulating water system, temperature changes in the flowing coolant can cause dissolved metal ions and particulates to deposit on metal surfaces. In a nuclear reactor, such deposition can have many undesired consequences. Deposit build up in steam generator tubing leads to reduced heat transfer efficiency. Corrosion products transported into the reactor core, or formed in-situ in the case of zirconium alloys, can be neutron activated and converted to radioactive isotopes (e.g., [54]Mn, [58]Co, ^{59}Fe, ^{60}Co, [95]Zr). Subsequent transport

and deposition of these radioactive isotopes on piping outside of the biological shielding of the reactor core creates a radiological hazard (*7*).

Radiolytic decomposition products of water are chemically reactive. Therefore, their steady-state concentrations in the solution phase can be easily affected by solution parameters such as pH, temperature and the presence of other chemical species, either intentionally or un-intentionally introduced. The introduction of chemical additives to nuclear coolant systems is a standard practice for chemistry control. Chemical additives may effectively push the system toward an optimal redox condition which can enhance the lifetime of reactor components and minimize other corrosion consequences.

Water radiolysis under long-term irradiation is also an important consideration in safety assessments of nuclear reactors and particularly for post-accident management in the unlikely event of a severe accident. Postulated (but extremely unlikely) severe accidents are characterized by the release of radioactive material from the reactor core into the surrounding containment building. The safety analysis of severe accidents includes prediction of gaseous radioiodine concentrations in the reactor containment building over a long period of time following an accident. The concern is the possible radiolytic conversion of normally involatile radioactive iodine to a volatile gaseous radioiodine species that might escape the containment building. Initially, iodine is released from failed fuel elements as an iodide that will dissolve in water ubiquitously present during an accident. Conversion of this iodide to volatile I_2 or volatile organic iodides may be driven by reactions of the iodide in the water with water radiolysis products (*8*, *9*).

Water radiolysis can also play an important role in controlling chemistry and corrosion at other locations in the nuclear fuel cycle. These include corrosion of containers used for spent fuel waste storage, as well as corrosion of materials and equipment used in fuel recycling and waste stream treatment. Understanding and limiting hydrogen production by water radiolysis in these environments is another concern.

The primary water radiolysis yields and the rates of elementary reactions of the primary radiolysis products with each other, with solvent molecules, and with various solute species have been studied extensively (*10–16*). However, how the combination of these elementary reactions influences the aqueous chemistry during long term radiation exposure is not well understood (*17–28*). The interfacial and surface reactions, and the transport processes that dictate materials degradation and corrosion product transport in nuclear reactor environments, in general, have high activation energies and occur over a long time scale. For these slower processes, the steady-state concentrations of the radiolytic decomposition products of water will be most important.

Systematic studies of the chemistry of complex systems as they evolve under long-term irradiation conditions have been very limited. However, some key experimental studies, in combination with computational radiolysis kinetic model simulations, have been performed to develop a quantitative understanding of the effects of corrosion products and pH- and redox-controlling agents on water radiolysis under conditions relevant to nuclear reactor systems.

2. Background

2.1. Short-Term Radiolysis Processes

The ionizing radiation that we are concerned with here is the radiation emitted from nuclear fission and from radioactive fission products or neutron activation products. It includes charged particles (α- and β-particles) and electromagnetic radiation (x- and γ-rays) with each particle or photon having an energy in the range of 50 keV to 10 MeV. These types of radiation, when passing through a fluid, lose energy almost continuously through a large number of small energy transfers to the interacting matter (*10*). The energy transfer is mainly via inelastic collisions between the radiation particles/photons and the electrons in the matter (*10*). For x-rays and γ-rays, the energetic photons transfer energy via photoelectric and Compton scattering, creating high energy electrons which, like β-particles, then subsequently undergo a series of energy transfers via particle-particle collisions with the electrons in the matter. The initial interaction with matter is thus to ionize the molecules or atoms on the particle/photon path. The probability of interacting directly with nuclei is very low, compared to the interaction of fast neutrons with matter. For the fast neutrons, atomic displacement must be considered in evaluating their impact on materials degradation. The chemical impacts of neutron radiation are beyond the scope of this study and are not further discussed here.

Since ionizing radiation interacts with matter initially via collisions with the electrons in the matter, the initial energy transfer rate depends on the density of electrons in the target matter. Since the electron density is nearly proportional to the mass density (except for H), the energy transfer rate per unit mass is nearly the same for all types of matter, independent of the physicochemical nature of the matter. That is, all species in a solution on a per-mass basis have an equal chance of absorbing the radiation energy. In dilute solutions typical of coolant systems, the radiation energy will thus be initially transferred almost entirely to the water and the probability of direct interaction of the radiation with any solute species present (e.g., trace levels of metallic corrosion products) is very small. As a consequence, the chemical impact of radiolysis on solute species occurs via reactions with radiolytic decomposition products of solvent molecules. The interaction of ionizing radiation with matter is thus referred to as a non-selective, solvent-oriented process. This contrasts with the selective and solute-oriented process that occurs in photolysis, where the energy of photons is on the order of a few eVs and can be tuned to the excitation energy of a target solute molecule. One important implication of this difference is that dilute chemical species in reactor coolant (deliberate or otherwise) will influence the coolant chemistry primarily via their reactions with radiolytic decomposition products of the solvent water. Their direct absorption of the radiation energy can be neglected.

In assessing radiation-induced chemical effects in the interacting medium, the rate of radiation-energy transfer per unit length (or the rate of linear energy transfer, LET) is a more useful parameter than energy absorbed per unit mass (since chemical reaction and transport rates depend on concentration, or more precisely activity, and not on mass). The LET depends on the mass of the radiation particle and is higher for α-particles than β-particles or γ-photons. The LET, dependent on

the elastic collision or scattering probability, determines the penetration depth of the radiation, with the penetration depth ranging from $20 - 25$ μm for α-particles and $0.5 - 1.0$ cm for β-particles and fast electrons, to tens of cm for γ-rays in water at room temperature. Due to the small volume in which its energy is deposited, α-radiation is important only in volumes very near the radiation source. Thus, α-radiation-induced aqueous processes may be important for materials in direct contact with a radiation source, e.g., fuel cladding, but not for corrosion of other reactor system materials. For the latter, β- or γ-radiation is of more importance.

The initial consequence of the interaction between a radiation particle (or energetic electron from a γ-photon) and water molecules is to form ion pairs ($H_2O^{\bullet+}$ and e^-_{hot}) and excited species (H_2O^*) along the radiation track where e^-_{hot} represents an energetic electron (*10*, *17*). These hot electrons may themselves have sufficient energy to produce secondary ion pairs ($H_2O^{\bullet+}$ and e^-) and excited species before they are thermalized. Any secondary ionization that they produce will be situated close (within a few nm or a few atom lengths) to the original ionization, in a small cluster, or spur, of excited and ionized species. The number of ion pairs (including excited species) in a spur depends on the LET rate and the effective ionization energy of the matter. For water molecules, typically 2-3 ion pairs or excited species are formed in a spur. This cluster formation of $H_2O^{\bullet+}$, e^- and H_2O^* typically occurs in $< 10^{-14}$ s. Different LET rates lead to different spur densities along the track. For high LET α-radiation spurs overlap, while for low LET β- or γ-radiation the distance between the spurs is large compared to spur length. The effect of the LET rate is less important in gas phase radiolysis because the spur density is much lower.

The ion-pair formation stage is followed by energy relaxation, dissociation ($H_2O^* \rightarrow [\bullet OH + \bullet H]$ or $[\bullet O + H_2]$), ion-molecule reaction ($H_2O^{\bullet+} + H_2O \rightarrow [\bullet OH + H_3O^+]$), or geminate recombination of locally 'trapped' radicals ($[\bullet OH + \bullet H] \rightarrow H_2O$) or ion pairs ($[H_3O^+ + e^-] \rightarrow [H_2O + \bullet H]$) in spurs or solvent cages. The trapped radicals and ions are spatially localized within spurs and interact weakly with the surrounding water molecules at first. The medium then relaxes to accommodate and solvate excess charge. Hydration (or solvation) of ions entails orientation of water molecules about the charged species. This occurs in about 10^{-11} s at 25°C, the relaxation time for dipoles in water. Electron hydration is a special case and electrons appear to become hydrated within about 10^{-12} s. While undergoing geminate recombination and solvation, the radicals and ions also diffuse out from the small volumes of the spurs and away from the influence of the geminate ion pairs. The probability of escaping geminate reactions to become free radicals and free ions depends on the Onsager radius of the solvent medium (*10*, *29*). Net radiation-induced chemical changes are smaller in a low dielectric medium because the Onsager distance is inversely proportional to the dielectric constant of the medium. Thus, in biphasic systems such as those encountered in aqueous corrosion (*3*) or aqueous-organic biphasic separation (*29*, *30*), the change in water chemistry and the interfacial reaction of water radiolysis products will be more important than the change due to the absorption of radiation energy by a metal or organic phase.

As the size of spurs expands and the absorbed energy is distributed within molecular energy states, the relative yields of the radiolysis products per absorbed

unit energy reach a uniform, homogeneous distribution along the track. In liquid water, these statistically averaged (over molecular energy states) and homogeneous yields are achieved on a 100 ns time scale following deposition of the radiation energy. The homogeneous yields are often referred to as the primary radiolysis yields, and expressed using G-values (in units of number of species produced per 100 eV absorbed energy, or μ-mol·J^{-1} in SI units). A schematic representation of the time progression of the size of the spurs and the chemical speciation is shown in Figure 1.

The spur density and the rates of the geminate recombination, solvation and diffusion determine the survival probability rates of free ions and free radicals, and, hence, the initial chemical yields at the onset of homogeneous distribution along the radiation track. These yields are a strong function of the nature of the solvent phase (such as dielectric constant) in addition to the LET rate. For example, the G-values (in brackets) for radiolysis of water at 25°C (*10*) are:

For α-radiolysis of liquid water:

$$H_2O(-2.28) \rightarrow \bullet OH(0.2),\ e_{aq}^-(0.2),\ H\bullet(0.1),\ H_2(1.2),\ H_2O_2(1.13),\ H_3O^+(0.2) \quad (1)$$

For γ-radiolysis of liquid water:

$$H_2O(-4.15) \rightarrow \bullet OH(2.7),\ e_{aq}^-(2.7),\ H\bullet(0.6),\ H_2(0.45),\ H_2O_2(0.7),\ H_3O^+(2.7) \quad (2)$$
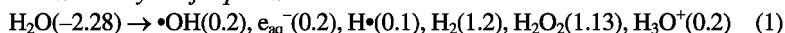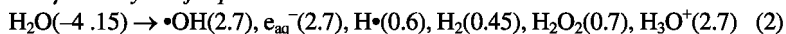
For γ-radiolysis of water vapour:

$$H_2O(-8.28) \rightarrow \bullet OH(8.2),\ e^-(3.0),\ H\bullet(7.2),\ H_2(0.48),\ H_2O_2(0.0),\ H^+(3.0) \quad (3)$$
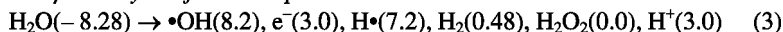
While the species formed at this stage are referred to as primary radiolysis products, they are not actually the first species formed upon the absorption of radiation energy. Note as well that the yields only apply to the irradiated volume which depends on the penetration depth.
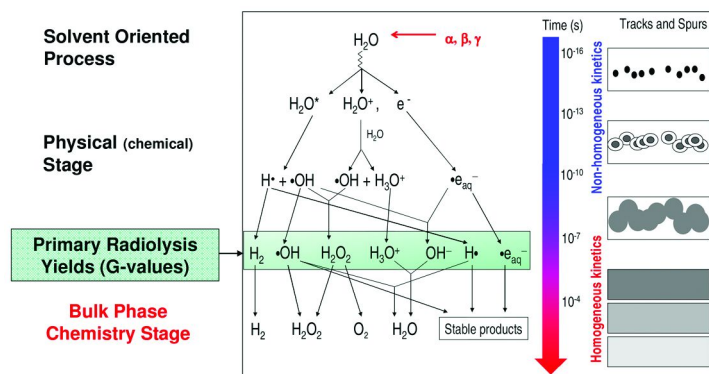
Figure 1. Schematic of chemical speciation and spur distribution at various stages following deposition of radiation energy. Adapted from (17)

2.2. Processes During Long-Term Chemistry Stage

The primary radiolysis products, once generated, undergo further chemical reactions with each other, solvent water molecules and any other chemically reactive species in solution. Hence, the solution chemistry will change with time following the establishment of the homogenous distribution of the primary products:

$$\bullet e_{aq}^- \;+\; H_3O^+ \;\longrightarrow\; \bullet H \;+\; H_2O \tag{4}$$

$$\bullet e_{aq}^- \;+\; H_2O_2 \;\longrightarrow\; OH^- \;+\; \bullet OH \tag{5}$$

$$\bullet OH \;+\; \bullet OH \;\longrightarrow\; \bullet O \;+\; H_2O \tag{6}$$

$$\bullet OH \;+\; H_2O_2 \;\longrightarrow\; \bullet HO_2 \;+\; H_2O \tag{7}$$

$$\bullet OH \;+\; H_2 \;\longrightarrow\; \bullet H \;+\; H_2O \tag{8}$$

$$H_2O_2 \;\longrightarrow\; \bullet OH \;+\; \bullet OH \tag{9}$$
etc.
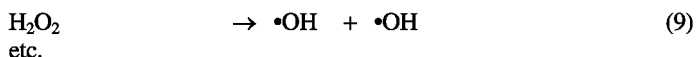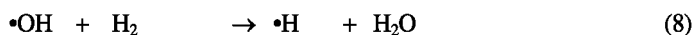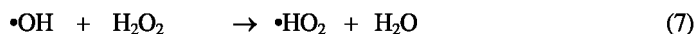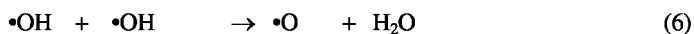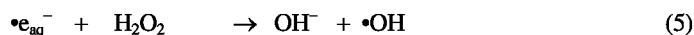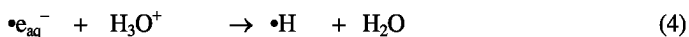
It has been shown that about 50 elementary reactions like those shown above and their rate constants adequately describe the radiolysis of water and its subsequent relaxation, Figure 2. The room temperature database can be found in references (*14*) *and* (*18*). The same set of elementary reactions applies at higher temperatures and the distribution of steady-state species that evolve is determined by the dependence of these reaction rate constants on temperature. The temperature dependence of the rate constants of most of these elementary reactions have been established (*15, 16, 18, 31*).
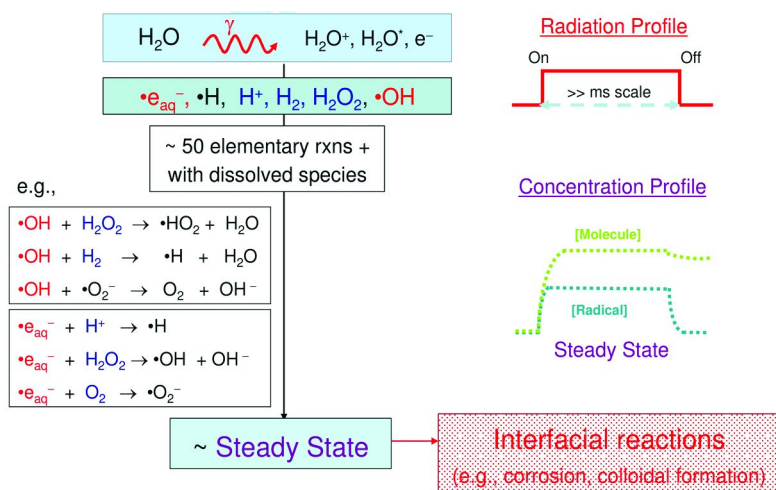
Figure 2. Schematic of homogeneous chemistry stage during long-term irradiation.

This later stage (at times > 100 ns) is often referred to as the chemistry stage and the reactions in this stage can be treated as homogeneous bulk-phase reactions within the irradiated volume (defined by the penetration depth of the radiation). Depending on the system of interest, additional processes may need to be considered, such as mass transport to connected unirradiated volumes and surface or interfacial reactions. The concentrations of individual primary radiolysis product species will evolve with time and these changes can be described using classical chemical reaction rate and mass transport equations (18–23, 25–28). These rate equations can be expressed using macroscopic properties such as concentration, temperature, or thermodynamic state properties and do not require exact knowledge of molecular or microscopic properties of the chemical system. Detailed information on molecular dynamics and the non-homogeneous distribution of radiolysis products within the short-term period prior to the establishment of the primary yield distribution is not necessary. Instead we can use the primary yields as the starting reactant concentrations and follow the radiolysis kinetics. Thus, the production of a primary radiolysis species is determined by its primary yield and the absorption dose rate, and its evolution is determined by its reactions with other species present. For example, the concentration of •OH within the irradiated volume during the chemistry stage is expressed by

$$\frac{d[\bullet OH]}{dt} = \text{production rate - removal rate} \tag{10}$$

The main production path for a primary radiolysis product, particularly the radical species, •e_{aq}^- and •OH can be approximated to:

$$\text{Production rate of} \bullet OH \approx C_R \cdot G_{\bullet OH} \cdot D_R \tag{11}$$

where $G_{\bullet OH}$ is the G-value for •OH production, D_R is the absorbed dose rate (in units of Gy·s^{-1}), and C_R is the unit conversion factor such that the rate of •OH production is in units of mol·dm^{-3}·s^{-1}. The removal or decomposition rate is expressed as:

$$\text{Removal rate of} \bullet OH = \sum_i k_{\bullet OH - i} \cdot [\bullet OH] \cdot [i] \tag{12}$$

where $k_{\bullet OH\text{-}i}$ is the rate constant for the reaction of •OH with chemical species i. If mass transport, such as diffusion, and interfacial/surface reactions become important they can be included in the rate equation (19–21).

The rate of an aqueous reaction varies depending on the reactivity of the partner species, and some solute species, even at impurity levels, can significantly alter the net removal rate of a radiolysis product. Temperature also significantly influences the rate. Although a dissolved species at a low concentration does not affect the primary radiolysis yields, it can have a profound influence on the fate of the radiolysis products in the chemistry stage.

The elementary chemical reactions of the primary radiolysis products with each other and other water-derived species have been studied extensively (10–16). Pulse radiolysis studies have been extremely useful for establishing the initial

homogeneous radiolysis yields and determining rate constants of the fast reactions of free radicals and ions. These studies have established that when irradiation ceases and the generation of the reactive radicals and ions stops, stable molecular products, H_2, O_2, H_2O_2 and H_2O form quickly.

Pulse radiolysis techniques are not as useful in studies of systems where mass transport or interfacial reactions are important. Compared to the aqueous reactions of radicals and ions which are typically diffusion controlled, interfacial mass transport and reactions on a surface or at an interface are much slower and occur on time scales much longer than those typically studied by pulse radiolysis techniques.

2.3. Speciation under Long-Term Irradiation

In a solution exposed to long-term continuous irradiation, the concentrations of the primary products initially increase linearly with time. However, as the concentrations of the primary products increase, the rates of their removal reactions increase. As a result, the concentrations of radiolysis products do not increase indefinitely but reach steady-state levels. Due to the chemically reactive nature of the primary radiolysis species, the irradiated aqueous system reaches steady state (or pseudo-steady state followed by a slower change toward a true steady state) relatively quickly. The pseudo-steady state or steady state then prevails as long as the irradiation remains constant, see Figure 2. Needless to say, the concentrations of radiolysis products at steady state can differ substantially from the concentrations expected when the same amount of dose is applied over a short duration, as in pulse radiolysis experiments.

Accurate description of the radiolysis kinetics during the homogeneous aqueous chemistry phase requires about 50 elementary reactions. Most steady-state radiolysis kinetic models, including ours, consist of a kinetic database of the elementary reactions and their rate constants (including the G-values), and the coupled differential rate equations are solved using numerical integration software (*18–23, 25–28*).

While solutions of computer models provide concentrations as a function of time and that can be used to understand and interpret experimental results, the chemistry can be sometimes be better appreciated by comparing the computer-generated numerical results with predictions of approximate analytical solutions to the chemical reaction kinetics. Analytical solutions to the complex reaction kinetics are impossible to obtain at early times ($< ms$), but solutions can be obtained at longer times using the steady-state approximation. This steady-state kinetic analysis provides more insight into the key reactions and chemistry occurring under long-term irradiation.

Steady state is reached when the loss (or removal) rate equals the production rate for the species. This condition can also be used for a pseudo-steady state, when the concentration of the species changes slowly compared to the speeds of the individual elementary reactions that control the net production and loss of the species. Hereafter, steady state is used to refer to both true- and pseudo-steady state conditions.
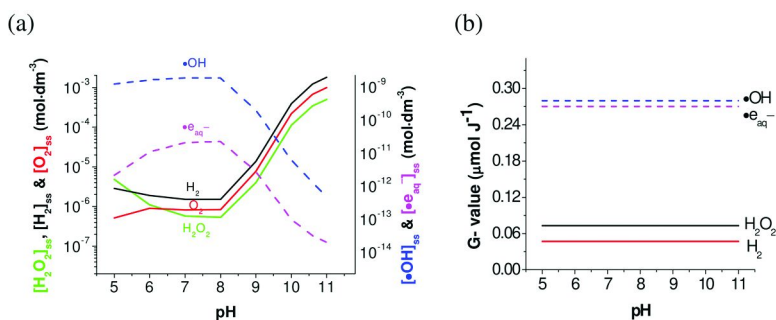
Figure 3. pH Dependence of (a) steady-state concentrations under continuous γ-irradiation (18) and (b) the primary radiolysis yields.

To understand how the concentration of a radiolysis product species might be affected by dissolved additives at impurity levels ($< 10^{-3}$ M) during long-term irradiation we need to understand the main production path(s) and the main loss path(s). For a primary radiolysis product species, the production rate is essentially constant (driven by the continuous radiation dose rate), but the loss rate increases as the species concentration increases. (For the primary species, contribution from secondary processes to its net production is negligible.) For example, the steady-state concentration of •OH under γ-irradiation can be expressed as:

$$[\bullet \text{OH}]_{ss} \approx \frac{C_R \cdot G_{\bullet OH} \cdot D_R}{\sum_i k_{\bullet OH-i} \cdot [i]} \tag{13}$$

since $\dfrac{d[\bullet \text{OH}]}{dt} = 0$ at steady state. $\tag{14}$

The steady-state concentration of a radiolysis product is inversely proportional to its net loss rate. Additives such as pH- or redox-controlling agents can significantly affect the steady-state concentrations of radiolysis products through their impact on the loss rates of different radiolysis products. (Note that the steady-state approximation can be used for systems in which the dose rate and the reaction rates are changing relatively slowly, hence the use of the approximately equal symbol in equation 13).

Evaluating the quantitative effect of pH agents or other chemical additives on steady-state behaviour is not straightforward since many different reaction paths are available for a given radiolysis product, and many of these reactions involve other radiolysis products. For example, •OH reacts with itself and other water decomposition products, H_2, H_2O_2, $\bullet O_2^-$ (reactions 6 to 9 and more), and may react with other dissolved additives, if present.

More importantly, the relative contributions of individual reactions to the net removal rate can vary considerably with the concentrations of species added to influence the pH. As shown in Figure 3, in the absence of any other added species, the steady-state concentrations of H_2, O_2 and H_2O_2 relative to those of $\bullet e_{aq}^-$ and •OH change by three orders of magnitude when the pH is raised from 6 to 10 (*22*). Such pH dependence is not expected based on the pH dependence of the primary

yields, Figure 3b, see further discussion later. Note that in this discussion pH < 3 and pH > 13 are not considered since the primary radiolysis yields are dependent on pH at these levels. At the extreme pHs, the concentrations of H^+ or OH^- are no longer negligible and, hence, affect the early radiolysis processes (*10*).

3. Long-Term γ-Radiolysis Behaviour

We have performed comprehensive studies of long-term γ-radiolysis chemistry as a function of pH, solute species concentration and temperature (*18*, *19*, *21*, *32–34*). The dissolved species studied include volatile molecules (dissolved H_2 (DH) and dissolved O_2 (DO)), transition metal ions (i.e., metal alloy corrosion products) and pH- and redox-controlling agents (nitrate/nitrite/ammonia/ hydrazine). These studies involved both experiments and long-term radiolysis kinetic model simulations.

In typical experiments, a continuous radiation source is provided by a ^{60}Co γ-cell in which vials containing water solutions are irradiated. The concentrations of radiolytically-produced molecular species, H_2, O_2, H_2O_2, and the other chemical species are analyzed as a function of irradiation time using various analytical techniques. The experimental details can be found elsewhere (*18*, *19*, *32–34*).

A suite of water radiolysis reactions, consisting of primary radiolysis product formation processes and ~50 subsequent chemical reactions (*18*) has been used in kinetic model simulations to interpret the experimental data. The models are supplemented with the reactions of any relevant additive species with the water radiolysis products depending on the experiment. These studies provide a mechanistic basis for extrapolation from the experiments to conditions inaccessible experimentally.

The experiments, and particularly those that explore the effect of pH and dissolved species on steady-state radiolysis, have been most extensively conducted at room temperature, and hence the following discussion is focused on that work. The results drawn from the room temperature studies can be extrapolated to predictions of behaviour at higher temperatures using the known temperature dependences included in the reaction kinetic database. However, these extrapolations should be used with caution and need be more fully validated by planned future steady-state radiolysis experiments at elevated temperatures.

3.1. Effect of pH on Steady-State Chemistry

The time required for an irradiated aqueous system to reach a true steady state depends on the system starting conditions. At room temperature, and in the absence of any other dissolved species, the effect of pH on radiolysis chemistry is illustrated by the results shown in Figure 4. In an initially deaerated solution, at pHs less than 8.5, steady state is reached relatively quickly. The steady-state concentrations of many molecular species (including H_2) at these pHs are below detection limits and the lines are only the model simulation results. At higher pHs, the concentrations of molecular radiolysis products, H_2 and H_2O_2 are much greater. They accumulate to the concentration levels reached at the lower pHs very quickly.

These fast increases are followed by a slower increase, taking several hours to reach a true steady-state level. (Note that the changes in pH due to irradiation were small in these experiments: within ± 0.5 when the initial pH was 6.0 ± 0.3, and within ± 0.2 when the initial pH was 10.6 ± 0.2.)

Experiments and analysis have shown that there are three distinctive pH regions: pH < 4.5, 4.5 < pH < 9.7 and pH > 9.7. These are delimited by the pKa values of two key equilibria:

$$HO_2\bullet \; \leftrightarrows \; H^+ + \bullet O_2^- \qquad\qquad pKa = 4.5 \qquad\qquad (15)$$

$$\bullet H \; \leftrightarrows \; H^+ + \bullet e_{aq}^- \qquad\qquad pKa = 9.7 \qquad\qquad (16)$$

As mentioned earlier, the extreme pHs, i.e., pH < 3 and pH > 13 are not considered since at extreme pHs, the primary radiolysis yields will be affected by the concentrations of H^+ or OH^- initially present.

In the pH range between the pKa of $HO_2\bullet$ (4.5) and the pKa of $\bullet H$ (9.7), the steady-state speciation does not depend on pH but, near the pKa of $\bullet H$, the concentrations of molecular products, such as H_2O_2, H_2 and O_2, dramatically increase while the concentrations of radicals such as $\bullet OH$ and $\bullet e_{aq}^-$ decrease by a similar magnitude (see Figure 3a). This pH dependence is attributed to a switch-over in the main removal path for $\bullet e_{aq}^-$. At pH < pKa of $\bullet H$, the main removal path for $\bullet e_{aq}^-$ is the reaction with H^+. At the higher pHs, this reaction becomes too slow and $\bullet e_{aq}^-$ reacts mainly with the secondary radiolysis product O_2, which is formed from the disproportionation reaction of $\bullet O_2^-$ (/$HO_2\bullet$). The concentration of O_2 at early times is low at all pHs. However, at very low H^+ concentrations (high pHs), O_2 at a low concentration level can compete effectively with H^+ for hydrated electrons, reaction 17, while O_2 is regenerated by reaction 18:

$$\bullet e_{aq}^- + O_2 \qquad \rightarrow \bullet O_2^- \qquad\qquad (17)$$

$$\bullet O_2^- + \bullet OH \qquad \rightarrow O_2 + OH^- \qquad\qquad (18)$$
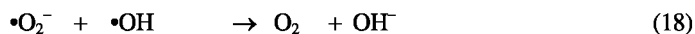
Once the reaction loop is established, O_2 reacts as a catalyst for the removal of the radicals. The net production of the reactive radicals $\bullet e_{aq}^-$ and $\bullet OH$ is suppressed, which in turn reduces the removal rates of molecular species due to reactions with these radicals (reactions 5, 6 and 8). The net effect is to increase the concentrations of H_2 and H_2O_2. At higher pHs, the reaction loop also allows the secondary product O_2 to accumulate to a significant level. The contribution of reactions 17 and 18 to the removal of $\bullet e_{aq}^-$ increases exponentially, resulting in the rapid increase in the concentrations of key molecular species and the decrease in radical species with increasing pH seen in Figure 3a.
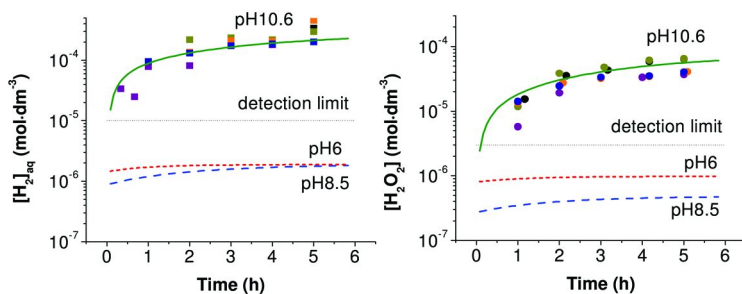
Figure 4. Radiolytic production of H_2 and H_2O_2 as a function of time at various pHs. The water samples were initially deaerated and irradiated at 2.0 $Gy·s^{-1}$. The lines are model calculation results and the symbols are data from several sets of experiments (18).

Figure 3a also shows that regardless of the pH level, there exists an inverse relationship between the concentrations of molecular and radical species. This inverse relationship arises because the main loss paths for radicals are via reactions with molecular species while the loss paths for molecular species are via reactions with radical species. However, it is not a one-to-one relationship, and hence the relationship is not exactly inverse. For example, •OH reacts mainly with H_2 and H_2O_2, and •e_{aq}^- reacts with H_2O_2 and O_2. On the other hand, H_2O_2 reacts with •OH and •e_{aq}^-, O_2 reacts with •e_{aq}^- and •H, and H_2 reacts with •OH. Quantitative relationships between the molecular and radical species concentrations as a function of pH have been established (*18*, *19*).

The inverse relationship between molecules and radicals appears to hold even when other species are present and become involved in the reactions (*32–34*). Because we now understand this relationship, the concentrations of radicals that are impossible to measure practically during radiolysis can be derived from the concentrations of more stable molecular products such as H_2 and O_2 (and H_2O_2 at room temperature) that can be readily measured by post-irradiation analyses.

At pH > 9.7 the overall reactivity of the molecular species present is greater than that of radical species. Thus, in the absence of any other reactive species, the key agents at high pHs controlling the redox potential of irradiated water are the molecular water radiolysis products (*3*). At lower pHs (< 8) the radical radiolysis products may be still important. An observation here is that this pH dependence would not have been predicted from short-term pulse radiolysis studies since the yields of primary radiolysis products and their short-term reaction behaviour are insensitive to pH over a wide range of pH (Figure 3b).

3.2. Effect of Dose Rate on Steady-State Concentrations

The inverse relationship between the radical and molecular concentrations is also responsible for an approximately **square-root dependence** of the steady-state concentration on dose rate predicted by computer modeling, Figure 5 (*18*). This model has been tested against experiments performed over a range of dose rates as well as other parameters (*9*, *18*, *19*, *21*, *23*, *25*).
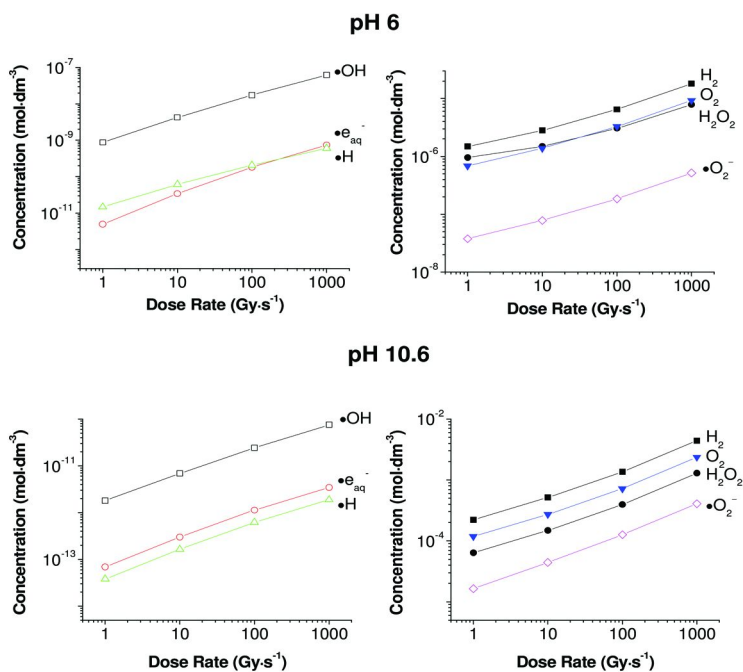
Figure 5. Dose rate dependence of the steady-state concentrations of γ-radiolysis products. The slopes are ~0.5 for most products, corresponding to a square-root dependence on dose rate (18).

Recalling that the parameter used to characterize radiation-induced effects is normally the total absorbed energy, for high LET radiation such as α-particles, the total absorbed energy may be an appropriate parameter. However, the results presented in Figure 5 show that the parameter needed to describe the effect of continuous γ-irradiation is not the total absorbed energy, but rather the dose rate. This applies to both β-particles or fast electrons, which yield nearly the same primary yields, and γ-irradiation since the main difference between these forms of radiation is the penetration depth. This is dealt with by appropriate measure of the dose rate in the irradiated volume.

For high LET radiation, the pH dependence seen for low LET γ-irradiation should not be present because the primary yields for radicals from high LET radiation are much smaller than the yields of molecular products, reaction 2. As a consequence, the concentrations of molecular species are significantly larger than those of radical species, even at low pHs, and the impact of reactions 17 and 18 is diminished. The smaller radical yields also lead to the accumulation of molecular species over long times and the thermal reactions of these species can dominate the evolution of the system chemistry. For example, thermal decomposition of H_2O_2, not its reaction with radicals, is the main loss path for H_2O_2 during long-term α-radiolysis. For high LET radiation, steady-state conditions will be reached much more slowly than for equivalent doses of low LET radiation.

Furthermore, the concentrations of the molecular species increase nearly linearly over time and are directly proportional to the total absorbed dose (*21*).

3.3. Effect of Dissolved Species

Dissolved species will react primarily with radical species (due to their high reactivity), indirectly influencing the molecular product concentrations. Dissolved species of interest during long-term irradiation are those that can react with water radiolysis products in a catalytic manner. These species include dissolved gases (oxygen and hydrogen), corrosion product ions and pH- or redox-controlling agents.

3.3.1. Dissolved O_2

Dissolved O_2 (in aerated water) reacts primarily with $\bullet e_{aq}^-$ (reaction 17) and the product of this reaction, $\bullet O_2^-$, reacts with $\bullet OH$ (reaction 18). The reduction in $[\bullet e_{aq}^-]$ and $[\bullet OH]$ increases the concentrations of H_2 and H_2O_2. At pH 6, the production of H_2 and H_2O_2 from γ-radiolysis of deaerated water is very low (below detection limits for conventional analytic techniques), but their production in aerated water is much greater, Figure 6 (*32*). An increase in the levels of these two species is less significant at pH > 9.7 since O_2 is already radiolytically produced in a relatively high concentration. The inverse relationship between the concentrations of molecular and radical species that is seen for deaerated water still holds with additional dissolved oxygen, Figures 6 **and** 7. At sufficiently high dissolved oxygen concentrations, the pH dependence of the steady-state concentrations of radiolysis products disappears and their concentrations are primarily determined by the oxygen level, Figure 7 (*32*).

The net effect of adding oxygen to water is conversion of the $\bullet e_{aq}^-$ radical to the less reducing species, $\bullet O_2^-$, $\bullet H$ and H_2, and conversion of $\bullet OH$ to the less oxidizing molecular species, H_2O_2 (*24*). However, since the less oxidizing and reducing species are more stable in the aqueous phase, they can accumulate to higher concentrations, and can be more effective in driving corrosion reactions with metals in contact with the irradiated solution.
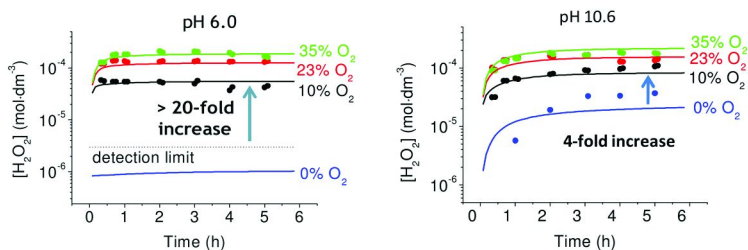
Figure 6. Effect of dissolved oxygen on the radiolytic production of H_2O_2 at pHs 6 and 10.6, at 2.0 Gy·s^{-1}. The lines are the calculation results and the symbols experimental data (32).
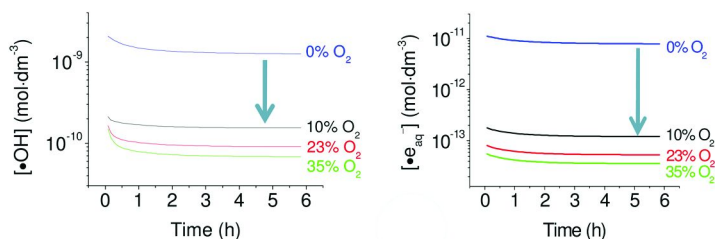
Figure 7. Calculated effect of dissolved oxygen on radical production at pH 6 and at 2.0 Gy·s⁻¹ (32).

3.3.2. Dissolved H₂

Dissolved H_2 reacts primarily with •OH (reaction 8) converting the oxidizing radical •OH to the reducing radical •H. The •H radical can react, as effectively as •e_{aq}^-, with O_2 to form •O_2^-, reaction 19. However, unlike •e_{aq}^-, •H also reacts with •O_2^- to form H_2O_2, reaction 20, and, thus, does not regenerate O_2. This secondary production of H_2O_2 is not significant compared to the primary radiolysis path for production of H_2O_2, reaction 2.

$$\bullet H \;+\; O_2 \;\;\rightarrow\; \{HO_2\bullet \;\leftrightarrows\; H^+ + \bullet O_2^-\} \tag{19}$$

$$\bullet H \;+\; \bullet O_2^- \;\;\rightarrow\; \{HO_2^- + H^+ \;\leftrightarrows\; H_2O_2\} \tag{20}$$
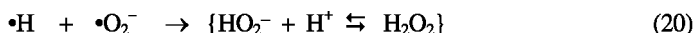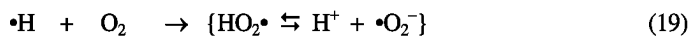
The increase in [•H] also increases [•e_{aq}^-] due to a shift in equilibrium 16. This increase in [•e_{aq}^-] decreases [H_2O_2] due to an increase in the rate of reaction 5, although the loss rate of H_2O_2 by reaction with •OH (reaction 7) is lower. Reaction 5 produces •OH which can then be consumed by H_2 and regenerate •H (reaction 8). The net effect of additional dissolved H_2 is thus to convert highly oxidizing •OH to reducing radicals •H and •e_{aq}^- which then suppresses the production of oxidizing O_2 and H_2O_2.

The ability of H_2 to suppress the production of the oxidizing species H_2O_2 and O_2 is of particular interest for reactor coolant water chemistry control and, hence, deliberate H_2 addition is practiced in some reactors. The minimum H_2 concentration required to suppress radiolytic production of O_2 is referred to as the Critical Hydrogen Concentration (CHC). The CHC has been determined empirically because in-reactor measurement is not easy. More importantly, there has been no systematic way of extrapolating the CHC value obtained for one set of coolant chemistry parameters to other conditions. Our improved understanding of the mechanisms whereby H_2 addition influences the production of O_2 provides a basis for determining the CHC as a function of system conditions.

The necessary condition for oxidizing species suppression is that •O_2^- reacts exclusively with •H (reaction 20) and not with •OH (reaction 18) since reaction 18 regenerates O_2. For this to happen we require,

$$k_{\bullet O_2^- \rightarrow \bullet H} \cdot [\bullet H] \gg k_{\bullet O_2^- \rightarrow \bullet OH} \cdot [\bullet OH] \tag{21}$$

where $k_{\bullet O_2^- \to \bullet H}$ and $k_{\bullet O_2^- \to \bullet OH}$ are the rate constants for the reactions of $\bullet O_2^-$ with $\bullet H$ and $\bullet OH$, respectively. Extensive model analysis of experimental studies shows that with this requirement, and considering the key decomposition reactions for the radiolysis products under high $[H_2]$ conditions, the CHC at pH 10.6 should have an approximate square-root dependence on dose rate (*32*):

$$CHC \propto \sqrt{D_R} \tag{22}$$

This is attributed to the competition between H_2 and O_2 in controlling the radiolysis behaviour. Since the (pseudo) steady-state concentration of O_2 has an approximate square root dependence, Figure 5, the necessary H_2 concentration to suppress the O_2 reactions needs to increase accordingly.

The studies also established the dependence of $[O_2]$ and $[H_2O_2]$ as a function of dissolved $[H_2]$. A unique value for CHC cannot be specified as it depends on the concentrations of O_2 and H_2O_2 to be suppressed (*32*). Nevertheless, equation 22 provides a mechanistic basis for extrapolating the observations from laboratory studies performed at low dose rates to the in-reactor chemistry present at much high dose rates.

3.3.3. Dissolved Metal Ions

Transitions metals such as Fe, Cr, Co, Ni and Mn are found in carbon steel and steel alloys. As these materials corrode, they release metal ions into the aqueous phase. Since transition metal atoms can exist in different oxidation states in the aqueous phase, they can catalytically interact with oxidizing and reducing water radiolysis products. For example, dissolved Fe^{2+} quickly reaches pseudo equilibrium with Fe^{3+} through oxidation with $\bullet OH$ and back reduction by $\bullet e_{aq}^-$ or $\bullet O_2^-$:

$$Fe^{2+} + \bullet OH \rightarrow Fe^{3+} + OH^- \tag{23}$$

$$Fe^{3+} + \bullet e_{aq}^- \rightarrow Fe^{2+} \tag{24}$$

$$Fe^{3+} + \bullet O_2^- \rightarrow Fe^{2+} + O_2 \tag{25}$$
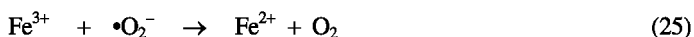
The metal ions also react with molecular species such as H_2O_2 and O_2, but those reaction rates are much slower. The rate constants for the reactions of ferric and ferrous irons with water radiolysis products at room temperature are well established (*35, 36*). Other transition metals undergo similar reactions but at different rates.

The catalytic cycling of metal ion redox couples can scavenge radical species leading to increased evolution of H_2 and H_2O_2 in irradiated iron-containing solutions. Due to the catalytic nature of the transition metal reactions, the impact of transition metal ions, even at small concentrations, can be significant, with the impact being more pronounced at lower pHs due to the higher radical concentrations at pHs < 9.7. However, the conversion between two oxidation

states of a transition metal ion can add another complication to the already complex system, due to the potentially different solubility of metal ion species at two different oxidation states – see further discussion below.

The production of H_2O_2 and H_2 as a function of the initial Fe^{2+} concentration has been measured at pHs in a range of 5 and 6 (*33*), and the results at pH 5.5 are shown in Figure 8. At all Fe^{2+} concentrations the $[H_2O_2]$ was below the detection limit; thus no experimental values are reported. Also shown in the figure are the model predictions, where the model consists of all the water radiolysis reactions and the reactions of ferrous and ferric ions with water radiolysis products (*33*).

The kinetic model simulations predict that the molecular radiolysis product concentrations, $[H_2]$ and $[H_2O_2]$, created in the solution during irradiation should rise from below the detection limit in pure water to experimentally detectable levels with the addition of initially dissolved Fe^{2+}. The concentrations are also predicted to increase as the initial dissolved $[Fe^{2+}]$ increases. However, the observed experimental results do not follow these trend. Instead, the measured $[H_2O_2]$ never exceeds the detection limit and the measured $[H_2]$ level is nearly independent of the initial dissolved iron concentration. The experimental data also suggest that Fe^{2+} reduces $[•OH]$ more effectively than $[•e_{aq}^-]$ since the addition of the iron affected the concentration of $H_2(aq)$ more than that of H_2O_2. This result would not be expected for a simple catalytic cycle involving oxidation of Fe^{2+} by $•OH$ and subsequent reduction of Fe^{3+} by $•e_{aq}^-$ and $•O_2^-$.

The discrepancy between the model predictions and the experimental observations is attributed to the formation of insoluble iron species that alter the balance in the concentrations of Fe^{2+} and Fe^{3+} and their relevant reaction rates. The solubility of transition metal ions in water depends on hydrolysis equilibria. For example, for Fe^{2+} these are:

$$Fe^{2+} \quad + \quad H_2O \quad \leftrightarrows \quad Fe(OH)^+ \quad + \quad H^+ \tag{26a}$$

$$Fe(OH)^+ \quad + \quad H_2O \quad \leftrightarrows \quad Fe(OH)_2 \quad + \quad H^+ \tag{26b}$$

$$Fe(OH)_2 \quad + \quad H_2O \quad \leftrightarrows \quad Fe(OH)_3^- \quad + \quad H^+ \tag{26c}$$
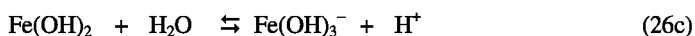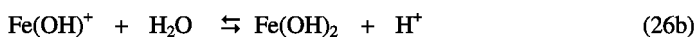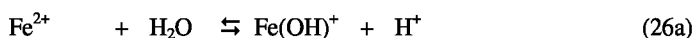
The solubilities of neutral $Fe(OH)_2$ and $Fe(OH)_3$ are a strong function of pH and the oxidation state of the metal, Figure 9a. The solubility of $Fe(OH)_3$ is can be several orders of magnitude lower than that of $Fe(OH)_2$ at pH < 12. Also shown in the figure are the concentrations of Fe^{2+} and Fe^{3+} species that were chemically determined for the tests discussed above (*33*), Figure 9b.

Thus, during irradiation, initially present soluble Fe^{2+} is converted to Fe^{3+} with the ratio of Fe^{3+}/Fe^{2+} quickly reaching steady state, Figure 9b. While this results in Fe^{3+} concentrations that are much higher than the nominal solubility limits for the Fe^{3+} species (under the studied conditions) no bulk precipitation of Fe^{3+} was observed. Instead, observed solution colour and clarity changes indicate that a suspended particulate or colloid was formed. The loss of the Fe^{3+} species from solution explains the behaviour of [H2] shown in Figure 8b. UV-absorption and fluorescence and Fourier Transform Infrared (FTIR) Spectroscopy studies confirmed the formation of colloidal Fe^{3+} oxy-hydroxide

species (*33*). Transmission electron microscope (TEM) images and particle size measurements found the particles were tens of nm in size with a very narrow size distribution, and sometimes aggregated to form particulates of ~100 nm. It is evident that steady-state irradiation promotes the formation of nano-scale colloids. Based on the concentrations of H_2, H_2O_2, Fe^{2+} and Fe^{3+} and the size of colloid observed as a function of irradiation time, a mechanism for the radiation-induced iron-oxide colloid formation has been proposed (*33*).
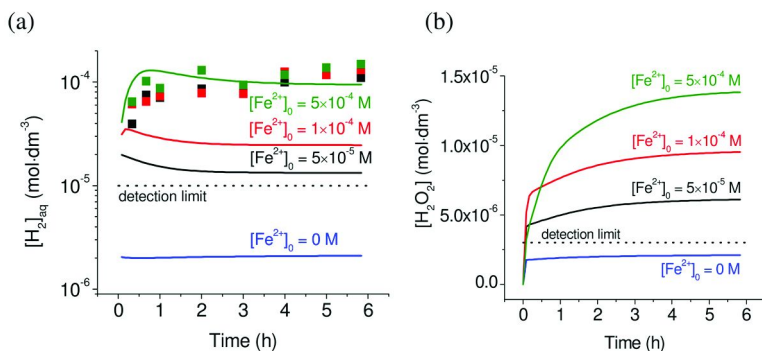
Figure 8. The concentrations of (a) H_2(aq); and (b) H_2O_2 evolved as a function of irradiation time for de-aerated $[Fe^{2+}]_0$ solutions of 0, 5×10^{-5}, 1×10^{-4}, and 5×10^{-4} M (0, 3, 6, 28 ppm) at pH 5.5 and a dose rate of 2.0 Gy·s⁻¹. Experimental results are shown as data points (H_2O_2 values were below the detection limit) and model simulation results are shown as solid lines (25).
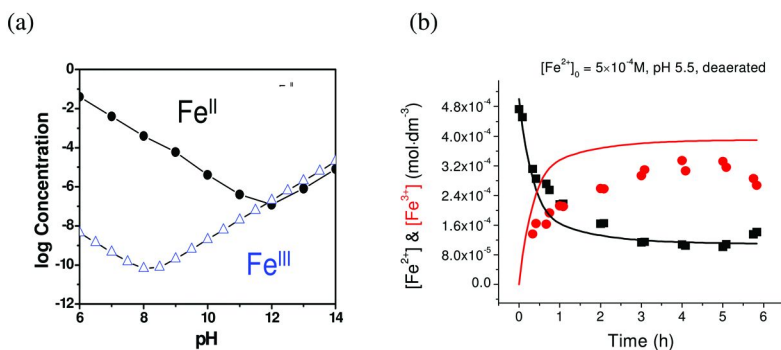
Figure 9. (a) Solubility of $Fe(OH)_2$ and $Fe(OH)_3$ as a function of pH at 25°C; and (b) experimentally observed (symbols) and calculated (lines) conversion of Fe^{2+} to Fe^{3+} as a function of irradiation time at pH 5.5 and 2.0 Gy·s⁻¹. The initial concentration $[Fe^{2+}]_0$ was 5×10^{-4} M, and $[Fe^{2+}]$ and $[Fe^{3+}]$ were chemically determined (33).

The dissolution and precipitation of inorganic ions are central phenomena in the corrosion of metals in water. Colloidal particles are particularly important as an intermediate physical state for suspension of inorganic elements in solution. Competition between precipitation on bulk surfaces and precipitation to form colloidal particles can affect local electrochemical conditions and the build-up of oxides on surfaces (and their thickness and porosity). The formation of colloids can impede the salting out of less soluble species on surfaces and transport the metallic species further out from the reactor core than expected in the absence of colloidal formation may be an important parameter to consider in assessing crud and activity transport in nuclear reactors.

Recent studies show that water radiolysis can alter the solubility and transport of metal species in very complex ways, beyond the participation of the metal ions in reactions with radiolysis products. The new results on the formation of stable colloidal particles have important implications for predictions of the transport and deposition or precipitation of corrosion products on structural surfaces.

3.3.4. Dissolved Nitrogen Species

Radiolytic decomposition of dissolved nitrogen species are of particular interest since such chemicals are routinely used in various chemical control, purification and processing applications. Dissolved nitrogen species can also inadvertently arise in trace levels as a result of unplanned air ingress to a system. It is well known that NO_3^- and NO_2^- consume the reducing species $\bullet e_{aq}^-$ and $\bullet O_2^-$ to form compounds that are successively lower in oxygen content and more reduced than their precursors (34, 37–41). More reduced species (NH_3 and N_2H_4) can consume $\bullet OH$ and be oxidized to form nitrate and nitrite (38–41). This can lead to a semi-catalytic interaction between the water radiolysis products (42). Only the water radiolysis behaviour in solutions initially containing nitrate or nitrite are discussed here.

Dissolved nitrogen species can provide several additional reaction pathways for radical radiolysis products (34, 37–40). For example, for solutions initially containing nitrate or nitrite, the key additional reactions include:

$$\bullet e_{aq}^- + NO_3^- \rightarrow [\bullet NO_3^{2-} + H_2O] \rightarrow \bullet NO + 2\,OH^- \qquad (27)$$

$$\bullet e_{aq}^- + NO_2^- \rightarrow [\bullet NO_2^{2-} + H_2O] \rightarrow \bullet NO_2 + 2\,OH^- \qquad (28)$$

$$\bullet OH + NO_2^- \rightarrow \bullet NO_2 + OH^- \qquad (29)$$

$$\bullet O_2^- + NO_3^- \rightarrow [\bullet NO_3^{2-} + H_2O] \rightarrow \bullet NO_2 + 2\,OH^- + O_2 \qquad (30)$$

$$2\,\bullet NO_2 + H_2O \rightarrow NO_3^- + NO_2^- + 2\,H^+ \qquad (31)$$
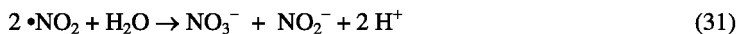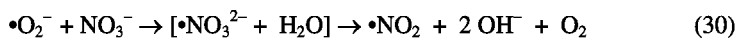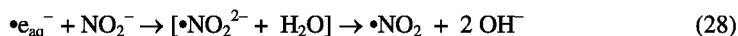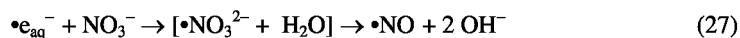
These nitrate and nitrite reactions can compete with the reactions of molecular water radiolysis products, reactions 7, 8 and 18, for $\bullet OH$ and reactions 4,5 and 17 for $\bullet e_{aq}^-$, and, at sufficient concentrations, can become the dominant removal paths

for the radicals. This will lower the net concentrations of $\bullet e_{aq}^-$ and $\bullet OH$, thereby reducing the decomposition of H_2 by reaction 8 and H_2O_2 by reactions 4 and 7.

As expected under all conditions studied, the addition of NO_3^- or NO_2^- was observed to increase the radiolytic production of H_2 and H_2O_2. Only the data obtained under pH 6 and deaerated conditions are shown in Figure 10. Those obtained under other conditions can be found elsewhere (*34*). The addition of nitrate ions increased the H_2O_2 production slightly more than the addition of nitrite ions, while adding nitrite increased the H_2 production more than nitrate, see Figure 10a versus 10**b**. These differences can be partially attributed to the different rate constants of the reactions of NO_3^- and NO_2^- with the radicals, reactions 27 to 30. However, the differences in $[H_2]$ and $[H_2O_2]$ are smaller than those expected based on the differences in the relevant elementary reaction rate constants. The reaction of NO_3^- with $\bullet e_{aq}^-$ has a larger rate constant than the reaction of NO_2^- with $\bullet e_{aq}^-$ and a larger increase in $[H_2O_2]$ would be expected for radiolysis of nitrate solutions than nitrite solutions. Similarly, nitrite solutions would be expected to yield a higher $[H_2]$ than nitrate solutions since NO_2^- is a good scavenger for $\bullet OH$ whereas no reaction of $\bullet OH$ with NO_3^- has been observed (*37*). Despite this the $[H_2]$ increases in the solution initially containing 10^{-3} M NO_3^-.
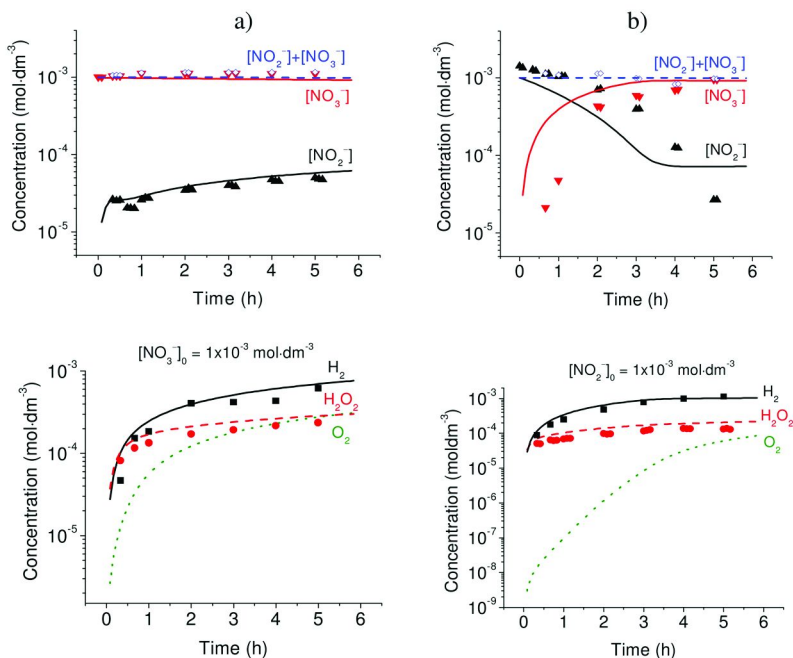
Figure 10. The time-dependent speciation of NO_3^- ($\blacktriangledown$, —) and NO_2^- ($\blacktriangle$, —), the overall mass balance of nitrogen species ($\diamondsuit$,---), and the time-dependent concentrations of $H_2(aq)$ ($\blacksquare$, —), H_2O_2 ($\bullet$,---) and O_2 (····) at pH 6.0 de-aerated condition are shown for aqueous solutions containing (a) 1×10^{-3} M $[NO_3^-]_0$; and (b) 1×10^{-3} M $[NO_2^-]_0$. Data points represent the experimental data and the lines are the model simulation results.

The small difference in the effects of nitrate and nitrite on the net radiolytic production of H_2 and H_2O_2 can be explained by the radiolytically induced conversion between nitrate and nitrite. Nitrate and nitrite ions undergo a series of redox reactions with reducing (e.g., $\bullet e_{aq}^-$, $\bullet O_2^-$) and oxidizing (e.g., $\bullet OH$, $HO_2\bullet$) species, reactions 27 to 30. Under continuous irradiation, this will result in interconversion between nitrate and nitrite until the system reaches a steady state, thereby establishing a reaction loop for ongoing reactions with radical species. The observed nitrogen speciation at this pseudo-steady state, after which the relative changes in concentrations are small, is nearly independent of whether the initial nitrogen species is NO_3^- or NO_2^- confirming this situation. This explains the small dependence in the net radiolytic production of H_2 and H_2O_2 on the initial nitrogen species.

The relative increases in $[H_2]$ and $[H_2O_2]$ with addition of nitrate or nitrite compared to pure water are larger at pH 6.0/de-aerated than at pH 10.6 (either aerated or de-aerated) (*34*). However, their steady-state concentrations at long times become nearly independent of pH or the presence of initial dissolved oxygen (i.e., aerated or de-aerated). This is consistent with reactions of NO_3^- and NO_2^- as the main removal paths for $\bullet e_{aq}^-$ and $\bullet O_2^-$ (or $HO_2\bullet$ at pH < 4.5). The dissolved oxygen concentration in fully aerated solutions at 1 atm and 25°C is $\sim 2.5 \times 10^{-4}$ M and the rate constant of the reaction of O_2 with $\bullet e_{aq}^-$ is 2.2×10^{10} M$^{-1}\cdot$s^{-1}. Thus, the rate for the reaction of $\bullet e_{aq}^-$ with 10^{-3} M nitrate in solution will be twice that for removal by oxygen while the initial rate for reaction of $\bullet e_{aq}^-$ with 10^{-3} M nitrite in solution is about the same as that for reaction of $\bullet e_{aq}^-$ with oxygen. However, nitrite can also react with $\bullet OH$ very effectively. Due to catalytic reactions of the nitrogen compounds or dissolved oxygen with the radicals, small differences in the rates can determine the balance of the reactions and control the overall radiolysis chemistry. The presence of nitrate or nitrite at levels near 10^{-3} M can compete effectively with reactions between O_2 and the radical primary radiolysis products. At sufficiently large concentrations of nitrate and nitrite the steady-state concentrations of generated during long-term continuous water radiolysis are primarily determined by the reactions with nitrate or nitrite.

Approximate analytical solutions for the (pseudo-) steady-state concentrations using the steady-state approximation have been developed and compared with the computer predictions. These kinetic analyses have provided an approximate solution for the steady-state ratios of NO_2^- and NO_3^- (*34*):

$$\frac{\left[NO_2^-\right]_{ss}}{\left[NO_3^-\right]_{ss}} \approx \frac{k_{27}\left[\bullet e_{aq}^-\right] + k_{30}\left[\bullet O_2^-\right]}{k_{29}\left[\bullet OH\right]} \tag{32}$$

The ratio of NO_2^- to NO_3^- at steady state is a function of the concentrations of three radical species, $\bullet e_{aq}^-$, $\bullet O_2^-$, and $\bullet OH$, and the pH dependence of the ratio mainly arises from the dependence of the radical concentrations on pH.

The results of experiments have been used to develop a simplified kinetics model that covers the inter-conversion of the most oxidized nitrogen species (NO_3^-) to the most reduced species (NH_4^+) under long-term irradiation. This model can be used to provide guidance for redox control (through addition of H_2)

in a nuclear plant and to set action limits (in response to measured NO_2^-/NO_3^- levels).

4. Conclusions

Aqueous chemistry driven by continuous low LET irradiation is very different from the short-term chemistry conditions created by pulse radiolysis. The fundamental parameter controlling the aqueous chemistry under continuous irradiation is not the total absorbed energy, but rather the dose rate. The main production paths for primary radiolysis products are proportional to the energy deposition (or radiation dose) rate. However, because the main removal paths are reactions with other primary radiolysis products, the steady-state concentrations have a square root dependence on the dose rate.

We now have a good understanding of the chemical kinetics arising during continuous irradiation of dilute water systems and can use this knowledge to predict the ways in which the redox chemistry will evolve and respond to the presence of chemicals added to a system. We know how key solution parameters, notably the pH and dissolved reactive impurities, can impact steady-state concentrations of molecular species important to redox chemistry. Using this knowledge, the concentrations of these species can be controlled by additives that will react with primary radiolysis radicals. Preliminary experiments on the behaviour of systems with dissolved transition metal ions have shown that their impact on water chemistry during radiolysis is unfortunately complex. In addition to participating in reactions with the water radiolysis products that control redox chemistry, the metal species can aggregate and precipitate — processes important to consider in corrosion chemistry. We have the tools for understanding the basis of steady-state water chemistry during continuous radiolysis, but we still have an interesting path to follow as we learn how to use these tools effectively to fully understand and predict corrosion behaviour.

References

1. Shoesmith, D. W. Kinetics of Aqueous Corrosion. In *ASM Handbook on Corrosion*; American Society for Metals: Metals Park, OH, 2003.
2. Xu, W.; Daub, K.; Zhang, X.; Noël, J. J.; Shoesmith, D. W.; Wren, J. C. *Electrochim. Acta* **2009**, *54* (24), 5727–5738.
3. Daub, K.; Zhang, X.; Noël, J. J.; Wren, J. C. *Electrochim. Acta* **2009**, *55*, 2767–2776.
4. Fujita, N.; Matsuura, C.; Saigo, K. *Radiat. Phys. Chem.* **2000**, *58*, 139–147.
5. Yamamoto, T.; Tsukui, S.; Okamoto, S.; Nagai, T.; Takeuchi, M.; Takeda, S.; Tanaka, Y. *J. Nucl. Mater.* **1996**, *228*, 162–167.
6. Ishigure, K.; Fujita, N.; Tamura, T.; Oshima, K. *Nucl. Technol.* **1980**, *50*, 169–177.
7. Woods, R. J.; Pikaev, A. K. In *Applied Radiation Chemistry: Radiation Processing*; John Wiley & Sons, Inc.: New York, 1994.
8. McFarlane, J.; Wren, J. C.; Lemire, R. J. *Nucl. Technol.* **2002**, *138*, 162–178.
9. Wren, J. C.; Ball, J. M.; Glowa, G. A. *Nucl. Technol.* **2000**, *129*, 297–325.
10. Spinks, J. W. T.; Woods, R. J. In *An Introduction to Radiation Chemistry*; Wiley: New York, 1990.
11. Allen, A. O. In *The Radiation Chemistry of Water and Aqueous Solutions*; Van Nostrand: Princeton, NJ, 1961.
12. Draganic, I. G.; Draganic, Z. D. In *The Radiation Chemistry of Water*; Academic Press: New York, 1971.
13. Farhataziz; Rodgers, M. A. J. In *Radiation Chemistry: Principles and Applications*; VCH Publishers: New York, 1987.
14. Buxton, G. V.; Greenstock, C. L.; Helman, W. P.; Ross, A. B. *J. Phys. Chem. Ref. Data* **1988**, *17*, 513–883.
15. Elliot, A. J.; Buxton, G. V. *J. Chem. Soc., Faraday Trans.* **1992**, *88* (17), 2465–2470.
16. Elliot, A. J.; Bartels, D. M. *The Reaction Set, Rate Constants and G-Values for the Simulation of the Radiolysis of Light Water over the Range 20° to 350 °C Based on Information Available in 2008*; 153-127160-450-001; Nuclear Platform Research and Development, Atomic Energy of Canada, Ltd.: Mississauga, Ontario, Canada, 2009.
17. Buxton, G. V. In *Radiation Chemistry*; Spotheim-Maurizot, M., Mostafavi, M., Douki, T., Belloni, J., Eds.; EDP Sciences: Les Ulis, France, 2008; pp 3−16.
18. Joseph, J. M.; Choi, B.-S.; Yakabuskie, P.; Wren, J. C. *Radiat. Phys. Chem.* **2008**, *77* (9), 1009–1020.
19. Yakabuskie, P. A.; Joseph, J. M.; Wren, J. C. *Radiat. Phys. Chem.* **2010**, *79*, 777–785.
20. Nielson, F.; Jonsson, M *J. Nucl. Mater.* **2006**, *359* (1−2), 1–7.
21. Wren, J. C.; Shoesmith, D. W.; Sunder, S. *J. Electrochem. Soc.* **2005**, *152*, B470–B481.
22. McCracken, D. R.; Zhang, J. *Simulations of Coolant Radiolysis in NRU Experiments*; COG-95-580/RC-1543; Atomic Energy of Canada, Ltd.: Mississauga, Ontario, Canada, 1997.

23. Stuart, C. R.; Ball, J. M.; Glowa, G. A. *Sensitivity Analysis of the Pure Water Radiolysis Dataset for Predicting ACR HTS Core Outlet Chemistry*; 108-127160-440-004; Atomic Energy of Canada, Ltd.: Mississauga, Ontario, Canada, 2003.
24. Stefanic, I.; LaVerne, J. A. *J. Phys. Chem. A.* **2002**, *106*, 447.
25. Wren, J. C.; Ball, J. M. *Radiat. Phys. Chem.* **2001**, *60*, 577–596.
26. Buxton, G. V.; Lynch, D. A. *Phys. Chem. Chem. Phys.* **1999**, *1*, 3293.
27. Buxton, G. V.; Sellers, R. M. *J. Chem. Soc., Faraday Trans.* **1985**, *81*, 449.
28. Boyd, A. W.; Carver, M. B.; Dixon, R. S. *Radiat. Phys. Chem.* **1980**, *15*, 177.
29. Wishart, J. F. In *Ionic Liquids as Green Solvents*; Rogers, R. D., Seddon, K. R., Eds.; ACS Symposium Series 856; American Chemical Society: Washington, DC, 2003; pp 381−396.
30. Joseph, J. M.; Howett, S.; Yakabuskie, P. A.; Wren, J. C. The University of Western Ontario: London, Ontario, Canada, 2010, to be submitted for publication.
31. Marin, T. W.; Takahashi, K.; Jonah, C. D.; Chemerisov, S. D.; Bartels, D. M. *J. Phys. Chem. A.* **2007**, *111*, 11540–11551.
32. Yakabuskie, P. A; Joseph, J. M.; Wren, J. C. The University of Western Ontario: London, Ontario, Canada, 2010, to be submitted for publication.
33. Joseph, J. M.; Yakabuskie, P. A.; Noël, J. J.; Wren, J. C. The University of Western Ontario: London, Ontario, Canada, 2010, to be submitted for publication.
34. Yakabuskie, P. A; Joseph, J. M.; Stuart, C.; Wren, J. C. The University of Western Ontario: London, Ontario, Canada, 2010, to be submitted for publication.
35. Lundstrom, T.; Christensen, H.; Sehested, K. *Radiat. Phys. Chem.* **2004**, *69*, 211.
36. Rush, J. D.; Bielski, H. J. *J. Phys. Chem.* **1985**, *89*, 5062.
37. Mezyk, S. P.; Bartels, D. M. *J. Phys. Chem. A.* **1997**, *101*, 6233.
38. Buxton, G. V.; Stuart, C. R. *J. Chem. Soc., Faraday Trans.* **1996**, *92*, 1519.
39. Buxton, G. V.; Stuart, C. R. *J. Chem. Soc., Faraday Trans.* **1997**, *93*, 1535.
40. Buxton, G. V.; Lynch, D. A.; Stuart, C. R. In *Water Chemistry of Nuclear Reactor Systems 7*; British Nuclear Energy Society: London, 1996; pp 150−152.
41. Buxton, G. V.; Lynch, D. A. *J. Chem. Soc., Faraday Trans.* **1998**, *94*, 3271.
42. It is termed semi-catalytic since the conversion from nitrate to nitrite or back requires many intermediate steps and, under irradiation conditions, the forward and reverse conversions are not via the same routes. The net redox conversion of nitrate and nitrite is also relatively slow. At much longer time scales than we used in our studies, the further conversion of nitrite to NO, N_2 and NH_3 will occur.

Repository Chemistry

Chapter 23

Bridging the Gap in the Chemical Thermodynamic Database for Nuclear Waste Repository: Studies of the Effect of Temperature on Actinide Complexation

Linfeng Rao,[*,1] **Guoxin Tian,**[1] **Yuanxian Xia,**[2] **Judah I. Friese,**[2] **PierLuigi Zanonato,**[3] **and Plinio Di Bernardo**[3]

[1]Lawrence Berkeley National Laboratory, Berkeley, CA 94720, USA
[2]Pacific Northwest National Laboratory, Richland, WA 99352, USA
[3]Dipartimento di Scienze Chimiche,
Università di Padova, 35131 Padova, Italy
[*]lrao@lbl.gov

Recent results of thermodynamic studies on the complexation of actinides (UO_2^{2+}, NpO_2^+ and Pu^{4+}) with F^-, SO_4^{2-} and $H_2PO_4^-/HPO_4^{2-}$ at elevated temperatures are reviewed. The data indicate that, for all systems except the 1:1 complexation of Np(V) with HPO_4^{2-}, the complexation of actinides is enhanced by the increase in temperature. The enhancement is primarily due to the increase in the entropy term ($T\Delta S$) that exceeds the increase in the enthalpy (ΔH) as the temperature is increased. These data bridge the gaps in the chemical thermodynamic database for nuclear waste repository where the temperature could remain significantly higher than 25°C for a long time after the closure of the repository.

Introduction

One of the strategies for the safe management of nuclear wastes is to store the high-level nuclear wastes (HLW) in underground geological repositories such as the proposed Yucca Mountain (YM) repository in U.S.A. According to the estimated inventory of the YM repository, some radionuclides, including [238]U, [235]U, [234]U, [233]U, [239]Pu, [237]Np, [241]Am, [129]I, ^{99}Tc, [79]Se and [36]Cl, are considered to

be the most important contributors to dose at different times after the closure of the repository (*1*). Among these, uranium is the most abundant and neptunium is one of the few most soluble radionuclides that might be mobilized from the degraded waste forms and carried out of the repository. This could happen if the engineered barrier systems (waste packages and drip shields) gradually deteriorate and eventually lose the integrity (*2*). A scenario projected by both the TSPA-SR (Total System Performance Assessment for Site Recommendation) and the TSPA-LR models (Total System Performance Assessment for License Application) indicate that ^{237}Np, ^{129}I and ^{99}Tc are the major contributors to the total annual dose beyond 10,000 years and the fractional dose attributed to ^{237}Np will reach 67% at 75,000 years (*2, 3*). As a result, the migration of actinides, particularly neptunium (because of its high mobility and significant fractional dose in a long-term) as well as uranium (because of its abundance in the source term) in the postclosure chemical environment of nuclear waste repositories is of great concern to long-term repository performance.

The postclosure chemical environment is expected to be at near neutral pH, slightly oxidizing, and at elevated temperatures (*2*). As an example, Figure 1 shows that the projected temperature in the vicinity of the waste form in the YM Repository is around 80-100°C one thousand years after the closure of the repository (*2*). As a result, predictions of the migration behavior of actinides in the repository cannot be made without taking into consideration the effect of temperature on the complexation of actinides with the ligands that may exist in the groundwater of the repository (e.g., OH^-, F^-, SO_4^{2-}, PO_4^{3-} and CO_3^{2}).

Until recently, there had been very few thermodynamic data on the complexation of actinides at temperatures above 20-25°C (*4–6*) so that gaps exist in the thermodynamic database available for the performance assessment of nuclear waste repositories. Consequently, the chemistry model currently used for the proposed YM repository relies on the reaction paths calculated at 25°C (*2, 7, 8*). In the cases where the equilibrium constant and the enthalpy of complexation at 25°C are available, the Van't Hoff approach assuming a constant enthalpy could be used to extrapolate the equilibrium constant to higher temperatures. However, such extrapolation could introduce high uncertainties in the calculated concentrations of actinides, or even result in erroneous data if the enthalpy of complexation is significantly temperature-dependent and/or the temperature range for extrapolation is wide. Therefore, the dissolved concentration limits calculated by the model used for the performance assessment of the repository inherently have high uncertainties, which could lead to decisions that are too conservative with unnecessarily large and costly safety margins. For example, a recently revised estimation of the solubility limits of ^{237}Np and other nuclides could easily reduce the total annual dose by a factor of more than five (*2, 8*).
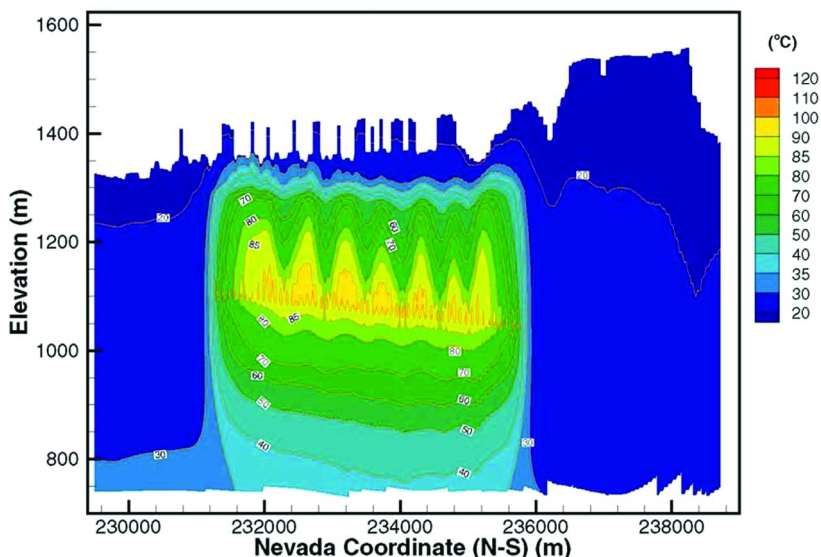
Figure 1. Temperature profile at 1,000 years along NS#2 cross section of the proposed Yucca Mountain Repository (with ventilation) from the Mountain-Scale Thermal-Hydrologic Model (2).

To help achieve more accurate predictions of the transport behavior of actinides in the HLW repository, bridge the gap in the thermodynamic data on actinide complexation at elevated temperatures, and improve our fundamental understanding of the thermodynamic principles governing the release of key radionuclides from the waste packages, recent studies have been conducted on the complexation of actinides with a few ligands, including OH^-, F^-, SO_4^{2-} and PO_4^{3-}, at elevated temperatures (*9–21*)). This paper summarizes the thermodynamic data for the systems of F^-, SO_4^{2-} and PO_4^{3-}, and discusses the effect of temperature on the speciation of actinides under conditions relevant to the waste repositories such as the proposed YM repository.

Base Concentrations of the Ligands Considered for the Proposed YM Repository

Based on the strength of complexation with actinides and the chemical composition of the groundwater on the YM site, the model used for the YM project defines three categories of ligands: primary (OH^-, CO_3^{2-}), secondary (F^-, SO_4^{2-}, HPO_4^{2-}), and tertiary (Cl^-, NO_3^-). The primary ligands, including OH^- and HCO_3^-/CO_3^{2-}, form strong complexes with actinides and their concentrations are dependent on the fugacity of carbon dioxide (f_{CO2}) and pH. The secondary ligands, including F^-, SO_4^{2-} and $H_2PO_4^-/HPO_4^{2-}/PO_4^{3-}$, form actinide complexes with moderate strength and could affect actinide solubilities if they are present in sufficiently high concentrations. The tertiary ligands, including Cl^- and NO_3^-,

are not considered in the modeling because they form very weak complexes with actinides and do not occur in sufficiently high concentrations (*8*).

"Base" concentrations of the ligands were selected as the starting point to develop the solubility models for the YM project. However, the concentrations of ligands could vary significantly in different scenarios, including 1) commercial spent nuclear fuel (CSNF) waste package breached under normal conditions or by seismic activity, 2) codisposal waste package with alteration by water from condensation only, and 3) codisposal waste package with alteration by seepage water and CSNF waste package breached by igneous activity. Therefore, concentrations of 1, 10, 100 and 1000 times of the base concentrations were used to accommodate different scenarios and test the sensitivity of the models (*8*). The base concentrations of a few ligands are shown in Table I.

Table I. Base concentrations of the ligands (*8*)

Component	Concentration (mg/L)
F^-	2.18
SO_4^{2-}	18.4
$H_2PO_4^-/HPO_4^{2-}/PO_4^{3-}$	0.1
pH	7.41
Alkalinity (HCO_3^-)	128.9

Complexation of Actinides with Fluoride at Variable Temperatures

The concentration of fluoride, a fairly strong complexant, in the groundwater of the proposed YM repository is in the range of 0.1 mM, but could be much higher than this in the presence of various breached waste packages. Therefore, its complexation with actinides could play an important role in the speciation and transport of actinides in the repository. However, few studies on the complexation of actinides with fluoride had been conducted at elevated temperatures and the data of enthalpy of complexation directly determined by calorimetry were very scarce (*4–6*).

Recently, equilibrium constants and the enthalpy of complexation have been determined for U(VI)/fluoride complexes by spectrophotometry (*11*), for Np(V)/fluoride complexes by spectrophotometry (*12*) and solvent extraction (*13*), and for Pu(IV)/fluoride complexes by solvent extraction (*15*), in the temperature range from 25 to 70°C. The data are summarized in Table II and Figure 2.

U(VI)/Fluoride

Four successive U(VI)/fluoride complexes (UO_2F^+, $UO_2F_2(aq)$, $UO_2F_3^-$, and $UO_2F_4^{2-}$) have been identified by absorption spectroscopy and the stability constants of the four complexes at 25, 40, 55 and 70°C have been calculated

(Table II) (*11*). The data indicate that the complexation of U(VI) with fluoride is fairly strong and becomes stronger at higher temperatures. When the temperature is increased from 25°C to 70°C, the stability constants of UO_2F^+, $UO_2F_2(aq)$, $UO_2F_3^-$ and $UO_2F_4^{2-}$ increase by about 2, 3, 8 and 11-fold, respectively. The enthalpies of complexation for UO_2F^+, $UO_2F_2(aq)$, $UO_2F_3^-$ and $UO_2F_4^{2-}$ at 25°C are directly measured by titration calorimetry and the entropies of complexation are calculated from the stability constants and the enthalpy of complexation.

The enthalpy and entropy data in Table II indicate that the complexation of U(VI) with fluoride is slightly endothermic. The positive entropy of complexation is the thermodynamic driving force for the formation of U(VI)/fluoride complexes. Release of water molecules from the hydration spheres of both UO_2^{2+} and F^- to the bulk water contributes to the overall entropy of complexation.

Np(V)/Fluoride

In a study by spectrophotometry (*12*), the absorption spectra in the near IR region were best-fitted with successive formation of 1:1 and 1:2 complexes represented by eq.1 and eq.2. The stability constants of $NpO_2F(aq)$ and $NpO_2F_2^-$ at 10, 25, 40, 55 and 70°C were listed in Table II. In the tables and figures of this manuscript, *I* donotes the ionic strength of the solution.

$$NpO_2^+ + F^- = NpO_2F(aq) \tag{1}$$

$$NpO_2^+ + 2F^- = NpO_2F_2^- \tag{2}$$

However, only the first complex, $NpO_2F(aq)$, was observed in the study by solvent extraction (*13*). Also, the stability constants of $NpO_2F(aq)$ obtained by solvent extraction are somewhat larger than those obtained by spectrophotometry (*12*) at corresponding temperatures (Table II). The reason for the difference probably lies in the neglect of the formation of $NpO_2F_2^-$ in fitting the data from solvent extraction. Nevertheless, both studies show that the complexation of Np(V) with fluoride is enhanced by the increase in the temperature: a 2-fold and 5-fold increase in the stability constants of $NpO_2F(aq)$ and $NpO_2F_2^-$, respectively, as the temperature is increased from 10 to 70°C.

The enthalpy of complexation at different temperatures was determined by variable-temperature calorimetry and found to become increasingly endothermic at higher temperatures (*12*). With these results, it was possible to calculate the heat capacities of complexation for $NpO_2F(aq)$ (76 ± 30 J·K^{-1}·mol^{-1}) and $NpO_2F_2^-$ (860 ± 100 J·K^{-1}·mol^{-1}). Including the values of heat capacity of complexation in the thermodynamic data base for the nuclear waste repository could lead to more accurate predictions of the temperature effect than assuming that the heat capacity is zero and the enthalpy of complexation is constant.

Table II. Thermodynamic parameters for the complexation of actinides with fluoride

Actinide	Reaction	t °C	log β I = 1.0 M	log β° I = 0	ΔH kJ·mol^{-1}	ΔS J·K^{-1}·mol^{-1}	Ref.
U(VI)	$UO_2^{2+} + F^- \leftrightarrows UO_2F^+$	25	4.60 ± 0.02	5.20 ± 0.07	2.8 ± 0.4		(11)
		40	4.62 ± 0.02	5.25 ± 0.07			
		55	4.67 ± 0.04	5.32 ± 0.07			
		70	4.80 ± 0.02	5.45 ± 0.07			
	$UO_2^{2+} + 2F^- \leftrightarrows$ $UO_2F_2(aq)$	25	8.07 ± 0.04	8.74 ± 0.07	5.2 ± 0.8		
		40	8.21 ± 0.04	8.91 ± 0.07			
		55	8.32 ± 0.06	9.06 ± 0.08			
		70	8.52 ± 0.02	9.31 ± 0.06			
	$UO_2^{2+} + 3F^- \leftrightarrows$ $UO_2F_3^-$	25	10.62 ± 0.04	11.25 ± 0.09	3.4 ± 1.1		
		40	10.78 ± 0.04	11.44 ± 0.09			
		55	11.21 ± 0.06	11.91 ± 0.10			
		70	11.55 ± 0.02	12.29 ± 0.09			
	$UO_2^{2+} + 4F^- \leftrightarrows$ $UO_2F_4^{2-}$	25	11.92 ± 0.14	12.01 ± 0.18	0.2 ± 3.3		
		40	12.27 ± 0.02	12.38 ± 0.11			
		55	12.59 ± 0.06	12.73 ± 0.12			
		70	12.95 ± 0.04	13.12 ± 0.11			

Actinide	Reaction	t °C	log β I = 1.0 M	log β° I = 0	ΔH kJ·mol⁻¹	ΔS J·K⁻¹·mol⁻¹	Ref.
Np(V)	$NpO_2^+ + F^- \leftrightarrows$ $NpO_2F(aq)$	10	1.19 ± 0.05	1.32 ± 0.12			(*12*)
		25	1.25 ± 0.05	1.39 ± 0.12	8.1 ± 1.0	51 ± 5	
		40	1.36 ± 0.05	1.51 ± 0.12	8.8 ± 0.6	54 ± 4	
		55	1.39 ± 0.05	1.55 ± 0.12	10.2 ± 0.5	58 ± 4	
		70	1.44 ± 0.05	1.62 ± 0.12	11.2 ± 2.6	60 ± 11	
		25	1.42 ± 0.10		20.8	97	(*13*)
		35	1.63 ± 0.03				
		50	1.77 ± 0.04				
		60	1.80 ± 0.03				
	$NpO_2^+ + 2F^- \leftrightarrows$ $NpO_2F_2^-$	10	1.37 ± 0.10	1.50 ± 0.15			(*12*)
		25	1.77 ± 0.09	1.92 ± 0.14	14.2 ± 3.1	82 ± 12	
		40	1.99 ± 0.10	2.15 ± 0.15	18.6 ± 1.6	98 ± 7	
		55	2.04 ± 0.08	2.21 ± 0.13	36.0 ± 1.4	149 ± 7	
		70	2.11 ± 0.09	2.30 ± 0.14	40.8 ± 8.8	159 ± 32	

Continued on next page.

Table II. (Continued). Thermodynamic parameters for the complexation of actinides with fluoride

Actinide	Reaction	t °C	log β I = 1.0 M	log β° I = 0	ΔH kJ·mol⁻¹	ΔS J·K⁻¹·mol⁻¹	Ref.
Pu(IV)	$Pu^{4+} + F^- \leftrightarrows PuF^{3+}$	25		8.86 ± 0.21	9.4 ± 5.0	201 ± 17	(*15*)
		40		8.95 ± 0.20			
		55		9.01 ± 0.20			
	$Pu^{4+} + 2F^- \leftrightarrows PuF_2^{2+}$	25		15.91 ± 0.21	15.0 ± 8.0	355 ± 27	
		40		16.02 ± 0.20			
		55		16.15 ± 0.20			

Similar to the complexation of U(VI) with fluoride, the thermodynamic parameters (ΔH and ΔS) indicate that the complexation of Np(V) with fluoride is entropy driven. As the temperature is increased, both the enthalpy and entropy of complexation increase. The favorable contribution from the entropy term ($T\Delta S$) exceeds the unfavorable contribution from the enthalpy (ΔH), resulting in the enhancement of complexation at higher temperatures.

Pu(IV)/Fluoride

Complexation of Pu(IV) with fluoride was studied by solvent extraction at 25, 40 and 55°C in 2.2 mol·kg^{-1} HClO$_4$ (*15*). Two complexes, PuF^{3+} and PuF$_2^{2+}$, were identified under the conditions in this work and the stability constants at 25, 40 and 55°C were determined from the distribution data. The enthalpies of complexation were calculated from the Van't Hoff plot of the stability constants at variable temperatures. Data from this work indicate that the complexation of Pu(IV) with fluoride is also enhanced by the increase in the temperature (Table II). Similar to the complexation of U(VI) and Np(V) with fluoride, the complexation of Pu(IV) with fluoride is endothermic and entropy-driven. This is typical of the formation of inner-sphere complexes and is not surprising because both Pu^{4+} and F$^-$ ions are strongly hydrated and a significant amount of energy is expected to be spent on dehydrating the ions, resulting in unfavorable enthalpy. Meanwhile, the dehydration of both the cation and anion and the re-arrangement of the water structure in the vicinity of the complex (PuF^{3+} and PuF$_2^{2+}$) as well as in the bulk creates a high degree of disorder, resulting in large positive entropy.

Complexation of Actinides with Sulfate at Variable Temperatures

Sulfate, one of the inorganic constituents in the groundwater of nuclear waste repository, could affect the migration of radioactive materials by forming complexes even under acidic conditions. In recent studies, equilibrium constants and the enthalpy of complexation have been determined for U(VI)/sulfate complexes by spectrophotometry (*16*), for Np(V)/sulfate complexes by spectrophotometry (*14, 18*) and solvent extraction (*13*), and for Pu(IV)/sulfate complexes by solvent extraction (*19*), in the temperature range from 25 to 70°C. The data are summarized in Table III and and Figure 3.

Table III. Thermodynamic parameters for the complexation of actinides with sulfate

Actinide	Reaction	$t\ °C$	$\log\ \beta$ $I = 1.0\ M\ NaClO_4$	$\log\ \beta°$ $I = 0$	ΔH $kJ\cdot mol^{-1}$	ΔS $J\cdot K^{-1}\cdot mol^{-1}$	Ref.
U(VI)	$UO_2^{2+} + SO_4^{2-} \rightleftarrows$ $UO_2SO_4(aq)$	25	1.96 ± 0.06	3.23 ± 0.08	17.7 ± 0.3	96 ± 1	(16)
		40	2.04 ± 0.06	3.35 ± 0.08	21.0 ± 0.4	106 ± 1	
		55	2.20 ± 0.06	3.56 ± 0.08	22.8 ± 0.6	111 ± 2	
		70	2.32 ± 0.03	3.74 ± 0.08	25.9 ± 0.7	120 ± 2	
	$UO_2^{2+} + 2SO_4^{2-} \rightleftarrows$ $UO_2(SO_4)_2^{2-}$	25	2.97 ± 0.03	4.22 ± 0.15	43.2 ± 0.9	201 ± 3	
		40	3.34 ± 0.03	4.63 ± 0.15	37.8 ± 0.4	184 ± 1	
		55	3.71 ± 0.06	5.06 ± 0.16	38.2 ± 1.2	187 ± 4	
		70	3.94 ± 0.15	5.34 ± 0.16	37.5 ± 0.7	184 ± 2	
Np(V)	$NpO_2^{+} + SO_4^{2-} \rightleftarrows$ $NpO_2SO_4^{-}$	10	0.43 ± 0.11	0.92 ± 0.22			(18)
		25	0.53 ± 0.14	1.03 ± 0.25	21 ± 7	81 ± 25	
		40	0.56 ± 0.04	1.09 ± 0.15	24 ± 5	87 ± 17	
		55	0.60 ± 0.12	1.15 ± 0.20	34 ± 2	115 ± 9	
		70	0.62 ± 0.08	1.21 ± 0.18	53 ± 5	166 ± 18	
		25	0.49 ± 0.31		17.8	69	(13)
		40	0.65 ± 0.19				
		50	0.73 ± 0.16				

Actinide	Reaction	t °C	$\log \beta$ $I = 1.0\ M\ NaClO_4$	$\log \beta°$ $I = 0$	ΔH $kJ \cdot mol^{-1}$	ΔS $J \cdot K^{-1} \cdot mol^{-1}$	Ref.
Pu(IV)	$Pu^{4+} + SO_4^{2-} \leftrightarrows PuSO_4^{2+}$	25	3.78 ± 0.05[a]	6.82 ± 0.12[b]	23.0[c]	149	(19)
		40	3.93 ± 0.03[a]	7.08 ± 0.12[b]			
		55	4.15 ± 0.03[a]	7.40 ± 0.12[b]			
	$Pu^{4+} + 2SO_4^{2-} \leftrightarrows$ $Pu(SO_4)_2(aq)$	25	6.73 ± 0.04[a]	9.30 ± 0.18[b]	25.6[c]	214	
		40	6.94 ± 0.04[a]	9.58 ± 0.18[b]			
		55	7.14 ± 0.04[a]	9.78 ± 0.18[b]			

[a] $I = 2.0\ M\ HClO_4$. [b] Calculated by using the ion interaction parameters for U(IV)/sulfate complexation from ref (4, 5). [c] Calculated by using the Van't Hoff equation.
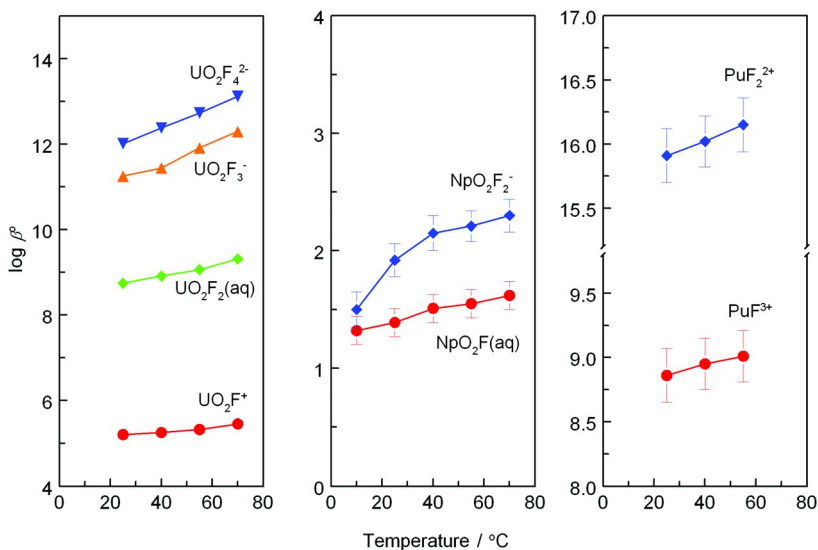
Figure 2. Recent data on the complexation of U(VI) (11), Np(V) (12) and Pu(IV) (15) with fluoride at variable temperatures (I = 0).

U(VI)/Sulfate

Results from spectrophotometric titrations show that U(VI) forms moderately strong complexes with sulfate, $UO_2SO_4(aq)$ and $UO_2(SO_4)_2^{2-}$, and the complexes become stronger as the temperature is increased: 2-fold and 10-fold increases in the stability constants of $UO_2SO_4(aq)$ and $UO_2(SO_4)_2^{2-}$, respectively, when the temperature is increased from 25°C to 70°C (Table III).

The results from calorimetric measurements at different temperatures indicate that the complexation is endothermic. The enthalpy of complexation for $UO_2SO_4(aq)$ increases as the temperature is higher (17.7 kJ·mol^{-1} at 25°C, 25.9 kJ·mol^{-1} at 70°C), while the enthalpy of complexation for $UO_2(SO_4)_2^{2-}$ remains nearly constant (Table III). From these data, the heat capacities (ΔC_p) of the complexation of $UO_2SO_4(aq)$ and $UO_2(SO_4)_2^{2-}$ are calculated to be 180 ± 14 J·K^{-1}·mol^{-1} and ~ 0 J·K^{-1}·mol^{-1}, respectively.

Data in Table III show that, in the temperature range from 25°C to 70°C, both the enthalpy and entropy of complexation of U(VI) with sulfate are positive. Therefore, the complexation is entropy-driven, characteristic of "hard acid" and "hard base" interactions and inner-sphere complexation (*22*). Dehydration of both the cations (UO_2^{2+}) and anions (SO_4^{2-}) plays the most significant roles in the complexation, the energy required for dehydration contributing to the positive enthalpy and the number of water molecules released from the hydration spheres contributing to the positive entropy. For the formation of $UO_2SO_4(aq)$, both the enthalpy and entropy of complexation increases as the temperature is increased, making opposite contributions to the temperature effect on the Gibbs free energy (and thus on the stability of the complex). The complexation is enhanced at higher temperatures because the increase in the entropy term ($T\Delta S$) exceeds the increase

in the enthalpy. The increase of entropy with the temperature in interpreted as the consequence of a more disordered bulk water structure at higher temperatures due to the perturbation by thermal movements. In the process of complexation, the solvating water molecules are released to an already expanded and more disordered bulk solvent (23). As a result, the net gain in the complexation entropy is larger at higher temperatures.

Np(V)/Sulfate

Results from spectrophotometric titrations show that the complexation of Np(V) with sulfate is weak but slightly enhanced by the increase in temperature (18). The stability constants of $NpO_2SO_4^-$ at 10, 25, 40, 55 and 70°C are listed in Table III. Data from calorimetric titrations show that the complexation of Np(V) with sulfate is endothermic and becomes increasingly endothermic at higher temperatures (18). From the temperature dependency of the enthalpy, the heat capacity of complexation is calculated to be (720 ± 170) $J \cdot K^{-1} \cdot mol^{-1}$.

The ΔH and ΔS values for the complexation of Np(V) with sulfate ($NpO_2^+ + SO_4^{2-} = NpO_2SO_4^-$) are both significantly larger (more positive) than those for the complexation of Np(V) with fluoride ($NpO_2^+ + F^- = NpO_2F(aq)$) (see Table II). This could be rationalized by assuming that the desolvation of SO_4^{2-} (-2 charge) requires more energy than the desolvation of F^- (-1 charge). In addition, SO_4^{2-} could complex metal ions in mono- and bi-dentate modes while F^- is a monodentate ligand. More water molecules would be released from the solvation spheres of bidentate SO_4^{2-} ligand and the metal ions, creating larger entropy changes upon complexation with SO_4^{2-}.

Pu(IV)/Sulfate

The complexation of plutonium(IV) with sulfate at variable temperatures from 25° C to 55° C has been investigated by the solvent extraction method (19). The decrease of the distribution ratio of Pu(IV) between the organic and aqueous phases was interpreted as being due to the formation of 1:1 and 1:2 Pu(IV)-SO_4^{2-} complexes in the aqueous phase and the stability constants of $Pu(SO_4)^{2+}$ and $Pu(SO_4)_2(aq)$ at different temperatures were accordingly calculated.

The stability constants of $Pu(SO_4)^{2+}$ and $Pu(SO_4)_2(aq)$ increase with increasing temperature. The enthalpies of complexation calculated with the Van't Hoff equation were positive. Again, the complexation of Pu(IV) with sulfate is entropy driven, similar to the complexation of Pu(IV) with fluoride, as well as the complexation of U(VI) and Np(V) with sulfate and fluoride. The dehydration of both the cations and anions plays important roles in the energetics of complexation.
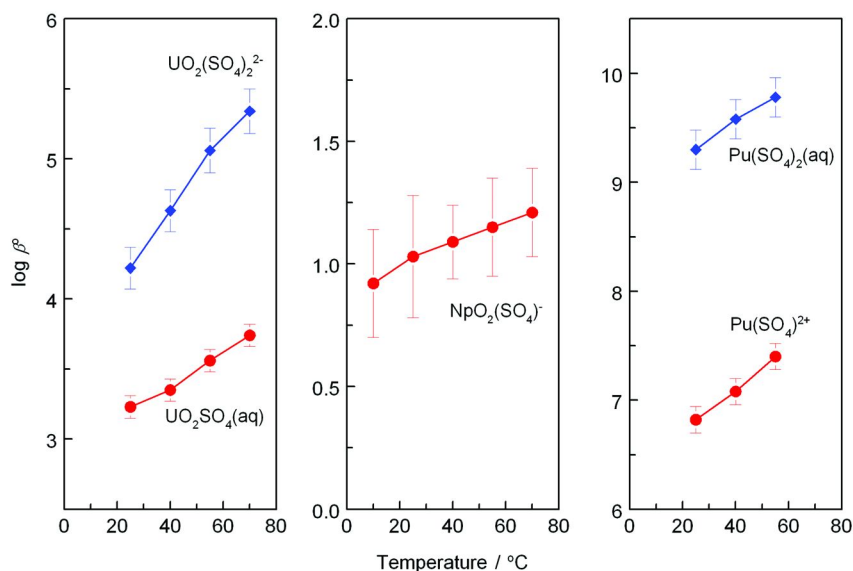
Figure 3. Recent data on the complexation of U(VI) (16), Np(V) (18) and Pu(IV) (19) with sulfate at variable temperatures (I = 0).

Table IV. Thermodynamic parameters for the complexation of actinides with phosphate

Actinide	Reaction	t °C	log β I = 1.0 M	ΔH kJ·mol⁻¹	ΔS J·K⁻¹·mol⁻¹	Ref.
Np(V)	$NpO_2^+ + HPO_4^{2-} \leftrightarrows$ $NpO_2(HPO_4)^-$	25	2.32 ± 0.04	-20.7	-25	(20)
		40	2.08 ± 0.06			
		55	1.99 ± 0.13			
	$NpO_2^+ + 2HPO_4^{2-} \leftrightarrows$ $NpO_2(HPO_4)_2^{3-}$	25	3.78 ± 0.35	27.7	165	(20)
		40	4.14 ± 0.25			
		55	4.22 ± 0.24			
Np(V)	$NpO_2^+ + H_2PO_4^- \leftrightarrows$ $NpO_2(H_2PO_4)(aq)$	25	1.18 ± 0.10	28.1	117	(21)
		40	1.39 ± 0.06			
		55	1.63 ± 0.03			

Complexation of Actinides with Phosphate at Variable Temperatures

In slightly acidic and near neutral solutions, $H_2PO_4^-$ and HPO_4^{2-} are the major species of phosphate. Data on the complexation of actinides with phosphate at elevated temperatures are extremely scarce. In the recent studies, complexation of Np(V) with $H_2PO_4^-$ and HPO_4^{2-} in the temperature range of $25 - 55°C$ were studied by solvent extraction. The stability constants and enthalpy of complexation are shown in Table IV and Figure 4.

Np(V)/HPO$_4$$^{2-}$

Stability constants of two complexes, $NpO_2(HPO_4)^-$ and $NpO_2(HPO_4)_2^{3-}$, at 25, 40 and 55°C were calculated from the solvent extraction data. The stability constants of $NpO_2(HPO_4)_2^{3-}$ from this work (*20*) are the first such data at temperatures above 25°C. The results show that the stability constant of $NpO_2(HPO_4)^-$ decreases at higher temperatures while the stability constant of $NpO_2(HPO_4)_2^{3-}$ increases at higher temperatures (Table IV). The enthalpies of complexation were calculated to be -20.7 kJ·mol^{-1} for $NpO_2(HPO_4)^-$ and 27.7 kJ·mol^{-1} for $NpO_2(HPO_4)_2^{3-}$. The negative enthalpy of complexation for $NpO_2(HPO_4)^-$, opposite to the positive enthalpies for all other complexation systems discussed in this paper, seems to support the hypothesis that this complex is of the "outer-sphere" type where minimum dehydration of the cation and anion is required. However, future studies of the complexation of Np(V) with phosphate in a wider temperature range and/or using different techniques are necessary to test the hypothesis.

Np(V)/H$_2$PO$_4$$^-$

$H_2PO_4^-$ is the dominant species of phosphate in slightly acidic aqueous solutions. Data from solvent extraction indicate that one Np(V) complex, $NpO_2(H_2PO_4)(aq)$, forms in aqueous solutions of pH ~ 5. The stability constant increases by about 3 times as the temperature is increased from 25°C to 55°C. The enthalpy of complexation was calculated by the Van't Hoff approach to be 28.1 kJ·mol^{-1}. As the data in Table IV show, the complexation of Np(V) with $H_2PO_4^-$ is entropy-driven, suggesting that the energy for the dehydration of the cation and anion is the dominant component in the energetics of the complexation (*21*).
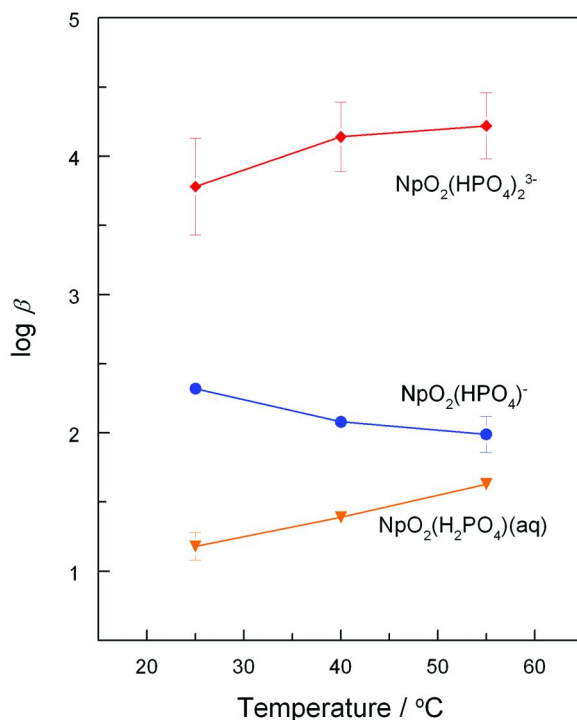
Figure 4. Recent data on the complexation of Np(V) with HPO_4^{2-} (20) and $H_2PO_4^-$ (21) at variable temperatures (I = 1.05 mol·kg^{-1}).

Effect of Temperature on the Speciation of Actinides

The recent data of the stability constants of actinide complexes at different temperatures allow us to calculate the speciation of actinides at variable temperatures in solutions containing the major inorganic ligands. Figures 5 and 6 show the speciation of U(VI) and Np(V) at 25°C and 70°C in the presence of fluoride and sulfate ($I = 0$).

Speciation of U(VI)

The species that were considered in the calculations include UO_2^{2+}, UO_2F^+, $UO_2F_2(aq)$, $UO_2F_3^-$, $UO_2F_4^{2-}$, $UO_2(SO_4)(aq)$, $UO_2(SO_4)_2^{2-}$, $UO_2(OH)^+$, $(UO_2)_2(OH)_2^{2+}$ and $(UO_2)_3(OH)_5^+$. The equilibrium constants for the hydrolysis of U(VI) at 25°C and 70°C are taken from the literature (9).

At 25°C and in the presence of 1 mM fluoride and sulfate (Figure 5A), the fluoride complexes (UO_2F^+ and $UO_2F_2(aq)$) are the dominant U(VI) species and $UO_2(SO_4)(aq)$ amounts to about 10% when pH is below 5. When pH is above 5.5, the complexation of U(VI) with fluoride and sulfate at 1 mM cannot compete with the hydrolysis of U(VI) and the $(UO_2)_3(OH)_5^+$ species becomes dominant (Figure 5A). In contrast, at 25°C and in the presence of 10 mM fluoride and

sulfate, all U(VI) is in fluoride complexes and the hydrolysis of U(VI) is effectively suppressed in the pH region up to 6 (Figure 5B).

At 70°C, the trends in speciation as the concentrations of fluoride and sulfate are increased from 1 mM (Figure 5C) to 10 mM (Figure 5D) are similar to those observed at 25°C. However, because both the hydrolysis of U(VI) and the complexation of U(VI) with fluoride and sulfate are enhanced at higher temperatures, the speciation at 70°C differs from that at 25°C. In particular, the higher hydrolyzed species ($(UO_2)_3(OH)_5^+$) becomes dominant at a lower pH (~ 5) in the presence of 1 mM fluoride (Figure 5C), while the higher fluoride complexes (especially $UO_2F_3^-$) becomes more important in the presence of 10 mM fluoride (Figure 5D). Again, the presence of 10 mM fluoride completely suppresses the hydrolysis of U(VI) at 70°C in the pH region up to 6.
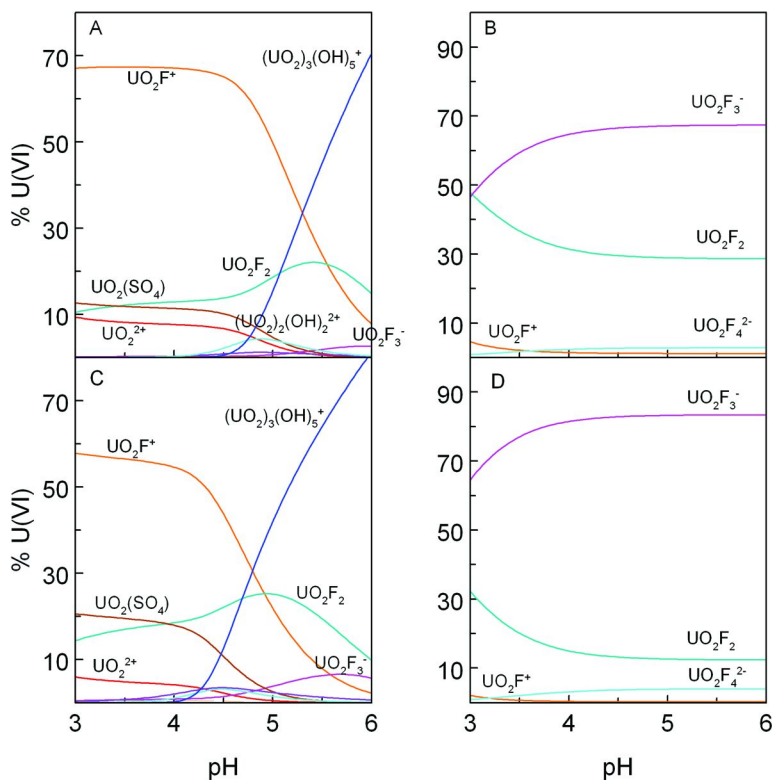
Figure 5. Speciation of U(VI) in aqueous solutions containing fluoride and sulfate at different temperatures (C_U = 1 mM). (A) – 25°C, $C_{fluoride}$ = $C_{sulfate}$ = 1 mM; (B) – 25°C, $C_{fluoride}$ = $C_{sulfate}$ = 10 mM; (C) – 70°C, $C_{fluoride}$ = $C_{sulfate}$ = 1 mM; (D) – 70°C, $C_{fluoride}$ = $C_{sulfate}$ = 10 mM.
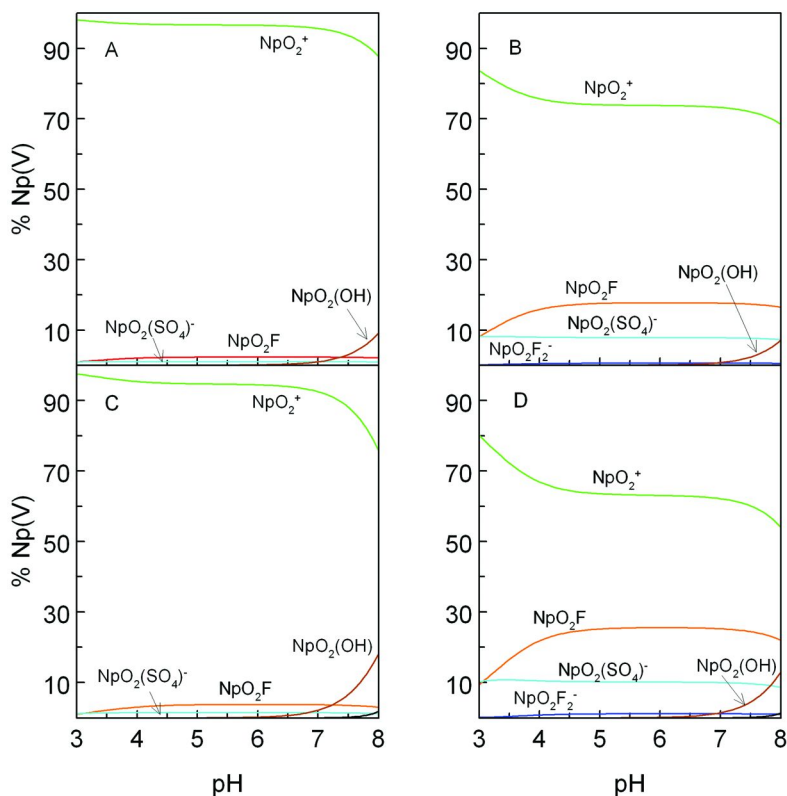
Figure 6. Speciation of Np(V) in aqueous solutions containing fluoride and sulfate at different temperatures (C_{Np} = 1 mM). (A) – 25°C, $C_{fluoride}$ = $C_{sulfate}$ = 1 mM; (B) – 25°C, $C_{fluoride}$ = $C_{sulfate}$ = 10 mM; (C) – 70°C, $C_{fluoride}$ = $C_{sulfate}$ = 1 mM; (D) – 70°C, $C_{fluoride}$ = $C_{sulfate}$ = 10 mM.

Speciation of Np(V)

The species that were considered in the calculations include NpO_2^+, $NpO_2F(aq)$, $NpO_2F_2^-$, $NpO_2(SO_4)^-$, $NpO_2(OH)(aq)$ and $NpO_2(OH)_2^-$. The equilibrium constants for the hydrolysis of Np(V) at 25°C and 70°C are taken from the literature (*10*).

The tendency of Np(V) toward hydrolysis and the complexation of Np(V) with fluoride and sulfate are much weaker than that of U(VI). Therefore, when the concentrations of fluoride and sulfate are low (1 mM), free NpO_2^+ remains to be the dominant species in the pH region up to 8, where the first hydrolyzed species ($NpO_2(OH)(aq)$) starts to form. The percentages of $NpO_2F(aq)$ and $NpO_2(SO_4)^-$ are slightly higher at 70°C (Figure 6C) than those at 25°C (Figure 6A), but are less than 5% at both temperatures.

In the presence of higher concentrations of fluoride and sulfate (10 mM), the percentage of $NpO_2F(aq)$ increases to 16% (25°C) and 25% (70°C), while that of $NpO_2(SO_4)^-$ increases to 8% (25°C) and 11% (70°C). For both fluoride and sulfate,

the importance of ligand complexation increases as the temperature is increased (Figure 6B and 6D).

Summary

Recent studies have generated thermodynamic data on the complexation of actinides with inorganic ligands at elevated temperatures. These data, while bridging the gaps in the thermodynamic database for the proposed nuclear waste repository, help to evaluate the effect of temperature on the speciation of actinides and achieve more accurate prediction of actinide speciation at elevated temperatures that are likely to be encountered in nuclear waste repositories.

Acknowledgments

References

1. *Solicitation for Submission of Project Proposals from National Laboratories and the U.S. Geological Survey*; OCRWM Report; Office of Scientific and Technical Information (OSTI), Office of Civilian Radioactive Waste Management (OCRWM): Washington, DC, January 19, 2005.
2. *Yucca Mountain Science and Engineering Report*; DOE/RW-0539-1; Office of Civilian Radioactive Waste Management (OCRWM): North Las Vegas, NV, 2002; Rev.1.
3. *Total System Performance Assessment: License Application Methods and Approach*; TDR-WIS-PA-000006REV 00, ACC:MOL.20020923.0175; Bechtel SAIC Company, LLC: Las Vegas, NV, 2002.
4. Grenthe, I.; Fuger, J.; Konings, R. J. M.; Lemire, R. J.; Muller, A. B.; Nguyen-Trung, C.; Wanner, H. In *Chemical Thermodynamics of Uranium*; Wanner, H., Forest, I., Eds.; Elsevier Science Publishers B.V.: Amsterdam, 1992.
5. Guillaumont, R.; Fanghanel, T.; Fuger, J.; Grenthe, I.; Neck, V.; Palmer, D. A.; Rand, M. H. In *Update on the Chemical Thermodynamics of Uranium, Neptunium, Plutonium, Americium, and Technetium*; Mompean, F. J., Illemassene, M., Domenech-Orti, C., Ben Said, K., Eds.; Elsevier Science Publishers B.V.: Amsterdam, 2003.
6. Rao, L. *Chem. Soc. Rev.* **2007**, *36*, 881–892.

7. *In-Package Environment and Waste Form Degradation and Solubility*; Technical Basis Document No.7; Bechtel SAIC Company, LLC: Las Vegas, NV, July 2004; Rev. 1.

8. *Dissolved Concentration Limits of Radioactive Elements*; ANL-WIS-MD-000010, Radioactive Waste Management System Management and Operation Contractor (CRWMS M&O) Technical Document; Office of Civilian Radioactive Waste Management (OCRWM): North Las Vegas, NV, November 2004; Rev. 03.

9. Zanonato, P.; Di Bernardo, P.; Bismondo, A.; Liu, G.; Chen, X.; Rao, L. *J. Am. Chem. Soc.* **2004**, *126*, 5515–5522.

10. Rao, L.; Srinivasan, T. G.; Garnov, A. Yu.; Zanonato, P.; Di Bernardo, P.; Bismondo, A. *Geochim. Cosmochim. Acta* **2004**, *68*, 4821–4830.

11. Tian, G.; Rao, L. *Inorg. Chem.* **2009**, *48*, 6748–6754.

12. Tian, G.; Rao, L.; Xia, Y.; Friese, J. I. *J. Therm. Anal. Calorim.* **2009**, *95*, 415–419.

13. Xia, Y.; Friese, J. I.; Moore, D. A.; Rao, L. *J. Radioanal. Nucl. Chem.* **2006**, *268*, 445–451.

14. Rao, L.; Tian, G.; Xia, Y.; Friese, J. I. *Thermodynamics of Neptunium(V) Fluoride and Sulfate at Elevated Temperatures*. Proceedings of the 11th International High-Level Radioactive Waste Management Conference (IHLRWM), Las Vegas, NV, April 30–May 4, 2006; pp 374−378.

15. Xia, Y.; Friese, J. I.; Rao, L.; Moore, D. A.; Bachelor, P. P. *Radiochim. Acta*, in press.

16. Tian, G.; Rao, L. *J. Chem. Thermodyn.* **2009**, *41*, 569–574.

17. Rao, L.; Tian, G. The Effect of Temperature on the Speciation of U(VI) in Sulfate Solutions. In *Uranium, Mining, and Hydrogeology*; Merkel, B. J., Hasche-Berger, A., Eds.; Springer-Verlag: Berlin, Heidelberg, 2008; pp 763−769.

18. Rao, L.; Tian, G.; Xia, Y.; Friese, J. I. *J. Therm. Anal. Calorim.* **2009**, *95*, 409–413.

19. Xia, Y.; Friese, J. I.; Moore, D. A.; Bachelor, P. P.; Rao, L. *J. Radioanal. Nucl. Chem.* **2007**, *274*, 79–86.

20. Xia, Y.; Friese, J. I.; Moore, D.; Bachelor, P. P.; Rao, L. *J. Radioanal. Nucl. Chem.* **2009**, *280*, 599–605.

21. Xia, Y.; Friese, J. I.; Moore, D.; Rao, L. *Stability Constants of Np(V) Complexes with Phosphate at Variable Temperatures*. Proceedings of the 11th International High-Level Radioactive Waste Management Conference (IHLRWM), Las Vegas, NV, April 30–May 4, 2006; pp 716−721.

22. Rizkalla, E. N.; Choppin, G. R. Lanthanides and Actinides Hydration and Hydrolysis. In *Handbook on the Physics and Chemistry of Rare Earths*; Gschneider, K. A., Jr., Eyring, L., Choppin, G. R., Lander, G. H., Eds.; Elsevier Science Publishers B.V.: Amsterdam, 1994; Vol. 18, Lanthanides/Actinides: Chemistry.

23. Di Bernardo, P.; Zanonato, P.; Tian, G.; Tolazzi, M.; Rao, L. *J. Chem. Soc., Dalton Trans.* **2009**, *23*, 4450–4457.

Chapter 24

Evaluation of THOR™ Mineralized Waste Forms (Granular and Monolith) for the DOE Advanced Remediation Technologies (ART) Phase 2 Project

C. L. Crawford[*] and C. M Jantzen

Savannah River National Laboratory (SRNL), Savannah River Nuclear Solutions (SRNS), Aiken, SC 29808
[*]**charles.crawford@srnl.doe.gov**

Fluidized Bed Steam Reforming (FBSR) processing of Hanford Low Activity Waste (LAW) and Waste Treatment Plant Secondary Waste (WTP-SW) simulants were performed in 2008 by THOR™ Treatment Technologies LLC (TTT). Testing was performed at the Hazen Research Inc. (HRI) Engineering Scale Technology Demonstration (ESTD) pilot plant facilities in Golden, CO. FBSR mineralized aggregate products from pilot tests on simulated waste representative of the Hanford LAW and the WTP-SW were characterized and leach tested at SRNL. Aggregates were monolithed using several different binders at various monolith scales including 2" cubes and 2"x 4", 3"x 6" and 6"x 12" cylinders. Monoliths were compression tested upon curing up to 28 days and also characterized and leach tested. A geopolymer formulation using flyash gives optimal monolith performance relative to compressive strength, durability and toxic metal retention.

Background and Introduction

FBSR offers a moderate temperature (700-750 °C) continuous method by which a wide variety of wastes can be processed into a mineral waste form. The process destroys any organics and/or nitrates in the waste. The mineral hosts can accommodate sulfates/sulfides, halides, and radionuclides, especially Tc-99,

Sr-90, I-129, and Cs-137. The granular waste form that is produced is as durable as glass. Monolithing of the granular product can be used to prevent dispersion during transport or burial/storage. A variety of monoliths have been shown to be feasible (*1–3*). In the sodium aluminosilicate (NAS) FBSR mineral structures, the contaminants such as Tc-99 are bound in cage (sodalite, nosean) or ring (nepheline) structures to surrounding aluminosilicate tetrahedra (*4*). The NAS minerals form by reaction between the waste and a processing additive (clay), which provides the SiO_2 and Al_2O_3. The NAS FBSR minerals are formed by destabilization of the clay at the moderate processing temperature: the clay becomes amorphous at the nanoscale and reactive. The cations in the waste react with the unstable clay molecules and rearrange to a crystalline (mineral) lowest free energy configuration. In mineral waste forms, as in glass, the molecular structure controls contaminant release by establishing the distribution of ion exchange sites, hydrolysis sites, and the access of water to those sites. Durability testing using ASTM C1285 (*5*) of the FBSR mineral waste form has shown that the FBSR product is as durable as glass and that an Al-buffering mechanism controls the release of alkali (Na, K, and Cs) elements and the solution pH controls the release of the other constituents like Re (simulant for Tc-99), S, and Si. The aluminosilicate buffereing mechanism is known to occur in nature during weathering of aluminosilicate minerals.

In this study six as-received Product Receiver (PR) from the Denitration and Mineralization Reformer (DMR) granular/powder samples and six High Temperature Filter (HTF) powder samples were received by SRNL for initial characterization and testing. FBSR PR samples had been taken from the Product Receiver Tank, while the HTF samples were the fines collected as carryover from the DMR. The process operated at high fluidizing velocities during the mineralization test such that nearly all of the product collected was from the HTF (*6*). Initial testing on the mineralized aggregates determined which mineral product blends (mixtures of the PR and HTF aggregates) were selected for further monolith studies. Initial monolith studies using small 2" cubes with various binders determined which binders to further study using larger cylinder monoliths (2"x 4", 3"x 6" and 6"x 12").

Experimental

The ESTD operational summary for the Hazen runs is shown in Table I. The first eight tests were performed on LAW using a DMR temperature of 725°C and different ratios of clay:simulant of 675 g or 640 g of OptiKast clay per liter of simulant. The last four tests were performed on WTP-SW (originally referred to as LAW-Recycle) using a DMR temperature in the range of 680°C to 700°C with a mixture of 45/55 Sagger/OptiKast clay with 307 g clay/L simulant. Detailed simulant compositions for the LAW and WTP-SW FBSR feeds have been reported (*6*). The major components common to both the LAW and WTP-SW feeds are Na^+, Al^{3+}, Si^{4+}, NO_3^-/NO_2^-, CO_3^{2-} and OH^-. The WTP-SW is higher in F^- and Cl^- and lower in SO_4^{2-} and PO_4^{2-} vs. the LAW. The components B, NH_4^+ and Zn^{2+} are only in the WTP-SW and it does not contain any organics ($C_2O_4^{2-}$, CH_3COO^-) that are in the LAW. The WTP-SW contains more 'trace' components than the LAW, e.g.,

10 trace components present in the WTP-SW at < 0.2 g/L vs. only 4 in the LAW present at < 0.2 g/L. Coal feed rates used in the FBSR processing were 16.6, 14.9, 16.1, 19.9 kg/hr, respectively for the Phase-1A, Phase-1B, Phase-2A, Phase-2B tests. SphereOX® iron-containing component was also added as a Cr reductant in both the LAW and WTP-SW processing. A total of 48 kg of Fe was added during LAW processing, and 49 kg of Fe was added during WTP-SW processing.

Table I. ESTD Operational Summary

Sample Description	Sample Log #	Date Sample Obtained	Test Phase	Hours of Operation at Test Conditions Before Sample Obtained	DMR Temp.
HTF	5280	4/27/2008 21:42	P-1A / LAW	17.7	725°C
PR	5274	4/28/2008 5:15	P-1A / LAW	25.3	725°C
HTF	5297	4/28/2008 17:28	P-1A / LAW	37.5	725°C
PR	5316	4/29/2008 3:54	P-1A / LAW	47.9	725°C
HTF	5351	4/30/2008 12:00	P-1B / LAW	28	725°C
HTF	5357	4/30/2008 19:44	P-1B / LAW	35.7	725°C
PR	5359	4/30/2008 22:55	P-1B / LAW	38.9	725°C
PR	5372	5/1/2008 7:00	P-1B / LAW	47	725°C
HTF	5471	5/5/2008 0:20	P-2A / WTP-SW	70.3	680°C
PR	5475	5/5/2008 4:00	P-2A / WTP-SW	74	680°C
HTF	5520	5/6/2008 10:00	P-2B / WTP-SW	26.5	700°C
PR	5522	5/6/2008 10:00	P-2B / WTP-SW	26.5	700°C

Single kilogram quantities of each HTF or PR aggregate product were initially analyzed and leach tested at SRNL. Product aggregates were screened to below 18 mesh to remove any large particulates of residual coal. Elemental and anion compositions of the steam reforming aggregate PR and HTF materials were measured for as-received samples after heating of the samples at 525 °C in air overnight in a muffle furnace. Loss on ignition (LOI) values were determined from mass loss. The <200 mesh (<74 μm) PCT-prepared powders were used for the dissolutions for analyses in all testing (aggregate and all various monoliths). Elemental and anion analyses were performed on lithium tetraborate fusion (1000 °C) and sodium peroxide digestion (650 °C), respectively. These methods used nominally 0.1 g of powder solid sample to 0.1 L of dissolved solution, and 0.15 g of powder solid to 0.250 L of dissolved solution, respectively. Digestion methods for elemental (cation) analysis involved the use of acids for dissolution. A KOH fusion method with water uptake was used for sample dissolution to obtain anion analyses using typically 0.25 g of solid powder to 0.1 L of dissolved solution. All elemental concentrations (except for I, Re and Cs) were determined by Inductively Coupled Plasma Atomic Emission Spectroscopy (ICP-AES). The Re, Cs and I were measured by Inductively Coupled Plasma Mass Spectroscopy (ICP-MS).

Chemical durability of the steam reformer products was determined using the Product Consistency Test (PCT) ASTM procedure C 1285-02 (*5*). Prior to sizing and washing, carbon was removed from the aggregate PR and HTF material by heating overnight at 525 °C . The PR and HTF product samples were sized between (-) 100 and (+) 200 mesh (< 149 μm and > 74 μm), which is the same size fraction used to express glass waste form performance. The sized material was washed six times (2 with rinse/decant, and 4 with rinse/sonication/decant) with 100% ethanol to remove electrostatic fines, followed by overnight drying in an oven at 90°C. Water was not used for washing so no potential water soluble phases would be removed prior to leaching as cautioned by the ASTM C1285-02 procedure. Portions of the washed and dried PR and HTF powders were analyzed using Microtrac – S3000 instrumentation for particle size analysis by laser light scattering. Brunauer, Emmett, Teller (BET) surface area measurements via gas adsorption was also performed on the sieved/washed/dried portions of the powders used for PCT. Both a low and high surface area standard were typically run in parallel for the BET surface area instrument. The low surface area standard used NIST-traceable silicon nitride powder with a certified 2.05 ± 0.09 m^2/g surface area. The high surface area standard used silica – alumina from Micromeritics with a certified 214 ± 6 m^2/g surface area. For all samples, ASTM Type I water was used as leachant, a constant leachate to sample ratio of 10 cm^3/g was used, the test temperature was 90 °C, and the test duration was seven days. Test duration and temperature are the nominal test conditions used for testing glass waste form performance under the PCT-A. In this program the original aggregate PR and HTF powders were all heat-treated to remove carbon. All subsequent PCTs (blends and monoliths) were performed on materials that did not receive any heat-treatment, i.e., residual FBSR carbon material remained in the samples that were chemically analyzed and leach-tested with PCT.

The method for surface area to volume determination for this work involves a measurement of the surface area by the BET method. In this method, the amount

of an inert gas that condenses on a powdered sample of known mass is measured at a temperature near the boiling point of the gas. The amount of gas condensed on the sample is measured by the pressure change in the system upon exposure to the sample. This method measures all open pores, inclusions, irregularities, etc. that are penetrable by the inert gas.

The Hanford LAW is a listed waste under the United States Environmental Protection Agency US-EPA Resource Conservation and Recovery Act (RCRA). When treated, the waste form must retain the hazardous components at the Universal Treatment Standard (UTS) limits (7). The Land Disposal Restrictions (LDRs) will apply to shallow land burial at Hanford. All PR and HTF samples were evaluated for retention of the hazardous metals by the EPA Toxicity Characteristic Leaching Procedure, Method 1311 (TCLP) (8). Greater than 100 g samples of as-received material were submitted to GEL Laboratories, LLC of Charleston, SC, an EPA-certified laboratory. In the leaching procedure, 100 g samples are extracted by a buffered acetic acid fluid for 18 hours. The extraction fluid (leachate) is then filtered and analyzed for elements of interest. Since organics are destroyed in the FBSR process, only the following RCRA hazardous inorganic species were measured: As, Ba, Cd, Cr, Pb, Se, Ag, Ni, Sb, Tl and Zn. If the concentration of a hazardous inorganic species from the simulated waste form is higher than the UTS limits, then it is assumed that a real waste treated in a similar manner would fail the UTS limits and require further remediation. FBSR blends from the LAW and WTP-SW tests, as well as the monoliths formed from the blends were also submitted for TCLP analyses. Milligram quantities of the dissolved aggregate powders were also measured for REDuction/OXidation (REDOX) using UV-VIS absorption spectroscopy for complexed iron.

After individual aggregates were studied, larger amounts of blended samples rich in HTF material were received for both LAW P1B and WTP-SW P2B. These blends had been pre-screened to < 18 mesh before shipment. Monolith studies with these blends involved the various cements and binders shown in Table II. All cement binder recipes used ASTM-I water (resistivity >18 Mohm-cm at 25 °C). Geopolymers also used Fisher reagent grade sodium hydroxide (NaOH) solutions and D™ Sodium Silicate solution from the PQ Corporation (Valley Forge, PA). The ordinary Portland cement composition is made up of various calcium silicates, aluminates and aluminoferrites. The high alumina-containing 'calcium aluminate cements' are made up of various calcium aluminates along with calcium aluminum silicates and calcium aluminum ferrites. The high alumina cement binders were supplied from Kerneos Inc. of Chesapeake, VA. Ceramicrete ingredients were obtained from Argonne National Laboratory (ANL) and consist of MgO and KH_2PO_4. No flyash was used in the ceramicrete for these studies. Some ceramicrete formulations used trace boric acid powder as set retarder. Geopolymer formulations for this project were based on earlier SRNL Laboratory Directed Research & Development (LDRD) studies completed in 2007 (9). Troy metakaolin clays were the main clays used in all geopolymer recipes. Later recipes used a Barden heat-treated clay, and a different set of geopolymer recipes used flyash as additive in place of the clay. A recent review of flyash uses in geopolymers for waste stabilization is available in the open literature (10).

Table II. Cements and Binders Used for Monoliths

Monolith System	Additives	Nominal Constituents/Conditions
Ordinary Portland Cement	OPC binder	SiO_2 (19-23wt%), Al_2O_3 (3-7wt%), Fe_2O_3 (1.5-4.5wt%), CaO (63-67wt%), other metal (Mg,K,Na,S)-oxides trace
High Alumina Cements	Tradenames: Ciment Fondu® Secar® 51 Secar® 71	$CaO•Al_2O_3$ $CaO•2Al_2O_3$ $12CaO•7Al_2O_3$ $2CaO•Al_2O_3•SiO_2$ $4CaO•Al_2O_3•Fe_2O_3$
Ceramicrete	MgO and KH_2PO_4	$MgO + KH_2PO_4 + 5\ H_2O = MgKPO_4.6H_2O$
Geopolymer	Troy and Barden heat-treated clays; flyash; sodium silicate solution; NaOH solution	Solids (aggregate waste and either clay or flyash) premixed; Sodium silicate liquid added, followed by caustic and final water addition

The 2" x 2" cubes were formulated by mixing the solid and liquid ingredients by hand in plastic bowls with a spatula for mixing. Final fresh blend was transferred from the plastic mix bowl to the cube mold with a spatula since these blends were typically thick and not easily poured. These monoliths were stored in capped cube molds for curing. All of the 2" x 4" and 3" x 6" cylinders were formulated using a Hobart (Troy, OH) mixer mill (Model N-50, 3-speed, 1/6th HP) fitted with an ~ 5 quart stainless steel bowl. A larger Hobart mixer mill (Model D-300) fitted with an ~ 30 quart stainless steel bowl was used for the 6" x 12" cylinder formulations. The Hobart mixers were fitted with a flat beater multipurpose agitator. All cylinder monoliths made in this project used standard plastic molds with fitted plastic caps. No heat treatment was applied to any of the monoliths in this project. Duplicate 6" x 12" cylinders were formulated and mixed at ambient laboratory temperatures of 20 °C +/- 5 °C. A single sample from each duplicate set was fitted with a K-type thermocouple located on the centerline of the cylinder with the TC tip placed in the vertical center. All the 6" x 12" cylinders were allowed to cure in a constant temperature and humidity room that was maintained at 23 °C +/- 2 °C and 95% minimum humidity. These are the ASTM-specified conditions for curing temperature and humidity for hydraulic cements and concretes per ASTM C31 'Standard Practice for Making and Curing Concrete Test Specimens in the Field' and ASTM C511 'Standard Specification for Mixing Rooms, Moist Cabinets, Moist Rooms, and Water Storage Tanks Used in the Testing of Hydraulic Cements and Concretes'. The 2" cubes were compression tested using ASTM C109 'Standard Test Method for Compressive Strength of Hydraulic Cement Mortars (Using 2-in. or [50-mm] Cube Specimens)' and the cylinders were compression tested using ASTM C39 'Standard Test Method for Compressive Strength of Cylindrical Concrete Specimens'.

Results and Discussion

Initial mineralized aggregates and blends were analyzed for LOI, REDOX, bulk density, particle size distribution and crystalline phases. The LOI values for the HTF and PR aggregates were in the ranges of 8.6 to 13, and ~ 2.1 wt%, respectively. Blended LAW and WTP-SW had LOI values of 1.7 and 11.1 wt%, respectively. The HTF aggregates have lower bulk density (0.65 g/cc) and higher REDOX ($Fe^{2+}/Fe_{Total} = 0.8 - 0.9$) than the PR aggregates at 1.0 g/cc and REDOX of 0.4 - 0.5. Particle size distribution for the LAW P1B blends were in the range of 2 to 383 microns and for the WTP-SW in the range of 2 to 204 microns. Crystalline phases determined from powder XRD are shown in Table III. Other minor components identified in the minerals were Al_2O_3, SiO_2, TiO_2 and graphite.

Table III. Crystalline Phases Identified by XRD

	Low-Carnegieite[i]	*Nepheline*[ii]	*Nosean*[iii] *and/or Sodalite*[iv]
LAW Minerals			
PR 5274 (P1A)	Y	Y	
PR 5316 (P1A)	Y	Y	
HTF 5280 (P1A)	Y	Y	
HTF 5297 (P1A)	Y	Y	Y
PR 5359 (P1B)	Y	Y	
PR 5372 (P1B)	Y	Y	
HTF 5351 (P1B)	Y	Y	
HTF 5357 (P1B)	Y	Y	
Blend (P1A)	Y	Y	
Blend (P1B)	Y	Y	
WTP-SW Minerals			
PR 5475 (P2A)	Y	Y	Y
HTF 5471 (P2A)	Y	Y	
PR 5522 (P2B)	Y	Y	Y
HTF 5520 (P2B)	Y	Y	
Blend (P2B)	Y	Y	Y

[i] $NaAlSiO_4$ or $Na_{1.45}Al_{1.45}Si_{0.55}O_4$. [ii] $(K_{0.25}Na_{0.75})AlSiO_4$, $Na_{0.89}Al_{0.9}Si_{1.1}O_4$, $NaAlSiO_4$, $Na_{1.53}Al_{0.92}Si_{0.92}O_4$. [iii] $Na_6[Al_6Si_6O_{24}](Na_2SO_4)$. [iv] $Na_6[Al_6Si_6O_{24}](2NaCl)$, $Na_6[Al_6Si_6O_{24}](2NaI)$, $Na_6[Al_6Si_6O_{24}](2NaF)$.

Table IV. Normalized PCT Data for Aggregates/Blends

	pH	BET (m²/g)	SA/V (m⁻¹)	Al, Cs (g/m²)	I, Na (g/m²)	Re, S (g/m²)	Si (g/m²)
5280 HTF P1A	11.6	5.28	528,480	1.9E-03 / 5.4E-03	1.5E-03 / 1.5E-02	3.1E-02 / 1.3E-01	4.7E-04
5297 HTF P1A	11.5	5.55	554,620	2.4E-03 / 6.6E-03	2.3E-03 / 1.3E-02	2.4E-02 / 1.2E-01	3.2E-04
5351 HTF P1B	11.5	5.26	525,904	1.6E-03 / 9.5E-03	1.1E-03 / 1.3E-02	7.0E-03 / 7.7E-02	5.1E-04
5357 HTF P1B	11.7	4.76	475,670	2.1E-03 / 8.0E-03	1.0E-03 / 1.6E-02	3.3E-02 / 1.3E-01	5.6E-04
5471 HTF P2A	10.0	5.56	555,550	2.9E-03 / 1.2E-02	5.9E-03 / 1.3E-02	1.5E-02 / 8.6E-02	1.1E-04
5520 HTF P2B	10.0	5.15	515,200	3.2E-03 / 1.4E-02	1.4E-02 / 1.5E-02	2.2E-02 / 9.7E-02	1.1E-04
5274 PR P1A	11.3	4.04	404,180	2.0E-03 / 1.3E-02	1.1E-03 / 1.0E-02	8.3E-03 / 4.8E-02	6.5E-04
5316 PR P1A	11.4	4.76	476,410	1.7E-03 / 1.2E-02	1.3E-03 / 1.2E-02	9.1E-03 / 6.1E-02	6.0E-04
5359 PR P1B	11.4	4.11	410,570	1.9E-03 / 1.8E-02	7.6E-04 / 1.5E-02	5.1E-03 / 5.8E-02	6.3E-04
5372 PR P1B	11.5	4.36	436,000	1.9E-03 / 1.1E-02	8.6E-04 / 1.4E-02	4.8E-03 / 7.0E-02	6.6E-04
5475 PR P2A	10.8	4.35	435,000	3.4E-03 / 1.6E-02	1.1E-02 / 1.3E-02	6.0E-03 / 5.4E-02	1.4E-04
5522 PR P2B	10.6	3.80	380,000	4.0E-03 / 1.9E-02	1.5E-02 / 1.3E-02	8.2E-03 / 4.4E-02	1.9E-04
LAW, P-1B	11.8	5.62	562,000	2.0E-03 / 9.6E-03	2.3E-03 / 1.3E-02	2.3E-02 / 8.0E-02	6.0E-04
WTP-SW, P-2B	10.1	4.89	488,940	4.2E-03 / 4.1E-02	1.3E-02 / 1.8E-02	5.0E-02 / 3.9E-02	1.4E-04

PCT data is shown in Table IV. The final leachate pHs were all in the range of 10.0 to 11.7. Surface areas of the 100-200 mesh powders were in the range of 3.8 to 5.6 m²/g. These surface areas are higher than similar sized glass fines (typically 0.04 m²/g) due to the porous nature of the aggregate minerals. Normalized releases from the PR and HTF samples were all less than 0.08 and 0.14 g/m², respectively, with normalized sulfur showing highest of the measured elements. The normalized release is calculated by dividing the analyzed leach ate concentrations by the elemental fraction in the waste form and the surface area to volume ratio.

Based on comparison of the normalized release for the various components shown in Table I with emphasis on Re as surrogate for Tc-99, the LAW P1B and the WTP-SW P2B blends were deemed to be the most durable of the aggregates and were carried forward in 2" cube monolith studies. Summary data for the 2" monoliths made with the various binder agents is shown in Table V. Waste loadings reported are on a dry basis calculated by dividing the mass of FBSR product by the FBSR product plus all other solids added from the binders and liquids. These data show that with few exceptions, monoliths containing nominally 65 to 85 wt% FBSR can be made to pass the 500 psi compressive strength lower limit. The 2" cubes were analyzed and leach tested using the PCT to produce normalized release data shown in Table VI (all values $< \sim 0.08$ g/m^2) that are comparable to the original aggregate and blends.

Table V. Summary Data for 2" Cubes

Monolith 2" Cube	Waste Loading	Compressive Strength (psi)	Cure Time (days)	Bulk Monolith Density (g/cc)
OPC-1	80.0	1,630	12	1.64
OPC-2	85.1	573	28	1.61
FON-1	68.6	770	7	1.77
FON-2	74.2	490	7	1.75
S41-1	68.6	672	7	1.75
S41-2	74.2	340	15	1.70
S71-1	68.6	1,120	7	1.70
S71-2	74.2	550	15	1.65
GEO-1	67.5	1,510	11	1.87
GEO-2	72.1	860	14	1.87
GEO-3	67.5	1,270	11	1.81
GEO-4	71.2	410	11	1.84
GEO-5	62.9	950	7	1.88
GEO-6	66.8	1,080	7	1.82
CER-1	66.7	520	8	1.81
CER-2	72.7	550	28	1.81

Table VI. Normalized PCT Data for 2" Cubes

2" Cube Monoliths	pH	BET m²/g	SA/V m⁻¹	Al/Cs (g/m²)	I/Na (g/m²)	Re/S (g/m²)	Si (g/m²)
FON-1	12.08	20.0	2E6	4.4E-03 6.2E-03	1.3E-03 1.2E-02	1.7E-02 1.9E-02	1.8E-05
FON-2	12.26	15.5	1.5E6	5.0E-03 8.3E-03	3.0E-03 1.6E-02	1.4E-02 3.4E-02	3.9E-05
S41-1	12.14	10.7	1.1E6	8.5E-03 1.1E-02	3.0E-02 2.2E-02	4.6E-02 4.8E-02	1.8E-05
S41-2	12.19	10.7	1.1E6	9.5E-03 4.3E-03	1.7E-02 2.5E-02	2.3E-02 5.8E-02	4.0E-05
S71-1	12.26	13.1	1.3E6	5.6E-03 1.7E-02	3.1E-02 2.0E-02	4.9E-02 4.0E-02	2.2E-05
S71-2	11.94	9.2	9E5	8.0E-03 2.8E-02	1.1E-02 2.1E-02	1.1E-02 4.5E-02	1.4E-04
OPC-1	12.23	31.5	3.1E6	8.5E-04 2.2E-03	5.4E-03 9.3E-03	3.2E-02 3.7E-02	4.3E-05
OPC-2	12.37	21.3	2.1E6	6.0E-04 9.1E-04	2.0E-03 9.1E-03	1.9E-02 4.5E-02	9.0E-05
GEO-1	12.12	15.2	1.5E6	6.9E-05 8.9E-04	1.3E-03 1.4E-02	8.9E-04 4.2E-02	2.5E-03
GEO-2	12.15	17.3	1.7E6	6.1E-05 5.4E-04	1.2E-03 1.3E-02	8.6E-03 3.8E-02	2.4E-03
GEO-3	12.29	10.9	1.1E6	2.2E-04 1.7E-03	2.2E-03 2.2E-02	1.0E-02 5.1E-02	4.2E-03
GEO-4	12.36	6.2	6E5	5.0E-04 3.7E-03	2.4E-03 4.3E-02	1.0E-02 8.3E-02	7.5E-03
GEO-5	12.30	10.6	1.1E6	5.6E-05 8.8E-04	8.9E-04 2.4E-02	6.4E-03 5.3E-02	9.9E-03
GEO-6	12.27	10.0	1E6	5.7E-05 4.0E-04	1.8E-03 2.1E-02	1.1E-02 6.1E-02	7.1E-03
CER-1	9.86	32.2	3.2E6	1.1E-04 5.6E-03	8.2E-04 6.3E-03	4.4E-02 3.1E-02	1.9E-05
CER-2	9.62	27.7	2.8E6	1.0E-04 6.3E-03	7.3E-04 5.4E-03	1.0E-02 2.9E-02	1.9E-05

Three of the monolith formulations were carried forward for further larger scale monolith studies involving 2"x4", 3"x6" and 6"x12" cylinders. A geopolymer matrix made with flyash in place of clay was also added. Summary data for the various cylinders is shown in Table VII. These data for the larger cylinder monoliths again show that monoliths containing FBSR at 65 to 74 wt% loading can pass the 500 psi limit.

Table VII. Summary Data for Cylinder Monoliths

Binder & Size	Comp. Strength (psi)	Cure Time (days)	Bulk Monolith Density (g/cc)	Waste Loading
LAW				
FON-2, 3" x 6"	580	28	1.69	74
6" x 12"	370	28	1.69	74
S71-2, 3" x 6"	660	17	1.68	74
6" x 12"	550	19	1.70	74
GEO-1, 3" x 6"	1,690	14	1.85	67
6" x 12"	1,530	14	1.82	67
GEO-7, 3" x 6"	2,500	14	1.90	65
6" x 12"	1,920	18	NM	65
WTP-SW				
FON-2, 3" x 6"	570	18	1.68	74
6" x 12"	420	28	1.67	74
S71-2, 3" x 6"	820	17	1.67	74
6" x 12"	660	19	1.66	74
GEO-1, 3" x 6"	890	14	1.83	67
6" x 12"	1,710	19	1.83	67
GEO-7, 3" x 6"	1,980	14	1.83	65
6" x 12"	520	28	NM	65

PCT data for all the cylinders were comparable to the previous 2" cube and aggregate/blend data. Normalized release for all elements in the three cylinder sizes were less than 0.04 g/m². Temperature profiles from centerline curing were measured for the largest 6" x 12" cylinders. The geopolymer matrix gave prompt temperature increases approaching 45 °C immediately after setting in the plastic molds. The calcium aluminate cements also attained the ~ 45 °C maximum temperature but on a longer timescale of several hours.

Conclusions

Characterization of these crystalline powder samples indicates they are primarily Al, Na and Si, with < 1wt% Fe, K and S also present. The PR samples contained less than 2.1 wt% carbon with a bulk (aggregate) density of ~ 1 g/cc, and the HTF samples ranged from 8.6 to 13 wt% carbon with estimated bulk (aggregate) density of 0.65 g/cc. Bulk density of the aggregates was determined simply by placement of known mass into a graduated cylinder with some gentle

tapping. Crystalline phases observed in the aggregate and blends from the Hazen ESTD testing show Low-Carnegieite, Nepheline, Nosean and Sodalite structures that are similar to previous FBSR testing results previously performed by SRNL. The as-received PR and HTF samples were roasted in air to determine loss on ignition and to prepare the samples for durability testing. Durability testing of the PR and HTF samples using the ASTM C1285 Product Consistency Test (PCT) 7-day leach test at 90°C was performed along with several reference glass samples. Normalized elemental releases from the PR and HTF samples were all less than 0.08 and 0.14 g/m^2, respectively. Measured leachate values were normalized using BET surface areas that measured in the range of 3.8 to 5.5 m^2/g for the 100-200 mesh fractions obtained from the FBSR aggregates.

A blend of the PR and HTF samples from the Phase 1-B LAW testing were chosen for monolith studies based on normalized elemental PCT release with emphasis given to Re as surrogate for Tc-99. The P1B blends contained 1.72 wt% and 11.06 wt% residual carbon, respectively, for the LAW and WTP-SW. TCLP was performed on the blends to show that these products meet the criteria for the EPA RCRA Universal Treatment Standards for all of the constituents except for Cd and Sb. However, these elements along with other toxic metals (Ba, Se and Tl) had been added to the FBSR feed simulant at ~ 1,000X the expected concentration to allow for adequate detection in the products.

Monolith studies were initially performed on P-1B LAW aggregate to make 2" cubes using ordinary Portland cement, high aluminum cements, ceramicrete and geopolymers. Based on compression data, PCT and TCLP performance, four monolith recipes from the 2"x 2" LAW cubes were carried forward into both 3"x 6" cylinders and 6"x 12" cylinders that were made from both LAW and WTP-SW. Curing temperatures were measured for the 6" x 12" cylinders using centerline thermocouples. PCT durability testing of the best candidate monolith forms shows average normalized release values below 0.04 g/m^2. Statistical analysis of the data indicate that the 95% confidence level is less than or equal to ~ 0.1 g/m^2. Finally, a single geopolymer formulation containing flyash was chosen from these monolith studies to produce 24 replicate WTP-SW containing 2"x 4" cylinders that measured > 2,200 psi after 28 days of curing. All of these fly ash-containing geopolymer 'GEO-7' formulations that used WTP-SW P2B blend (3" x 6", 6" x 12" and 2" x 4" cylinders) passed TCLP for all elements. Results of these studies carried out at SRNL and the FBSR pilot facilities at Hazen, CO have successfully demonstrated the capabilities of the THOR™ FBSR process as a potential means to treat and prepare the Hanford LAW and WTP-SW for disposal at the Hanford Integrated Disposal Facility (IDF).

References

1. Jantzen, C. M.; Lorier, T. H.; Pareizs, J. M.; Marra, J. C. *Fluidized Bed Steam Reformed (FBSR) Mineral Waste Forms: Characterization and Durability Testing*; WSRC-STI-2006-00317; U.S. Department of Energy: Washington, DC, 2006. http://www.osti.gov/bridge/index.jsp.

2. Jantzen, C. M. *Durability Testing of Fluidized Bed Steam Reforming (FBSR) Waste Forms*, Rev. 0; WSRC-MS-2006-00015; Waste Management 2006 Symposium Proceedings, Tuscon, AZ, February 26−March 2, 2006; U.S. Department of Energy: Washington, DC. http://www.osti.gov/bridge/index.jsp.

3. Crawford, C. L.; Jantzen, C. M. *Durability Testing of Fluidized Bed Steam Reformer (FBSR) Waste Forms for Sodium Bearing Waste (SBW) at Idaho National Laboratory (INL)*, Rev. 0; WSRC-STI-2007-00319; U.S. Department of Energy: Washington, DC, August 2007. http://www.osti.gov/bridge/index.jsp.

4. Jantzen, C. M. *Mineralization of Radioactive Wastes by Fluidized Bed Steam Reforming (FBSR): Comparisons to Vitreous Waste Forms and Pertinent Durability Testing*, Rev. 0; WSRC-STI-2008-00268; Savannah River National Laboratory for U.S. Department of Energy: Aiken, SC, December 2008.

5. *Standard Test Methods for Determining Chemical Durability of Nuclear, Hazardous, and Mixed Waste Glasses and Multiphase Glass Ceramics: The Product Consistency Test (PCT)*; ASTM C 1285-02; ASTM International: West Conshohocken, PA, 2002.

6. *Report for Treating Hanford LAW and WTP SW Simulants: Pilot Plant Mineralizing Flowsheet*, Rev. 1; Project Number 29387, Document Number RT-21-002; THOR Treatment Technologies for U.S. Department of Energy: Denver, CO, April 2009. http://www.thortt.com/.

7. Land Disposal Restrictions. *Code of Federal Regulations*, Part 268, Title 40, 2004.

8. *Test Methods for Evaluating Solid Waste, Physical/Chemical Methods*, 3rd ed.; EPA 530/SW-846, TCLP Method 1311; Office of Solid Waste, U.S. Environmental Protection Agency: Washington, DC, 1986.

9. Jantzen, C. M.; Jurgensen, A. R.; Burket, P. R.; Missimer, D. M.; Crawford, C. L. Low Temperature Waste Forms and Containment: Geopolymers. In *SRNL LDRD Annual Report for 2007*; SRNS-STI-2008-00533; Savannah River National Laboratory for U.S. Department of Energy: Aiken, SC, December 16, 2008. http://www.osti.gov/bridge/index.jsp.

10. Ferna´ndez Pereira, C.; Luna, Y.; Querol, X.; Antenucci, D.; Vale, J. Waste stabilization/solidification of an electric arc furnace dust using fly ash-based geopolymers. *Fuel 88* **2009**, 1185–1193.

Effects of Organic Acids on Biotransformation of Acinides

**Toshihiko Ohnuki,*,[1] Naofumi Kozai,[1] Takuo Ozaki,
Fuminori Sakamoto,[1] Yoshinori Suzuki,[1] and Takahiro Yoshida[1,2]**

**[1]Advanced Science Research Center, Japan Atomic Energy Agency,
Tokai, Ibaraki 319-1195, Japan
[2]Present address: Radioactive Waste Management Funding and Research
Center, Tsukishima, Chuo-ku, Tokyo 104-0052, Japan
*ohnuki.toshihiko@jaea.go.jp**

The effects of organic materials on the biotransformation of actinides should be elucidated to estimate the impact of potential release of actinides from waste forms disposed in geologic formation. Biotransformation includes adsorption, degradation, and reduction of the complexes of actinides with organic acids. We have conducted the loboratory experiments to elucidate the effects of organic materials secreted from a algal cells and a siderophore on the adsorption of trivalent actinides and lanthanides, and organic acids on the reduction of U(VI) to U(IV). The biodegradation of the complexes of organic acids with trivalent lanthanides have also been studied.

Introduction

The presence of actinides in nuclear reactors and radioactive wastes is a major environmental concern due to their long radioactive half-lives, their high energy radiation emissions, and their chemical toxicity. In order to estimate the potential impact of actinides on human beings, the mobility of actinides has been examined in terms of its interactions with soils and subsoils composed of abiotic and biotic components, principally minerals and bacteria (*1–7*). Among the biotic components, some microorganisms have cells whose surfaces sorb actinides (*6–11*). The high capacity of microbial surfaces to bind actinides may affect environmental behavior of actinides. The interaction of actinides

with microorganisms involves (i) adsorption, (ii) oxidation/reduction, and (iii) degradation of actinide-organic complexes. The interaction of actinides with microorganisms results in changes in the chemical state of actinides (biotransformation).

Naturally occurring chelating substances have the potential to enhance the solubility and mobility of various toxic metals and radionuclides by forming complexes in the environment (*12*). However, we have a limited knowledge on the effects of organic materials on the biotransformation.

The microbiology research group of JAEA is conducting basic scientific research on microbial interactions with actinides. Fundamental research on the effects of organic materials on the microbial transformations of actinides involves elucidating the mechanisms of adsorption, degradation, and redox of actinides by aerobic or anaerobic microorganisms under relevant microbial process conditions.

Effect of Organic Acids on Adsorption

Various microorganisms excrete organic acids. One of the famous exudates is a siderophore to solubilize Fe(III) and then utilize it for life. These exudates with chelating ability may solubilize lanthanides and actinides of low solubility in groundwater of neutral pH. However, effects of the exudates on the adsorption of lanthanides and actinides are scarcely known. We have examined the effects of the exudates from *Chlorella vulgaris* of unicellular eukaryote bacterium on the adsorption of Eu(III) and Cm(III) (*13*). We also conducted the experiments to elucidate the effects of desferrioxamine B (DFO) of trihydroxamate siderophore on the adsorption of Eu(III) and Pu(IV) by *Pseudomonas fluorescens* of Gram-negative soil bacterium (*14*, *15*).

Effects of Exudates on the Adsorption of Eu(III) and Cm(III) on *C. vulgaris*

Adsorption kinetics and distribution coefficient (K_d) of Eu(III) and Cm(III) were obtained as function of pH. Approximately 0.1 g dry weight of *C. vulgaris* was exposed in the 0.5% NaCl solution containing 1×10^{-6} mol·L^{-1} ^{152}Eu or 1×10^{-8} mol·L^{-1} ^{244}Cm at pH 5.0 ± 0.1 for 20 min. To measure distribution coefficient, 0.025 g dry weight of *C. vulgaris* was contacted with 5 ml solution of Eu and Cm, the pHs were adjusted between 2 and 9. Adsorption of Eu and Cm on cellulose which is major component of cell envelop of *C. vulgaris* was measured using cellulose powder obtained from Kanto Chemical, Tokyo, Japan. The cellulose was used without purification. Fifty mg of cellulose was mixed with 5 ml of solution containing Eu or Cm at pH 4, 5, and 6. The concentration of Eu and Cm were measured by radioactivity. The solutions were filtered through 0.20-μm membrane to obtain the supernatant solutions. The distribution coefficient, Kd (cm^3·g^{-1}) was calculated by the following equation (1)

$$K_d = (C_0 - C)V/CM \qquad (1)$$

where C_0 is the initial concentration of the metal ion in the aqueous phase; C, the equilibrium concentration of the metal ion in the aqueous phase; V, the volume of the aqueous phase (cm^3); and, W, the dry-weight of the microbial cells (g).

Time dependent adsorbed fractions of Eu and Cm (Fig. 1) (13) showed immediate increase after exposure to Eu or Cm solution, followed by gradual descent with increasing time up to 20 min. No marked differences in adsorption kinetics were observed between Eu and Cm. The log K_d of Cm by algal cells was approximately 3 at pH 2, and slightly increased with increasing pH to approximately 4 around pH 3, then gradually decreased to 2.1with increasing pH up to 8. The log K_d of Cm by cellulose was less than 1 at pH 2, and increased to approximately 5 with increasing pH around 6, then gradually decreased up to 4 around pH 8. The pH dependence of the log K_d for Eu by algal cells and cellulose was nearly the same as that of Cm (Data not shown). These results indicated that the pH dependence of log K_d of Eu and Cm differs between algal cells and cellulose, even though major component of cell envelop of algal cells was cellulose.

The amounts of total organic carbon (TOC) excreted from algal cells into solution containing no Eu and Cm were approximately 19, 20, and 21 ppm at pHs 4, 5, and 6, respectively. The log K_ds for Cm between cellulose and exudates solution collected from algal cells measured at pH 4, 5, and 6 are shown in Fig. 1b (cellulose + exudates). The K_d was 2.3 at pH 4, and slightly decreased to 1.7 with increasing pH up to 6. This log K_d was lower than that of cellulose alone, and the tendency with pH was different from that of cellulose, indicating that amounts of Cm adsorbed by cellulose was descent by the formation of complexes with the exudates from algal cells. The tendency of log K_d with pH resembled to that of algal cells. These findings suggest that the difference in the tendency of log K_d for unicellular eukaryote of *C. vulgaris* and cellulose reflects the sequestration of Eu and Cm by the formation of complex with the exudates.

We measured organic materials excreted from *Saccharomyces cerevisiae* one of the unicellular eukaryote by SEC-HPLC-ICPMS without acidification to examine the existence of Eu bound to organic ligands. Separation of organic molecules was performed with a 10.7 φ × 300 mm SEC column (GL-W540, Hitachi chemical Co., Ltd) safeguarded with a guard column (GL-W500, Hitachi chemical Co., Ltd). Ultraviolet 280 nm absorbance of size-excluded fractions was monitored as an indicator of benzene nucleus contained in proteins before introduction to ICP-MS (Agilent4500).

The SEC separation makes it possible to estimate the molecular weight (MW) of unknown peaks for UV 280 nm absorbance from correlation of the retention time and MW using known MW standards (16). The chromatogram of the UV 280 nm absorbance (Fig. 2: UV) shows one strong peak with weak peak around 20 min, and insect in Fig. 2 shows very weak peak around 8 min. These peaks at 20 min correspond to MW ranging around several kDa. The other peak around 8 min corresponds to region out of the limit of size exclusion for the SEC column, it means that at least organic molecules having MW more than 670 kDa were excreted from *S. cerevisiae*. Eu shows strong peak around 8 min, and weak peak around 20 min, indicating that Eu was bound to the exudates from the cells to be formed complexes.
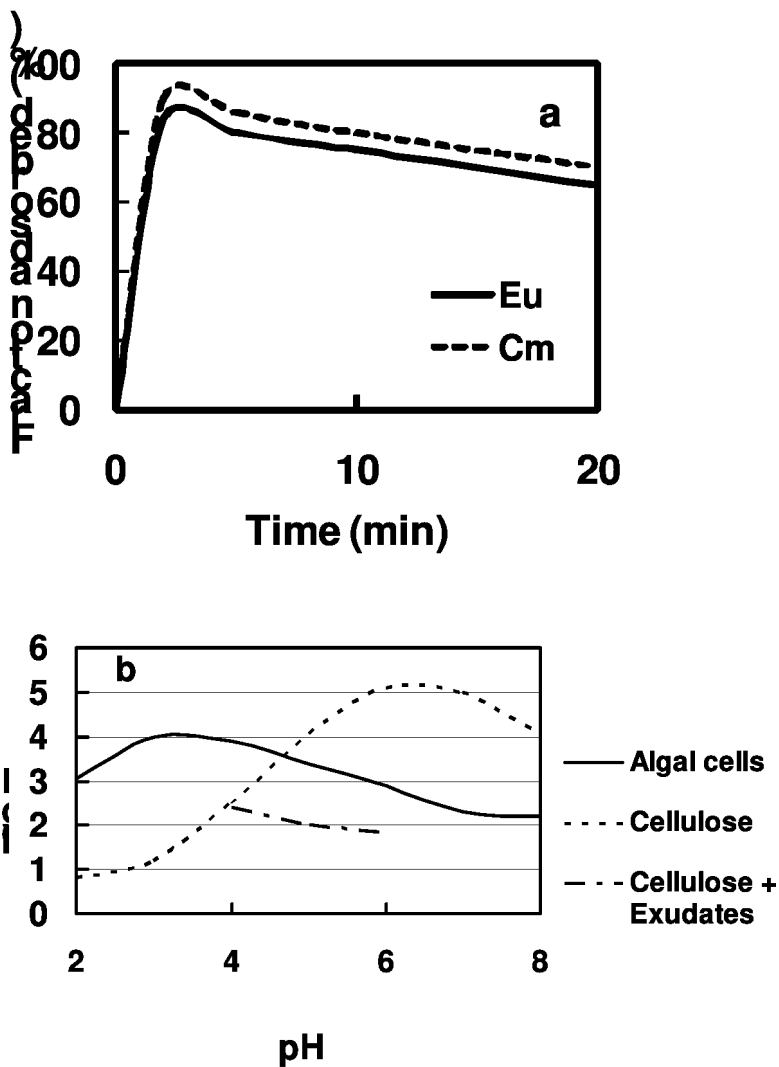
Figure 1. (a) Time dependent adsorbed fractions of Eu and Cm by algal cells at pH 5, and (b) logarithmic distribution coefficient of Cm by algal cells, cellulose, and cellulose in the exudates solution (13).
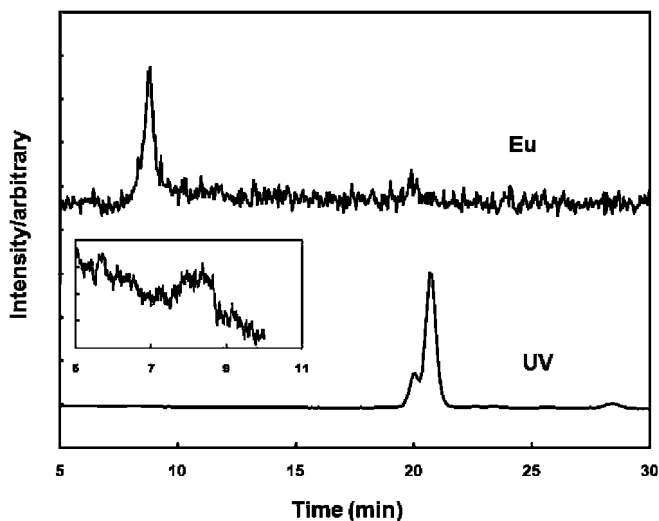
Figure 2. Profiles of Eu signals detected by ICP-MS and that of UV 280 nm absorbance detected by SEC-HPLC. UV 280 nm absorbance around 8 min is shown in inset.

Therefore, the exudates can have large impact on the environmental behavior of Eu and Cm, because the complex of trivalent actinides and lanthanides with exudates move much more widely with water flow.

Effects of DFO on the Adsorption of Eu(III), Th(IV), and Pu(IV) on Bacteria

As mentioned above, exudates from microorganisms reduce the sorption of Cm(III) and Eu(III) by microorganisms. Naturally occurring chelating substances also have the potential to reduce the sorption of actinides and lanthanides by forming complexes in the environment. Siderophores, produced by microorganisms, access insoluble cations and form complexes not only with Fe but also with actinides, causing their solubility to increase (*17*). Yoshida et al. (*14*, *15*) have studied the effects of desferrioxamine (DFO) B on the sorption of trivalent and tetravalent lanthanides and actinides by soil bacteria of *P. fluorescens* and *B. subtilis*.

The sorption density of Pu(IV) and Th(IV) on the both bacterial cells, and Fe(III) and Eu(III) on *P. fluorescens* in the presence of DFO are shown in Fig. 3 as a function of the stability constants of the metal-DFO complexes (Pu(IV) (log K = 30.8) (*18*), Fe(III) (log K = 30.6) (*19*), Th(IV) (log K = 26.6) (*20*), and Eu(III) (log K = 15) (*21*). Adsorption density of Eu(III), Th(IV), Fe(III), and Pu(IV) on the both bacterial cells decreased with increasing of the stability constant of the DFO complexes. Sorption of metals ion at pH 4 from approximately 50 to 15 μM g^{-1} with a increase of log K from 15 to 30, while that at pH 6 from approximately 40 to 6 μM g^{-1}. On the contrary, adsorption of DFO on both species was negligible at 3 hours after contact of the 1:1 Th(IV)-DFO complex with *P. fluorescens* or *B. subtilis* cells at pH 5.5. No DFO was sorbed on *P. fluorescens* cells from Eu(III)-

DFO complexes. These results indicate that Th(IV), Pu(IV), and Eu(III) were dissociated from DFO by the contact with cells, after which the metal ions are sorbed.

Adsorption of Eu(III) cation on *P. fluorescens* cells does not change significantly at pH 3 – 8 (*8, 22*), indicating that the affinity of *P. fluorescens* cell surfaces with metal cations is not changed significantly at these pHs. These facts indicate that ligand exchange reaction predominates the adsorption of the complexes of trivalent actinides and lanthanides with DFO by the bacterial cells.

Effect of DFO on the Adsorption of Rare Earth Elements on *P. fluorescens* –Anomaly of Ce Adsorption-

The effect of DFO on the adsorption of REEs (La, Ce, Pr, Nd, Sm, Eu, Gd, Tb, Dy, Ho, and Er) was examined by using cells of *P. fluorescens*. The percent fractions of adsorbed REEs by the cells determined after 30 minutes' contact with 1.0 mg dm^{-3} of each REE and 0.5 mmol dm^{-3} DFO decreased roughly along with the atomic number except Ce (Fig. 4). The percent fraction adsorbed of Ce was significantly lower than those of the neighboring REEs, La(III) and Pr(III). If Ce is present as Ce(III) in the solution, Ce anomaly should not observed. Because, the stability constant of the Ce(III)-DFO complex is expected to be intermediate or comparable to that of the La(III)-DFO and Pr(III)-DFO complexes. XANES study showed that the oxidation state of Ce in the DFO complex was tetravalent (*14*). The anomalously in lower Ce adsorption was due to the higher stability of the Ce(IV)-DFO complex than that of the Ce(III)-DFO complex.
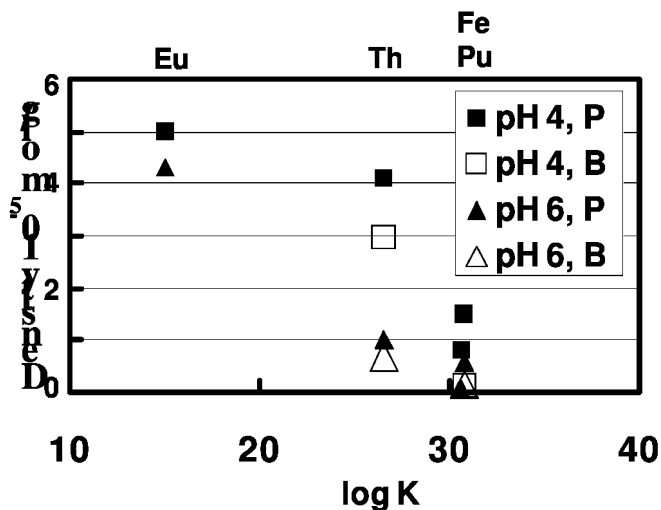
Figure 3. Sorption density of Th(IV) and Pu(IV) on P. fluorescens and B. subtilis in the presence of DFO as a function of a function of the stability constants of the metal-DFO complexes. Initial concentrations of Fe(III), Eu(III), Th(IV), Pu(IV), and DFO were 20 mM. P indicates P. fluorescens, and B, B. subtilis. Data are plotted based on refs. (17).
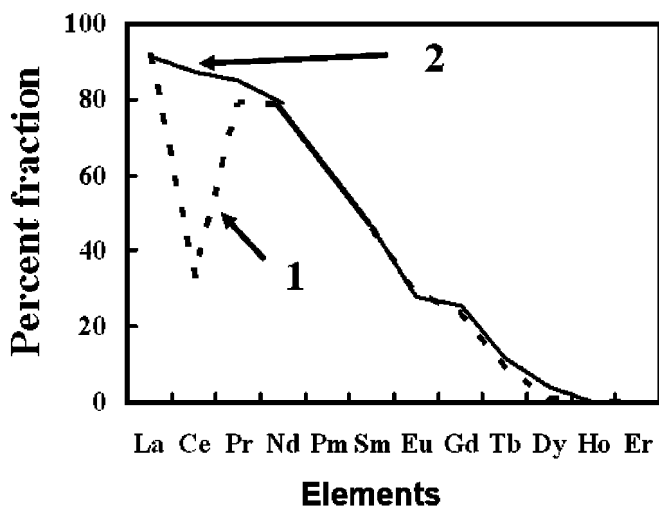
Figure 4. Percent fraction adsorbed of REEs complexed with DFO after exposure to P. fluorescens cells. 1: without hydroxylammonium and 2: with hydroxylammonium. Data modified after (14).

By adding hydroxylammonium, which is a reducing reagent, the Ce anomaly disappeared. The distribution of trivalent REEs between water and particles shows a gradual variation along with their atomic number because of the lanthanide contraction. Cerium is the only REE with tetravalent oxidation state at ambient aquatic conditions (*23*). The spontaneous oxidation of Ce in the DFO complex is due to the extremely large ratio in the stability between Ce(IV)-DFO and Ce(III)-DFO (*15*). The REE patterns for environmental waters often show a lower abundance of Ce compared with the neighboring REEs, which is called the negative Ce anomaly, resulting from the higher tendency of Ce(IV) in adsorption on particles than trivalent REEs (*14*). Our results indicated that DFO of siderophore can contribute to a positive Ce anomaly in environmental waters.

Biodegradation of Organic Acids

Effects of metals on the biodegradability of organic substances have been widely examined. Most investigations focused on the organic substances with a high chelating ability, such as NTA and EDTA (*24*, *25*). However, organic substances with a low chelating ability are rarely focused. Organic substances, such as lactic acid and ascorbic acid with relatively low chelating abilities with REEs are reported to affect their uptake by plants (*26*). We have studied the effects of Eu(III) on the degradation of malic acid by *Pseudomonas fluorescens*. For comparison the effects of Eu(III) on the degradation of citric acid of high chelating reagent were examined.

Biodegradation of Citric and Malic Acids with Eu(III)

The medium containing 1×10^{-3} mol L^{-1} of citric acid and 1.5×10^{-4} mol L^{-1} $EuCl_3$ or 1×10^{-2} mol L^{-1} malic acid and 1.0×10^{-4} mol L^{-1} $EuCl_3$ was contacted with *P. fluorescens* at 30 ± 1 °C for 240 h. The culture media contained citric acid or malic acid as a sole carbon source. The withdrawn suspensions were filtered through a 0.20 μm membrane filter, and the concentration of citric acid, malic acid, and Eu(III) in the filtrate was determined. The concentration of Eu(III) was measured by inductively-coupled plasma-atomic emission spectroscopy (ICP-AES) (Shimadzu ICPS-7000, Shimadzu Corporation, Kyoto, Japan), and the concentration of citric acid and malic acid was determined by HPLCMS using an organic acid column (Waters, P/N 023694).

Europium(III) showed different effects on the biodegradation behavior of malic acid and citric acid by *P. fluorescens*. The concentration of citric acid decreased with time until it reached that of Eu(III) in each medium (Fig. 5). Slower decreasing rates were observed in the media with Eu(III) than in control medium containing no Eu(III), while almost no change was observed in the Eu(III) concentration (*27*). These results show a 1:1 Eu(III)-citric acid complex is recalcitrant to degradation by *P. fluorescens*.

Attempts have been made to elucidate the factors which determine the degradability of a particular metal-organic acid complex. Klüner et al. showed that the biodegradability of metal-EDTA complexes by certain bacteria is not completely in good accordance with their stability (*25*). Firestone and Tiedje suggested that the structure of complexes determines the biodegradability of NTA (*24*). Joshi-Tope and Francis also claimed that the biodegradability of metal-citric acid complexes by *P. fluorescens* depends on the structure of the complex, showing that mononuclear bidentate complexes are readily degraded, whereas mononuclear tridentate, binuclear, and polynuclear complexes are recalcitrant (*28*). Unfortunately, the reason for the recalcitrancy of Eu(III)-citrate complex was not clarified so far.

The concentration of malic acid decreased with increasing time in the medium, and attained to be almost 0 mol L^{-1} at 180 h after exposure (*29*). The Eu(III) concentration in the medium did not change despite the complete degradation of malic acid in the media. Time course of the absorption intensity of malic acid and pyruvic acid in the malic acid medium was measured by organic acid column (Waters, P/N 023694) with a photodiode array at 200–400 nm after exposure to *P. fluorescens* (Fig. 6). Malic acid was degraded within 100 h in the absence of Eu(III), and pyruvic acid was generated and degraded within 100 h. On the contarary, pyruvic acid was present up to 250 h after exposure, even though malic acid was degraded within 100 h in the presence of Eu(III). Since the solubility of cationic species of Eu(III) is very low in neutral pH solution, Eu(III) should be complexed with some organic materials in the solution. Pyruvic acid is one of the host to dissolve Eu(III) in the solution by forming complex.

These findings strongly suggest that Eu(III) changes its chemical species during degradation of organic materials of weak chelating reagents by bacteria.
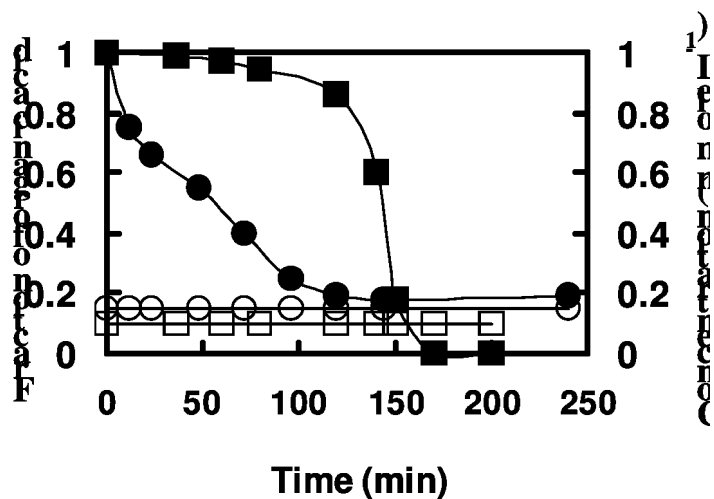
Figure 5. Time courses of fraction of citric (●)and malic (■) acids present in the solution after exposure to the solution containing organic acid and Eu(III) (30). The concentrations of Eu in citric (○) and malic (□) acids are shown.
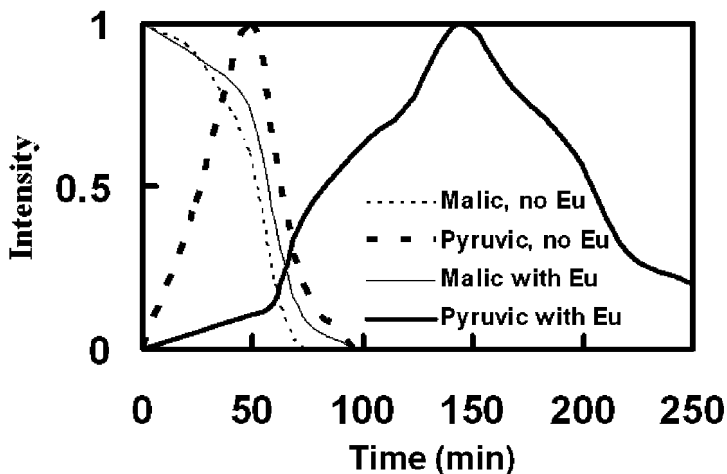
Figure 6. Time course of the absorption intensity of malic acid and pyruvic acid in the malic acid medium detected byorganic acid column after exposure to P. fluorescens (29). The intensity is normalized by the highest intensity in each profile.

Effects of Organic Acids on Bioreduction of U(VI)

Uranium, one of the actinides, have a number of oxidation states in a solution, and in higher oxidation states of +5 and +6, they form oxygenated species, UO^+ and UO_2^{2+}, respectively. Chemical properties of uranium considerably depend on their oxidation states (*30*). For that reason, it is important to elucidate the redox properties of the actinides to estimate their mobility in the environment. The reduction of UO_2^{2+} to UO_2^+ in the presence of organic acid has been studied polarographically (*31*). These results suggest that organic acids affect the bioreduction. Ganesh et al. (*32*) examined kinetics of U(VI) reduction by *Desulfovibrio desulfuricans* and *Shewanella alga* in the presence of acetate, malonate, oxalate, and citrate. In their study, the different effects of the complexation were observed in the reduction by the two bacterial species. Haas and Northup (*33*) have investigated the reductive precipitation rate of U(VI) by *Shewanella putrefaciens* in the presence of various organic acid and observed that the rates were correlated with stability constans of 1:1 aqueous U(VI)-organic complexes. However, we have limited knowledge of bioreduction of U(VI) in the presence of organic acids. We investigated the redox behavior of UO_2^{2+} in organic acid solutions by electrochemically (*34*) and biologically (*35*).

Electrochemical Reduction of U(VI) with Organic Acids

We investigated the redox behavior of UO_2^{2+} in organic acid solutions of oxalic [$(COOH)_2$], malonic ($HOOCCH_2COOH$), succinic [$HOOC(CH_2)_2COOH$], adipic [$HOOC(CH_2)_4COOH$], L-malic [$HOOCCH(OH)CH_2COOH$], and L-tartaric acid [$HOOCCH(OH)CH(OH)COOH$] by cyclic voltammetry to understand the effect of organic complex formation on the redox behavior in terms of the stability constants of the complexes. Cyclic voltammograms were measured under the nitrogen atmosphere using an ALS/CHI Electrocemical Analyzer Model 600C (CH Instruments, Inc., USA). A three-electrode system composed of a glassy carbon working electrode (surface areas $=12.56$ mm^2), a Pt counter electrode, and an Ag-AgCl/saturated KCl reference electrode was utilized.

Figure 7 shows a plot of the peak potentials of the cathodic peak at v of 0.025 V s^{-1} vs. logarithmic stability constant of the 1:1 complex of U(VI) with organic acid, $\beta^{VI}_{1,1}$ (*34*). The peak potentials decreased linearly with an increase in the $\beta^{VI}_{1,1}$. These results show that UO_2^{2+} is more difficult to be reduced by complexation in the presence of organic acid which forms stronger complex with UO_2^{2+}. Essentially, the redox potential of UO_2^{2+}/UO_2^+ in the presence of organic acid depends on the ratio of complex formation constants of UO_2^{2+} and UO_2^+ with organic acids (β^V and β^{VI}), and we need to plot the redox potentials against a log (β^V/β^{VI}). We obtained a good linear relationship between the peak potentials and the log $\beta^{VI}_{1,1}$. The stability constants of UO_2^+ complexes are generally much smaller than those of UO_2^{2+} complexes (*36*), and the effect of UO_2^+ complexes formation on the redox potential is small comparing to that of UO_2^{2+} complexes. This tendency is useful to predict the potential UO_2^{2+} may be reduced in the presence of an organic acid whose stability constant is already known.
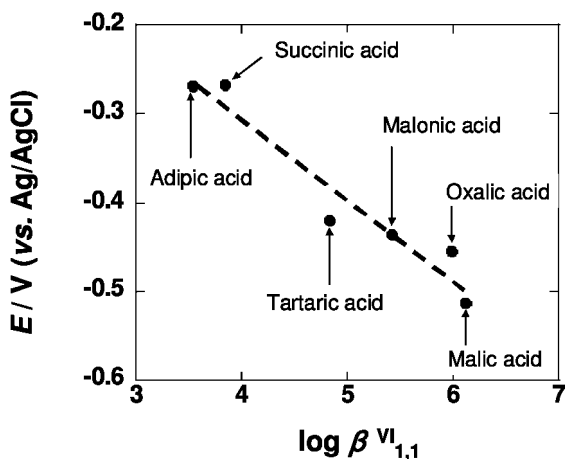
Figure 7. The plots of the cathodic peak potentials at the scan velocity of 0.025 V s⁻¹ vs. the log βⱽᴵ₁, ₁ of the complex of UVI) with organic acids (34).

Bioreduction of U(VI) in the Presence of Organic Acids

Batch experiments were performed using four kinds of media to evaluate the influence of strong complexation reagents on the bioreduction on U(VI). The one contained sodium lactate as an electron donor, 1 mM $UO_2(NO_3)_2$ as an electron accepter. The other contained additionally 100 mM organic acid (citric acid, NTA or EDTA) as strong complexation reagnts (citrate, NTA or EDTA media, respectively). Ultraviolet-visible spectra, total dissolved U concentrations, and pH of the solutions were measured. Concentrations of dissolved U(IV) were determined from UV-VIS spectra obtained by using a UV-VIS spectrophotometer (UV-2500PC, Shimazu Co, Kyoto, Japan). Uranium(IV) has a sharp absorption peak between 600 and 700 nm whereas U(VI) does not in the area. The precipitates formed in the medium were collected at the end of the batch experiments by centrifugation and analyzed by U L_{III}-edge ($\approx$17166 eV) X-ray absorption near-edge structure (XANES) spectroscopy.

Figures 8a and 8b show, respectively, the UV-VIS spectra of control (a) and citrate media (b). At initial state (0 h), an absorption peak attributable to U(VI) was observed between 400 and 500 nm in the both media. The broad absorption band increased up to 4 h and then decreased. Finally, that disappeared and the solution was colorless after 21 h incubation. The precipitates were observed in control medium. Oxidation state of U in the precipitates was attributed to IV by XANES, indicating formation of UO_2. In the citric medium, the peak attributable to U(VI) decreased and four main peaks attributable to U(IV) appeared between 400 and 700 nm (Fig. 8b). In the NTA and EDTA media, descent of the peak of U(VI) and ascent of four main peaks attributable to U(IV) were observed as like in the citrate medium. Concentrations of U(IV) in the citrate, NTA, and EDTA media were estimated by the absorption peak at 600-700 nm and the time courses of the dissolved U(IV) fractions are illustrated in Fig. 9. Fractions of U(IV) in the

NTA and EDTA media increased rapidly with time and reached more than 97% after 8 h incubation. On the other hand, fraction of U(IV) in the citrate medium increased gradually and reached about 67% after 50 h incubation. The rates in the NTA and EDTA media were 5 times faster than that in the citrate medium.
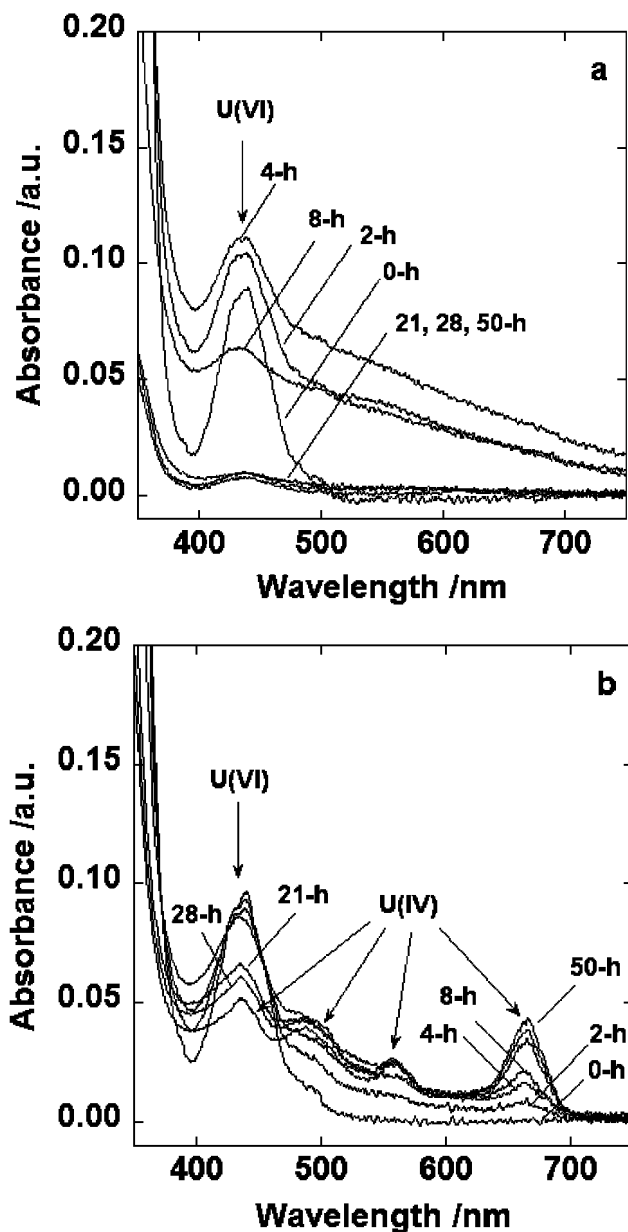
Figure 8. UV-VIS spectra of (a) control and (b) citrate media (35).
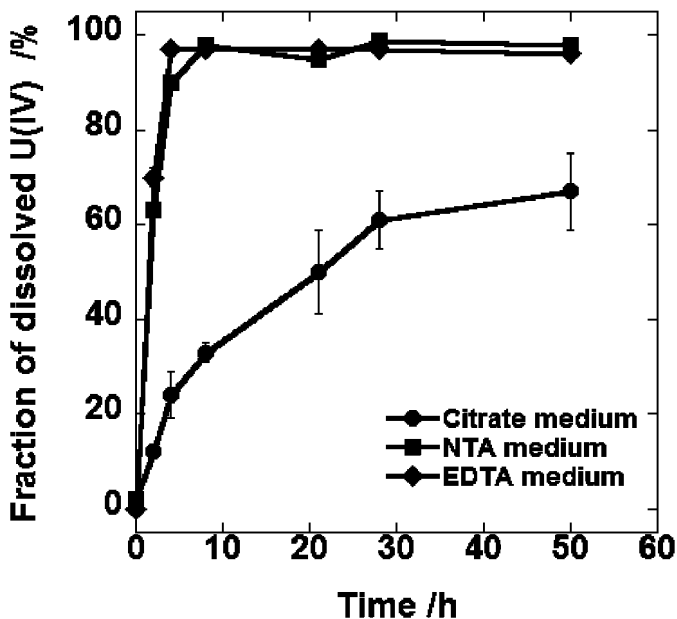
Figure 9. Concentrations of U(IV) in the citrate, NTA, and EDTA media (35).

The stability constants of 1:1 U(VI)-citrate, -NTA and EDTA are, respectively, 8.96, 9.56 and 13.7 (*37*, *38*). The citrate complex is the weakest and, therefore, a faster reduction rate would be expected, but it was the slowest in the present study. Previous work examined the reduction behavior of U(VI)-citrate complexes by an electrochemical method indicated that the reduction of U(VI) is more difficult by polymerization of U(VI) with citric acid (*34*). Uranium(VI) forms polynuclear complexes with citrate at neutral pH, e.g. $(UO_2)_3Cit_3^{3-}$, $(UO_2)_6Cit_6(OH)_{10}^{16-}$ (*39*, *40*), while it forms mononuclear complex with NTA and EDTA ((*40*, *41*)). These acts suggest that formation of polynuclear U(VI)-citrate complexes is one of the reasons for the lower reduction rate in the citrate media than those in the NTA and EDTA media. It has been reported that bioavailability of metal-citrate complexes for biodegradation depends on the structure of the complexes rather than the stability constants (*28*, *42*). In the reduction of U(VI)-organic complexes by *S. putrefaciens*, the geometries of the complexes may be one of the key factors of bioavailability.

Conclusions

The effects of organic acids on the adsorption, degradation, and reduction of the complexes of actinides with organic acids have been studied by laboratory experiments. We found that organic materials secreted from a algal cells reduced the adsorption of trivalent actinides and lanthanides. A siderophore caused Ce anomaly in the adsorption of all REE elements on bacterial cells, that is opposite anomaly observed in nature. Presence of trivalent Eu inhibits the degradation of citric and malic acids. Citric acids delay the electrochemical and biological

reduction of U(VI) to U(IV). These results indicate that organic acids affect on the biotransformation actinides in the environments.

Acknowledgments

References

1. Ticknor, K. V. *Radiochim. Acta* **1994**, *64*, 229.
2. Waite, T. D.; Davis, J. A.; Payne, T. E.; Waychunas, G. A.; Xu, N. *Geochim. Cosmochim. Acta* **1994**, *58*, 5465.
3. Sylwester, E. R.; Hudson, E. A.; Allen, P. G. *Geochim. Cosmochim. Acta* **2000**, *64*, 2431.
4. Dent, A. J.; Ramsay, J. D.; Swanton, S. W. *J. Colloid Interface Sci.* **1992**, *150*, 45.
5. Francis, A. J.; Gillow, J. B.; Dodge, C. J.; Harris, R.; Beveridge, T. J.; Papenguth, H. W. *Radiochim. Acta* **2004**, *92*, 481.
6. Fowle, D. A.; Fein, J. B.; Martin, A. M. *Sci. Technol.* **2000**, *34*, 3737.
7. Haas, J. H.; Dichristina, T. J.; Wade, R., Jr. *Chem. Geol.* **2001**, *180*, 33–54.
8. Suzuki, Y.; Nankawa, T.; Yoshida, T.; Ozaki, T.; Ohnuki, T.; Francis, A. J.; Tsushima, S.; Enokida, Y.; Yamamoto, I. *J. Nucl. Radiochem. Sci.*, **2005**, *6*, 91−93.
9. Brantley, S. L.; Liermann, L.; Bau, M. *Geomicrobiol. J.* **2001**, *18*, 37.
10. Panak, P. J.; Nitsche, H. *Radiochim. Acta* **2001**, *89*, 499.
11. John, S. G.; Ruggiero, C. E.; Hersman, L. E.; Tung, C. S.; Neu, M. P. *Environ. Sci. Technol.* **2001**, *35*, 2942.
12. McCarthy, J. F.; Sanford, W. E.; Stafford, P. L. *Environ. Sci. Technol.* **1998**, *32*, 3901.
13. Ozaki, T.; Kimura, T.; Ohnuki, T.; Yoshida, Z.; Francis, A. J. Association mechanisms of europium(III) and curium(III) with *Chlorella vulgaris*. *Environ. Toxicol. Chem.* **2003**, *22*, 273–278.
14. Yoshida, T.; Ozaki, T.; Ohnuki, T.; Francis, A. J. *Radiochim. Acta* **2004**, *92*, 749–753.
15. Yoshida, T.; Ozaki, T.; Ohnuki, T.; Francis, A. J. *Chem. Geol.* **2004**, *212*, 239–246.
16. Malavolta, M.; Piacenza, F.; Costarelli, L.; Giacconi, R.; Muti, E.; Cipriano, C.; Speziab, S.; Mocchegiania, E. *J. Anal. Atom Spectrom.* **2007**, *22*, 1193–1198.
17. Brainard, J. R.; Strietelmeier, B. A.; Smith, P. H.; Langston-Unkefer, P. J.; Barr, M. E.; Ryan, R. R. *Radiochim. Acta* **1992**, *58-59*, 357.
18. Jarvis, N. V.; Hancock, R. D. *Inorg. Chim. Acta* **1991**, *182*, 229.
19. Schwarzenbach, G.; Schwarzenbach, K. *Helv. Chim. Acta* **1963**, *46*, 1390.
20. Whisenhunt, D. W.; Neu, M. P.; Hou, Z.; Xu, J.; Hoffman, D. C.; Raymond, K. N. *Inorg. Chem.* **1996**, *35*, 4128.

21. Brainard, J. R.; Strietelmeier, B. A.; Smith, P. H.; Langston-Unkefer, P. J.; Barr, M. E.; Ryan, R. R. *Radiochim. Acta* **1992**, *58/59*, 357.

22. Yoshida, T.; Ozaki, T.; Ohnuki, T.; Francis, A. J. *Eu(III) Adsorption by Pseudomonas fluorescens in the Presence of Organic Ligands*. Proceedings of the International Symposium on Radioecology and Environmental Dosimetry; Inaba, J., Tsukada, H., Takeda, A., Eds.; Institute of Environmental Sciences: Aomori, Japan, 2003, p 296.

23. Shlokovitz, E. R.; Landing, W. L.; Lewis, B. L. *Geochim. Cosmochim. Acta* **1994**, *58*, 1567–1579.

24. Firestone, M. K.; Tiedje, J. M. *Appl. Microbiol.* **1975**, *29*, 758–764.

25. Kluner, T.; Hempel, D. C.; Nörtemann, B. *Appl. Microbiol. Biotechnol.* **1998**, *49*, 194–201.

26. Ozaki, T.; Ambe, S.; Enomoto, S.; Minai, Y.; Yoshida, S.; Makide, Y. *Radiochim. Acta* **2002**, *90*, 303–307.

27. Suzuki, Y.; Nankawa, T.; Yoshida, T.; Ozaki, T.; Ohnuki, T.; Francis, A. J.; Tsushima, S.; Enokida, Y.; Yamamoto, I. Biodegradation of Eu(III)-citrate complexes by *Pseudomonas fluorescens*. *J. Radioanal. Nucl. Chem.* **2005**, *266*, 199–204.

28. Joshi-Tope, G.; Francis, A. J. *J. Bacteriol.* **1995**, *177*, 1989–1993.

29. Nankawa, T.; Suzuki, Y.; Ozaki, T.; Ohnuki, T.; Francis, A. J. Degradation of Eu(III)-malic acid complexes by *Pseudomonas fluorescens*. *J. Alloy Compd.* **2006**, 408–412, 1329–1333.

30. Silva, R. J.; Nitsche, H. Actinide environmental chemistry. *Radiochim. Acta* **1995**, *70−71*, 377.

31. Koltoff, I. M.; Harris, W. E. The polarograhy of uranium. II. Polarography in strongly acid solution. *J. Am. Chem. Soc.* **1946**, *68*, 1175.

32. Ganesh, R; Robinson, K. G.; Reed, G. D.; Sayler, G. S. Reduction of hexavalent uranium from organic complexes by sulfate- and iron-reducing bacteria. *Appl. Environ. Microbiol.* **1997**, *63*, 4385–4391.

33. Hass, J. R.; Northup, A. Effects of aqueous complexation on reductive precipitation of uranium by *Shewanella putrefaciens*. *Geochem. Trans.* **2004**, *5*, 41–48.

34. Suzuki, Y.; Nankawa, T.; Ozaki, T.; Ohnuki, T.; Francis, A. J.; Enokida, Y.; Yamamoto, I. Electrochemical studies on uranium in the presence of organic acids. *J. Nucl. Sci. Technol.* **2007**, *44*, 1227–1232.

35. Suzuki, Y.; Tanaka, K.; Kozai, N.; Ohnuki, T. Effects of citrate, NTA, and EDTA on the reduction of U(VI) by *Shewanella putrefaciens*. *Geomicrobiol. J.* **2010**, *27*, 245−250.

36. Smith, R. M.; Martell, E. *Critical Stability Constants*; Plenum Press: New York, 1989; Volume 6.

37. Hummel, W.; Anderegg, G.; Puigdomench, I.; Rao ,L.; Tochiyama, O. Chemical Thermodynamics of Compounds and Complexes of U, Np, Pu, Am, Tc, Se, Ni, and Zr with Selected Organic Ligands. In *Chemical Thermodynamics*; Organisation for Economic Co-operation and Development: Paris, 2005; Volume 9.

38. Smith, R. M.; Martell, A. E.; Motekaitis, R. J. *NIST Standard Reference Database 46*; National Institute of Standards and Technology (NIST): Gaithersburg, MD, 2003.

39. Rajan, K. S.; Martell, A. E. Equilibrim studies of uranyl complexes. III. Interaction of uranyl ion with citric acid. *Inorg. Chem.* **1965**, *21*, 462–469.

40. Pasilis, S. P.; Pemberton, J. E. Speciation and coordination chemistry of uranyl(VI)-citrate complexes in aqueous solution. *Inorg. Chem.* **2003**, *42*, 6793–6800.

41. Stefano, C. D.; Gianguzza, A.; Milea, D.; Pettignano, A.; Sammartano, S. Sequestering ability of polyaminopolydarboxylic ligands towards dioxouranium(VI) cation. *J. Alloys Compd.* **2006**, *424*, 93–104.

42. Francis, A. J.; Dodge, C. J.; Gillow, J. B. Biodegradation of metal citrate complexes and implications for toxic-metal mobility. *Nature* **1992**, *356*, 140–142.

Chapter 26

The Role of Dissolved Hydrogen on the Corrosion/Dissolution of Spent Nuclear Fuel

M. E. Broczkowski, D. Zagidulin, and D. W. Shoesmith*

The University of Western Ontario, London Ontario, Canada N6A 5B7
***dwshoesm@uwo.ca**

The literature on nuclear fuel dissolution and radionuclide release studies in aqueous solutions containing dissolved hydrogen has been reviewed. These studies include investigations with spent PWR and MOX fuels, fuel specimens doped with alpha emitters to mimic "aged" fuels, SIMFUELs fabricated to simulate spent fuel properties, and unirradiated uranium dioxide pellets and powders. In all these studies, dissolved hydrogen was shown to suppress fuel corrosion and in spent fuel studies to suppress radionuclide release. A number of mechanisms have been either demonstrated or proposed to explain these effects, all of which involve the activation of hydrogen to produce the strongly reducing H· radical, which scavenges radiolytic oxidants and suppresses fuel oxidation and dissolution (i.e., corrosion). Both gamma and alpha radiation have been shown to produce H· surface species. With gamma radiation this could involve the absorption of gamma energy by the solid leading to water decomposition to OH· and H· radicals, with the OH· radical subsequently reacting with hydrogen to yield an additional H·. This latter radical then suppresses fuel oxidation and scavenges radiolytic oxidants. With alpha radiation, the need to neutralize oxygen vacancies generated by recoil events can initiate the same process by decomposing water. In the absence of radiation fields activation can occur on the surface of noble metal (epsilon) particles. Since these particles are galvanically-coupled to the fuel matrix they act as anodes for hydrogen oxidation (which proceeds through surface H· species) and forces the UO_2 to adopt a low potential. Also, there is some evidence to suggest that H_2 can be activated on

the UO_2 surface in the presence of hydrogen peroxide, but the process appears to be inefficient.

Depending on the radiation fields present and the number density of epsilon particles, complete suppression of fuel corrosion appears possible even for hydrogen pressures as low as 0.1 to 1 bar. Since the corrosion of steel liners within failed waste containers could produce hydrogen pressures up to 50 bar, fuel corrosion could be completely suppressed under the long-term conditions expected in sealed repositories.

Introduction

The selected approach for long-term management of used nuclear fuel in Canada is Adaptive Phased Management (*1*). This approach includes centralized containment and isolation of the used fuel in a deep geological repository in a suitable rock formation. The repository concept is based on multiple barriers, and provides reasonable assurance in the long-term containment and isolation of the fuel bundles. One of these barriers is the robust copper shell-steel lined container (*2–5*). However, it is judicious to assume containers will eventually fail, thereby, exposing the used fuel bundles to groundwater. Since the used fuel contains the residual radioactivity, its behaviour in contact with groundwater is important for long-term safety assurance.

The release of > 90% of radionuclides contained within the used nuclear fuel will be governed by the corrosion/dissolution of the fuel (UO_2) matrix. The rate of this process will be related to, but not necessarily directly proportional to, the solubility of uranium in the groundwater contacting the fuel. At repository depths, groundwaters are inevitably oxygen-free. Furthermore, any oxygen introduced during repository construction and operation prior to sealing will be rapidly consumed by mineral and biochemical reactions in the surrounding clays and by minor corrosion of the copper container (*2–5*).

If anoxic conditions were maintained in the repository, the solubility of the UO_2 waste form would be in the region of $\sim 10^{-9.5}$ mol/L, which is very low (*6–13*). However, the radiolysis of water due to the radiation fields in the fuel will establish oxidizing conditions at the fuel surface. Under oxidizing conditions the solubility of uranium (as UO_2^{2+}) increases by many orders of magnitude (*7*). Thus, the rate of fuel dissolution (which is a corrosion reaction when oxidants are consumed to produce soluble UO_2^{2+}) will depend on the redox condition (*14–16*), which will be established by the radiation fields associated with the fuel and how they decay with time. This is illustrated in Figure 1, which shows the evolution of radiation dose rates with time for a typical CANDU fuel bundle. This evolution in solution redox conditions makes the fuel corrosion process (and, hence, the radionuclide release process) very dependent on the time to failure of the waste container.
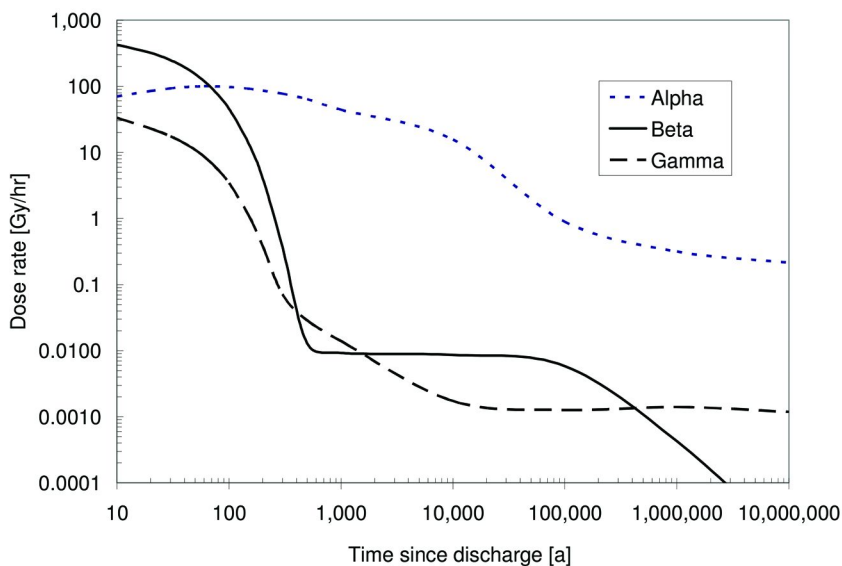
Figure 1. Alpha, beta, and gamma radiation dose rates calculated as a function of time for a layer of water in contact with a CANDU fuel bundle with a burnup of 220 MWh/kgU

In this report the influence of redox conditions on fuel corrosion/dissolution inside a failed waste container will be discussed with a special emphasis on the effect of dissolved H_2. Significant pressures of H_2 are expected to develop as the steel liner within the container corrodes, since its escape through the surrounding compacted clay and host rock will be very slow.

The Dependence of the Fuel Corrosion/Dissoluton Rate on Redox Conditions

The dependence of fuel corrosion/dissolution rate on redox conditions is now well established based on electrochemical measurements (*14, 17–19*), measurements of corrosion rates (or rate constants) in the presence of oxidants (*20–27*) and dissolution/corrosion rate measurements in the presence of radiation fields (*16, 26, 28–34*).

Based on this data and additional electrochemical evidence (*35, 36*), the fuel behaviour can be specified as a function of redox conditions, see Figure 2. In this plot, the potential axis is the corrosion potential (E_{CORR}), which specifies the response of the fuel surface to the redox condition (E_h) in the exposure environment. (Although not shown here, a plot of measured and predicted fuel corrosion rates as a function of potential has also been determined (*14, 37*)). The vertical dashed line in Figure 2 (at -0.4V [vs SCE]) indicates the threshold for the onset of fuel corrosion. Descriptions of the experimental procedures used to establish this threshold have been described elsewhere (*35, 36, 38*). Above this potential there is the possibility of fuel corrosion at a rate controlled by

the concentration of radiolytically-produced oxidants. For potentials below this threshold, fuel dissolution, and hence the mobilization of radionuclides, can only occur by chemical dissolution of the UO_2 fuel (to yield soluble U^{IV}).

While the above studies establish the corrosion nature of the fuel dissolution/radionuclide release process and its dependence on redox conditions in the presence of radiolytically decomposed water, other processes occurring within a failed container would influence the redox conditions at the fuel surface.

The key reactions anticipated within a failed, groundwater-flooded container are illustrated in Figure 3.

Two corrosion fronts exists, one on the fuel surface driven by the radiolytic oxidants and a second one on the surface of the carbon steel liner sustained by reaction with water to produce Fe^{2+} and H_2. In this illustratin, H_2O_2 is taken to be the primary radiolytic oxidant driving fuel corrosion (39–41), although the production of O_2 via H_2O_2 decomposition would introduce a second oxidant.
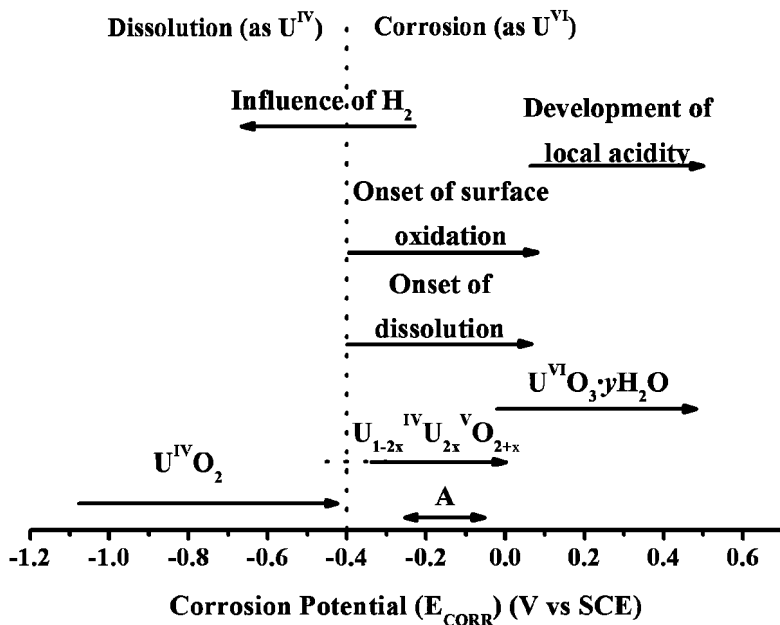
Figure 2. The composition of a UO₂ surface as a function of potential. The arrow A indicates the corrosion potential range predicted by a mixed potential model to describe fuel corrosion due to the alpha radiolysis of water inside a failed waste container (37). The upper limit of this range represents the expected E_{CORR} if the container fails soon after emplacement in the repository, and the lower limit represents the E_{CORR} predicted if the container fails after 10^6 years.
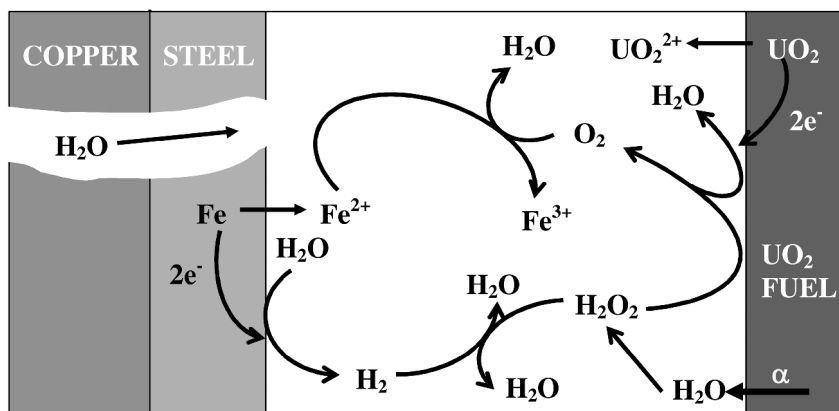
Figure 3. Illustration showing the key chemical and electrochemical reactions anticipated inside a groundwater flooded waste container.

The illustration in Figure 4 shows the differences in redox conditions established at these two fronts. The value of E_h is the solution redox condition in alpha radiolytically-decomposed water which will vary depending on radiation dose rate. The very positive value of E_h is an indication of the oxidizing potential of H_2O_2 which will control the redox condition at the fuel surface. Providing radiolytically-produced H_2O_2 does not reach the steel, redox conditions at this surface will be established by the water reduction process, for which the equilibrium potential is very low. Consequently, the corrosion processes on the two surfaces will occur at distinctly different E_{CORR} values as illustrated in Figure 4. E_{CORR} for the steel, $(E_{CORR})_{Fe}$, will be ≤ -800 mV under anoxic conditions (*42–45*) whereas E_{CORR} for the fuel, $(E_{CORR})_{UO2}$, will be > -400 mV if corrosion by radiolytic oxidants is occurring (Figure 2). This large separation introduces the possibility of a number of redox processes between the oxidants produced by radiolysis (H_2O_2), H_2O_2 decomposition (O_2), and fuel corrosion (UO_2^{2+}), and the potential reductants (Fe^{2+}, H_2) formed by steel corrosion. The simplified illustration in Figure 3 suggests the scavenging of oxidants will involve only a series of homogeneous reactions, but the studies to be described below will show this to be a major oversimplification in the case of H_2.

Under the anoxic conditions anticipated within a failed waste container, carbon steel or iron will react with water to produce Fe^{2+} and H_2, and the corrosion product magnetite (Fe_3O_4),

$$Fe + 2H_2O \rightarrow Fe^{2+} + H_2 + 2OH^- \tag{1}$$

$$3Fe + 4H_2O \rightarrow Fe_3O_4 + 4H_2 \tag{2}$$

Many studies on the influence of Fe and Fe corrosion products on fuel corrosion have been published (*37, 46–56*), and inevitably show that the presence of Fe suppresses corrosion and radionuclide release.
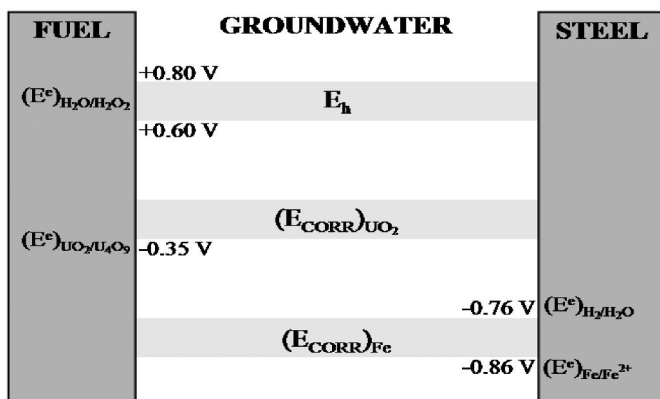
Figure 4. Illustration showing the two corrosion fronts existing within a failed, groundwater-flooded waste container, one on the fuel surface established by reaction with radiolytic oxidants and a second one on the steel surface established by reaction with water. The zone marked E_h indicates the redox condition expected due to the alpha radiolysis of water. The E_{CORR} zones indicate the range of corrosion potentials measured on fuel and steel electrodes.

It is not possible to separate the redox-controlling influences of Fe^{2+} and H_2 in experiments involving steel or iron and considerable effort has been expended in studying them separately. Ferrous ion is well known to regulate redox conditions in natural waters (*57*), and a number of direct attempts have been made to determine the influence of Fe^{2+} and Fe_3O_4, both experimentally (*52–56*) and via model calculations (*58–60*). The calculations of Jonsson et al. (*60*), based on experimentally determined rate constants, indicate that the consumption of H_2O_2 via the Fenton reaction

$$Fe^2 + H_2O_2 \rightarrow Fe^{3+} + OH^\bullet + OH^- \tag{3}$$

$$Fe^{2+} + OH^\bullet \rightarrow Fe^{3+} + OH^- \tag{4}$$

could suppress UO_2 dissolution by a factor of > 40.

However, there is a considerable amount of evidence that H_2 has a much larger effect on fuel dissolution than Fe^{2+}. Even relatively small amounts of dissolved H_2 can have a very major influence on fuel corrosion/dissolution, and hydrogen pressures of up to 5 MPa are expected to develop quickly within a failed container (*61, 62*). Consequently, this review will focus on the influence of H_2 on fuel corrosion/dissolution.

Influences of Hydrogen on Fuel Corrosion

A considerable database of information on the influence of H_2 has now been accumulated on a wide range of materials:

(a) spent fuels, in particular PWR and MOX fuels;

(b) fuel specimens doped with different quantities of α-emitters to simulate the much lower alpha radiation dose rates expected in spent fuel after long disposal times;

(c) SIMFUELS, which are unirradiated analogues of used fuel produced by doping UO_2 with a series of stable elements (Ba, Ce, La, Mo, Sr, Y, Rh, Pd, Ru, Nd, Zr) in proportions appropriate to simulate different degrees of reactor burn-up; and

(d) UO_2 pellets and powder, sometimes incorporating the noble metal Pd.

This information is described and discussed below.

Spent Fuels

The results of the latest experimental work carried out in a large European research project on spent fuel stability in the presence of H_2 (*63*) have recently been reported (*16*). The early studies in the European program, conducted on high burn-up spent fuel in the presence of powdered Fe and its corrosion products (*47*) showed that the release rates of all important radionuclides (Sr, Cs, Pu) decreased as the H_2 pressure, from Fe corrosion, in the experimental vessel increased to up to 2.8 bar over the 1,049 days of the experiment. Simultaneously, the dissolution of the UO_2 matrix, taken to be indicated by the rate of release of the Sr inventory in the fuel, appeared to slow down and eventually stop. While this study clearly demonstrated an effect of Fe corrosion on fuel dissolution and radionuclide release it did (could) not separate the influences of Fe^{2+} and H_2.

To avoid this ambiguity, a further 1,095 day static corrosion experiment was conducted in 5.0 mol/L NaCl under an overpressure of 3.2 bar of H_2 (*16*). In the early stages of this experiment, when the system was only Ar-purged, the Sr release rate, again used as an indicator of the matrix dissolution rate, was a factor of ~ 14 higher than after the H_2 pressure was eventually applied. This influence of H_2 persisted over the entire subsequent duration of the test during which the solution concentrations of the redox-sensitive radionuclides (Tc, Np, Pu) decreased. The Sr releases rates for this experiment (after H_2 addition) and the original experiment (with Fe powder present) were considerably lower than with only Ar-purging.

To determine whether the aqueous uranium was equilibrating with U^{VI} or U^{IV} solids, the analyzed uranium concentrations were compared to calculated solubilities for UO_2, and for U^{VI} solids that could feasibly form in the solution used. These calculations were made using the available thermodynamic data-set for U^{IV} and U^{VI} aqueous species and the solids UO_2, metaschoepite ($UO_3 \cdot 2H_2O$), and sodium diuranate ($NaU_2O_7 \cdot 6H_2O$)) (*9*, *64*, *65*). For the pressurized H_2 experiment, the measured solubilities were considerably lower than those calculated for U^{VI} solids and essentially coincided with the calculated UO_2 solubility.

For both experiments, analyzed O_2 levels in the reaction vessel were below the detection limit, and E_h values were as low as -500 mV (vs Ag/AgCl) compared to >200 mV when the atmosphere was Ar only. Since a considerable amount of radiolytic O_2 should have been produced at the radiation dose rates present in the fuel specimens, a very efficient scavenging of oxidants must have occurred. The

possibility that Fe corrosion by O_2 could account for this scavenging in the first experiment (*66*) was ruled out by XRD and EDX analyses of the iron corrosion products. Only magnetite (Fe_3O_4), and possibly a small amount of green rust, were observed. Magnetite is the expected corrosion product for the anoxic corrosion of iron/steel (*43, 44*) and the traces of green rust are an indication that only very low levels of O_2 could have been present (*45, 67*). For the amounts of O_2 calculated to be radiolytically-produced in this experiment, considerable amounts of Fe_2O_3 and α- FeOOH would be expected if the O_2 reacted with the iron (*68*). The only other available scavenger in both experiments would be H_2.

A leaching experiment with MOX fuel with a high average burn-up of 48 MWd/KgU (in 10 mM NaCl + 2mM HCO_3^-) showed that the dissolution of even highly α-active fuel could be completely suppressed with a sufficiently high H_2 pressure (53 bar, equivalent to a dissolved H_2 concentration of 4.3×10^{-2} mol/L) (*16*). No dissolution rate could be calculated since, once the preoxidized layer present on commencement of the experiment had dissolved, no further U release was observed over the 494 days of the experiment. Again, the U concentration approached the solubility of the unoxidized UO_2 matrix, a value of 3×10^{-10} mol/L finally being achieved. The redox-sensitive radionuclides initially released appeared to be reduced and reprecipitated. That no oxide dissolution occurred was strongly supported by the Cs release behaviour. Once the initial Cs release was over (presumably from exposed grain boundaries), no further release was observed over the final 300 days of the experiment.
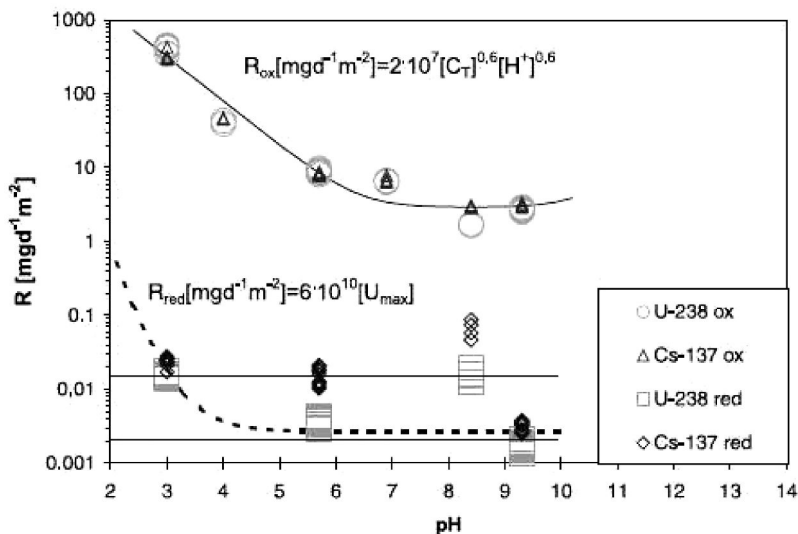
Figure 5. Used fuel dissolution rates as a function of pH for oxidizing and reducing conditions. Oxidizing conditions: solution purged with 20% O_2 /0.03% CO_2 / 80% Ar; Reducing conditions, solution bubbled with H_2 containing 0.03% CO_2 over a Pt foil (69). The two horizontal lines are extrapolations of electrochemically measured corrosion rates to -0.35 V and -0.45 V (vs. SCE) (38).

Such high concentrations of dissolved H_2 are not essential for the suppression of spent fuel corrosion rates. In a flow-through experiment, a decrease in dissolution rate of 3 to 4 orders of magnitude was achieved in the presence of only 8 x 10^{-4} mol/L of dissolved H_2 (equivalent to a H_2 pressure of about 1 bar) compared to rates measured under oxidizing conditions, Figure 5 (69). By performing a series of experiments as a function of pH (3 to ~ 9.5), it was demonstrated that the rates under oxidizing conditions exhibited the pH dependence expected from controlled laboratory experiments with UO_2 (14, 23, 70). By contrast, in the H_2-purged experiments the lack of a pH dependence at low pH (< 6) and the extremely low rates are consistent with a chemical dissolution process. In support of this claim, the measured spent fuel dissolution rates under reducing conditions were shown to be similar to those predicted for potentials around the –400 mV (vs SCE) threshold (Figure 2) below which only chemical dissolution is possible (38).

Many of these observations are consistently observed in other published studies on spent fuel in the presence of H_2 (54, 71–75), and the key observations can be summarized.

(I) Despite short-term ambiguities introduced by the presence of preoxidized layers, U concentrations decrease to very low levels with time. The time taken to reach these low levels depends largely on the initial condition of the fuel surface, and how it is treated, either prior to, or during, the initial stages of the experiment.

(II) These low U levels are well below the solubilities of U^{VI} solids which could feasibly have deposited in the leaching environment. Comparison of measured U levels to calculated solubilities for UO_2 shows this to be the only solid that could equilibrate with the solution at these concentrations.

(III) The concentrations of radiolytically-produced O_2 is generally around or below the detection limit of 10^{-8} mol/L, and there is considerable evidence to show these low concentrations are maintained by reaction with H_2 to produce water. At the low temperatures generally employed in spent fuel experiments a reaction between O_2 and H_2 would not be expected to occur in the absence of catalysis by the UO_2 surface.

(IV) It is dubious as to whether the Sr release rate can be used as an indicator of the fuel dissolution rate. Under oxidizing conditions, when a significant amount of dissolution occurs, the correlation between these rates appears to be good (76, 77). However, when only minimal dissolution occurs in the presence of H_2, the release behaviour of Sr appears to be complicated by release of its small grain boundary inventory, which would have been swamped by release from the fuel matrix under oxidizing conditions. In addition, changes in surface properties thought to be induced by its reduction by H_2 may also influence Sr release (16, 78).

(V) The concentrations of redox sensitive radionuclides decrease throughout the leaching experiments consistent with their reduction and reprecipitation by reaction with H_2.

Alpha-Doped UO₂ Specimens

Since container lifetimes are expected to be long, spent fuel is unlikely to be exposed to groundwater over the 300 to 1,000 year period over which γ/β radiation fields are significant, Figure 1. Beyond this period, α-radiation fields will dominate and be the source of oxidants for fuel corrosion via the α-radiolysis of water. To study the influence of α-radiation without interference from γ/β fields, α-doped UO₂ specimens have been used. These specimens contain different fractions of α-emitters ([238]Pu, [239]Pu, [233]U) to simulate the levels of α-activity in spent fuels after various periods of containment (*16, 30, 55, 56, 63, 79*). Based on studies with α-emitters and a number of spent fuel studies, a dependence of fuel corrosion rate on α-activity is now well established, Figure 6, and has been discussed in detail (*63*).
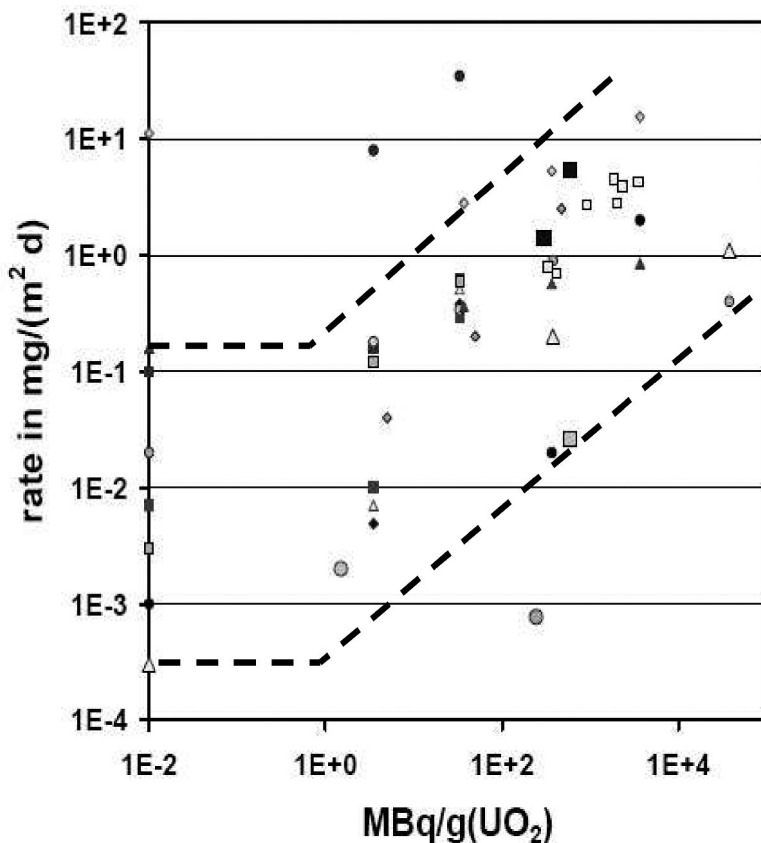
Figure 6. Corrosion rates measured for alpha-doped UO₂, non-doped UO₂ (0.01 MBq/g) and spent fuel specimens as a function of alpha activity (63). The sources of the individual data points are given in the reference. The dashed lines are arbitrary and drawn to emphasize the approximate alpha-strength below which no influence of alpha radiation is observed (1 MBq/g).
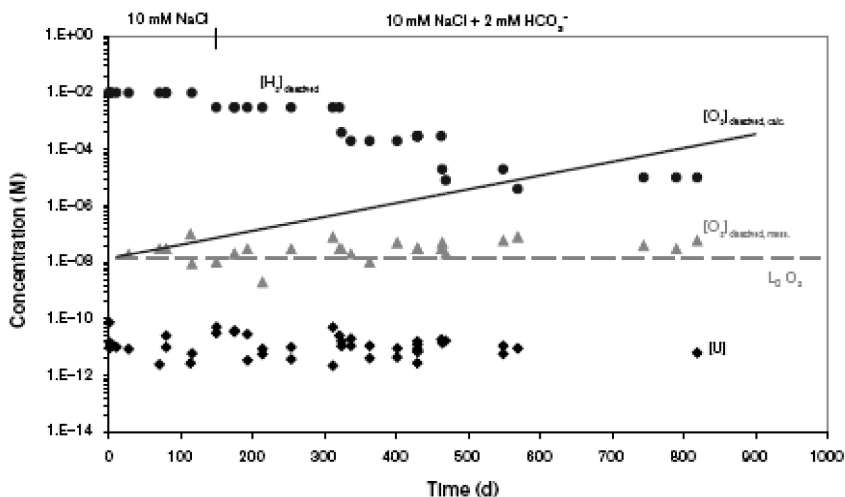
Figure 7. Measured H₂, O₂ and total U concentrations, as a function of time, in a pressure vessel leaching experiment of a 10% ^{233}U-doped UO₂ in 10^{-2} mol/L NaCl (0 to 114 days) and 10^{-2} mol/L NaCl + 2 x 10^{-2} mol/L HCO₃⁻ (114 days onwards) as the H₂ overpressure was periodically changed. The red line shows the calculated radiolytic O₂ concentrations (16).

Experiments performed with ^{233}U-doped UO₂ (1% and 10% ^{233}U) in a carbonate-dominated water ($\sim 10^{-3}$ mol/L, pH = 7.5) containing no H₂ showed no measureable influence of α-radiation at the 1% doping level (over 46 days) suggesting the alpha activity of this specimen represents an approximate threshold below which solubility-controlled, as opposed to radiolytically-controlled, dissolution would prevail (Figure 2), as suggested by Poinssot et al. (*63*) and indicated by the break in the dashed lines in Figure 6. The rates measured at this threshold are very similar to those predicted using a simple extrapolation of electrochemical data (*17*) to the E_{CORR} threshold shown in Figure 2. This consistency adds credibility to the claim that a threshold does exist and can be used to interpret the influence of H₂ on fuel dissolution rate. A repeat of these experiments in the presence of an Ar/6% H₂-purge (equivalent to a H₂ concentration of 5 x 10^{-5} mol/L) showed that even this small concentration of H₂ suppressed the dissolution rate below this threshold; i.e., no U release was observed with the 1% ^{233}U-doped UO₂ sample.

Subsequently, using the 10% ^{233}U-doped UO₂ an experiment was conducted in a solution containing 2 x 10^{-3} mol/L NaCl and 2 x 10^{-3} mol/L HCO₃⁻ in which the H₂ pressure was varied in stages from an initial value of 16 bar (about 10^{-2} mol/L dissolved H₂) to a final value of 0.01 bar (10^{-5} mol/L dissolved H₂) (*16*). All the indicators that corrosion/dissolution were completely suppressed were observed, Figure 7.

(I) The U concentration was extremely low ($\leq 10^{-10}$ mol/L), indicating solubility-control over the full 2.2 years of the experiment.

(II) The E_h, initially –100 mV (vs SHE), decreased over the first 50 days to ≤ –300 mV and remained well below –300 mV thereafter, only rising over the final days of the last period when the H_2 concentration was at its lowest. This final increase was not accompanied by an increase in U concentration, indicating that reducing conditions were maintained at the fuel surface even at this very low final H_2 concentration.

(III) Measured O_2 concentrations were in the region of 10^{-8} mol/L throughout the experiment, even though the amount of radiolytically-produced O_2 should have been many orders of magnitude greater by the end of the experiment.

(IV) The absence of any surface oxidation of the UO_2 was confirmed by X-ray photoelectron spectroscopy (XPS). Also, although the presence of UO_2 fragments in the vessel made analyses somewhat ambiguous, there was no evidence for the redeposition of dissolved U.

Since no change in U concentration occurred over the full two years of the experiment, no dissolution rate could be calculated and it could be concluded that dissolution had been completely suppressed.

This conclusion is strongly supported by the XPS results, which are consistent with previous XPS analyses of UO_2 surfaces exposed to radiation under Ar-purged and H_2-purged (0.1 to 1 bar) conditions (*80*). These authors showed that, in the absence of radiation at 100°C the extent of oxidation of a UO_2 surface was the same in the presence of H_2 as it was in an Ar-purged system. However, when the UO_2 (a disc cut from a CANDU fuel pellet) was placed close to a ^{241}Am source, surface oxidation occurred in Ar-purged solution, but in the presence of H_2, the extent of oxidation of the UO_2 surface decreased as the α-source strength increased

These results were qualitatively confirmed by the dissolution rates determined electrochemically (by a standard Tafel extrapolation and by electrochemical impedance spectroscopy (EIS)) (*16*), which showed a dependence of dissolution rate on α-activity and a suppression of the rate for both 1% ^{233}U and 10% ^{233}U electrodes in the presence of H_2. These rates are included in Figure 6, and are high compared to other rates; i.e., outside the area encompassed by the dashed lines. This probably reflects the difficulties inherent in making EIS measurements on an electrode with a bulk resistance of 10^5 ohms.

Given the absence of any UO_2 corrosion the lack of radiolytic oxygen cannot be attributed to its consumption by fuel corrosion, leaving its consumption by H_2 catalyzed by the fuel surface as the only alternative explanation.

The Role of Gamma Radiation in the Activation of H_2

It is clear from these studies on spent fuels and α-doped specimens that dissolved H_2 can suppress fuel corrosion completely, even at low concentrations. Also, H_2 can reduce the concentrations of radiolytic oxidants down to their analytical detection limits. At the low temperatures employed it has been shown that H_2 cannot act as a homogeneous solution reductant; e.g., for U^{VI} (*78*), Np^V (*81*) and Tc^{VII} (*82*). To act as a reductant H_2 must be activated; i.e., dissociated into reactive H atoms, a process that can be achieved either radiolytically or on

catalytic surfaces. For the present systems a combination of these two modes is possible.

The homogeneous activation of H_2 by low energy transfer (LET) radiation, which generates $OH^{\bullet}$ radicals, to produce reactive hydrogen radicals

$$OH^{\bullet} + H_2 \rightarrow H_2O + H^{\bullet} \tag{5}$$

has been demonstrated computationally (*83*) and experimentally (*84, 85*). H_2 concentrations in the range found to suppress fuel corrosion (10^{-4} to 10^{-5} mol/L) have been shown to scavenge molecular radiolytic oxidants to below detection limits as well as consume small amounts of added H_2O_2. While this can readily explain the scavenging of radiolytic oxidants in spent fuel experiments, it is insufficient to explain the complete absence of fuel dissolution, as well as a number of other laboratory observations made on UO_2 electrodes exposed to gamma irradiated solutions.

King et al. (*86*) studied the effect of γ-radiation on the E_{CORR} of UO_2 (CANDU) in the presence of either a 5 MPa over pressure of H_2 (equivalent to ~ 4 x 10^{-2} mol/L of dissolved H_2) or Ar. A comparison of the E_{CORR} values obtained under irradiation in the presence of H_2 to the values in the presence of Ar is shown in Figure 8. The range of values recorded in unirradiated solutions for both gases are shown as a vertical bar (*87*). Under irradiation, E_{CORR} values in the presence of H_2 were consistently more negative, and those in the presence of Ar consistently more positive, than values measured in the absence of radiation. This increase in E_{CORR} in Ar is expected due to a slight radiolytic oxidation of UO_2 when a radiation field is present.
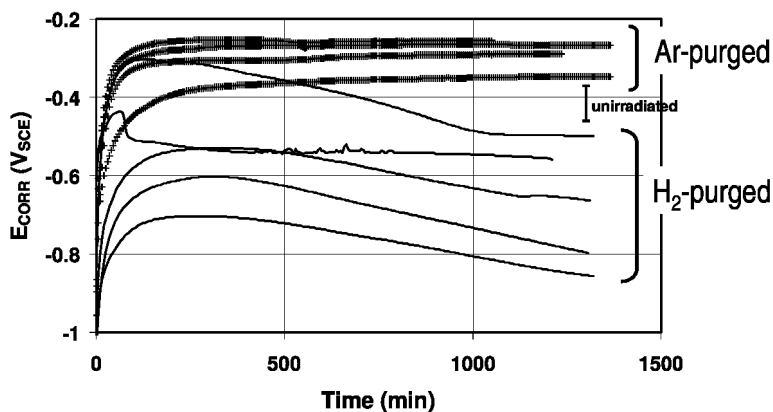
Figure 8. Time dependence of the corrosion potential (E_{CORR}) of a UO_2 electrode in gamma-irradiated 0.1mol/L NaCl (pH~9.5) at room temperature in the presence of either 5MPa of H_2 or Ar. The results of four or five replicate tests are shown for each set of conditions. The range of E_{CORR} values recorded in unirradiated solutions for both gases is shown as the vertical bar (87).
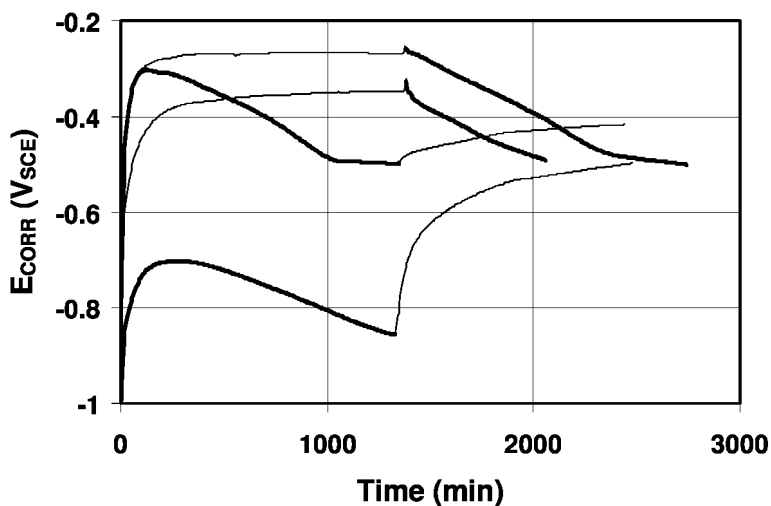
Figure 9. Effect of changing from H₂ (heavy line) to Ar (light line) overpressure on the E_{CORR} of UO₂ in γ-irradiated 0.1 mol dm⁻³ NaCl solution (pH 9.5) at room temperature (86).

However, the influence of H_2 is more dramatic than can be explained by just the homogeneous solution scavenging of radiolytic oxidants. Comparison of the absolute values in Figure 8 with the threshold potential for surface oxidation of UO_2, Figure 2, shows that E_{CORR} is suppressed to values up to 400 mV more negative than the threshold for oxidation/corrosion, and approaches the reversible potential for the reaction

$$H_2 \leftrightarrows 2H^+ + 2e^- \qquad (6)$$

which proceeds on surfaces through reactive H· radical intermediates. A general observation in these experiments is the peak in the E_{CORR} versus time relationship in the presence of H_2, the decrease in E_{CORR} at longer times suggesting that the state of the UO_2 surface is slowly changing. Since the electrodes were pre-treated electrochemically to remove air-formed U^{VI} oxides, this change cannot be attributed to the reduction of a pre-oxidized surface layer. The most probable, but unproven, explanation is that γ-assisted decomposition of H_2 produces H· radicals which subsequently reduce U^V surface states, present in residual slightly non-stoichiometric sites, to U^{IV},

$$U^V + H^\bullet \rightarrow U^{IV} + H^+ \qquad (7)$$

This surface reduction appears to be partially irreversible as shown in Figure 9, which shows the E_{CORR} response to changes in the pressurizing gas during the experiment. The critical observation in these experiments is that, after exposure to H_2, E_{CORR} does not recover to the value measured on first exposure to an Ar purge, suggesting that the UO_2 surface may have been permanently reduced by radiolytically-produced H· radicals on the surface.

A surface reduction step, as described in reaction 7, must simultaneously involve the extraction of an interstitial O^{2-} ion from the $(U^{IV})_{1-2x}(U^V)_{2x}O_{2+x}$ lattice in order to maintain electrical neutrality in the surface. This would likely be achieved by consumption of the proton produced. Consequently, a reduction reaction of this type can be considered as a defect annealing process since the primary defect in slightly non-stoichiometric UO_{2+x} is the O^{2-} interstitial ion occupying vacancies in the UO_2 fluoride structure (88).

For gamma radiation it is also feasible that enhanced radiolytic effects at the oxide/solution interface involving the creation of excitons is involved (89). Excitons are produced by the absorption of radiation in the solid. Providing the oxide band gap is sufficiently large (5 eV) that these excitons have sufficient energy to break H-O-H bonds (5.1 eV), they can act as a source of OH• and H• radicals. Reaction of the OH• radical with H_2 would create an additional H• radical,

$$OH^{\bullet} + H_2 \rightarrow H_2O + H^{\bullet} \qquad (8)$$

These H• radicals can scavenge radiolytic oxidants and suppress fuel oxidation/corrosion. In the reduced state, when the 5f level is fully occupied, UO_2 does possess the 5 eV band gap which allows formation of the high energy excitons.

The Role of Alpha Radiolysis in the Activation of H_2

While this combination of γ-radiolysis and γ-activation of H_2 on the UO_2 surface offers an explanation for the scavenging of radiolytic oxidants and suppression of radiolytic corrosion of spent fuels, it cannot explain the similar results obtained with α-doped specimens when γ/β radiation fields are absent. In the case of α-radiation, it has been shown (85) that even quite large amounts of H_2 (up to 1 bar, equivalent to 8×10^{-4} mol/L) did not influence the production of radiolytic oxidants in the absence of UO_2. Practically equal amounts were produced with and without H_2, in solutions irradiated with 5 MeV He atoms. Also, while radiolysis models developed for spent fuels show that the combination of γ/β/α radiation and H_2 can lead to the consumption of radiolytically-produced molecular oxidants (90–92), the continuous generation of molecular oxidants by α-radiolysis means conditions remain locally oxidizing even at high H_2 pressures. Thus, no argument can be made that the homogeneous solution scavenging of radiolytic oxidants alone can completely suppress radiolytic corrosion of UO_2.

Thus, a surface activation of H_2 to produce reactive H• radicals similar to that observed in the presence of γ-radiation must be available on α-doped UO_2 surfaces. Evidence exists to show that H_2 and O_2 can be recombined on α-active $^{239}PuO_2$ surfaces at 25°C (93). In addition, radiolytic H_2 gas generation via the decomposition of water on NpO_2 (doped with the α-emitter ^{244}Cm) achieves a steady-state indicative of a balance between H_2O decomposition and the reverse H_2/O_2 recombination process. A similar mechanism can be anticipated on α-doped UO_2 even though no water production was detected in an H_2/O_2 mixture on depleted UO_2 (which would have effectively negligible α-activity (94)).

Catalysis on UO_2 surfaces is well characterized and catalytic activity is considerably enhanced on defective surfaces. Defective surfaces can be created by Ar ion sputtering which, for an actinide oxide like UO_2, leads to preferential ejection of the much lighter O atom and the creation of an oxygen vacancy. The need to repair this site can lead to the extraction of oxygen from, and hence the reduction of, absorbed species. The actinide oxides are particularly reactive, especially U, since hybridization between the 5f and 6d electronic orbitals allow the creation of multiple oxidation states (+3 to +6) in the solid state. These features have lead to uranium oxides being studied for the catalysis of many reactions including dehydrogenation (*95*), oxidation (*96*, *97*), ammoxidation (*98*, *99*), oxidative coupling (*100*) and etherification (*101*). Most pertinent to the present discussion is the demonstration that water decomposition involving the oxidative healing of defects in the reduced surface occurs on UO_2 and is promoted when the surface defect density is increased by Ar ion sputtering (*102*). Alpha emission will also produce surface defects by the preferential ejection of the lighter O atom leading to reduced (U^{III}) states. Subsequent oxidation of the surface by H_2O, leading to the reincorporation of O^{2-}, would yield a proton and leave a $H^\bullet$ available to scavenge radiolytic oxidants. This provides one possible mechanism by which radiolytic oxidants can be consumed at the location where they are produced for as long as α-radiolysis persists and H_2 is present.

The Role of Noble Metal (Epsilon [ε]) Particles in the Control of Surface Redox Conditions

In-reactor irradiation has a significant influence on the chemical and physical properties of the fuel due to the production of a wide range of radionuclides (*104*, *105*). Of key importance from the present perspective are the rare earths (RE) (e.g., Nd, Eu, Gd) which reside in the fuel lattice as RE^{III} cations and create additional U^V species leading to an increase in matrix electrical conductivity (*88*), and the elements which are unstable as oxides (Mo, Ru, Pd, Rh, Tc), which segregate to form noble metal particles known as ε-particles.

Noble metals are well known as catalysts for oxidation/reduction reactions, especially the $H_2/H^\bullet/H^+$ reaction, and three of the four predominant components of ε-particles (Rh, Pd, Ru) are exceptionally good catalysts for this reaction as evidenced by their exchange current densities, Table 1 (*106*, *107*).

Thus, it would be expected that these particles could act as galvanically-coupled anodes (for H_2 oxidation) and cathodes (e.g., for H_2O_2 reduction). Thus, H_2 activation on these particles is likely more effective in suppressing fuel corrosion than the utilization of defects produced by α-recoil or the γ-excitation of H_2 (*38*, *108*, *109*). The function of these particles has been investigated electrochemically using SIMFUEL specimens with different degrees of simulated burn-up (*106*, *110–112*). SIMFUELS are unirradiated analogues of used nuclear fuel, produced by doping the UO_2 matrix with a series of stable elements (Ba, Ce, La, Mo, Sr, Y, Rh, Pd, Ru, Nd and Zr) in proportions appropriate to simulate the chemical effects caused by in-reactor irradiation to various levels of burn-up. This fabrication process reproduces the increase in matrix conductivity due to RE dopants and the creation of noble metal particles.
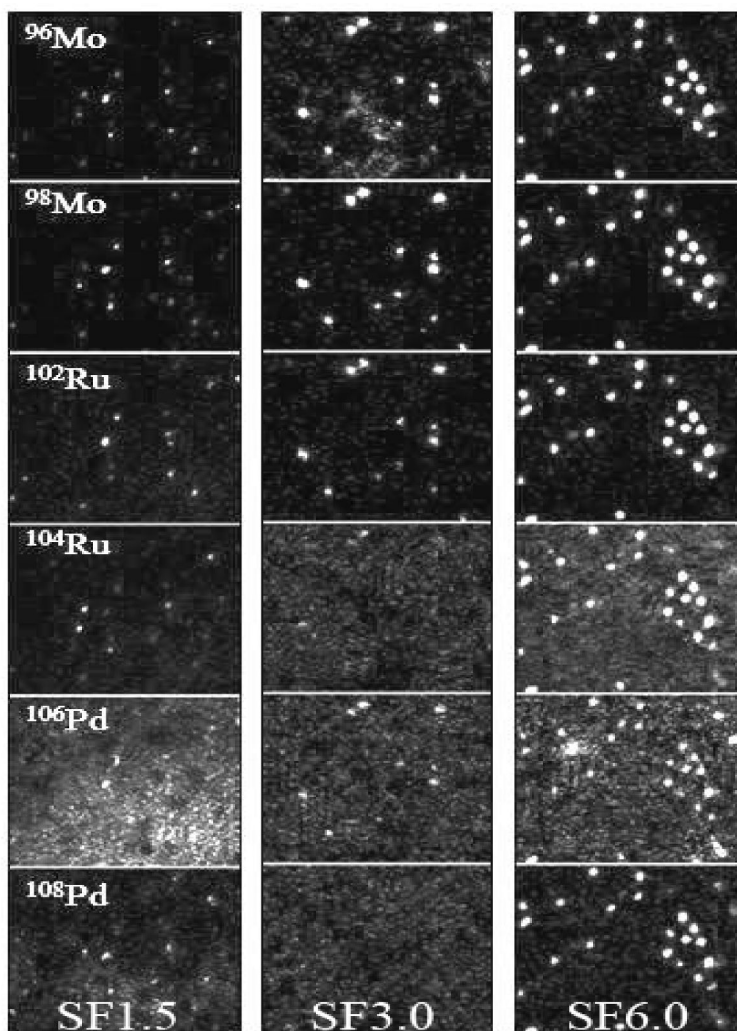
Figure 10. SIMS images showing the elements $^{96,\ 98}$Mo, $^{102,\ 104}$Ru, and $^{106,\ 108}$Pd detected in three SIMFUEL specimens (SF) with various degrees of simulated burn-up (expressed as an atomic %). No map for Rh is shown due to its low concentration. Each individual area is 50 μm x 50 μm.

Figure 10 shows the distribution of epsilon particles for three SIMFUELS with various degrees of simulated burn-up covering the range from the level expected in CANDU fuel (1.5 at %) to that expected for a very high burn-up enriched fuel (6 at %). This distribution was obtained from SIMS analysis for the individual elements in the particles. The increase in size and number density of particles with the increase in degree of simulated burn-up is clear.

The E_{CORR} on SIMFUELS is very responsive to variations in redox conditions, Figure 11. In the presence of dissolved O_2 (aerated solutions) oxidation of the

fuel surface is catalyzed by O_2 reduction on the ε-particles. A similar catalysis of H_2O_2 reduction occurring on Pd particles dispersed throughout UO_2 was also demonstrated to cause enhanced corrosion (*113*). However, the presence of even small amounts of dissolved H_2 (purging with 5% H_2/95% Ar) suppressed E_{CORR} well below the value measured under purely anoxic conditions (Ar-purging) even for a low density of ε-particles (1.5 at % SIMFUEL, Figure 11).

The value of E_{CORR} decreased with the number density of ε-particles present, Figure 12, and XPS analyses confirmed that the extent of oxidation of the UO_2 surface decreased as E_{CORR} decreased, Figure 13.

For the 6 at % SIMFUEL, with a high number density of ε-particles, E_{CORR} was suppressed to a value of –400 mV (vs SCE), the threshold below which corrosion of UO_2 does not occur, Figure 2. This effect can be attributed to the reversible dissociation of H_2 to H· radicals on the ε-particles that act as galvanically-coupled anodes within the fuel matrix. When E_{CORR} reaches, or is suppressed below, this threshold, the UO_2 is fully galvanically protected and thermodynamically immune to corrosion. This process is illustrated schematically in Figure 14. That immunity to oxidation, and hence corrosion, is achieved is confirmed by the XPS analyses which show that the surface composition is as reduced as that achieved by electrochemical reduction of the electrode at potentials < - 1V (vs SCE) (*106*). That this mechanism is similarly active in the presence of γ–irradiated solutions has also been recently demonstrated (*114*).
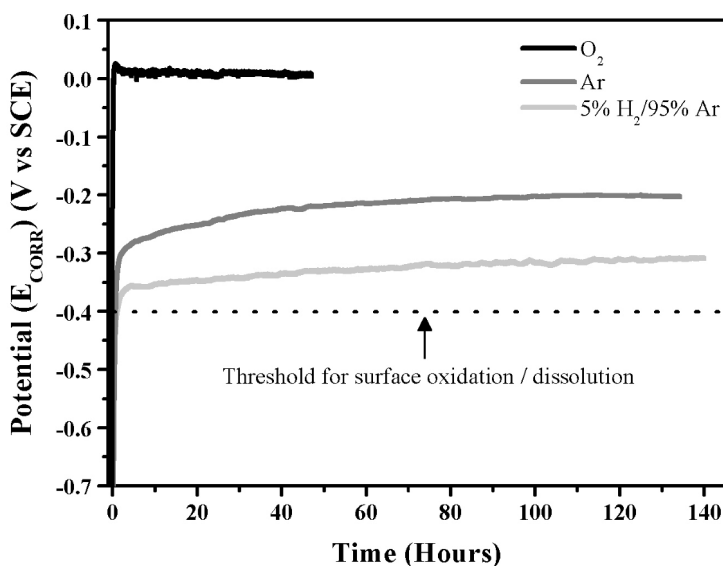
Figure 11. E_{CORR} measurements on a SIMFUEL electrode (SF1.5, with an extent of simulated burn-up of 1.5 at%) in a 0.1 mol/L KCl solution (pH = 9.5) purged with various gases at 60°C. The electrode was electrochemically-cleaned prior to the start of each experiment. The dashed line shows the potential threshold for corrosion (Figure 2) (110).
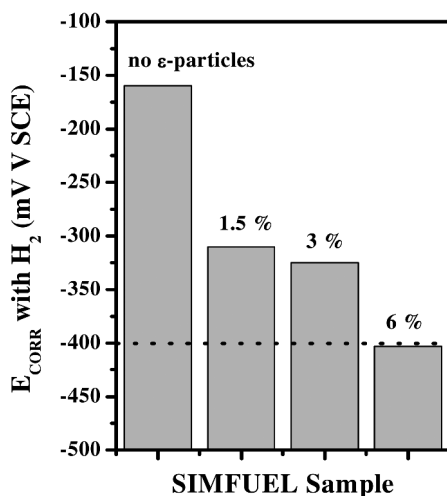
Figure 12. The influence of the increasing number and size of epsilon particles in SIMFUELS with different degrees of simulated burnup (expressed as an atomic %) on the corrosion potential (E_{CORR}) measured in H_2-purged 0.1mol/L KCl solution (pH = 9.5) at 60°C. The horizontal line shows the potential threshold for corrosion (Figure 2) (38).

Table 1. Exchange current densities for the proton reduction reaction for the four predominant epsilon particle constituents

Element	Exchange Current Densities (A.cm^{-2})
Pd	$10^{-3.0}$
Rh	$10^{-3.6}$
Ru	$10^{-3.3}$
Mo	$10^{-7.1}$

Measurements performed in a pressure vessel show that E_{CORR} can be suppressed well below the threshold even on 1.5 at % SIMFUEL, providing the pressure of H_2 is increased sufficiently, Figure 15. It is worth noting that the potential achieved under these conditions approaches the reversible potential for the $H_2/H^\bullet/H^+$ reaction as observed on UO_2 containing no ε-particles in the presence γ-radiation, Figure 8. For this condition, the $H_2/H^\bullet/H^+$ reaction becomes reversible on the ε-particles and the UO_2 matrix is completely inert.

Since noble metals are catalytic for both the reduction of potential fuel oxidants, such as H_2O_2, as well as the reductant H_2, it is not surprising that it can be shown that ε-particles will catalyze the reaction between H_2O_2 and H_2 to produce water; i.e., ε-particles will catalyze the scavenging of radiolytic oxidants by H_2. Nilsson and Jonsson (*109*) showed that Pd, present as a powder, acted as a catalyst for this reaction and Broczkowski has shown that a similar catalysis

occurs on the ε-particles in 1.5 at % SIMFUEL (*106*). The reaction was shown to be diffusion controlled on Pd which could account for the very strong effect of H_2 on spent fuel dissolution at very modest concentrations (10^{-5} to 10^{-4} mol/L) (*16*).
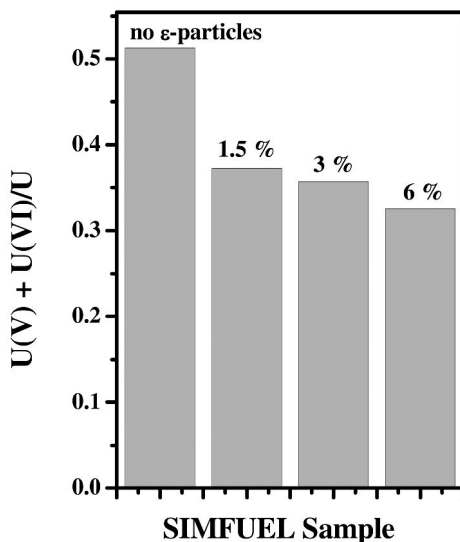
Figure 13. The influence of the increasing number and size of epsilon particles in SIMFUELS with different degrees of simulated burnup (expressed as an atomic %) on the degree of oxidation of the surface (determined by XPS) in H_2-purged 0.1mol/L KCl (pH = 9.5) at 60°C.
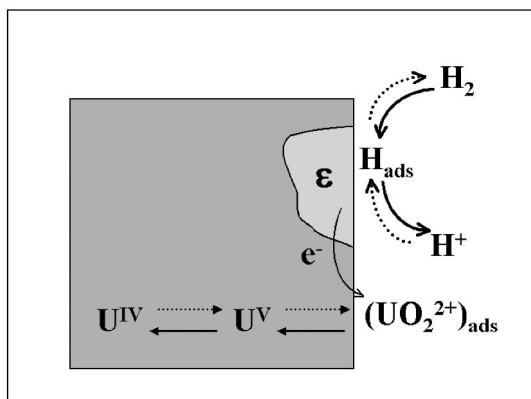
Figure 14. Illustration showing the galvanic coupling of epsilon particles to the fuel matrix in H_2-containing solutions (110).
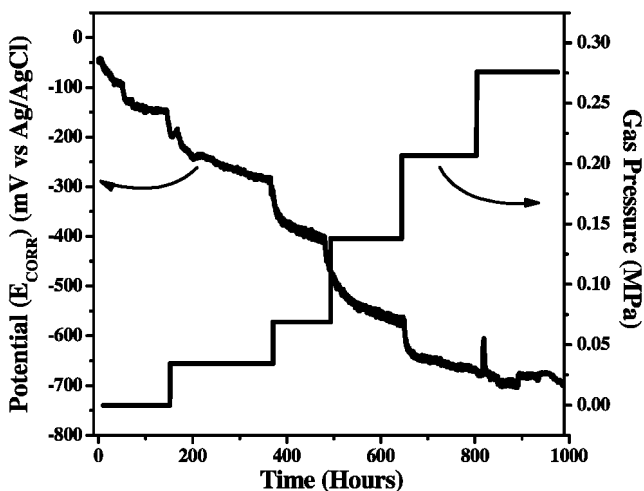
Figure 15. The influence of H$_2$ solution overpressure on the E$_{CORR}$ of a SIMFUEL electrode with 1.5% of simulated burn-up (SF1.5) measured in a 0.1 mol/L KCl solution (pH = 9.5) at 60°C. The system was initially purged with Ar only at atmospheric pressure, and then with a series of increasing 5% H$_2$/Ar pressures (110).
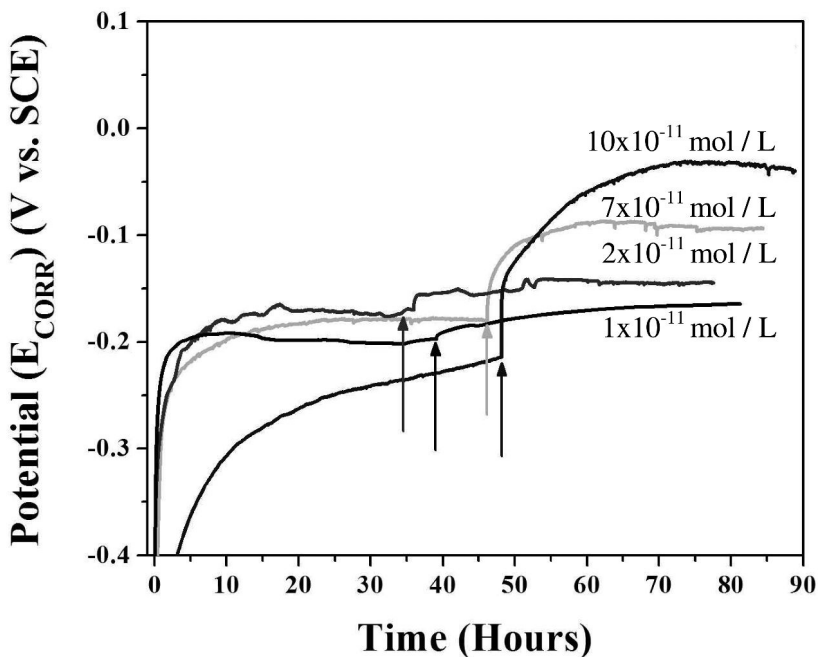
Figure 16. E$_{CORR}$ recorded on a SIMFUEL with 1.5% of simulated burn-up (SF1.5) in a 0.1 mol·L^{-1} KCl solution (pH 9.5) purged with Ar at 60°C. The arrows indicate the times when H$_2$O$_2$ was added in the individual experiments (106).

Figures 16 and 17 show the E_{CORR} response of a 1.5 at % SIMFUEL surface to the addition of small concentrations of H_2O_2 under Ar-purged conditions, Figure 16, and with a 5% H_2/95% Ar purge (~4.5 x 10^{-5} mol/L of dissolved H_2), Figure 17. In the absence of H_2, E_{CORR} increases to a new steady-state value which increases with increasing H_2O_2 concentration, and XPS analyses show that the extent of oxidation of the surface increases accordingly (*106*). The addition of similar concentrations of H_2O_2 in the presence of H_2 initially stimulated an increase, but eventually a decrease, in E_{CORR} for sufficiently low H_2O_2 concentrations. Note the steady-state E_{CORR} in this experiment prior to H_2O_2 addition is lower than that in the Ar-purged solution (Figure 16), which reflects the dissociation of H_2 on the ε-particles and its galvanically-coupled effect on the UO_2

XPS analyses confirm that no permanent oxidation of the surface occurred except at a H_2O_2 concentration of 10^{-9} mol/L, when E_{CORR} did not fully recover to the value measured prior to H_2O_2 addition, Figure 18. In this figure the lines indicate the $U^{IV}/U^V/U^{VI}$ levels in the UO_2 surface under H_2-purged conditions (i.e., before H_2O_2 addition) and the data points show the surface composition after the addition of H_2O_2 and completion of E_{CORR} excursions similar to those shown in Figure 17.

This E_{CORR} behaviour cannot be attributed solely to H_2O_2 scavenging by H_2 on ε-particles, independently of the galvanic coupling effect. While it is possible that the positive excursion in E_{CORR} lead to a temporary oxidation of the UO_2 surface, the XPS results demonstrate that this was not sustainable. Irrespective of whether the H_2O_2 was eventually consumed in these experiments, the absence of UO_2 oxidation confirms that galvanic protection of the UO_2 was maintained or eventually reestablished. In fact, the XPS analyses suggest the UO_2 surface is actually reduced to a level below its original composition, Figure 18. The suppression of UO_2 dissolution by H_2O_2 in the presence of H_2 and Pd particles has also recently been demonstrated analytically (*109*, *114*).

The Role of the UO_2 Surface in the Control of Surface Redox Conditions

A remaining question is whether or not the UO_2 surface itself can activate H_2 in the absence of ε-particles and/or radiation fields. Wren et al. (*34*) claimed that a $U_{1-2x}^{IV} U_{2x}^V O_{2+x}$ surface could catalyze the reaction between H_2 and H_2O_2 based on the slow rate of oxidation of UO_2 surfaces in close proximity to an Au-plated ^{241}Am α-source. These experiments were conducted in 0.1 mol/L $NaClO_4$ (pH = 9.5) solutions at room temperature. The oxidation rate was up to two orders of magnitude lower in the presence of α-radiolysis than when H_2O_2 was added chemically and approximately one order of magnitude lower than oxidation by the considerably slower oxidant, O_2. It was speculated that the surface catalyzed decomposition of H_2O_2

$$H_2O_2 + e^- \rightarrow {}^\bullet OH + OH^- \tag{9}$$

$$U^{IV} \rightarrow U^V + e^- \tag{10}$$

proceeded through a ·OH surface species which could subsequently be consumed by α-radiolytically produced H_2 confined in the 25 μm thick layer of solution separating the UO_2 and Au-plated α-source,

$$H_2 + OH^\bullet \rightarrow H_2O + H^+ + e^- \qquad (11)$$

$$U^V + e^- \rightarrow U^{IV} \qquad (12)$$

However, Nilsson and Jonsson (*115*) could find no evidence for this reaction in a system containing 2 x 10^{-4} mol/L H_2O_2 and up to 40 bar of H_2 (≥ 2 x 10^{-2} mol/L of dissolved H_2). Additionally, the observation that H_2 will reduce UO_2^{2+} when Pd is present (*115*), but not when UO_2 alone is present (*39*), also suggests the UO_2 surface cannot activate H_2.
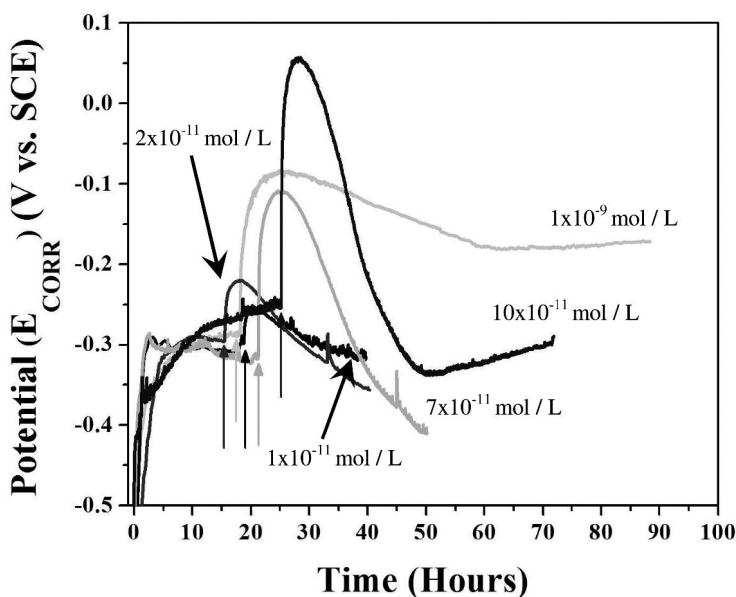
Figure 17. E_{CORR} recorded on a SIMFUEL with 1.5% of simulated burn-up (SF1.5) in a 0.1 mol·L^{-1} KCl solution (pH 9.5) purged with 5% H_2/95% Ar at 60°C. The vertical arrows indicate the times when H_2O_2 was added in the individual experiments (106).
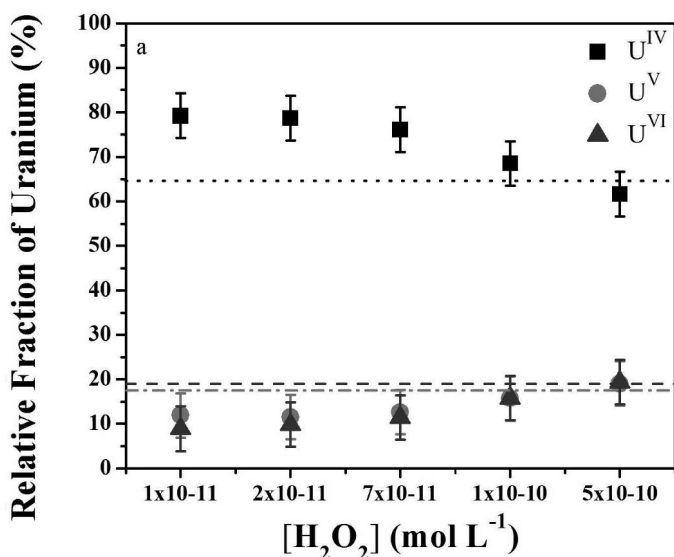
Figure 18. Surface composition measured (by XPS) on a SIMFUEL with 1.5% of simulated burn-up (SF1.5) after E_{CORR} measurements in 5% H_2/95% Ar-purged 0.1 mol/L KCl solution (pH = 9.5) at 60°C. The horizontal dotted lines refer to the fraction of U^{IV} (black), U^V (light grey), and U^{VI} (dark grey) measured after E_{CORR} experiments with no H_2O_2 added (106).
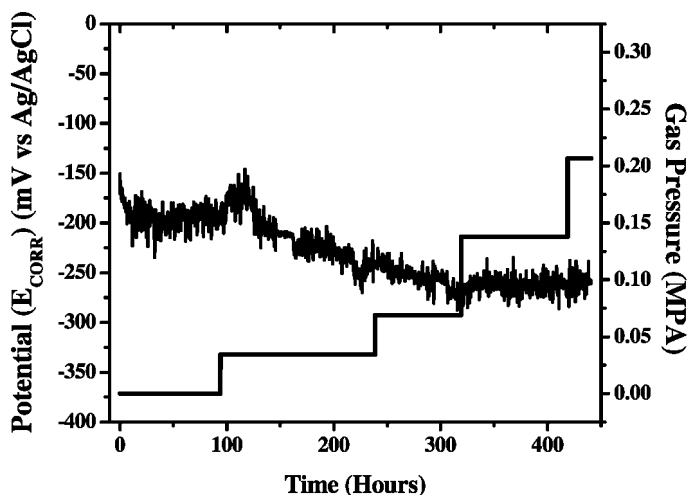
Figure 19. The influence of H_2 overpressure on the E_{CORR} of a SIMFUEL electrode with 3.0% simulated burn-up, but containing no epsilon particles, in a 0.1 mol/L KCl solution (pH = 9.5) at 60°C. The system was initially purged with Ar only at atmospheric pressure, and then with a series of increasing 5% H_2/Ar pressures (110).
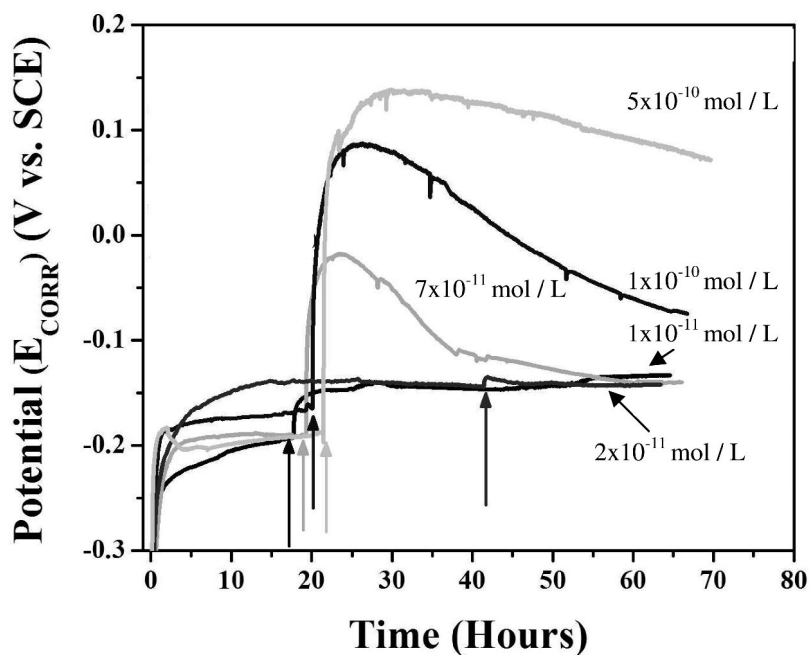
Figure 20. E_{CORR} measured on a SIMFUEL with 3 at% simulated burn-up, but containing no epsilon particles in a 0.1 mol/L KCl solution (pH 9.5) purged with 5%H_2/95% Ar at 60°C. The vertical arrows indicate the times when H_2O_2 was added in the individual experiments (106).

That H_2 cannot be activated, or activated only to a minor degree, on UO_2 appears to be confirmed by the results in Figure 19, in which the influence of an increase in H_2 pressure on E_{CORR} measured on a rare-earth doped SIMFUEL without ε-particles is shown (*106*). As opposed to measurements on SIMFUEL with ε-particles, when E_{CORR} was suppressed to values well below the –400 mV threshold value for UO_2 oxidation/corrosion, Figure 15, E_{CORR} showed only a minor change with increasing H_2 pressure indicating no significant change in the properties of the surface had occurred.

However, a series of experiments in which small additions of H_2O_2 were made to 5% H_2/95% Ar-purged solutions showed that the E_{CORR} measured on the SIMFUEL with no ε-particles exhibited similar behavior, Figure 20, to that observed for the 1.5 at % SIMFUEL, Figure 16. The rapid increase in E_{CORR} on first adding the H_2O_2 was reversed, as observed when ε-particles were present. This reversal in E_{CORR} suggests the H_2O_2 is being consumed by reaction with H_2 on the UO_2 surface. Unfortunately, although XPS analyses showed slight differences between the electrodes exposed to either Ar-purged or H_2/Ar-purged solutions, the differences were too small to indicate a clear difference in composition.

However, the results strongly suggest that, while H_2 may not dissociatively absorb on UO_2, H_2O_2 does, and that the $\cdot OH$ radical species formed can then be scavenged by H_2 leading to H_2O_2 consumption rather than fuel oxidation. Good electrochemical evidence exists to show that the first electron transfer to H_2O_2

involves the creation of an OH• radical (*116*, *117*). The results in Figure 20 show that, for this scavenging process to occur, the concentration ratio $[H_2]/[H_2O_2]$ needs to be $>10^5$. This may explain why a similar effect was not observed by Nilsson and Jonsson (*115*) since their concentration ratio was only $\sim10^2$.

It can be concluded that the scavenging of low concentrations of radiolytic oxidants would occur on the UO_2 surface in the presence of a sufficient H_2 concentration. However, the process appears to be kinetically slow when compared to the reaction rate on ε-particles or when H_2 is radiolytically activated.

Summary and Conclusions

The results of corrosion/dissolution studies on spent fuels, α-doped UO_2 specimens, SIMFUELs and undoped UO_2 specimens have been reviewed, and the mechanisms proposed to explain the ability of dissolved H_2 to completely suppress fuel corrosion and radionuclide release discussed.

The primary reductant leading to the protection of the fuel against corrosion is the H• radical species which can be produced by a number of activation steps depending on the composition of the fuel and the form of the radiation present. The potential mechanisms include the following:

(I)   A combination of γ-radiation and dissolved H_2 can produce H• radicals on the UO_2 surface. This may involve the adsorption of γ energy in the surface to produce high energy excitons which decompose water to OH• and H• surface species. Scavenging of OH• by H_2 can then create an additional H•. These radicals can then suppress corrosion and scavenge radiolytic oxidants.

(II) Similar inhibition and scavenging processes are possible when only α-radiation is present. In this case the dissociation of water could be caused by the need to neutralize the oxygen vacancy caused by the ejection of an O atom from the surface caused by an α-recoil event.

(III) In the absence of any radiation fields, experiments on SIMFUELs show that H_2 activation can occur rapidly on epsilon particles. Since these particles are galvanically-coupled to the rare earth-doped (and, hence, conducting) UO_2 matrix, they act as anodes forcing the matrix to adopt a low potential. For either a sufficiently high extent of simulated burn-up (number density of particles) at low $[H_2]$ or a sufficiently high $[H_2]$ at a low extent of simulated burn-up, this galvanic coupling can render the UO_2 unreactive.

(IV) It is also possible that the UO_2 could activate H_2 in the presence of H_2O_2, although evidence for this is weak. If oxidation/corrosion of the surface by H_2O_2 involves OH•, these could be scavenged by reaction with H_2 and hence prevented from causing fuel oxidation.

The studies show that even small pressures of H_2 (0.1 to 1 bar) can effectively suppress fuel corrosion. Since the production of H_2 will commence as soon as waste containers fail and groundwater contacts the carbon steel liner, and, in sealed

repositories, H_2 pressures up to 50 bar are anticipated, this influence of H_2 has the potential to shut down fuel corrosion very rapidly. This suppression will be at least partially effective even for early failure when oxidizing conditions would be maintained by gamma/beta radiolysis of water. It is possible therefore that the conditions for extremely slow chemical dissolution of fuel would be rapidly established and that dissolution and radionuclide release would be extremely slow almost from the time of container failure irrespective of when it occurred.

Acknowledgments

References

1. Nuclear Waste Management Organization (NWMO). www.nwmo.ca.
2. McMurry, J.; Dixon, D. A.; Garroni, J. D.; Ikeda, B. M.; Stroess-Gascoyne, S.; Baumgartner, P.; Melnyk, T. *Evolution of a Canadian Deep Geologic Repository: Base Scenario*; 06819-REP-01200-10092-R00; Ontario Power Generation, Nuclear Waste Management Division: Toronto, Ontario, Canada, 2003.
3. King, F.; Kolar, M. *The Copper Container Corrosion Model Used in AECL's Second Case Study*; 06819-REP-01200-10041-R00; Ontario Power Generation: Toronto, Ontario, Canada, 2000.
4. Kolar, M.; King, F. *Mater. Res. Soc. Symp. Proc.* **1996**, *412*, 547–554.
5. Maak, P. *Mater. Res. Soc. Symp. Proc.* **2004**, *807*, 447–451.
6. Parks, G. A.; Pohl, D. C. *Geochim. Cosmochim. Acta* **1988**, *52*, 863–875.
7. Grenthe, I. J.; Fuger, J.; Konings, R. J.; Lemire, R. J.; Muller, A. B.; Nguen-Trung, C.; Wanner, H. *Chemical Thermodynamics of Uranium*; Elsevier Science Publishing Co. : Amsterdam, The Netherlands, 1992.
8. Fuger, J. *J. Nucl. Mater.* **1993**, *201*, 3–14.
9. Neck, V.; Kim, J. I. *Radiochim. Acta* **2001**, *89*, 1–16.
10. Rai, D.; Yui, M.; Moore, D. A. *J. Solution Chem.* **2003**, *32*, 1–17.
11. Yajima, T.; Kawamura, Y.; Ueta, S. *Mater. Res. Soc. Symp. Proc.* **1995**, *353*, 1137–1142.
12. Rai, D.; Felmy, A. R.; Ryan, J. L. *Inorg. Chem.* **1990**, *29*, 260–264.
13. Guillamont, R.; Fanghanel, T.; Grenthe, I. J.; Neck, V.; Palmer, D.; Rand, M. H. *Update on the Chemical Thermodynamics of Uranium, Neptunium, Plutonium, Americium and Technetium,*; Nuclear Energy Agency (NEA)/Organisation for Economic Co-operation and Development (OECD): Amsterdam, The Netherlands, 2003; Vol. 5; pp 182−187.
14. Shoesmith, D. W. *J. Nucl. Mater.* **2000**, *282*, 1–31.

15. Werme, L. O.; Johnson, L. H.; Oversby, V. M.; King, F.; Spahiu, K.; Grambow, B.; Shoesmith, D. W. *Spent Fuel Performance under Repository Conditions: A Model for Use in SR-Can*; TR-04-19; Svensk Kaernbraenslehantering AB: Stockholm, Sweden, 2004.

16. Carbol, P.; Cobos-Sabate, J.; Glatz, J. P.; Ronchi, C.; Rondinella, V.; Wegen, D. H.; Wiss, T.; Loida, A.; Metz, V.; Kienzler, B.; Spahiu, K.; Grambow, B.; Quinones, J. *The Effect of Dissolved Hydrogen on the Dissolution of ^{233}U Doped $UO_2(s)$, High Burn-Up Spent Fuel and MOX Fuel*; TR-05-09; ITU: Sweden, 2005.

17. Shoesmith, D. W.; Sunder, S. *An Electrochemistry-Based Model for the Dissolution of UO_2*; AECL-10488; Atomic Energy of Canada, Ltd.: Toronto, Ontario, Canada, 1991.

18. Sunder, S.; Miller, N. H.; Shoesmith, D. W. *Corros. Sci.* **2004**, *46*, 1095–1111.

19. Shoesmith, D. W.; Sunder, S.; Bailey, M. G.; Wallace, G. J. *Corros. Sci.* **1989**, *29*, 1115–1128.

20. Ekeroth, E.; Jonsson, M. *J. Nucl. Mater.* **2003**, *322*, 242–248.

21. Hossain, M. M.; Ekeroth, E.; Jonsson, M. *J. Nucl. Mater.* **2006**, *358*, 202–208.

22. Gimenez, J.; Baraj, E.; Torrero, M. E.; Casas, I.; de Pablo, J. *J. Nucl. Mater.* **1996**, *238*, 64–69.

23. de Pablo, J.; Casas, I.; Gimenez, J.; Marti, V.; Torrero, M. E. *J. Nucl. Mater.* **1996**, *232*, 138–145.

24. de Pablo, J.; Casas, I.; Clarens, F.; El Aamrani, F.; Rovira, M. *Mater. Res. Soc. Symp. Proc.* **2001**, *663*, 409–426.

25. Clarens, F.; de Pablo, J.; Diez-Perez, I.; Casas, I.; Gimenez, J.; Rovira, M. *Environ. Sci. Technol.* **2004**, *38*, 6656–6661.

26. Corbel, C.; Sattonnay, G.; Guilbert, S.; Garrido, F.; Barthe, M. F.; Jegou, C. *J. Nucl. Mater.* **2006**, *348*, 1–17.

27. de Pablo, J.; Casas, I.; Gimenez, F.; Clarens, F.; Duro, L.; Bruno, J. *Mater. Res. Soc. Symp. Proc.* **2004**, *807*, 1–6.

28. Jegou, C.; Broudic, V.; Poulesquen, A.; Bart, J. M. *Mater. Res. Soc. Symp. Proc.* **2004**, *807*, 391–396.

29. Mennecart, T.; Grambow, B.; Fattahi, M.; Blondiaux, G.; Andriambololona, Z. *Mater. Res. Soc. Symp. Proc.* **2004**, *807*, 403–408.

30. Stroes-Gascoyne, S.; Betteridge, J. S. *The Effects of Doping Level, Carbonate, Fe and H_2 on the Corrosion Potential and Dissolution Rate of ^{238}Pu-Doped UO_2.* Canadian Nuclear Society Meeting on Waste Management, Decommissioning and Environmental Restoration for Canada's Nuclear Activities: Current Practices and Future Needs, Ottawa, Ontario, 2005.

31. Bailey, M. G.; Johnson, L. H.; Shoesmith, D. W. *Corros. Sci.* **1985**, *25*, 233–238.

32. Sunder, S.; Shoesmith, D. W.; Christensen, H.; Miller, N. H. *J. Nucl. Mater.* **1992**, *190*, 78–86.

33. Sunder, S.; Shoesmith, D. W.; Kolar, M.; Leneveu, D. M. *J. Nucl. Mater.* **1997**, *250*, 118–130.

34. Wren, J. C.; Shoesmith, D. W.; Sunder, S. *J. Electrochem. Soc.* **2005**, *152*, B470–B481.
35. Santos, B. G.; Nesbitt, H. W.; Noel, J. J.; Shoesmith, D. W. *Electrochim. Acta* **2004**, *49*, 1863–1873.
36. Shoesmith, D. W.; Noel, J. J.; Garisto, F. *Mater. Res. Soc. Symp. Proc.* **2004**, *824*, 81–87.
37. Shoesmith, D. W.; Kolar, M.; King, F. *Corrosion* **2003**, *59*, 802–816.
38. Shoesmith, D. W. *Used Fuel and Uranium Dioxide Dissolution Studies: A Review*; NWMO TR-2007-03; Nuclear Waste Management Organization: Toronto, Ontario, 2007.
39. Ekeroth, E.; Jonsson, M.; Eriksen, T. E.; Ljungqvist, K.; Kovacs, S.; Puigdomenech, I. *J. Nucl. Mater.* **2004**, *334*, 35–39.
40. Ekeroth, E.; Roth, O.; Jonsson, M. *J. Nucl. Mater.* **2006**, *355*, 38–46.
41. Nielson, F.; Jonsson, M. *J. Nucl. Mater.* **2006**, *359*, 1–7.
42. Blackwood, D. J.; Naish, J. J.; Platts, N.; Taylor, K. J.; Thomas, M. I. *The Anaerobic Corrosion of Carbon Steel in Granitic Groundwaters*; TR-95-03; Swedish Nuclear Fuel and Waste Management Company (SKB): Stockholm, Sweden, 1995.
43. Smart, N. R.; Blackwood, D. J.; Werme, L. *Corrosion* **2002**, *58*, 547–559.
44. Smart, N. R.; Blackwood, D. J.; Werme, L. *Corrosion* **2002**, *58*, 627–637.
45. Lee, C. T.; Qin, Z.; Odziemkowski, M.; Shoesmith, D. W. *Electrochim. Acta* **2006**, *51*, 1558–1568.
46. Loida, A.; Grambow, B.; Geckeis, H. *J. Nucl. Mater.* **1996**, *238*, 11–22.
47. Grambow, B.; Loida, A.; Dressler, P.; Geckeis, H.; Gago, J.; Casas, I.; de Pablo, J.; Gimenez, J.; Torrero, M. E. *Long-Term Safety of Radioactive Waste Disposal: Chemical Reaction of Fabricated and High-Burnup Spent UO_2 Fuel with Saline Brines*; FZKA 5702; Inst. Nukleare Entsorgungstech, Forschungszent: Karlsruhe, Germany, 1996.
48. El Aamrani, F.; Casas, I.; Martin, C.; Rovira, M.; de Pablo, J. *Effect of Iron and Canister Corrosion Products on the Dissolution of UO_2*. Proceedings of Spent Fuel Workshop, Las Vegas, NV, 1998.
49. Loida, A.; Kelm, M.; Kienzler, B.; Geckeis, H.; Bauer, A. *Mater. Res. Soc. Symp. Proc.* **2006**, *932*, 473–480.
50. Albinsson, Y.; Odegaard-Jensen, A.; Oversby, V. M.; Werme, L. O. *Mater. Res. Soc. Symp. Proc.* **2003**, *757*, 407–413.
51. Cui, D.; Spahiu, K.; Wesrsin, P. *Mater. Res. Soc. Symp. Proc.* **2003**, *787*, 427–432.
52. Loida, A.; Grambow, B.; Geckeis, H. *Mater. Res. Soc. Symp. Proc.* **2002**, *663*, 417–426.
53. Quinones, J.; Serrano, J. A.; Diaz Arocas, P. P.; Rodriguez Almazan, J. L.; Cobos, J.; Esteban, J. A.; Martinez-Esparza, A. *Mater. Res. Soc. Symp. Proc.* **2000**, *663*, 435–439.
54. Ollila, K.; Albinsson, Y.; Oversby, V.; Cowper, M. *Dissolution Rates of Unirradiated UO_2, UO_2 Doped with ^{233}U, and Spent Fuel under Normal Atmospheric Conditions and under Reducing Conditions Using an Isotope Dilution Method*; TR-03-13; VTT Processes: Jyvaskyla, Finland, 2003.

55. Stroes-Gascoyne, S.; King, F.; Betteridge, J. S.; Garisto, F. *Radiochim. Acta* **2002**, *90*, 603–609.

56. Stroess-Gascoyne, S.; King, F.; Betteridge, J. S. *The Effects of Alpha-Radiolysis on UO$_2$ Dissolution Determined from Electrochemical Experiments with ^{238}Pu-Doped UO$_2$*; 06819-REP-01300-10030-R00; Ontario Power Generation, Nuclear Waste Management Division: Toronto, Ontario, Canada, 2002.

57. Stumm, W. *Aquatic Chemical Kinetics: Reaction Rates of Processes in Natural Waters*; John Wiley: New York, 1990.

58. King, F.; Kolar, M. *Validation of the Mixed-Potential-Model for Used Fuel Dissolution against Experimental Data*; 06819-REP-01200-10077-R00; Ontario Power Generation, Nuclear Waste Management Division: Toronto, Ontario, Canada, 2002.

59. King, F.; Kolar, M. *Sensitivity Analysis of the Factors Affecting the Effective G-Value G_{eff} in the Mixed-Potential Model for Used Fuel Dissolution*; 06189-REP-01300-10044-R00; Ontario Power Generation, Nuclear Waste Management Division: Toronto, Ontario, Canada, 2002.

60. Jonsson, M.; Nielsen, F.; Roth, O.; Ekeroth, E.; Nilsson, S.; Hossain, M. M. *Environ. Sci. Technol.* **2007**, *41*, 7087–7093.

61. Liu, L.; Neretnieks, I. *Nucl. Technol.* **2002**, *138*, 69–78.

62. Sellin, P. *Mater. Res. Soc. Symp. Proc.* **2002**, *663*, 755–763.

63. Poinssot, C.; Ferry, C.; Kelm, M.; Grambow, B.; Martinez-Esparza, A.; Johnson, L.; Andriambololona, J.; Bruno, J.; Cachoir, C.; Cavedon, J.-M.; Christensen, H.; Corbel, C.; Jegou, C.; Lemmens, K.; Loida, A.; Lovera, P.; Miserque, F.; De Pablo, J.; Poulesquen, A.; Quinones, J.; Rondinella, V.; Spahiu, K.; Wegen, D. *Spent Fuel Stability under Repository Conditions: Final Report of the European Project*; CEA-R-6093; CEA/Saclay: Cedex, France, 2005.

64. Fanghanel, Th.; Neck, V. *Pure Appl. Chem.* **2002**, *74*, 1895–1907.

65. Neck, V.; Altmaier, M.; Muller, R.; Schlieker, M.; Fanghanel, T. *Solubility of U(VI) in NaCl and MgCl$_2$ Solutions*. Ninth International Conference on Chemistry and Migration Behaviour of Actinides and Fission Products in the Geosphere, Migration '03, Gyeongju, Korea, 2003; p 47.

66. Grambow, B.; Smailos, E.; Geckeis, H.; Muller, R.; Hentschel, H. *Radiochim. Acta* **1996**, *74*, 149–154.

67. Hansen, H. C. B. In *Layered Double Hydroxides: Present and Future*; Rives, V., Ed.; Nova Science Publishers: New York, 2002; pp 413−434.

68. King, F.; Stroess-Gascoyne, S. *An Assessment of the Long-Term Corrosion Behaviour of C-Steel and the Impact on the Redox Conditions inside a Nuclear Fuel Waste Disposal Container*; 06819-REP-01200-10028-R00; Ontario Power Generation: Toronto, Ontario, Canada, 2000.

69. Rollin, S.; Spahiu, K.; Eklund, U. B. *J. Nucl. Mater.* **2001**, *297*, 231–243.

70. Torrero, M. E.; Baraj, E.; de Pablo, J.; Gimenez, J.; Casas, I. *Int. J. Chem. Kinet.* **1997**, *29*, 261–267.

71. Grambow, B.; Loida, A.; Martinez-Esparza, A.; Diaz-Arocas, P.; de Pablo, J.; Marx, G.; Glatz, J. P.; Lemmens, K.; Ollila, K.; Christensen, H. *Source Term for Performance Assessment of Spent Fuel as a Waste Form*; EUR

19140 EN; Nuclear Science and Technology, European Commission: Brussels, Belgium, 2000.

72. Spahiu, K.; Eklund, U. B.; Cui, D.; Lundstrom, M. *Mater. Res. Soc. Symp. Proc.* **2002**, *713*, 633–638.
73. Spahiu, K.; Cui, D.; Lundstroem, M. *Radiochim. Acta* **2004**, *92*, 625–629.
74. Fors, P.; Carbol, P.; Van Winckel, S.; Spahiu, K. *J. Nucl. Mater.* **2009**, *394*, 1–8.
75. Carbol, P.; Fors, P.; Van Winckel, S.; Spahiu, K. *J. Nucl. Mater.* **2009**, *392*, 45–54.
76. Grambow, B.; Forsyth, R. S.; Werme, L. O.; Bruno, J. *Nucl. Technol.* **1990**, *92*, 204–213.
77. Loida, A.; Kienzler, B.; Geckeis, H. *Mater. Res. Soc. Symp. Proc.* **2002**, *757*, 433–439.
78. Spahiu, K.; Devoy, J.; Cui, D.; Lundstroem, M. *Radiochim. Acta* **2004**, *92*, 597–601.
79. Muzeau, B.; Jqgou, C.; Delaunay, F.; Broudic, V.; Brevet, A.; Catalette, H.; Simoni, E.; Corbel, C. *J. Alloys Compd.* **2009**, *467*, 578–589.
80. Sunder, S.; Boyer, G. D.; Miller, N. H. *J. Nucl. Mater.* **1990**, *175*, 163–169.
81. Cui, D.; Eriksen, T. *Reduction of Tc(VII) and Np(V) in Solution by Ferrous Ion: A Laboratory Study of Homogeneous and Heterogeneous Redox Processes*; TR-96-03; Swedish Nuclear Fuel and Waste Management Company (SKB): Stockholm, Sweden, 1996.
82. Guppy, R. M.; Atkinson, A.; Valentine, T. M. *Studies of the Solubility of Technetium under a Range of Redox Conditions*; AERE-R-13467, DOE-RW-89.102; Materials Development Division, Harwell Laboratory, UKAEA: Oxfordshire, U.K., 1989.
83. Tait, J. C.; Johnson, L. H. *Computer Modeling of Alpha Radiolysis of Aqueous Solutions in Contact with Used Uranium Dioxide Fuel*; Whiteshell Nuclear Research Establishment, Atomic Energy of Canada, Ltd.: Pinawa, Manitoba, Canada, 1986; pp 611−615.
84. Pastina, B.; Isabey, J.; Hickel, B. *J. Nucl. Mater.* **1999**, *264*, 309–318.
85. Pastina, B.; LaVerne, J. A. *J. Phys. Chem. A* **2001**, *105*, 9316–9322.
86. King, F.; Quinn, M. J.; Miller, N. H. *The Effect of Hydrogen and Gamma Radiation on the Oxidation of UO_2 in 0.1 $mol.dm^{-3}$ NaCl Solution*; TR-99-27; Whiteshell Laboratories, Atomic Energy of Canada, Ltd.: Pinawa, Manitoba, Canada, 1999.
87. King, F.; Shoesmith, D. W. *Electrochemical Studies of the Effect of H_2 on UO_2 Dissolution*; TR-04-20; Integrity Corrosion Consulting, Ltd.: Calgary, Alberta, Canada, 2004.
88. Shoesmith, D. W.; Sunder, S.; Hocking, W. H. In *Electrochemistry of Novel Materials*; Lipkowski, J., Ross, P. N., Eds.; VCH Publishers: New York, 1994; pp 297−337.
89. Petrik, N. G.; Alexandrov, A. B.; Vall, A. I. *J. Phys. Chem. B* **2001**, *105*, 5935–5944.
90. Eriksen, T. *Radiolysis of Water within a Ruptured Fuel Element*; U-96-29; Swedish Nuclear Fuel and Waste Management Company (SKB): Stockholm, Sweden, 1996.

91. Jonsson, M.; Nielsen, F.; Ekeroth, E.; Eriksen, T. E. *Mater. Res. Soc. Symp. Proc.* **2004**, *807*, 385–390.
92. Grambow, B.; Mennecart, T.; Fattahi, M.; Blondiaux, G. *Radiochim. Acta* **2004**, *92*, 603–609.
93. Haschke, J. M.; Allen, T. H.; Stakebake, J. L. *J. Alloys Compd.* **1996**, *243*, 23–35.
94. Devoy, J.; Haschke, D.; Cui, D.; Spahiu, K. *Mater. Res. Soc. Symp. Proc.* **2003**, *807*, 41–46.
95. Madhavaram, H.; Idriss, H. *J. Catal.* **1999**, *184*, 553–556.
96. Taylor, S. H.; Heneghan, C. S.; Hutchings, G. J.; Hudson, I. D. *Catal. Today* **2000**, *59*, 249–259.
97. Heneghan, C. S.; Hutchings, G. J.; O'Leary, S. R.; Taylor, S. H.; Boyd, V. J.; Hudson, I. D. *Catal. Today* **1999**, *54*, 3–12.
98. Graselli, R. K.; Burrington, J. D.; Suresh, D. D.; Friedrich, M. S.; Hazle, M. A. S. *J. Catal.* **1981**, *68*, 109.
99. Graselli, R. K.; Suresh, D. D. *J. Catal.* **1972**, *25*, 273–291.
100. Madhavaram, H.; Idriss, H. *J. Catal.* **2002**, *206*, 155–158.
101. Ai, M. *J. Catal.* **1983**, *83*, 141–150.
102. Senanyake, S. D.; Waterhouse, G. I. N.; Chan, A. S. Y.; Madey, T. E.; Mullins, D. R.; Idriss, H. *Catal. Today* **2007**, *120*, 151–157.
103. Kleykamp, H. *J. Nucl. Mater.* **1985**, *131*, 221–246.
104. Kleykamp, H. *Nucl. Technol.* **1988**, *80*, 412–422.
105. Johnson, L. H.; Shoesmith, D. W. Spent Fuel. In *Radioactive Waste Forms for the Future*; Elsevier Science Publishers: Amsterdam, The Netherlands, 1988.
106. Broczkowski, M. E. Ph.D. Thesis, The University of Western Ontario, London, Ontario, Canada, 2008.
107. Norskov, J. K.; Bligaard, T.; Logadottir, A.; Kitchin, J. R.; Chen, J. G.; Pandelov, S.; Stimming, U. *J. Electrochem. Soc.* **2005**, *152*, J23–J26.
108. Cui, D.; Low, L.; Sjostedt, K.; Spahiu, K. *Radiochim. Acta* **2004**, *92*, 551–555.
109. Nilsson, S.; Jonsson, M. *J. Nucl. Mater.* **2008**, *372*, 160–163.
110. Broczkowski, M. E.; Noel, J. J.; Shoesmith, D. W. *J. Nucl. Mater.* **2005**, *346*, 16–23.
111. Broczkowski, M. E.; Zhu, R.; Ding, Z.; Noel, J. J.; Shoesmith, D. W. *Mater. Res. Soc. Symp. Proc.* **2006**, *932*, 449–456.
112. Broczkowski, M. E.; Noel, J. J.; Shoesmith, D. W. *J. Electroanal. Chem.* **2007**, *602*, 8–16.
113. Nilsson, S. Ph.D. Thesis, KTH Chemical Science and Engineering, Stockholm, Sweden, 2008.
114. Trummer, M.; Roth, O.; Jonsson, M. *J. Nucl. Mater.* **2008**, *383*, 226–230.
115. Nilsson, S.; Jonsson, M. *J. Nucl. Mater.* **2008**, *374*, 290–292.
116. Goldik, J. S.; Noel, J. J.; Shoesmith, D. W. *J. Electroanal. Chem.* **2005**, *582*, 241–248.
117. Goldik, J. S.; Noel, J. J.; Shoesmith, D. W. *J. Electrochem. Soc.* **2006**, *153*, E151–E159.

Chapter 27

Integrated Repository Science for the Long-Term Prediction of Nuclear Waste Disposal

Patricia Paviet-Hartmann* and Thomas Hartmann

University of Nevada Las Vegas, 4505 Maryland Parkway, Box 454009, Las Vegas, NV 89154
***patricia.paviet-hartmann@unlv.edu**

Performance assessment of nuclear salt repositories may vary depending on the model and the variability of the parameters. It seems important to lower the degree of freedom of repository models by implementing reasonable constraints based on experimental data. The authors will present data encompassing an integration of different scientific disciplines describing the overall processes that occur under repository conditions. Scenarios of post-closure radioactive releases involving hydrologic transport of radionuclides in brines will be discussed by showing examples of Cm(III) and U(VI) complexation in brines. Laboratory research conducted to determine the behavior of ^{239}Pu in brines after exposure to MgO backfill will be presented to illustrate the importance of backfill material. Finally, any long-term prediction of a nuclear waste repository cannot omit the importance of radiolysis which will be introduced by the application of 5 MeV Helium ion beam line experiments.

Introduction

The quality of a disposal strategy for nuclear waste is determined by its isolation capacity towards the actinide elements, which are considered the most radiotoxic radionuclides. As an administrative measure, the quality of the disposal strategy is evaluated by performance assessment, which should include experimental data like thermodynamic and kinetics, unfolding the most

dominant processes relevant to potential mobilization of radionuclides from the primary waste-forms, to the retention in secondary actinide-host phases, to their migration towards the biosphere. The generally accepted conception for nuclear waste disposal is burial in deep geologic formation (salt, tuff, hard rock or clay) chosen to ensure that the radiotoxic constituents of nuclear waste will remain confined as a result of the geochemical constitution and the addition of engineered barriers. These natural and engineered barriers will impede or at least minimize the potential release of radionuclides to the environment. Hereby, one of the greatest concerns and a potential worst-case scenario for environmental sound disposal is groundwater intrusion. Groundwater intrusion into a nuclear waste repository may affect the constitution and composition of the geological barrier by the inundation of the repository by the surrounding aquifers. Therefore geo-engineered barriers like periclase-based MgO backfill material used at the Waste Isolation Pilot Plant (WIPP) repository are designed to minimize waste-form groundwater interaction, to delay the development of mobile actinide species, and to sequester microbial gas generated. However, the impact of periclase-based backfill material on repository performance is not fully understood. Furthermore, in case of water intrusion into a generic salt repsotiory, exposure of chloride-dominated brines to radiation from degraded nuclear waste will probably take place. For instance, in a generic salt repository groundwater or brines, alpha- and gamma radiation emitted from light actinides will induce the formation of radiolytic species such as hypochlorite (OCl^-) hypochlorous acid (HOCl), hypobromite (HOBr) which, in the absence of reductants, can cause higher redox potentials, enhance waste-forms dissolution rates, and furthermore promote higher actinide oxidation states, as well as higher actinide solubilities.

The objectives here is to demonstrate that laboratory experiments are crucial for the development and evaluation of a generic salt repository model because the generated data will provide reasonable uncertainty ranges for long-term actinide speciation and actinide concentration resulting in a durable repository performance assessment of the long-term exposure of the public. Therefore, an integration of the different scientific disciplines (e.g. radiochemistry, geochemistry, and materials science) appears necessary for the accurate determination of the overall processes expected within a geological repository receiving nuclear waste and for an increased reliability in the forecast of long-term repository performance.

Overview of Back Fill Material Studies

As post-closure conditions progress, brine-waste interactions and subsequent dissolution and transport of actinides in brines could occur such that actinides may become available to enter possible intrusion pathways generated in the future. Strong chemical sorption and precipitation of radionuclides, as well as weak dissolution behavior for radionuclides in the initial contaminant materials, are the major processes for immobilization of actinides in repository sites.

Most radioactive waste disposal programs are considering the use of repository backfill materials to enhance the containment of radioactive waste. The concepts include the use of backfill to provide well-defined chemical conditions,

favorable hydraulic conductivity, and desirable physical characteristics within the disposal facility. The backfill materials have been classified into two groups according to their primary properties, including chemical backfills such as cementitious materials and magnesium oxide (MgO), and hydrological/physical backfills such as clay, salt and cementitious materials. Cementitious materials have been used as both chemical and physical backfill. A chemical backfill has the ability to buffer the chemistry of the repository to conditions that favor low radionuclide solubility and has the ability to sorb or incorporate radionuclides and, therefore, retard their release from the repository. In the UK, the backfill material, Nirex Reference Vault Backfill (NRVB) (*1*), a mixture of 40% of OPC (ordinary Portland cement), 15% lime and 45% crushed limestone has been proposed for intermediate level radioactive waste (ILW) disposal to maintain a high-pH aqueous environment in the repository. The high pH lowers the solubility of important radionuclides and the high surface area of surface-active minerals in the NRVB promotes radionuclide sorption. In Switzerland, cementitious materials have been used as a repository backfill for low level and intermediate level radioactive wastes. This material has large micro-porosity and internal surfaces, which in turn provide lager reaction and sorption sites for radionuclides. It also has a high pH, which lowers the solubility of radionuclides (*2*).

A hydrological/physical backfill, with its low hydraulic conductivity and diffusivity, has the ability 1- to minimize access of groundwater to the waste and limit radionuclide migration, 2- to ensure repository stability and support waste packages, whereas the dissipation of heat away from the waste is effectively promoted through its thermal conductivity. Canada's concept for nuclear fuel waste disposal is based on a multiple barrier system. The nuclear fuel waste would be disposed in an engineered excavation at a depth of 500 m to 1000 m in the granite of the Canadian Shield. Based on their concepts, clay-based buffer and backfill and cement-based sealing materials were studied (*3*). They found that clay-, cement- and bitumen-based backfill materials can minimize water flow around the container to limit corrosion and waste-form dissolution, and provide enhanced seals at hydraulically critical points in a vault. These materials can decrease the hydraulic conductivity so that the radionuclide transport is diffusion-controlled, and the radionuclide release is delayed by incorporating materials that inhibit water movement and entrap radionuclides. In Germany, rock salt formation has been extensively studied for the final disposal of both radioactive waste and hazardous chemically toxic waste. The thermal and mechanical behavior of salt and its radiolytic stability were investigated and adequate models exist to describe the long-term behavior of salt (*4–6*).

MgO Back Fill Material Used at WIPP

MgO is the engineered backfill recognized by the environmenral Protection Agency (EPA) in the WIPP repository. Its introduction was motivated by the need to mitigate the effect of microbial CO_2 generation on actinide mobility in a post-closure repository environment (*7, 8*). MgO will sequester CO_2 and buffer brine pH at a moderately basic level, thus minimizing actinide solubilities in WIPP

brines. Water uptake by MgO will delay the development of mobile actinides and gas generation by microbes and corrosion. Reduced gas generation will reduce or even eliminate spallings releases. As MgO hydrates, it swells, reducing porosity and permeability, which will inhibit gas flow in the repository, in turn reducing spallings releases. Hydration will also result in a self-sealing mechanism by which water uptake and swelling of MgO adjacent to a groundwater seep cuts off further seepage. Reaction with some groundwaters will produce cementitious materials, which will help to cement waste particles or produce a cohesive solid mass. Larger particles are less likely to be entrained in a spallings release. If sufficient water eventually accumulates in a repository to support microbial gas generation, magnesium carbonate cements will form; also producing good cohesion and strength (*9*).

Extensive studies, conducted by several researchers, have led to a better understanding of the behavior of MgO, along with its carbonation and hydration products (*10–15*). Grambow *et al.* (*4*), found that with MgO addition, alkaline pH values > 8 could only be achieved if no additional chloride- or sulfate-based Mg-minerals would be dissolved. Magnesium oxide sequestered CO_2 generated by microbial degradation of organic materials in the waste, with the formation of relatively insoluble carbonate solids (*8, 9*). Moreover, MgO reduced the amounts of free liquid in the repository through hydration reactions. It was reported (*9*) that MgO was effective in absorbing water and CO_2, although it indicated that conversion of MgO to hydroxycarbonate was limited by the formation of mineral rinds. The hydration reaction was associated with an increase in pH, volumetric expansion, and the production of heat. Magnesium oxide may react with potential intruding brines and form $Mg(OH)_2$ or Mg-hydroxychlorides (e.g., $Mg_3(OH)_5Cl \cdot 4H_2O$) (*4*). Bynum *et al.* (*7*) reported that the use of MgO as the backfill material not only controlled the pH of the expected fluids, but also effectively removed carbonate from the system. If CO_2 were present, magnesite or hydromagnesite would be formed. It was reported that magnesite controlled the maximum carbonate concentrations in most brines of the hexary system of oceanic salt solids (*4*).

The technical MgO backfill material introduced into the WIPP repository is produced through calcination of magnesium carbonate and contains as the main phase: periclase (MgO) with about 90 to 96 wt.-% and as the minor phases: lime (CaO) and the silicates forsterite (Mg_2SiO_4), and monticellite ($CaMgSiO_4$). The oxides periclase and lime are well crystallized, their X-ray peak profiles and lattice parameters can be refined to good quality figures and their quantification using X-ray diffraction-based analysis is consistent. The precise quantification of forsterite and especially monticellite is not possible based on their poor crystallinity and low contents. But beside some inconsistencies in the relative quantification of the silicates using Rietveld refinement, the associated lattice parameter refinement always confirms the unit cells of forsterite and monticellite (Table I). It should be mentioned that both silicates could form solid solutions by partly replacing Mg^{2+} with Fe^{2+} that will impact unit cell dimensions and the structure factors, but also crystallinity when annealing is not sufficient. MgO backfill samples were obtained from Sandia National Laboratories (SNL). A representative MgO sample was fractionated into a fraction (A) > 1 mm and (B) < 1 mm. A part of fraction

(B) was exposed to air under ambient conditions for two weeks (sample (C)) before XRD analysis. The samples were ground to sizes of approximately 10 – 30 microns and placed in a standard sample holder to be used in the 9-position sample stage. The samples were analyzed by X-ray diffraction using a D8-11 Advance from Bruker AXS using Cuk$\alpha_{1/2}$ irradiation at 40 kV and 40 mA. All measurements were conducted in step-scan mode with step sizes of 0.02°2θ and step time of 3 to 5 seconds. To improve resolution the system was equipped with primary and secondary 2.3 ° Soller slits and the variable slit system was set to 1° for the divergence slit and 0.5° for the anti-scatter slit. The receiving slit was set to be 0.1 mm and to minimize fluorescence-related background, a graphite secondary monochromator in combination with a scintillation counter was used. No internal standards were used; the correction for goniometer off-set and sample displacement, line positioning and line profiles were verified by the use of NIST SRM silicon 640c (*a* = 5.4311646(92) Å) and a NIST SRM LaB$_6$ 660a (*a* = 4.1569162(97) Å) line standards prior to the measurements.

The X-ray patterns were analyzed qualitatively by using the EVA evaluation software package associated with the X-ray powder data-base ICDD-PDF 1-50, and analyzed quantitatively by using the TOPAS-2 Rietveld refinement software package combined with single-crystal X-ray data using the ICSD inorganic crystal structure database from FIZ Karlsruhe.

In Figures 1 and 2, the measured X-ray patterns are compared with the total calculated patterns based on the phase-specific scattering functions through Rietveld refinement. The difference-intensity functions (measured intensities - calculated intensities) are displayed and the theoretical phase-specific line positions indicated (periclase (1), lime (2), forsterite: (3), monticellite (4)).

By using X-ray diffraction combined with least-square and Rietveld refinement techniques the crystalline solid phase constitution of technical MgO in the grain size fraction < 1mm can be quantified to a high confidence level. The sample (A) contains (a) 95-96 wt.-% periclase (MgO), (b) 0.7-1 wt.-% lime (CaO), 1-2 wt.-% forsterite (Mg$_2$SiO$_4$), and 1-2 wt.-% monticellite (CaMgSiO$_4$). The profile parameter of the oxides and forsterite were refined based on symmetric pseudo-Voigt (PV) functions. The poor crystallinity of the silicate monticellite does not allow refining PV profile parameter. In all MgO samples, impurities of an unknown phase (black arrow) in the range between d = 2.67 Å and d = 2.68 Å were identified. These impurities may represent another silicate-phase of a sulfate-containing phase, which has to be proven by chemical analysis.

Table I. Refinement results of MgO Backfill for the WIPP repository (*16*)

Refined Results	MgO sample A	MgO sample B	MgO Sample C	
Main Phase	**Periclase MgO**	**Periclase MgO**	Periclase MgO	Reference PDF 45-946
Spacegroup	Fm-3m	Fm-3m	Fm-3m	Fm-3m
Lattice parameter a (Å)	4.21072	4.20868	4.20664	4.2112
Wt. %	96.09275	94.62323	91.90251	
Cell Mass	161.24	161.24	161.24	161.24
Cell Vol (Å^3)	74.65681	74.54848	74.4399	74.68
R Bragg	3.380	6.885	17.107	
Minor Phase	**Lime CaO**	**Lime CaO**	**Lime CaO**	**Reference PDF 37-1497**
Spacegroup	Fm-3m	Fm-3m	Fm-3m	Fm-3m
a (Å)	4.80326	4.80152	4.79687	4.81059(9)
Wt. %	0.7899773	0.7651397	1.624722	
Cell Mass	224.32	224.32	224.32	224.32
Cell Vol (Å^3)	110.8174	110.6969	110.3757	111.33
R Bragg	17.932	11.491	11.239	
Minor Phase	**Forsterite Mg₂SiO₄**	**Forsterite Mg₂SiO₄**	**Forsterite Mg₂SiO₄**	**Reference PDF 34-189**
Spacegroup	Pnma	Pnma	Pnma	Pnma
a (Å)	10.19384	10.21049	10.21786	10.1978(8)
b (Å)	5.98369	5.97657	5.97032	5.9817(5)
c (Å)	4.75064	4.77051	4.76895	4.7553(3)
Wt. %	2.320575	2.375034	2.510675	
Cell Mass	562.84	562.84	562.84	562.84
Cell Vol (Å^3)	289.7736	291.114	290.9249	290.07
R Bragg	25.450	14.905	20.518	
Minor Phase	**Monticellite CaMgSiO₄**	**Monticellite CaMgSiO₄**	**Monticellite CaMgSiO₄**	**Reference PDF**
Space group (standard setting)	Pnma	Pnma	Pnma	Pnma
a (Å)	11.06060	10.99066	10.97537	11.074(1)
b (Å)	6.34199	6.36305	6.36352	6.3666(6)
c (Å)	4.80999	4.79581	4.79432	4.8224(6)
Wt. %	1.543196	2.236597	3.962094	
Cell Mass	625.92	625.92	625.92	625.92
Cell Vol (Å^3)	337.4026	335.391	334.8446	340.0
R Bragg	26.492	20.914	23.283	
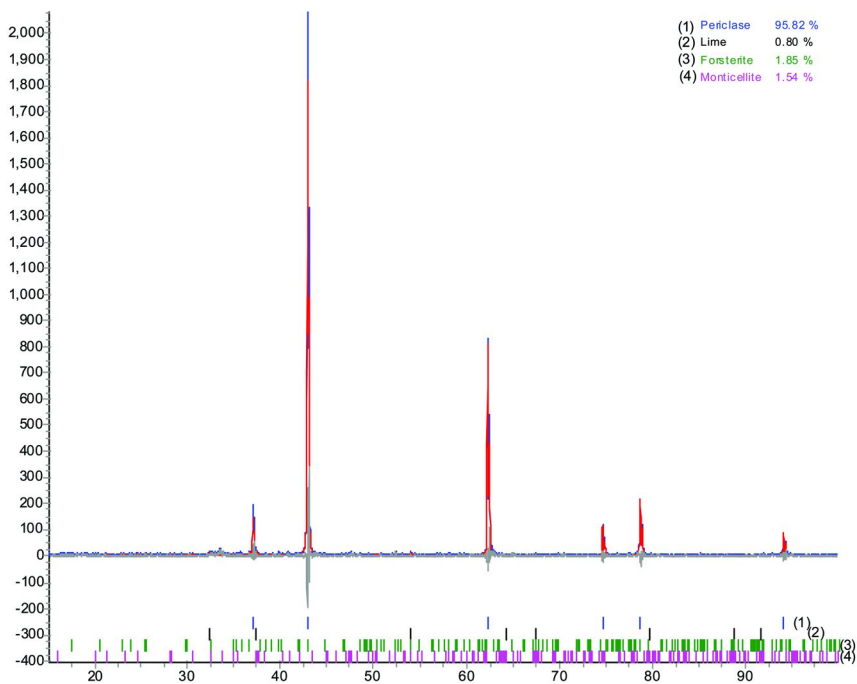
Figure 1. X-ray Diffraction Pattern of MgO Sample (A) > 1 mm, 15 to 100°2θ
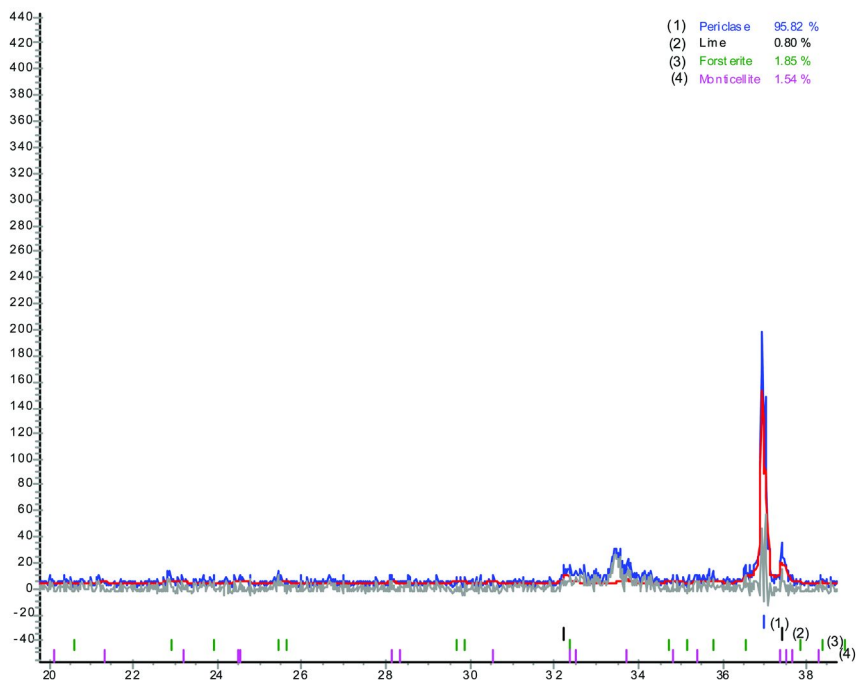
Figure 2. X-ray Diffraction Pattern of MgO Sample (A) > 1 mm, 20 to 39°2θ

Solid Phase Constitution of MgO in Contact with Synthetic WIPP Brines

Technically processed MgO (90-95 wt.-% periclase) was immersed into synthetic WIPP brine for several weeks and changes in phase constitution were quantified by using Rietveld refinement on X-ray diffraction powder data. The crystalline phases formed as a result of the MgO-brine interaction may dominate the sorption- and de-sorption of actinides as well as actinide precipitation and actinide fixation through actinide-host-phase formation within the life cycle of the repository. These interactions can only be understood through realistic (hot) experiments. The assumptions of the long-term geochemical and radiochemical repository conditions through geochemical modeling is only successful if input data (crystalline phase formation and Gibbs energies) are available and in compliance with experimental data. As shown in Figure 3, the reacted sample showed stratographic separation and the sample holders exhibited swelling and rupturing within the zone of maximum hydration and Sorel cement formation associated with high crystallization pressure.

The different sample locations represent different reaction conditions for MgO backfill to convert into either (1) Sorel cement (Bischofite, Tachyhydrite, Korshunovskite, and/or $Mg_3(OH)_5Clx4H_2O$) (2) Brucite and (3) Gypsum. While Bischofite was most likely formed via gel-formation apart from the solid sample (Figure 3, -10-0 mm), the formation of Korshunovskite might be considered as the dominant sub-reaction when MgO is in contact with $MgCl_2$ solution and the major product of the hydration and chlorination of MgO. The phase contents of Korshunovskite and Periclase exhibit reciprocal relations to each other and the content of Korshunovskite rises approximately linear with MgO turnover and reaction progress. The concentrations of calcium and sulfate present in the backfill and the brine define the quantity of the phases Tachyhydrite and Gypsum formed. This phase constitution is associated with a white topographic separation on top of the sample. The formation of Tachyhydrite is limiting the calcium concentration in $MgCl_2$ solution to allow hydration and chlorination of MgO into Korshunovskite. The Tachyhydrate formation may also serve to a more important purpose. Tachyhydrate has the potential to incorporate plutonium into its crystal structure to partly substitute calcium from its lattice site. As an important consequence, the Tachyhydrate formation may significantly limit actinide (plutonium) concentration in the repository by forming a Tachyhydrite-like $(Ca_{1-x}Pu_x)Mg_2Cl_6x12H_2O)$ host phase. It would be wise to investigate the potential formation of a most-likely Tachyhydrite-like actinide host phase based on its impact on the radiochemical conditions of a generic salt repository.
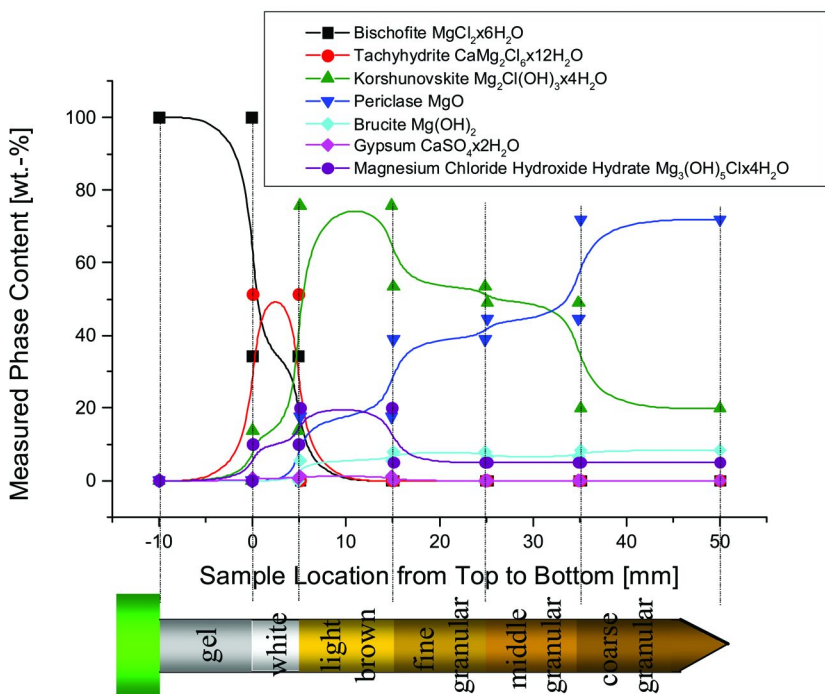
Figure 3. Phase constitution of WIPP MgO backfill in contact with 3.7 M MgCl$_2$ for several weeks. The content of the individual identified phases are quantified by Rietveld refinement of X-ray powder data and the specific sample position from sample top (0 mm) and sample bottom (50 mm) are marked. The absolute content of magnesium chloride hydroxide hydrate (Mg$_3$(OH)$_5$Clx4H$_2$O) is only roughly estimated since crystal structure date of this phase are not available.

The formation of Korshunovskite (Figure 4) might reflect the thermodynamics and also the kinetics of the transformation of MgO in MgCl$_2$ solution into Sorel cement. To further understand the impact of the also present magnesium chloride hydroxide hydrate (Mg$_3$(OH)$_5$Clx4H$_2$O) phase on the Sorel cement formation, its crystal structure should be determined. Despite an early assumption that MgO would buffer pH and sequester microbiological and radiolytical CO$_2$, there is no obvious reason for Sorel cement phases as determined here to undergo significant carbonation and to buffer the pH in the geochemical system. Tachyhydrate CaMg$_2$Cl$_6$ x 12 H$_2$O not only lowers Ca-concentration, it may have the potential to incorporate Pu into its crystal structure and to form a stable host phase for actinides: e.g."*Ca$_{1-x}$(Pu,U,Th)$_x$Mg$_2$Cl$_6$x12H$_2$O*".
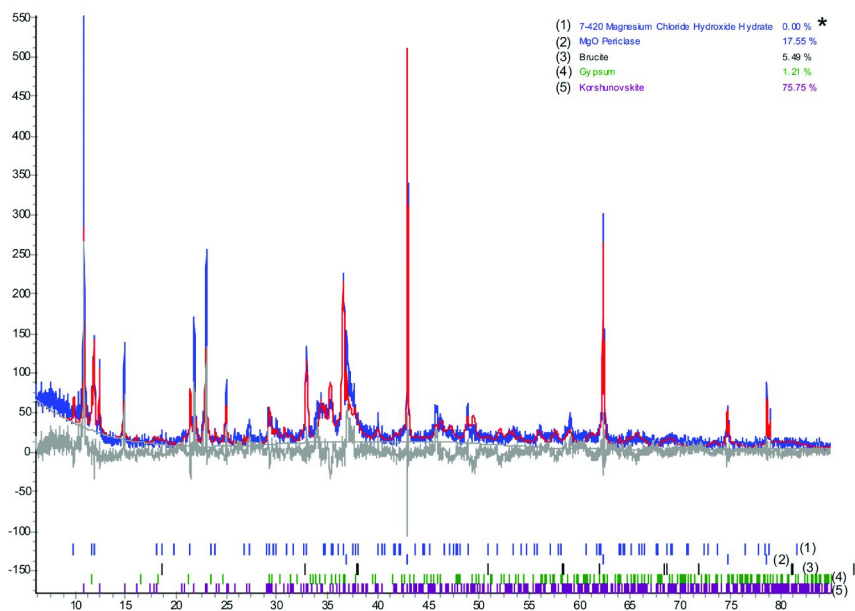
*Figure 4. Phase constitution of MgO backfill reacted with MgCl₂ – based brine. Zone of maximum hydration and chlorination X-ray diffraction analysis by Rietveld refinement. *: Phase content of magnesium chloride hydroxide hydrate could not be calculated since the crystal structure is unknown*

Back Fill MgO Brines Interaction with Plutonium

A separate, but related issue concerns the heterogeneity of a generic salt repository in terms of rewetting after closure and new phase formation in the backfill. Questions such as how long rewetting may take place in a repository, or by which paths the infiltrating water may pass through, are answered in most cases with an intrusion of water scenario. After closure, if a generic salt repository is partially inundated, portions of the repository may become wetted to various degrees and the backfill may undergo phase changes, whereas, other portions may not be wetted at all.

Villarreal *et al.* (*17*) reported that an addition of MgO to a CO_2 pressurized WIPP brine increased pcH from 4.48 to 7.7; the concentration of Pu with all other actinides were reduced by 90% to 95%. Farr et al. (*18*) reported that brucite $(Mg(OH)_2)$ rapidly sorbed near 100% of aqueous Pu(IV) from pH 8 to pH 13, and the presence of citrate did not affect the sorption of Pu(IV). The X-ray photoelectron spectroscopy (XPS) results indicated Pu(IV) was incorporated in the subsurface of brucite. Experiments on the effectiveness of MgO on sorption and desorption of actinides (especially [239]Pu) from Pu-MgO-brine and Pu-MgO-chloride mixtures demonstrate that the impact of MgO-backfill on actinide chemistry is rather complex (*19*).

Several experiments on 1) the effect of MgO backfill on the chemical properties of synthetic brines, 2) the behavior of [239]Pu(VI) in MgO pore solutions after MgO backfill was equilibrated with brines and chloride solutions; and 3) the desorption of [239]Pu from a Pu-MgO-brine and Pu-MgO-chloride conglomerates are presented in the following sections to illustrate the backfill MgO brines interactions with plutonium.

Behavior of [239]Pu - Sorption and Precipitation

The discussion about plutonium sorption and precipitation is focused on the scenario where MgO backfill is fully inundated with the brines, which is a major concern for potential actinide migration from a repository towards the biosphere. In $MgCl_2$-rich solutions, both adsorption and precipitation processes of plutonium might occur simultaneously at a pH greater than 7, but less than 8. Under this pH range, Pu(VI) is not stable and is reduced to Pu(IV) (*20*). When the solution pH is less than 8.0, the predominant species of plutonium in the solution may include plutonium chloride such as $PuCl^{3+}$, $PuCl_2^{2+}$ and $PuCl_3^+$ (*21*), plutonium oxide PuO_2^0 and plutonium hydroxide such as $Pu(OH)_4^0$. The species of PuO_2^0 and $Pu(OH)_4^0$ are insoluble (*21*) and they would be precipitated. The species of plutonium chloride, $PuCl^{3+}$, $PuCl_2^{2+}$ and $PuCl_3^+$, are soluble, but would likely be adsorbed by the MgO backfill. However, in NaCl based brines solutions, the precipitation of plutonium might be the major process, resulting in the reduction of Pu(VI) from the solutions due to pH values greater than 9.5 −13+. In solutions with high pH, the primary species of plutonium are tetrahedral valence oxides and hydroxide such as PuO_2^o and $Pu(OH)_4^0$ (*20*), which are insoluble. This results in almost all of the introduced plutonium being precipitated. To confirm the influence of pH on the solubility of Pu(VI) in brines, first two synthetic WIPP brines solutions were prepared (Table II) and two tests were performed. Generic WIPP Brine (GWB) and Egnergy Research and Development Adminsitration (WIPP Well) (ERDA brine) were used to simulate WIPP brines in this study. In the first test, the pH of Pu(VI)-GWB solution containing $10^{-7}M$ Pu(VI) was adjusted to 8.5 and the pH of the Pu(VI)-ERDA solution containing $10^{-7}M$ Pu(VI) was adjusted to 12.0. In the second test, 1 mL of $10^{-7}M$ Pu(VI)-GWB and 1 mL of $10^{-7}M$ Pu(VI)-ERDA was added to 10 mL of the solutions that were collected from the MgO-GWB and the MgO-ERDA solids at MgO to water ratios of 1:0.25 and 1:10, respectively. At the end of both tests, the final solutions were mixed thoroughly and the final pH values were measured again. Afterwards, the solutions were centrifuged at 38,300 g for 1 h. The [239]Pu activity in the supernatant was counted using a liquid scintillation counter.

Table II. Chemical composition of two synthetic WIPP brines (*19*)

Reagent	GWB or Brine G (Salado Brine) (g)	ERDA-6 or Brine E (Castile brine) (g)
Na_2SO_4	23.972	22.515
NaBr	2.602	1.074
$Na_2B_4O_7 \cdot 10\ H_2O$	14.305	22.515
NaCl	170.630	248.558
KCl	33.093	6.869
$MgCl_2 \cdot 6H_2O$	196.698	3.667
LiCl	0.177	N/A
$CaCl_2 \cdot 2H_2O$	1.930	1.76
Total volume	1000.00 mL	1000.00 mL

Table III. Influence of pH on the solubility of ^{239}Pu(VI) in brines

Sample ID	Final pH	% Reduction of Pu	Observation
Pu(VI)-GWB working solution	*8.5	13.9	A small amount of white precipitates was observed after the solution was centrifuged
Pu(VI)-ERDA working solution	*12.0	99.7	White precipitates were formed at pH ~8.5. The solution became a white gel at pH 11.0
MgO-GWB 25%	**8.28	81.4	Visible white precipitates were easily observed
MgO-GWM 1:10	**8.32	67.7	White precipitates were formed
MgO-ERDA 25%	**10.02	97.5	Visible white precipitates were easily observed
MgO-ERDA 1:10	**8.41	54.8	A small amount of white precipitates was observed after the solution was centrifuged

* The pH values were the final pH after pH adjustment using NaOH.   ** The pH values were the final pH after addition of $10^{-7}M$ of Pu(VI) to the pore solutions.

When the pH of Pu(VI)-GWB solution containing $10^{-7}M$ Pu(VI) was adjusted to 8.5, a small amount of white precipitate was observed after the solution was centrifuged and 13.9% of the Pu(VI) was reduced. The reduction of hexavalent plutonium was confirmed by UV Visible spectrophotometry. When the pH of Pu(VI)-ERDA solution containing $10^{-7}M$ Pu(VI) was adjusted, white precipitates were formed at a pH of ~8.5 and formation of a white gel started at pH> 8.5. All of the solution became a white gel at pH 11.0. Approximately 99.7% of Pu was removed from the solution after centrifugation. When 1 mL of $10^{-7}M$ Pu(VI)-GWB and 1 mL of $10^{-7}M$ Pu(VI)-ERDA were added to the solutions collected from MgO-GWB and MgO-ERDA solids, respectively, white precipitates were observed. Approximately 68% to 81% of Pu was removed from the MgO-GWB pore solution after centrifugation, while approximately 55% to 97% of Pu was removed from the MgO-ERDA pore solutions (Table III). These results confirm that solution pH is the major factor controlling the solubility of Pu. Therefore, increases in solution pH by use of MgO backfill significantly control the Pu migration in the repository.
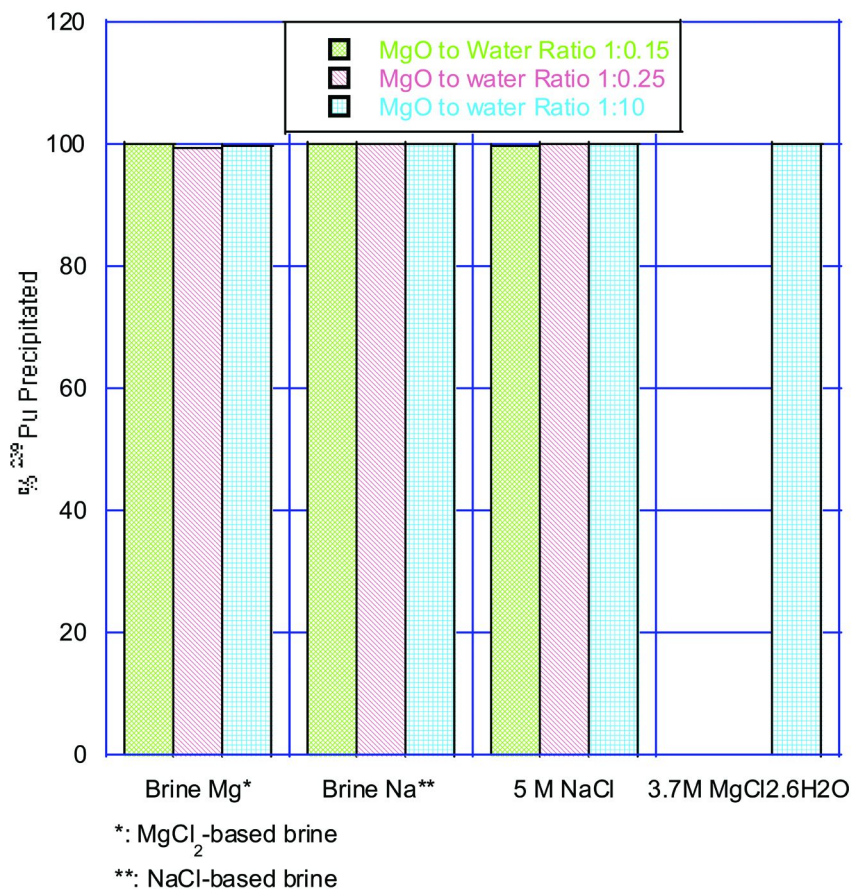
Figure 5. Pu(VI) precipitation in the presence of MgO in contact with chloride solutions and synthetic brines after 68 days, at three different MgO to water ratios: 1:0.15, 1:0.25, and 1:10 (19).

Behavior of Pu-239 - Release of [239]Pu

Desorption of plutonium from Pu-loaded MgO conglomerates, which were collected from the MgO backfill that was equilibrated with 15%, 25% and 1:10 of [239]Pu(VI) brines, was performed. These desorption experiments were performed to examine the release of Pu from MgO conglomerates after exposure of Pu(VI)-brines to MgO backfill for 68 days. Data show that at least 99% of Pu was removed from the solutions by precipitation and/or adsorption in all water levels (Figure 5).

The desorption experiments were conducted using Pu-free solutions in the presence or absence of 3.2 x $10^{-5}M$ NaOCl solution, at room temperature under agitated and non-agitated conditions. Hypochlorite may be one of the radiolysis by-product formed after irradiation of sodium chloride solutions by alpha emitters as described in the next section on radiolysis. After 36-day agitating extraction (shaking at 100 rpm), the presence of hypoclorite (OCl^-) did not significantly influence the release of Pu from the Pu-loaded MgO conglomerates (Figure 6). When the Pu-loaded MgO conglomerates, which were collected from MgO backfill that had been in contact with Pu(VI) solutions (at a MgO to water ratio of 1:0.25), were used for desorption, as much as 30% of the Pu was released. The release rate of Pu follows the order of MgO-GWB > MgO-ERDA> MgO-NaCl > MgO-$MgCl_2 \cdot 6H_2O$.

However, under non-agitated conditions, regardless of the presence or absence of hypochlorite, small amounts of Pu were released from the Pu-loaded MgO-GWB conglomerate, and no Pu was released from the Pu-loaded MgO-ERDA conglomerates after 110 days (Figure 7).

The studied MgO backfill material has an ability to sorb or incorporate plutonium and other actinides, therefore retarding their release from the WIPP repository site. However, accidental intrusion in a generic salt repository (eventually through oil and gas explorations), with the consequence of inundation, may cause a potential release of plutonium.

Radiolysis

Groundwater intrusion into a designated nuclear generic salt repository causes the repository to be at least partly inundated with brine, which further is exposed to radiation from the nuclear waste. The obvious impact of radiolysis on repository performance is not greatly considered in performance assessment efforts. In absence of potential reductants (e.g. metal-ions from corrosion of container materials), radiolysis by-products such as hypochlorite (OCl^-), hyprochlorous acid (HOCl), hyprobromous acid (HOBr) favor higher redox potentials, enhancement of waste-form dissolution, and more importantly, oxidation of actinides to their higher oxidation state, which is usually the most soluble (*23–25*). In actual groundwater, the situation is more complex because natural chloride-based salt brines contain certain amounts of bromides that could have a drastic effect on the radiolytic oxidation of chlorides and the induced formation of radiolytic bromide species (*26–28*).
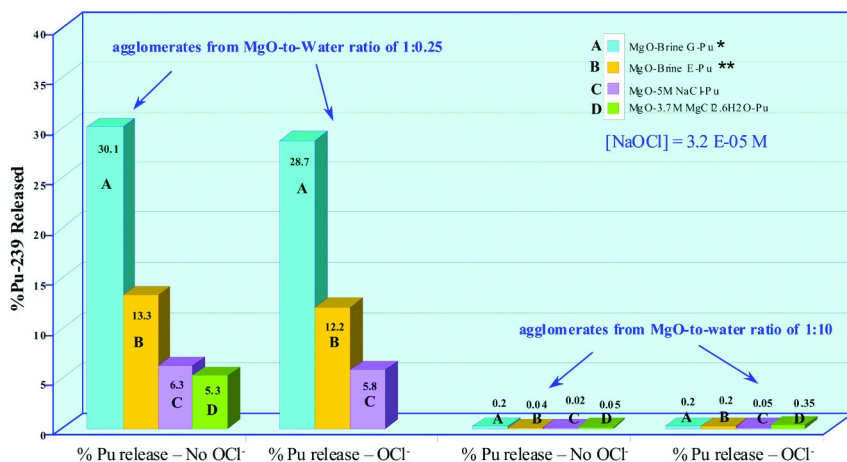
Figure 6. Desorption of ^{239}Pu from Pu-loaded MgO WIPP backfill material after 36-day in agitated conditions (22). MgO-Brine-G Pu*: $MgCl_2.6H_2O$ based Brine MgO-Brine-E Pu**: NaCl based Brine
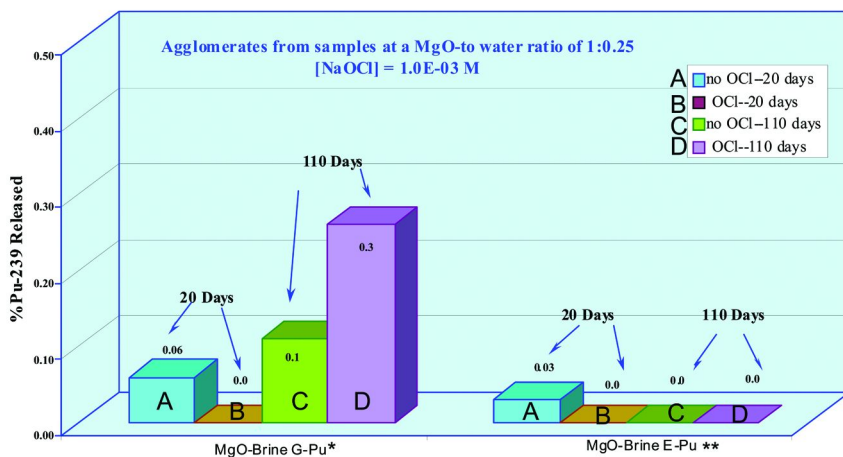
Figure 7. Desorption of $^{239}Pu(VI)$ from Pu-loaded MgO-brine agglomerates under non-agitated conditions (22) MgO-Brine G-Pu*: $MgCl_2.6H_2O$ based brine MgO-Brine-E Pu**: NaCl based Brine

The aim of the experiments as presented here is to develop a fast method to determine formation rates of radiolytic species in repository related groundwater or brines. A "cold" experimental approach is used to determine radiation-induced formation rates of radiolytic species by applying beam-line experiments irradiation on liquid media by treating 5 M NaCl and synthetic NaCl-based brine (Brine E described in Table II) with 4.9 MeV protons and 5.2 MeV Helium ions. In a first accelerator-based experiment the results show that ion-irradiation of 5 M NaCl solution with 12 μC (12 μC = charge of 5.20126 10^{11} electrons) of 4.9 MeV protons was already sufficient to induce the hypochlorite formation indicated by

UV-visible absorption spectra at 292 nm, associated with an absorbed dose of 2.96 kGy (Figure 8A). A total absorbed dose of 7.41 kGy was achieved and the formation of hypochlorite followed an approximately linear trend as a function of total absorbed dose (Figure 9A). The irradiation of a more complex NaCl-based brine (Brine E) by 5 MeV helium ions on the other hand, produced different radiolytic species which were unexpected. The irradiation of brine E led to the formation of Br_2Cl^- and Br_3^- associated with a peak at 247 nm and 266 nm, respectively (Figure 8B). Each incremental irradiation step of 6 μC of 5.2 MeV He^{++} is associated with radiation energy of 15.49 J, to step-wise increase the absorbed irradiation dose in the test cell by 651 Gy. The achieved total absorbed dose was 5.86 kGy. Incrementally introducing 651 Gy doses into the 20 mL brine solution induced the formation of Br_2Cl^- and Br_3^- species and linearly increased concentrations as a function of total absorbed dose (Figure 9B).

The main objective of these irradiation experiments is to determine the formation rates of radiolytic species (G-value, 100eV yield) as input data for the overall geochemical and radiochemical repository model. The measured G-value for the formation of OCl^- in a 20 mL quartz cell containing 5 M NaCl solution, irradiated by 5 MeV protons was determined to be 0.0949 molecules /100 eV, which is in good agreement with the data published by Kelm et al. (*29*) of 0.0965 applying alpha-self-irradiation using plutonium solutions of 3.7 GBq/L (0.1Ci/L).

The irradiation of NaCl-based synthetic brine E by 5.2 MeV He^{++} ions up to a total absorbed radiation dose of 5.86 kGy, led to the formation of tribromide (Br_3^-) and bromide-chloride species (Br_2Cl^-) (Figure 8B). The G-value for the formation of Br_2Cl^-, $G(Br_2Cl^-)$, obtained by irradiating the brine solution with 5.2 MeV helium ions is determined to be $3.51*10^{-3} \pm 0.04*10^{-3}$ (molecules per 100 eV), while the G-value for the formation of Br_3^-, $G(Br_3^-)$, is determined to be $2.67*10^{-3} \pm 0.04*10^{-3}$.
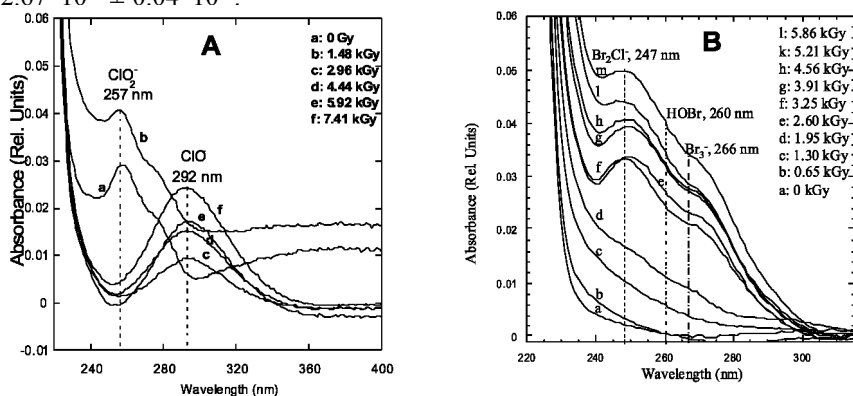
*Figure 8. **A**: Ion-irradiation induced formation of ClO_2^- and OCl^- in 5 M NaCl (pH 13) introducing 4.9 MeV protons. The UV Vis absorption spectra were taken after each incremental dose of 1.48 kGy. The final irradiation dose was 7.41 kGy. **B**: UV Vis absorption spectra of chloro-bromide species in synthetic NaCl-based brine E, pH 7.83. The brine was irradiated with incremental steps of 6 μC 5.2 MeV He^{++} ions introducing irradiation doses of 651 Gy per step. The final irradiation dose was 5.86 kGy.*
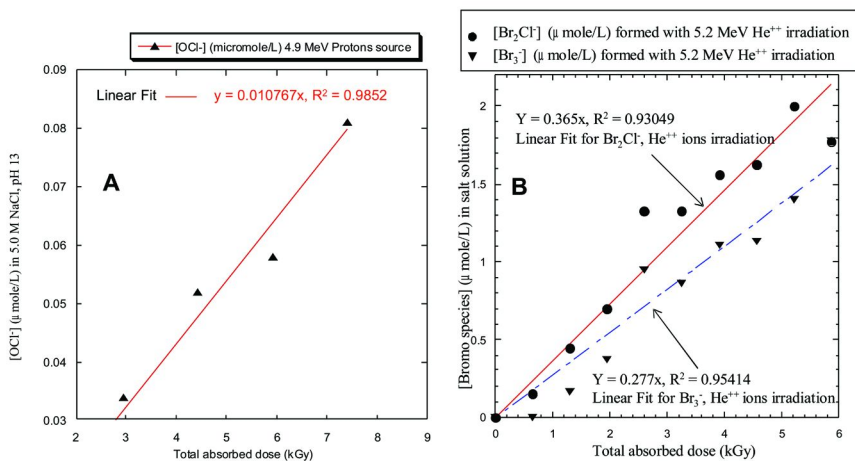
*Figure 9. Irradiation-induced formation of radiolytic products. **A**:
Proton-irradiation-induced hypochlorite formation as a function of total
absorbed dose while irradiating 20 mL of 5 M NaCl solution with 4.9 MeV
proton ions; **B**: Irradiation-induced formation of ClBr₂⁻ and Br₃⁻ as a function of
absorbed dose. 20 mL of synthetic WIPP Castile brine E was irradiated with 5.2
MeV He⁺⁺ ions.*

The resulting concentrations of radiolytic species with increasing dose will
follow a logarithmic function and reaching plateau-type saturation on a long
term. This long-term steady-state concentration of radiolytic species as a result of
radiation-induced formation and their likely catalytic or photolytic decomposition
are dependent on radiation dose rates, while primary formation rates defined as
G-values (100 eV yields) as determined here are basically independent of (*alpha*)
dose rates. However, this short-term irradiation experiment demonstrates that the
radiation-induced formation of Br_2Cl^- and Br_3^- is activated at rather low absorbed
doses and their concentrations are initially rising in a linear fashion (Figures 9A
and 9B).

Speciation of Actinides

Without recycling, actinides, in particular plutonium, along with fission
products such as technetium-99 make the largest contribution to the radiotoxicity
of radioactive waste over an extremely long time period (Figure 10). For this
reason, investigation of their geochemical behavior is a priority research around
the scientific community. The ultimate goal is to derive thermodynamic data
of complexation and association equilibria in the aqueous phase (formation of
mobile radionuclides species). As the concentration of actinides in repository
relevant aquatic systems is in the trace range (nanomole), highly sensitive direct
spectroscopic speciation methods are developed and applied. Advances have
been significant in the last decade in characterization of chemical elements in
complex chemical systems by the application of species-sensitive techniques in
combination with species-determining techniques.
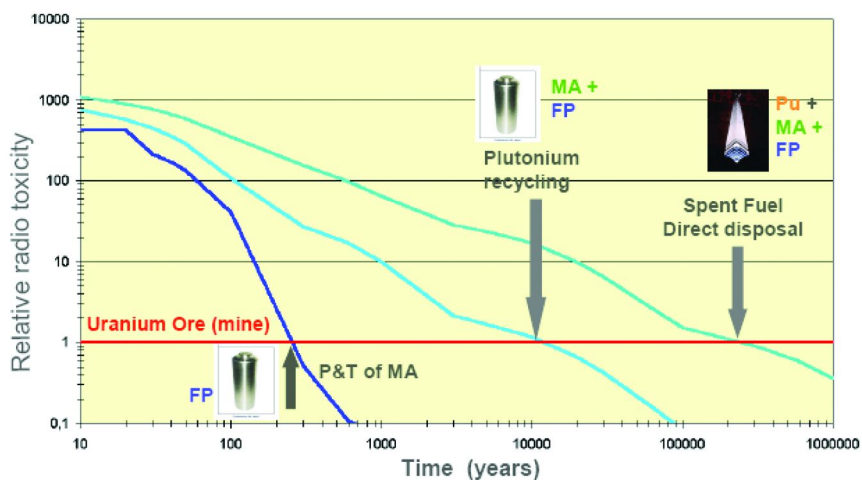
Figure 10. Relative radiotoxicity of used fuel as a function of time (30)
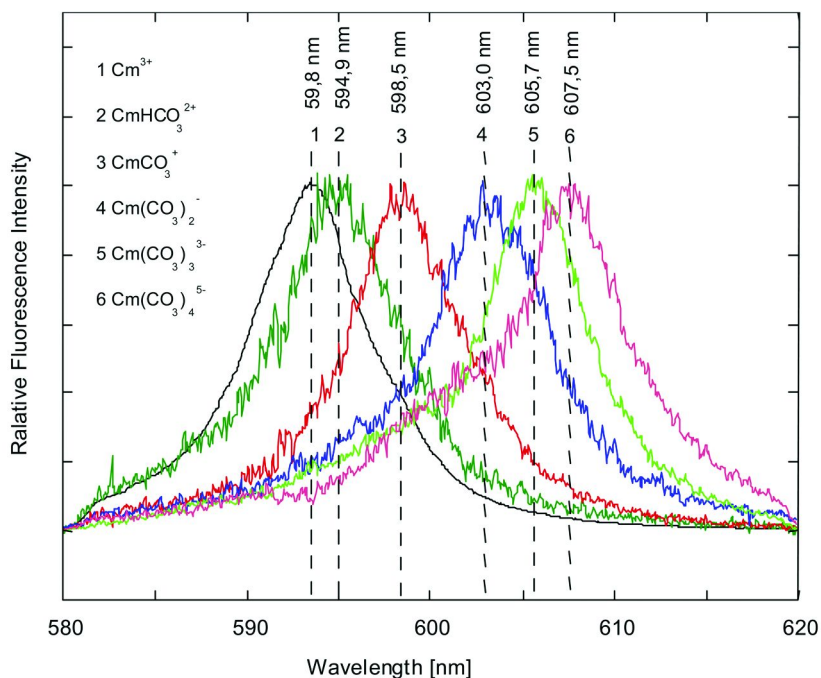
Figure 11. Selected fluorescence emission spectra of Cm (III) in carbonate media. Mixture 0.01 m Na_2CO_3 - 1.0 m $NaHCO_3$. Spectra are scaled to the same peak area.

Table IV. Limit of detection for the main element of interest by TRLFS (*31*) (with permission)

Element	Detection limit (M)
Uranium	5.10^{-9}
Curium	10^{-8}
Americium	10^{-6}
Europium	10^{-8}

Table V. Spectroscopic characteristics of aqueous, sulfate, carbonate, and silica-sorbed curium species

Species	Emission (nm)	FWHM (nm)	Lifetime (µs)	n H_2O	Ref.
Cm^{3+}	593.8	7.7	68 ± 3	8.7 ± 0.4	(*32*)
$Cm(OH)^{2+}$	598.8	11.5	72 ± 3	8.1 ± 0.4	(*32*)
$Cm(OH)_2^+$	603.5	11.2	80 ± 10	7.2 ± 0.7	(*32*)
$CmSO_4^+$	596.2	9.5	88 ± 2	6.5 ± 0.6	(*33*)
$Cm(SO_4)_2^-$	599.5	8	95 ± 8	5.9 ± 0.7	(*33*)
$Cm(SO_4)_3^{3-}$	602.2	5.5	195 ± 3	2.5 ± 0.5	(*33*)
$CmH(CO_3)^{2+}$	594.9	8.6			(*34*)
$Cm(CO_3)^+$	598.5	8.4	85 ± 4	6.8 ± 0.5	(*34, 35*)
$Cm(CO_3)_2^-$	603.0	7.5	105 ± 5	5.3 ± 0.6	(*34, 35*)
$Cm(CO_3)_3^{3-}$	605.7	7.1	215 ± 6	2.1 ± 0.5	(*34, 35*)
$Cm(CO_3)_4^{5-}$	607.5	11.7			(*34*)
$\equiv SiOCm(I)$	602.3	8	220 ± 14	2.1 ± 0.5	(*35*)
$\equiv SiOCm(II)$	604.9	13.2	740 ± 35	≈ 0	(*35*)

These methods allow identifying the chemical form (speciation) of radionuclides. Time Resolved Laser Fluorescence Spectroscopy (TRLFS) is the method of choice for actinide speciation in the nanomolar concentration range because of its high sensitivity resulting from laser excitation, rapidity (few minutes analysis), and direct information obtained (spectral and temporal) on complexes present in solutions. The following criteria: (1) excitation wavelength 375 nm for Cm (III) as an example (with the correct choice of the dye laser), (2) emission selectivity since each element studied gives a characteristic fluorescence spectrum, and (3) time resolution parameters, permitsdiscrimination of long lifetime fluorescence against undesirable short lifetime fluorescence. Table IV lists the limit of detection of speciation for U, Cm, Am, and Eu.
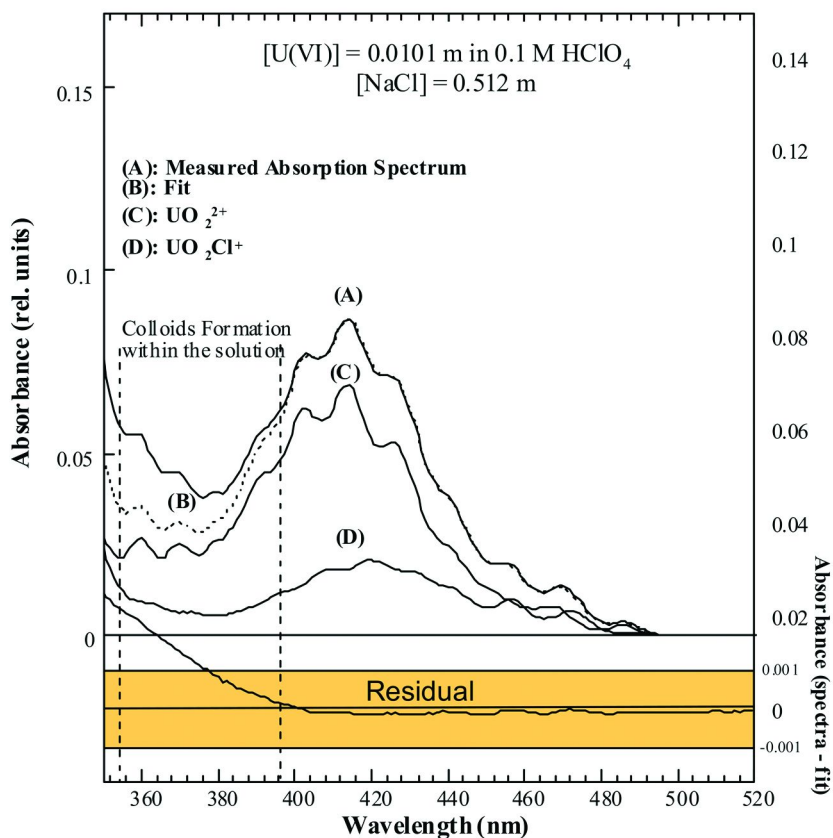
Figure 12. Peak deconvolution of a mixed spectrum, [U(VI)] = 0.0101m, [NaCl] = 0.512m

Some selected fluorescence emission spectra of Cm(III) ions and its complexation by carbonate in very dilute solutions in the wavelength range from 580 to 620 nm are presented in Figure 11. At 0 molal ligand concentration, the emission spectrum represents the Cm^{3+} ion. The ligand concentration increase is associated with a shift of the fluorescence emission spectrum towards higher wavelength and a change in the shape of the spectrum. These noticeable changes are attributed to the formation of Cm(III) complexes.

The experimentally observed spectroscopic characteristics for the individual curium(III) species under different conditions and in different media are is listed in Table V.

Complexation of dioxouranium (VI) chloride is presented to illustrate actinide speciation studies studied by UV Vis spectrophotometry (Figure 12). The complex formation of dioxouranium (VI) chloride complexes in NaCl solution was investigated, because the understanding of the uranium chemical behavior in brines is an important task to further predict overall generic salt repository performance and requires additional comprehension in regard to the interaction between UO_2^{2+} and chloride ions (*36–38*). As shown in Figure 12, the spectrum

of [UO$_2$CO$_3$] = 0.0101m measured at a chloride molality of 0.512 mol/kg H$_2$O is plotted together with the spectra of the individual components UO$_2^{2+}$, UO$_2$Cl$^+$, and UO$_2$Cl$_2^0$. The residual of the profile fit as the difference between the measured spectrum and the sum of the spectra of the individual species, as well as the fitted overall spectra are displayed.

Complexation reactions of actinides in groundwater solutions or brines are highly diverse. The understanding of chemical speciation of actinides such as Cm(III) or U(VI) under generic salt repository conditions is crucial in order to perform accurate safety analysis and to extrapolate performance assessment of potential nuclear repository for the time to come. Actinide sorption/desorption, coprecipitation, secondary phase formation, mineralization, and most importantly migration under the conditions of the repository are determined by their chemical form, and their speciation.

Conclusion

Scientific integration of the following disciplines, geochemistry, mineralogy, radiolysis, and actinide chemistry are essential for the accurate evaluation of long-term exposure and the support of performance assessment of any nuclear repository, independently of the geologic formation (salt, tuff, hard rock or clay). Data on the interaction of backfill material and the geologic medium, actinide sorption / desorption under repository relevant conditions, radiolytic product formation, and actinide speciation under repository conditions demonstrate that these data are crucial in order to understand the complex chemistry involved in any repository system. For now, the uncertainty in the assessment of long-term geochemical and radiochemical repository conditions as well as in the approximation of long-term exposure is rather high and it seems necessary to lower their degree of freedom by implementing a broader array of experimental data.

Latest techniques on the quantification of solid phase formation by Rietveld refinement have been applied, new approach to determine formation rates of radiolytic species using an ion-accelerator have been developed, and furthermore new speciation techniques such as laser spectroscopy have been utilized to provide new insights on actinide chemical reactions in the nanomole range and under natural aquatic conditions to reflect the geochemical situation of a generic salt repository. If nuclear recycling is considered as a viable option, the maximum dose resulting from the disposal of high level waste from various fuel cycle scenarios will not significantly change from one scenario to the other. Even though, we may used advanced recycling technologies such as TALSPEAK process or DIAMEX/SANEX process, and build fast neutron reactors by 2040, the availability of nuclear repositories will not be an option but a necessity and a reality. For all considered repositories worldwide: clay in France, tuff in USA, hard rock in Sweden and Finland, salt in USA and Germany, an integrated repository science program encompassing some of the techniques and experiments described here is strongly recommended to fully master and understand all the geochemical, radiochemical, chemical reactions that may be involved.

References

1. Duerden, S. L.; Hooper, A. J.; Trivedi, D. P.; Humphreys, P. N. *Radioactive Waste Disposal in the United Kingdom: Use and Application of Cements and Backfill Materials*; R&D Technical Report P178; International Workshop on the Uses of Backfill in Nuclear Waste Repositories, Carlsbad, NM, May 1998; pp 2-136−2-153.

2. Zuidema, P.; Berner, U. *Cementitious Backfill: The Swiss View*; R&D Technical Report P178; International Workshop on the Uses of Backfill in Nuclear Waste Repositories, Carlsbad, NM, May 1998; pp 2-121−2-124.

3. Stroes-Gascoyne, S.; Johnson, L. H. *Clay- and Cement-Based Backfill and Sealing Materials Designed for Use in a Canadian Nuclear Fuel Waste Disposal Vault*; R&D Technical Report P178; International Workshop on the Uses of Backfill in Nuclear Waste Repositories, Carlsbad, NM, May 1998; pp 2-15−2-31.

4. Geckeis, H.; Metz, V.; Kienzler, B. Geochemical behaviour of radionuclides in the multi-barrier system of a nuclear waste repository. *Nachrichten–Forschungszentrum Karlsruhe, Forschungszentrum Karlsruhe* **2004**, *36* (2), 110−115.

5. Brewitz, W.; Noseck, U. *Comptes Rend. Phys.* **2002**, *3* (7−8), 879–889.

6. Loida, A.; Kienzler, B.; Metz, V *High Level Waste Forms for Repositories in Rock Salt and Argillaceous Rocks: Concepts for Future Investigations*. Tagungsbericht−Jahrestagung Kerntechnik 2007, Institut fuer Nukleare Entsorgung, Forschungszentrum Karlsruhe GmbH: Karlsruhe, Germany, 2007; pp 387−390.

7. Bynum, R.; Stockman, V.; Papenguth, H.; Wang, Y.; Peterson, A.; Krumhansl, J.; Nowak, E.; Cotton, J.; Patcher, S.; Chu, M. *Identification and Evaluation of Appropriate Backfills for the Waste Isolation Pilot Plant (WIPP)*; Report SAND-98-1026C; International Workshop on the Uses of Backfill in Nuclear Waste Repositories, Sandia National Laboratory: Albuquerque, NM, 1998; pp 1−12.

8. Krumhansl, J.; Molecke, M. A.; Papenguth, H. W.; Brush, L. H. *A Historical Review of Waste Isolation Pilot Plant Backfill Development*. 7th International Conference Proceedings on Radioactive Waste Management and Environmental Remediation, Nagoya Japan, September 26−30, 1999; American Society of Mechanical Engineers: New York, 1999; pp 530−537.

9. Kelly, J. W.; Krumhansl J. L.; Papenguth, H. W.; Bynum, R. V.; Nowak, E. J.; Stockman, C. T.; Wang, Y. *MgO-Backfill Effects on the Chemical Conditions in the WIPP*. 8th International Conference Proceedings on High-Level Radioactive Waste Management, Las Vegas, NV, May 11−14, 1998; American Nuclear Society: La Grange Park, IL, 1998; pp551−553.

10. Atkins, M.; Glasser, F. P.; Kindness, A. *Cem. Concr. Res.* **1991**, *22* (3), 241–246.

11. Berner, U. R. *Radiochim. Acta* **1988**, *44−45*, 387–393.

12. Bonen, D. *J. Am. Ceram. Soc.* **1992**, *75*, 2904–2906.

13. Königsberger, E; Königsberger, L. C.; Gamsjäger, H. *Geochim. Cosmochim. Acta* **1999**, *63*, 3105–3119.

14. Pokrovsky, O. S.; Schott, J.; Thomas, F. *Geochim. Cosmochim. Acta* **1999**, *63*, 863−880.

15. Zheng, L.; Xuehua, C.; Mingshu, T. *Cem. Concr. Res.* **1991**, *21* (6), 1049–1057.

16. Hartmann, T. *Phase Constitution, Phase Formation and Reaction Products of Designated MgO Backfill Material for the WIPP Repository in Contact with Synthetic WIPP Brines*; Report LA-UR-02-2797; Los Alamos National Laboratory: Los Alamos, NM, 2002; pp 1−46.

17. Villarreal, R.; Morzinski, A.; Bergquist, J.; Leonard, S. *The Actinide Source-Term Waste Test Program (STTP)*, unpublished.

18. Farr, J. D.; Schulze, R. K.; Honeyman, B. D. *Radiochim. Acta* **2000**, *88*, 675–678.

19. Lu, N.; Conca, J.; Hartmann, T.; Paviet-Hartmann, P.; Parker, G.; Martinez, B.; Strietelmeier, E. *Solution Chemistry and Plutonium-239 Behavior in Synthetic Brines and Chloride Solutions after Exposure to Magnesium Oxide Backfill*; Report LAUR-02-3665; Los Alamos National Laboratory: Los Alamos, NM, 2002; pp 1−33.

20. Langmuir, D. In *Aqueous Environmental Geochemistry*; Prentice-Hall, Inc.: Upper Saddle River, NJ, 1997; pp 529−530.

21. Cleveland, J. M. In *The Chemistry of Plutonium*; American Nuclear Society: La Grange Park, IL, 1979; p 107.

22. Paviet-Hartmann, P; Hartmann T. *Optimizing Nuclear Waste Repository Development by Implementing Experimental Data on Radiolysis*. Conference Proceedings Global 2007, Boise, ID, September 9−13, 2007.

23. Hartmann, T.; Paviet-Hartmann, P.; Wetteland, C.; Lu, N. *Rad. Phys. Chem.* **2003**, *66*, 335–341.

24. Hartmann, T.; Wetteland, C.; Ware, D.; Lu, N.; Sage, S.; Walthall, M.; Moir, D.; Paviet-Hartmann, P. *Spectroscopic Investigation of the Formation of Hypochlorite, Radiolysis By-Product in 5 M NaCl Featuring High-Energy Proton Beam Line Experiments*. International Conference Proceedings Spectrum 2002, Reno, NV, August 4−8, 2002; American Nuclear Society: La Grange Park, IL.

25. Kelm, M.; Bohnert, E. *Nucl. Technol.* **2000**, *129*, 123–130.

26. Ershov, B.; Janata, E.; Kelm, M. *Meendeleev Commun.* **2001**, *4*, 149–150.

27. Ershov, B.; Kelm, M.; Gordeev, A.; Janata, E. *Phys. Chem. Chem. Phys.* **2002**, *4*, 1872–1875.

28. Ershov, B.; Kelm, M.; Janata, E.; Gordeev, A.; Bohnert, E. *Radiochim. Acta* **2002**, *90* (9−11), 617–622.

29. Kelm, M.; Pashalidis, I.; Kim, J. I. *Appl. Radiat. Isot.* **1999**, *51*, 637–642.

30. Bouchard, J. *International Energy Agency Workshop on Energy Technology Roadmaps*; International Energy Agency (IEA): Paris, May 15−16, 2008.

31. Moulin, C. *Evaluation of Speciation Technology*; Nuclear Energy Agency (NEA), Organisation for Economic Co-operation and Development (OECD): Paris, 1999; pp 51−59.

32. Fanghänel, Th.; Kim, J. I.; Paviet, P.; Klenze, R.; Hauser, W. *Radiochim. Acta* **1994**, *66−67*, 81–87.

33. Paviet, P.; Fanghänel, Th.; Klenze, R.; Kim, J. I. *Radiochim. Acta* **1996**, *74*, 99–103.
34. Fanghänel, Th.; Weger, H. T.; Könnecke, Th.; Neck, V.; Paviet-Hartmann, P.; Steinle, E.; Kim, J. I. *Radiochim. Acta* **1998**, *82*, 47–53.
35. Paviet-Hartmann, P.; Fanghänel, Th.;Klenze, R.; Könnecke, Th.; Kim, J. I.; Hauser,W.; Weger, H.; Park, K. K.; Chung, K. H. *Evaluation of Speciation Technology*; Nuclear Energy Agency (NEA), Organisation for Economic Co-operation and Development (OECD): Paris, 1999; pp 221−229.
36. Lin, M. R.; Paviet-Hartmann, P.; Xu, Y.; Tait, C. D.; Runde, W. H. *Abstr. Pap., Am. Chem. Soc.* **1998**, *216* (1−3), 65.
37. Paviet-Hartmann, P.; Lin, M. R. *Mat. Res. Soc. Symp. Proc.* **1999**, *556*, 977–984.
38. Paviet-Hartmann, P.; Lin, M. R *Abstr. Pap., Am. Chem. Soc.* **2002**, *224* (1), U712.

Indexes

Subject Index

H

I

L

M

N